Tarik Mitran
Ram Swaroop Meena
Abhishek Chakraborty *Editors*

Geospatial Technologies for Crops and Soils

Springer

Geospatial Technologies for Crops and Soils

Tarik Mitran • Ram Swaroop Meena •
Abhishek Chakraborty
Editors

Geospatial Technologies for Crops and Soils

Springer

Editors
Tarik Mitran
Soil and Land Resources Assessment Division
National Remote Sensing Centre
Department of Space, ISRO
Hyderabad, Telangana, India

Abhishek Chakraborty
Agroecosystem and Modeling Division
Agricultural Sciences and Applications Group, National Remote Sensing Centre
Department of Space
ISRO
Hyderabad, Telangana, India

Ram Swaroop Meena
Department of Agronomy, Institute of Agricultural Science
Banaras Hindu University
Varanasi, Uttar Pradesh, India

ISBN 978-981-15-6863-3 ISBN 978-981-15-6864-0 (eBook)
https://doi.org/10.1007/978-981-15-6864-0

This Springer imprint is published by the registered company Springer Nature Singapore Pte Ltd.
The registered company address is: 152 Beach Road, #21-01/04 Gateway East, Singapore 189721, Singapore

Foreword

THE OHIO STATE UNIVERSITY

School of Environment and Natural Resources
Ohio Agricultural Research and Development Center

Carbon Management and Sequestration Center (C-MASC)
210 Kottman Hall | 2021 Coffey Rd, Columbus, OH 43210
lal.1@osu.edu | cmasc.osu.edu | 614-292-9069 Phone | 614-292-7432 Fax

The ever-growing world population will lead to enormous pressure on land resources to produce food for 10 billion people in 2050. However, to meet the future challenges of feeding the world population, there is a need for a continuous assessment and prioritized intervention to halt the declining trends in crop productivity, minimizing the rate of land degradation, reducing the environmental damage, and enhancing farm income through a sustainable resource development plan. The adoption of Geospatial Technologies encompassing techniques and tools related to Remote Sensing (RS), Geographic Information System (GIS), Global Positioning System (GPS), advanced data processing, Information Technology (IT)-driven outreach, and web-services might play the much-needed role of a fulcrum to increase future agricultural productivity. Geospatial technologies can pave way for significant

improvements in efficiency of input-use, resulting in cost savings on inputs and precious resources. Geospatial tools can be used for soil profiling, satellite imagery, and mapping results to assess nutrient deficiencies in site-specific location and fine tune products (i.e., area-specific fertilizer mixtures for crops), which can help promote judicious and balanced use of fertilizers rather than blanket applications that can lead to several environmental issues .The goal is to develop agricultural resources management options for advancing global food security, adapting and mitigating climate change, and promoting "Sustainable Development Goals" of the United Nations.

Therefore, this book is timely and highly pertinent because it addresses the applications of geospatial technologies for crops and soils. It also provides information about cost-effective measures, easy-to-understand interpretation, and the documentation needed to formulate sustainable action plans to achieve effective resource management at global, national, regional, and farm level. The information collated in this book is based on joint efforts of many scientists, professors, experts, and researchers. It is a reflection of long years of professional experience of the authors in reviewing, analyzing, and synthesizing the vast and dynamic field of expertise and innovations. The authors have focused on many case studies that review a variety of modern tools and techniques for data collection, storage, analysis, update, integration, interpretation, and representation for informed decision making. Specifically, the book highlights availability and use of various spatial, temporal, and spectral data to formulate sustainable resources development plans and associated challenges. The authors have explored and examined numerous advances such as those related to precision farming, crop monitoring, crop production, soil moisture, soil quality, land degradation, digital soil mapping, agricultural land use, etc.

Above all, authors have highlighted the use of proximal sensing, unmanned aerial vehicle (UAV), and various modelling approaches to assessing crops and soils. They have also described the applications of GIS which is considered one of the important tools for decision making in a problem-solving environment dealing with geo-information. They have elucidated that such technologies can monitor the overall prospect of agriculture through its capabilities to provide decision support scenarios. Hence, the book is a major contribution to the field of crop and soil science by highlighting the importance of applied research. Finally, the contributors have prepared the volume encompassing latest developments in the field of geospatial technologies. This book is a pertinent reference material for policymakers, researchers, students, and practitioners in soil science, agronomy, ecology, and management of natural resources with specific focus on some global

issues such as food and nutritional security, adaptation and mitigation of climate change, soil quality, biodiversity, and the action plan for advancing the "Sustainable Development Goals" of the United Nations.

Sincerely,

Rattan Lal

Distinguished University Professor of Soil Science, SENR; Director, Carbon Management and Sequestration Center, The Ohio State University, Columbus, OH, USA

May 11, 2020

Preface

Human civilization has started facing an unprecedented situation towards the sustainable use of natural resources for the ever-increasing population. The situation is further complicated by the changes in temperature and rainfall patterns, increasing extreme weather events, altered pest and disease profiles, and rapid degradation of land and soil quality. So there is a need to introduce the latest technologies in agriculture to enhance its production and also help policymakers make informed decisions. Geospatial technologies and tools which includes Remote sensing (RS), Geographical Information System (GIS), Global Positioning System (GPS), mobile and web applications, etc., would provide unique capabilities to analyze multi-scale multi-temporal datasets and generate decision supports to sustainable development, food, nutritional environmental, and economic security. Satellite RS images of an optical, microwave, thermal, and hyperspectral domain could provide a unique instrument allowing a regular and synoptic coverage of crop and soil resources at a continental or regional level. Hence, it proved to be a powerful tool to assess crop and soil properties in varying spatial and temporal scales with cost-effectiveness.

This book is a compilation of the development in the field of geo-spatial technologies towards monitoring and assessment of crops and soils. The focus has been given on the crop monitoring, crop growth and yield simulation modeling, crop yield estimation, crop production estimation, retrieval of crop biophysical and biochemical parameters, precision agriculture, etc. Moreover, soil moisture estimation, land degradation assessment, soil quality assessment, digital soil mapping, hyperspectral, and microwave remote sensing for crops and soils assessment have also been discussed in detail. Further, special emphasis is provided to integrate multi-dimensional, multi-temporal, multi-scale data, and its analytics towards informed decision making. The objective of this book is to document the applications of space-based technologies for crops and soil assessment for sustainable development of agriculture.

In general, this book is suitable for agronomists, soil scientists, environmentalists, researchers, policymakers, and students who wish to simultaneously enhance the production and profitability of land resources. Moreover, the editors have provided a road map to achieve sustainable crops and soil management using geo-spatial

technologies. All chapters are well-illustrated with case studies, figures, appropriately placed data tables and photographs, and supported with extensive and most recent references.

Hyderabad, Telangana, India — Tarik Mitran
Varanasi, Uttar Pradesh, India — Ram Swaroop Meena
Hyderabad, Telangana, India — Abhishek Chakraborty

Contents

About the Editors

Tarik Mitran is a Soil Scientist working in Soil and Land Resources Assessment Division, National Remote Sensing Centre, Indian Space Research Organisation (ISRO), Hyderabad, India. He completed his Ph.D. in Agricultural Chemistry and Soil Science in 2012 at Bidhan Chandra Krishi Viswavidyalaya, West Bengal, India, with Prestigious "Maulana Azad National Fellowship" funded by University Grant Commission, India. In 2017, he completed his postdoctoral research on "Soil Carbon Modeling Using Geospatial Techniques" under Prof. Rattan Lal, World Food Prize 2020 Laureate, Distinguished Scientist and Director of Carbon Management and Sequestration Centre (CMASC), The Ohio State University (OSU), USA. Dr. Mitran has published 25 articles in reputed peer-reviewed journals, 8 book chapters, 15 conference papers as well as number of technical bulletins, popular articles, and scientific reports. He has been awarded prestigious "INDO-US Post-doctoral Fellowship" in 2016 by Science and Engineering Research Board (SERB) and Indo-U.S. Science and Technology Forum (IUSSTF), Department of Science and Technology (DST), India. Dr. Mitran has also received "Certificate of Recognition" from Office of International Affairs, OSU, USA; "Junior Scientist of the Year 2017" by IFEE and Confederation of Indian Universities (CIU), New Delhi; "Clean Environment Education and Promotion Award" by International Benevolent Research Foundation (IBRF), Kolkata; and Best Poster Presentation Award twice by Indian Society of Soil Science, New Delhi. He has qualified National

Eligibility Test (NET) in Soil Science twice, conducted by Indian Council of Agricultural Research (ICAR). Dr. Mitran has also received University Merit Scholarship, Junior/Senior Research Fellowship during his studies. He is actively involved as a Principle Investigator/ Co-Principle Investigator in various National, Operational, as well as technology development projects at National Remote Sensing Centre, ISRO, India. His current areas of research is soil carbon assessment, soil CO_2 efflux assessment and its role in climate change, soil fertility and spatial mapping, predictive soil mapping, hyperspectral remote sensing of soils, land degradation assessment using remote sensing, soil erosion modelling, land use and land cover assessment using remote sensing, etc. Dr. Mitran is also acting as a reviewer for various peer-reviewed international journals and is member of scientific societies.

Ram Swaroop Meena is working as an Assistant Professor in the Department of Agronomy, Institute of Agricultural Sciences, BHU, Varanasi (UP). Dr. Meena has secured first division in all the classes with triple NET, Junior Research Fellowship (JRF), and Senior Research Fellowship (SRF) from the Indian Council of Agricultural Research (ICAR) and RGNF Award from the University Grants Commission (UGC), Government of India. Dr. Meena has been awarded Raman Research Fellowship by the Ministry of Human Resource Development (MHRD), GOI. He has completed his postdoctoral research on soil carbon sequestration under Prof. Rattan Lal, World Food Prize 2020 Laureate, Distinguished Scientist and Director of Carbon Management and Sequestration Centre (CMASC), The Ohio State University, USA. Dr. Meena is working on soil sustainability, crop productivity, and resources use efficiency under the current climatic era. Dr. Meena has supervised 20 postgraduate and 5 Ph.D. students, and he has 10 years of research and teaching experience at the undergraduate/postgraduate/Ph.D. level. He is working on the three externally funded running projects from DST, MHRD, and ICAR (GOI) and involved in many academic and administrative activities going on at the institute/university level. Dr. Meena has published more than 110 research and review papers in peer-reviewed reputed journals up

to 7.2 impact factor with H-index 38. He has published 4 books at the national level and another 12 books at the international level and contributed to 15 book chapters at national and 35 at international levels. Dr. Meena has worked as an expert in the National Council of Educational Research and Training (NCERT), MHRD, GOI, to develop the two books for school education at XI and XII standards. Dr. Meena has been awarded several awards, namely, Young Scientist, Young Faculty, Global Research, Excellence in Research, Honorable Faculty Award, etc. Dr. Meena is a member of 9 reputed national and international societies and is working as a general secretary, editor, and member of the editorial board in 12 national and international peer-reviewed reputed journals and has attended several national and international conferences in the country and abroad. Dr. Meena is contributing to the agricultural extension activities on farmers' level as associate coordinator in trainings, meetings, workshops, and farmers' fair.

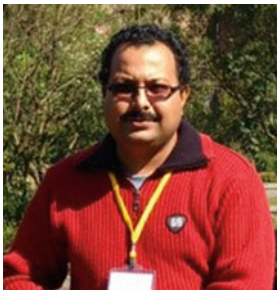

Abhishek Chakraborty is working as a Senior Scientist at the National Remote Sensing Centre (NRSC), Indian Space Research Organisation, Hyderabad, India. He has completed his B.Sc. (Hon) in Agriculture at Bidhan Chandra Krishi Viswavidyalaya, West Bengal, India, and obtained his M.Sc. and Ph.D. degrees from the Division of Agricultural Physics, Indian Agricultural Research Institute, New Delhi. Dr. Chakraborty has more than 15 years' experience in the applications of geospatial technologies in agriculture. He has been working under several projects of national importance funded by DST, ISRO, Central/State Ministries, etc. He is responsible for establishing a network of eddy covariance flux towers over different agro-ecosystems to study the dynamics of carbon/moisture fluxes. Dr. Chakraborty has developed a geo-portal (BHUVAN -JAIVOORJA) to assess spatial distribution of biomass potential from crop residues over India to facilitate site suitability of biofuel/biomass power plants. He played a significant role in National Agricultural Drought Monitoring and Assessment System of India and developed two new indices for detection of early season drought.

Dr. Chakraborty has also assessed long-term changes/shift in the weather patterns vis-a-vis crop phenology using time series satellite and weather data. He is recipient of ISSS gold medal for best doctoral thesis and four best paper awards in conferences. Dr. Chakraborty has co-guided two M. Tech. students and presently guiding a Ph.D. student. He has published more than 30 research papers in peer-reviewed reputed journals and conferences and more than 50 scientific reports. Dr. Chakraborty is life member of two national scientific societies. Presently, he is heading Agroecosystem and Modelling Division of NRSC.

Chapter 1
Geospatial Technologies for Crops and Soils: An Overview

Tarik Mitran, Ram Swaroop Meena, and Abhishek Chakraborty

Contents

Abstract Natural resource monitoring and assessment is a vital step to formulate a sustainable development plan. The introduction of various modern geospatial techniques and tools like Remote Sensing (RS), Geographic Information System (GIS), Global Positioning System (GPS), and information technology (IT) have provided

T. Mitran (✉)
Soil and Land Resources Assessment Division, National Remote Sensing Centre, Department of Space, ISRO, Hyderabad, Telangana, India
e-mail: tarikmitran@nrsc.gov.in

R. S. Meena
Department of Agronomy, Institute of Agricultural Science, Banaras Hindu University, Varanasi, Uttar Pradesh, India
e-mail: meenars@bhu.ac.in

A. Chakraborty
Agroecosystem and Modeling Division Agricultural Sciences and Applications Group, National Remote Sensing Centre Department of Space, ISRO, Hyderabad, Telangana, India
e-mail: abhishek_c@nrsc.gov.in

T. Mitran et al. (eds.), *Geospatial Technologies for Crops and Soils*,
https://doi.org/10.1007/978-981-15-6864-0_1

powerful approaches of surveying, identifying, classifying, mapping, monitoring, and characterization of the composition, extent, and distribution of various natural resources. Geospatial techniques deal with the acquirement, storage, processing, production, presentation, and dissemination of geoinformation. The information obtained from RS, GPS, and through conventional methods could be used effectively to create database in GIS platform for various spatial and temporal analysis related to sustainable management of land resource and formulate environment-friendly action plans. Major applications of geospatial technologies related to crops and soils are crop inventory and monitoring, crop production estimates and forecasting, crop growth simulation modeling, crop yield estimation, precision agriculture, soil mapping, land degradation assessment, soil erosion assessment, soil quality assessment, digital soil mapping, digital terrain modeling, soil-landscape modeling, land use/land cover mapping, agricultural land use planning, etc., which have a far-reaching impact on mapping, monitoring, and management of crop and land resources on sustainable basis. Geospatial approaches have made inroads across different sectors both in private and public domain in various countries across the world. Selected tools can help to restore the soil health, stop exploitation of the natural resources, reduce energy consumption, carbon and water footprints, and improve the productivity and sustainability under changing climate. Geospatial technologies for crops and soils a novel tool for the food, nutritional, environmental, and economic security for the future generations under limited natural resources. This book will be helpful for the producers, researchers, teachers, and policymakers to deal with the future alarming issues.

Keywords Agriculture · Geospatial · Geographic Information System · Information Technology · Remote Sensing

Abbreviations

AI	Artificial Intelligence
ALOS	Advance Land Observing Satellite
APEX	Airborne PRISM Experiment
AVIRIS	Airborne Visible Infrared Imaging Spectrometer
CA	Conservation Agriculture
CNSA	China National Space Administration
CSA	Climate-Smart Agriculture
DESIS	DLR Earth Sensing Imaging Spectrometer
DGPS	Differential Global Positioning System
EM	Electromagnetic
ENVISAT	Environmental Satellite
ESA	European Space Agency
EWT	Equivalent Water Thickness

FAO	Food and Agricultural Organization
FAPAR	Fraction of Absorbed Photosynthetically Active Radiation
GHGs	Greenhouse Gasses
GIS	Geographical Information System
GPS	Global Positioning System
HSI	Hyperspectral Imager
ISRO	Indian Space Research Organization
IT	Information Technology
JAXA	Japan Aerospace Exploration Agency
LAI	Leaf Area Index
LANDSAT	Land Satellite
MODIS	Moderate-resolution Imaging Spectrometer
MRS	Microwave Remote Sensing
NASA	National Aeronautics and Space Administration
NAVSTAR	Navigation System with Time and Ranging
NDRI	Normalized Difference Red Edge Index
NDVI	Normalized Difference Vegetation Index
NIR	Near Infrared
PA	Precision Agriculture
PALSAR	Phased Array Type L-band Synthetic Aperture Radar
PF	Precision Farming
RDVI	Renormalized Difference Vegetation Index
RISAT	Radar Imaging Satellite
RS	Remote Sensing
SAR	Synthetic Aperture Radar
SAVI	Soil Adjusted Vegetation Index
SIF	Sun Induced Fluorescence
SPAD	Soil Plant Analysis Development
SPOT	Système Pour l'Observation de la Terre
SWIR	Shortwave Infrared Region
TIR	Thermal Infrared
TM	Thematic Mapper
TRS	Thermal Remote Sensing
UAV	Unmanned Aerial Vehicles
UN	United Nation
USGS	United States Geological Survey
VRT	Variable Rate Technology

1.1 Introduction

For about 2.5 million years, human species fed themselves by hunting animals and gathering plants. Human ecological footprint was minimal. Nearly about 10,000 years ago, human started controlling and manipulating few animals and plants species for their benefit. This leads to development of agrarian society with concept of advance food security. It translated into population explosion and more tilling for the extra food. Since then humans have been facing this cyclic phenomenon and surprisingly surviving it. But in the present scenario, horizontal expansion of agricultural activities is limited. Hence, our sole effort has been directed toward vertical expansion under limited resources.

The latest United Nations (UN) projections reveal that the world population will rise from 6.8 billion to 9.1 billion in 2050, which leads to an increase in demand for agricultural produces by 60% (Alexandratos and Bruinsma 2012). Other constraints like fragmented land holdings, land degradation, deterioration of soil health, the declining trend of the total crop productivity, as well as global climatic variations have posed serious threats in agricultural growth and development. However, to meet up with the future challenges to feed the 9 billion people of the world, there is a need to halt the declining trend of the total crop productivity, minimizing the rate of degradation of natural resources, and enhancing farm incomes through sustainable resources development plan. The adoption of newly emerged technology and tools like remote sensing (RS), geographic information System (GIS), global positioning system (GPS) and information technology (IT) might play a major role to enhance agricultural productivity in the future (Hakkim et al. 2016) through continuous monitoring and assessment of the natural resources. The gamut of all these technologies and tools, termed as geospatial technology, is a rapidly growing and changing field that assists the user in the collection, storage, analysis, interpretation, and dissemination of spatial data. It is a cost-effective approach which includes acquisition of real-time satellite images through RS, data analysis and management through GIS, location services and geo-referencing through GPS, and web services and outreach through IT. The advances in RS generate data for detailed inventory, mapping, and monitoring of crop, land, and water resources on a large scale (Gerhards et al. 2019). Satellite RS coupled with GIS and mobile app–based positional information has emerged as an efficient tool for the sustainable development in agriculture sector by optimizing input resources, minimizing the cost of production, and risk of biotic/abiotic in nature. Such technologies have the capabilities to provide "Decision Support Scenarios" which could be vital for monitoring the overall health of the agricultural sector and facilitate informed decision-making. Some of the major applications of geospatial technologies related to agriculture are crop inventory and monitoring (Schmedtmann and Campagnolo 2015; Ghazaryan et al. 2018; Heupel et al. 2018), crop growth simulation modeling, crop yield estimation (Huang et al. 2019; Ban et al. 2019; Phung et al. 2020), PA (Friedl 2018; Neupane and Guo 2019), soil mapping (Manchanda et al. 2002; Mulder et al. 2011), assessment of soil erosion (Woldemariam et al. 2018; Meena et al. 2018;

Zabihi et al. 2019); assessment of soil quality (Paz-Kagan et al. 2014, 2015), digital soil mapping (Ma et al. 2019; Wadoux et al. 2019), water management for irrigated agriculture (Taghvaeian et al. 2018; Tazekrit et al. 2018; Ojo and Ilunga 2018), agricultural land use planning (Ambika et al. 2016; Useya et al. 2019; Pareeth et al. 2019), etc. The medium and coarse resolution RS datasets can provide a regular and synoptic coverage of crop and soil resources at a continental or regional level. Whereas the fine-resolution satellite data helps in micro-level or farm-level agricultural activities such as water resources mapping, drainage pattern, management of fertilizers, pesticides, variable rate technology, crop insurance, crop damage assessment, etc. RS data of optical, microwave, thermal, and hyperspectral domain has proved to be a powerful tool to assess crop and soil properties in varying spatial and temporal scales. Several researchers (Mulla 2013; Pareeth et al. 2019; Rotairo et al. 2019; Phung et al. 2020) have shown the usefulness of RS technology to get spatially and temporally variable information for agriculture. A large number of satellite RS data are available nowadays to the researcher for natural resources management such as Moderate-Resolution Imaging Spectrometer (MODIS), Land Satellite (Landsat), Sentinel, Resourcesat-2, Cartosat-1, Cartosat-2, Planet, and QuickBird, etc. The number of satellite missions by various space agencies like National Aeronautics and Space Adminstration (NASA), European Space Agency (ESA), Japan Aerospace Exploration Agency (JAXA), China National Space Administration (CNSA), Indian Space Research Organization (ISRO), etc., dedicated to RS, has increased space resources sgnificantly over the past decades and will further increase over the coming decades and beyond. Nowadays several countries from the Asia-Pacific, South Asia, North America, and Europe are creating an Agricultural Market Information System which utilizes geospatial tools to fuse basic socioeconomic and crop statistics for the overall management of agriculture produce and demand–supply chain. In nutshell, geospatial technology has become part and parcel of agriculture management system. The technology has proven its potential and effectiveness, and also provides scope of future development.

1.2 Current Challenges in Agriculture: Global Perspective

Agriculture, in generic sense, is harvesting of sunlight toward conversion of carbon dioxide and water into carbohydrate/sugar. This basic translation is modulated by prevailing weather, pests and diseases, soil, and plant resources. Often agriculture is livelihood, not a profitable business, particularly in the third world countries. Hence, agriculture is done sub-optimally with limited resources in majority of the global arable land. This caters the biggest challenges as well as the opportunities of agriculture.

Feeding 9 billion of human population by 2050 is the target set by FAO (Alexandratos and Bruinsma 2012). It requires increase of agricultural produce by 60% from present status. The target is really challenging and further complicated by the changing global climatic pattern (Meena et al. 2018a). The world scientific

community has reached to a broad consensus that the concentration of atmospheric greenhouse gases, mainly carbon dioxide, has been increasing unprecedently, and more so in the last few decades. This resulted in significant warming of global climate as evident from rise in global average air and ocean temperature, widespread melting of snow and ice, and rise in global average sea level. Studies across the globe have reported these changes over European region (Hasanean 2001; Domonkos and Tar 2003; Feidas et al. 2004), China (Liu et al. 2004), Japan and Korean peninsula (Chung and Yoon 2000; Yue and Hashino 2003), Malaysia (Tangang et al. 2007), Alaska (Stafford et al. 2000), and India (Revadekar et al. 2012; Chakraborty et al. 2017; Chakraborty et al. 2018). The warming pattern has also caused change in rainfall pattern, increase in extreme weather events, altered pest and disease profiles along with the crop phenology, and rapid degradation of land and soil quality (Cleland et al. 2007; Das et al. 2013; Chakraborty et al. 2014). The phenomena of the changing climatic and ecosystem condition have been found to be global in nature, though they do exhibit considerable spatial and temporal variability at local level.

To meet the demands of higher production, overexploitation of land may lead to land degradation. At present 33% of arable land suffers from various kinds of degradation processes. It is a global threat which leads to reduction in area and productivity of 13.4 billion ha of global cultivable land (Reddy 2003). Agricultural production is deleteriously affected due to inappropriate land care strategies in maximum portions of the world (Lambin and Meyfroidt 2011; Lambin et al. 2013). Sometimes direct impact of land degradation may appear in rapid desertification of semi-arid and arid region, frequent and intense drought occurrence, and loss of productive topsoil and biodiversity (Gibbs et al. 2010; Lambin and Meyfroidt 2011; Meena et al. 2020). Besides land degradation, volatile weather and extreme events would change the growing seasons; limit the availability of water; allow weeds, pests, and disease to thrive; and reduce crop productivity drastically. Apart from all the above-mentioned issues, some of the biggest problems facing the agricultural sector in developing and under-developed countries are low yield, fragmented land holdings, poor infrastructure, low use of appropriate and best farming techniques, a decline in soil fertility etc., which are leading contributors to low agricultural productivity. Hence, countries need to prioritize agriculture and growing food with more sustainable methods.

1.3 Importance of Geospatial Technologies

To meet up with the future challenges to feed the 9 billion people of the world, there is a need to continue investing in appropriate technologies to arrest the declining trend of the total crop productivity, minimizing the rate of degradation of natural resources, reducing environmental damage (including greenhouse gas emission), and enhancing farm incomes through a sustainable resources development plan. Over the few decades, the innovation in digital agricultural technologies such as

precision farming (PF), crop monitoring and surveillance system, artificial intelligence (AI) in agricultural decision supports, IT-driven extensions are gaining more importance. The adoption of such newly emerged technology and tools into the entire agriculture value chain might play major role in increasing agricultural productivity in the future (Hakkim et al. 2016; Mitran et al. 2018a). These technologies help in continuous monitoring and assessment of the condition and availability of the agricultural resources and simultaneously transformed agriculture into a sustainable ecosystem. Further, it can also reduce the impact of agriculture on the global environment by optimizing the use of water, fertilizer, fossil fuel, and land for food production. The greenhouse gas emissions contributed by agriculture can also be mitigated through adopting climate-smart practices.

1.4 Geospatial Tools and Techniques

The modern geospatial technologies include RS, GIS, GPS, proximal sensing, mobile technology, etc., which can be used efficiently for agricultural resources management and precision farming. The overall idea and integration of such technologies are presented in Fig. 1.1.

1.4.1 Remote Sensing

RS is the "science of making inferences about material objects from measurements, made at distance, without coming into physical contact with the objects under study" (Lillesand et al. 2015). A RS system consists of a platform (satellite, rocket, balloon, etc.), where a sensor can be mounted to collect and or emit radiation/signal (Sabins 1997). RS can be "active" when a signal is emitted by a satellite and its reflection by the object is detected by the sensor and "passive" when the object is illuminated by sunlight and its reflection/emission is detected by the sensor (Ran et al. 2017a, b). RS imagery along with GIS to process, alter, manipulate, store, and retrieve can very effectively used for natural resource management. RS images can be obtained either from sensor in satellite platform or boarded on small aircraft as aerial photography (Mulla 2013). Aerial photography is the original form of RS and remains the most widely used method until recently. It has few advantages, that is, aerial images are generally of high resolution depending on the flight height (3–5 km). They are relatively immune to the cloudiness, and acquiring time of the image can be scheduled at will. Aerial photographs are different types such as black and white, high- or low-altitude photographs, vertical/oblique, infrared, multi-spectral, etc. The selection of aerial photographs depends on the purpose of the study. These photographs are very useful in small areas for micro-level investigation. Vertical aerial photographs are mostly used in land use planning, cartography, specifically in photogrammetric surveys, to generate topographic maps (Twiss et al. 2001). Oblique

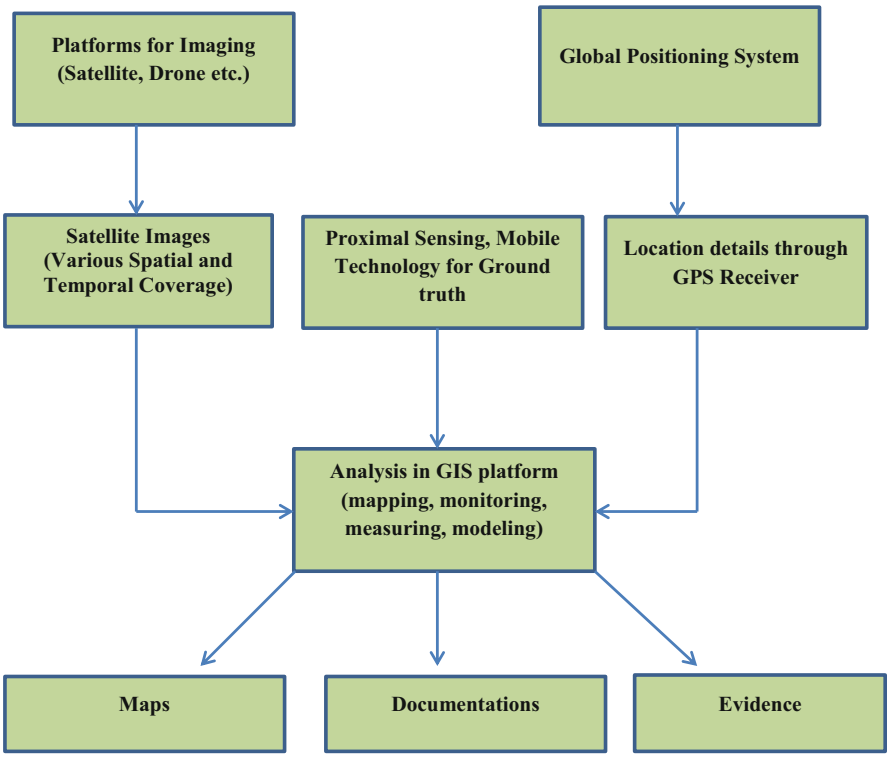

Fig. 1.1 A schematic diagram on geospatial technologies

aerial photography is useful for environmental studies (Stewart et al. 2014). The satellite RS for systematic natural resources management began with the launch of the Earth Resources Technology Satellite (ERTS-1) by the USA in 1972, later renamed as LANDSAT. Remote sensors, such as on-board radiometers or spectro-radiometers allows the observation of large areas of the Earth surface (synoptic capability) at different wavelengths (optical, infrared, thermal, etc.) of the electro-magnetic (EM) radiation (multispectral capability) and at a frequent time interval (multi-temporal capability). Optical RS deals with collecting radiation reflected and emitted from the object under study within the EM spectrum of visible (0.4 μm), near-infrared (NIR) and thermal infrared (TIR, 15 μm). Landsat, Sentinel-2, Resourcesat, Quickbird, and SPOT satellites are the well-known multispectral satellite sensors. Optical RS is one of the suitable technologies for the analysis, surveying, mapping, and monitoring of soils and crops. However, using optical RS datasets for mapping have several limitations. Instrument calibration, atmospheric correction, and cloud screening for data especially during the monsoon period are major limitations for optical RS. However, the introduction of microwave remote sensing (MRS) overcame few issues such as monitoring the Earth's surface,

irrespective of day/night and even in cloudy weather conditions which make it more effective and useful (Navalgund et al. 2007). The main advantages of MRS are its ability to penetrate the clouds, rain, vegetation, and even very dry soil surfaces. EM waves having frequencies between 109 and 1012 Hz are generally considered as microwaves. Radar is an active MRS system in which the terrain is illuminated using EM energy and the scattered energy returning from the terrain (known as radar return or backscatter) is detected and recorded as images. Examples of radar RS instruments include Synthetic Aperture Radar (SAR), scatterometers, altimeters, and radar sounders. MRS technology is been widely used for crop monitoring during the rainy season, soil moisture estimation, and land cover analysis. Sentinel-1, Radarsat-1&2, Radar Imaging Satellite (RISAT-1), Environmental Satellite (ENVISAT), Advance Land Observing Satellite–Phased Array type L-band Synthetic Aperture Radar (ALOS-PALSAR) are the well-known satellite sensors that use microwave sensors. Nowadays hyperspectral remote sensing is gaining more importance because of choice for more bands (>200 bands) as compared to multispectral imagery (between 3 and 10 bands). Hyperspectral imaging sensors measures surface reflectance with a given spatial resolution, covering an area instead of a single point (Gerighausen et al. 2012) and providing spectral information at high spatial density (Franceschini et al. 2015). Hyperspectral datasets have a greater potential to detect differences among land and water features. For example, multispectral imagery can be used to map cropped areas, while hyperspectral imagery can be used to map crop type too. The growing demand for large-scale investigations related to natural resources management and environmental issues has required the development of air- and spaceborne imaging spectroscopy. Currently, airborne hyperspectral sensors predominate over spaceborne imaging spectroscopy (Transon et al. 2018). Airborne sensors such as Airborne Visible Infrared Imaging Spectrometer (AVIRIS), DLR Earth Sensing Imaging Spectrometer (DESIS), and Airborne PRISM Experiment (APEX) have excellent potential for imaging spectroscopy (Rast and Painter 2019). Airborne hyperspectral data has been widely used for crops and soil assessment such as discrimination of crop type, retrieval of crop biophysical parameters, determination of soil mineral content, organic matter, nitrogen, salinity status, iron oxide content, and carbonate by using diagnostic absorption features of hyperspectral bands. Upcoming spaceborne sensors with high revisit time (from 3 to 5 days), higher spatial resolution, from several countries, are planned for launch in the coming years.

Besides hyperspectral RS, thermal remote sensing (TRS) is also gaining importance for natural resources and environmental studies. Thermal infrared radiation refers to EM waves with a wavelength of between 3 and 20 μm. Most of the TRS applications make use of 3–5 and 8–14 μm ranges. The major difference between the near infrared and thermal infrared is that NIR is the reflected energy where thermal infrared is emitted energy. The principle of TRS in agriculture is based on the emission of radiation responding to the temperature of the leaf and canopy. However, the emission of radiation varies with air temperature and the rate of evapotranspiration (Maes and Steppe 2012; Gerhards et al. 2019). TRS is widely used for the detection of plant responses to environmental and water stresses (Gago et al. 2015; Ramoelo et al. 2015; Khanal et al. 2017; Huang et al. 2018).

RS technology has a great potential to acquire high spatial, spectral, and temporal resolution data as input for PA (Gerhards et al. 2019). The advances in RS technology generate data for detailed inventory, mapping, and monitoring of crop, land, and water resources on large scale (Gerhards et al. 2019). A RS data user should be aware of various data products and their use in respective domains in order to choose a dataset. A variety of remote sensing satellite datasets with their specifications is distributed through different websites from manufacturers, satellite operators, data providers, and is presented in Table 1.1.

1.4.2 Proximal Sensing

Besides remote sensing, proximal sensing is also getting attention in agriculture especially in precession farming. To overcome the constraints of satellite-based remote sensing, modern world is emphasizing on the use of proximal sensing techniques in PA to assess the growth and stress of crops. In proximal sensing, the platforms are mostly handheld, tractor based, stationary installation, and robotics managed, etc., and the sensors are in close contact to the object. The types of sensors used in this case can be simple RGB or gray-level imaging, multispectral, hyperspectral imaging, or IR-thermography (Rossel and Behrens 2010; Mulla 2013). Apart from reflectance, transmittance, and absorption, plant leaves can also emit energy by fluorescence (Apostol et al. 2003) or thermal emission (Cohen et al. 2005). Sensors have significant uses in the field of agriculture, especially in the field of plant monitoring. The information collected through the proximal and remote sensors is always tied to efficient data analysis approaches such as advance machine learning, data mining, spectral soil, and vegetation indices–based algorithms, identification of specific wavelength and feature, etc. The proximal RS is able to provide information on both biotic and abiotic stresses such as nutrient deficiency, pests, and diseases, etc. A number of proximal sensors such as Soil Plant Analysis Development (SPAD) meter (Schepers et al. 1992), green seeker (Raun et al. 2002), crop spec (Reusch et al. 2010), H-sensor artificial intelligence (Partel et al. 2019), etc. have been developed for crop assessment. Besides crop sensors, proximal soil sensors are also getting more attention in precision farming. Proximal soil sensors allow inexpensive and rapid collection of quantitative, precise, high-resolution data, which can be used to better understand soil temporal and spatial variability. Rossel et al. (2011) provided description of proximal soil sensing techniques used and the soil properties that can be measured by these technologies. The characterization of the temporal and spatial variation of soil at field and landscape level using point-based observation is time-consuming, expensive, and impractical. The remotely sensed satellite images, as well as aerial photos, can provide excellent spatial coverage; however, the measurement is, indirect, involves large uncertainties and typically limited to the surface to surface soil (5–6 cm), hence not appropriate to measure spatial and temporal variability at farm level. Such limitations make the proximal soils sensing increasingly popular by filling the data gap between the lower

Table 1.1 The list of major satellite data available for agricultural and land resources assessment

Satellite data	Spatial resolution	Temporal resolution (days)	Spectral coverage	Date range of acquisition	Provider/ developer	Uses	Source
Landsat 7 ETM+	15, 30, 60 m	16	Band 1: 450–515 nm (30 m), Band 2: 525–605 nm (30 m), Band 3: 630–690 nm (30 m), Band 4: 750–900 nm (30 m), Band 5: 1550–1750 nm (30 m), Band 6: 1040–1250 nm (60 m), Band 7: 2090–2350 nm (30 m), Band 8: 520–900 nm (15 m)	Since April 15, 1999	NASA/USGS	Vegetation types, crop classification, crop stress, crop water use, crop residue, land surface phenology, biomass content, water resources assessment, land use and land cover, land degradation, soil map, etc.	https://www.usgs.gov/land-resources/nli/landsat
ASTER	15–90 m	4–16	Band 1: 520–600 nm (15 m), Band 2: 630–690 nm (15 m), Band 3: 760–860 nm (15 m), Band 4: 760–860 nm (15 m), Band 5: 1600–1700 nm (30 m), Band 6: 2145–2185 nm (30 m), Band 7: 2185–2225 nm (30 m), Band 8: 2235–2285 nm (30 m),	Since December 18, 1999	NASA, USA Government of Japan	Vegetation, ecosystem dynamics, crop stress, change detection, Earth science, land cover analysis, etc.	https://asterweb.jpl.nasa.gov/eos.asp

(continued)

Table 1.1 (continued)

Satellite data	Spatial resolution	Temporal resolution (days)	Spectral coverage	Date range of acquisition	Provider/ developer	Uses	Source
			Band 9: 2295–2365 nm (30 m), Band 10: 2360–2430 nm (30 m), Band 11: 8125–8475 nm (90 m), Band 12: 8475–8825 nm (90 m), Band 13: 8925–9275 nm (90 m), Band 14: 10250–10,950 nm (90 m), Band 15: 10950–11,650 nm (90 m)				
ASTER GDEM Version 3	30 m		Created by compiling VNIR images	Version 3: August 2019	METI, Govt. of JAPAN and NASA, USA	Elevation, slope, terrain analysis, topographic analysis, watershed management, land suitability, soil erosion, cartographic applications	https://asterweb.jpl.nasa.gov/eos.asp
MODIS	250 m (B1-B2) 500 m (B3-B7) 1000 m (B8-B36)	1–2	Band 1: 620–670 nm, Band 2: 841–876 nm Band 3: 459–479 nm; Band 4: 545–565 nm, Band 5:	Terra: December 18, 1999 Aqua: May 4, 2002	NASA	Land boundaries and properties, vegetation types, agricultural crop monitoring,	https://modis.gsfc.nasa.gov/

			1230–1250 nm, Band 6: 1628–1652 nm, Band 7: 2105–2155 nm, Band 8: 405–420 nm, Band 9: 438–448 nm, Band 10: 483–493 nm, Band 11: 526–536 nm, Band 12: 546–556 nm, Band 13: 662–672 nm, Band 14: 673–683 nm, B15: 743–753 nm, Band 16: 862–877 nm, Band 17: 890–920 nm, Band 18: 931–941 nm, Band 19: 915–965 nm, Band 20: 3660–3840 nm, Band 21: 3929–3989 nm, Band 22: 3.929–3.989 nm, Band 23: 4020–4080 nm, Band 24: 4433–4498 nm, Band 25: 4482–4549 nm, Band 26: 1360–1390 nm, Band 27: 6535–6895 nm, Band 28: 7175–7475 nm, Band 29: 8400–8700 nm, Band 30: 9580–9880 nm, Band			drought assessment, regional crop stress, vegetation phenology, crop residues, land use and land cover, long-term changes, primary productivity, ecosystem fluxes, Crop biophysical parameter, evapotranspiration, forest fire, global climate change, atmospheric correction, aerosol, ice and snow study, snow melt run-off, etc.	

(continued)

Table 1.1 (continued)

Satellite data	Spatial resolution	Temporal resolution (days)	Spectral coverage	Date range of acquisition	Provider/ developer	Uses	Source
			31: 10780–11,280 nm, Band 32: 11770–12,270 nm, Band 33: 13185–13,485 nm, Band 34: 13485–13,785 nm, Band 35: 13785–14,085 nm, Band 36: 14085–14,385 nm				
Landsat 8 OLI (B1-B9) TIRS (B10-B11)	15, 30, 60, 100 m	16	Band 1: 433–453 nm (30 m), Band 2: 450–515 nm (30 m), Band 3: 525–600 nm (30 m), Band 4: 630–680 nm (30 m), Band 5: 845–885 nm (30 m), Band 6: 1560–1660 nm (60 m), Band 7: 2100–2300 nm (30 m), Band 8: 500–680 nm (15 m), Band 9: 1360–1390 nm (30 m), Band 10: 1060–1120 nm (100 m) (IR), Band 11:	Since February 11, 2013	NASA/USGS	Vegetation types, crop classification, crop stress, crop water use, crop residue, land surface phenology, vegetation biomass content, water resources assessment, land use and land cover, land degradation, soil map, etc.	https://www.usgs.gov/land-resources/nli/landsat

			1150–1250 nm (100 m) (IR)				
ResourceSat	AWiFS: 56 m	AWiFS: 2–3; LISS-III: 12–13; LISS-IV:25–26	AWiFS: 56 m (ResourceSat 1, ResourceSat 2, 2A)	ResourceSat-1 October 17, 2003, ResourceSat-2 April 20, 2011, ResourceSat- 2A December 7, 2016,	ISRO	Crop monitoring, crop classification, drought monitoring, horticulture, water resource assessment, land use land cover, soil map, wasteland mapping, land degradation, etc.	https://www.isro.gov.in
	LISS-III:23.5 m		Band 2: 520–590 nm				
	LISS-IV:5.8 m		Band 3: 620–680 nm				
			Band 4: 770–860 nm				
			Band 5: 1,550–1700 nm				
			LISS-III:23.5 m (ResourceSat 1, ResourceSat 2, 2A)				
			Band 2: 520–590 nm				
			Band 3: 620–680 nm				
			Band 4: 770–860 nm				
			Band 5: 1,550–1700 nm				
			LISS-IV:5.8 m 1 (mono), 3 (MX) (ResourceSat 2, 2A)				
			Band 2: 520–590 nm				
			Band 3: 620–680 nm				
			Band 4: 770–860 nm				
Sentinel 2	10, 20 or 60 m	5	Band 1: 421–457 nm (60 m), Band 2: 439–535 nm (10 m), Band 3: 537–582 nm	Sentinel 2A: 2015.	ESA	Vegetation types, crop classification, crop stress, crop water use, crop	https://sentinels.copernicus.eu/web/sentinel/missions/sentinel-2
				Sentinel 2B in 2017.			

(continued)

Table 1.1 (continued)

Satellite data	Spatial resolution	Temporal resolution (days)	Spectral coverage	Date range of acquisition	Provider/ developer	Uses	Source
			(10 m), Band 4: 646–685 nm (10 m), Band 5: 694–714 nm (20 m), Band 6: 731–749 nm (20 m), Band 7: 768–796 μm (20 m), Band 8: 767–908 nm (10 m), Band 8a: 848–881 nm (20 m), Band 9: 931–958 nm (60 m), Band 10: 1338–1414 nm (60 m), Band 11: 1539–1681 nm (20 m), Band 12: 2072–2312 nm (20 m)			residue, land surface phenology, vegetation biomass content, water resources assessment, land use and land cover, land degradation, soil map, etc.	
WorldView-2	0.5 m and 1.84 m	1.1	Pan: 450–800 nm	October 8, 2009	Digital Globe, USA	Farm level crop monitoring, crop damage assessment, crop parameter retrieval, precision farming, crop insurance, micro-watershed assessment, farm asset mapping,	https://spacedata.copernicus.eu/web/cscda/missions/worldview-2
			Coastal: 400–450 nm				
			B: 450–510 nm				
			G: 510–580 nm				
			Y: 585–625 nm				
			R: 630–690 nm				
			Red Edge: 705–745 nm				
			NIR 1: 770–895 nm				

			NIR 2: 860–1040 nm			horticulture, irrigation infrastructure, etc.	
Rapid Eye	6.5 m	5.5	B: 440–510 nm G: 520–590 nm R: 630–680 nm Red Edge: 690–730 nm NIR: 760 – 850 nm	August 29, 2008	Rapid Eye AG, Germany	Farm-level crop monitoring, crop damage assessment, crop parameter retrieval, precision farming, crop insurance, micro-watershed assessment, farm asset mapping, horticulture, irrigation infrastructure, etc.	https://earth.esa.int//web/guest/missions/3rd-party-missions/current-missions/rapideye
Ikonos	80 cm B/W 3.2 m RBGiR	1–3	B/W: 445–900 nm, B: 445–516 nm, G: 506–595 nm, R: 632–698 nm, NIR: 757–853 nm	Launch September 24, 1999	Digital Globe, USA	Farm-level crop monitoring, crop damage assessment, crop parameter retrieval, Precision farming, crop insurance, micro-watershed assessment, farm asset mapping,	https://directory.eoportal.org/web/eoportal/satellite-missions/i/ikonos-2

(continued)

Table 1.1 (continued)

Satellite data	Spatial resolution	Temporal resolution (days)	Spectral coverage	Date range of acquisition	Provider/ developer	Uses	Source
						horticulture, irrigation infrastructure, etc.	
SPOT	Spot 6, 7: Panchromatic – 1.5 m Multispectral – 6.0 m (B,G,R, NIR)	1–4	B/W: 455–745 nm, R: 625–695 nm, G: 530–590 nm, B: 450–520 nm, NIR: 760–890 nm	SPOT 6: September 9, 2012; SPOT 7: June 30, 2014	Centre national d'études spatiales (CNES), SSTC and Swedish National Space Board	Crop monitoring, crop classification, drought monitoring, horticulture, water resource assessment, land use, land cover, soil map, wasteland mapping, land degradation, etc.	https://earth.esa.int/web/guest/data-access/browse-data-products/-/article/spot-6-and-7-archive-and-new
Cartosat	Cartosat-1: 2.5 m Cartosat-2 and 2A: 0.8 m	5	Cartosat-1, 2 and 2A: panchromatic band (500–850 nm)	CartoSat-1: May 5, 2005, CartoSat 2–2: January 10, 2007, CartoSat-2A: April 28, 2008.	ISRO	Cartographic applications, rural applications, coastal land use, creation of land use maps, precision farming, horticulture, farm asset mapping, encroachment, etc.	https://www.isro.gov.in
CartoDEM	10 m		Cartosat-1 stereo data	May 5, 2005	ISRO	Elevation, slope, terrain analysis, topographic analysis, cartographic	https://www.isro.gov.in

						applications, quantitative analysis of run-off and soil erosion, etc.	
KOMPSAT (Korea Multiple-Purpose Satellite)	KOMPSAT-3: 0.70 m	1.4	KOMPSAT 3: PAN: 450–900 nm, MS1 (Blue): 450–520 nm, MS2 (Green): 520–600 nm, MS3 (Red): 630–690 nm, MS4 (NIR): 760–900 nm	KOMPSAT 3: May 17, 2012;	Korea Aerospace Research Institute (KARI)	Farm-level crop monitoring, crop damage assessment, crop parameter retrieval, precision farming, crop insurance, micro-watershed assessment, farm asset mapping, horticulture, irrigation infrastructure, etc.	https://spacedata.copernicus.eu/web/cscda/missions/kompsat-3
	KOMPSAT-3A:0.55 m		KOMPSAT 3A: same as KOMPSAT 3 with MWIR: 3300–5200 nm	KOMPSAT 3A: March 25, 2015			
Sentinel 1	Strip Map: 5*5 m;	6–12	C-band synthetic-aperture radar (5.405 GHz)	Sentinel-1A: April 3, 2014,	ESA	Agricultural monitoring, soil moisture assessment etc., soil erosion studies	https://sentinels.copernicus.eu/web/sentinel/missions/sentinel-1
	Interferometric Wide:5*20; Extra Wide Swath:25*100;			Sentinel-1B: April 25, 2016			
	Wave (WV) Mode:5*20						
RADARSAT	8–100 m	3	Synthetic Aperture Radar (SAR)	RADARSAT 1 launched on November 4, 1995.	Canadian Space Agency	Hydrology, agricultural monitoring, soil moisture, rice crop mapping, crop biophysical parameters, etc.	www.asc-csa.gc.ca/eng/satellites/radarsat
	3 × 1 m–100 × 100 m		RADARSAT 1 and 2: C-band (5.6 cm)	RADARSAT 2 launched on December 14, 2007			

(continued)

Table 1.1 (continued)

Satellite data	Spatial resolution	Temporal resolution (days)	Spectral coverage	Date range of acquisition	Provider/ developer	Uses	Source
RISAT	RISAT 2: 50 m RISAT 1: 1 m,	RISAT-1: 25	RISAT 2: X-band SAR	RISAT 2: April 20, 2009	ISRO	Surface topography and costal change; land use monitoring, agricultural monitoring, rice crop mapping, etc.	https://www.isro.gov.in
	RISAT 2B: 0.5*0.3 m	RISAT 2 and 2B: 3 to 4	RISAT 1: C-band SAR (5.35 GHz)	RISAT 1: April 26, 2012,			
			RISAT 2B: X Band	RISAT-2B: May 22, 2019			
ALOS-PALSAR 2	Stripmap:3,6 and 10 m	14	L band SAR (1.2 GHz)	May 24, 2014	JAXA	Cartographic applications, environmental monitoring	https://www.jaxa.jp/projects/sat/alos2/index_j.html
	ScanSAR: 60 and 100 m						
EO 1 Hyperion	30 m	16	422–2395 nm	November 21, 2000; Deactivated on March 30, 2017	NASA/GSFC	Crop monitoring, crop condition, crop pest and disease assessment, crop nutrient stress, soil mapping, land degradation assessment, etc.	https://archive.usgs.gov/archive/sites/eo1.usgs.gov/index.html
HJ-A/HSI	100 m	–	450–950 nm	September 5, 2008	Academy of Space Technology China	Agriculture, crop assessment, land classification, monitoring, soil salinity assessment, etc.	www.cresda.com
SRTMShuttle Radar Topography Mission	30 and 90 m	–	X band: 3.1 cm	February 11, 2000	NASA	Elevation, slope, terrain analysis, topographic analysis, cartographic applications	https://www2.jpl.nasa.gov/srtm/
			C band: 5.6 cm				

resolution remotely sensed data and high-resolution point data (Adamchuk 2011; Rossel et al. 2011). A number of the proximal sensors as well as methods such as ground-penetrating radar, EM induction, electrical resistivity, magnetometry, optical reflectance, gamma-ray spectroscopy, etc., have been used for farm- and landscape-level soil survey to indirectly measure the spatial and temporal variability of soil properties. Various soil physical and chemical properties such as soil texture, porosity, pH, bulk density, soil structure, salinity, organic carbon, moisture content, $CaCO_3$ content, cation-exchange capacity, ionic composition, plant-available nutrients, as well as metal content in contaminated soil, etc. can be assessed using various proximal soil sensing methods (Doolittle and Brevik 2014; Dao 2018).

1.4.3 Geographic Information System

GIS is a computerized system for gathering information of Earth features with a geographic reference system (latitude, longitude, coordinates, projection). Visual representation either through map generation or any other digital image format makes it a unique one to the users. It is a blend of computer technology and mapping science of geography – regarded as computational geography (Kavita and Patil 2011). Many other terms synonymously used in place of GIS include spatial data handling system (Marble and Peuquet 1983), geographic data system (White 1984), spatial information system, geo-data system, geo-based information system, natural resource information system (Clarke 1986), multipurpose cadastre, etc. The basic functions of GIS are collection of Earth's information, analysis, update, manipulation, storage, complex relation and integration of data, interpretation and visual representation for further decision-making through a systematic way integrating personnel, institutions, hardware, data, and software (Supuwiningsih and Rusli 2017). What GIS does is basically capturing location-specific information and its facile displaying to the user for better understanding, interpretation, and informed decision-making.

GIS is an assemblage of computer hardware, software, storage device, modeling or logical interface, operating personnel, and geographic information collected through capturing device or remotely sensed tools (Chang et al. 2009; Pendleton 2012). GIS is dished out into two major groups (Gangwar 2013):

(i) Base data or core data or framework data (common for all applications): Data includes information about elevation, natural or constructed features of the Earth's surface, geodetic frameworks for navigation, etc.
(ii) Thematic data (application-specific data): This data varies according to the user's application, for example, socioeconomic data from planning and censuses, natural resource data, or modified forms of base data, etc.

GIS contains a database management system to handle two types of data: spatial (real-world geo-referenced information) and attribute data (a characteristic feature of objects). It undergoes spatial analysis to find out trends, patterns, shapes, and

relationships of data. Spatial analysis is of different types like overlay analysis (superimposing thematic layers to go insight of the data), proximity analysis (to find out how much features are close to each other), buffer analysis (this is a type of proximity analysis which is determined through distance around features and applied to points, lines, or polygons to discover areas in or outside the buffer area) (Farkas et al. 2016), etc. GIS incorporates only two kinds of data, namely vector- and raster-featured data. Vector and raster featured data describe discrete and continuous features, respectively. Vector-featured data comprises point (no dimension), line (one dimension), and area or polygon (two dimensions), while raster-featured data includes grid cells and pixels (Wieczorek and Delmerico 2009). Point is displayed on screen or maps by reducing its scale as a symbol. For example, the corner of a building is shown by a point as a representative of coordinates. Line, on the other hand, connects two points and thus represents one dimension. For instance, the boundary of a water body can be marked by a line. The area, as well as polygon, represents two-dimensional specifications (community land or water body or vegetation land uses) by incorporating at least three connecting lines through different points (Chang et al. 2009). Polygons have an area and perimeter values and are used to represent a wide range of physical (types of soil, forests, and water bodies), anthropogenic (land parcels, administrative boundaries), and other features (Sugumaran and DeGroote 2011). In raster GIS, a unique reference coordinate or cell address represents discrete attribute data contained a grid cell or pixel at a corner or center. Raster format superimposes imageries over grid cells for better features' identification, and pixel size or grid decides the resolution of images. Unlike vector format, raster GIS undergoes scalar operations on spatially explicit data and requires conversion into vector format before further operations. Nowadays, many GIS software like ArcGIS, QGIS, Maptitude, GeoMedia, etc. can easily transform those formats into each other. GIS provides data output and presentation through charts and maps as these communicate better than words. Chart expresses the tabular data in some graphical diagrams like area, bar, column, line, scatter, and pie. GIS-based software has dynamic charts for automatic updating. On another side, maps like planimetric, topographic, cadastral, image, thematic, etc. represent features related to Earth through pictorial or symbolized formats embodied by scales, coordinates, etc. A list of GIS software used for spatial data analysis is presented in Table 1.2.

1.4.4 Global Positioning System

GPS is a satellite-based navigation system, capable of locating any positions on the Earth. It can supply real-time, three-dimensional data regarding positions, navigation, and timing continuously 24 h/day. The development of GPS was primarily

Table 1.2 A list of GIS software for spatial data analysis

GIS software	Developer	Country	References
ArcGIS	Environmental Systems Research Institute (ESRI)	Redlands, California, USA	https://www.esri.com/en-us/arcgis
GeoMedia (Hexagon)	Intergraph	Madison, Alabama, United States	https://geospatial.intergraph.com/products/GeoMedia
QGIS	Open Source Geospatial Foundation	Chicago, USA	https://qgis.org/en/site
SAGA-GIS	Department of Physical Geography, University of Gottingen,	Germany	https://www.saga-gis.org/en
GRASS GIS	GRASS Development Team	Chicago, USA	https://grass.osgeo.org/
gvSIG	Open Source Geospatial Foundation	Chicago, USA	https://www.gvsig.org
ENVI	Harris Geospatial Solutions	Broomfield, Colorado, United States	https://www.harrisgeospatial.com
MapInfo Professional	Pitney Bowes	Stamford, Connecticut, USA	https://www.mapinfo.com
Global Mapper	Blue Marble Geographics	Hallowell, Maine, USA	https://www.bluemarblegeo.com/products/global-mapper.php
Manifold GIS	Manifold Software Limited	USA	https://www.manifold.net
Smallworld	GE Energy Connections	Cambridge, England	https://www.ge.com
Bentley Map	Bentley Systems, Incorporated	Exton, Pennsylvania, USA	https://www.bentley.com
MapViewer and Surfer	Golden Software LLC	Golden, Colorado, USA	https://www.goldensoftware.com
Maptitude	Caliper Corporation	Newton, Massachusetts, USA	https://www.caliper.com
SuperGIS	Supergeo Technologies	Taipei, Taiwan	https://www.supergeotek.com
Super Map	SuperMap Software Co., Ltd	Beijing, China	https://www.supermap.com
PCIGeomatica	PCI Geomatics	Markham, Ontario, Canada	https://www.pcigeomatics.com
IDRISI	Clark Laboratories	Worcester, MA USA	https://clarklabs.org
AutoCAD Map 3D	Autodesk	San Rafael, California, United States	https://autodesk.com
Tatuk GIS	TatukGISSp	Gdynia, Poland	https://www.tatukgis.com
MicroImages (TNTgis)	MicroImages, Inc	Lincoln, Nebraska, USA	https://www.microimages.com

(continued)

Table 1.2 (continued)

GIS software	Developer	Country	References
MapMaker Pro (MapMaker)	Map Maker Limited	Argyll, Scotland, UK	https://www.mapmaker.com
MapRite	Envitia	Reston, VA, USA	https://www.envitia.com
Ilwis	52°North ILWIS Community	Netherlands	https://www.52north.org

made for military applications and it started mainly as a Navigation System with Time and Ranging Global Positioning System (NAVSTAR GPS), but it was made available for civilian use since the 1980s. There are at least 24 GPS satellites in action for all the times which synchronize operations so that these repeated signals are transmitted at the same instance. It can calculate its position in three dimensional space when the receiver estimates the distance to at least four GPS satellites also referred to as trilateration. Most of the handheld GPS have 20 m positional and 1 m location accuracy. However, submeter location accuracy could also be obtained by using Differential GPS (DGPS). There are no subscriptions or setup charges required to use GPS. Hence, it can be accessed by anyone for any application which needs location coordinates. This has opened many new avenues for spatial data analyses. Nowadays farmers could access the GPS to perform site-specific farm activities. In GPS, several satellites are involved in the identification of the actual position of farm equipment within the field. GPS is a real-time, accurate, all-weather, economic, and continuously available positioning system. Hence, it has emerged as a unique surveying technique with wide range of applications in various domain. The major applications of GPS in agriculture are as follows:

I. Geophysical and cadastral surveys
II. Determination of the precise location in the field for spatial variability assessment
III. Determination of the precise location in the field for site-specific input applications
IV. Yield mapping
V. Integration of all field-based variables such as the intensity of weeds, crop yield, and soil moisture, etc. with RS data using DGPS
VI. Crop insurance value chain
VII. Agricultural supply chain
VIII. Disaster management and support

1.5 Role of Geospatial Technologies in Sustainable Agriculture

The discoveries in the field of science and technology during the twentieth and twenty-first centuries, especially geospatial technology, have enabled farmers to effectively use farm inputs to maximize crop yield. Geospatial technologies play a vital role in major agriculture application areas such as crop, soils, land, water, climate, and risk-related studies with data, models, and analytics. The geospatial technologies are playing a meaningful role in agriculture in the following ways:

(a) Easy and timely data acquisition
(b) Near real-time visualization and assessment of natural resources
(c) High-resolution and accurate mapping and assessment
(d) Optimize planning tools and techniques for agricultural activities (seeding, irrigation, fertilization etc.)
(e) Facilitate real-time mapping and monitoring of farm operations
(f) Improve yield and productivity of crops
(g) Centralized management of spatial and nonspatial data at farm level
(h) In-season crop damage assessment
(i) Support to the crop insurance value chain
(j) Easy dissemination of agricultural data through web
(k) Improving farm incomes while minimizing risk

There are various approaches to optimize agricultural activities through geospatial technologies such as climate-smart agriculture (CSA), precision farming (PF), conservation agriculture (CA), etc. Such approaches can optimize the use of farm inputs and resources which helps to reduce the cost of production and minimize agricultural risk and hazards, hence, improve the crop productivity and farm income. CSA coined by FAO is described as "agriculture that sustainably increases productivity, resilience (adaptation), reduces/removes greenhouse gases (GHGs) (mitigation), and enhances achievement of national food security and development goals". The adoption of CSA by farmers can improve crop production, increase economic growth, reduce greenhouse gas emission, create jobs, and hence decline hunger and poverty. PF is the use of geospatial tools and techniques to assess spatial and temporal variability associated with crop production factors to enhance crop performance and environmental quality (Pierce and Nowak 1999). It is also known as satellite agriculture, PF can relate to an agricultural production system with a robust set of technologies, including RS, GIS, GPS, and Variable Rate Technology (VRT) which can propel agriculture into the computerized information-based world. Nowadays geospatial technologies are playing a crucial role in CA. The real-time spatial and temporal satellite data analysis helps in the formulation of a series of land management practices that include soil management practices to reduce land degradation, introduce cover crops, retention of crop residues, recommended suitable cropping sequences, etc.

1.6 Crop and Soil Factors Influencing Remote Sensing

There are several crop and soil attributes that influence remote sensing signal. The amount of energy absorbed and transmitted by a plant leaf is affected principally by the amount and type of chlorophyll content, leaf internal structure, leaf water content, and leaf biomass content etc. It is further modulated by leaf area per unit land, leaf arrangement (leaf angle distribution), background soil reflectance, sun-sensor geometry at canopy level. Leaf-level synthetic spectral reflectance generated by PROSPECT-D model using different input parameters are presented in Fig. 1.2 (http://opticleaf.ipgp.fr/index.php?page=prospect). Among the plant pigments, chlorophyll-a and chlorophyll-b absorb radiation strongly in the visible wavelength range (400–700 nm) specifically 430 (blue) and 660 (red) nm for chlorophyll-a; and 450 (B) and 650 (R) nm for chlorophyll-b. Both chlorophyll-a and -b absorb light, but chlorophyll-a plays a dominant and critical role in converting light energy to chemical energy (Pinter et al. 2003). Due to the absorption of chlorophyll, the healthy green leaf shows very low reflectance values (~5–10%) in the blue and red region of the EM spectrum. The green region exhibits comparatively higher reflectance (~10–15%) making the plant leaf green in color. Sudden surge in reflectance is observed (~40–50%) in the near-infrared (700–1000 nm) due to well-developed leaf internal structure of spongy parenchyma and air space (Salama 2011). This is followed by two weak water absorption bands (970, 1200 nm) in

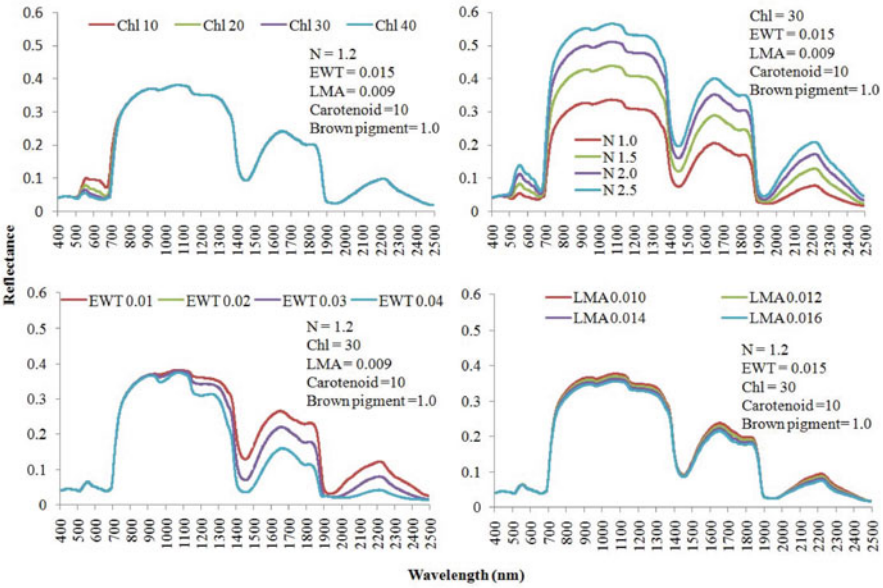

Fig. 1.2 Spectral response vegetation as influenced by chlorophyll$_{a+b}$ content (Chl) in μg cm^{-2}, leaf structural parameters (N), equivalent water thickness (EWT) in cm, leaf mass per unit area (LMA) g cm^{-2}; carotenoid content in μg cm^{-2}, brown pigment (arbitrary unit)

NIR and two strong water absorption bands (1450, 1940 nm) in Shortwave Infrared Region (SWIR). The response of leaf reflectance spectra with the variation of the major inputs are presented in Fig. 1.2. Keeping other factors constant, the leaf chlorophyll content has been varied from 10 to 40 μg cm^{-2} and the effect on the reflectance spectra is observed in the visible region only (400–700 nm). The absorption at blue and red bands has increased with the increase in the chlorophyll content. The reflectance at green region has also decreased as the higher chlorophyll content turn the leaf darker. The leaf internal structure (N) parameter is found to be highly sensitive. The N parameter has been increased from 1 to 2.5 keeping other inputs as constant, and the spectral reflectance is found to increase drastically. The effect was found across the spectral band but more pronounced in the reflection peaks than the absorption regions. The leaf wetness parameters, that is, Equivalent Water Thickness (EWT) is found to have effect on the NIR and SWIR of the spectrum. The spectral response with the increase of EWT from 0.01 to 0.04 cm, keeping other variables constant, is presented in Fig. 1.2. With the increase in EWT, the depth of the water absorption bands have increased. It has effectively brought down the whole spectra from NIR to SWIR proportionately. The effect of leaf mass per unit area (LMA) was found in NIR to SWIR with marginal effect. The reflectance is found to be marginally decreased with no change in the absorption region. As other parameters are kept constant, the increase in LMA made the leaf internal structure more compact with less airspace. This results in a decrease of reflectance in the NIR and SWIR regions, as depicted in Fig. 1.2. Please be informed that the driving parameters of leaf reflectance act simultaneously and produce a mix response in practical scenarios.

An interesting observation revealed that when a plant goes to the senescence stage, reflectance begins to downhill in the near-infrared region (collapse of leaf internal structure) and uphill in the red regions (loss of leaf chlorophyll). The absorption mechanism of EM radiation in the pigments of green vegetation is attributed to atomic excitation by photon, where the electron is bumped into higher energy orbital that lies further from the nucleus (Jensen et al. 2008; Salama 2011). On the contrary, a high value of plant reflectance in the near-infrared (NIR 700–1300 nm) region is an effect of leaf density and canopy arrangement. During the senescence stage, a relatively faster degradation of chlorophylls compared to carotenoids causes a significant increase in reflectance in the red wavelength. However, a low value of reflectance at the NIR region is due to collapsing of the spongy-mesophyll layer as the leaf comes under stress. In this decaying phase of the plant, carotenes absorb blue and reflect green and red, resulting in the yellow appearance of the leaves. Due to the death of brown pigments known as tannins, leaf reflectance and transmittance in 400–700 nm decrease (Fourty et al. 1996; Salama 2011). This distinct difference in reflectance behavior between the red and NIR portions of the spectrum is the stimulus for the generation of spectral indexes (Sripada et al. 2006). These indexes are very frequently used to assess various plant canopy attributes such as biomass, chlorophyll and moisture content, leaf area index (LAI), Nitrogen (N) content, etc.

The most important contributing soil factors are moisture and organic matter content which affect the amount of radiation reflected by bare soils. Reflection of radiation from bare soil is also affected by soil texture, $CaCO_3$, calcium, and iron oxides (Rossel et al. 2006). Each soil property has its own specific spectral region where reflectance is the strongest (Ben-Dor et al. 2007). In cultivated land, bare soil and crop canopies are often both present. The mixing of the spectral signatures from bare soil as well as crop canopies often confuses the interpretation of the reflectance data. A few techniques are available to isolate information about plant characteristics from the mixture of reflectance, which includes spectral indexes that adjust for soil effects (Haboudane et al. 2004), spectral unmixing algorithm (Huete and Escadafal 1991), and derivative spectra (Demetriades-Shah et al. 1990).

1.7 Application of Geospatial Technologies in Crop Science

During late twentieth and early twenty-first centuries, the applications of RS and GIS in crop science are gaining more attention through crop inventory/mapping and management. RS is capable of providing spatially explicit and efficient crop inventory (crop map, crop acreage estimation, crop production estimates etc.) and management (crop condition, crop damage, drought monitoring and assessment, precision farming, cropping system analysis, etc.) as it can capture information at wide ranges of spatial and temporal scales with wall-to-wall coverage (Liaghat and Balasundram 2010). Typical vegetation signature across the EM domain (400–2500 nm) is presented in Fig. 1.2. The leaf-level signature is principally governed by the leaf pigments, leaf water content, leaf biomass, and internal structures as discussed earlier. Hence, the crops having differences in these parameters produce unique signature of spectral reflectance. Further at the canopy level, the signature is modulated by the unique crop spacing, canopy architecture, background soil exposure, etc. The crop signature can also be separated using the temporal frame of the crop-growing season. Global- and regional-scale crop maps have been successfully generated with considerable accuracy using the aforementioned spectral and temporal signatures. This becomes the basis of successful monitoring and assessment of crop. The functionality of GIS enables integration of other thematic services like soil maps, weather maps, and other resources maps which facilitate rapid and reliable decision-making. The satellite remote sensing application in crop science begins with the classification of land cover types with major emphasis on crop types. However, nowadays the focus has been shifted more toward the characterization of plant biophysical parameter, yield prediction, and crop production forecasting. RS of agricultural has provided valuable insights into various agronomic parameters such as start of the season, end of the season, seasonal greenness, crop condition anomalies, crop damage, etc. One of the main advantages of RS techniques is considered to be repeated information retrieval without any destructive sampling of crops. The response of vegetation cover to different spectral bands varies depending on the change in physical and biological properties of the

vegetation canopies of different crops. Hence, various multispectral, broadband vegetation indices such as Normalized Difference Vegetation Index (NDVI), Normalized Difference Red Edge Index (NDRI), Soil-Adjusted Vegetation Index (SAVI), etc. along with weather parameters derived from surface and satellite observations have been widely used for crop studies (Schmedtmann and Campagnolo 2015; Lira Melo de Oliveira Santos et al. 2019; Zortea and Rodrigues 2019). Nowadays the introduction of hyperspectral remote sensing enables researchers to a more detailed analysis of crops such as crop classification, crop condition, retrieval of crop biophysical and biochemical attributes, crop stress (Ennouri and Kallel 2019; Virnodkar et al. 2020), as well as disease and pest etc. (Bhattarai et al. 2019; Yones et al. 2019). Several researchers have developed narrow-band vegetation indices using hyperspectral information for analysis and monitoring of crops and retrieval of different biophysical and biochemical variables of a plant (Shelestov et al. 2017; Pasqualotto et al. 2019; Darvishzadeh et al. 2019). Accurate estimates of crop biophysical as well as biochemical variables like LAI, fraction of absorbed photosynthetically active radiation (FAPAR), leaf moisture and chlorophyll content, primary production, sun-induced fluorescence (SIF) from RS can assist in determining vegetation physiological status (Penuelas et al. 1995). The study of crop phenology and its seasonal dependence, and seasonal dependence (Belanger et al. 1995), may serve as bioindicators of vegetation stress (Zarco-Tejada et al. 2001), and are crucial for sustainable agriculture. The introduction of microwave data enables the researcher to assess crops mainly in the rainy season during kharif. The development in the field of satellite and sensor in the last few decades makes a remote sensing–based approach as the most trusted and efficient tool to pre-harvest crop production estimation. Geospatial tools along with various modeling approaches such as machine learning, principle component analysis, lambda–lambda models, stepwise discriminant analysis, artificial intelligence, pattern recognition, mobile computing, etc. have opened a new dimension in crop science (Thenkabail et al. 2004). Similarly, process-based crop growth simulation models using RS and GIS-based inputs have been proven potential tools for analyzing crop behavior and yield prediction in various spatial and temporal scales. Nowadays, the modern world is emphasizing on the use of proximal remote sensing techniques in PA to assess the growth and stress of crops. Besides, unmanned aerial vehicle (UAV) or drone is showing its potential in farm resource management by capturing quality images of various aspects of crop cultivation especially monitoring the crop health at relatively cheaper expenditure over other remote sensing tools (Primicerio et al. 2012). Several researchers have reported the usage of geospatial technologies in different aspects of crop science which is presented in Table 1.3.

Table 1.3 Major applications of geospatial technologies in crop and soil science

Sl. no.	Application	Description	References
Crop Science			
1.	Crop identification, crop type mapping	Multispectral satellite datasets are capable of identifying and mapping a crop by considering changes in reflectance as a function of plant phenology	Schmedtmann and Campagnolo (2015), Ghazaryan et al. (2018), Heupal et al. (2018), Lira Melo de Oliveira Santos et al. (2019), Zortea and Rodrigues (2019) and Sun et al. (2019)
2.	Crop acreage estimation	The manual estimation of areas under crop is laborious and time consuming due to vast size of lands. Geospatial techniques can play a crucial role the estimation of the farmland on which a crop has been planted	Li et al. (2011), Pan et al. (2012), Craig and Atkinson (2013) and Rotairo et al. (2019)
3.	Crop stress (nutrient, moisture, etc.) and crop condition health assessment	RS can play an important role in crop health monitoring and the extent to which the crop has withstood stress. Specific absorption bands of the plant pigment, crop moisture, and crop vigor are useful to assess crop condition	Katsoulas et al. (2016), Mee et al. (2017), Ennouri and Kallel (2019) and Virnodkar et al. (2020)
4.	Crop yield and production forecasting and modeling	The expected crop yield and production over a given area or farmland can be estimated before harvesting of the crop using RS and GIS over a given period of time. It uses various crop information such as crop phenology, agronomic practices, crop weather, moisture level in the crops, soils map, etc. Nowadays crop yields are forecasted using RS input in combination with various statistical and machine learning approach using vegetation indices, phenology matrices, crop maps and yield proxies, etc. Crop growth simulation model enabled with in-season RS based crop biophysical parameters is an efficient tool in this aspect	Maki et al.(2017), Kasampalis et al. (2018), Huang et al. (2019), Ban et al. (2019) and Phung et al. (2020)

(continued)

Table 1.3 (continued)

Sl. no.	Application	Description	References
5.	Horticulture crop assessment and management	High-resolution satellite or aerial images are found to be highly suitable for mapping of horticultural and plantation crops. Due to its unique tree canopy and spacing, horticultural crop produce typical textural parameters of the image. This is utilized for rapid mapping and monitoring of the horticultural crops. The production estimates of horticultural crops are still under research and development	Trout et al. (2008), Usha and Singh (2013) and Marinelli et al. (2019)
6.	Crop damage assessment	Crop damage can be due to unseasonal rainfall, hailstorm, pest and diseases, drought, and flood, etc. RS can be used to assess the crop area damage if there is large-scale destruction of crop canopy or leaf pigment. Current year anomalies with respect to normal year can also be a reasonable proxy for this purpose	Prabhakar et al. (2013), Zhou et al. (2016), Boschetti et al. (2015), Surek and Nador (2015) and Sawant et al. (2019)
7.	Retrieval of crop biophysical parameters	The multispectral and hyperspectral indices are very useful for quantification of different biophysical and biochemical parameters like LAI, leaf chlorophyll contents and leaf moisture content, etc. Different canopy reflectance models are used for this purpose	Clevers and Kooistra (2011), Verrelst et al. (2015), Shelestov et al. (2017), Pasqualotto et al. (2019) and Darvishzadeh et al. (2019)
8.	Crop insurance	High-resolution satellite data, drone, aerial images, proximal sensor can be used to assess crop growth, yield and extent of crop damage, delay in crop sowing, and moral hazards at farm level, and allow policymakers to provide insurance-related information for claim settlement. Geospatial technology can also provide objective solution of crop cutting experiment	De Leeuw et al. (2014), Borgogno-Mondino et al. (2019), Banerjee and Pandey (2019) and Valverde-Arias et al. (2020)

(continued)

Table 1.3 (continued)

Sl. no.	Application	Description	References
9.	Precision farming	PF can improve crop productivity with the aid of RS, GIS, and GPS, etc. It can help in analysis and management of spatial and temporal variability of farm inputs such as seeds, fertilizer, water, chemical, etc. within the field	Andreo (2013), Qiu et al. (2014), Mulla and Miao (2016), Hakkim et al. (2016), van Evert et al. (2017), Nabi et al. (2017), Castillejo-González (2018), Friedl (2018) and Neupane and Guo (2019)
10.	Identification of pest and diseases infestation	RS approach particularly hyperspectral remote sensing can play a vital role in the monitoring pest and diseases infestation in the crop field and provide valuable data to adopt more accurate pest and diseases control mechanisms. Disease and pest forewarning system can also be developed using satellite and weather-based information	Ghobadifar et al. (2016), Mahlein (2016), Bhattarai et al. (2019) and Yones et al. (2019)
11.	Identification of harvesting and planting dates	RS can monitor and observe weather pattern, crop climate, soil type, soil moisture, etc. which are useful to predict the planting and harvesting seasons of various crop based on area favorable for crop sowing. Time series satellite data analysis can also provide crop phenological metrics such as start of the season and end of the season	Chen et al. (2011) and Rolim et al. (2019)
12.	Mapping of agricultural land use and crop sown area	The multispectral satellite data is useful to map land use and land cover for various functions such as crop growing and landscaping, etc. It can help in PA where specific land soils are used for specific purposes	Wu et al. (2014), Ambika et al. (2016), Useya et al. (2019) and Pareeth et al. (2019)
	Crop intensification	RS can be used to identify the in-season fallow area and also the single and double cropping systems. It can also be used to assess the suitability of taking up crops in the fallow land	Estel et al. (2016), Bégué et al. (2018), Löw et al. (2018) and Dimov et al. (2019)

(continued)

Table 1.3 (continued)

Sl. no.	Application	Description	References
13.	Crop biomass estimation	The rapid, reliable, and accurate economical estimation of crop above-ground biomass is possible through high-resolution spatial and temporal satellite data, hyperspectral data, drone, aerial images	Niu et al. (2019), Dayananda et al. (2019) and Han et al. (2019)
	Crop residues biomass	Geospatial technology along with crop statistics at administrative level can be used assess the spatial distribution of the surplus crop residue biomass and facilitate utilization of the same for biofuel/biomass power plants	Wang et al. (2013) and Chakraborty et al. (2019)
Soil Science			
1.	Soil survey and mapping	The most common and important application of RS in soil domain is soil mapping. Soil information as a form of map is useful for PA, crop growth simulation model, water balance studies, irrigation requirement, crop suitability assessment, etc.	Dwivedi (2001), Manchanda et al. (2002) and Mulder et al. (2011)
2.	Soil moisture monitoring	RS techniques provide an alternative way to measure the spatial and temporal variability of soil moisture. Soil moisture can be retrieved either from optical/thermal/microwave sensors or fusion of these sensors. Such data helps in estimation of the amount of moisture present in the soil and hence the type of crop that can be grown in the soil	Magagi et al. (2012), Wagner et al. (2013), Akbar and Moghaddam (2015), Zhang and Zhou (2016), Mohanty et al. (2017), Saha et al. (2018) and Mohamed et al. (2019)
3.	Irrigation monitoring and management of irrigated agriculture	RS provides information about amount of soil moisture present in soil spatially and temporally. Such data can be used to determine whether a particular soil is moisture deficient or not which helps in irrigation scheduling	Taghvaeian et al. (2018), Tazekrit et al. (2018) and Ojo and Ilunga (2018)

(continued)

Table 1.3 (continued)

Sl. no.	Application	Description	References
4.	Wasteland mapping and land degradation assessment; identification of problematic soils	The advanced techniques such as microwave and hyperspectral and proximal ground-based sensor data with multivariate statistical algorithm have increased the efficiency of classification and mapping of degraded lands, problematic soils, etc. This allows experts to identify the areas under degradation and areas that are still intact. Such data are useful to develop action plan for land degradation neutrality for optimum productivity	Yiran et al. (2012), Mohamed et al. (2013), Vicente-Serrano et al. (2015) and Mao et al. (2018)
5.	Soil erosion assessment and modeling	Satellite-derived environment parameters, DEM, LULC, vegetation cover, grid weather data are very useful to predict annual field-scale erosion rates through modeling approaches. Various process-based models, such as LISEM, EPIC, etc., are using space-based inputs to model soil erosion	Pandey et al. (2009), Karaburun (2010), Mitasova et al. (2013), Woldemariam et al. (2018) and Zabihi et al. (2019)
6.	Digital/predictive soil mapping	Availability of DEM and high-resolution images and different environmental covariates allow to predict and generate spatial soil property map with the assistance of computer-based systems, modeling, or GIS. Such maps are very useful for precision farming and landscape and environmental modeling	Carré et al. (2007), Minasny and McBratney (2016), Sreenivas et al. (2016), Camera et al. (2017), Forkuor et al. (2017), Mitran et al. (2018b), Ma et al. (2019) and Wadoux et al. (2019)
7.	Spatial variability of soil properties/nutrients	GIS is a very useful tool to generate spatial soil map from point-based field observation. This helps in assessing spatial variability of soil parameters, nutrient content which allow farmers to adopt site-specific nutrient management	Zhang et al. (2003), Vasu et al. (2017), Usowicz and Lipiec (2017), Teng et al. (2017) and Sharma and Sood (2020)

(continued)

Table 1.3 (continued)

Sl. no.	Application	Description	References
8.	Soil quality assessment	Geospatial techniques involving the use of RS, GPS, and GIS provide new approaches for studying various soil quality aspects in different spatial as well as temporal domains. Soil health assessment through spectral soil quality indexing is of major focus nowadays	Ben-Dor and Banin (1995), de Paul Obade and Lal (2013) and Paz-Kagan et al. (2014, 2015)
9.	Soil fertility assessment and management	RS and GIS are important in the determination of soil management practices based on the soil fertility data collected from the fields	Blaes et al. (2016), AbdelRahman et al. (2016), Song et al.(2018), Molin and Tavares (2019) and Patel and Ghosh (2019)
10.	Land suitability and capability assessment	Soil survey information coupled with RS data can be integrated in the GIS to evaluate crop suitability for different soils or vice versa. This helps in PA where specific soils are used for specific purposes	AbdelRahman et al. (2016), Yohannes and Soromessa (2018), Memarbashi et al. (2017), Parry et al. (2018), Purnamasari et al. (2019) and Murti (2019)
11.	Soil nutrient deficiency	RS and GIS techniques can be used to determine the extent of soil and crop nutrient deficiency and facilitate the agricultural expert and farmers to come up with remedies that would increase the nutrients level in crops via soil hence improved the overall crop yield	Meng et al. (2015), Hengl et al. (2017) and Yousfi et al. (2019)

1.8 Application of Geospatial Technologies in Soil Science

The conventional method of soil assessment is based on regular soil sampling design, sample collection, sample preparation, and subsequent chemical analysis in the laboratory. However, this approach is time-consuming, laborious, and costly to assess soil over a large area. Moreover, such a method can give you point-based information. Traditionally this information is represented as soil maps knowledge is represented as soil maps conforming to the discrete model of spatial variation (Heuvelink and Webster 2001). It shows polygons (represents homogeneous soils) with boundaries where changes in soil parameters are considered to be abrupt. However, the complete and accurate spatial information on soils is required for

proper land use planning, soil management, and other activities linked to environmental protection. In nature soil properties are spatially variable therefore it should be estimated as a continuous variable rather than point values to have higher accuracy and wide applications. The recent advancement of RS, GIS, and GPS has enabled the researchers to assess land resources spatially and temporally. The availability of wide ranges of spatial and temporal satellite datasets make soil survey easier in the form of soil mapping. It can provide complete information about soil resources of an area which is utmost important for an effective agricultural research and advisory program. However, many soil properties can be better modeled with a continuous model of spatial variation using digital mapping approaches. The RS-based inputs along with secondary datasets such as slope, vegetation, climate, etc. allow for a more quantitative approach to soil survey producing continuous surfaces based on soil-forming factors which called "predictive" or digital mapping technique (Carré et al. 2007; Sreenivas et al. 2016; Mitran et al. 2018b). Besides, this approach gives spatial estimates of the uncertainty of the predictions. It uses a regression analysis between in situ point measurements of soil quality data and exhaustive satellite-derived indices to predict and upscale to larger areas spatially. The digital soil maps are also an ideal input for spatially distributed models. The satellite data along with digital soil map, land use, slope, and rainfall data derived from RS data can help in delineating major land degradation processes such as water and wind erosion, salt-affected soils, waterlogging, etc. along with its severity such as undegraded, moderately degraded, degraded, and severely degraded (Mohamed et al. 2013; Vicente-Serrano et al. 2015; Mao et al. 2018). A number of researchers have used RS and GIS techniques for soil taxonomic study or soil classification. GIS is also playing an important role in land resource inventories by assessing spatial variability of soil properties through interpolation techniques, that is kriging (Usowicz and Lipiec 2017; Teng et al. 2017; Sharma and Sood 2020). Nowadays introduction of hyperspectral remote sensing enables researchers to a more detailed analysis of soil fertility and quality (Paul Obade and Lal 2013; Paz-Kagan et al. 2014, 2015; Molin and Tavares 2019; Patel and Ghosh 2019). The quantitative prediction of soil properties, soil salinity, soil organic carbon content, $CaCO_3$ content, nutrient deficiency, etc. using hyperspectral data helps in formulating optimum soil management practices. The availability of microwave data helps in soil moisture estimation (Mohanty et al. 2017; Saha et al. 2018; Mohamed et al. 2019) and soil erosion studies (Woldemariam et al. 2018; Zabihi et al. 2019). RS and GIS have also played a crucial role in land suitability and capability assessment by identifying the problems associated with the soils (Memarbashi et al. 2017; Parry et al. 2018; Purnamasari et al. 2019; Murti 2019). Several researchers have reported the application of geospatial technologies in various aspects of soil science which is presented in Table 1.3.

1.9 Geospatial Technologies in Agriculture: Status and Challenges

The application of geospatial technologies and tools for sustainable resources management especially in agriculture has been advancing quite rapidly over the last decade in the Asia-Pacific region (Indonesia, Australia, Malaysia, Japan, etc.), South Asia (India), East Asia (China), Europe (Spain, Belgium, Netherlands), and in North America (USA, Mexico). A global survey was carried out by geospatial media and communication (2015) across the world (www.geospatialworld.net) and reported that 29% of the response to the survey use geospatial technologies for agricultural land use land cover mapping; 20% for crop inventory, acreage production, harvesting and storage; 19% for mapping of soil, water, and land; 13% for variable-rate technology; 7% for groundwater mapping and management; 12% for site suitability analysis. In the Asia-Pacific region, RS and GIS are mostly used for mapping of crops. Malaysia is mostly using RS and GIS for rice crop mapping and monitoring. Indonesia is using such technologies for producing digital maps and for land distribution of paddy field types. In Australia, these techniques are mostly used for mapping of oil palms and sugarcane. In India, satellite images are using for large-scale agricultural land use mapping, crop inventory, acreage estimation, crop production, storage, and harvesting studies. However, in Europe, these technologies are using for the automation of machinery and farm equipment, crop and water management, soil properties at a macro level, whereas agricultural land uses land cover mapping, wasteland mapping, etc. at a micro-level. Although the major RS data source in China is multispectral, they are using much higher spatial resolution data as well as hyperspectral data for agricultural monitoring. The major RS applications in agriculture in China are precision farming, crop yield, agricultural survey, and disaster forecasting. In North America, agricultural land use land cover mapping is the major use of geospatial techniques at a macro level, whereas crop disease assessment and site suitability analysis is at a micro level. The major micro-level applications of geospatial techniques are variable rate application and management of farm inputs (seeds, fertilizers, chemicals, etc.), groundwater zonation for irrigation suitability, drainage patterns, etc.

Geospatial technologies play an influential role in the agriculture sector by increasing yields, managing resources, prediction of outcomes, and improving farm practices. However, the application and adoption of geospatial technologies in agriculture are facing many problems and challenges, which vary from region to region across the globe. The challenges can be technology related, farm related, data related, and organization related. The major challenges at the organization level are lack of proper geospatial policies, skilled manpower, financial resources, etc. The lack of recent satellite images, topographic data, the spatial scale of data, unavailability of cloud-free data, data interoperability, and different data format are the major data-related challenges facing the agriculture sector to adopt geospatial techniques. Technology-related issues involved compatibility and high cost of hardware and software, lack of understanding in the correct application of the

technology, inadaptability by the farmers at the grassroots, etc. Besides, a small landholding of the farmers, environmental issues, and farm ownership issues, identification and estimation of area and production of short-duration crops grown in fragmented landholdings, in particular during kharif/monsoon season, makes the geospatial technology application more challenging.

1.10 Conclusions and Future Prospective

The rapid development in the field of geospatial technologies especially the remote sensing and geographic information system play a key role to the sustainable management of natural resources through extraction of the precise and desired information to save the costly and infinitive natural resources for the future generation. Remote sensing data at the optical, microwave, thermal, and hyperspectral domain has proved to be a powerful tool to assess the crop and soil properties in varying spatial and temporal scales with cost-effectiveness. Remote sensing satellite images can be used efficiently for crop growth monitoring, crop condition assessment, crop acreage and yield estimation, precision farming, crop biomass estimation, identification of pest and diseases infestation, soil survey and mapping, land degradation assessment, soil moisture estimation, soil quality assessment, etc. Geographic Information System is considered one of the important tools for decision-making in a problem-solving environment dealing with geo-information. Such technologies and tools can be used effectively for developing optimum management strategies or suitable action plans to maintain the agricultural sustainability of any province. It is a novel approach to save the energy consumption directly and indirectly, reduce input and footprints of the ecosystems, and enhance the eco-intensification of the natural resources for the food, nutritional, environmental, and economic security to the growing population.

References

AbdelRahman MA, Natarajan A, Hegde R (2016) Assessment of land suitability and capability by integrating remote sensing and GIS for agriculture in Chamarajanagar district, Karnataka, India. Egypt J Remote Sens Space Sci 19(1):125–141

Adamchuk V (2011) On-the-go soil sensors–are we there yet. McGill University, Ste-Anne-de-Bellevue, p 63

Akbar R, Moghaddam M (2015) A combined active–passive soil moisture estimation algorithm with adaptive regularization in support of SMAP. IEEE Trans Geosci Remote Sens 53 (6):3312–3324

Alexandratos N, Bruinsma J (2012) World agriculture towards 2030/2050: the 2012 revision, ESA working paper no. 12–03. FAO, Rome

Ambika AK, Wardlow B, Mishra V (2016) Remotely sensed high resolution irrigated area mapping in India for 2000 to 2015. Sci Data 3(1):1–4

Andreo V (2013) Remote sensing and geographic information systems in precision farming. Available: http://aulavirtual.ig.conae.gov.ar/moodle/pluginfile.php/513/mod_page/content/71/seminario_andreo_2013.pdf. Retrieved April 16, 2015

Apostol S, Viau AA, Tremblay N, Briantais JM, Prasher S, Parent LE, Moya I (2003) Laser-induced fluorescence signatures as a tool for remote monitoring of water and nitrogen stresses in plants. Can J Remote Sens 29(1):57–65

Ban HY, Ahn JB, Lee BW (2019) Assimilating MODIS data-derived minimum input data set and water stress factors into CERES-Maize model improves regional corn yield predictions. PLoS One 14(2)

Banerjee S, Pandey AC (2019) Crop insurance model to consolidate academia-industry cooperation: a case study over Assam, India. Spat Inf Res 27(6):719–731

Bégué A, Arvor D, Bellon B, Betbeder J, De Abelleyra D, PD Ferraz R, Lebourgeois V, Lelong C, Simões M, R Verón S (2018) Remote sensing and cropping practices: a review. Remote Sens 10 (1):99

Belanger MJ, Miller JR, Boyer MG (1995) Comparative relationships between some red edge parameters and seasonal leaf chlorophyll concentrations. Can J Remote Sens 21(1):16–21

Ben-Dor E, Banin A (1995) Near-infrared analysis (Nira) as a method to simultaneously evaluate spectral featureless constituents in soils. Soil Sci 159(4):259–270

Ben-Dor E, Feingersh T, Filin S, Schläpfer D (2007) Better analysis of hyperspectral images by correcting reflectance anisotropy. SPIE Newsroom. 2010 Apr 7

Bhattarai GP, Schmid RB, McCornack BP (2019) Remote sensing data to detect hessian fly infestation in commercial wheat fields. Sci Rep 9(1):1–8

Blaes X, Chomé G, Lambert MJ, Traoré PS, Schut AG, Defourny P (2016) Quantifying fertilizer application response variability with VHR satellite NDVI time series in a rainfed smallholder cropping system of Mali. Remote Sens 8(6):531

Borgogno-Mondino E, Sarvia F, Gomarasca MA (2019) Supporting insurance strategies in agriculture by remote sensing: a possible approach at regional level. In: International conference on computational science and its applications 2019. Springer, Cham, pp 186–199

Boschetti M, Nelson A, Nutini F, Manfron G, Busetto L, Barbieri M, Laborte A, Raviz J, Holecz F, Mabalay MR, Bacong AP (2015) Rapid assessment of crop status: an application of MODIS and SAR data to rice areas in Leyte, Philippines affected by Typhoon Haiyan. Remote Sens 7 (6):6535–6557

Camera C, Zomeni Z, Noller JS, Zissimos AM, Christoforou IC, Bruggeman A (2017) A high resolution map of soil types and physical properties for Cyprus: a digital soil mapping optimization. Geoderma 285:35–49

Carré F, McBratney AB, Mayr T, Montanarella L (2007) Digital soil assessments: beyond DSM. Geoderma 142(1–2):69–79

Castillejo-González IS (2018) Mapping of olive trees using pan sharpened quick bird images: an evaluation of pixel- and object-based analyses. Agronomy 8:288. https://doi.org/10.3390/agronomy8120288

Chakraborty A, Seshasai MV, Dadhwal VK (2014) Geospatial analysis of the temporal trends of kharif crop phenology metrics over India and its relationships with rainfall parameters. Environ Monit Assess 186(7):4531–4542

Chakraborty A, Seshasai MV, Rao SK, Dadhwal VK (2017) Geospatial analysis of temporal trends of temperature and its extremes over India using daily gridded (1× 1) temperature data of 1969–2005. Theor Appl Climatol 130(1–2):133–149

Chakraborty A, Seshasai MV, Reddy CS, Dadhwal VK (2018) Persistent negative changes in seasonal greenness over different forest types of India using MODIS time series NDVI data (2001–2014). Ecol Indic. https://doi.org/10.1016/j.ecolind.2017.11.032

Chakraborty A, Biswal A, Pandey V, Murthy CS, Rao PVN, Chowdhury S (2019) Spatial disaggregation of the bioenergy potential from crop residues using geospatial technique. ISPRS WG III/10, GEOGLAM, ISRS Joint International Workshop on Earth Observation for Agricultural Monitoring, February 18–20, New Delhi, India

Chang AY, Parrales ME, Jimenez J, Sobieszczyk ME, Hammer SM, Copenhaver DJ, Kulkarni RP (2009) Combining google earth and GIS mapping technologies in a dengue surveillance system for developing countries. Int J Health Geogr 8(1):1–11

Chen J, Huang J, Hu J (2011) Mapping rice planting areas in southern China using the China Environment Satellite data. Math Comput Model 54(3–4):1037–1043

Chung YS, Yoon MB (2000) Interpretation of recent temperature and precipitation trends observed in Korea. Theor Appl Climatol 67:171–180

Clarke KC (1986) Advances in geographic information systems. Comput Environ Urban Syst 10 (3–4):175–184

Cleland EE, Chuine I, Menzel A (2007) Shifting plant phenology in response to global change. Trends Ecol Evol 22(7):357–365

Clevers JG, Kooistra L (2011) Using hyperspectral remote sensing data for retrieving canopy chlorophyll and nitrogen content. IEEE J Sel Top Appl Earth Obs Remote Sens 5(2):574–583

Cohen S, Raveh E, Li Y, Grava A, Goldschmidt EE (2005) Physiological responses of leaves, tree growth and fruit yield of grapefruit trees under reflective shade screens. Sci Hortic 107(1):25–35

Craig M, Atkinson D (2013) A literature review of crop area estimation. Accessed July 2013; 2:2018

Dao TH (2018) Sensing soil and foliar phosphorus fluorescence in Zea mays in response to large phosphorus additions. Precis Agric 18(5):685–700

Darvishzadeh R, Wang T, Skidmore A, Vrieling A, O'Connor B, Gara TW, Ens BJ, Paganini M (2019) Analysis of Sentinel-2 and rapidEye for retrieval of leaf area index in a saltmarsh using a radiative transfer model. Remote Sens 11(6):671

Das PK, Chakraborty A, Sesha Sai MVR (2013) Spatial analysis of temporal trend of rainfall and rainy days during Indian summer monsoon season using daily gridded (0.50 × 0.50) rainfall data for the period of 1971–2005. Meteorol Appl 19. https://doi.org/10.1002/met.1361

Dayananda S, Astor T, Wijesingha J, Chickadibburahalli Thimappa S, Dimba Chowdappa H, Nidamanuri RR, Nautiyal S, Wachendorf M (2019) Multi-temporal monsoon crop biomass estimation using hyperspectral imaging. Remote Sens 11(15):1771

De Leeuw J, Vrieling A, Shee A, Atzberger C, Hadgu KM, Biradar CM, Keah H, Turvey C (2014) The potential and uptake of remote sensing in insurance: a Review. Remote Sens 6 (11):10888–10912

de Paul Obade V, Lal R (2013) Assessing land cover and soil quality by remote sensing and geographical information systems (GIS). Catena 104:77–92

Demetriades-Shah TH, Steven MD, Clark JA (1990) High resolution derivative spectra in remote sensing. Remote Sens Environ 33(1):55–64

Dimov D, Löw F, Uhl JH, Kenjabaev S, Dubovyk O, Ibrakhimov M, Biradar C (2019) Framework for agricultural performance assessment based on MODIS multitemporal data. J Appl Remote Sens 13(2):025501

Domonkos P, Tar K (2003) Long term changes in observed temperature and precipitation series 1901–1998 from Hungary and their relations to large scale changes. Theor Appl Climatol 75:131–147

Doolittle JA, Brevik EC (2014) The use of electromagnetic induction techniques in soils studies. Geoderma 223:33–45

Dwivedi RS (2001) Soil resources mapping: a remote sensing perspective. Remote Sens Rev 20 (2):89–122

Ennouri K, Kallel A (2019) Remote sensing: an advanced technique for crop condition assessment. Math Probl Eng 2019:1–8

Estel S, Kuemmerle T, Levers C, Baumann M, Hostert P (2016) Mapping cropland-use intensity across Europe using MODIS NDVI time series. Environ Res Lett 11(2):024015

Farkas D, Hilton B, Pick J, Ramakrishna H, Sarkar A, Shin N (2016) A tutorial on geographic information systems: a ten-year update. Commun Assoc Inf Syst 38(1):9

Feidas H, Makrogiannis T, Bora-Santa E (2004) Trend analysis of air temperature time series in Greece and their relationship with circulation using surface and satellite data: 1955–2001. Theor Appl Climatol 79:185–208

Forkuor G, Hounkpatin OK, Welp G, Thiel M (2017) High resolution mapping of soil properties using remote sensing variables in south-western Burkina Faso: a comparison of machine learning and multiple linear regression models. PLoS One 12(1)

Fourty T, Baret F, Jacquemoud S, Schmuck G, Verdebout J (1996) Leaf optical properties with explicit description of its biochemical composition: direct and inverse problems. Remote Sens Environ 56(2):104–117

Franceschini MH, Demattê JA, da Silva Terra F, Vicente LE, Bartholomeus H, de Souza Filho CR (2015) Prediction of soil properties using imaging spectroscopy: considering fractional vegetation cover to improve accuracy. Int J Appl Earth Obs Geoinf 38:358–370

Friedl MA (2018) Remote sensing of croplands. Compr Remote Sens:78–95

Gago J, Douthe C, Coopman R, Gallego P, Ribas-Carbo M, Flexas J, Escalona J, Medrano H (2015) UAVs challenge to assess water stress for sustainable agriculture. Agric Water Manag 153:9–19

Gangwar S (2013) Flood vulnerability in India: a remote sensing and GIS approach for warning, mitigation and management. Int J Environ Sci Dev Monit 4(2):77–79

Gerhards M, Schlerf M, Mallick K, Udelhoven T (2019) Challenges and future perspectives of multi-/hyperspectral thermal infrared remote sensing for crop water-stress detection: a review. Remote Sens 11(10):1240

Gerighausen H, Menz G, Kaufmann H (2012) Spatially explicit estimation of clay and organic carbon content in agricultural soils using multi-annual imaging spectroscopy data. Appl Environ Soil Sci 2012

Ghazaryan G, Dubovyk O, Löw F, Lavreniuk M, Kolotii A, Schellberg J, Kussul N (2018) A rule-based approach for crop identification using multi-temporal and multi-sensor phenological metrics. Eur J Remote Sens 51(1):511–524

Ghobadifar F, Aimrun W, Jebur MN (2016) Development of an early warning system for brown planthopper (BPH) (Nilaparvata lugens) in rice farming using multispectral remote sensing. Precis Agric 17(4):377–391

Gibbs HK, Ruesch AS, Achard F, Clayton MK, Holmgren P, Ramankutty N, Foley JA (2010) Tropical forests were the primary sources of new agricultural land in the 1980s and 1990s. Proc Natl Acad Sci 107(38):16732–16737

Haboudane D, Miller JR, Tremblay N, Pattey E, Vigneault P (2004) Estimation of leaf area index using ground spectral measurements over agriculture crops: prediction capability assessment of optical indices. In: XXth ISPRS congress: "Geo-imagery bridging continents". Istanbul, Turkey, 2004 July 12, pp 12–23

Hakkim VA, Joseph EA, Gokul AA, Mufeedha K (2016) Precision farming: the future of Indian agriculture. J Appl Biomater Biomech:68–72

Han L, Yang G, Dai H, Xu B, Yang H, Feng H, Li Z, Yang X (2019) Modeling maize above-ground biomass based on machine learning approaches using UAV remote-sensing data. Plant Methods 15(1):10

Hasanean HM (2001) Fluctuations of surface air temperature in the Eastern Mediterranean. Theor Appl Climatol 68(1–2):75–87

Hengl T, Leenaars JG, Shepherd KD, Walsh MG, Heuvelink GB, Mamo T, Tilahun H, Berkhout E, Cooper M, Fegraus E, Wheeler I (2017) Soil nutrient maps of Sub-Saharan Africa: assessment of soil nutrient content at 250 m spatial resolution using machine learning. Nutr Cycl Agroecosyst 109(1):77–102

Heupel K, Spengler D, Itzerott S (2018) A progressive crop-type classification using multitemporal remote sensing data and phenological information. PFG–J Photogramm Remote Sens Geoinf Sci 86(2):53–69

Heuvelink GB, Webster R (2001) Modelling soil variation: past, present, and future. Geoderma 100 (3–4):269–301

http://opticleaf.ipgp.fr/index.php?page=prospect

https://archive.usgs.gov/archive/sites/eo1.usgs.gov/index.html

https://asterweb.jpl.nasa.gov/eos.asp

https://autodesk.com

https://clarklabs.org
https://directory.eoportal.org/web/eoportal/satellite-missions/i/ikonos-2
https://earth.esa.int//web/guest/missions/3rd-party-missions/current-missions/rapideye
https://earth.esa.int/web/guest/data-access/browse-data-products/-/article/spot-6-and-7-archive-and-new
https://geospatial.intergraph.com/products/GeoMedia
https://geospatialmedia.net
https://grass.osgeo.org/
https://modis.gsfc.nasa.gov/
https://qgis.org/en/site
https://sentinels.copernicus.eu/web/sentinel/missions/sentinel-1
https://sentinels.copernicus.eu/web/sentinel/missions/sentinel-2
https://spacedata.copernicus.eu/web/cscda/missions/kompsat-3
https://spacedata.copernicus.eu/web/cscda/missions/worldview-2
https://www.52north.org
https://www.bentley.com
https://www.bluemarblegeo.com/products/global-mapper.php
https://www.caliper.com
https://www.envitia.com
https://www.esri.com/en-us/arcgis
https://www.ge.com/digital/applications/geospatial-network-modeling-solutions-utilities
https://www.gvsig.org
https://www.harrisgeospatial.com
https://www.isro.gov.in
https://www.mapinfo.com
https://www.mapmaker.com
https://www.microimages.com
https://www.pcigeomatics.com
https://www.saga-gis.org/en
https://www.supergeotek.com
https://www.supermap.com
https://www.tatukgis.com
https://www.usgs.gov/land-resources/nli/landsat
https://www2.jpl.nasa.gov/srtm/

Huang B, Zhao B, Song Y (2018) Urban land-use mapping using a deep convolutional neural network with high spatial resolution multispectral remote sensing imagery. Remote Sens Environ 214:73–86

Huang J, Gómez-Dans JL, Huang H, Ma H, Wu Q, Lewis PE, Liang S, Chen Z, Xue JH, Wu Y, Zhao F (2019) Assimilation of remote sensing into crop growth models: current status and perspectives. Agric For Meteorol 276:107609

Huete AR, Escadafal R (1991) Assessment of biophysical soil properties through spectral decomposition techniques. Remote Sens Environ 35(2–3):149–159

Jensen L, Aikens CM, Schatz GC (2008) Electronic structure methods for studying surface-enhanced Raman scattering. Chem Soc Rev 37(5):1061–1073

Karaburun A (2010) Estimation of C factor for soil erosion modeling using NDVI in Buyukcekmece watershed. Ozean J Appl Sci 3(1):77–85

Kasampalis DA, Alexandridis TK, Deva C, Challinor A, Moshou D, Zalidis G (2018) Contribution of remote sensing on crop models: a review. J Imaging 4(4):52

Katsoulas N, Elvanidi A, Ferentinos KP, Kacira M, Bartzanas T, Kittas C (2016) Crop reflectance monitoring as a tool for water stress detection in greenhouses: a review. Biosyst Eng 151:374–398

Kavita KM, Patil G (2011) Geographic information system (GIS)–for business analytics. Int J Sci Eng Res 2(11):1–6

Khanal S, Fulton J, Shearer S (2017) An overview of current and potential applications of thermal remote sensing in precision agriculture. Comput Electron Agric 139:22–32

Lambin EF, Meyfroidt P (2011) Global land use change, economic globalization, and the looming land scarcity. Proc Natl Acad Sci 108(9):3465–3472

Lambin EF, Gibbs HK, Ferreira L, Grau R, Mayaux P, Meyfroidt P, Morton DC, Rudel TK, Gasparri I, Munger J (2013) Estimating the world's potentially available cropland using a bottom-up approach. Glob Environ Chang 23(5):892–901

Li Q, Wu B, Jia K, Dong Q, Eerens H, Zhang M (2011) Maize acreage estimation using ENVISAT MERIS and CBERS-02B CCD data in the North China Plain. Comput Electron Agric 78 (2):208–214

Liaghat S, Balasundram SK (2010) A review: the role of remote sensing in precision agriculture. Am J Agric Biol Sci 5(1):50–55

Lillesand T, Kiefer RW, Chipman J (2015) Remote sensing and image interpretation. Wiley

Lira Melo de Oliveira Santos C, Augusto Camargo Lamparelli R, Kelly Dantas Araújo Figueiredo G, Dupuy S, Boury J, Luciano AC, Torres RD, Le Maire G (2019) Classification of crops, pastures, and tree plantations along the season with multi-sensor image time series in a subtropical agricultural region. Remote Sens 11(3):334

Liu B, Xu M, Henderson M, Ye Q, Yiging L (2004) Taking China's temperature: daily range, warming trend and regional variation, 1955–2000. J Clim 17(22):4453–4462

Löw F, Biradar C, Dubovyk O, Fliemann E, Akramkhanov A, Narvaez Vallejo A, Waldner F (2018) Regional-scale monitoring of cropland intensity and productivity with multi-source satellite image time series. GISci Remote Sens 55(4):539–567

Ma Y, Minasny B, Malone BP, Mcbratney AB (2019) Pedology and digital soil mapping (DSM). Eur J Soil Sci 70(2):216–235

Maes WH, Steppe K (2012) Estimating evapotranspiration and drought stress with ground-based thermal remote sensing in agriculture: a review. J Exp Bot 63(13):4671–4712

Magagi R, Berg AA, Goïta K, Belair S, Jackson TJ, Toth B, Walker A, McNairn H, O'Neill PE, Moghaddam M (2012) Canadian experiment for soil moisture in 2010 (CanEx-SM10): overview and preliminary results. IEEE Trans Geosci Remote Sens 51(1):347–363

Mahlein AK (2016) Plant disease detection by imaging sensors–parallels and specific demands for precision agriculture and plant phenotyping. Plant Dis 100(2):241–251

Maki M, Sekiguchi K, Homma K, Hirooka Y, Oki K (2017) Estimation of rice yield by SIMRIW-RS, a model that integrates remote sensing data into a crop growth model. J Agric Meteorol 73 (1):2–8

Manchanda ML, Kudrat M, Tiwari AK (2002) Soil survey and mapping using remote sensing. Trop Ecol 43(1):61–74

Mao D, Wang Z, Wu B, Zeng Y, Luo L, Zhang B (2018) Land degradation and restoration in the arid and semiarid zones of China: Quantified evidence and implications from satellites. Land Degrad Dev 29(11):3841–3851

Marble DF, Peuquet DJ (1983) The computer and geography: some methodological comments. Prof Geogr 35(3):343–344

Marinelli MV, Scavuzzo CM, Giobellina BL, Scavuzzo CM (2019) Geoscience and remote sensing on horticulture as support for management and planning. Aust J Agric Res 2(2):43

Mee CY, Balasundram SK, Hanif AH (2017) Detecting and monitoring plant nutrient stress using remote sensing approaches: a review. Asian J Plant Sci 16:1–8

Meena RS, Mitran T, Kumar S, Yadav G, Bohra JS, Datta R (2018) Application of remote sensing for sustainable agriculture and forest management. Inform Process Agric 5:295–297

Meena RS, Kumar V, Yadav GS, Mitran T (2018a) Response and interaction of *Bradyrhizobium japonicum* and Arbuscular mycorrhizal fungi in the soybean rhizosphere: a review. Plant Growth Regul 84:207–223

Meena RS, Lal R, Yadav GS (2020) Long term impacts of topsoil depth and amendments on soil physical and hydrological properties of an Alfisol in Central Ohio, USA. Geoderma 363:1141164

Memarbashi E, Azadi H, Barati AA, Mohajeri F, Passel SV, Witlox F (2017) Land-use suitability in Northeast Iran: application of AHP-GIS hybrid model. ISPRS Int J Geo Inf 6(12):396
Meng JH, You XZ, Cheng ZQ (2015) Evaluating soil available nitrogen status with remote sensing. In: Precision agriculture'15 2015 July 1. Wageningen Academic Publishers, pp 337–344
Minasny B, McBratney AB (2016) Digital soil mapping: a brief history and some lessons. Geoderma 264:301–311
Mitasova H, Barton CM, Ullah I, Hofierka J, Harmon RS (2013) GIS-based soil erosion modeling. In: Treatise on geomorphology. Elsevier Inc, pp 228–258
Mitran T, Lal R, Mishra U, Meena RS, Ravisankar T, Sreenivas K (2018a) Climate change impact on soil carbon stocks in India. In: Lal R, Stewart BA (eds) Soil and climate. Advances in soil science. Taylor and Francis, Boca Raton, 301–322
Mitran T, Mishra U, Lal R, Ravisankar T, Sreenivas K (2018b) Spatial distribution of soil carbon stocks in a semi-arid region of India. Geoderma Reg 15:e00192. https://doi.org/10.1016/j.geodrs.2018.e00192
Mohamed ES, Belal A, Saleh A (2013) Assessment of land degradation east of the Nile Delta, Egypt using remote sensing and GIS techniques. Arab J Geosci 6(8):2843–2853
Mohamed ES, Ali A, El-Shirbeny M, Abutaleb K, Shaddad SM (2019) Mapping soil moisture and their correlation with crop pattern using remotely sensed data in arid region. Egypt J Remote Sens Space Sci. https://doi.org/10.1016/j.ejrs.2019.04.003
Mohanty BP, Cosh MH, Lakshmi V, Montzka C (2017) Soil moisture remote sensing: State-of-the-science. Vadose Zone J 16(1)
Molin JP, Tavares TR (2019) Sensor systems for mapping soil fertility attributes: challenges, advances, and perspectives in Brazilian tropical soils. Eng Agrícola 39(SPE):126–147
Mulder VL, De Bruin S, Schaepman ME, Mayr TR (2011) The use of remote sensing in soil and terrain mapping – a review. Geoderma 162(1–2):1–9
Mulla DJ (2013) Twenty-five years of remote sensing in precision agriculture: key advances and remaining knowledge gaps. Biosyst Eng 114:358–371
Mulla DJ, Miao Y (2016) Precision farming. In: Thenkabail PS (ed) Land resources monitoring, modeling, and mapping with remote sensing. CRC Press, Boca Raton, pp 161–178
Murti SH (2019) Agroecosystem zone mapping as a baseline for land suitability evaluation based on remote sensing image processing and geographic information systems in Temanggung regency, Central Java province. In: Remote sensing for agriculture, ecosystems, and hydrology XXI 2019 Oct 21, vol 11149. International Society for Optics and Photonics, p 111491W
Nabi A, Narayan S, Afroza B, Mushtaq F, Mufti S, Ummyiah HM, Malik A (2017) Precision farming in vegetables. J Pharmacogn Phytother 6(6):370–375
Navalgund RR, Jayaraman V, Roy PS (2007) Remote sensing applications: an overview. Curr Sci 93:12
Neupane J, Guo W (2019) Agronomic basis and strategies for precision water management: a review. Agronomy 9(2):87
Niu Y, Zhang L, Zhang H, Han W, Peng X (2019) Estimating above-ground biomass of maize using features derived from UAV-based RGB imagery. Remote Sens 11(11):1261
Ojo OI, Ilunga F (2018) Geospatial analysis for irrigated land assessment, modeling and mapping. Multi-purp Appl Geosp Data 9:65
Pan Y, Li L, Zhang J, Liang S, Zhu X, Sulla-Menashe D (2012) Winter wheat area estimation from MODIS-EVI time series data using the Crop Proportion Phenology Index. Remote Sens Environ 119:232–242
Pandey A, Mathur A, Mishra SK, Mal BC (2009) Soil erosion modeling of a Himalayan watershed using RS and GIS. Environ Earth Sci 59(2):399–410
Pareeth S, Karimi P, Shafiei M, De Fraiture C (2019) Mapping agricultural land use patterns from time series of Landsat 8 using random forest based hierarchical approach. Remote Sens 11 (5):601

Parry JA, Ganaie SA, Bhat MS (2018) GIS based land suitability analysis using AHP model for urban services planning in Srinagar and Jammu urban centers of J&K, India. J Urban Manag 7 (2):46–56

Partel V, Kakarla SC, Ampatzidis Y (2019) Development and evaluation of a low-cost and smart technology for precision weed management utilizing artificial intelligence. Comput Electron Agric 157:339–350

Pasqualotto N, Delegido J, Van Wittenberghe S, Rinaldi M, Moreno J (2019) Multi-crop green LAI estimation with a new simple Sentinel-2 LAI Index (SeLI). Sensors 19(4):904

Patel AK, Ghosh JK (2019) Soil fertility status assessment using hyperspectral remote sensing. In: Remote sensing for agriculture, ecosystems, and hydrology XXI 2019 Oct 21, vol 11149. International Society for Optics and Photonics, p 111490E

Paz-Kagan T, Shachak M, Zaady E, Karnieli A (2014) A spectral soil quality index (SSQI) for characterizing soil function in areas of changed land use. Geoderma 230:171–184

Paz-Kagan T, Zaady E, Salbach C, Schmidt A, Lausch A, Zacharias S, Notesco G, Ben-Dor E, Karnieli A (2015) Mapping the spectral soil quality index (SSQI) using airborne imaging spectroscopy. Remote Sens 7(11):15748–15781

Pendleton PM (2012) GIS-based incident mapping and analysis within the CSU Northridge Department of Police Services. Doctoral dissertation, California State University, Northridge

Penuelas J, Filella I, Gamon JA (1995) Assessment of photosynthetic radiation-use efficiency with spectral reflectance. New Phytol 131(3):291–296

Phung HP, Nguyen LD, Thong NH, Thuy LT, Apan AA (2020) Monitoring rice growth status in the Mekong Delta, Vietnam using multitemporal Sentinel-1 data. J Appl Remote Sens 14 (1):014518

Pierce FJ, Nowak P (1999) Aspects of precision agriculture. In: Advances in agronomy, vol 67. Academic, pp 1–85

Pinter PJ Jr, Hatfield JL, Schepers JS, Barnes EM, Moran MS, Daughtry CS, Upchurch DR (2003) Remote sensing for crop management. Photogramm Eng Remote Sens 69(6):647–664

Prabhakar M, Prasad YG, Desai S, Thirupathi M, Gopika K, Rao GR, Venkateswarlu B (2013) Hyperspectral remote sensing of yellow mosaic severity and associated pigment losses in Vigna mungo using multinomial logistic regression models. Crop Prot 45:132–140

Primicerio J, Di Gennaro SF, Fiorillo E, Genesio L, Lugato E, Matese A, Vaccari FP (2012) A flexible unmanned aerial vehicle for precision agriculture. Precis Agric 13(4):517–523

Purnamasari RA, Noguchi R, Ahamed T (2019) Land suitability assessments for yield prediction of cassava using geospatial fuzzy expert systems and remote sensing. Comput Electron Agric 166:105018

Qiu B, Fan Z, Zhong M, Tang Z, Chen C (2014) A new approach for crop identification with wavelet variance and JM distance. Environ Monit Assess 186:7929–7940

Ramoelo A, Dzikiti S, Van Deventer H, Maherry A, Cho MA, Gush M (2015) Potential to monitor plant stress using remote sensing tools. J Arid Environ 113:134–144

Ran Y, Li X, Jin R, Kang J, Cosh MH (2017a) Strengths and weaknesses of temporal stability analysis for monitoring and estimating grid-mean soil moisture in a high-intensity irrigated agricultural landscape. Water Resour Res 53(1):283–301

Ran L, Zhang Y, Wei W, Zhang Q (2017b) A hyperspectral image classification framework with spatial pixel pair features. Sensors 17(10):2421. https://doi.org/10.3390/s17102421. PMC 5677443

Rast M, Painter TH (2019) Earth observation imaging spectroscopy for terrestrial systems: an overview of its history, techniques, and applications of its missions. Surv Geophys 40 (3):303–331

Raun WR, Solie JB, Johnson GV, Stone ML, Mullen RW, Freeman KW et al (2002) Improving nitrogen use efficiency in cereal grain production with optical sensing and variable rate application. Agron J 94:815–820

Reddy VR (2003) Land degradation in India extent, costs and determinants. Econ Polit Wkly 38 (44):4700–4713

Reusch S, Jasper J, Link A (2010) Estimating crop biomass and nitrogen uptake using Cropspec, a newly developed active crop-canopy reflectance sensor. In: Proceedings of the 10th international conference on Positron Annihilation (ICPA), Denver, CO, USA, 18–21 July 2010, p 381
Revadekar JV, Kothawale DR, Patwardhan SK, Pant GB, Kumar KR (2012) About the observed and future changes in temperature extremes over India. Nat Hazards 60(3):1133–1155
Rolim J, Navarro A, Vilar P, Saraiva C, Catalao J (2019) Crop data retrieval using earth observation data to support agricultural water management. Engg Agrícola 39(3):380–390
Rossel RV, Behrens T (2010) Using data mining to model and interpret soil diffuse reflectance spectra. Geoderma 158(1–2):46–54
Rossel RV, Walvoort DJ, McBratney AB, Janik LJ, Skjemstad JO (2006) Visible, near infrared, mid infrared or combined diffuse reflectance spectroscopy for simultaneous assessment of various soil properties. Geoderma 131(1–2):59–75
Rossel RV, Adamchuk VI, Sudduth KA, McKenzie NJ, Lobsey C (2011) Proximal soil sensing: an effective approach for soil measurements in space and time. In: Advances in agronomy 2011 Jan 1, vol 113. Academic, pp 243–291
Rotairo L, Durante AC, Lapitan P, Rao LN (2019) Use of remote sensing to estimate paddy area and production: a handbook. Asian Development Bank
Sabin FF (1997) Remote sensing: principles and interpretation, 3rd edn. WH Freeman and Company, New York
Saha A, Patil M, Goyal VC, Rathore DS (2018) Assessment and impact of soil moisture index in agricultural drought estimation using remote sensing and GIS techniques. In: Multidisciplinary digital publishing institute proceedings, vol 7, p 2
Salama RB (2011) Remote sensing of soils and plants imagery. Encycl Agrophy:681–692
Sawant S, Mohite J, Sakkan M, Pappula S (2019) Near real time crop loss estimation using remote sensing observations. In: 2019 8th international conference on Agro-Geoinformatics (Agro-Geoinformatics) 2019 July 16. IEEE, pp 1–5
Schepers JS, Francis DD, Vigil M, Below FE (1992) Comparison of corn leaf nitrogen concentration and chlorophyll meter readings. Commun Soil Sci Plant Anal 23:2173–2187
Schmedtmann J, Campagnolo ML (2015) Reliable crop identification with satellite imagery in the context of common agriculture policy subsidy control. Remote Sens 7(7):9325–9346
Sharma R, Sood K (2020) Characterization of spatial variability of soil parameters in apple orchards of Himalayan region using geostatistical analysis. Commun Soil Sci Plant Anal 25:1–3
Shelestov A, Kolotii A, Skakun S, Baruth B, Lozano RL, Yailymov B (2017) Biophysical parameters mapping within the SPOT-5 Take 5 initiative. Eur J Remote Sens 50(1):300–309
Song YQ, Zhao X, Su HY, Li B, Hu YM, Cui XS (2018) Predicting spatial variations in soil nutrients with hyperspectral remote sensing at regional scale. Sensors 18(9):3086
Sreenivas K, Dadhwal VK, Kumar S, Harsha GS, Mitran T, Sujatha G, Suresh GJ, Fyzee MA, Ravisankar T (2016) Digital mapping of soil organic and inorganic carbon status in India. Geoderma 269:160–173
Sripada RP, Heiniger RW, White JG, Meijer AD (2006) Aerial color infrared photography for determining early in-season nitrogen requirements in corn. Agron J 98(4):968–977
Stafford JM, Wendler G, Curtis J (2000) Temperature and precipitation of Alaska: 50-year trend analysis. Theor Appl Climatol 67:33–44
Stewart ID, Oke TR, Krayenhoff ES (2014) Evaluation of the 'local climate zone'scheme using temperature observations and model simulations. Int J Climatol 34(4):1062–1080
Sugumaran R, Degroote J (2011) Spatial decision support systems. Int J Geogr Inf Sci 25(11):1–2
Sun C, Bian Y, Zhou T, Pan J (2019) Using of multi-source and multi-temporal remote sensing data improves crop-type mapping in the subtropical agriculture region. Sensors 19(10):2401
Supuwiningsih NN, Rusli M (2017) Prediction of decreasing agricultural land based on geographic information system case study: Denpasar city. Int J Comput Appl 162(9):0975–8887
Surek G, Nádor G (2015) Monitoring of damage in sunflower and maize parcels using radar and optical time series data. J Sens 2015. https://doi.org/10.1155/2015/548506

Taghvaeian S, Neale CM, Osterberg JC, Sritharan SI, Watts DR (2018) Remote sensing and GIS techniques for assessing irrigation performance: case study in Southern California. J Irrig Drain Eng 144(6):05018002

Tangang FT, Juneng L, Ahmad S (2007) Trend and interannual variability of temperature in Malaysia: 1961–2002. Theor Appl Climatol 89(3–4):127–141

Tazekrit I, Benslimane M, Simonneaux V, Hartani T, Hamimed A (2018) Estimation of irrigation water pumping by remote sensing: application of the SAMIR model to citrus under Mediterranean climate conditions. Rev Bras Meteorol 33(3):391–400

Teng M, Zeng L, Xiao W, Huang Z, Zhou Z, Yan Z, Wang P (2017) Spatial variability of soil organic carbon in Three Gorges Reservoir area, China. Sci Total Environ 599:1308–1316

Thenkabail PS, Enclona EA, Ashton MS, Van Der Meer B (2004) Accuracy assessments of hyperspectral waveband performance for vegetation analysis applications. Remote Sens Environ 91(3–4):354–376

Transon J, d'Andrimont R, Maugnard A, Defourny P (2018) Survey of hyperspectral earth observation applications from space in the sentinel-2 context. Remote Sens 10(2):157

Trout TJ, Johnson LF, Gartung J (2008) Remote sensing of canopy cover in horticultural crops. Hortic Sci 43(2):333–337

Twiss SD, Thomas CJ, Pomeroy PP (2001) Topographic spatial characterisation of grey seal Halichoerus grypus breeding habitat at a sub-seal size spatial grain. Ecography 24(3):257–266

Useya J, Chen S, Murefu M (2019) Cropland mapping and change detection: toward Zimbabwean cropland inventory. IEEE Access 7:53603–53620

Usha K, Singh B (2013) Potential applications of remote sensing in horticulture – a review. Sci Hortic 153:71–83

Usowicz B, Lipiec J (2017) Spatial variability of soil properties and cereal yield in a cultivated field on sandy soil. Soil Tillage Res 174:241–250

Valverde-Arias OR, Esteve P, Tarquis AM, Garrido A (2020) Remote sensing in an index-based insurance design for hedging economic impacts on rice cultivation. Nat Hazards Earth Syst Sci 20(1):345–362

van Evert FK, Gaitán-Cremaschi D, Fountas S, Kempenaar C (2017) Can precision agriculture increase the profitability and sustainability of the production of potatoes and olives? Sustainability 9:1863. https://doi.org/10.3390/su9101863

Vasu D, Singh SK, Sahu N, Tiwary P, Chandran P, Duraisami VP, Ramamurthy V, Lalitha M, Kalaiselvi B (2017) Assessment of spatial variability of soil properties using geospatial techniques for farm level nutrient management. Soil Tillage Res 169:25–34

Verrelst J, Camps-Valls G, Muñoz-Marí J, Rivera JP, Veroustraete F, Clevers JG, Moreno J (2015) Optical remote sensing and the retrieval of terrestrial vegetation bio-geophysical properties – a review. ISPRS J Photogramm Remote Sens 108:273–290

Vicente-Serrano SM, Cabello D, Tomás-Burguera M, Martín-Hernández N, Beguería S, Azorin-Molina C, Kenawy AE (2015) Drought variability and land degradation in semiarid regions: assessment using remote sensing data and drought indices (1982–2011). Remote Sens 7 (4):4391–4423

Virnodkar SS, Pachghare VK, Patil VC, Jha SK (2020) Application of machine learning on remote sensing data for sugarcane crop classification: a review. In: ICT analysis and applications 2020. Springer, Singapore, pp 539–555

Wadoux AM, Padarian J, Minasny B (2019) Multi-source data integration for soil mapping using deep learning. Soil 5(1):107–119

Wagner W, Hahn S, Kidd R, Melzer T, Bartalis Z, Hasenauer S, Figa-Saldaña J, de Rosnay P, Jann A, Schneider S (2013) The ASCAT soil moisture product: a review of its specifications, validation results, and emerging applications. Meteorol Z 22(1):5–33

Wang W, Liu Y, Zhang L (2013) The spatial distribution of cereal bioenergy potential in China. GCB Bioenergy 5:525–535

White MS Jr (1984) Technical requirements and standards for a multipurpose geographic data system. Am Cartogr 11(1):15–26

Wieczorek WF, Delmerico AM (2009) Geographic information systems. Wiley Interdiscip Rev Comput Stat 1(2):167–186

Woldemariam GW, Iguala AD, Tekalign S, Reddy RU (2018) Spatial modeling of soil erosion risk and its implication for conservation planning: the case of the Gobele watershed, east Hararghe zone, Ethiopia. Land 7(1):25

Wu B, Meng J, Li Q, Yan N, Du X, Zhang M (2014) Remote sensing-based global crop monitoring: experiences with China's crop watch system. Int J Digital Earth 7(2):113–137

www.asc-csa.gc.ca/eng/satellites/radarsat

Yiran GA, Kusimi JM, Kufogbe SK (2012) A synthesis of remote sensing and local knowledge approaches in land degradation assessment in the Bawku East District, Ghana. Int J Appl Earth Obs Geoinf 14(1):204–213

Yohannes H, Soromessa T (2018) Land suitability assessment for major crops by using GIS-based multi-criteria approach in Andit Tid watershed, Ethiopia. Cogent Food Agric 4(1):1470481

Yones MS, Khdery GA, Dahi HF, Farg E, Arafat SM, Gamil WE (2019) Early detection of pink bollworm Pectinophora gossypiella (Saunders) using remote sensing technologies. In: Remote Sensing for Agriculture, Ecosystems, and Hydrology XXI 2019 Oct 18, vol 11149. International Society for Optics and Photonics, p 111491C

Yousfi S, Gracia-Romero A, Kellas N, Kaddour M, Chadouli A, Karrou M, Araus JL, Serret MD (2019) Combined use of low-cost remote sensing techniques and δ13C to assess bread wheat grain yield under different water and nitrogen conditions. Agronomy 9(6):285

Yue S, Hashino M (2003) Temperature trends in Japan: 1900–1996. Theor Appl Climatol 75:15–27

Zabihi M, Pourghasemi HR, Motevalli A, Zakeri MA (2019) Gully erosion modeling using GIS-based data mining techniques in northern Iran: a comparison between boosted regression tree and multivariate adaptive regression spline. In: Natural hazards GIS-based spatial modeling using data mining techniques 2019. Springer, Cham, pp 1–26

Zarco-Tejada PJ, Miller JR, Noland TL, Mohammed GH, Sampson PH (2001) Scaling-up and model inversion methods with narrowband optical indices for chlorophyll content estimation in closed forest canopies with hyperspectral data. IEEE Trans Geosci Remote Sens 39 (7):1491–1507

Zhang D, Zhou G (2016) Estimation of soil moisture from optical and thermal remote sensing: a review. Sensors 16(8):1308

Zhang S, He Y, Fang H (2003) Spatial variability of soil properties in the field based on GPS and GIS. Nongye Gongcheng Xuebao. Trans Chin Soc Agric Eng 19(2):39–44

Zhou J, Pavek MJ, Shelton SC, Holden ZJ, Sankaran S (2016) Aerial multispectral imaging for crop hail damage assessment in potato. Comput Electron Agric 127:406–412

Zortea M, Rodrigues ER (2019) Crop identification using superpixels and supervised classification of multispectral CBERS-4 wide-field imagery. In: Remote Sensing for Agriculture, Ecosystems, and Hydrology XXI 2019 Oct 21, vol 11149. International Society for Optics and Photonics, p 111491U

Chapter 2
Remote Sensing and Geographic Information System: A Tool for Precision Farming

Pabitra Kumar Mani, Agniva Mandal, Saikat Biswas, Buddhadev Sarkar, Tarik Mitran, and Ram Swaroop Meena

Contents

P. K. Mani (✉) · A. Mandal · B. Sarkar
Department of Agricultural Chemistry and Soil Science, Bidhan Chandra Agricultural University, Mohanpur, India

S. Biswas
Department of Agronomy, Bidhan Chandra Agricultural University, Mohanpur, India

T. Mitran
Soil and Land Resources Assessment Division, National Remote Sensing Centre, ISRO, Hyderabad, Telangana, India
e-mail: tarikmitran@nrsc.gov.in

R. S. Meena
Department of Agronomy, Institute of Agricultural Sciences, Banaras Hindu University, Varanasi, India
e-mail: meenars@bhu.ac.in

T. Mitran et al. (eds.), *Geospatial Technologies for Crops and Soils*,
https://doi.org/10.1007/978-981-15-6864-0_2

Abstract The right time application of the right amount of input is a prerequisite to optimizing profitability and sustainability with a lesser impact on environmental degradation. Such can be achieved through precision farming (PF). It can offer a great potential to minimize the yield gap by optimizing food production using best management practices. It can also help to maintain the consumption of natural resources at an ecologically benign and environmentally sustainable level. PF is a holistic approach to enhance crop productivity with the aid of satellite-based technology and information technology (IT) to assess and manage the spatial and temporal variability of resources and inputs such as seeds, fertilizers, chemicals, etc. within the field. Application of remote sensing (RS) and geographic information system (GIS) shows a great promise to precision agriculture (PA) because of its role in monitoring spatial variability overtime at high resolution. This chapter highlights various applications of RS and GIS techniques in PA or smart agriculture.

Keywords Decision support system · Geographic information system · Remote sensing · Satellite farming

Abbreviations

AIEM	Advanced Integral Equation Model
ALI	Advanced Land Imager
ARVI	Atmospherically Resistant Vegetation Index
ASTER	Advance Spaceborne Thermal Emission and Reflection Radiometer
AVHRR	Advance Very High Resolution Radiometer
AVIRIS	Airborne Visible Infrared Imaging Spectrometer
AWS	Amazon Web Services
CASI	Compact Airborne Spectrographic Imager
DCNI	Double-peak Canopy Nitrogen Index
DEM	Digital Elevation Model
DGPS	Differential Global Positioning System
DSSAT	Decision Support System for Agrotechnology Transfer
DVI	Difference Vegetation Index
EO	Earth Observing
EOS	Earth Observing System
EROS	Earth Resources Observation and Science
ERS	European Remote Sensing satellite
FASAL	Forecasting Agricultural Output Using Space, Agrometeorology and Land Based Observations
FIS	Farm Information Systems
GDVI	Green Difference Vegetation Index

GI	Greenness Index
GIS	Geographic Information System
GNDVI	Green Normalized Difference Vegetation Index
GNSS	Global Navigation Satellite System
GOSAVI	Green Optimized Soil-Adjusted Vegetation Index
GPS	Global Positioning System
GRVI	Green–Red Vegetation Index
GSAVI	Green Soil–Adjusted Vegetation index
GWR	Geographically Weighted Regression
HH	Horizontal Transmit and Horizontal Receive
HNDVI	Hyperspectral Normalized Difference Vegetation Index
HV	Horizontal Transmit and Vertical Receive
HVI	Hyperspectral Vegetation Index
IEM	Integral Equation Model
IRS	Indian Remote Sensing
IRSS	Indian Remote Sensing Satellite
IT	Information Technology
JERS	Japanese Earth Resource Satellite
LAI	Leaf Area Index
LANDSAT	Land Satellite
LASSIE	Low-Altitude Stationary Surveillance Instrumental Equipment
LIDAR	Light Detection and Ranging
LORIS	Local Resources Information System
MCAR	Modified Chlorophyll Absorption Ratio
MCARI	Modified Chlorophyll Absorption Ratio Index
MODIS	Moderate-resolution Imaging Spectrometer
MSAVI	Modified Soil-Adjusted Vegetation Index
MSR	Modified Simple Ratio
MSS	Multispectral Sensor
MTVI	Modified Triangular Vegetation Index
MZ	Management Zone
NAOC	Normalized Area Over Reflectance Curve
NASA	National Aeronautics and Space Administration
NDI	Normalized Difference Index
NDNI	Normalized Difference Nitrogen Index
NDRE	Normalized Difference Red Edge
NDVI	Normalized Difference Vegetation Index
NDWI	Normalized Difference Water Index
NG	Normalized Green
NGNDVI	Normalized Green Normalized Difference Vegetation Index
NR	Normalized Red
NUE	Nitrogen Use Efficiency

OLS	Ordinary Least Square
OMNBR	Optimal Multiple Narrow Band Reflectance Indexes
OSAVI	Optimized Soil-Adjusted Vegetation Index
PA	Precision Agriculture
PCA	Principal Component Analysis
PF	Precision Farming
PFDC	Precision Farming Development Center
PLS	Partial Least Squares
PSSR	Pigment Specific Simple Ratio
PVI	Perpendicular Vegetation Index
RDVI	Renormalized Difference Vegetation Index
RGRI	Red–Green Ratio Index
RIICE	Remote Sensing–based information and Insurance for Crops in Emerging Economics
RISAT	Radar Imaging Satellite
RS	Remote Sensing
RVI	Ratio Vegetation Index
RVSI	Red-Edge Vegetation Stress Index
SAR	Synthetic Aperture Radar
SAVI	Soil-Adjusted Vegetation Index
SNR	Signal-to-Noise Ratio
SOC	Soil Organic Carbon
SOM	Soil Organic Matter
SPAD	Soil Plant Analysis Development
SPOT	Système Pour l'Observation de la Terre
SR	Simple Ratio
SRM	Satellite-based Rice Monitoring
SRTM	Shuttle Radar Topography Mission
SWIR	Shortwave Infrared Region
TCARI	Transformed Chlorophyll Absorption Reflectance Index
TKK	Tata Kisan Kendra
TM	Thematic Mapper
TVI	Triangular Vegetation Index
TVIMSR	Triangular Vegetation Index Modified Simple Ratio
UAV	Unmanned Aerial Vehicles
USDA	United States Department of Agriculture
VH	Vertical Transmit and Horizontal Receive
VNIR	Visible Near Infrared
VRT	Variable Rate Technology
VV	Vertical Transmit and Vertical Receive
WDVI	Weighted Difference Vegetation Index

2.1 Introduction

Innovative discoveries in the fields of science and technology and their subsequent application in the agriculture field have enabled farmers to utilize their valuable natural resources effectively and efficiently for obtaining maximum yield. These developments have further been greatly supported by the use of sophisticated machine, adoption of new planting practices, judicious use of manures and fertilizers, integrated pest management by using herbicides and pesticides, etc. (Andreo 2013). However, to meet up with the future challenges to feed the 9 billion people of the world, there is a need to stop the declining trend of the total crop productivity, minimizing the rate of degradation of natural resources, and enhancing farm incomes. Other constraints like fragmented land holdings, trade liberalization on agriculture, as well as global climatic variations have posed serious threats in agricultural growth and development. The role of newly emerged technology adoption might play major instruments to increase agricultural productivity in the future (Hakkim et al. 2016). Therefore, the success of large-scale farming depends on the culmination of information based on satellite remote sensing (RS) data with well-documented spatial maps obtained through geographic information system (GIS) which are the basis of precision farming (PF) (Brisco et al. 1998; Carr et al. 1991; Palmer 1996).

PA is defined as the "the application of technologies and principles to manage spatial and temporal variability associated with all aspects of agricultural production to improve crop performance and environmental quality" (Pierce and Nowak 1999). The efficient management of various farm inputs in a particular location requires a qualitative and quantitative assessment of the infield variability (both, spatial and temporal) (Khosla 2001; Patil and Bhalerao 2013). PF is considered as one of the breakthroughs in agriculture (Crookston 2006), ranking below conservation tillage, fertilizer and herbicide management, and improved crop genetics, and is a holistic approach to improve crop productivity with the aid of information technology (IT) and satellite-based technology (Finch et al 2014). The right time application of the right amount of input in right location is a prerequisite to optimizing profitability and sustainability with a lesser impact on environmental degradation (Mondal et al. 2004; Mondal and Tewari 2007). Linsley and Bauer (1929) were credited to drill the seed by adopting PF. However, the works of Johnson et al. (1983) and Matthews (1983) initiated the modern PF (Stafford 2000).

2.1.1 Concept and Principle of Precision Farming

Precision farming (PF) or precision agriculture (PA) is an integrated information– and production-based farming system utilizing adequate information, appropriate technology, and proper management. The goal of precision PA is to enhance long-term, site-specific and whole farm production efficiency, productivity, and net return

without incurring any severe impact on the ecosystem of the surroundings (Earl et al. 1996; Andreo 2013). PF, as it is practiced today, had its beginnings in the mid-1980s with two contrasting philosophies, namely, farming by soil (Larson and Robert 1991) versus grid soil sampling for delineation of management zones (MZs) (Bhatti et al. 1991b; Mulla 1991, 1993; Mulla and Miao 2016).

PF is a breakthrough from the traditional management practice of soil and crop to sophisticated management considering spatial and temporal variability within the same field. It is a fine-tuning of total field management, where management decisions are considered according to the variations in resource conditions. The PF can be statistically represented as $P = 1-SD$, where, SD is standard deviation. If SD is 0, then $P = 1$, indicating a highly homogeneous field and if SD is 1, then $P = 0$, denoting maximum variability of field (Patil and Bhalerao 2013).

The basic principle of PF is to maximize the use efficiency of inputs considering spatial and temporal variability within a field and reflected by the quantity and quality of outputs. The five "R" concepts may be used in PA encompassing the "right amount of input at the 'right place' at the 'right time, from 'right source' with 'right manner'" (Khosla 2008). In this sense, PF can relate to an agricultural production system with a robust set of technologies, including RS, GIS, Global Positioning System (GPS), and Variable Rate Technology (VRT), which can propel agriculture into the computerized information–based world. The application of such technologies can optimize production efficiency, quality, reducing production costs, and reducing negative environmental impacts of farm practices – all at the location-specific, site-specific, zonal level (Earl et al. 1996; Andreo 2013).

Farm machinery and equipment for PF are available for various farm operations, including the tillage operation, sowing, transplanting, mechanical weeding, fertilizer distribution, as well as spraying of pesticides, etc. (Fig. 2.1). Nowadays global navigation satellite system (GNSS)–based vehicle guidance has been the most widely adopted PA technology in developed countries (Heraud and Lange 2009). GNSS-based navigation system auto steers the operation of tractors and other machinery to minimize gaps and overlaps on the predefined paths. Several aviation tools were used to guide operators to allow agricultural vehicles to use visual feedback such as light bars or graphical displays. However, nowadays auto-guidance systems steer agricultural vehicles under operation without direct input from operators. Autonomous agricultural vehicles known as Field Robots are the next logical step in the automation of crop production system (Gebbers and Adamchuk 2010).

PF offers several benefits, including improved efficiency of farm management inputs, increases in crop productivity or quality, and reduced transport of fertilizers and pesticides beyond the edge of a field (Mulla et al. 1996).

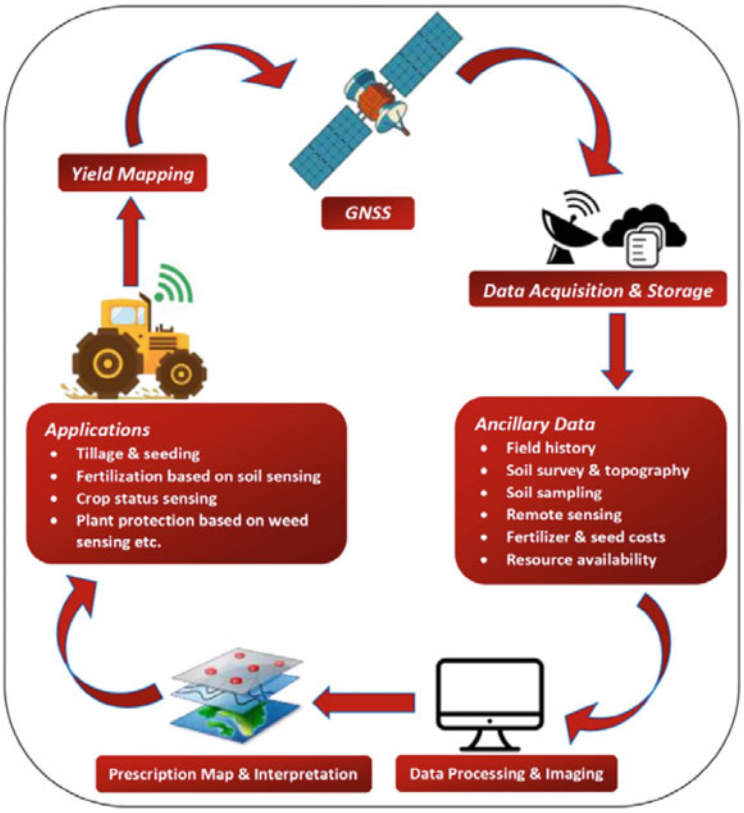

Fig. 2.1 Flow diagram depicting precision agriculture in crop production

2.1.2 Objectives of Precision Farming

2.1.2.1 Increased Profitability and Sustainability

Maximum profit can be obtained in each zone or site in a field by balancing precise amount of farm inputs (seeding rate, variety, herbicide, and insecticide) as per crop needs, which can be determined by weather, soil characteristics (nutrient availability, texture, and drainage) and historic crop performance. At the very same time, PF aims at sustaining this profitability (Van Evert et al. 2017; Nabi et al. 2017; Meena et al. 2018) PA has an advantage for both farmers and society as a whole. For the farming community, PA is expected to provide positive returns on investment, leading to an increase in profitability; while for society, PA is attractive because it may increase the sustainability of the farming (Pierce and Nowak 1999; Fleming et al. 2000; Gebbers and Adamchuk 2010; Foley et al. 2011; Banu 2015; Basso et al. 2016).

2.1.2.2 Production Efficiency Optimization

The basic objective of PF is to optimize economic returns across a field. There is a need to adopt the differential management approach to get optimum production at each site or within each "zone." The identification of variability in yield potential is a prerequisite of PF, assuming a uniform yield potential of the field (Nabi et al. 2017). MZs are used in PF to divide field regions which differ in their requirements for farm inputs (Mulla 1991, 1993; Mulla and Miao 2016). The response of fertilizer, irrigation, or pesticides can be delineated based on variations in crop yield, soil type, topography, and soil properties (moisture content, pH, organic matter, etc.). RS has been used to delineate MZs based on variations in soil organic matter (SOM) content (Mulla 1997; Fleming et al. 2004; Christy 2008). Boydell and McBratney (2002) used 11 years of Landsat Thematic Mapper imagery for a cotton field to identify MZs based on yield stability.

2.1.2.3 Optimizing Product Quality

Optimization of product quality is another important concern for PF. This can be achieved through sensors that detect the quality attributes of the crop and thus inputs are to be applied accordingly (Hakkim et al. 2016). If quality premiums exist in production systems, they may alter the quantity of input required to get optimum profitability and agronomic response (Pierce and Nowak 1999; Gebbers and Adamchuk 2010; Whelan and Taylor 2013; Nabi et al. 2017).

2.1.2.4 Efficient Use of Farm Inputs

PF involves efficient use of farm inputs, that is, fertilizer, chemicals, seeds, etc., according to the yield potential of the soil and judicious use of site-specific variable rate application (VRA) of these agrochemicals (i.e. herbicides, insecticides) where the problem appears (Nabi et al. 2017).

2.1.2.5 Soil Conservation, Water, Energy Surface, and Groundwater Protection

A comprehensive approach to PF begins from crop planning and thus includes such tillage practices that conserve the soil or disturb the soil to its minimum. Besides, water is efficiently applied through techniques like drip irrigation, etc. In all these cases, very less energy is used and thus PA leads to conservation of energy too (Nabi et al. 2017). PF aims at safeguarding the environment by way of efficient use of inputs like chemical fertilizers, etc. This prevents their leaching through groundwater or as runoff through surface water.

2.1.2.6 Minimizing Environmental Impact

In PF, farmers follow precise management practices which may reduce the environmental risk associated with uniform/blanket field treatments (Whelan and Taylor 2013). A better management decisions lead to judicious use of inputs to optimize production needs, resulting decrease in the net loss of any inputs to the environment. Though there may be possibilities of potential unintentional damages to the environment associated with the production system. However, such damage risk can be minimized through adoption of such a hi-tech method (Pierce and Nowak 1999; Gebbers and Adamchuk 2010; Nabi et al. 2017).

2.1.2.7 Minimizing Risk

Most of the farmers considered risk management from two contrasting points of view – assured income and environmental impact. Farmers frequently practice risk management by committing an error by applying extra low-cost inputs (Whelan and Taylor 2013). To ensure that the produce is harvested/sold on time and to get guaranteed assured returns, farmers often follow the practice of extra spraying of chemicals, extra fertilizer addition, buying more machinery, or hiring extra labor. PF attempts to offer a risk management solution that may allow both income and environment parameters to be considered. Thus, improved management strategy depends on a better understanding of the soil–plant–animal–environment interaction and more detailed use of emerging and existing information technologies (Pierce and Nowak 1999; Whelan and Taylor 2013; Nabi et al. 2017).

2.1.3 Components of Precision Farming

2.1.3.1 Remote Sensing Technique

The science that makes inferences about material object from measurement made at distance without coming into physical contact with the object under study is called RS. RS comprises sensors to collect the reflected radiation from the object and a platform such as an aircraft, balloon, rockets, satellite, or even a ground-based sensor-supporting stand onto which the sensors could be attached. Various aircraft and spacecraft imaging systems along with RS sensors are used nowadays. Indian Remote Sensing Satellites (IRSS), French National Earth Observation Satellite (i.e., SPOT), IKONOS, etc. are some of the recent notable imaging system used in spacecraft platforms. RS is a promising technology for PA as it effectively monitors spatial variability overtime at high resolution (Moran et al. 1997). Various researchers have reported the usefulness of RS technology to obtain spatially and temporally variable information in PF (Hanson et al. 1995; Moran et al. 1997). Moran et al. (1997) summarized the various application of RS as a source of various

types of information for PF. However, there are several limitations found in using RS data for mapping. The major limitations are calibration of the instrument, atmospheric correction, and normalization of off-nadir effects on optical data. However, during the monsoon period, cloud screening for data and image processing from various airborne video and digital cameras also create a disadvantage of optical RS (Moran et al. 1997).

A relatively cheap, available and marketable RS technology for PA is the need of the hour in developing countries. Some of the pertinent requirements are as follows:

- Turnaround time should be low (24–48 h).
- Data cost should be less (~100 INR/acre/season).
- Spatial resolution should be high (minimum 2 m multispectral).
- Spectral resolution should be high (<25 nm).
- Temporal resolution should be high (minimum 5–6 data per season).

However, the delivery of analytical products in a simpler format may creat interest among the users to purchase it in developing countiries (Ray et al. 2010; Sahoo 2011).

2.1.3.2 Geographic Information System

GIS could be referred to as a computerized data storage and retrieval system that could be used for managing and analyzing spatial data. GIS presents analyzed information in the form of maps that provides a better understanding of various crop growth factors and soil fertility, pests, weeds, and other factors determining yield. GIS map is useful for decision-making based on spatial relationship. Several GIS software with various functionality and price are available nowadays. Many farm information systems (FIS) are available where simple programs are used to produce a farm-level database. Local Resources Information System (LORIS) is one of such FIS. LORIS includes many modules capable of importing data, generating raster files through different gridding methods, storing raster data in a database, generating digital agro-resource maps, creating operational maps, etc. (Schroder et al. 1997).

A comprehensive farm GIS contains base maps of topography, soil types, and properties, etc. Information and data on yield, crop rotation, tillage, chemicals, fertilizers, etc. could be stored in the system for obtaining useful information. Thus, GIS could be useful for preparing the fertility and weed and pest intensity maps based on which further recommendations of application rates of inputs could be inferred.

2.1.3.3 Global Positioning System

GPS could be referred to as a satellite-based navigation system capable of locating any positions on the Earth. Real-time, three-dimensional data regarding positions,

navigation, and timing could be obtained through GPS continuously (24 h/day). The development of GPS was primarily made for military applications, but it was made available for civilian use since the 1980s. No charges for subscription or setup are needed for using GPS. The system can be accessed with a GPS by anyone and can be used in any application that requires location coordinates. The public availability of the global positioning system (GPS) has opened many new avenues for spatial data analyses.

Nowadays farmers access the GPS to perform site-specific activities. In GPS, several satellites are involved in the identification of the actual position of farm equipment within the field. When detection is done in single receiver mode (autonomous navigation), the accuracy of the GPS could be degraded due to various errors. In PA, where a higher degree of accuracy is needed, the operation of the GPS has to be done in a differentially corrected positioning mode, for instance by Differential Global Positioning System (DGPS). DGPS is mostly used for yield mapping and VRA in PA. GPS plays a significant role to determine the precise location in the field for the study of spatial variability as well as for site-specific input applications. The positional accuracy of the GPS is around 20 m with location accuracy of 1 m and submeter could also be obtained by using DGPS. The availability of GPS approaches to the farming system will make all field-based variables to be integrated. The integration among field variables such as the intensity of weeds, soil moisture content, yield, and RS data could be achieved by the use of GPS more specifically by the use of DGPS.

2.1.3.4 Variable Rate Techniques

Variable Rate Technique is an equipment which is capable of altering the rate of application of fertilizers, seeds, irrigation, chemicals, etc. according to the site- and soil-specific requirement across the field. Adjustments in pesticides, herbicides, nutrients, lime, and even seeding rates could be done according to the status or problems of soils and the areas (Adamchuck and Mulliken 2005). VRT consists of a variable rate control system having application equipment that performs a site-specific application of inputs at the precise time. Management practices commonly used in PF include variable-rate fertilizer (Diacono et al. 2013) or pesticide application, variable rate seeding or tillage, and variable rate irrigation. Sylvester-Bradley et al. (1999) reported that VRT is best fitted where prior knowledge of identified large heterogeneity and predicted treatment zone is available. Besides, the lack of appropriate sensor is the major problem (Goulding 2002). Murrell (2004) observed that the application of variable N rates enhanced N use efficiency (NUE) over fixed rates, but did not respond to increase in yield. Farmers are more likely to accept those practices that increase yields as well as NUE (Murrell 2004; Olesen et al. 2004; Goulding et al. 2008).

2.1.3.4.1 Components of VRT

The VRT is consist of many technical components (Fig. 2.2). The basic component of a typical map-based variable rate system is a cab-computer of controller equipped with application software, an actuator that works according to the direction of computer and controls the input rates, and a DGPS receiver that helps in geo-referencing by providing the information about the position of the vehicle or cab. After receiving the positional information through DGPS, the computer sets the required application rate as a function of vehicle position by harmonizing with other preexisting information and then sends a setpoint signal to the controller that regulates the desired rate of application. Actual application rates for GPS position could also be recorded by a VRT (Sökefeld 2010), which could be stored as a record and could be reviewed further for future recommendation.

2.1.3.4.2 Variable Rate Application Methods

Variable Rate Application (VRA) methods could be classified into two groups based on the use of GPS system in it or not. The two methods are map-based VRA and sensor-based VRA (Table 2.1).

2.1.3.4.3 Map-Based VRA

This VRA method uses a GPS receiver and an electronic map or prescription map to control the rate of application. An electronic map, also known as a prescription map, is an electronic data file containing all important and specific information regarding the input rates required for a particular field or condition. With the movement of the applicator across the field (using the field position from GPS receiver), the input concentration changes by matching with the desired rate preset of the particular positions in the prescription map (by harmonizing the positions obtained from DGPS receiver). Map-based VRA also uses map-based previous measurements that are then implemented by employing several strategies which are based on crops, soils, and location-specific information like yield of crops, topography, soil properties, RS datasets, and others (Grisso et al. 2011).

2.1.3.4.4 Sensor-Based VRA

GPS or prescription maps are not used in this method. In this case, soil properties and crop characteristics are assessed by the sensors attached to applicators and the report

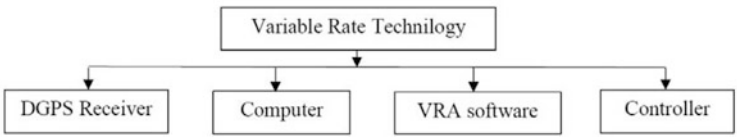

Fig. 2.2 Basic components of variable rate technology (VRT)

Table 2.1 Comparisons between map- and sensor-based VRA

S. No.	Parameter	VRA (map based)	VRA (sensor based)
1	Brief method of approach	Grid sampling followed by lab analysis and generation of site-specific maps. Finally the use of VRA	Field information based on real-time sensor, feedback control measures, and finally the use of VRA
2	Requirement of DGPS/GPS	Important	Not so important
3	Soil and plant sample analysis in laboratory	Required	Not required
4	Mapping	Important	Not necessary
5	Requirement of time	More	Less
6	Constraints	Cost of soil sampling and analysis	Lack of appropriate sensors to obtain soil- and plant-related data
7	Operation procedure	Difficult	Easy
8	Operation skills	Required	Required
9	Sampling size	2–3 acres	Individual spot
10	Acceptance among the farmers	It is popular in developing countries	It is popular in developed countries

Modified, Patil and Shanwad (2009)

is then transferred to the control system where calculations of input rates are made. The control system then relays the computed information of input rate to the controller, based on which the final inputs are done to the specific site. One of the notable advantages of sensor-based VRA is the use of real-time data using real-time sensors instead of previously collected data in map-based VRA.

2.2 Usefulness of Remote Sensing Data in Precision Farming

Applications of RS knowledge in the agricultural field have attracted a variety of endeavors (Moran et al. 1997; Mani 2000; Pinter et al. 2003; Adamchuk et al. 2004; Andreo 2013). The major endeavors are monitoring and mapping of soil properties like organic matter and clay content, moisture percentage, pH and salinity level (Corwin and Lesch 2003; Christy 2008; DeTar et al. 2008; Gomez et al. 2008); crop yield and biomass study of canola, corn, cotton, sorghum, and wheat (Lelong et al. 1998; Yang et al. 2000, 2001; Shanahan et al. 2001; Seelan et al. 2003; Warren and Metternicht 2005; Zhao et al. 2007); crop species classification (Rao 2008); crop nutrient and water stress (Lelong et al. 1998; Erickson et al. 2004; Clay et al. 2006;

Moller et al. 2007; Tilling et al. 2007); infestations of weeds and their monitoring (Lamb and Brown 2001; Thorp and Tian 2004; Scotford and Miller 2005; Gutierrez et al. 2008); and plant diseases and infestation of insects (Seelan et al. 2003).

2.3 Satellite Remote Sensing in Precision Farming

Since the early 1970s literature reveals that satellites have been successfully utilized for RS imagery in the field of agriculture (Bauer and Cipra 1973; Doraiswamy et al. 2003; Jewel 1989; Mulla 2013) (Table 2.2). Identification and inventorization of

Table 2.2 List of satellites and their suitability in precision agriculture

Satellite (year)	Spectral bands with spatial resolution	Return frequency (d)	Suitability in precision agriculture
LiDAR (1995)	VIS (vertical RMSE 10 cm)	N/A	High
Radar SAT (1995)	C-band radar (30 m)	1–6	Medium
IKONOS (1999)	Panchromatic, B, G, R, NIR (1–4 m)	3	High
Landsat 7 ETM + (1999)	B, G, R, NIR, 2 SWIR, Panchromatic, TIR (15, 30, 60 m)	16	Medium
SRTM (2000)	C/X-band radar (30 m)	N/A	Medium
Terra EOS ASTER (2000)	G, R, NIR and 6 MIR, 5 TIR bands (15–90 m)	16	Medium
EO-1 Hyperion (2000)	400–2500 nm, 10 nm bandwidth (30 m)	16	High
Rapid Eye (2008)	B, G, R, red edge, NIR (6.5 m)	5.5	High
World View-2 (2009)	P (0.5 m), B, G, Y, R, red edge, NIR (1.84 m)	1.1	High
Cartosat 1 and Cartosat 2, Cartosat 2A (2005, 2007, 2009)	Panchromatic (0.5–0.85 μm) Cartosat 1: 2.5 Cartosat 2, 2A: 0.8 m	5	High
Landsat 8 OLI (2013)	B, G, R, NIR, 2 SWIR (30 m), Panchromatic (15 m), 2 TIR (100 m)	16	Medium
SPOT 6 and 7 (2012 and 2014)	Panchromatic (1.5 m), B, G, R, NIR (6.0 m)	1–4	High
Resourcesat 2 and 2A (2011 and 2016)	AWiFS (56 m), LISS-III (23.5 m), LISS-IV (5.6 m), B, G, R, NIR, MIR	2–3, 12–13, 25–26	High
KOMPSAT 3 and 3A (2012 and 2015)	Panchromatic, B, G, R, NIR, MWIR (KOMPSAT 3A: 0.55 and KOMPSAT 3:0.70 m)	1.4	High
Sentinel 2A and 2B (2015 and 2017)	B, G, R (10 m), 3 red edge (20 m), 2 NIR (10, 20 m), 3 SWIR (20 and 60 m)	5	High

P = purple, B = blue, G = green, R = red, IR = infrared, NIR = near infrared, MIR = mid infrared, TIR = thermal infrared. Suitability classes L, M and H refer to low, medium and high respectively

crops could be done with Landsat MSS and Thematic Mapper (TM) data within certain limits (Morain and Williams 1975; Hanuschak et al. 1980; Ryerson et al. 1985; Ehrlich et al. 1990; Oetter et al. 2000; Blaes et al. 2005), SPOT imagery (Buttner and Csillag 1989; Hanna et al. 2004; Xavier et al. 2005), and Indian Remote Sensing (IRS) satellite data (Dutta et al. 1994; Panigrahy and Sharma 1997). Satellite RS has created huge availability of remotely sensed data for research and various applications (Liu 2015; Chi et al. 2016). Their use was generally observed in large-scale classifications of crops (Bauer and Cipra 1973; Jewel 1989; Panigrahy and Sharma 1997), monitoring of impacts on tillage (Casady and Palm 2002), as well as to understand the effect of environmental factors like infestation and outbreaks of diseases (Yang et al. 2005). The measurement of reflectance from the surface soils with the help of Landsat TM data is a significantly efficient and accurate method for topsoil organic carbon (SOC) content estimation (Baumgardner et al. 1985; Henderson et al. 1989; Frazier 1989; Huang et al. 2007; Jaber and Al-Qinna 2011; Yang et al. 2015). Based on Landsat imagery of bare soil, initiation of use of RS data in PA was made to understand and study the spatial patterns of soil organic matter (SOM) content (Bhatti et al. 1991a; Frazier and Jarvis 1990; Wilcox et al. 1994). Mulla (1997) also reported the use of Landsat imagery data as auxiliary data coupled with ground truth information for assessing the spatial patterns of soil phosphorus as well as grain yield of wheat.

Satellite imaging systems with the fine spatial resolution with revisit cycles of a very short period are generally used in researches regarding PA (Table 2.2) (Mulla 2013). Images with high spatial resolution provide provisions of identification and area estimation of crops more accurately over the traditional practice. Attempts of preparing maps of SOC contents using satellite multispectral imagery have been made using 4-m IKONOS (Sullivan et al. 2005), and 10 and 20 m SPOT (Campbell 1996; Vaudour et al. 2013). In the past few years, the data of IKONOS and Quick Bird data have been used for several applications (Mumby and Edwards 2002; Sawaya et al. 2003; Wang et al. 2004). Notable operations including assessment of nitrogen (N) deficiency in sugar beet, the efficiency of fungicides in wheat, etc. have been made using IKONOS through spectral information of visible and near-infrared bands (Seelan et al. 2003). Bausch and Khosla (2010) estimated values of normalized green normalized difference vegetation index (NGNDVI) (Gitelson et al. 1996a, b) in irrigated maize from Quick Bird data which strongly correlates with spatial patterns in N sufficiency. Quick Bird images (spatial resolution of 2.4 m) were also found to be effective for determining olive plantation area, numbers of trees, spatial patterns of tree canopies in concerned area and yields of olive (García Torres et al. 2008; Castillejo-González 2018). Further, improvement in the processing capability was noted as a result of the incorporation of additional spectral information like the use of red-edge spectral wavelength (obtained from WorldView-2) in PA. Performance of simulated WorldView-2 red-edge-based spectral indices were used by Li et al. (2014) to assess concentration and uptake of N in summer maize (*Zea mays L*). Enhanced availability of high-resolution optical satellite data opens the avenues of new opportunities in PF through crop mapping

and assessment (Turker and Ozdarici 2011; Yang et al. 2011; Drusch et al. 2012; Hornacek et al. 2012; Li et al. 2013; Esch et al. 2014; Qiu et al. 2014).

Several trends could be noted on the uses of satellite-based RS data (Table 2.2). First, the improvement is observed on spatial resolution from 80 m (Landsa) to submeter in GeoEye and WorldView (Mulla 2013). Secondly, the improvement on the frequency of revisit is noticed in WorldView as compared to Landsat which took 18 days. Third, an increase in number of spectral bands, that is, eight or more (bandwidths >40 nm) in WorldView from four in case of Landsat (bandwidths >60 nm) is observed. The introduction of hyperspectral sensors such as Hyperion has provided further superior spectral resolution, (400–2500 nm with interval of 10 nm). With the betterment of spectral and spatial resolution of satellite datasets, the use of reflectance data from these platforms has become more effective and reliable in PA (Table 2.2).

The suitability of various spectral and spatial images in case of PA depends on several factors like crop management practices, the capacity of farm equipment, variation in farm inputs, farm unit area, and water resources, etc. (Olson 1998; Al-Kufaishi et al. 2006; Lindblom et al. 2017; Friedl 2018; Neupane and Guo 2019). Improved spatial and spectral resolutions (1–3 m) are useful for estimating spatial patterns of crop biomass or yield than computing variable rate of fertilization (5–10 m). Accuracy of VRA of fertilizers is often limited by delay times of fertilizer spreader (Chan et al. 2004). Improved spatial and spectral resolutions (0.5–1 m) are generally useful in case of variable rate spraying of herbicides for spot weed control as compared to variable rate irrigation (5–10 m) (Chan et al. 2004). In developing countries mostly financially strong larger commercial farms are able to obtain higher spatial and spectral resolution RS datasets compared to smaller farms (Mulla 2013).

Normalized Difference Vegetation Index (NDVI)–based estimation of spatial patterns in crop biomass (Yang et al. 2000) and potential crop yield (Doraiswamy et al. 2003) is becoming familiar in PA. NDVI is calculated based on the ratios in the red and NIR portion of spectrum (Rouse et al. 1973) using the formula $NDVI = (NIR - Red)/(NIR + Red)$. It ranges from 0 to 1 as normalization processes are used to calculate the index. NDVI exhibits a sensitive response toward green vegetation even for areas with low vegetation covers (Xue and Su 2017). Hence, use of this index is often observed in the assessment of regional and global vegetation. NDVI shows a significant relation not only with the canopy structure and LAI but also with canopy photosynthesis (Gamon et al. 1995; Grace et al. 2007). Despite being used widely, various limitations are associated with NDVI (Thenkabail et al. 2010). Introduction of yield monitors capable to provide measurements of yield in finer-scale resolution across large spatial areas could augment the capacity of RS in the prediction of structural characteristics of crop, namely, LAI, biomass, and yield (Karnieli et al. 2010; Sripada et al. 2005; Zhang et al. 2012). However, calibration in RS is another important step as factors such as soil brightness, soil color, atmosphere, cloud, cloud shadow, and leaf canopy shadow could affect the values of NDVI (Xue and Su 2017).

Apart from NDVI, several broadband spectral indices (Table 2.3) have used in PA (Sripada et al. 2006, 2008; Miao et al. 2009). The normalized red (NR) index is

Table 2.3 Use of different multispectral, broadband vegetation indices in precision agriculture

Index	Definition	References
NG	G/(NIR + R + G)	Sripada et al. (2005)
NR	R/(NIR + R + G)	Sripada et al. (2005)
GRVI	NIR/G	Sripada et al. (2005)
GSAVI	1.5 × [(NIR − G)/(NIR + G + 0.5)]	Sripada et al. (2005)
GOSAVI	(NIR − G)/(NIR + G + 0.16)	Sripada et al. (2005)
NDRE	$(R_{790} - R_{720})/(R_{790} + R_{720})$	Barnes et al. (2000)
WDVI	NIR − (C.red)	Clevers (1997)
GNDVI	(NIR − G)/(NIR + G)	Gitelson et al. (1996a, b)
OSAVI	(NIR − R)/(NIR + R + 0.16)	Rondeaux et al. (1996)
ARVI	(NIR − RB)/(NIR + RB)	Kaufman and Tanre (1992)
MSAVI2	0.5 × [2 × (NIR + 1) − SQRT((2 × NIR + 1)^2– 8 × (NIR − R))]	Qi et al. (1994)
SAVI	1.5 × [(NIR − R)/(NIR + R + 0.5)]	Huete (1988)
DVI	NIR − R	Tucker (1979)
GDVI	NIR − G	Tucker (1979)
PVI	$SQRT((\rho_{soil}-\rho_{veg})^2_R-(\rho_{soil}-\rho_{veg})^2_{NIR})$	Richardson and Weigand (1977)
NDVI	(NIR − R)/(NIR + R)	Rouse et al. (1973)
RVI	NIR/R	Jordan (1969)

Modified, Mulla (2013)
G = green reflectance, NIR = near infrared, and R = red reflectance, RB = difference between Blue and Red channel, C = ratio between NIR and red reflectance of soil

generally concerned with the portion of the spectrum where chlorophyll strongly absorbs radiation. Contrarily, the normalized green (NG) index is associated with the portion of the spectrum where absorption of radiation occurs through pigments other than chlorophyll. Ratio vegetation index (RVI) is the ratio of NIR to red reflectance (Jordan 1969) whereas the green–red vegetation index (GRVI) (Tucker 1979) is the ratio of NIR to green reflectance. There are two types of NDVI, one usually deals with NIR and R reflectance while the other is green normalized difference vegetation index (GNDVI), which deals with NIR and G reflectance (Gitelson et al. 1996a, b). The difference between reflectance in the NIR and R bands is generally considered to compensate for the effects of soil reflectance to formulate difference vegetation index (DVI) (Tucker 1979). Better performance of these indices was noted than NIR and R ratio indices such as NDVI and RVI where compensation of soil effects is not considered. According to Sripada et al. (2006), green difference vegetation index (GDVI) (NIR-G) exhibited a better correlation with an economically optimum N rate in corn than DVI (NIR-R). The main function of vegetation indices, other than NDVI, is a compensation of the effects factors like soil background and atmospheric conditions that hamper the vegetation spectral reflectance of crop characteristics such as type of crops, leaf area index (LAI), or canopy biomass (Bouman 1995). Exclusion of diminution of the effect of soil brightness (as the pixels in the image is a

combination of vegetation and soil information) could be done by using distance-based vegetation indices in cases where vegetation is sparse (Huete and Jackson 1988). Perpendicular vegetation index (PVI) (Richardson and Weigand 1977) and SAVI are notable distance-based vegetation indices in recent days (Thiam and Eastmen 1999). Many other indices have also been reported that are capable to compensate the undesirable soil effects which include soil-adjusted vegetation index (SAVI) (Huete 1988), modified soil-adjusted vegetation index (MSAVI) (Qi et al. 1994), optimized soil-adjusted vegetation index (OSAVI) (Rondeaux et al. 1996), green soil-adjusted vegetation index (GSAVI, Sripada et al. 2005), green optimized soil-adjusted vegetation index (GOSAVI), etc. On the other hand, the atmospherically resistant vegetation index (ARVI) is another type of index capable of considering atmospheric effect (Kaufman and Tanre 1992).

Major challenges regarding the use of satellite RS in PA were summarized by Moran et al. (1997) and Yao et al. (2010), and according to them RS images in the visible and NIR bands are restricted to cloud-free days when irradiance is relatively consistent across time. Cloud cover could not affect only the radar imagery obtained from satellites or airplanes. Calibration of raw digital numbers to true surface reflectance, atmospheric corrections, geo-rectification of data by GPS-based ground control locations are other notable challenges regarding this.

2.3.1 Satellite-Based Rice Monitoring (SRM) – A Case Study

The combined knowledge of integrated RS, crop modeling, and ICT tools in the satellite-based rice monitoring (SRM) system (Fig. 2.3) is useful for the effective dissemination of near-real-time and accurate information of growth and yield of rice. Information regarding abiotic and biotic stresses under rice cultivation may be generated which will be useful for end-users. Remote Sensing–Based Information and Insurance for Crops in Emerging Economies (RIICE) technology is capable of providing timely and accurate is capable of providing information about rice-planted areas at village level. This information is about the start of the season and its variability with geography, expected and actual yield, and the impact of any disaster on specific rice-growing areas. The use of precise and real-time information obtained from RIICE in the implementation of crop insurance programs has become a trend in several countries (i.e., the Republic of India and the Socialist Republic of Vietnam). In rice cultivation, for monitoring, mapping, and forecasting purposes such projects have already shown significant success. A combination of RS, crop modeling, web geographic information system (GIS), smartphone, unmanned aerial vehicles (UAV), and Amazon Web Services (AWS) made such systems promising in various countries. In 2016, over 24.5 million hectares of land under rice cultivation have been monitored through these integrated systems with more than 85% accuracy while the coverage area was only 1.6 million ha in the initial stages in 2012 (Sylvester 2018).

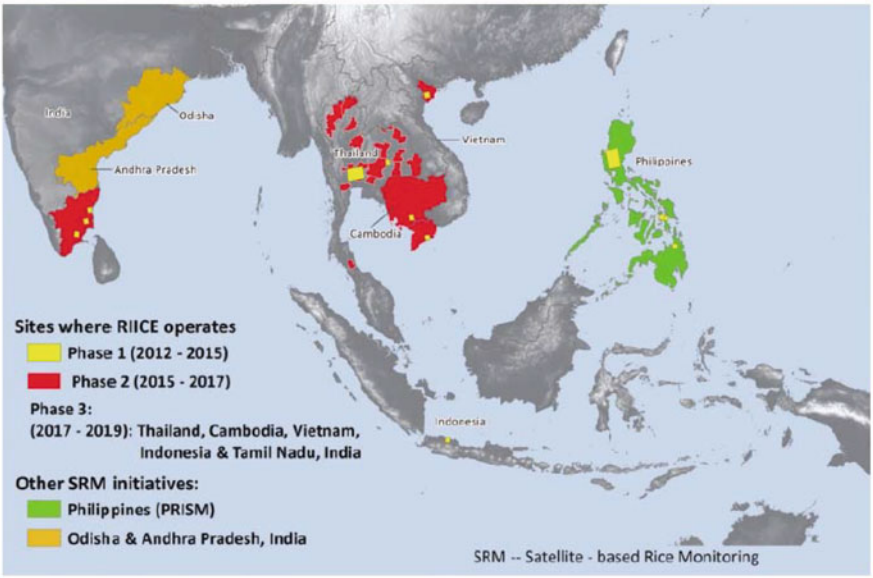

Fig. 2.3 Satellite-based rice monitoring (SRM) sites in South Asia and Southeast Asia. (Adopted, Sylvester (2018)

2.3.2 Proximal Remote Sensing of Crops in Precision Farming

To overcome the constraints of satellite-based RS, modern world is emphasizing on the use of proximal RS techniques in PA to assess the growth and stress of crops. Proximal RS is also an integrated system having components like sensors mounted on tractors, spreaders, sprayers, or irrigation booms which combinedly could monitor and conduct the real-time site-specific management of fertilizers, pesticides, or irrigation (Hummel et al. 1996). Schepers et al. (1992) were the pioneers of assessment of crop status through proximal sensing over RS where they had used a Minolta soil plant analysis development (SPAD) meter for determining chlorophyll contents of maize at silking stage under a range of N treatments by measuring leaf greenness. After that, a significant number of sensors and spectral indexes were invented for monitoring various crop properties (Table 2.4) associated with N stress in plants and to set the basis for VRT.

Unavailability of direct estimation of the amount of N fertilizer needed to overcome crop N stress is a notable constraint of the chlorophyll meter, Green Seeker, Yara N, and Crop Circle sensors (Samborski et al. 2009). To overcome this drawback, comparisons of sensor readings with reference strips values of crops receiving sufficient N fertilizer were made by scientists (Blackmer and Schepers 1995; Kitchen et al. 2010; Raun et al. 2002; Sripada et al. 2008). These data were used to develop N fertilizer response functions related to sensor readings to

Table 2.4 Developments in remote and proximal leaf sensing in precision agriculture

Year	Innovation	References
1992	SPAD meter (650, 940 nm) used to detect N deficiency in corn	Schepers et al. (1992)
1995	Nitrogen sufficiency indices	Blackmer and Schepers (1995)
1996	Optical sensor (671, 780 nm) used for on-the-go detection of variability in plant nitrogen stress	Stone et al. (1996)
2002	Yara N sensor	Link et al. (2002)
2002	Green Seeker (650, 770 nm)	Raun et al. (2002)
2002	CASI hyperspectral sensor–based index measurements of chlorophyll	Haboudane et al. (2002, 2004)
2002	MSS remote sensing of agriculture fields with UAV	Herwitz et al. (2004)
2003	Fluorescence sensing for N deficiencies	Apostol et al. (2003)
2004	Crop Circle (590, 880 nm or 670, 730, 780 nm)	Holland et al. (2004)
2004	LASSIE (Real-time images of crop and soil surfaces)	Lilienthal et al. (2004)
2005	Cropscan2000H – grain quality sensor	Long et al. (2005)
2006	Field Spec (325–1075 nm)	Rodriguez et al. (2006)
2010	CropSpec – Crop Canopy Sensor (735, 808 nm)	Reusch et al. (2010) Topcon.
2010	The Multiplex – fluorescence-based optical sensor	Ghozlen et al. (2010) FORCE-A, Orsay, France
2011	OptRx (670, 730, 780 nm)	Sudduth et al. (2011) AgLeader
2013	HandySpec (360–900 nm or 400–1100 nm)	Weis et al. (2013) HandySpec Field, Tec5, Oberursel, Germany
2013	Weedseeker – automatic spot spray system	Weis et al. (2013) N-Tech, Trimble
2014	ISARIA – real-time VR nitrogen sensor (670, 700, 740, 780 nm)	Haas (2014) Fritzmeier Umwelttechnik
2017	See and Spray – smart spraying by artificial intelligence	Chostner (2017) Blue River Technology, USA
2019	H-sensor artificial intelligence (deep and transfer learning)	Partel et al. (2019) Agricon GmbH, Germany

recommend the required amount of N fertilizer to mitigate N stress in crops (Scharf et al. 2011). Further experiments are still needed in this regard for getting superior crops, site, and climate-specific responses.

2.3.3 Hyperspectral Remote Sensing in Precision Farming

Hyperspectral imaging is widely known as imaging spectroscopy. According to Goetz et al. (1985), hyperspectral remote sensing (HRS) could be classically defined as "The acquisition of images in hundreds of continuous registered spectral bands

such that for each pixel a radiant spectrum can be derived." Rather than the number of bands available in the image, the narrow and continuous wavelength nature makes it hyperspectral (Shippert 2004; Mohan and Porwal 2015). Reflectance data over a wide spectral range are generally collected at small spectral increments (typically 10 nm) in HRS (Goetz et al. 1985). Pointing out of the particular frequency is the crucial function in this technique with more number of bands to reduce the redundancy (Bandyopadhyay et al. 2017), which improves the capability to assess the spectral response of soils and vegetated surfaces in a more precise way. This opens the avenue of a detailed insight regarding the spatial and spectral variability of bare as well as vegetated surfaces (Mulla 2013).

National Aeronautics and Space Administration (NASA) launched the airborne visible/infrared imaging spectrometer (AVIRIS) in 1987, which was the first hyperspectral sensor (Goetz 1987; Tan 2017) and it was able to provide continuous imagery from 380 to 2500 in bands with a spectral resolution of 10 nm and spatial resolution of 20 m. AVIRIS became highly successful along the time, and in a majority of hyperspectral analyses it is the principal source of data nowadays (Vorovencii 2009) . In 2000, NASA launched a satellite-based Hyperion sensor (spectral coverage 0.40–2.50 μm), EO-1 for capturing hyperspectral images from space mainly with the primary issue of mineralogical mapping (Kruse 2003). However, these hyperspectral datasets are also very useful for crop- and soil-related studies. Datt et al. (2003) reported that hyperspectral data obtained from Advanced Land Imager (ALI) predicted spatial patterns in case of rice yield more precisely with the help of derivative indexes and red-edge position as compared to the predictions made by NDVI. Wu et al. (2010) in China observed that chlorophyll content in the canopy and leaf area index could be measured in a nondestructive way for a considerable range of crops by using vegetative indexes formulated based upon red-edge reflectance data collected by hyperspectral ALI. Again, for assessing the green leaf area index, the Compact Airborne Spectrographic Imager (CASI), an aerial hyperspectral imaging system has also been used (Haboudane et al. 2002, 2004). Some handheld, boom-mounted, hyperspectral, and multispectral imaging systems are also there in this regard, for example, The Crop Scan sensor (CROPSCAN Inc., Rochester, MN, USA) (Andreo 2013).

Continuity, range, and spectral resolution of bands are the main factors that make differences between hyperspectral and multispectral imaging. A number of plant and soil parameter such as chlorophyll, cellulose, LAI, carotenoids, crop biomass, soil moisture, soil nutrient, and organic matter can be sensed using hyperspectral data (Haboudane et al. 2002; Goel et al. 2003; Oppelt and Mauser 2004; Zarco-Tejada et al. 2004). A specific wavelength is most sensitive to a particular soil or crop parameters. The crop LAI and biomass can be retrieve with a red band centered at 687 nm, whereas crop moisture content can be assessed with a NIR band centered at 970 nm (Thenkabail et al. 2010). Thenkabail et al. (2010) reported linkages of 33 more hyperspectral reflectance bands with certain characteristics of soils and crops. Contrarily, there are limitations in the case of multispectral imaging which could analyze based on single broadband combinations. Hence it is insensitive to measure chlorophyll and others plant attributes at LAI values exceeding 3.0

(Thenkabail et al. 2000). Another problem of this constraint is the interference of the reflectance of bare soil at lower LAI values. According to Thenkabail et al. (2000), three general categories of predictive spectral indices could be formulated using hyperspectral data: (1) optimal multiple narrow-band reflectance indexes (OMNBR), (2) narrow band NDVI, and (3) SAVI. The requirement of narrow bands is only two to four in case of OMNBR to depict plant characteristics. However, the most important information regarding plant parameters can be obtaining from shorter green wavelength (500–550 nm), longer red wavelength (650–700 nm), red-edge (720 nm), and two NIR (900–940 and 982 nm), spectral bands. This band-based information is only available in narrow increments of 10–20 nm and cannot be sensed in broad multispectral bands that are associated with older satellite imaging systems. Improved statistical methods like partial least squares (PLS) (Viscarra Rossel et al. 2006) and principal components analysis (PCA) (Geladi 2003) were found useful for chemometric analysis of hyperspectral data. Besides, pattern recognition and classification such as object-based (Frohn et al. 2009) decision tree (Wright and Gallant 2007) approaches are also useful. A range of narrowband hyperspectral indexes (Table 2.5) have been used in PA (Haboudane et al. 2002, 2004; Li et al. 2010; Miao et al. 2007, 2009). Similar forms as broadband spectral indices have also observed among many of these but they vary in terms of reflectance bands for hyperspectral indices that are narrower. Such indices exhibited effective responses to the canopy or leaf attributes such as LAI, chlorophyll, specific pigments, or nitrogen stress etc. Along with the existing indices, continuous assessments and innovations are also being made for the development of new hyperspectral indices (Li et al. 2010; Thenkabail et al. 2011).

Several researchers (Yao et al. 2010; Thenkabail et al. 2011) studied promising applications of HRS in PA. These applications include a diverse range of crops and their biophysical and biochemical variables, such as yield (Wang et al. 2008), chlorophyll a and b (Zhu et al. 2007; Delegido et al. 2010), total chlorophyll (Haboudane et al. 2004), nitrogen content (Rao et al. 2007), carotenoid pigments (Blackburn 1998), plant stress (Zhao et al. 2007), plant moisture (Penuelas et al. 1995), aboveground biomass (Thenkabail et al. 2004a, b), and biophysical variables (Darvishzadeh et al. 2008; Thenkabail et al. 1994a, b; Alchanatis and Cohen 2010).

Application of HRS for variable-rate techniques, particularly nitrogen fertilization depending on spatial patterns in chlorophyll content, could be considered as its most concerning use in PF. As, in China, the performance of the MCARI/OSAVI705 index has been proved significantly superior over all other vegetation indexes in terms of chlorophyll content assessment of a diverse range of agricultural canopy types (Wu et al. 2010).

2.3.4 Microwave Remote Sensing in Precession Farming

Microwave remote sensing (MRS) can monitor the earth's surface, irrespective of atmospheric conditions and day/night which makes it more effective and useful

Table 2.5 Hyperspectral narrow-band vegetation indices commonly used in precision agriculture

Index	Definition	References
SR5	$R_{675}/(R_{700} \times R_{650})$	Chappelle et al. (1992)
SR2	NIR/green $= R_{800}/R_{550}$	Buschman and Nagel (1993)
DI1	$R_{800} - R_{550}$	Buschman and Nagel (1993)
NDI3	$(R_{734} - R_{747}) /(R_{715} + R_{726})$	Vogelmann et al. (1993)
SR4	R_{740}/R_{720}	Vogelmann et al. (1993)
MSAVI	$0.5[2R_{800} + 1 - SQRT((2R_{800} + 1)2–8(R_{800} - R_{670}))]$	Qi et al. (1994)
SR3	R_{700}/R_{670}	McMurtrey et al. (1994)
Greenness index (G)	R_{554}/R_{677}	Smith et al. (1995)
RDVI	$(R_{800} - R_{670})/SQRT(R_{800} + R_{670})$	Rougean and Breon (1995)
HVI	R_{743}/R_{692}	Gitelson et al. (1996a, b)
MCARI	$[(R_{700} - R_{670}) - 0.2(R_{700} - R_{550})] (R_{700}/R_{670})$	Daughtry et al. (2000)
NDVI	$(R_{800} - R_{680})/(R_{800} + R_{680})$	Lichtenthaler et al. (1996)
NDWI	$(R_{857} - R_{1241})/(R_{857} - R_{1241})$	Gao (1996)
OSAVI	$(1 + 0.16) (R_{800} - R_{670})/(R_{800} + R_{670} + 0.16)$	Rondeaux et al. (1996)
MSR	$(R_{800}/R_{670} - 1) /SQRT(R_{800}/R_{670} + 1)$	Chen (1996)
SR6	$R_{672}/(R_{550} \times R_{708})$	Datt (1998)
SR7	$R860/(R550 \times R708)$	Datt (1998)
NDI1	$(R_{780} - R_{710})/(R_{780} - R_{680})$	Datt (1999)
NDI2	$(R_{850} - R_{710})/(R_{850} - R_{680})$	Datt (1999)
PSSRa	R_{800}/R_{680}	Blackburn (1998)
PSSRb	R_{800}/R_{635}	Blackburn (1998)
RVSI	$0.5(R_{722} + R_{763}) - R_{733}$	Merton and Huntington (1999)
RGRI	R_{red}/R_{green}	Gamon and Surfus (1999)
SR1	NIR/red $= R_{801}/R_{670}$	Daughtry et al. (2000)
Green NDVI (GNDVI)	$(R_{801} - R_{550})/(R_{800} + R_{550})$	Daughtry et al. (2000)
TVI	$0.5 \times [120 \times (R_{750} - R_{550}) - 200 \times (R_{670} - R_{550})]$	Broge and Leblanc (2000)
TCARI	$3 \times [(R_{700} - R_{670}) - 0.2 \times (R_{700} - R_{550}) (R_{700}/R_{670})]$	Haboudane et al. (2002)

(continued)

Table 2.5 (continued)

Index	Definition	References
TCARI/OSAVI	$\frac{3 \times [(R_{700} - R_{670}) - 0.2(R_{700} - R_{550})]\ (R_{700}/R_{670})}{(1 + 0.16)\ (R_{800} - R_{670})/(R_{800} + R_{670} + 0.16)}$	Haboudane et al. (2002)
NDNI	$\left[\frac{\log\ (1/R_{1510} - \log\ (1/R_{1680})]}{[\log\ (1/R_{1510} - \log\ (1/R_{1680})]}\right.$	Serrano et al. (2002)
MCARI/ OSAVI	$\frac{[(R_{700} - R_{670}) - 0.2(R_{700} - R_{550})]\ (R_{700}/R_{670})}{(1 + 0.16)\ (R_{800} - R_{670})/(R_{800} + R_{670} + 0.16)}$	Zarco-Tejada et al. (2004)
MTVI	$1.2 \times [1.2 \times (R_{800} - R_{550}) - 2.5 \times (R_{670} - R_{550})]$	Haboudane et al. (2004)
MCARI2	$\frac{1.5[2.5(R_{800} - R_{670}) - 1.3(R_{800} - R_{550})]}{\sqrt{\left[(2R_{800} + 1)^2 - \left(6R_{800} - 5\sqrt{R_{670}}\right) - 0.5\right]}}$	Haboudane et al. (2004)
NAOC*	$\text{NAOC} = 1 - \frac{\int_a^b \rho d\lambda}{\rho_{\max}(b-a)}$	Delegido et al. (2010)
DCNI	(R720 − R700)/(R700 − R670)/ (R720 − R670 + 0.03)	Chen et al. (2010)

R = reflectance at the wavelength (nm) in subscript. NIR = near-infrared reflectance. *(ρ refers to reflectance, λ the wavelength, $\rho_{\max=}$ maximum far-red reflectance, corresponding to reflectance at the wavelength "b," and "a" and "b" are the integration limits surrounding the chlorophyll well centered at ~670 nm)

(Navalgund et al. 2007). Electromagnetic waves having frequencies between 109 and 1012 Hz are generally considered as microwaves. Radar is an active MRS system (Reddy 2018) in which the terrain is illuminated using electromagnetic energy and the scattered energy returning from the terrain (known as radar return) is detected and recorded as images. In the case of both aircraft- and satellite-based systems, radar return intensity varies with characteristics of terrain and radar systems (Gupta and Jangid 2010). The various sensor parameters such as polarization, incidence angle, etc. (Henderson and Lewis 1998; Sahebi et al. 2002; Gupta and Jangid 2010) and physical parameters such as surface roughness, feature orientation, and electrical (dielectric constant) property of the target (Ulaby et al. 1978; Dobson and Ulaby 1986; Baghdadi et al. 2008; Sahebi and Angles 2010) generally governs the microwave signatures. Terrain properties affect the frequency of radar scattering (Reddy 2018). A given surface will appear very rough at higher frequency compared to a lower frequency. Usually, a rise in the backscattering coefficient occurs with an increase in frequency while the signal penetration depth rises with a rise in wavelength in the microwave region. Multifrequency data are capable of distinguishing types of roughness (Reddy 2018). The polarization of the incident wave also influences the backscattering. The multiple scattering and volume scattering from a complex surface, such as forest, cause depolarization. The radar backscattering coefficient is greatly influenced by the angle of the incident energy. This dependency of the backscattering coefficient toward the angle of the incident is mainly due to surface roughness (Ulaby et al. 1986; Fung 1994).

The soil moisture estimation using MRS is mostly based on the strong dependence of radar backscatter on the dielectric constant of soil. The dielectric constant of

dry soil at microwave frequency is about 3, while it is about 80 for water. The radar backscattering coefficient (σ°) is strongly related to soil moisture due to high dielectric constant of a mixture of soil and water (Wang 1980).

The linear increase in the backscattering coefficient could be observed with the increase in soil moisture content. The development of a significant number of site-specific empirical models has been made based on the relationship between the backscattering coefficient and soil moisture content. The two factors that influence the backscattering coefficient are soil surface moisture and soil roughness (Panciera et al. 2013; Zhao et al. 2016; Huang et al. 2019). Many contradictions are there regarding the effects of soil surface roughness and soil moisture content on the backscattering coefficient where some consider that the effects of soil surface roughness are greater than that of soil moisture content while others consider them the same (Satalino et al. 2002; Rahman et al. 2008).

Several researchers effectively devoted their time in the incorporation of the effect of surface roughness and crop cover using a theoretical approach based on physical models (the integral equation model (IEM) (Fung et al. 1992; Fung 1994; Srivastava et al. 2006) and advanced IEM (AIEM) (Chen et al. 2003; Pettinato et al. 2013; Choker et al. 2017; He et al. 2017). The development of some semiempirical models over bare soils was also reported (Oh 2004; Dubois et al. 1995). The Oh model is dependent upon the ratios of the measured backscatter coefficients HH/VV and HV/VV for estimating volumetric soil moisture (mv) and surface roughness (Hrms). The backscatter coefficients in HH and VV polarizations to the soil's dielectric constant and surface roughness were used in the model proposed by Dubois (Baghdadi et al. 2016). Derivation of soil moisture over vegetated areas could be made by the models used in bare land along with the vegetation scattering models. Water Cloud Model is the most widely used vegetation scattering model (Lievens and Verhoest 2011). The generalization of these empirical models over a wide area results in problems of sensitivity limitation toward other target parameters, including soil texture, surface roughness, and vegetation cover (Bertoldi et al. 2014).

For accomplishing various applications, the aforesaid interaction of microwaves is widely used. Under rice cultivation, a distinctive pattern in backscatter could be noticed throughout the growth stage. This is might be due to the result of interaction between rice canopy structure, canopy water content, soils, and surface with SAR properties such as band, polarization, and incident angle (Le Toan et al. 1997; Chakraborty et al. 2005; McNairn and Shang 2016; Fikriyah et al. 2019). The estimation of rice area is generally made based on the physical basis formed, depending upon the characteristic temporal increase in backscattering coefficient from rice transplanting stage to maximum vegetative stage (Patel et al. 1995; Panigrahy et al. 1997, 2000; Parihar and Oza 2006). Three main mechanisms of scattering that could explain the interactions between SAR and rice canopy structure are (a) direct volume scattering from the rice canopy, (b) surface scattering from the ground, and (c) multiple scattering (double-bounce) from the interaction between the rice canopy and the ground surface (Bouvet and Le Toan 2011; Koppe et al. 2013). Quad-polarization (VH, VV, HH, and HV) data provided by RADARSAT-2 were found potent enough to retrieve parameters regarding rice canopy and to determine

the biomass associated with the crop yield (Wu et al. 2011; Yang et al. 2012). For monitoring the rice phenology, the sensor acts as an ideal data source. The exploitation of the relationships of the backscattering coefficients and their combinations versus the phenology of rice helps to measure HH/VV, VV/VH, and HH/VH ratios, which are effective for monitoring of rice phenology (He et al. 2017).

In various studies where space and airborne SAR scatterometers and simulations model are involved are found efficient for retrieving soil parameters (roughness and moisture) and, to a lesser extent, the soil's textural composition (Shi et al. 1997; Oh 2004; Holah et al. 2005; Zribi et al. 2005; Baghdadi et al. 2006, 2007; Srivastava et al. 2006, 2009). In western Rajasthan, for detecting paleo-channel having high moisture content at a depth of 45–75 cm covered by dry sand, the subsurface penetration capability of radar has been used (Mehta et al. 1993).

Mohan et al. (1990) studied optimal sensor configuration based on different ground-based scatterometer data for application in soil moisture and vegetation purposes. However, radar signal obeys a logarithmic function with the soil-surface roughness irrespective of SAR configuration (Fung 1994; Ulaby et al. 1986). More sensitivity of SAR data toward soil roughness could be observed at a higher angle of incidence (Baghdadi et al. 2008; Baghdadi and Zribi 2006). Broadly, low frequency (C, L band) and low incidence angle (7°–17°) are associated with soil moisture applications.

The higher angle of incidence (>40°), higher the frequency (X, C) with multi-polarization (HH, VV and HV) capability is required for crop inventory. At the time of the monsoon period and flood inundation, the Radar Imaging Satellite (RISAT) has been effective for monitoring crops in PF (Das and Paul 2015). SAR interferometry merges two SAR images of the identical scene captured from variable positions and/or times required to map topography DEM generation and tracks out small coherent movements (differential interferometry). Numerous researchers have demonstrated the potential of SAR interferometry for various RS applications like plant density mapping, plant height estimation, and surface water extent in adverse weather conditions which could be used in PF. A few important findings of using SAR interferometry for agricultural crop studies are presented in Table 2.6. Synthetic aperture radar (SAR) images can be potentially used in the agricultural sector for identification of crops and the on-field conditions, soil moisture, tilled conditions, forecasting of yield and residue assessment, zone mapping and management, etc. (McNairn and Brisco 2004).

2.4 Utility and Applications of GIS

GIS operations and functionality were reviewed by several authors (Maguire et al. 1991; Martin 1991; Bernhardsen 1992 and Environmental Systems Research Institute 1993). Laurini and Thompson (1998) compiled 10 major functions of GIS as follows:

Table 2.6 Use of radar remote sensing for research in precision agriculture

SAR technique	Sensor parameters	Biophysical parameters of agricultural crop							Author(s)
	Frequency	LAI	Biomass	Yield	Density	Height	Water content	Crop inventory	
Backscatter coefficient	X, Ku, and Ka bands	√							Ulaby et al.(1984)
Backscatter coefficient	C and L bands		√						Ulaby et al. (1999)
Backscatter coefficient	X band						√		Qi et al. (2004)
SAR Interferometry	C band					√			Srivastava et al. (2006)
Backscatter coefficient	C and L bands				√				Patel et al. (2006a)
Backscatter coefficient	C band			√					Patel et al. (2006b)
Polarimetric SAR Interferometry	S, C, and X bands					√			Lopez-Sanchez et al. (2007)
Polarimetric SAR	L band							√	Tan et al. (2011)
Backscatter coefficient	C band		√			√			Wu et al. (2011)
Polarimetric SAR	C and L band							√	Skriver (2012)
Backscatter coefficient	C band							√	Jang et al. (2012)
Backscatter coefficient	X, C, and L bands						√		Kim et al. (2012)
Backscatter coefficient	C band	√	√					√	Moran et al. (2012)
Backscatter coefficient	L and X bands		√						Paloscia et al. (2012)
SAR Interferometry	C band							√	Engdahl (2013)
Backscatter coefficient	X band	√							Fontanelli et al. (2013)
Backscatter coefficient	X band	√	√						Inoue and Sakaiya (2013)
Polarimetric SAR	C band		√						Patel and Srivastava (2013)
Polarimetric SAR	C band		√			√			Haldar et al. (2014)

(continued)

Table 2.6 (continued)

SAR technique	Sensor parameters	Biophysical parameters of agricultural crop							Author(s)
	Frequency	LAI	Biomass	Yield	Density	Height	Water content	Crop inventory	
Backscatter coefficient	L, X, C, and Ku bands						√		Emmerik et al. (2015)
Polarimetric SAR	C band							√	Uppala et al. (2015)
Backscatter coefficient, SAR Interferometry, and Polarimetric SAR Interferometry	X band					√			Erten et al. (2016)
Polarimetric SAR	C band	√	√			√	√		Srivastava et al. (2016)
Backscatter coefficient	C band							√	Sonobe et al. (2017)
Polarimetric SAR	L band	√	√			√			Hariharan et al. (2018)
Polarimetric SAR	C and X band							√	Liu et al. (2019)
Backscatter coefficient	C band	√	√			√			Valcarce-Diñeiro et al. (2019)

Modified, Sivasankar et al. (2018)

(i) Automated Mapping: Replicating paper maps or toposheets into digital format
(ii) Thematic Mapping: Using target's information and demographic data
(iii) Map Overlay or Composite Mapping: Mapping from stacked data layers
(iv) Spatial Querying: Gathering information about particular condition from a database through identification
(v) Spatial Browsing: Searching information about particular condition from a database through identification
(vi) Spatial Problem-Solving: Using deductive reasoning or eliminating irrelevant spatial information for addressing the particular problem-solving and decision-making
(vii) Spatial Data Analysis: Testing the spatially explicit data for interpretation
(viii) Implementing Spatial Statistics: Using statistical tools for assessment of spatial attributes of interest
(ix) Spatial Statistical Analysis: Testing statistically the spatial attributes of interest
(x) Spatial Analysis: Carrying out simulation through a wide range of spatial statistical tools available for further representation of spatial phenomena (Foley et al. 1990; Laurini and Thompson 1992; Bonham-Carter 1994).

A typical GIS contains information about the usual features of a location, unique or discriminate features within that location, changing trend of particular observation parameters over time, spatial or landscape patterns of that location, and prediction of the target's change in future (Gangwar 2013). Its importance is widespread over various disciplines and implementation sectors like agriculture, IT sectors, telecommunication, mining and exploration, environmental and ecological exploration and maintenance, strategic studies for renewable energy resources, natural resource identification, and management, as well as any other particulars associated with earth's spatial dwelling. Some potential management and decision-making applications of GIS in the agricultural sector are in PF, addressing pests and diseases, land use planning, biodiversity assessment, resource identification, and mapping, crop area marking and yield prediction, watershed and irrigation management, genetic resources management, etc. (Mulla 1993; Mulla and McBratney 2000; Oliver 2010; Mulla and Khosla 2015). GIS application in natural resource management has already documented by many scientists such as forest pest impact modeling (White 1984), modeling of narcotic crop sites (Waltz and Holm 1986), waste disposal site modeling (Buckley and Hendrix 1986), water quality assessment (Welch et al. 1986), CO2 effect analysis (Brekke 1986), etc. GIS enriches knowledge and reduces uncertainty to improve and expedite decision-making, prevent mistakes, and save cost. The integration of GIS with simulation modeling and RS tools ensures a high range of applications in different scientific fields.

2.4.1 Geostatistics: A Tool for Spatial Variability Assessment

Geostatistics has been evolved basically to characterize incompletely known spatial features of the earth by incorporating multiple numerical techniques through probabilistic models or pattern recognition techniques (Olea 2009). It always uses sampling location details to find out the spatial correlation between measurements, which makes it a distinct from classic statistical concepts. In the 1950s, the seminal idea about geostatistics was put forwarded by Danie Krige to address doubt during decision-making for carrying out expensive operations in mining and petroleum industries (Zhang 2011). Later, mining industries' data interpolation through geostatistics was proposed by Matheron (1962). Gradually, geostatistics has extended its prevalence in other earth science fields like forestry, soil mapping, meteorology, ecology, hydrogeology, geomorphology, hydrology, geophysics, geography, soil sciences, landscape ecology, epidemiology, environmental monitoring and assessment, oceanography, sedimentology, agronomy, geochemistry, atmospheric sciences, or any other discipline with spatial data (Myers 2008; Fischer 2015). In recent years, it has been successfully combined with RS and GIS for accelerating its efficiency and broad coverage in the scientific arena. The term "spatiotemporal statistics" (the scientific branch that analyses and interprets spatial and temporal data) is often synonymously used instead of geostatistics (Journel 1986). Geostatistics has specifically expressed interpolation of scalar values, such as strain ellipticity (Mukul 1998), soil properties, vectors treatments (Young 1987; Lajaunie et al. 1997), curvilinear geometrical analysis (Xu 1996), kriging interpolation for three-dimensional geometrics of earth surfaces (Lajaunie et al. 1997), etc. Certainly, geostatistics is different from conventional statistics. Conventional statistics provide analysis and interpretation of uncertainty occurrences due to limited and error sampling. It does not quantify the space, magnitude, or other factors associated with variability of uncertainty. It mainly considers discrete or individual data points. Conversely, apart from the data distribution, geostatistics further employs tools to determine spatial relationships, and thus provides accurate and bulk information from limited and error sampling. Additionally, it predicts the probability of spatial distribution of properties and minimizes uncertainty in data sampling. It mainly considers differences in value and spatial locations of data points. Geostatistics is based on the fact that at some scale autocorrelation of properties of an object occurs, that is, in close proximity, data has homogeneity. It measures the sample (called supports) to represent a population. This sample can be one or mean of several others.

Principles of geostatistics mostly rely on Kriging. Kriging is defined as a linear regression method for determining point values (or spatial means) at a random location of earth from observations of its value from adjacent locations. The concept of kriging was first put forward by Matheron (1962) for data points' interpolation and termed as an optimal prediction of a variable by interpolating its location with data points in close proximity (Cressie 1990). Unlike other regression models, kriging allows estimation of a single realization of the unbiased, random field.

Kriging method is divided into five major types: simple kriging, ordinary kriging (mostly used), anisotropic kriging (for analysis of geometric anisotropy), universal kriging (analysis of local pattern or trends), and co-kriging (analysis using two or more regionalized input variables) (Hendrikse 2000). Other types include indicator kriging, disjunctive kriging, and log-normal kriging. Simple kriging assumes stationarity of the first moment over the domain with known averages. Universal kriging assumes polynomial trend (three steps: removal of drift in a specified distance, kriging of secondary residuals, and outcome or estimated residuals from secondary residuals' kriging combined with a drift to determine properties of the real surface) while indicator kriging incorporates indicator functions either in separate form or in combination to predict transition probabilities. Disjunctive kriging is a nonlinear expression of kriging. Lognormal kriging uses a logarithmic technique to interpolate positive data. Ordinary kriging considers an unknown mean (constant) over neighborhood search for data estimation of the target location. Anisotropic kriging uses variogram surface inspection with various pixel sizes and the result varies with scale change. Co-kriging is a combination of ordinary kriging operations to identify and estimate poorly sampled variables (predict and) using well-sampled variables (co-variable). The co-variables should be correlated either positively or negatively. Studies conducted on the prediction of spatial variability in chemical properties by Nourzadeh et al. (2012) revealed that Cokriging was the best method for interpolating the chemical properties of soil. Kriging till date has spread its application in various disciplines like the spatial variability maps of soil properties (Franzen and Peck 1995; Hengl et al. 2004; Santra et al. 2008; Liu et al. 2008; García-Tomillo et al. 2017), environmental science (Lajaunie 1984; Zirschky 1985; Webster and Oliver 2007), hydrology (Mulla and Hammond 1988; Moslemzadeh et al. 2011; Danilov et al. 2018), mining (Pan et al. 1993), natural resources for the management of nutrients (Vieira et al. 2007; Chatterjee et al. 2015; Fathi and Mirzanejad 2015; Metwally et al. 2019), RS (Mulla 1991; Oliver 2010; Mulla 2016), and modeling of microwave devices. Kriging not only provides spatial autocorrelation, but also can replace stratified sampling if aggregates size is greater than the distance between two sampling points (Webster and Oliver 2007). It compensates for the data clustering and gives estimates of estimation error. Its uniformity in all types of sampling and properties has made its broad range of applications (Oliver and Carroll 2004; Oliver 2010, 2013). Oliver (2013) had conducted a case study on a field which has complex geography with variations in topography and soils in the Yattendon Estate in Berkshire. Based on variogram and kriging, he generated various digital maps related to yield of crops, soil properties to aid the farmer in decision-making, etc. He presented the short-range (30 m) and long-range (130 m) spatial variations in wheat yield through interpolation technique (Fig. 2.4).

The short-range variation is due to the management effects. However, the long-range variation in yield is mostly related with the soil texture, that is, sand and clay content and slope, hence the plateau area has the highest yield.

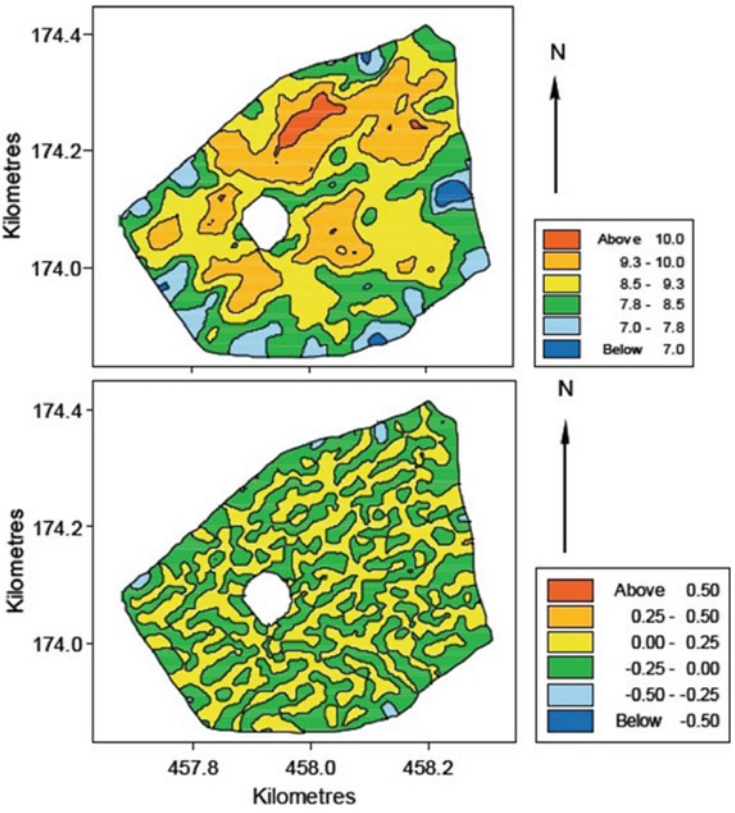

Fig. 2.4 The long-range (top) and short-range (below) spatial variation in yield. (Modified, Oliver 2013)

2.4.2 Spatial Econometry

Compared with the above mentioned, spatial econometry is relatively a new discipline in the scientific field (Arbia 2015). The idea was pioneered by Belgian economist Jean Paelinck just 40 years ago (Paelinck and Klaassen 1979). It has accelerated its speed from the last two decades due to the flood of problems associated with digitization and explosive revolution of data in information and technology and communication sectors. Spatial econometry is a scientific field that offers analytical techniques for identifying interdependence of geographically neighbor observations (areas or points) (LeSage 2005). This subfield of econometrics (i.e., application of statistical tools to make a quantitative analysis of actual economic phenomena based on observations and understanding to formulate inference about economic relationships) using regression models undergoes spatial autocorrelation and heterogeneity for cross-sectional and panel data (Paelinck and Klaassen 1979; Anselin 1988). Spatial interaction means a sample correlation about the location of

observations. Spatial heterogeneity means the variability of econometric relationships according to space. It has been spreading the essence of success, as it recalls Gauss–Markov assumptions what the traditional econometrics forgot (LeSage 1999). Spatial econometrics though in adolescence stage, already has several application fields like regional economics, real estate, criminology, demography, agricultural economics, land use land cover, urban planning, industrial organization, political sciences, psychology, demography, epidemiology, managerial economics, education, economic development, health economics, public finance, innovation diffusion, history, labor, resources, energy economics, transportation, social sciences, food security, marketing, environmental studies, etc. (Arbia 2015). With the help of various geostatistical and spatial data analysis tools and models, spatial econometry interprets different economic phenomenon, namely interactions, spatial concentration, external factors, etc.

2.4.3 Spatial Regression

Regression is a statistical process to evaluate the relationship between a variable of interest (dependent) and one or more explanatory variables (predictors or independent variables). The spatial dependence of observations is determined through spatial autocorrelation (data attributes generated in response to the spatial pattern in values). The spatial pattern is estimated with the help of global (Moran's I, Geary's C, Getis/Ord Global G) as well as local (LISA and others) statistical methods. The regression model of such characteristics (i.e., spatial autocorrelation) is called a spatial regression model (Srinivasan 2015). Spatial autocorrelation is observed when observations that are closer to each other in space have related values. Spatial regression analysis aims to model, examine, and explore spatial relationships and explains factors responsible for the spatial pattern. Ordinary least square (OLS) is the best regression technique used so far. OLS provides a global model of variable or process for further interpretation and prediction (Arc GIS Pro, v. 10.7) using a single regression equation. Another important technique that has a long use in geography and other associated disciplines is the geographically weighted regression method (GWR). GWR provides a local model of variable or process for prediction or interpretation by fitting the regression equation to every aspect in the dataset (Kupfer and Farris 2007). Both OLS and GWR effectively estimate liner relationships (either positive or negative). Spatial regression has address two issues: (a) geographic features that are not spatially autocorrelated (Lark 2000) and (b) nonstationary nature of properties that user wants to model (Paciorek and Schervish 2006; Risser and Calder 2015; Risser et al. 2019).

2.4.4 Delineation of Management Zones

PF is a time- or location (site)-specific farming method that relies on four "R" principles: Right product, Right rate, Right time, and Right place. It aims in managing spatial soil variability by addressing only the requirements for soil and crop rather than the entire field (Doerge 1999; Mzuku et al. 2005). PF thus requires a practical management approach to delineate its MZs. Similar MZs are the homogeneous areas having an analogous trend of yield limitation or improvement through similar key factors in each case (Doerge 1999; Khosla and Shaver 2001; Fridgen et al. 2004; Basso et al. 2007). However, delineation of such subfields is hard as there exist strong interrelationships of biotic, abiotic, and climatic factors. Already several approaches such as topography, soil properties through survey maps (Carr et al. 1991), soil sampling (Mulla 1991), terrain features through DEM (McCann et al. 1996; Lark 1998; Nolan et al. 2000), aerial photography (Fleming et al. 2000) remotely sensed imageries (Bhatti et al. 1991b; Moulin et al. 1998), invasive (Mulla 1991) and noninvasive samplings (Johnson and Richard 2003), etc. are in practice to delineate management zones. Each management zone is unique (may it be in requirements or results). The most important spatial information for demarcating MZs has the characteristics of stability, quantitativeness (numerical), being rigorous and nonstop sampled and should pose a relationship with crop yield and performance directly. For the development of the management zone to carry out the PF, several data on previous crop history, previous years' yield map, soil properties, and fertility, drainage, microclimate, pest problem, etc. about every portion of the field is required. If some subregions of the field show similarity to each other, they are marked as a particular management zone and, thus, the entire field is separated by different types of management zones. As complex relationships among several factors are continuously occurring in the field, the constraint arises on maintenance and update of recorded data for making zone-wise application map for the next uses. The problem further arises with the combined use of more than one variable (say, for example, weed control and fertilizer management, organic nutrition and irrigation, etc.). Therefore, a good management zone always requires help from flexible and advanced GIS tools (Royal 1998). A proper combination of all types of collected field information, knowledge about marking MZs, and modification or change of formula with temporal variability of MZs are needed to address the challenge further. GIS users for determining MZs should be ready for change and flexible enough to convert the management layer in raster or vector format for running selected variable rate applicators. The most effective management zone strategy changes with region and growers. Available data on soil and crop conditions along with experience of farmers and profound knowledge of users in computer and software handling, etc., all help to select ideal management zone.

2.5 Geoinformatics in Precision Agriculture

Geoinformatics is part of scientific and technological field, which collects, differentiates, stores, analyses, depicts, and transfuses information about the structure and characteristic features of location in a secured way for the users to interpret well (Raju 2003). On the other hand, Ehlers (2003) has stated that it is not only a branch of science and technology, but also an art for acquiring spatial information to analyze, store, visually represent, and transfuse further. There are several coined definitions of Geoinformatics worldwide. Geoinformatics is a multidisciplinary field and consists of several disciplines such as RS for acquiring images through earth observation sensors, GIS for processing, interpretation of geoinformation, and visually depicting outcomes through sheets or digitally for decision-making. Besides, it provides an opportunity to prepare spatial databases, framing information systems, modeling through manual–digital interaction using various wired and wireless network interfaces. Geocomputation, cartographic technology, GPS, GIS, web-mapping, geodesy, RS, photogrammetry, and geo-visualization are used in Geoinformatics for geoinformation analysis. Geoinformatics is becoming more efficient and acceptable in several sectors due to combining the improved analytical efficiency, latest telecommunications opportunities, in a wide range of information, and recent upgradation of image processing tools such as RS, GPS and GIS. The flow chart of the working principle of Geoinformatics in a decision support system is presented in Fig. 2.5. Nowadays Geoinformatics provides benefit to many regular services such as urban planning and land uses, car transports, aviation, and maritime transports, public health, meteorology and climatology, environmental modeling and analysis, military, agriculture, oceanography, business planning, architecture, and archaeological studies, telecommunications, and many more. In industrial, environmental, commercial, and agricultural sectors and in various regional, national, and international public or private organizations, in the field of research, survey, mapping, emergency support, etc., currently Geoinformatics plays a crucial role in better decision-making and goal achievements.

2.5.1 Yield Monitoring and Mapping

Since yield is a major parameter representing the impacts of different on-field agronomic factors, monitoring, mapping, as well as their relationship with spatial and temporal variability of other agronomic attributes would help in the formation of future strategy (Mondal et al. 2004). Thus, yield monitoring and mapping consist of a vital and logical part for the system required for practicing PA. From the aspect of PA, yield monitoring could be simply defined as a technique capable of generating adequate information that could be used by the farmers for making better decisions in the field (Wang 1999). Grain yield could be assessed field- or load-wise by yield monitors. Some monitoring systems used in the case of forage crops collect

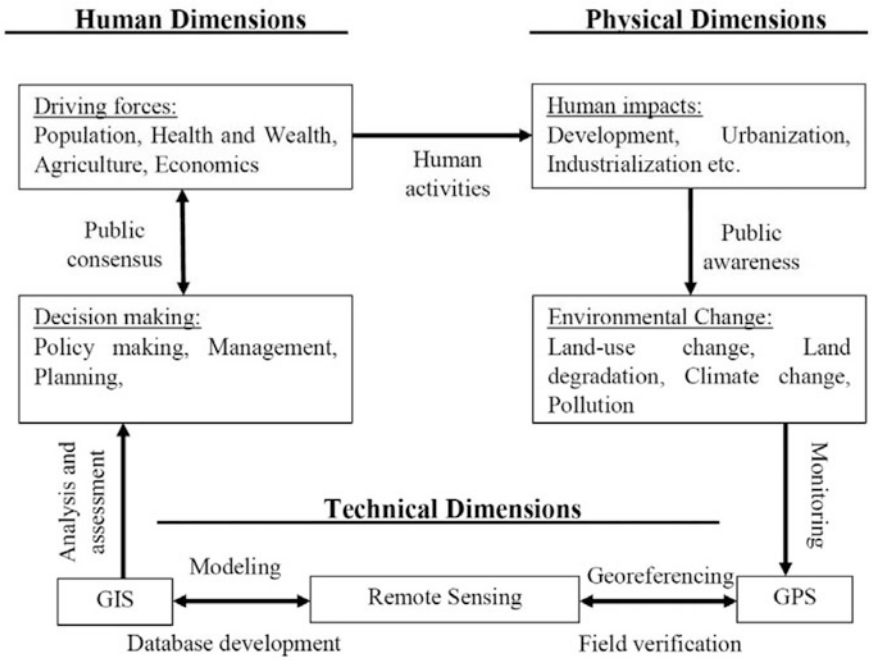

Fig. 2.5 Flowchart of the working principle of geoinformatics in a decision support system. (Modified, Murai 1999)

information such as weight, water content, and several other parameters bale wise (Davis et al. 2005).

2.5.1.1 Yield Monitoring in Precision Farming

The yield monitoring system provides the farmer with greater flexibility with instant information about the condition of the field and crops based on which farmers could take necessary steps (Thylen and Murphy 1996). In recent days, yield monitors enable farm equipment to acquire a large range of information of grain yield, moisture level, and soil properties and so on through their association with the equipment (Fig. 2.6) which eventually made the decision-making process easier for the farmers. So, the time of harvesting (Vellidis et al. 2001; Yang and Everitt 2002) fertilizer application, irrigations could be easily assessed along with the mitigation of potential threat through improved understanding of yield-related traits by analyzing geo-referenced data of particular field (Grisso et al. 2002). This information is generally collected in data storage devices, which could be further transferred and stored in personal computers in a variety of formats.

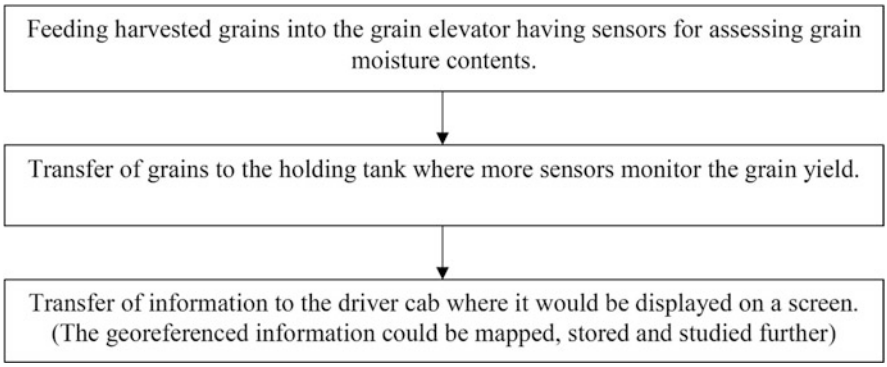

Fig. 2.6 Flowchart of the steps of yield-monitoring process

2.5.1.2 Yield Mapping in Precision Farming

The whole process of measurement, compilation, and presentation of georeferenced crop yield data and other parameters such as grain moisture content in a consolidated effective form such as in the form of a map is called yield mapping. Several sensors dedicated to several parameters are generally employed in this whole process. These sensors along with the DGPS receiver assess several sets of instantaneous data points of several parameters based on which yield maps are developed (Arslan and Colvin 2002; Fulton et al. 2018). Many automated elements are involved in this system. For instance, as a combine operator guides the farmers for crop cultivation and its harvesting only, yield data collection is an automated system in the process of yield mapping. So the flow of grain through the chute is continuously recorded along with the recording of the field position of the harvester. Georeferenced yield information is then transferred in a computerized system for interpolating with the help of special software to generate yield maps of the field. The binary format is most preferable as it is capable of storing digital data efficiently. But the conversion of this binary data into standard text format is necessary as most of the software cannot process the raw binary data. One cannot get the reason of yield variation from the yield map as it only offers the information depicting the superior and inferior parts of the field in terms of yield or it may provide an overview of variation of grain moisture content in the field which would help farmers to decide whether to harvest or not in that particular part of the field (Stoorvogel et al. 2016). Hence, farmers are asked to apply their experience, indigenous knowledge, and supplementary information to describe yield maps for upgrading their decision regarding crop management to get maximum profit. Thus, the PF system is mainly the assemblage of different elements and technologies in one effective system for performing successful PA (Pfost et al. 1998, 1999; Blackmore et al. 2003; Zhang et al. 2008; Colaco et al. 2015; Fulton et al. 2018).

2.5.2 *Fertilizer Recommendation*

Recommendations of fertilizers depending on the analysis of soil and plant are generally introduced for the betterment of productivity in agriculture as they are of high efficiency mainly focused on the practical scientific techniques that deal with the data obtained from the soil and plant analysis (Xia et al. 2011). The soil testing and fertilizer recommendation methods are commonly implemented to improve fertilizer efficiency for obtaining an augmented yield along with mitigating the detrimental effects of long-term fertilization for specific crops (Black 1992; Wang et al. 1998). The increase in crop growth due to better fertilization could also contribute to building soil organic carbon content, which in turn influences the distribution of nutrients in the soil as well as nutrient cycling. Thus, fertilizer recommendation based on soil and plant analyses not only helps in promoting crop productivity to meet the ever-increasing need of rising population but also helps to maintain environmental sustainability. Hence, the use of this essential and effective technique in modern agriculture not only ensures a steady production but also facilitates optimum use of fertilizers which makes it a source-efficient and environment-friendly approach (Xia et al. 2011; Wei and Qi 2013).

Traditionally over the years, the soil is sampled and tested in the laboratory for a recommendation of fertilizers which is not only uneconomical but also time-consuming. With the use of geospatial analysis, cost-saving and increment of work efficiency can be successfully achieved (Tang et al. 2007).

The wide use of computers as a computing device in experiments and researches regarding fertilizers was started between the 1970s and 1980s in the western world (Haynes 1986). An increase in concerns regarding the development and application of a various range of fertilizers was noted since the 1980s (Black 1992) and computer-based fertilization decision systems were established by several developed countries at that time. Auburn University coined a recommendation system containing 52 fertilization standard types while the Agro Services International Inc. starred to use a software-based system to determine the optimal nutrient requirement and were able to give consultancy regarding 11 nutrients for 140 numbers of crops. “Crop-environment resources information system” was developed by Richie and people got the recommendation of nitrogen-based on climates, crop varieties, physiological characteristics, moisture and nutrient status for wheat and corn cultivation (Haynes 1986; Black 1992). The emergence of the agricultural production decision system integrating several systems such as scientists’ expertise, simulation models, GIS, and RS took part in the development of technology. AE-GIS, a decision support system equipped with crop models and GIS, was developed by Florida State University agricultural and environmental studies. The Decision Support System for Agrotechnology Transfer (DSSAT) was then developed by the University of Hawaii, which was capable of assessing the effects of different environmental factors by using simulation models to help take appropriate decisions further regarding management practices. In a similar period, GPFARM developed by the United States Department of Agriculture (USDA) became a potent

organization to support production decision-makers as it took economy, environment, and sustainability together into consideration.

Over time scientists developed expert systems on fertilizer recommendation for crops based on the soil nutrient status of the field. Previously soil samples had to collect in a scientific way, which was very cumbersome to the farmers (Ren et al. 2002; Wang et al. 2010). Application of Resource Information Database helped to overcome such problems to some extent. Thus, this system of scientists' expertise was able recommend fertilization by cutting down complicated and time-consuming procedures including soil sampling and analysis (Tang et al. 2007). Because of the mutation of the past few decades, a combination of spatial information with soil nutrient content database became necessary to study the distribution of nutrients in agricultural fields (Mao and Zhang 1991; Qi et al. 2009).

Latest interventions like high-resolution satellite information, GPS, GIS, and information technology hold good prospects of monitoring soil nutrient status and in fertilizer management, land use planning which can be sustained for the future. The satellite covers many types of information, namely landforms, geological features, soil categories, erosion, land use, groundwater, and soil moisture which increases the potential of the fertilizer recommendation process. The combined use of RS, GPS, and GIS imparts positively on digital analysis and mapping of the distribution of different nutrients in soils of a vast area quickly. RS, GIS and GPS in recent days could assess the spatial variance of soil nutrients where geostatistics forms the foundation of soil resource information database. Depending on laboratory analysis and previous literature, soil testing and fertilizer recommendation models and indices are made (Tang et al. 2007; Li et al. 2008). After indexing the nutrient status of a particular field in the database of soil resources, scientists' expertise concludes fertilizer recommendation, dose, and application scheme for a specific crop (Tang et al. 2007).

2.5.3 Digital Soil Mapping

Soil maps could be simply defined as mapping units where a specific type of soil having characteristic properties is believed to be located. Digital soil mapping with the assistance of computer-based systems covers various features or properties of soil in the generated maps (Kumar 2018). Thus, digital soil mapping is nothing but making databases of georeferenced information about the soil under certain resolution based on field observations and laboratory analysis along with environmental considerations. Statistical and mathematical models are generally used to combines soil observations and information dealing with correlation among RS data and environmental attributes. Unlike soil mapping, soil-landscape mapping delivers a land resource survey that deals with similar or associated soil types and repeating patterns of landscapes (Schoknecht et al. 2004). Soil-landscape mapping is an important tool for better and firm decision-making under variable management practices, as land resource interpretation lowers the risk of implication of various

practices. It also enhances the better understanding of biophysical processes, and helps in strategies for land use planning in large-scale environmental regulation, trading, monitoring, and mapping of natural resources, such as distribution and prediction of soil carbon storage (Pieri 1997). Geospatial technologies in which satellite-based imageries are used for simple monitoring purposes, such as soil productivity, fertility, moisture status, etc., would help farmers to make future decisions precisely.

Soil and landscape analyses have been significantly influenced by the advancement of GIS-based digital terrain modeling (Mahmoudabadi et al. 2017). For soil characteristics prediction, development of soil-landscape models have also been made by combined use of both statistical modeling and digital terrain analysis (Moore et al. 1993; McSweeney et al. 1994). In these cases, images acquired through RS devices act as data source support for digital soil mapping (Ben-Dor et al. 2008; Slaymaker 2001). For analyzing and modeling the land surface as well as studying the relations between several components of the landscape such as topography, anthropogenic, hydrological, geological, and biological components, digital terrain analyses are generally used. Despite being a profitable and potent technology, soil spectroscopy has not still been regularly applied during survey or monitoring. With computer software's upgradation, digital elevation models (DEMs) have become popular. DEMs generally use remotely sensed data to produce 3-D landscape models that are capable of delineating geomorphological and land surface features in a precise way through visual interpretation. DEMs are also able to provide several information regarding elevation, slopes, aspect maps, etc. with the help of which efficiency of soil mapping can be augmented. Hence, for this purpose, logical integration of remotely sensed imagery, soil data obtained from sampling, and digital elevation models (DEMs) could upgrade the efficiency of the DSM system to interpret and predict the soil properties (Grunwald 2009), and automated soil mapping using DEMs has also been started. Significant positive correlation and predictive features among terrain attributes and different soil properties have been observed by Moore et al. (1993) and Gessler et al. (1995). Thus, the use of terrain attributes along with soil features can act as secondary variables that could enhance the interpolation accuracy of present soil information (Kumar and Singh 2016).

2.6 Modern Trend in Precision Farming: Use of Drones

The modern trend in monitoring natural resources, vegetation, and agrarian belts is to adopt drones, that is, unmanned aerial vehicles (UAVs) that possess miniaturized sensors (Jin et al. 2009; Wang and Wu 2010; Salami et al. 2014). They are rapid in turnaround and offer very high-resolution imagery because of the proximity of sensors to the surface to be monitored (Berni et al. 2009; Green 2013; Vanac 2014). As agriculture is the backbone for many developing countries like India, there is an urgent need to incorporate RS in this sector at a cheap cost (~100 INR/acre/season) with improved spatial (2 m multispectral or more), spectral (<25 nm),

Table 2.7 Differences of UAVs from various remote sensing tools

Tools	Field of view	Spatial resolution	Usability	Payload	Data acquisition cost
UAV	50–500 m	0.5–10 cm	#	X	*
Helicopters	0.2–2 km	5–50 cm	##	X	**
Airborne	0.5–5 km	0.1–2 m	##	√	***
Satellite	10–50 km	1–25 m	–	–	****

Modified, Candiago et al. (2015)
√: Unlimited, X: Limited, *Very low, **Medium, ***High, ****Very High, #Very good, ##Pilot mandatory

and temporal (minimum five to six times in each season) resolutions, reduced turnaround time (24–48 h) for delivering analytical observations in simple and easy to understand the way in case of PF (Hunt et al. 2005; Lelong et al. 2008; Nebiker et al. 2008; Rango et al. 2009; Hardin and Hardin 2010; Xiang and Tian 2011). Unmanned aerial systems (UAS) have a great potential of capturing images of spatial phenomena from a low altitude (Swain et al. 2007) and therefore this young technology is now gaining attention in the agricultural sector in place of others.

One of the most active emerging areas of research in PA uses cameras mounted on UAVs (Berni et al. 2009; Zhang and Kovacs 2012; Huang et al. 2018). An Unmanned Aerial Vehicle (UAV) can be fully automated or instructed to be automated or manually operated (Sylvester 2018). The development of UAV platforms linked with various sensors (image, position, range, etc.) can effectively capture multispectral images at a cm-level resolution which holds good prospects in PF (Lelong et al. 2008; Turner et al. 2011; Guo et al. 2012; Primicerio et al. 2012; Bendig et al. 2012; Lucieer et al. 2014; Nex and Remondino 2014; Colomina and Molina 2014; Bansod et al. 2017), agriculture, and forestry management (Grenzdörffer et al. 2008). Nowadays, UAVs are showing their potential in farm resource management by capturing quality images of various aspects of crop cultivation, especially monitoring the crop health at relatively cheaper expenditure over other RS tools (Primicerio et al. 2012). The UAVs are relatively inexpensive, can be deployed rapidly at low altitudes when crop stress is starting to appear, and have the flexibility to be flown during windy or partly cloudy conditions (Mulla and Miao 2016). In Table 2.7, differences of UAV from other RS tools are mentioned.

The successful use of UAVs or drones in PF is now gaining importance. For instances, UAVs have potential applications in tracking out small weed zones (in rangelands) (Hardin et al. 2007); crop water stress (Berni et al. 2009); biomass monitoring (Hunt et al. 2005; Swain et al. 2010); in figuring out vineyard vigor (Primicerio et al. 2012); in the identification of crop types such as rice (Swain et al. 2007, 2010), coffee (Johnson et al. 2004), wheat (Hunt et al. 2010), corn (Hunt et al. 2005), etc.; and in evaluating the effect of nutrient management on crops, etc. Reports from Hunt et al. (2005) and Swain et al. (2007) showed the evidence of identification capabilities of drones about the effects of the application of different doses of nitrogen on crops.

2.7 Major Challenges in Precision Farming

A well-documented improvement in crop yield, profitability, or environmental quality remains rare in scientific literature, despite a large number of success stories on PF. There are many technology-related, farm-related, data related, and organization related issues, which are associated with the adoption of PF. The major challenges as are follows:

- Technology-related issues involve compatibility and high cost of hardware and software, and a lack of understanding in the correct application of the technology.
- Lack of reliable and inexpensive sensors, cloud-free data, different data formats, etc.
- Most of the available sensors provide indirect measurement of soil and plant attributes; however producers are looking for sensors which can provide direct input for existing prescription algorithms (Dobermann et al. 2004).
- Issues with data interoperability: Farmers and researchers can easily collected huge information within short span of time, but assessment, interpretation, and transformation of these quality data into meaningful management decisions, beneficial potentialities, and related risks have proven to be a difficult task.
- The major constraints for implementation of technology in farmers' fields include lack of awareness about current policies, lack of skills, and their uneducated backgrounds.
- Inadaptability by the farmers at the grassroots: In developing countries, most of the farmers have small and marginal landholdings and they are financially weak, and thus afraid of the risks of change, so they reluctantly accept technological interventions.

2.8 Conclusions and Future Perspectives

Remote sensing technology has a great potential to acquire various spatial, spectral, and temporal resolution datasets which can be used as input for precision agriculture. Remote sensing data at optical, microwave, thermal, and hyperspectral domains prove to be a powerful tool to assess crop and soil properties in varying spatial and temporal scales with cost-effectiveness. Satellite RS coupled with GIS and mobile app-based positional information has emerged as an efficient tool for the sustainable development in precision agriculture resources by optimizing input resources, minimizing the cost of production, and risk of biotic/abiotic in nature. Modernization and advancement in space and information technologies have created a suitable environment for the implication of PF in many countries. In most of the developing countries, the problem of adoption of PF is due to small landholdings, so the adoption of precision farming through community farming approach would be a better option. The full potential of precision farming can only be exploited if the soil scientists, agronomists, agricultural economists, and engineers develop simple and robust methodologies and technologies for farmers.

References

Adamchuck VI, Mulliken J (2005) Site specific management of soil pH (FAQ). University of Nebraska-Lincoln, Extension EC05705

Adamchuk VI, Hummel JW, Morgan MT, Upadhyaya SK (2004) On-the-go soil sensors for precision agriculture. Comput Electron Agric 44:71–79

Alchanatis V, Cohen Y (2010) Spectral and spatial methods of hyperspectral image analysis for estimation of biophysical and biochemical properties of agricultural crops. Ch. 13. In: Thenkabail PS, Lyon JG, Huete A (eds) Hyperspectral remote sensing of vegetation. CRC Press, Boca Raton, p 705

Al-Kufaishi SAA, Blackmore BSS, Sourell H (2006) The feasibility of using variable rate water application under a central pivot irrigation system. Irrig Drain Syst 20:317–327

Andreo V (2013) Remote sensing and geographic information systems in precision farming. Available: http://aulavirtual.ig.conae.gov.ar/moodle/pluginfile.php/513/mod_page/content/71/seminario_andreo_2013.pdf. Retrieved 16 April 2015

Anselin L (1988) Spatial econometrics: methods and models. Kluwer Academic, Dordrecht

Apostol S, Viau AA, Tremblay N, Briantais JM, Prasher S, Parent L, Moya I (2003) Laser-induced fluorescence signatures as a tool for remote monitoring of water and nitrogen stresses in plants. Can J Remote Sens 29:57–65

Arbia G (2015) Spatial econometrics: a broad view. Found Trends Econometrics 8(3–4):1–121

Arslan S, Colvin TS (2002) Grain yield mapping: yield sensing, yield reconstruction, and errors. Precis Agric 3:135–154

Baghdadi N, Zribi M (2006) Evaluation of radar backscatter models IEM, OH and Dubois using experimental observations. Int J Remote Sens 27(18):3831–3852

Baghdadi N, Holah N, Zribi M (2006) Soil moisture estimation using multi-incidence and multi-polarization ASAR data. Int J Remote Sens 27(10):1907–1920

Baghdadi N, Cerdan O, Zribi M, Auzet V, Darboux F, El Hajj M, Bou Kheir R (2007) Operational performance of current synthetic aperture radar sensors in mapping soil surface characteristics in agricultural environments: application to hydrological and erosion modeling. Hydrol Process 22 (1):9–20

Baghdadi N, Cerdan O, Zribi M, Auzet V, Darboux F, El Hajj M, Kheir RB (2008) Operational performance of current synthetic aperture radar sensors in mapping soil surface characteristics in agricultural environments: application to hydrological and erosion modelling. Hydrol Process Int J 22:9–20

Baghdadi N, Choker M, Zribi M, El Hajj M, Paloscia S, Verhoest NEC, Lievens H, Baup F, Mattia F (2016) A new empirical model for radar scattering from bare soil surfaces. Remote Sens 8 (920):1–14. https://doi.org/10.3390/rs8110920

Bandyopadhyay D, Bhavsa D, Pandey K, Gupta S, Roy A (2017) Red edge index as an indicator of vegetation growth and vigor using hyperspectral remote sensing data. Proc Natl Acad Sci India Sect A Phys Sci. https://doi.org/10.1007/s40010-017-0456-4

Bansod B, Singh R, Thakur R, Singhal G (2017) A comparison between satellite based and drone based remote sensing technology to achieve sustainable development: a review. J Agric Environ Int Dev 111(2):383–407. https://doi.org/10.12895/jaeid.20172.690

Banu S (2015) Precision agriculture: tomorrow's technology for today's farmer. J Food Process Technol 6:468–473

Barnes EM, Clarke TR, Richards SE, Colaizzi PD, Haberland J, Kostrzewski M, Waller P, Choi C, Riley E, Thompson T, Lascano RJ, Li H, Moran MS (2000) Coincident detection of crop water stress, nitrogen status and canopy density using ground based multispectral data. In: Robert PC, Rust RH, Larson WE (eds) Proceedings of the fifth international conference on precision agriculture. ASA, Madison, pp 1–15

Basso B, Bertocco M, Sartori L, Martin EC (2007) Analyzing the effects of climate variability on spatial of yield in a maize-wheat-soybean rotation. Eur J Agron 26:82–91

Basso B, Dumont B, Cammarano D, Pezzuolo A, Marinello F, Sartori L (2016) Environmental and economic benefits of variable rate nitrogen fertilization in a nitrate vulnerable zone. Sci Total Environ 545–546:227–235

Bauer M E, Cipra J E (1973) Identification of agricultural crops by computer processing of ERTS MSS data (LARS Technical Reports. Paper 20. http://docs.lib.purdue.Edu/larstech/20). In: The laboratory for applications of remote sensing Purdue University, West Lafayette, Indiana, pp 1–9

Baumgardner MF, Silva LF, Biehl LL, Stoner ER (1985) Reflectance properties of soils. Adv Agron 38:1–44. https://doi.org/10.1016/S0065-2113(08)60672-0

Bausch WC, Khosla R (2010) QuickBird satellite versus ground-based multi-spectral data for estimating nitrogen status of irrigated maize. Precis Agric 11:274–290

Bendig J, Bolten A, Bareth G (2012) Introducing a low-cost mini-UAV for thermal- and multispectral-imaging. Int Arch Photogramm Remote Sens Spat Inf Sci 39(B1):345–349

Ben-Dor E, Taylor RG, Hill J, Demattê JAM, Whiting ML, Chabrillat S, Sommer S (2008) Imaging spectrometry for soil applications. Adv Agron 97:321–392

Bernhardsen T (1992) Geographic information systems. VIAK IT and Norwegian Mapping Authority, Arendal

Berni JAJ, Zarco-Tejada PJ, Suarez L, Gonzalez-Dugo V, Fereres E (2009) Remote sensing of vegetation from UAV platforms using lightweight multispectral and thermal imaging sensors. Retrieved March 12, 2012 from: http://www.ipi.uni-hannover.de/fileadmin/institut/pdf/isprs-Hannover2009/Jimenez_Berni-155.pdf

Bertoldi G, Chiesa SD, Notarnicola C, Pasolli L, Niedrist G, Tappeiner U (2014) Estimation of soil moisture patterns in mountain grasslands by means of SAR RADARSAT2 images and hydrological modeling. J Hydrol 516:245–257

Bhatti AU, Mulla DJ, Frazier BE (1991a) Estimation of soil properties and wheat yields on complex eroded hills using geostatistics and thematic mapper images. Remote Sens Environ 37:181–191

Bhatti AU, Mulla DJ, Koehler FE, Gurmani AH (1991b) Identifying and removing spatial correlation from yield experiments. Soil Sci Soc Am J 55:1523–1528

Black CA (1992) Soil fertility evaluation and control. LEWIS Publishers, Bockaton

Blackburn GA (1998) Quantifying chlorophylls and carotenoids at leaf and canopy scales: an evaluation of some hyperspectral approaches. Remote Sens Env 66(3):273–285

Blackmer TM, Schepers JS (1995) Use of a chlorophyll meter to monitor nitrogen status and schedule fertigation for corn. J Prod Agric 8:56–60

Blackmore BS, Godwin RJ, Fountas S (2003) The analysis of spatial and temporal trends in yield map data over six years. Biosyst Eng 84(4):455–466

Blaes X, Vanhalleb L, Defourny P (2005) Efficiency of crop identification based on optical and SAR image time series. Remote Sens Environ 96:352–365

Bonham-Carter GF (1994) Geographic information systems for geoscientists: modelling with GIS. Pergamon, Ontario

Bouman BAM (1995) Crop modeling and remote sensing for yield prediction. J Agric Sci 43:143–161

Bouvet A, Le Toan T (2011) Use of ENVISAT/ASAR wide-swath data for timely rice fields mapping in the Mekong River Delta. Remote Sens Environ 115:1090–1101

Boydell B, McBratney A (2002) Identifying potential within field management zones from cotton-yield estimates. Precis Agric 3(1):9–23

Brekke EB (1986) Use of GIS to analyze impacts of $C0_2$ gas development on elk calving areas. In: Proceedings of Third National MOSS Users Workshop, Bureau of Land Management, Denver, Colorado, 236 p

Brisco B, Brown RJ, Hirose T, McNairn H, Staenz K (1998) Precision agriculture and the role of remote sensing: a review. Can J Remote Sens 24(3):315–327

Broge NH, Leblanc E (2000) Comparing prediction power and stability of broadband and hyperspectral vegetation indices for estimation of green leaf area index and canopy chlorophyll density. Remote Sens Environ 76:156–172

Buckley DJA, Hendrix WG (1986) Use of geographic information systems in assessment of site suitability for land application of waste. In: Proceedings of Geographic Information Systems in Government. U.S. Army Engineer Topographic Laboratory, Ft. Belvoir, p 968

Buschman C, Nagel E (1993) In-vivo spectroscopy and internal optics of leaves as a basis for remote sensing of vegetation. Int J Remote Sens 14:711–722

Buttner G, Csillag F (1989) Comparative study of crop and soil mapping using multitemporal and multispectral SPOT and Landsat Thematic Mapper data. Remote Sens Environ 29:241–249

Campbell JB (1996) Introduction to remote-sensing, 2nd edn. The Guiford Press, London, p 622

Candiago S, Remondino F, De Giglio M, Dubbini M, Gattelli M (2015) Evaluating multispectral images and vegetation indices for precision farming applications from UAV images. Remote Sens 7(4):4026–4047

Carr PM, Carlson GR, Jacobsen JS, Nielsen GA, Skogley EO (1991) Farming soils, not fields: a strategy for increasing fertilizer profitability. J Prod Agric 4:57–61

Casady WW, Palm HL (2002) Precision agriculture, remote sensing and ground truthing. University of Missouri-Colombia EQ 453. www.muextension.missouri.edu/xplor/

Castillejo-González IS (2018) Mapping of olive trees using pansharpened quickbird images: an evaluation of pixel- and object-based analyses. Agronomy 8:288. https://doi.org/10.3390/agronomy8120288

Chakraborty M, Manjunath KR, Panigrahy S, Kundu N, Parihar JS (2005) Rice crop parameter retrieval using multi-temporal, multi-incidence angle Radarsat SARdata. ISPRS J Photogramm Remote Sens 59(5):310–322

Chan CW, Schueller JK, Miller WM, Whitney JD, Cornell JA (2004) Error sources affecting variable rate application of nitrogen fertilizer. Precis Agric 5:601–616. https://doi.org/10.1007/s11119-004-6345-2

Chappelle EW, Kim MS, McMurtrey JE III (1992) Ratio analysis of reflectance spectra (RARS): an algorithm for the remote estimation of the concentrations of chlorophyll a, chlorophyll b and carotenoids in soybean leaves. Remote Sens Environ 39(3):239–247

Chatterjee S, Santra P, Kaushik K, Ghosh D, Das I, Sanyal SK (2015) Geostatistical approach for management of soil nutrients with special emphasis on different forms of potassium considering their spatial variation in intensive cropping system of West Bengal, India. Environ Monit Assess 187:183

Chen J (1996) Evaluation of vegetation indices and modified simple ratio for boreal applications. Can J Remote Sens 22:229–242

Chen KS, Wu TD, Tsang L, Li Q, Shi J, Fung AK (2003) Emission of rough surfaces calculated by the integral equation method with comparison to three-dimensional moment method simulations. IEEE Trans Geosci Remote Sens 41:90–101

Chen P, Haboudane D, Tremblay N, Wang J, Vigneault P, Li B (2010) New spectral indicator assessing the efficiency of crop nitrogen treatment in corn and wheat. Remote Sens Environ 114:1987–1997

Chi M, Plaza A, Benediktsson JA, Sun Z, Shen J, Zhu Y (2016) Big data for remote sensing: challenges and opportunities. In: Proceedings of the IEEE, pp 2207–2219

Choker M, Baghdadi N, Zribi M, El Hajj M, Paloscia S, Verhoest NEC, Lievens H, Mattia F (2017) Evaluation of the Oh, Dubois and IEM backscatter models using a large dataset of SAR data and experimental soil measurements. Water 9:38

Chostner B (2017) See and spray: the next generation of weed control. Resour Manag 24:4–5

Christy CD (2008) Real-time measurement of soil attributes using on-the-go near infrared reflectance spectroscopy. Comput Electron Agric 61:10–19

Clay DE, Kim KI, Chang J, Clay SA, Dalsted K (2006) Characterizing water and nitrogen stress in corn using remote sensing. Agron J 98:579–587

Clevers JGPW (1997) A simplified approach for yield prediction of sugar beet based on optical remote sensing data. Remote Sens Environ 61(2):221–228

Colaco AF, Trevisan RG, Karp FHS, Molin JP (2015) Yield mapping methods for manually harvested crops. In: Stafford JV (ed) Precision Agriculture '15. Academic Publishers, Wageningen, pp 225–232
Colomina I, Molina P (2014) Unmanned aerial systems for photogrammetry and remote sensing: a review. Remote Sens 92:79–97
Corwin DL, Lesch SM (2003) Application of soil electrical conductivity to precision agriculture: theory, principles, and guidelines. Agron J 95:455–471
Cressie NAC (1990) The origins of Kriging. Math Geol 22:239–252
Crookston K (2006) A top 10 list of developments and issues impacting crop management and ecology during the past 50 years. Crop Sci 46:2253–2262
Danilov A, Pivovarova I, Krotova S (2018) Geostatistical analysis methods for estimation of environmental data homogeneity. Hindawi Sci World J 2018:1–7
Darvishzadeh R, Skidmore A, Schlerf M, Atzberger C, Corsi F, Cho M (2008) LAI and chlorophyll estimation for a heterogeneous grassland using hyperspectral measurements. ISPRS J Photogramm Remote Sens 63:409–426
Das K, Paul PK (2015) Soil moisture retrieval model by using RISAT-1, C-band data in tropical dry and sub-humid zone of Bankura district of India. Egypt J Remote Sens Space Sci 18(2):297–310
Datt B (1998) Remote sensing of chlorophyll a, chlorophyll b, chlorophyll ab and total carotenoid content in eucalyptus leaves. Remote Sens Environ 66(2):111–121
Datt B (1999) Visible/near infrared reflectance and chlorophyll content in eucalyptus leaves. Int J Remote Sens 20(14):2741–2759
Datt B, Jupp D, McVicar T, Van Niel T (2003) Time series analysis of EO-1 Hyperion data for yield estimation at an agricultural site. Geosci Remote Sens Symp, IGARSS Proc IEEE Int 1:564–566
Daughtry CST, Walthall CL, Kim MS, de Colstoun EB, McMurtrey JE (2000) Estimating corn leaf chlorophyll concentration from leaf and canopy reflectance. Remote Sens Environ 74:229–239
Davis G, Massey R, Massey R (2005) Precision agriculture: an introduction. www.muextension.missouri.edu/explore/envqual/wq0450.html
Delegido J, Alonso L, Gonzalez G, Moreno J (2010) Estimating chlorophyll content of crops from hyperspectral data using a normalized area over reflectance curve (NAOC). Int J of Applied Earth Observation and Geoinfo 1;12(3):165–74
DeTar WR, Chesson JH, Penner JV, Ojala JC (2008) Detection of soil properties with airborne hyperspectral measurements of bare fields. Trans Am Soc Agric Biol Eng 51(2):463–470
Diacono M, Rubino P, Montemurro F (2013) Precision nitrogen management of wheat: a review. Agron Sustain Dev 33:219–241
Dobermann A, Blackmore S, Cook S E, Adamchuk VI (2004) Precision farming: challenges and future directions. In: Proceedings of the 4th International Crop Science Congress, New directions for a diverse planet, 26 Sep–1 Oct 2004, Brisbane, Australia
Dobson MC, Ulaby FT (1986) Active microwave soil moisture research. IEEE Trans Geosci Remote Sens GE-24(1):23–36. https://doi.org/10.1109/TGRS.1986.289585
Doerge TA (1999) Defining management zones for precision farming. Crop Insight 8:21. Pioneer Hi-Bred International Inc
Doraiswamy PC, Moulin S, Cook PW, Stern A (2003) Crop yield assessment from remote sensing. Photogramm Eng Remote Sens 69:665–674
Drusch M, Del Bello U, Carlier S, Colin O, Fernandez V, Gascon F, Hoersch B, Isola C, Laberinti P, Martimort P, Meygre A, Spoto F, Sy O, Marchese F, Bargellini P (2012) Sentinel-2: ESA's optical high-resolution mission for GMES operational services. Remote Sens Environ 120:25–36
Dubois PC, Van Zyl J, Engman T (1995) Measuring soil moisture with imaging radars. IEEE trans. Geosci Remote Sens 33:915–926
Dutta S, Sharma SA, Khera AP, Ajai YM, Hooda RS, Mothikumar KE, Manchanda ML (1994) Accuracy assessment in cotton acreage estimation using Indian remote sensing satellite data. ISPRS J Photogramm Remote Sens 49(6):21–26

Earl R, Wheeler PN, Blackmore BS, Godwin R (1996) Precision farming – the management of variability. J Inst Agric Eng 51:18–23
Ehlers M (2003) Geoinformatics and digital earth initiatives: a German perspective. Int J Digit Earth (IJDE) 1(1):17–30
Ehrlich D, Estes J, Scepan J (1990) Improving crop type determination using satellite imagery: a study for the regione del veneto, Italy. Geocarto Int 5(2):35–47
Emmerik T, Steele-Dunne SC, Judge J, van de Giesen N (2015) Impact of diurnal variation of vegetation in vegetation water content on radar backscatter from maize during water stress. IEEE Trans Geosci Remote Sens 53(7):3855–3869
Engdahl M (2013) Multi-temporal in SAR in land-cover mapping and vegetation mapping. Doctoral Thesis. Aalto University, pp 1–119
Environmental Systems Research Institute (1993) Understanding GIS: the ARC/INFO method. Longmans, London
Erickson BJ, Johannsen CJ, Vorst JJ, Biehl LL (2004) Using remote sensing to assess stand loss and defoliation in maize. Photogram Eng Remote Sens 70:717–722
Erten E, Lopez-Sanchez JM, Yuzugullu O, Hajnsek I (2016) Retrieval of agricultural crop height from space: a comparison of SAR techniques. Remote Sens Environ 87:130–144
Esch T, Metz A, Marconcini M, Keil M (2014) Combined use of multi-seasonal high and medium resolution satellite imagery for parcel-related mapping of cropland and grassland. Int J Appl Earth Obs Geoinf 28:230–237
Fathi H, Mirzanejad M (2015) Spatial variability of agricultural characteristics to evaluate productivity potential in Iran. J Environ Sci Technol 8(1):13–24
Fikriyah VN, Darvishzadeh R, Laborte A, Khan NI, Nelson A (2019) Discriminating transplanted and direct seeded rice using Sentinel-1 intensity data. Int J Appl Earth Obs Geoinf 76:143–153
Finch HJS, Samuel AM, Lane GPF (2014) Precision farming. In: Lockhart and Wiseman's crop husbandry including grassland. Woodhead Publishing, Sawston, pp 235–244
Fischer MM (2015) Spatial analysis in geography. Int Encycl Soc Behav Sci 23:94–99. https://doi.org/10.1016/b978-0-08-097086-8.72054-x
Fleming KL, Westfall DG, Wiens DW, Brodah MC (2000) Evaluating farmer developed management zone maps for variable rate fertilizer application. Precis Agric 2:201–215
Fleming K, Heermann DF, Westfall DG (2004) Evaluating soil color with farmer input and apparent soil electrical conductivity for management zone delineation. Agron J 96:1581–1587
Foley JD, Van Dam A, Feiner SK, Hughes JF (1990) Computer graphics, principles and practice. Addison-Wesley, Reading
Foley JA, Ramankutty N, Brauman KA, Cassidy ES, Gerber JS, Johnston M, Mueller ND, O'Connell C, Ray DK, West PC, Balzer C, Bennett EM, Carpenter SR, Hill J, Monfreda C, Polasky S, Rockström J, Sheehan J, Siebert S, Tilman D, Zaks DPM (2011) Solutions for a cultivated planet. Nature 478:337–342
Fontanelli G, Paloscia S, Zribi M, Chahbi A (2013) Sensitivity analysis of X-band SAR to wheat and barley leaf area index in the Merguellil basin. Remote Sens Lett 4(11):1107–1116
Franzen DW, Peck TR (1995) Field soil sampling density for variable rate fertilization. J Prod Agric 8:568–574
Frazier BE (1989) Use of Landsat thematic mapper band ratios for soil investigations. Adv Space Res 9(1):155–158
Frazier BE, Jarvis CR (1990) A Landsat TM ratio transformation to show soil variation, Agronomy abstract 291. American Society of Agronomy, Madison
Fridgen JJ, Kitchen NR, Sudduth KA, Drummond ST, Wiebold WJ, Fraisse CW (2004) Management zone analyst (MZA): software for subfield management zone delineation. Agron J 96:100–108
Friedl MA (2018) Remote sensing of croplands. In: Comprehensive remote sensing. CRC Press, Boca Raton, pp 78–95
Frohn R, Reif M, Lane C, Autrey B (2009) Satellite remote sensing of isolated wetlands using object-oriented classification of LANDSAT-7 data. Wetlands 29:931–941

Fulton J, Hawkins E, Taylor R, Franzen A, Shannon DK, Clay DE, Kitchen NR (2018) Yield monitoring and mapping. In: Shannon DK, Clay DE, Kitchen NR (eds) Precision agriculture basics. American Society of Agronomy, Crop Science Society of America, and Soil Science Society of America, Madison, pp 63–77. https://doi.org/10.2134/precisionagbasics.2016.0089

Fung AK (1994) Microwave scattering and emission models and their applications. Artech House, Boston

Fung AK, Li Z, Chen KS (1992) Backscattering from a randomly rough dielectric surface. IEEE Trans Geosci Remote Sens 30:356–369

Gamon JA, Surfus JS (1999) Assessing leaf pigment content and activity with a reflectometer. New Phytol 143:105–117

Gamon JA, Field CB, Goulden ML, Griffin KL, Hartley AE, Joel G, Peñuelas J, Valentini R (1995) Relationships between NDVI, canopy structure, and photosynthesis in three Californian vegetation types. Ecol Appl 5(1):28–41

Gangwar S (2013) Geographical Information System (GIS) in geography: a conceptual analysis. Int J Inf Comput Technol 3(7):23–728

Gao B (1996) NDWI: a normalized difference water index for remote sensing of vegetation liquid water from space. Remote Sens Env 58:257–266

García Torres L, Peña-Barragán JM, López-Granados F, Jurado-Expósito M, Fernández-Escobar R (2008) Automatic assessment of agro-environmental indicators from remotely sensed images of tree orchards and its evaluation using olive plantations. Comput Electron Agric 61:179–191

García-Tomillo A, Mirás-Avalos JM, Dafonte-Dafonte J, Paz-González A (2017) Mapping soil texture using geostatistical interpolation combined with electromagnetic induction measurements. Soil Sci 182(8):278–284

Gebbers R, Adamchuk VI (2010) Precision agriculture and food security. Science 327:828–831

Geladi P (2003) Chemometrics in spectroscopy. Part 1. Classical chemometrics. Spectrochim Acta B 58:767–782

Gessler PE, Moore ID, McKenzie NJ, Ryan PJ (1995) Soil-landscape modelling and spatial prediction of soil attributes. Int J Geogr Inf Sci 9(4):421–432

Ghozlen NB, Cerovic ZG, Germain C, Toutain S, Latouche G (2010) Non-destructive optical monitoring of grape maturation by proximal sensing. Sensors 10:10040–10068. https://doi.org/10.3390/s101110040

Gitelson AA, Kaufmann YJ, Merzlyak MN (1996a) Use of a green channel in remote sensing of global vegetation from EOS-MODIS. Remote Sens Environ 58:289–298

Gitelson AA, Merzlyak MN, Lichtenthaler HK (1996b) Detection of red edge position and chlorophyll content by reflectance measurements near 700 nm. J Plant Physiol 148:501–508

Goel PK, Prasher SO, Landry JA, Patel RM, Bonnell RB, Viau AA, Miller JR (2003) Potential of airborne hyperspectral remote sensing to detect nitrogen deficiency and weed infestation in corn. Comput Electron Agric 38:99–124

Goetz A (1987) The portable instant display and analysis spectrometer (PIDAS). In: Proceedings of the third Airborne Imaging Spectrometer data analysis workshop, vol 87–30. JPL Publication, Pasadena, pp 8–17

Goetz AFH, Vane G, Solomon JE, Rock BN (1985) Imaging spectrometry for Earth remote sensing. Science 228(4704):1147–1153

Gomez C, Lagacherie P, Coulouma G (2008) Continuum removal versus PLSR method for clay and calcium carbonate content estimation from laboratory and airborne hyperspectral measurements. Geoderma 148:141–148

Goulding KWT (2002) Minimising losses of nitrogen from intensive agricultural systems. In: Lynch JM, Schepers JS, Ünver I (eds) Innovative soil-plant systems for sustainable agricultural practices. Proceedings of an international workshop organized by the University of Ankara, Faculty of Agriculture, Department of Soil Science 3–7 June 2002, Izmir, Turkey, pp 477–499

Goulding KWT, Jarvis S, Whitmore A (2008) Optimizing nutrient management for farm systems. Philos Trans R Soc B 363:667–680. https://doi.org/10.1098/rstb.2007.2177

Grace J, Nichol C, Disney M, Lewis P, Quaife T, Bowyer P (2007) Can we measure terrestrial photosynthesis from space directly, using spectral reflectance and fluorescence? Glob Chang Biol 13(7):1484–1497

Green M (2013) Unmanned drones may have their greatest impact on agriculture, pp 1–4. http://www.thedailybeast.com/articles/2013/03/26unmanned-drones-may-havetheir-greatest-impact-on-agriculture.html#stash.c36uDpsT.dpuf

Grenzdörffer GJ, Engel A, Teichert B (2008) The photogrammetric potential of low-cost UAVs in forestry and agriculture. Int Arch Photogramm Remote Sens Spatial Inf Sci 37(B1):1207–1214

Grisso RD, Jasa PJ, Schroeder MA, Wilcox JC (2002) Yield monitor accuracy: successful farming magazine case study. Appl Eng Agric 18(2):147–151

Grisso R, Alley M, Thomason W, Holshouser D, Roberson GT (2011) Precision farming tools: variable-rate application. Blacksburg, Virginia Cooperative Extension, College of Agriculture and Life Sciences, Virginia Polytechnic Institute and State University

Grunwald S (2009) Multi-criteria characterization of recent digital soil mapping and modelling approaches. Geoderma 152:195–207

Guo T, Kujirai T, Watanabe T (2012) Mapping crop status from an unmanned aerial vehicle for precision agriculture applications. Int Arch Photogramm Remote Sens Spatial Inf Sci 39 (B1):485–490. https://doi.org/10.5194/isprsarchives-XXXIX-B1-485-2012

Gupta VK, Jangid RA (2010) Estimation of radar backscattering coefficient of soil surface with moisture content at microwave frequencies. Int J Pure Appl Phys 6(4):509–516

Gutierrez PA, Lopez-Granados F, Jurado-Exposito JMPM, Hervas-Martinez C (2008) Logistic regression product-unit neural networks for mapping Ridolfia segetum infestations in sunflower crop using multitemporal remote sensed data. Comput Electron Agric 64:293–306

Haas T (2014) Measuring device for determining a vegetation index value of plants. US Patent No. 8823945

Haboudane D, Miller JR, Tremblay N, Zarco-Tejada PJ, Dextraze L (2002) Integrated narrow-band vegetation indices for prediction of crop chlorophyll content for application to precision agriculture. Remote Sens Environ 81:416–426

Haboudane D, Miller JR, Pattey E, Zarco-Tejada PJ, Strachan IB (2004) Hyperspectral vegetation indices and novel algorithms for predicting green LAI of crop canopies: Modeling and validation in the context of precision agriculture. Remote Sens Environ 90:337–352

Hakkim VMA, Joseph EA, Gokul AJA, Mufeedha K (2016) Precision farming: the future of Indian agriculture. J Appl Biol Biotechnol 4(06):68–72

Haldar D, Chakraborty M, Manjunath KR, Parihar JS (2014) Role of polarimetric SAR data for discrimination/biophysical parameters of crops based on canopy architecture. Int Arch Photogram Remote Sens Spatial Inf Sci XL-8:737–744

Hanna R, Allah M, Berry A, Sharobeem Y (2004) Crop estimation using satellite based and ground-based surveys (comparative study). In: Proceedings of ASAE Annual International Meeting, St. Joseph, Michigan. American Society of Agricultural Engineers, Ottawa

Hanson LD, Robert PC, Bauer M (1995) Mapping wild oats infestation using digital imagery for site specific management. In: Proceedings of site-specific management for agricultural system 27–230, March, 1994, Minneapolis, MN. ASA-CSA-SSSA, Madison, pp 495–503

Hanuschak GA, Sigman R, Craig ME, Ozga M, Luebbe RC, Cook PW, Kleweno DD, Miller CE (1980) Crop-area estimates from Landsat: transition from research and development to timely results. IEEE Trans Geosci Remote Sens GE-18(2):160–166

Hardin PJ, Hardin TJ (2010) Small-scale remotely piloted vehicles in environmental research. Geogr Compass 4:1297–1311

Hardin PJ, Jackson MW, Anderson VJ, Johnson R (2007) Detecting squarrose knapweed (Centaurea virgata Lam. Ssp. Squarrosa Gugl.) using a remotely piloted vehicle: a Utah case study. GI Sci Remote Sens 44:203–219

Hariharan S, Mandal D, Tirodkar S, Kumar V, Bhattacharya A, Lopez-Sanchez JMA (2018) Novel phenology based feature subset selection technique using random forest for multi temporal PolSAR crop classification. J Selec Top Appl Earth Observ Remote Sens 11(11):4244–4257. https://doi.org/10.1109/JSTARS.2018.2866407

Haynes RJ (1986) Mineral nitrogen in the plant-soil system. Academic Press, New York
He L, Jing MC, Chen KS (2017) Simulation and SMAP observation of sun-glint over the land surface at the L-band. IEEE Trans Geosci Remote Sens Lett 55:2589–2604
Henderson FM, Lewis AJ (1998) Principles and applications of imaging radar. Manual of remote sensing, 3rd edn. John Wiley and Sons, New York
Henderson TL, Szilagyi A, Baumgardner MF, Chen CT, Landgrebe DA (1989) Spectral band selection for classification of soil organic matter content. Soil Sci Soc Am J 53:778–784
Hendrikse J (2000) Geostatistics in ILWIS. Int Arch Photogram Remote Sens 33(B4):365–375
Hengl T, Heuvelink GBM, Stein A (2004) A generic framework for spatial prediction of soil variables based on regression-kriging. Geoderma 120(1–2):75–93
Heraud JA, Lange AF (2009) Agricultural automatic vehicle guidance from horses to GPS: how we got here, and where we are going, ASABE distinguished lecture series 33. American Society of Agricultural and Biological Engineers, St. Joseph, pp 1–67
Herwitz SR, Johnson LF, Dunagan SE, Higgins RG, Sullivan DV, Zheng J, Lobitz BM, Leung JG, Gallmeyer BA, Aoyagi M, Slye RE, Brass JA (2004) Imaging from an unmanned aerial vehicle: agricultural surveillance and decision support. Comput Electron Agric 44:49–61
Holah N, Baghdadi N, Zribi M, Bruand A, King C (2005) Potential of SAR/ENVISAT for the characterization of soil surface parameters over bare agricultural fields. Remote Sens Environ 96 (1):78–86
Holland KH, Schepers JS, Shanahan JF, Horst GL (2004) Plant canopy sensor with modulated polychromatic light. In: Mulla DJ (ed) Proceedings of 7th International conference on precision agriculture. (CDROM). University of Minnesota, Minneapolis
Hornacek M, Wagner W, Sabel D, Hong-Linh T, Snoeij P, Hahmann T, Diedrich E, Doubkova M (2012) Potential for high resolution systematic global surface soil moisture retrieval via change detection using Sentinel-1. IEEE J Select Topics Appl Earth Observ Remote Sens 5:1303–1311. https://doi.org/10.1109/JSTARS.2012.2190136
Huang XW, Senthilkurnar S, Kravchenko A, Thelen K, Qi JG (2007) Total carbon mapping in glacial till soils using near-infrared spectroscopy Landsat imagery and topographical information. Geoderma 141:34–42
Huang Y, Zhong-Xin C, Tao YU, Xiang-Zhi H, Gu XF (2018) Agricultural remote sensing big data: management and applications. J Integr Agric 17:1915–1931
Huang S, Ding J, Zou J, Liu B, Zhang J, Chen W (2019) Soil moisture retrieval based on Sentinel-1 Imagery under Sparse Vegetation Coverage. Sensors 19(3):589
Huete A (1988) A soil adjusted vegetation index (SAVI). Remote Sens Environ 25:295–309
Huete AR, Jackson RD (1988) Soil and atmosphere influences on the spectra of partial canopies. Remote Sens Environ 25:89–105
Hummel JW, Gaultney LD, Sudduth KA (1996) Soil property sensing for site-specific crop management. Comput Electron Agric 14:121–136
Hunt ER, Cavigelli M, Daughtry CST, McMurtrey JE, Walthall CL (2005) Evaluation of digital photography from model aircraft for remote sensing of crop biomass and nitrogen status. Precis Agric 6:359–378
Hunt ER, Hively WD, Fujikawa SJ, Linden DS, Daughtry CST, McCarty GW (2010) Acquisition of NIR-green-blue digital photographs from unmanned aircraft for crop monitoring. Remote Sens 2:290–305
Inoue Y, Sakaiya E (2013) Relationship between X-band backscatter coefficients from high resolution satellite SAR and biophysical variables in paddy rice. Remote Sens Lett 4 (3):288–295
Jaber SM, Al-Qinna MI (2011) Soil organic carbon modeling and mapping in a semi-arid environment using thematic mapper data. Photogramm Eng Rem Sens 77:709–719
Jang MW, Kim YH, Park NW, Hong SY (2012) Mapping paddy rice varieties using multi-temporal Radarsat SAR images. Korean J Remote Sens 28(6):653–660
Jewel N (1989) An evaluation of multi-date SPOT data for agriculture and land use mapping in the United Kingdom. Int J Remote Sens 10:939–951

Jin W, Du H, Xu X (2009) A review on unmanned aerial vehicle remote sensing and the applications. In: Remote sensing information (pp 1–8). http://en.cnki.com.cn/Article_en/CJFDTotal-NYGU201419025

Johnson RM, Richard EP (2003) Evaluation of crop and soil spatial variability in Louisiana sugarcane production systems. In: Robert PC et al (eds) Precision agriculture [CD-ROM]. Proceedings International Conference, 6th, Minneapolis, MN, 14–17 July 2002. ASA, CSSA, and SSSA, Madison

Johnson CE, Schafer RL, Young SC (1983) Controlling agricultural machinery intelligently. In: Agricultural electronics-1983 and beyond. Proceedings of the National Conference on Agricultural Electronics Applications. American Society of Agricultural Engineers, St Joseph, pp 14–119

Johnson LF, Herwitz SR, Lobitz BM, Dunagan SE (2004) Feasibility of monitoring coffee field ripeness with airborne multispectral imagery. Appl Eng Agric 20:845–849

Jordan CF (1969) Derivation of leaf area index from quality of light on the forest floor. Ecology 50:663–666

Journel AG (1986) Mining geostatistics. Math Geol 18:119–140

Karnieli A, Agam N, Pinker RT, Anderson M, Imhoff ML, Garik G, Gutman GG, Panov N, Goldberg A (2010) Use of NDVI and land surface temperature for drought assessment: merits and limitations. J Clim 23(3):618–633

Kaufman YJ, Tanre D (1992) Atmospherically Resistant Vegetation Index (ARVI) for EOS-MODIS. IEEE Trans Geosci Remote Sens 30(2):261–270

Khosla R (2001) Zoning in on precision agriculture. Colarado State Univ Agron Newslett 21(1):2–4

Khosla R (2008) Precision agriculture: challenges and opportunities in flat world. Opening ceremony presentation. In: The 9th International Conference on Precision Agriculture, July 20–23rd, 2008

Khosla R, Shaver T (2001) Zoning in on nitrogen needs. Colorado State Univ Agron Newslett 21:24–26

Kim Y, Jackson T, Lee H, Hong S (2012) Radar vegetation index for estimating the vegetation water content of rice and soybean. IEEE Geosci Remote Sens Lett 9(4):564–568

Kitchen NR, Sudduth KA, Drummond ST, Scharf PC, Palm HL, Roberts DF, Vories ED (2010) Ground-based canopy reflectance sensing for variable-rate nitrogen corn fertilization. Agron J 102:71–84

Koppe W, Gnyp ML, Hütt C, Yao Y, Miao Y, Chen X, Bareth G (2013) Rice monitoring with multi-temporal and dual-polarimetric Terra SAR-X data. Int J Appl Earth Obs Geoinf 21:568–576

Kruse F (2003) Mineral mapping with AVIRIS and EO-1 hyperion. In: Proceedings of the 12th JPL Airborne Geoscience Workshop. JPL Publication, Pasadena, pp 230–234

Kumar S (2018) Remote sensing for land resource monitoring and management. In: GPO R, Singh SK (eds) Geospatial technologies in land resources mapping, monitoring and management, geotechnologies and the environment, vol 21. Springer, Cham, pp 355–375

Kumar S, Singh RP (2016) Spatial distribution of soil nutrients in a watershed of Himalayan landscape using terrain attributes and geostatistical methods. Environ Earth Sci 75:473

Kupfer JA, Farris CA (2007) Incorporating spatial non-stationarity of regression coefficients into predictive vegetation models. Landsc Ecol 22:837–852

Lajaunie C (1984) A geostatistical approach to air pollution modelling. In: Verly G, David M, Journel AG, Marechal A (eds) Geostatistics for natural resources characterization, part 2. D Reidel Publishing, Dordrecht, pp 877–891

Lajaunie C, Courrioux G, Mmanuel L (1997) Foliation fields and 3D cartography in geology: principles of a method based on potential interpolation. Math Geol 29(4):571–584

Lamb DW, Brown RB (2001) Remote-sensing and mapping of weeds in crops. J Agric Eng Res 78:117–125

Lark RM (1998) Forming spatially coherent regions by classification of multivariate data: An example from the analysis of maps of crop yield. Int J Geogr Inform Sci 12:83–98

Lark RM (2000) Regression analysis with spatially autocorrelated error: simulation studies and application to mapping of soil organic matter. Int J Geo Inf Sci 14(3):247–264
Larson WE, Robert PC (1991) Farming by soil. In: Lal R, Pierce FJ (eds) Soil management for sustainability. Soil and Water Conservation Society, Ankeny, pp 103–112
Laurini R, Thompson D (1992) Fundamentals of spatial information systems. Academic Press, London
Laurini R, Thompson D (1998) Fundamentals of spatial information systems. A.P.I.C Series 37:1–673
Le Toan T, Ribbes F, Li-Fang W, Floury N, Kung-Hau D, Kong JA, Fujita M, Kurosu T (1997) Rice crop mapping and monitoring using ERS-1 data based on experiment and modeling results. IEEE Trans Geosci Remote Sens 35:41–56
Lelong CCD, Pinet PC, Poilvé H (1998) Hyperspectral imaging and stress mapping in agriculture: a case study on wheat in Beauce (France). Remote Sens Environ 66:179–191
Lelong CCD, Burger P, Jubelin G, Roux B, Labbe S, Barett F (2008) Assessment of unmanned aerial vehicles imagery for quantitative monitoring of wheat crop in small plots. Sensors 8:3557–3585
Lesage JP (1999) Spatial Econometrics using MATLAB: a manual for the spatial econometrics toolbox functions, available at https://www.spatial-econometrics.com
Lesage JP (2005) Spatial Econometrics. In: Kempf-Leonard K (ed) The encyclopedia of social measurement, volume 3. Elsevier, Amsterdam, pp 613–619
Li FY, Li XM, Chen LY, Guo B, Qi ZP (2008) The analysis of soil nutrient situations in Wanning of Hainan Province. Chinese J Soil Sci 29:1284–1287
Li F, Miao Y, Hennig SD, Gnyp ML, Chen X, Jia L, Bareth G (2010) Evaluating hyperspectral vegetation indices for estimating nitrogen concentration of winter wheat at different growth stages. Precis Agric 11:335–357
Li Y, Gong JH, Wang DC, An LP, Li R (2013) Sloping farmland identification using hierarchical classification in the Xi-He region of China. Int J Remote Sens 34:545–562
Li F, Miao Y, Feng G, Yuan F, Yue S, Gao X, Liu Y, Liu B, Ustin SL, Chen X (2014) Improving estimation of summer maize nitrogen status with red edge-based spectral vegetation indices. Field Crops Res 157:111–123
Lichtenthaler HK, Lang M, Sowinska M, Heisel F, Miehé JA (1996) Detection of vegetation stress via a new high resolution fluorescence imaging system. J Plant Physiol 148(5):599–612
Lievens H, Verhoest NEC (2011) On the retrieval of soil moisture in wheat fields from L-band SAR based on water cloud Modeling, the IEM, and effective roughness parameters. IEEE Trans Geosci Remote Sens Lett 8:740–744
Lilienthal H, Ponomarev M, Schnug E (2004) Application of LASSIE to improve agricultural field experimentation. Landbauforschung Voelkenrode 1:21–26
Lindblom J, Lundström C, Ljung M, Jonsson A (2017) Promoting sustainable intensification in precision agriculture: review of decision support systems development and strategies. Precis Agric 18:309–331
Link A, Panitzki M, Reusch S (2002) Hydro N-sensor: tractormounted remote sensing for variable nitrogen fertilization. In: Robert PC (ed) Precision agriculture [CD-ROM]. Proceedings of 6th international conference on precision agriculture. ASA, CSSA, and SSSA, Madison, pp 1012–1018
Linsley CM, Bauer F (1929) Illinois Agricultural Experiment Station. Circular. University of Illinois, Urbana, p 346
Liu P (2015) A survey of remote-sensing big data. Front Environ Sci 3:1–6
Liu X, Zhao K, Xu J, Wang F (2008) Spatial variability of soil organic matter and nutrients in paddy fields at various scales in southeast China. Environ Geol 53:1139–1147
Liu C, Chen Z, Wang D, Li D (2019) Assessment of the X- and C-band polarimetric SAR data for plastic-mulched farmland classification. Remote Sens 11(6):660. https://doi.org/10.3390/rs11060660

Long DS, Engel RE, Carpenter FM (2005) On-combine sensing and mapping of wheat protein concentration. Crop Manag. https://doi.org/10.1094/CM-2005-0527-01-RS

Lopez-Sanchez JM, Ballester-Berman D, Marquez-Moreno Y (2007) Model limitations and parameter estimation methods for agricultural applications of polarimetric SAR interferometry. IEEE Trans Geosci Remote Sens 45(11):3481–3493

Lucieer A, Malenovsky Z, Veness T, Wallace L (2014) HyperUAS-imaging spectroscopy from a multirotor unmanned aircraft system. J Field Robotics 31(4):571–590

Maguire DJ, Goodchild MF, Rhind DW (eds) (1991) Geographical information systems: principles and applications (2 Volumes). Longman Scientific and Technical, Harlow

Mahmoudabadi E, Karimi A, Haghnia GH, Sepehr A (2017) Digital soil mapping using remote sensing indices, terrain attributes, and vegetation features in the rangelands of northeastern Iran. Environ Monit Assess 89(10):500

Mani PK (2000) Remote sensing –a modern tool for agricultural resource management. Everyman's Sci 35(2):57–62

Mao DR, Zhang CD (1991) Studies on the model and experimental design for recommendation of fertilization. Chinese J Soil Sci 22(5):216–218

Martin D (1991) Geographic information systems and their socioeconomic applications. Routledge, London

Matheron G (1962) Traite de geostatistiqueappliquee. Mermoires du Bureau de Researches Geologiqueset Mminieres. Tome I, No. 14, Editions Technip, Paris, Tome II: le krigeage, No. 24. Editions BRGM, Paris

Matthews J (1983) Some challenges for engineers in agriculture. J R Agric Soc Engl 144:146–158

McCann BL, Pennock DJ, Van Kessel C, Walley FL (1996) The development of management units for site specific farming. In: Robert PC, Rust RH, Larson WE (eds) Precision agriculture. Proceedings of International Conference, 3rd, Minneapolis, MN, 23–26 June 1996. ASA, CSSA, and SSSA, Madison, pp 295–302

McMurtrey JE, Chappelle EW, Kim MS, Meisinger JJ, Corp LA (1994) Distinguish nitrogen fertilization levels in field corns (Zea mays L.) with actively induced fluorescence and passive reflectance measurements. Remote Sens Environ 47:36–44

McNairn H, Brisco B (2004) The application of C-band polarimetric SAR for agriculture: a review. Can J Remote Sens 30(3):525–542

McNairn H, Shang J (2016) A review of multitemporal synthetic aperture radar (SAR) for crop monitoring. In: Ban Y (ed) Multitemporal remote sensing. Springer, Cham, pp 317–340

McSweeney KM, Gessler PE, Slater B, Hammer RD, Bell I, Peterson GW (1994) Towards a new framework for modelling the soil-landscape continuum. In: Factors of soil formation: a fiftieth anniversary retrospective, special publication 33. Soil Science Society of America, Madison, pp 127–145

Meena RS, Mitran T, Kumar S, Yadav G, Bohra JS, Datta R (2018) Application of remote sensing for sustainable agriculture and forest management. Inf Process Agric 5:295–297

Mehta NS, Rajawat AS, Bahuguna IM, Mehta DS, Srimal AK (1993) Geological potential of ERS-1 SAR data: observations in parts of Aravali and Thar Desert, western India. In: Proceedings of second ERS-1 symposium, space at the service of our environment, Hamburg, Germany, 11–14 October 1993, ESA-SP-361, pp 931–936

Merton R, Huntington J (1999) Early simulation results of the ARIES-1 satellite sensor for multi-temporal vegetation research derived from AVIRIS. ftp://popo.jpl.nasa.gov/pub/docs/workshops/99_docs/41.pdf. NASA Jet Propulsion Lab, Pasadena

Metwally MS, Shaddad SM, Liu M, Yao R, Abdo AI, Li P, Jiao J, Chen X (2019) Soil properties spatial variability and delineation of site-specific management zones based on soil fertility using fuzzy clustering in a hilly field in Jianyang, Sichuan, China. Sustainability 11(7084):1–19. https://doi.org/10.3390/su11247084

Miao Y, Mulla DJ, Randall GW, Vetsch JA, Vintila R (2007) Predicting chlorophyll meter readings with aerial hyperspectral remote sensing for in-season site-specific nitrogen management of

corn. In: Stafford JV (ed) Precision agriculture '07. Academic Publisher, Wageningen, pp 635–641
Miao Y, Mulla DJ, Randall G, Vetsch J, Vintila R (2009) Combining chlorophyll meter readings and high spatial resolution remote sensing images for in-season site-specific nitrogen management of corn. Precis Agric 10:45–62
Mohan BK, Porwal A (2015) Hyperspectral image processing and analysis. Curr Sci 108:833–841
Mohan S, Mehta NS, Patel P (1990) Radar remote sensing for land applications – a review. Scientific Report No ISRO-SAC-SR36–91. Space Applications Centre, Ahmedabad
Moller M, Alchanatis V, Cohen Y, Meron M, Tsipris J, Naor A et al (2007) Use of thermal and visible imagery for estimating crop water status of irrigated grapevine. J Exp Bot 58:827–838
Mondal P, Tewari VK (2007) Present status of precision farming: a review. Int J Agric Res 2 (1):1–10
Mondal P, Tewari VK, Rao PN, Verma RB, Basu M (2004) Scope of precision agriculture in India. In: Proceedings of international conference on emerging technologies in agricultural and food engineering, December 14–17, 2004. Department of Agricultural and Food Engineering, IIT, Kharagpur, p 103
Moore ID, Gessler PE, Nielsen GA, Peterson GA (1993) Soil attribute prediction using terrain analysis. Soil Sci Soc Am J 57(2):443–452
Morain SA, Williams DL (1975) Wheat production estimates using satellite images. Agron J 67:361–364
Moran MS, Inoue Y, Barnes EM (1997) Opportunities and limitations for image-based remote sensing in precision crop management. Remote Sens Environ 61:319–346
Moran MS, Alonso L, Moreno JF, Mateo MPC, Fernando de la Cruz D, Montoro A (2012) A RADARSAT-2 quad-polarized time series for monitoring crop and soil conditions in Barrax, Spain. IEEE Trans Geosci Remote Sens 50(4):1057–1070
Moslemzadeh M, Salarijazi M, Soleymani S (2011) Application and assessment of kriging and cokriging methods on groundwater level estimation. J Am Sci 7(7):34–39
Moulin AP, Beckie HJ, Pennock DJ (1998) Strategies for variable rate nitrogen fertilization in hummocky terrain. In: Robert PC, Rust RH, Larson WE (eds) Precision Agriculture. Proceedings of the Fourth International Conference. ASA/CSSA/SSSA, Madison, pp 839–846
Mukul M (1998) A spatial statistics approach to the quantification of finite strain variation in penetratively deformed thrust sheets: an example from the Sheeprock Thrust Sheet, Sevier Fold-and-Thrust belt, Utah. J Struct Geol 20(4):371–384
Mulla DJ (1991) Using geostatistics and GIS to manage spatial patterns in soil fertility. In: Kranzler G (ed) Automated agriculture for the 21st century. American Society of Agriculture Engineers, St. Joseph, pp 336–345
Mulla DJ (1993) Mapping and managing spatial patterns in soil fertility and crop yield. In: Robert P, Larson W, Rust R (eds) Soil specific crop management. American Society of Agronomy, Madison, pp 15–26
Mulla DJ (1997) Geostatistics, remote sensing and precision farming. In: Stein A, Bouma J (eds) Precision agriculture: spatial and temporal variability of environmental quality, Ciba foundation symposium 210. Wiley, Chichester, pp 100–119
Mulla DJ (2013) Twenty five years of remote sensing in precision agriculture: key advances and remaining knowledge gaps. Biosyst Eng 114:358–371
Mulla DJ (2016) Spatial variability in precision agriculture. In: Shekhar S, Xiong H, Zhou X (eds) Encyclopedia of GIS. Springer International Publishing, Cham. https://doi.org/10.1007/978-3-319-23519-6_1652-1
Mulla DJ, Hammond MW (1988) Mapping of soil test results from large irrigation circles, pp. 169–176. In: Proceedings 39th Annual far west regional fertilizer conference, Bozeman, MT, July 11–13
Mulla D, Khosla R (2015) Historical evolution and recent advances in precision farming. In: Lal R, Stewart BA (eds) Soil-specific farming: precision agriculture. CRC Press. Taylor and Francis Group, Boca Raton, pp 1–35
Mulla DJ, McBratney AB (2000) Soil spatial variability. In: Sumner ME (ed) Handbook of soil science. CRC Press, Boca Raton, pp A321–A352

Mulla DJ, Miao Y (2016) Precision farming. In: Thenkabail PS (ed) Land resources monitoring, modeling, and mapping with remote sensing. CRC Press, Boca Raton, pp 161–178
Mulla DJ, Perillo CA, Cogger CG (1996) A site-specific farm-scale GIS approach for reducing groundwater contamination by pesticides. J Environ Qual 25:419–425
Mumby PJ, Edwards AJ (2002) Mapping marine environments with IKONOS imagery: enhanced spatial resolution can deliver greater thematic accuracy. Remote Sens Environ 82:248–257
Murai S (1999) GIS work book: fundamental and technical courses, vols 1 & 2. National Space Development Agency of Japan (NASDA)/Remote Sensing Technology Center of Japan (RESTEC), Japan Association of surveyors
Murrell TS (2004) Using advanced technologies to refine nitrogen management at the farm scale: a case study from the US Midwest. In: Mosier AR, Syers JK, Freney JR (eds) Agriculture and the nitrogen cycle. Assessing the impacts of fertilizer use on food production and the environment. SCOPE 65. Ch. 11. Island Press, Washington, DC, pp 155–165
Myers DE (2008) Aniosotropic radial basis functions. Int J Pure Appl Math 42:197–203
Mzuku M, Khosla R, Reich R, Inman D, Smith F, MacDonald L (2005) Spatial variability of measured soil properties across site-specific management zones. Soil Sci Soc Am J 69:1572–1579
Nabi A, Narayan S, Afroza B, Mushtaq F, Mufti S, Ummyiah HM, Malik A (2017) Precision farming in vegetables. J Pharmacogn Phytochem 6(6):370–375
Navalgund RR, Jayaraman V, Roy PS (2007) Remote sensing applications: an overview. Curr Sci 93(12):1747–1766
Nebiker S, Annen A, Scherrer M, Oesch D (2008) A light-weight multispectral sensor for micro UAV: opportunities for very high resolution airborne remote sensing. Int Arch Photogramm Remote Sens Spatial Inf Sci 37(B1):1193–1200
Neupane J, Guo W (2019) Agronomic basis and strategies for precision water management: a review. Agronomy 9(2):87
Nex F, Remondino F (2014) UAV for 3D mapping application: a review. Appl Geomat 6:1–15
Nolan SC, Goddard TW, Lohstraeter G (2000) Assessing management units on rolling topography. In: Robert PC et al (eds) Precision agriculture. Proceedings International Conference, 5th, Bloomington, MN, 16–19 July 2000. ASA, CSSA, and SSSA, Madison
Nourzadeh M, Mahdian MH, Malakouti MJ, Khavazi K (2012) Investigation and prediction spatial variability in chemical properties of agricultural soil using geostatistics. Arch Agron Soil Sci 58 (5):461–475
Oetter DR, Cohen WB, Berterretch EM, Maiersperger TK, Kennedy RE (2000) Land cover mapping in an agricultural setting using multiseasonal Thematic Mapper data. Remote Sens Environ 76:139–155
Oh Y (2004) Quantitative retrieval of soil moisture content and surface roughness from multipolarized radar observations of bare soil surfaces. IEEE Trans Geosci Remote Sens 42 (3):596–601
Olea RA (2009) A practical primer on geostatistics: U.S. Geological Survey, Open-File Report 2009-1103. U.S. Geological Survey, Reston, p 346
Olesen JE, Sørensen P, Thomsen IK, Eriksen J, Thomsen AG, Berntsen J (2004) Integrated nitrogen input systems in Denmark. In: Mosier AR, Syers JK, Freney JR (eds) Agriculture and the nitrogen cycle. Assessing the impacts of fertilizer use on food production and the environment. SCOPE 65, ch. 9. Island Press, Washington, DC, pp 129–140
Oliver MA (2010) Geostatistical applications for precision agriculture. Springer, Dordrecht
Oliver MA (2013) Precision agriculture and geostatistics. How to manage agriculture more exactly. R Stat Soc 4:7–22
Oliver MA, Carroll ZL (2004) Description of spatial variation in soil to optimize cereal management. Project Report no. 330. Home-Grown Cereals Authority, London
Olson K (1998) Precision agriculture: current economic and environmental issues. In: Proceedings of the Sixth Joint Conference on Food, Agriculture, and the Environment, Minneapolis, MN, USA, 31 August–2 September 1998

Oppelt N, Mauser W (2004) Hyperspectral monitoring of physiological parameters of wheat during a vegetation period using AVIS data. Int J Remote Sens 25:145–159

Paciorek CJ, Schervish MJ (2006) Spatial modelling using a new class of nonstationary covariance functions. Environmetrics 17:483–506

Paelinck JHP, Klaassen LH (1979) Spatial Econometrics. Saxon House, Farnborough

Palmer RJ (1996) Positioning aspects of site-specific applications. In: Proceedings of site-specific management for agricultural system, 27–30 March, 1996. ASA-CSSA-SSSA, Madison, pp 613–618

Paloscia S, Pettinato S, Santi E (2012) Combining L-and X-band SAR data for estimating biomass and soil moisture of agricultural fields. Eur J Remote Sens 45:99–109

Pan G, Gaard D, Moss K, Heiner T (1993) A comparison between cokriging and ordinary kriging: case study with a Polymetallic deposit. Math Geol 25(3):377–398

Panciera R, Tanase MA, Lowell K, Walker JP (2013) Evaluation of IEM, Dubois, and Oh radar backscatter models using airborne L-band SAR. IEEE Trans Geosci Remote Sens 52:4966–4979

Panigrahy S, Sharma SA (1997) Mapping of crop rotation using multidate Indian remote sensing satellite digital data. ISPRS J Photogramm Remote Sens 52:85–91

Panigrahy S, Chakraborty M, Sharma SA, Kundu N, Ghose SC, Pal M (1997) Early estimation of rice acre using temporal ERS-1 synthetic aperture radar data – a case study for Howrah and Hooghly districts of West Bengal, India. Int J Remote Sens 18:1827–1833

Panigrahy S, Chakraborty M, Manjunath KR, Kundu N, Parihar JS (2000) Evaluation of RADARSAT ScanSAR synthetic aperture radar data for rice crop inventory and monitoring. J Indian Soc Remote Sens 28(1):59–65

Parihar JS, Oza MP (2006) FASAL: an integrated approach for crop assessment and production forecasting. In: Robert J, Kuligowski, Parihar JS, Saito G (eds) Proceedings of Society of Photo-Optical Instrumentation Engineers, Agricultural and hydrology applications (vol 6411), pp 641101–641113

Partel V, Kakarla SC, Ampatzidis Y (2019) Development and evaluation of a low-cost and smart technology for precision weed management utilizing artificial intelligence. Comput Electron Agric 157:339–350

Patel P, Srivastava HS (2013) RADARSAT-2 announcement of opportunity project on soil moisture, surface roughness and vegetation parameter retrieval using SAR polarimetry, Technical Report: SAC/EPSA/MPSG/CVD/TDP-R&D/01/13. Indian Space Research Organisation, Ahmedabad, pp 1–81

Patel NK, Medhavy TT, Patnaik C, Hussain A (1995) Multi-temporal ERS-1 SAR data for identification of rice crop. J Indian Soc Remote Sens 23:33–39

Patel P, Srivastava HS, Panigrahy S, Parihar JS (2006a) Comparative evaluation of the sensitivity of multi-polarized multifrequency SAR backscatter to plant density. Int J Remote Sens 27 (2):293–305

Patel P, Srivastava HS, Navalgund RR (2006b) Estimating wheat yield: An approach for estimating number of grains using cross polarized Envisat-1 ASAR data. Microwave Remote Sensing of the Atmosphere and Environment. In: Valinia A, Uratsuka S, Tapan Misra (eds). Proceedings of Soci Photo-Optical Instrument Engineers, 6410 (641009) pp 01–12

Patil SS, Bhalerao SA (2013) Precision farming: the most scientific and modern approach to sustainable agriculture. Int Res J Sci Eng 1(2):21–30

Patil VC, Shanwad UK (2009) Relevance of precision farming to Indian agriculture. In: Second national conference on agro-informatics and precision farming, December 2009

Penuelas J, Filella I, Lloret P, Munoz F, Vilajeliu M (1995) Reflectance assessment of mite effects on apple trees. Int J Remote Sens 16:2727–2733

Pettinato S, Santi E, Paloscia S, Pampaloni P, Fontanelli G (2013) The inter comparison of X-band SAR images from COSMO-SkyMed and TerraSAR-X satellites: case studies. Remote Sens 5:2928–2942

Pfost D, Cassady W, Shanon K (1998) Precision agriculture, Global Positiong System (GPS). Water quality, WQ 451. University Extension. University of Missouri-System, Columbia, pp 1–6
Pfost D, Casady W, Shannon K (1999) Global positioning system receivers. Site-specific management guidelines, 6th edn. Potash & Phosphate Institute, Norcross
Pierce FJ, Nowak P (1999) Aspects of precision agriculture. Adv Agron 67:1–85
Pieri C (1997) Planning a sustainable land management: the hierarchy of user needs. ITC J 3 (4):223–228
Pinter PJ Jr, Hatfield JL, Schepers JS, Barnes EM, Moran MS, Daughtry CST, Upchurch DR (2003) Remote sensing for crop management. Photogramm Eng Remote Sens 69:647–664
Primicerio J, Di Gennaro SF, Fiorillo E, Genesio L, Lugato E, Matese A, Vaccari FP (2012) A flexible unmanned aerial vehicle for precision agriculture. Precis Agric 13:517–523. https://doi.org/10.1007/s11119-012-9257-6
Qi J, Chehbouni A, Huete AR, Keer YH, Sorooshian S (1994) A modified soil vegetation adjusted index. Remote Sens Environ 48:119–126
Qi J, Wang C, Inoue Y, Zhang R, Gao W (2004) Synergy of optical and radar remote sensing in agricultural applications.In: Gao W, Shaw DR (ed) Ecosystems' dynamics, agricultural remote sensing and modeling, and site-specific agriculture. Proceedings of the international society for optical engineering (SPIE) August 2004, Bellingham, WA, 5153, p 153–158. https://doi.org/10.1117/12.514562
Qi ZP, Wei ZY, Li FY, Tang SM (2009) Chinese J Soil Sci 40:1292–1296
Qiu B, Fan Z, Zhong M, Tang Z, Chen C (2014) A new approach for crop identification with wavelet variance and JM distance. Environ Monit Assess 186:7929–7940
Rahman M, Moran M, Thoma D, Bryant R, Collins CH, Jackson T, Orr BJ, Tischler M (2008) Mapping surface roughness and soil moisture using multi-angle radar imagery without ancillary data. Remote Sens Environ 112:391–402
Raju PLN (2003) Fundamentals of geographic information systems. In: Sivakumar MVK, Roy PS, Harmsen K, Saha SK (eds) Workshop: satellite remote sensing and GIS applications in agricultural meteorology, India
Rango A, Laliberte AS, Herrick JE, Winters C, Havstad K, Steele C, Browning D (2009) Unmanned aerial vehicle-based remote sensing for rangeland assessment, monitoring, and management. J Appl Remote Sens 3(033542):1–15
Rao NR (2008) Development of a crop-specific spectral library and discrimination of various agricultural crop varieties using hyperspectral imagery. Int J Remote Sens 29:131–144
Rao NR, Garg PK, Ghosh SK (2007) Estimation of plant chlorophyll and nitrogen concentration of agricultural crops using EO-1 Hyperion hyperspectral imagery. J Agric Sci 146:1–11
Raun WR, Solie JB, Johnson GV, Stone ML, Mullen RW, Freeman KW et al (2002) Improving nitrogen use efficiency in cereal grain production with optical sensing and variable rate application. Agron J 94:815–820
Ray SS, Panigrahy S, Parihar JS (2010) Precision Farming in Indian Context. Geospatial World 12/08/2010. http://geospatialmedia.net
Reddy GPO (2018) Satellite Remote Sensing Sensors: Principles and Applications. In: Reddy GPO, Singh SK (eds). Geospatial technologies in land resources mapping, monitoring and management (pp 21–43). Springer International Publishing. https://doi.org/10.1007/978-3-319-78711-4
Ren GX, Yang GH, Zhang ZM, Nie JF (2002) Fertilizer application model on winter wheat with plastic film mulching in Weibei Dryland. J Northwest Sci-Tech, Univ Agric For 30:38–46
Reusch S, Jasper J, Link A (2010) Estimating crop biomass and nitrogen uptake using Cropspec, a newly developed active crop-canopy reflectance sensor. In: Proceedings of the 10th International Conference on Positron Annihilation (ICPA), Denver, CO, USA, 18–21 July 2010, p 381
Richardson AJ, Weigand C (1977) Distinguishing vegetation from soil background information. Photogramm Eng Remote Sens 43(12):1541–1552
Risser MD, Calder CA (2015) Regression-based covariance functions for nonstationary spatial modeling. Environmetrics 26:284–297

Risser MD, Caldery CA, Berrocalz VJ, Berrettx C (2019) Nonstationary spatial prediction of soil organic carbon: implications for stock assessment decision making. Ann Appl Stat 13 (1):165–188

Rodriguez D, Fitzgerald GJ, Belford R, Christensen LK (2006) Detection of nitrogen deficiency in wheat from spectral reflectance indices and basic crop eco-physiological concepts. Aust J Agric Res 57(7):781–790. https://doi.org/10.1071/ar05361

Rondeaux G, Steven M, Baret F (1996) Optimization of soil-adjusted vegetation indices. Remote Sen Environ 55:95–107

Rougean JL, Breon FM (1995) Estimating PAR absorbed by vegetation from bidirectional reflectance measurements. Remote Sens Environ 51:375–384

Rouse JW Jr, Hass RH, Schell JA, Deering DW (1973) Monitoring vegetation systems in the great plains with ERTS. In: Proceedings 3rd Earth Resources Technology Satellite (ERTS) symposium, vol 1. NASA SP-351, NASA, Washington, DC, pp 309–317

Royal K (1998) Creating good management zones: how to capitalize from flexible data integration. Modern Agric Fall:26–28

Ryerson RA, Dobbins RN, Thibault C (1985) Timely crop area estimates from Landsat. Photogramm Eng Remote Sens 51:1735–1743

Sahebi M, Angles J (2010) An inversion method based on multi-angular approaches for estimating bare soil surface parameters from RADARSAT-1. Hydrol Earth Syst Sci 14:2355–2366

Sahebi MR, Angles J, Bonn F (2002) A comparison of multi-polarization and multi-angular approaches for estimating bare soil surface roughness from spaceborne radar data. Can J Remote Sens 28:641–652

Sahoo RN (2011) Precision farming: concepts, limitations, and opportunities in Indian agriculture. In: Sharma AR, Behera UK (eds) Resource conserving techniques in crop production (pp 439–450). Scientific Publishers in India

Salami E, Berrado C, Pastor E (2014) UAV flight experiments applied to the remote sensing of vegetated areas. Remote Sens 6:11051–11081

Samborski SM, Tremblay N, Fallon E (2009) Strategies to make use of plant sensors-based diagnostic information for nitrogen recommendations. Agron J 101:800–816

Santra P, Chopra UK, Chakraborty D (2008) Spatial variability of soil properties and its application in predicting surface map of hydraulic parameters in an agricultural farm. Curr Sci 95:937–945

Satalino G, Mattia F, Davidson MW, Le Toan T, Pasquariello G, Borgeaud M (2002) On current limits of soil moisture retrieval from ERS-SAR data. IEEE Trans Geosci Remote Sens 40:2438–2447

Sawaya KE, Olmanson LG, Heinert NJ, Brezonik PL, Bauer ME (2003) Extending satellite remote sensing to local scales: land and water resource monitoring using high-resolution imagery. Remote Sens Environ 88:144–156

Scharf PC, Shannon DK, Palm HL, Sudduth KA, Drummond ST, Kitchen NR, Mueller LJ, Hubbard VC, Oliveira LF (2011) Sensor-based nitrogen applications out-performed producer-chosen rates for corn in on-farm demonstrations. Agron J 103:1683–1691

Schepers JS, Francis DD, Vigil M, Below FE (1992) Comparison of corn leaf nitrogen concentration and chlorophyll meter readings. Commun Soil Sci Plant Anal 23:2173–2187

Schoknecht N, Tille P, Purdie B (2004) Soil landscape mapping in south-western Australia. Overview of methods and outputs. Resource management technical report 280. Department of Agriculture, Government of Western Australia, Kensington

Schroder D, Haneklaus S, Schung E (1997) Information management in precisionagriculture with LORIS. In: Stafford JV (ed) Precision Agriculture'97, Technology, IT and management, vol II. BIOS Scientific Publishers Ltd, Oxford, pp 821–826

Scotford IM, Miller PCH (2005) Applications of spectral reflectance techniques in northern European cereal production: a review. Biosyst Eng 90:235–250

Seelan SK, Laguette S, Casady GM, Seielstad GA (2003) Remote sensing applications for precision agriculture: a learning community pproach. Remote Sens Environ 88:157–169

Serrano L, Penuelas J, Ustin SL (2002) Remote sensing of nitrogen and lignin in Mediterranean vegetation from AVIRIS data: decomposing biochemical from structural signals. Remote Sens Environ 81:355–364

Shanahan JF, Schepers JS, Francis DD, Varvel GE, Wilhelm WW, Tringe JM (2001) Use of remote sensing imagery to estimate corn grain yield. Agron J 93:583–589

Shi J, Wang J, Hsu AY, O'Neill PE, Engman ET (1997) Estimation of bare surface soil moisture and surface roughness parameter using L band SAR image data. IEEE Trans Geosci Remote Sens 35(5):1254–1266

Shippert P (2004) Why use hyperspectral imagery? Photogramm Eng Remote Sens 70(4):377–396

Sivasankar T, Kumar D, Srivastava HS, Patel P (2018) Advances in radar remote sensing of agricultural crops: a review. Int J Adv Sci Eng Inf Technol 8(4):1126–1137

Skriver H (2012) Crop classification by multitemporal C- and L-Band single- and dual-polarization and fully polarimetric SAR. IEEE Trans Geosci Remote Sens 50(6):2138–2149. https://doi.org/10.1109/TGRS.2011.2172994

Slaymaker O (2001) The role of remote sensing in geomorphology and terrain analysis in the Canadian Cordillera. Int J Appl Earth Obs Geoinf 3(1):11–17

Smith RC, Adams G, Stephens J, Hick PT (1995) Forecasting wheat yield in a Mediterranean-type environment from the NOAA satellite. Aust J Agric Res 46:113–125

Sökefeld M (2010) Variable rate technology for herbicide application herbicide application. In: Precision crop protection-the challenge and use of heterogeneity. Springer, Heidelberg, pp 335–347

Sonobe R, Yamaya Y, Tani H, Wang X, Kobayashi N, Mochizuki K (2017) Assessing the suitability of data from Sentinel-1A and 2A for crop classification. GI Sci Remote Sens 54 (6):918–938. https://doi.org/10.1080/15481603.2017.1351149

Srinivasan S (2015) Spatial regression models. In: Encyclopedia of GIS: living edition. Springer, Cham. https://doi.org/10.1007/978-2-319-23519-6_1294-2

Sripada RP, Heiniger RW, White JG, Weisz R (2005) Aerial color infrared photography for determining late-season nitrogen requirements in corn. Agron J 97(5):1443–1451

Sripada RP, Heiniger RW, White JG, Crozier CR, Meijer AD (2006) Attempt to validate a remote sensing-based late-season corn nitrogen requirement prediction system. Crop Manag 5(1). https://doi.org/10.1094/CM-2006-0405-01-RS

Sripada RP, Schmidt JP, Dellinger AE, Beegle DB (2008) Evaluating multiple indices from a canopy reflectance sensor to estimate corn N requirements. Agron J 100:1553–1561

Srivastava HS, Patel P, Navalgund RR (2006) Application potentials of synthetic aperture radar interferometry for land-use mapping and crop height estimation. Curr Sci 91(6):783–788

Srivastava HS, Patel P, Sharma Y, Navalgund RR (2009) Large area soil moisture estimation using multi-incidence-angle RADARSAT-1 SAR data. IEEE Trans Geosci Remote Sens 47 (8):2528–2534. https://doi.org/10.1109/TGRS.2009.2018448

Srivastava HS, Sivasankar T, Sharma PK (2016) Biophysical parameters retrieval using RISAT-1 hybrid polarimetric SAR data. In: National Symposium on Recent Advances in Remote Sensing and GIS with Special Emphasis on Mountain Ecosystems, Dehradun, India

Stafford JV (2000) Implementing precision agriculture in the 21st century. J Agric Eng Res 76:267–275

Stone ML, Solie JB, Raun WR, Whitney RW, Taylor SL, Ringer JD (1996) Use of spectral radiance for correcting in season fertilizer nitrogen deficiencies in winter wheat. Trans ASAE 39:1623–1631

Stoorvogel JJ, Kooistra L, Bouma J (2016) Managing soil variability at different spatial scales as a basis for precision agriculture. In: Lal R, Stewart BA (eds) Soil specific farming- precison agriculture. CRC Press, Boca Raton, pp 37–71

Sudduth KA, Kitchen NR, Drummond ST (2011) Nadir and oblique canopy reflectance sensing for N application in corn. Liccosec 7:162–172

Sullivan DG, Shaw JN, Rickman D (2005) IKONOS imagery to estimate surface soil property variability in two Alabama physiographies. Soil Sci Soc Am J 69:1789–1798

Swain KC, Jayasuriya HPW, Salokhe VM (2007) Suitability of low-altitude remote sensing images for estimating nitrogen treatment variations in rice cropping for precision agriculture adoption. J Appl Remote Sens 1:013547

Swain KC, Thomson SJ, Jayasuriya HPW (2010) Adoption of an unmanned helicopter for low altitude remote sensing to estimate yield and total biomass of a rice crop. Trans ASABE 53:21–27

Sylvester G (2018) E-agriculture in action: drones for agriculture. FAO and International Telecommunication Union, Bangkok, pp 1–112

Sylvester-Bradley R, Lord E, Sparkes DL, Scott RK, Wiltshire JJJ, Orson J (1999) An analysis of the potential of precision farming in Northern Europe. Soil Use Manag 15:1–8

Tan SY (2017) Developments in hyperspectral sensing. In: Pelton JN et al (eds) Handbook of satellite applications. Springer International Publishing, Cham. https://doi.org/10.1007/978-3-319-23386-4_101

Tan CP, Ewe HT, Chuah HT (2011) Agricultural crop-type classification of multi-polarization SAR images using a hybrid entropy decomposition and support vector machine technique. Int J Remote Sens 2(22):7057–7071

Tang QF, Yang AF, Wang TZ, Tang SM (2007) Spatial variation of soil main nutrients on arable land in Ding'an county. Chinese J Trop Crops 28:44–50

Thenkabail SP, Ward AD, Lyon JG, Merry CJ (1994a) Thematic mapper vegetation indices for determining soybean and corn crop growth parameters. Photogramm Eng Remote Sens 60 (4):437–442

Thenkabail SP, Ward AD, Lyon JG (1994b) LANDSAT-5 Thematic Mapper models of soybean and corn crop characteristics. Int J Remote Sens 15(1):49–61

Thenkabail PS, Smith RB, Ede P (2000) Hyperspectral vegetation indices and their relationships with agricultural crop characteristics. Remote Sens Environ 71:158–182

Thenkabail PS, Enclona EA, Ashton MS, Van Der Meer V (2004a) Accuracy assessments of hyperspectral waveband performance for vegetation analysis applications. Remote Sens Environ 91(2–3):354–376

Thenkabail PS, Enclona EA, Ashton MS, Legg C, Jean De Dieu M (2004b) Hyperion, IKONOS, ALI, and ETM+ sensors in the study of African rainforests. Remote Sens Environ 90:23–43

Thenkabail PS, Lyon JG, Huete A (2010) Hyperspectral remote sensing of vegetation and agricultural crops: knowledge gain and knowledge gap after 40 years of research. Ch. 28. In: Thenkabail PS, Lyon JG, Huete A (eds) Hyperspectral remote sensing of vegetation. CRC Press, Boca Raton, p 705

Thenkabail PS, Lyon JG, Huete A (2011) Advances in hyperspectral remote sensing of vegetation and agricultural croplands. In: Thenkabail PS, Lyon JG, Huete A (eds) Hyperspectral remote sensing of vegetation. CRC Press, Boca Raton, pp 3–36

Thiam S, Eastmen RJ (1999) Chapter on vegetation indices. In: Guide to GIS and image processing, volume 2; Idrisi Production. Clarke University, Worcester, pp 107–122

Thorp KR, Tian LF (2004) A review on remote sensing of weeds in agriculture. Precis Agric 5:477–508

Thylen L, Murphy DP (1996) The control of errors in momentary yield data from combine harvesters. J Agric Eng Res 64(4):271–278

Tilling SK, O'Leary GJ, Ferwerda JG, Jones SD, Fitzgerald GJ, Rodriguez D, Belford R (2007) Remote sensing of nitrogen and water stress in wheat. Field Crops Res 104:77–85. https://doi.org/10.1016/j.fcr.2007.03.023

Tucker CJ (1979) Red and photographic infrared linear combinations for monitoring vegetation. Remote Sens Environ 8:127–150

Turker M, Ozdarici A (2011) Field-based crop classification using SPOT4, SPOT5, IKONOS and QuickBird imagery for agricultural areas: a comparison study. Int J Remote Sens 32:9735–9768

Turner D, Lucieer A, Watson C (2011) Development of an unmanned aerial vehicle (UAV) for hyper resolution vineyard mapping based on visible, multispectral, and thermal imagery. In:

Abstracts of 34th International Symposium on Remote Sensing of Environment, Sydney, Australia, 10–15 April 2011
Ulaby FT, Batlivala PP, Dobson MC (1978) Microwave backscatter dependence on surface roughness, soil moisture, and soil texture: part I-bare soil. IEEE Trans Geosci Electron 16:286–295
Ulaby FT, Allen CT, Eger G, Kanemasu E (1984) Relating the microwave backscattering coefficient to leaf area index. Remote Sens Environ 14:113–133
Ulaby FT, Moore RK, Fung AK (1986) Microwave remote sensing: active and passive, vol. II. Artech House, Norwood
Ulaby FT, Sarabandi K, Dobson MC (1999) Development of SAR algorithm for mapping soil moisture and vegetation biomass, Technical Report 032601-F. University of Michigan, Ann Arbor, pp 1–24
Uppala D, Kothapalli RV, Poloju S, Mullapudi SSVR, Dadhwal VK (2015) Rice crop discrimination using single date RISAT-1 hybrid (RH, RV) polarimetric data. Photogramm Eng Remote Sens 81(7):557–563
Valcarce-Diñeiro R, Lopez-Sanchez JM, Sánchez N, Arias-Pérez B, Martínez-Fernández J (2019) Influence of incidence angle in the correlation of C-band polarimetric parameters with biophysical variables of rainfed crops. Can J Remote Sens. https://doi.org/10.1080/07038992.2019.1579051
van Evert FK, Gaitán-Cremaschi D, Fountas S, Kempenaar C (2017) Can precision agriculture increase the profitability and sustainability of the production of potatoes and olives? Sustainability 9:1863. https://doi.org/10.3390/su9101863
Vanac M (2014) Drones are the latest idea to improve farm productivity. The Columbus Dispatch. pp 1–3. http://www.dispatch.com/content/stories/business/2013/09/19/eyes-in-the-skies.html
Vaudour E, Bel L, Gilliot JM, Coquet Y, Hadjar D, Cambier P, Michelin J, Houot S (2013) Potential of spot multispectral satellite images for mapping topsoil organic carbon content over Peri-Urban croplands. Soil Sci Soc Am J 77:2122–2139. https://doi.org/10.2136/sssaj2013.02.0062
Vellidis G, Perry CD, Durrence JS, Thomas DL, Hill RW, Kvien CK, Hamrita TK, Rains G (2001) The peanut yield monitoring system. Am Soc Agric Eng 44(4):775–785
Vieira SR, Villa CE, Vázquez EV, González AP (2007) Geostatistical analysis of soil fertility data sampled in two consecutive years in Castilla, Spain. In: Stafford JV (ed) Precision agriculture '07. Academic Publishers, Wageningen, pp 257–263
Viscarra Rossel RA, Walvoort DJJ, McBratney AB, Janik LJ, Skjemstad JO (2006) Visible, near infrared, mid infrared or combined diffuse reflectance spectroscopy for simultaneous assessment of various soil properties. Geoderma 131:59–75
Vogelmann JE, Rock BN, Moss DM (1993) Red edge spectral measurements from sugar maple leaves. Int J Remote Sens 14:1563–1575
Vorovencii I (2009) The hyperspectral sensors used in satellite and aerial remote sensing. Bull Transilvania Univ Brasov 2(51) Series II: 51–56
Waltz FA, Holm EA (1986) Modeling narcotic crop-growing sites with MOSS. In: Proceedings Third National MOSS Users Workshop. Bureau of Land Management, Denver, p 236
Wang JR (1980) The dielectric properties of soil-water mixtures at microwave frequencies. Radio Sci 15:977–985
Wang MH (1999) Field information collection and process technology. Agric Mech 7:22–24
Wang F, Wu Y (2010) Research and applications of UAS Borne Remote Sensing, pp 1–8. http://en.cnki.com.cn/Article_en/CJFDTotal-NYGU201419025, pp 3–4
Wang XR, Chen XP, Zhang FS, Mao DR (1998) Application of fertilization model for fertilizer recommendation in China. Plant Nutr Fertil Sci 4:67–74
Wang L, Sousa WP, Gong P, Biging GS (2004) Comparison of IKONOS and QuickBird images for mapping mangrove species on the Caribbean coast of Panama. Remote Sens Environ 91:432–440
Wang FM, Huang J, Wang XZ (2008) Identification of optimal hyperspectral bands for estimation of rice biophysical parameters. J Integ Plant Biol 50(3):291–299

Wang H, Bai YL, Yang LP, Lu YL, Wang L (2010) Application of fertilizer recommendation based on ASI systematic approach in maize in Northeast China. Soil Fertil Sci China 5:31–37
Warren G, Metternicht G (2005) Agricultural applications of high-resolution digital multispectral imagery: evaluating within-field spatial variability of canola (Brassica napus) in Western Australia. Photogramm Eng Remote Sens 71:595–602
Webster R, Oliver MA (2007) Geostatistics for environmental scientists, 2nd edn. John Wiley and Sons Ltd, London
Wei Z, Qi Z (2013) The application of GIS techniques in soil testing and fertilizer recommendations: part I a review. Adv Mater Res 610–613:3693–3696
Weis M, Andujar D, Peteinatos GG, Gerhards R (2013) Improving the determination of plant characteristics by fusion of four different sensors. In: Stafford JV (ed) Precision agriculture '13. Academic Publisher, Wageningen, pp 63–69
Welch R, Remillard MM, Fung SS (1986) Monitoring aquatic vegetation and water quality with a geographic information system. In: Proeedings of Geographic Information Systems Workshop. American Society Photogrammetric Remote Sensing, Atlanta, Georgia, p 425
Whelan B, Taylor J (2013) Precision agriculture for grain production systems. CSIRO Publishing, Collingwood, pp 1–199
White MS (1984) Modeling forest pest impacts – aided by a GIS in a decision support system framework. In: Proceedings Third National MOSSUsers Workshop. Bureau of Land Management, Denver, p 236
Wilcox GH, Frazier BE, Ball ST (1994) Relationship between Soil Organic Garbon and Landsat TM Data in Eastern Washington. Photogramm Eng Remote Sens 60(6):777–781
Wright C, Gallant A (2007) Improved wetland remote sensing in Yellowstone National Park using classification trees to combine TM imagery and ancillary environmental data. Remote Sens Environ 107:582–605
Wu C, Wang L, Niu Z, Gao S, Wu M (2010) Nondestructive estimation of canopy chlorophyll content using Hyperion and Landsat/TM images. Int J Remote Sens 31:2159–2167
Wu F, Wang C, Zhang H, Zhang B, Tang Y (2011) Rice crop monitoring in South China with RADARSAT-2 quad-polarization SAR data. IEEE Geosci Remote Sensing Lett 8(2):196–200
Xavier B, Vanhalle L, Defourny P (2005) Efficiency of crop identification based on optical and SAR image time series. Remote Sens Environ 96:352–365
Xia FQ, Guo TW, Jiang XF, Zhang XC (2011) Research progress on soil testing and fertilizer recommendation. Gansu Agric Sci Technol 7:46–49
Xiang H, Tian L (2011) Method for automatic georeferencing aerial remote sensing (RS) images from an unmanned aerial vehicle (UAV) platform. Biosyst Eng 108:104–113
Xu W (1996) Conditional curvilinear stochastic simuation using pixel-based algorithms. Math Geol 28(7):937–949
Xue J, Su B (2017) Significant remote sensing vegetation indices: a review of developments and applications. J Sensors 2017:1–17
Yang C, Everitt JH (2002) Relationships between yield monitor data and airborne multidate multispectral digital imagery for grain sorghum. Precis Agric 3:373–388
Yang C, Everitt JH, Bradford JM, Escobar DE (2000) Mapping grain sorghum growth and yield variations using airborne multispectral digital imagery. Trans ASAE 43:1927–1938
Yang Z, Rao MN, Elliott NC, Kindler SD, Popham TW (2005) Using ground-based multispectral radiometry to detect stress in wheat caused by greenbug (Homoptera Aphididiae) infestation. Comput Electron Agric 47(2):121–135
Yang C, Everitt JH, Murden D (2011) Evaluating high resolution SPOT 5 satellite imagery for crop identification. Comput Electron Agric 75:347–354
Yang S, Zhao X, Li B, Hua G (2012) Interpreting RADARSAT-2 quad-polarization SAR signatures from rice paddy based on experiments. IEEE Geosci Remote Sens Lett 9:65–69
Yang R, Rossiter DG, Liu F, Lu Y, Yang F, Yang F, Zhao Y, Li D, Zhang G (2015) Predictive mapping of topsoil organic carbon in an alpine environment aided by Landsat TM. PLoS One 10 (10):e0139042

Yao HL, Tang L, Tian, Brown RL, Bhatnagar D, Cleveland TE (2010) Using hyperspectral data in precision farming applications. Ch. 25. In: Thenkabail PS, Lyon JG, Huete A (eds) Hyperspectral remote sensing of vegetation. CRC Press, Boca Raton, p 705

Young DS (1987) Random vectors and spatial analysis by geostatistics for geotechnical applications. Math Geol 19(6):467–479

Zarco-Tejada PJ, Miller JR, Morales A, Berjó NA, Aguera J (2004) Hyperspectral indices and model simulation for chlorophyll estimation in open-canopy tree crops. Remote Sens Environ 90:463–476

Zhang Y (2011) Introduction to geostatistics-course notes (pp 1–31)

Zhang C, Kovacs JM (2012) The application of small unmanned aerial systems for precision agriculture: a review. Precis Agric 13:693–712

Zhang M, Li MZ, Liu G, Wang MH (2008) Yield mapping in precision farming. In: Li D (ed) Computer and computing technologies in agriculture, The International Federation for Information Processing 259, vol 2. Springer, Boston, pp 1407–1410

Zhang B, Wu D, Zhang L, Jiao Q, Li Q (2012) Application of hyperspectral remote sensing for environment monitoring in mining areas. Environ Earth Sci 65(3):649–658

Zhao D, Huang L, Li J, Qi J (2007) A comparative analysis of broadband and narrowband derived vegetation indices in predicting LAI and CCD of a cotton canopy. ISPRS J Photogramm Remote Sens 62(1):25–33

Zhao X, Huang N, Song XF, Li ZY, Niu ZJ, Waves M (2016) A new method for soil moisture inversion in vegetation-covered area based on Radarsat 2 and Landsat 8. J Infrared Millim Waves 35:609–616

Zhu Y, Zhou D, Yao X, Tian Y, Cao W (2007) Quantitative relationships of leaf nitrogen status to canopy spectral reflectance in rice. Aust J Agric Res 58(11):1077–1085. https://doi.org/10.1071/AR06413

Zirschky J (1985) Geostatistics for environmental monitoring and survey design. Environ Int 11:515–524

Zribi M, Baghdadi N, Holah N, Fafin O (2005) New methodology for soil surface moisture estimation and its application to ENVISAT-ASAR multi-incidencedata inversion. Remote Sens Environ 96:485–496

Chapter 3
Retrieval of Crop Biophysical Parameters Using Remote Sensing

Nilimesh Mridha, Debasish Chakraborty, Anima Biswal, and Tarik Mitran

Contents

N. Mridha (✉)
ICAR-National Institute of Natural Fibre Engineering and Technology, ICAR, Kolkata, West Bengal, India
e-mail: nilimesh.mridha@gmail.com

D. Chakraborty
ICAR Research Complex for North Eastern Hill Region (ICAR-RC-NEH), Umiam, Meghalaya, India
e-mail: debasish.chakraborty@icar.gov.in

A. Biswal
Agroecosystem and Modeling Division, Agricultural Sciences and Applications Group, National Remote Sensing Centre, Department of Space, ISRO, Hyderabad, Telangana, India
e-mail: biswal_a@ncsc.gov.in

T. Mitran
Soil and Land Resources Assessment Division, National Remote Sensing Centre, Department of Space, ISRO, Hyderabad, Telangana, India
e-mail: tarikmitran@nrsc.gov.in

T. Mitran et al. (eds.), *Geospatial Technologies for Crops and Soils*,
https://doi.org/10.1007/978-981-15-6864-0_3

Abstract Consistent and near-real-time crop growth monitoring over a large scale is a very crucial step for digital agriculture. An efficient tool for accurate retrieval of different biophysical parameters is the basic requirement for crop growth monitoring. Quantitative estimation of various crop biochemical and biophysical variables with reliable accuracy is very useful for different applications related to agriculture, ecology, and climate. This chapter briefly describes different methods and models for the retrieval of various crop biophysical parameters using remote sensing (RS) approaches. Leaf area index (LAI) is a vital attribute in many land-surface vegetation and climate models which have many important applications. Leaf chlorophyll and leaf water content are key parameters in many ecological processes, such as photosynthesis, respiration, transpiration, and they also provide stress information. The fraction of absorbed photosynthetically active radiation (fAPAR) by crop vegetation is used as an essential climate variable (ECVs) and critical input in many land-surface, crop growth and climate, ecological, water, and carbon cycle models. This chapter highlights various retrieval methods of crop biophysical parameters, including empirical, semiempirical, hybrid, physically based models with various inversion algorithms like look-up table, neural network, genetic algorithms, Bayesian networks, support vectors, etc.

Keywords Biophysical · Crops · Chlorophyll · Leaf Area Index · Remote Sensing · fAPAR · Inversion

Abbreviations

ANN	Artificial Neural Network
DWI	Depth Water Index
CCC	Canopy Chlorophyll Content
CRM	Canopy Reflectance Model
ECVs	Essential Climate Variables
EM	Electromagnetic Spectrum
ETM	Enhanced Thematic Mapper
EWT	Equivalent Water Thickness
fAPAR	Fraction of Absorbed Photosynthetically Active Radiation
fCover	Fractional Cover
GA	Genetic Algorithm
GPR	Gaussian Processes Regression
IO	Iterative Optimization
LAI	Leaf Area Index
LCC	Leaf Chlorophyll Content
Landsat	Land Satellite
LUT	Lookup Table
MLRA	Machine Learning Regression Algorithms
NDWI	Normalized Difference Water Index
N	Nitrogen

NPP	Net Primary Productivity
OLI	Operational Land Imager
PAR	Photosynthetically Active Radiation
PCR	Principal Component Regression
PLSR	Partial Least Squares Regression
R^2	Coefficient of Determination
REGFLEC	Regularized Canopy Rfelectance Model
REP	Red-edge Position
RF	Random Forests
RMSE	Root Mean Square Error
RR	Ridge (Regulated) Regression
RS	Remote Sensing
RTM	Radiative Transfer Model
SAC	Spectral Angle Cosine
SMLR	Stepwise Multiple Linear Regression
SVM	Support Vector Machine
SVR	Support Vector Regression
SWI	Spectral Similarity Water Indices
SWIR	Shortwave Infrared
TIR	Thermal Infrared
TM	Thematic Mapper
UAV	Unmanned Aerial Vehicle
VIs	Vegetation Indices
WAAI	Water Absorption Area Index
WCM	Water Cloud Model
WDVI	Weighted Difference Vegetation Index
WSN	Wireless Sensor Networks

3.1 Introduction

Quantitative estimation of various crop biochemical and biophysical parameters with reliable accuracy is very useful for various application related to agriculture, ecology, and environment (Houborg et al. 2007; Sehgal et al. 2013). The distribution of these parameters over spatial and temporal scale plays a very significant role to develop improved prediction models of crop yield and abiotic stress detection at a regional level. Accurate estimation of crop biophysical as well as biochemical variables through RS can help in understanding the physiological status of vegetation (Peñuelas et al. 1994; Meena et al. 2018), phenology and seasonal dependence (Bélanger and Richards 1995), and serve as bioindicators of vegetation stress (Zarco-Tejada et al. 2001), which are crucial for sustainable agriculture. Among various parameters leaf area index (LAI), fraction of absorbed photosynthetically active radiation (fAPAR), chlorophyll content, and water content, etc. are of primary

importance. RS techniques provide unique capabilities like repetivity, stability, cost-effectiveness, and global to regional-level coverage which is enabling the widespread use of estimation of biophysical variables in studies of land surface and atmospheric processes (Houborg and Boegh 2008; Vohland et al. 2010). LAI, defined as one-sided leaf surface area per unit ground surface area (Chen and Black 1992), is used for understanding various ecological processes such as photosynthesis, transpiration, evapotranspiration, etc. and estimation of net primary production (NPP) of terrestrial ecosystems (Bonan 1993; Meena et al. 2018a). Researchers showed that LAI is a vital parameter for crop assessment, crop yield, and production as well as ecosystem productivity model both in global and regional scales (Rasmussen 1997; Running et al. 1989). It is also important for biosphere–atmosphere interaction in some general circulation models (Yao et al. 2008). Apart from LAI, parameters such as vegetation fraction and fAPAR have been included in the list of essential terrestrial climate variables (Baret et al. 2013; Shelestov et al. 2017). These parameters can be employed to monitor and quantify crop health status within agriculture monitoring tasks under the Global Agriculture Monitoring (GLAM) initiative (Becker-Reshef et al. 2010). It is also very efficient to estimate crop yield (Kogan et al. 2013; Kolotii et al. 2015) and predict crop production (Gallego et al. 2014). At the same time, monitoring spatial patterns of biochemical composition in plant foliage is required to understand growth dynamics in plant communities (Hilker et al. 2012) and serve as bioindicators of vegetation stress (Luther and Carroll 1999; Zarco-Tejada et al. 2001).

Plant biophysical parameter retrieval using RS techniques can be broadly classified as empirical (statistical or variable based) and analytical or physical (radiative) approaches (Ustin et al. 2004; Hilker et al. 2012). Both these approaches have their pros and cons. Empirical approaches are simple and computationally efficient, making them highly desirable for large area RS applications (Tucker 1980; Colombo et al. 2003; Souza et al. 2010). But these approaches lack generality, thereby restricting the scale of application (Baret 1991; Hall et al. 1995). The physical models describe the interaction of radiation within the canopy based on laws of physics, providing an explicit relation between the canopy variables (biophysical and biochemical) and canopy reflectance (Houborg and Boegh 2008; Verger et al. 2011). These techniques consider the relationship between the canopy variables with that of the surface reflectance anisotropy, making them scientifically robust (Bacour et al. 2002a; Pisek et al. 2011; Román et al. 2011; Chakraborty et al. 2015). These techniques are scientifically robust and possess the capability of generalization, but are limited by (a) the complexity of the process of canopy radiation interaction and (b) use of inversion methods (Combal et al. 2002; Walthall et al. 2004; Baret and Buis 2008; Yao et al. 2008). Therefore, a significant amount of research has been done to overcome both these limitations. Different model inversion techniques like numerical optimization, lookup table (LUT), artificial neural networks (ANN), genetic algorithm (GA), principal component inversion (PCI), support vector machines (SVM) regression, and several hybrid mechanisms are used (Jacquemoud et al. 2000; Fang et al. 2003; Meroni et al. 2004; Walthall et al. 2004; Satapathy and Dadhwal 2005; Durbha et al. 2007; Darvishzadeh et al. 2008; Kravchenko 2009;

Tuia et al. 2011; Sehgal et al. 2016). The objective of this chapter is to highlight various retrieval methods of crop biophysical parameters, including an empirical, semiempirical, hybrid, physically based model with various inversion algorithms.

3.2 Scope of Remote Sensing–Based Parameter Retrieval

Since 1972, with the launch of first civil earth observing satellite, Land Satellite 1 (LANDSAT-1), RS technology has evolved as a vital tool for spatial and temporal analysis of various bio-geophysical processes at different scales (Goward and Williams 1997). Programs like Large Area Crop Inventory Experiment (LACIE) and Agriculture & Resources Inventory Surveys through Aerospace Remote Sensing (Ag RISTARS) proved that RS techniques could be successfully used for crop identification, crop condition monitoring, acreage estimation, and production estimation (Moran et al. 1997). To serve all these purposes, the retrieval of biophysical parameters is the prerequisite step. Since the early days of the 1970s, researchers across the world have been developing various techniques and methods to retrieve the biophysical parameter using RS datasets. LAI, fractional cover (fCover), fAPAR, and chlorophyll contents are the most common biophysical attributes retrieved using RS-based approaches. Among all these, LAI representing the actual leaf surface available for energy and mass exchange between the canopy and atmosphere is the most frequently retrieved biophysical parameter. LAI is the key variable to model crop evapotranspiration, biomass assimilation, and partitioning and yield estimation (Broge and Mortensen 2002). fCover is related to gap fraction in the nadir direction and mostly used for decoupling vegetation and soil effects for modeling processes like evapotranspiration (Baret et al. 2006a). fAPAR is directly related to LAI and a key variable for various crop growth simulation models and the primary productivity model (Baret et al. 2006a, b). Plant chlorophyll content, an indicator of photosynthetic potential, is the most important biochemical constituent of the plant. Leaf chlorophyll content (LCC) is a sensitive indicator of crop response to nitrogen (N) stress, as N is an important constituent of chlorophyll structure and internal greenness of the leaf (Baret and Fourty 1997). Crop phenological information is the key variable controlling the partitioning of assimilates in all the crop models that simulate crop growth, development, and yield. Several researchers have used RS-based crop phenology information (such as the start of the season, seasonal greenness, the peak of the season, end of the season, etc.) that enhanced the agro-ecosystem model outputs (Xin et al. 2002; Karnieli 2003).

3.3 Approaches to Remote Sensing–Based Retrieval

Several approaches have been developed worldwide to retrieve biophysical attributes from RS datasets by many researchers. These approaches are broadly categorized into two groups: (i) empirical approach based on statistical regression models linking RS information with field-measured biophysical attributes (Pu and Cheng 2015; Kira et al. 2016); (ii) physical modeling approach based on radiative transfer models (RTMs) simulating the canopy reflectance followed by inversion of these RTMs to retrieve the targeted parameters (Campos-Taberner et al. 2016; Féret et al. 2017). In the empirical approach, linear statistical–based regression, nonlinear methods like machine learning (deep learning, random forest, etc.) and dimensionality reduction methods such as partial least square regression (PLSR) etc. are applied for retrieval process and mapping at a larger scale. This approach is based on the computation of various narrow and broadband spectral vegetation indices and spectral transformation, followed by the development of statistical models. Though it is computationally fast, it lacks transferability, making its application limited in varied spatial and temporal scales. On the other hand, physical approaches are based on RTM, which considers canopy reflectance–based non-leaf angle distribution, specular reflection of leaves, Lambertian characteristics of soil, and hotspot effects of vegetation canopy, etc. Hence, these models are robust and transferable than statistical models. At the same time, the major limitation in the physical approach is the "ill-posed problem," where a different combination of plant trait values can produce the same reflectance spectra. The parameters like chlorophyll contents, etc. are often retrieved by these models with higher accuracy as compared to biomass, protein content, etc. This remains a challenge because these traits do not have a prominent spectral signature (Homolova et al. 2013). The above-mentioned approaches expanded into subcategories and combinations further, with progress in data analytics, algorithms, and computational techniques. Hence, various retrieval approaches can be further categorized into four subcategories (Verrelst et al. 2015a, b), which are discussed in the following section.

3.3.1 Methods Based on Parametric Regression

RS-based parametric regression method is based on the assumption of an explicit relation between spectral observations and the biophysical parameters of interest. Typically, a band combination is selected followed by suitable arithmetic formulation. This includes computation of spectral vegetation indices (VIs) followed by fitting of linear or nonlinear functions with the crop biophysical parameter of interest. These VIs are mostly designed to enhance vegetation-sensitive spectral features by reducing background noise (Glenn et al. 2008; Clevers 2014). Traditionally these VIs are developed for sensors with broad spectral bands. A list of popular broadband and narrowband indices commonly used for crop biophysical parameter

retrieval is presented in Table 3.1. Researchers have proposed optimal band combinations using two-dimensional correlation matrices, developed based on various established spectral indices (Thenkabail et al. 2002; Mariotto et al. 2013; Rivera et al. 2014). A "best performing index" can be selected out of these so-called optimized or generic indices. At the same time, none of these VIs can potentially use all available spectral information from quasi-continuous spectral datasets in case of narrowband hyperspectral images. In this context, various "shape indices" are developed to extract valuable information from quasi-continuous narrow bands to the full extent.

The shape indices mostly used for crop monitoring are confined around the red-edge position (REP). It corresponds to the position of the wavelength at the maximum of the first derivative in the spectral reflectance curve in the red-edge region (670–780 nm). This REP is sensitive and related to the canopy variables like LAI, LCC, and canopy chlorophyll content (CCC), etc. These correlations have been used by several researchers to derive LAI, LCC, and CCC (Clevers and Kooistra 2012; Delegido et al. 2013). Many researchers have also proposed normalized index, taking finite integrals defined by specific spectral regions over visible and red-edge wavelengths (Mutanga et al. 2005; Malenovský et al. 2006; Delegido et al. 2010). Sometimes spectral derivatives are transformed into an index, instead of integration, to relate the crop biophysical parameters (Zarco-Tejada et al. 2002; Le Maire et al. 2004). Continuum removal (CR) is another technique generally applied over the full spectrum to get individual absorption features by normalizing it with a common baseline (Clark and Roush 1984). It is employed to generate various maps on chlorophyll content (Broge and Leblanc 2001), N content (Schlerf et al. 2010; Mitchell et al. 2012), grassland biomass (Cho et al. 2007), and foliar water content (Stimson et al. 2005), etc. Many researchers have also reported that the use of narrow-band indices which are originally developed from broadbands do not always improve the retrieval accuracy. In some cases, it may result in poor parameter prediction (Broge and Leblanc 2000; Broge and Mortensen 2002). Alternatively, the narrowband indices originally developed to retrieve leaf biochemical attributes are mostly better than the broadband (Haboudane et al. 2004; Zarco-Tejada et al. 2005).

Parametric methods usually end in the regression model calibrated with experimental data collected from a different environment, sensors set up at different scales, and hence, highly empirical. Their predictive performance is vulnerable to the different environmental and experimental setup, like change in surface properties or sun-sensor geometry (Verrelst et al. 2008, 2010), etc. Therefore, these models are most suitable and perform well under local conditions, and their application is limited in a broader operational setting. The selection of appropriate bands, formulation of suitable indices, and fitting appropriate parametric function are the basic criteria for parametric regression to retrieve biophysical parameters. However, Verrelst et al. (2015a, b) reported an important issue in using spectral VIs for retrieval of biophysical parameters under the empirical approaches. It is necessary to establish and validate the significant relationship between VIs and the biophysical parameters of interest to adopt such approaches. This often demands costly and

Table 3.1 List of major spectral indices used in crop biophysical parameter retrieval

Spectral index	Use	Formula	References
CAI	Applicable for exposed surface containing dried plant material	$0.5(\rho_{2000} + \rho_{2200}) - \rho_{2100}$	Daughtry (2001)
DVI	Distinguish between soil and vegetation, LAI retrieval	NIR − RED	Tucker (1979) and Yang et al. (2007)
EVI	Useful for higher LAI	$\frac{(\text{NIR} - \text{RED})}{(\text{NIR} + 6 * \text{RED} - 7.5 * \text{BLUE} + 1)}$	Huete et al. (2002)
GCI	Leaf chlorophyll content	$\left(\frac{\rho_{\text{NIR}}}{\rho_{\text{Green}}}\right) - 1$	Gitelson et al. (2003)
GNDVI	More sensitive to chlorophyll than NDVI	$\frac{(NIR - \text{GREEN})}{(\text{NIR} + \text{GREEN})}$	Gitelson and Merzlyak (1998)
NGRDI	Chlorophyll retrieval	$\frac{(\text{GREEN} - \text{RED})}{(\text{GREEN} + \text{RED})}$	Tucker (1979) and Singhal et al. (2019)
MCARI	Relative abundance of chlorophyll	$[(\rho_{700} - \rho_{670}) - 0.2 (\rho_{700} - \rho_{550})] * (\rho_{700}/\rho_{670})$	Daughtry et al. (2002)
MSI	Sensitive to leaf water content	$\left(\frac{\rho_{1599}}{\rho_{819}}\right)$	Ceccato et al. (2001)
NDVI	Measure of heathy and green vegetation, LAI retrieval	$\frac{(\text{NIR} - \text{RED})}{(\text{NIR} + \text{RED})}$	Rouse et al. (1974) and Tillack et al. (2014)
OSAVI	Used for sparse vegetation with soil background, canopy chlorophyll retrieval	$\frac{(NIR - RED)}{(NIR + \text{RED} + 0.16)}$	Rondeaux et al. (1996) and Clevers et al. (2017)
PRI	Sensitive to change in carotenoid pigment	$\left(\frac{\rho_{531} - \rho_{570}}{\rho_{531} + \rho_{570}}\right)$	Gamon et al. (1997)
RENDVI	Precision agriculture and crop stress detection	$\left(\frac{\rho_{750} - \rho_{705}}{\rho_{750} + \rho_{705}}\right)$	Gitelson and Merzlyak (1994)
REPI	Canopy stress detection, LAI retrieval	Wavelength of the maximum derivative of reflectance in red edge region (690–740 nm)	Curran et al. (1995); Pu et al. (2003); Sun et al. (2020)
SASI	Soil and vegetation moisture	Based on the NIR (858 nm) and SWIR (1240 and 1640 nm) MODIS bands	Khanna et al. (2007)
SAVI	Suppresses the effects of soil, LAI retrieval	$\frac{1.5(NIR - RED)}{(NIR + \text{RED} + 0.5)}$	Huete (1988); Broge and Leblanc (2000)
SR	Easy to understand and valid over wide range of LAI	$\frac{\text{NIR}}{\text{RED}}$	Birth and McVey (1968) and Eklundh et al. (2003)

(continued)

Table 3.1 (continued)

Spectral index	Use	Formula	References
TCARI	Relative abundance of chlorophyll	$3[(\rho_{700} - \rho_{670}) - 0.2 (\rho_{700} - \rho_{550}) * (\rho_{700}/\rho_{670})]$	Haboudane et al. (2004)

NB: The formula is designed on the reflectance value for the spectral region/specific wavelength; *DVI* Difference vegetation index, *EVI* Enhanced vegetation index, *NDVI* Normalized difference vegetation index, *NGRDI* Normalized green–red difference index, *GNDVI* Green normalized difference vegetation index, *SR* Simple ratio, *SAVI* Soil-adjusted vegetation index; *OSAVI* Optimized soil-adjusted vegetation index, *GCI* Green chlorophyll index, *MCARI* Modified chlorophyll absorption ratio index, *RENDVI* Red-edge normalized difference vegetation index; *REPI* Red-edge position index, *TCARI* Transformed chlorophyll absorption reflectance index, *PRI* Photochemical reflectance index, *MSI* Moisture stress index, *CAI* Cellulose absorption index, *SASI* Shortwave angle slope index

time-intensive measurement programs over a wide range of crops and varied canopy conditions along with combinations of view/sun geometry.

3.3.2 Nonparametric Regression Methods

Nonparametric methods are directly defining regression models based on RS-derived information. Hence, selection of spectral band explicitly and its transformation is not required like parametric methods. Linear nonparametric regression including stepwise multiple linear regression (SMLR), principal component regression (PCR), PLSR, and ridge regulated regression (RR), etc. are usually preferred because of their optimal performance and simplicity. SMLR is useful for the selection of appropriate spectral bands carrying important information on vegetation parameters (Dorigo et al. 2007). Ramoelo et al. (2011) employed both SMLR and PLSR to retrieve foliar N and phosphorus (P) in combination with CR techniques using field spectrometer measurements. Both SMLR and PLSR have been used successfully for retrieving soil properties particularly soil N content (Bartholomeus et al. 2012; Miphokasap et al. 2012). PLSR technique can be used to retrieve foliage nitrogen content using hyperspectral data (Coops et al. 2003; Huang et al. 2004). Many studies show potentialities of the PLSR technique to retrieve crop biophysical properties like LAI, stem biomass, and leaf nutrient concentrations, etc. (Cho et al. 2007; Im et al. 2009).

For the last few decades, a variety of nonparametric, nonlinear models also known as machine learning regression algorithms (MLRAs) have been developed and used extensively. Such techniques are capable to capture nonlinear relationships of image features without explicitly knowing the underlying data distribution, hence robust to work with various data types. They are also flexible enough to incorporate a priori knowledge and can pool different data types into the analysis. Breiman (2001) employed decision tree learning including Bagging Decision Trees (BDT) and

Random Forest (RF) approaches to improve the prediction accuracy of the retrieved crop biophysical parameter. However, decision trees are often used as a classification algorithm rather than in regression studies. Recently, RF approach has been successfully used for mapping various vegetation properties like biomass (Le Maire et al. 2011; Mutanga et al. 2012; Adam et al. 2014), LAI (Vuolo et al. 2013), canopy N (Li et al. 2014), etc. These studies demonstrated that the RF technique has performed better than conventional parametric linear or nonparametric methods. Similarly, artificial neural networks (ANN) is another popular nonlinear and nonparametric approach followed for parameter retrieval from RS datasets. Since the mid-1990s ANN has been successfully used for mapping vegetation parameters (Jin and Liu 1997; Paruelo and Tomasel 1997; Kimes et al. 1999). The most common type of ANN is a feed-forward structure, facilitating the information flow in a unidirectional forward mode where no cycling or looping is defined. This feed-forward ANN uses experimental (field) data for training the model. ANN is successfully used to estimate foliar N concentrations (Huang et al. 2004) and LAI (Jensen et al. 2012) using hyperspectral data. Other techniques like kernel method (Camps-Valls and Bruzzone 2009) are also reported in RS-based parameter retrieval in bio-geo sciences. SVM is a supervised learning model with associated learning algorithms and the most frequently used algorithm in nonparametric regression methods. Initially, it has introduced for image classification studies, however, later support vector regression (SVR) successfully utilized for retrieval of continuous vegetation parameters. Karimi et al. (2008) had applied SVR to retrieve crop biophysical attributes like plant height, foliar N concentration, and leaf chlorophyll content, etc. from hyperspectral RS data. Verrelst et al. (2012) had used SVR along with more recent kernel-based methods to retrieve bio-geophysical parameters such as LAI, LCC, and fCover from simulated Sentinel-2,3 datasets. Similarly, Bayesian networks (BNs) are recently developed probabilistic models, characterized by graphical structures representing information on domains of uncertainty (Cooper and Herskovits 1992). Kalacska et al. (2005) used BN models to retrieve LAI from Landsat ETM. Similarly, Mustafa et al. (2011, 2012) used BNs to improve LAI retrieval using MODIS and ASTER imageries. They have reported that LAI estimation accuracy was improved with a forest growth model. Strength and weaknesses of nonparametric regression methods were discussed in detail by Verrelst et al. (2015a, b). They have concluded that none of these nonparametric methods could be incorporated into an operational or global retrieval system with acceptable error. A schematic diagram of the process flow of retrieval of biophysical parameters through parametric as well as nonparametric regression is presented in Fig. 3.1.

3.3.3 Methods Based on Laws of Physics

Crop parameter retrieval based on physical model depends on laws establishing cause–effect relationships. These models are parametrized based on the information acquired through RTFs. Canopy reflectance model simulates reflectance based on

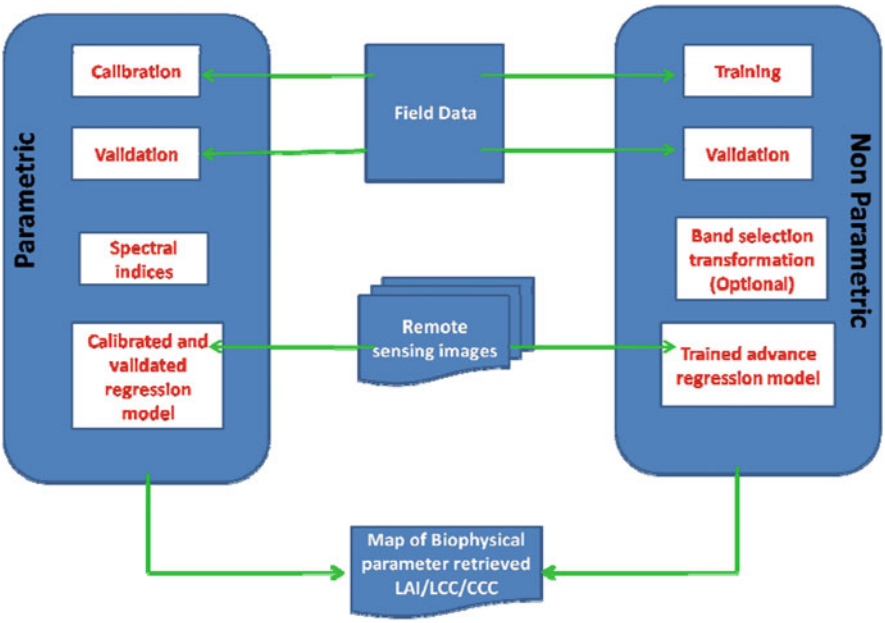

Fig. 3.1 Schematic diagram for retrieval of biophysical parameters by empirical approach

the interaction between solar radiation and the leaf-canopy attributes using physical laws. These models combine leaf optical model, canopy reflectance, and soil reflectance model to calculate the top of the canopy reflectance. This calculated reflectance has to be compared with observed reflectance recorded by RS data corrected for atmospheric influences. Another way for linking RS observation is to compute radiance from the radiation propagation model in the atmosphere (Verhoef and Bach 2003). However, in this chapter discussion will be confined to reflectance at canopy level, hence atmospheric models are not discussed here. Soil reflectance significantly contributes to the top of the canopy-simulated reflectance under sparse or low canopy coverage. Hence, soil reflectance models can play an important role in such circumstances. Again, soil reflectance is a function of soil moisture, soil color, surface roughness, soil organic matter, and inorganic carbon content, etc., and its parameters are often fixed by using simple empirical formulae and scaling factors (Atzberger et al. 2003; Baret et al. 2006a, b).

3.3.3.1 Leaf Optical Model

Leaf optical properties govern reflection, absorption, and transmission of radiation by a leaf. It requires a thorough understanding of leaf microstructure (palisade and spongy parenchyma), distribution of the biochemical constituents and air space, and the anisotropic scattering of leaves (Jacquemoud and Ustin 2001). Nevertheless, leaf

scattering and absorption properties are successfully explained more simply following different approaches and models by various researchers. Some of these models like the N-flux model, plate models, and ray tracing models are cited most often by many researchers. N-flux models proposed by Fukshansky et al. (1991) and Richter and Fukshansky (1996) are very simple models based on the concept of Kubelka–Munk theory that considers leaf as being a slab of absorbing and diffusing material. The inversion of this model is a complex process as it is very difficult to correlate the specific absorption coefficient of a leaf with its biochemical composition and concentration (Fukshansky et al. 1991). On the other hand, plate models are relatively simple to replicate, based on the assumption that the leaf biochemical elements are distributed homogeneously and responsible for absorption and Lambertian scattering. Hence it makes the retrieval of biochemical comparatively simpler through the inversion process. PROSPECT model is a very popular plate model that has been successfully used by various researchers (Jacquemoud and Baret 1990). Ray tracing models are based on Monte Carlo simulations. It is a most realistic accounting system for complex leaf internal structure by simulating the propagation of photons within leaf foliage (Govaerts et al. 1996). However, its usage is limited, as it requires a very detailed picture of individual cells along with their spatial arrangement and optical constants within the foliage (Dorigo et al. 2007). It makes the model computational-intensive both for forward simulation and subsequent inversion. In the radiosity model, the optical properties of a leaf are controlled by distinct reflecting and transmitting components with a defined shape, position, and orientation. The main advantage of this model is that leaf and canopy reflectance could be simulated for any given view angle and wavelength once the RTFs model equations are solved. However, the use of this model is also limited due to the initial high computational load to form the view factor matrix and finding a solution for the RTFs model. The algorithmic BDF model (ABM) proposed by Baranoski and Rokne (2005) is a popular radiosity model. The Markov chains–based stochastic model for leaf optical properties (SLOP) is also reported in the literature (Maier et al. 1999; Dorigo et al. 2007). Once again, these models demand higher computational facilities than plate and N-flux models, hence are not fit for direct inversion.

3.3.3.2 Canopy Reflectance Model

It is based on the radiative transfer approach, assuming canopy as a turbid medium where the canopy elements (leaves) are considered as a randomly distributed, small absorbing, and scattering elements. Such models are the best fit for addressing radiation propagation in most of the crops. The radiative transfer approaches are best fitted in heterogeneous canopies like orchards, row crops, etc, where the assumption of a horizontally homogenous and infinite canopy does not work properly. In sparse canopies where multiple scattering and shading are negligible because of low zenith angles, geometrical models have been proposed to describe radiation propagation (Chen and Leblanc 1997). The combination of radiative transfer and geometrical approaches gives hybrid models. It assumes canopy as a translucent

geometrical object (plants) where the turbid medium radiative transfer equation is employed. Such models are useful for representing sparse canopies or forests. Some of these 3D hybrid models such as the three-dimensional radiation interaction model (TRIM) (Goel and Grier 1988), GeoSAIL (Huemmrich 2001), and the invertible forest reflectance model (INFORM) (Schlerf and Atzberger 2006) are well documented in the literature.

3.3.3.3 Inversion of Canopy Reflectance Model

The main aim of CRM is to find a set of input parameters that leads to the best fit between simulated bidirectional and sensor measured reflectance (Combal et al. 2002). Therefore, the inversion problem is fixed to estimate the set of input parameters fed to CRM to achieve the best match between the two independent reflectance values (simulated and measured) of a given canopy. The inversion of canopy RTM with full-spectrum RS data is considered as a generic approach with a sound physical base (Dorigo et al. 2007). But in reality, this inversion is not straightforward and requires a careful trade-off between the realism and inversion possibility of the RTM (Fig. 3.2). Generally, complex models require fixing of many parameters and are more realistic but hard to invert. Whereas simpler models with fewer number of parameters may be easier to invert though they are less realistic. Several techniques

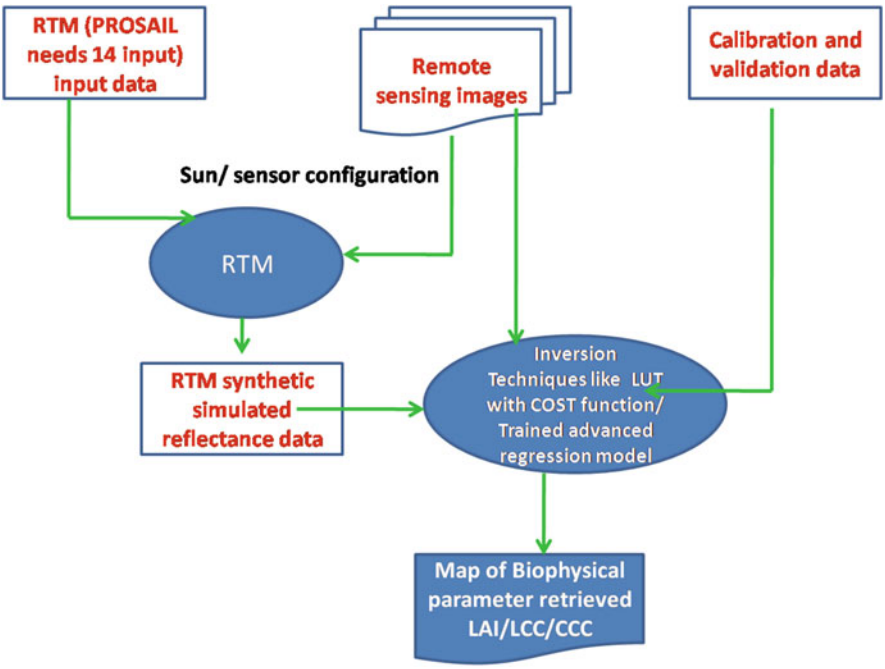

Fig 3.2 Flowchart of RTM-based inversion approaches for retrieval of biophysical parameters

have been used to find the best fit, such as lookup table approach (LUT), iterative optimization, ANN, etc. Iterative optimization (IO) is a classical technique to invert RTMs using RS data (Jacquemoud et al. 1995; Kuusk 1998; Zarco-Tejada et al. 2001).

The IO techniques use merit function minimization and optimization while searching for the best fit between the measured and simulated reflectance by iteratively running the canopy reflectance model using different sets of input parameters. A wide range of statistical and mathematical approaches such as quasi-Newton algorithms (Bacour et al. 2002b), Markov Chain Monte Carlo approaches (Zhang et al. 2005), and genetic algorithms (de Wit 1999) have used by many researchers for finding the global minima. Several researchers have successfully retrieved biophysical parameters using the IO method (Jacquemoud et al. 1995; Kuusk 1998; Zarco-Tejada et al. 2001). However, it is computationally too intensive to be used for operational retrieval programs. In the LUT approach, a large number of possible spectra are generated using different combinations of input parameters within a specified range. It is based on querying the LUT and applies a cost function for optimization (Liang 2007) which reduces the summed differences between measured and simulated reflectance throughout the defined spectrum. In this approach, the computationally most demanding step of the inversion process is performed before inversion itself (Dorigo et al. 2007), thus making it faster. LUT inversion is being successfully applied for retrieval of the biophysical parameters like LAI and fAPAR on a global scale using MISR/MODIS data (Knyazikhin et al. 1999).

The success of retrieval of crop biophysical attributes using CRM is highly dependent on the selection of appropriate model meeting the requirements of specific canopy under consideration. Further retrieval accuracy is strongly dependent on the selection of suitable inversion technique, an accurate canopy parameterization realization along with the availability and use of prior knowledge (Combal et al. 2002; Liang 2004). Various physical modeling approaches based on RTMs have demonstrated strong potential for retrieval of biophysical parameters. Nevertheless, there are several limitations such as higher computational requirement and a rigid parameterization. At the same time, ill-posed inversion problem arises when significantly varying input parameters of RTMs result in limited variability in simulated spectra, making the parameter retrieval more challenging (Atzberger 2004). In a physical modeling approach, RTMs account for the differences in canopy structure, background soil reflectance, illumination, and viewing geometries, hence, making it usable across multiple operational applications for canopy parameter retrieval (Bacour et al. 2006).

3.3.4 Hybrid Method

This approach combines the flexibility and computational efficacy of nonparametric methods with the generic properties of physically based RTM. Here, basically inverse mapping technique is followed along with a nonparametric model which is

trained with the RTMs simulated reflectance data. The hybrid approach uses all available data to train nonlinear, nonparametric regression model in which LUTs are used as input for machine learning. However, in LUT-based inversion approach, it seeks for a simulated spectrum as close as observed one. The hybrid methods based on ANN proved to be excellent algorithms which can deal with large datasets. Such algorithms trained with RTM-generated data is a well-accepted approach for retrieval of biophysical parameters from RS data (Baret et al. 1995; Kimes et al. 1998; Weiss and Baret 1999). PROSPECT-SAIL (PROSAIL) is the most popular model used retrieve canopy water content across the USA, using Moderate Resolution Imaging Spectroradiometer (MODIS) data (Trombetti et al. 2008). Richter et al. (2009) retrieved LAI using sentinel-2 data and PROSAIL–ANN hybrid approach. Yang et al. (2012) compared PCA approach with PROSAIL–ANN hybrid approach for hyperspectral data. Durbha et al. (2007) retrieved LAI using SVR model on Multiangle Imaging Spectroradiometer (MISR) data along with PROSAIL simulations.

The Sentinel-2 datasets provided by European Space Agency consists of 13 spectral bands covering the visible and NIR to SWIR region is very useful for crop biophysical parameter retrieval. It gives systematic coverage with better temporal resolution than many medium resolution optical sensors presently operating. The SNAP (Sentinel Application Platform) software based on ANN approach is designed to retrieve LAI, CCC, canopy water content (CWC), fAPAR, and fractional cover using instantaneous observations from Sentinel-2. Djamai et al. (2019) reported that it is possible to generate sub-weekly time series of vegetation biophysical parameters at medium resolution (~20 m) by using Sentinel-2-like synthetic surface reflectance data produced by merging clear-sky S2-multispectral imager data of Sentinel-2A with daily bi-direction reflectance distribution function (BRDF)–adjusted MODIS images. Brede et al. (2020) proposed a hybrid retrieval technique by combining canopy RTMs with nonparametric machine learning regression algorithms (MLRAs) as a fast and accurate method to retrieve LAI from data streams of Sentinel-2A Multispectral Instruments (MSI), Landsat 7 ETM+, and Landsat 8 OLI.

3.4 Retrieval of Biophysical and Biochemical Parameters of Crops

3.4.1 Retrieval of Leaf Area Index

LAI being the key structural characteristic of crops, because of its role in controlling many biological and physical processes in plant canopies, remains the most crucial parameter for retrieval (Darvishzadeh et al. 2008). It is widely used for crop phenology detection, crop health monitoring, and crop yield modeling. It can also serve as input for various climatic models to understand the land surface energy and mass exchanges. Further, the leaf area acts as a boundary between the underlying

plant microclimate and the atmosphere. This part of the plant is exposed, hence easier to capture directly by RS. LAI has been retrieved through several approaches, such as parametric regression approaches (red-edge position calculations, different integration-based indices covering specific spectral regions, etc.); nonparametric regression methods; linear nonparametric models like SMLR, PCR, PLSR, RR; nonlinear and nonparametric models such as RF, ANN, SVM, Gaussian processes regression (GPR); physically based RTM (PROSPECT, SAIL, PROSAIL, FLIGHT, INFORM, etc.); and hybrid methods (ANN along with RTM, alternative machine learning regression algorithms methods trained with RTM generated datasets, etc.) (Verrelst et al. 2015a). Many researchers have used several techniques to retrieve LAI using RS data (Table 3.2). Verrelst et al. (2015b) have compared all these techniques for retrieval of LAI based on root mean square error (RMSE), coefficient of determination (R^2), and processing speed (second) (Table 3.3).

Verrelst et al. (2015b) have observed that the range of RMSE was quite high (0.615–0.923) for parametric indices as compared to the nonparametric techniques (0.436–0.803), indicating more robustness in prediction for nonparametric techniques. The results of the coefficient of determination also showed a similar trend. But the range of processing speed for parametric methods was quite low, and in many cases they were faster than the nonparametric techniques, barring a few like PCR (processing speed 0.003), PLSR (processing speed 0.010), etc. In the case of inversion of physically based models the processing speed was quite higher as compared to both the techniques while the RMSE and R^2 were also similar. The parametric techniques are very fast and provide the results instantly, followed by nonparametric techniques while the application of physically based models is slow. Hence appropriate techniques should be chosen for different applications based upon the purpose, study area, and availability of computation facility.

3.4.2 Retrieval of Chlorophyll Content

Biochemical parameters of plants, that is, the pigments are mainly governed the photosynthetic and physiological activities (Cornelissen et al. 2003). Chlorophyll pigments which significantly regulate photosynthetic activities serve as the most critical leaf biochemical parameters (Clevers and Kooistra 2012; Inoue et al. 2016). Chlorophyll pigments can absorb solar radiation and help in photosynthetic light reactions using its two functional forms namely chlorophyll a and b, each having definite spectral properties (Lichtenthaler and Buschmann 2001). The total leaf chlorophyll content (mass per unit leaf area) is largely accountable for any photosynthetic activity in the leaf and plays a major role in the adaptation process and arresting the solar energy (Gitelson et al. 2006). Hence, it acts as a crucial indicator of crop growth and nutrition status to evaluate stress due to diseases or infestation, and heavy metal pollution in plants (Cui and Zhou 2017). Carotenoids (Car) and the red pigments, anthocyanins (Anth), are also very important as they prevent damage to the photosynthetic systems and leave from surplus lights respectively due to their

Table 3.2 Methods and types of remote sensing datasets used for LAI retrieval

Methods/ techniques	Crop/plant	Data used	Specific band/indices	Accuracy RMSE (m^2 m^{-2})	References
Parametric methods					
Parametric regression	Potato	Sentinel-2	WDVI	0.36	Clevers et al. (2017)
OSAVI, EVI, MTVI	Corn, soybean, wheat	Landsat TM 5 and Landsat 7ETM+	Red, green, blue, NIR	<0.60	Liu et al. (2012)
Parametric regression	Summer wheat, winter barley	Non-imaging hyperspectral data	WDVI	0.22	Kneubühler Mathias Naef and Itten Klaus (2000)
Nonparametric methods					
Nonparametric regression	Mixed crops (corn, sorghum, cotton, and soybean)	Landsat 5	Red and NIR	0.42–0.90	Gowda et al. (2015)
Nonparametric–neural network	Maize, fruit crops, mixed crops (cereals, alfalfa, pepper, artichokes, etc.)	Rapid Eye data	Five broadbands	0.61–0.91	Vuolo et al. (2010)
Physical inversion methods					
Radiative transfer model – PR OSAIL	Grassland/ saltmarsh	Sentinel-2 and RapidEye	All bands and their combination	0.84–0.90	Darvishzadeh et al. (2019b)
Radiative Transfer Model –PORO SAIL	Wheat	MODIS, Landsat TM, IRS LISS-3, and field-based hyperspectral data	All broadbands of multispectral data and hyperspectral data (400–2500 nm)	0.36–0.52	Mridha et al. (2014)
LUT inversion	Maize, fruit crops, mixed crops (cereals, alfalfa, pepper, artichokes, etc.)	Rapid Eye data	Five broad bands	0.35–0.93	Vuolo et al. (2010)
REGFLEC	Maize, Soybean	Landsat 5 TM and Landsat 7 ETM+	Green, Red, NIR	1.25	Houborg et al. (2015)
LUT inversion	Wheat	IRS LISS-3	All broadbands	0.56	Sehgal et al. (2016)

(continued)

Table 3.2 (continued)

Methods/ techniques	Crop/plant	Data used	Specific band/indices	Accuracy RMSE (m^2 m^{-2})	References
Hybrid methods					
Hybrid method, PROSAIL model, and MLRA	Mixed crops	–	–	$R^2 > 0.96$	Verrelst et al. (2016)
Hybrid-polarized SAR	Wheat	RISAT-1	SAR Backscatter Signatures (RH and RV)	0.41–0.77	Chauhan et al. (2018)
PROSAIL with machine learning (LSLR)	Wheat	Sentinel-2	Band 3 to 7, 8a, 11, and 12	0.68	Upreti et al. (2019)
Radiative transfer model with ANN	Cereal crops, broadleaf crops, grasses, forests, etc.	ENVISAT-MERIS	11 spectral bands	RMSE: 0.09	Bacour et al. (2006)

NB: *EVI* Enhanced vegetation index, *OSAVI* Optimized soil-adjusted vegetation index, *REGFLEC* Regularized canopy reflectance model, *LUT* Lookup table, *PLSR* Partial least square regression, *NIR* near-infrared, *MODIS* Moderate-Resolution Imaging Spectrometer, *MERIS* Medium-Resolution Imaging Spectrometer, *WDVI* Weighted-difference vegetation index; *MTVI* Modified triangular vegetation index, *LSLR* Least square linear regression, *MLRA* Multiple linear regression

Table 3.3 Comparison of performance of different LAI retrieval techniques

Techniques	RMSE	R^2	Processing speed (s)	Reference
Parametric indices	0.61–0.92	0.61–0.82	0.02–0.12	Verrelst et al. (2015b)
Nonparametric	0.43–0.80	0.68–0.90	0.003–28.32	
Physical model inversion	0.79–0.87	0.67–0.74	0.31–0.90	

photo-protective role (Gitelson et al. 2003). Due to its immense importance, environmentalists or ecologists use foliar chlorophyll content for various aspects of crop monitoring. These include an assessment of the interaction between vegetation health and biotic or abiotic environmental stress (Garnier et al. 2007), quality assessment of habitat and identification of tree species (Delegido et al. 2014), estimation of crop net primary production and precision farming (Navarro-Cerrillo et al. 2014), along with ecosystem productivity calculation of any vegetation system (Gitelson et al. 2006; Lavorel et al. 2011). Furthermore, LCC is recognized as one of the "essential biodiversity variables" or "critical factor" in understanding ecosystem response to climate change (Croft et al. 2017), where RS can play the vital role over its timely monitoring (Skidmore et al. 2015; Darvishzadeh et al. 2019a). Many researchers across the world have used various techniques and RS images for retrieval of crop CCC which is presented in Table 3.4.

Table 3.4 Methods and remote sensing datasets used for canopy chlorophyll retrieval

Methods/ models	Crops	Remote sensing data used	Specific band (s)/indices	Accuracy (RMSE)	References
Parametric methods					
Parametric regression	Potato	Sentinel-2	TCARI/ OSAVI	0.062–0.066 g m^{-2}	Clevers et al. (2017)
Green model (R_{NIR}/ R_{Green}) − 1	Soybean, maize, different species	MODIS, MERIS	NIR, green	Soybean: 0.18 gm m^{-2}, maize: 0.32 gm m^{-2} 0.25–0.70 gm m^{-2}	Gitelson et al. (2006)
Red-edge model (R_{NIR}/ $R_{Red\ edge}$) − 1	Soybean, maize, different species	MODIS, MERIS	NIR, red edge	Soybean: 0.15 gm m^{-2}, maize: 0.31 gm m^{-2} 0.08–0.60 gm m^{-2}	Gitelson et al. (2006)
NGRDI	Turmeric	UAV-mounted multispectral sensors	Green, red	0.13 mg/g	Singhal et al. (2019)
Nonparametric methods					
Kernel Ridge Regression	Turmeric	UAV-mounted multispectral sensors	Green, red, red edge and NIR	< 0.10 mg/g	Singhal et al. (2019)
Neural Network	Maize, fruit crops, mixed crops (cereals, alfalfa, pepper, artichokes, etc.)	Rapid Eye data	Five broad-bands blue, green, red, red-edge, and NIR	0.25–0.70 gm m^{-2}	Vuolo et al. (2010)
Physical inversion methods					
REGFLEC	Maize, soybean	Landsat 5 TM and Landsat 7 ETM+	Green, red, NIR	8.42 μg cm^{-2}	Houborg et al. (2015)
Radiative transfer model POROSAIL	Wheat	MODIS, Landsat TM, and IRS LISS-3 and field-based hyperspectral data	All broadbands of multispectral data and hyperspectral data (400–2500 nm)	0.34–0.36 g m^{-2}	Mridha et al. (2014)
LUT-inversion	Maize, Fruit crops, mixed	Rapid Eye data	Five broad bands blue,		

(continued)

Table 3.4 (continued)

Methods/ models	Crops	Remote sensing data used	Specific band (s)/indices	Accuracy (RMSE)	References
	crops (cereals, alfalfa, pepper, artichokes, etc.)		green, red, red-edge and NIR	RMSE: 0.31–0.50 gm m^{-2}	Vuolo et al. (2010)
LUT-inversion	Wheat	IRS LISS-3	All broadbands	0.35 gm m^{-2} 0.89	Sehgal et al. (2016)
Hybrid Method					
Hybrid method curve fitting, LS-SVR, RFR	Mixed crops (oats, corn, alfalfa, and others)	CHRIS datasets	Hyperspectral indices (50 nos.)	RMSE: 1.69–5.94 μg cm^{-2}	Liang et al. (2016)
PROSAIL with (machine learning) PLSR	Wheat	Sentinel-2	Band 3 to 7, 8a, 11, and 12	26.32 g cm^{-2}	Upreti et al. (2019)

NB: *TCARI* Transformed chlorophyll in reflectance index, *OSAVI* Optimized soil-adjusted vegetation index, *NGRDI* Normalized green–red difference index, *REGFLEC* Regularized canopy reflectance model, *LUT* Lookup table, *PLSR* Partial least square regression, *NIR* near-infrared, *MODIS* Moderate-Resolution Imaging Spectrometer, *MERIS* Medium-Resolution Imaging Spectrometer, *PSSR* Pigment-specific simple ratio, *RARS* ratio analysis of reflectance spectra, *LS-SVR* least squares support vector regression, *RFR* Random forest regression

Optical RS, especially the visible portion of the spectrum (400–700 nm), has a long history in delivering approaches for estimating either chlorophyll or nitrogen (N) in vegetation (Clevers and Kooistra 2012). As it is challenging to estimate biochemical concentrations at leaf level especially for satellite-based RS and large area approach, researchers prefer to focus on integrated biochemical contents at the canopy level (i.e., observed from a remotely sensed platform). Hence, in this case, the chemical concentration is expressed as the chemical amount per unit ground surface area (Jones et al. 2007). Potentially all the approaches described for LAI retrieval also apply for the retrieval of the pigment or specifically chlorophyll content of the plant. As the chlorophyll pigments have very specific spectral absorption bands, having robust scientific basis, hence very simple approaches like reflectance at certain bands or simple vegetation indices have been widely used for its successful retrieval (Gitelson et al. 2006). Apart from that, the inversion of a leaf to canopy radiative transfer models have also been used to accurately estimate the chlorophyll content by several researchers (Darvishzadeh et al. 2008; Clevers and Kooistra 2012). It is quite clear from Table 3.4 that plant CCC can be retrieved using RS

images through various modeling techniques with good accuracy. However, retrieval accuracy varies with the nature of canopy, that is, sole crops or a mixture of crops/species, retrieval techniques used, and the RS platform used (laboratory based, field scale, or satellite scale, etc.). Based upon the requirement of the users, proper approaches for estimation of chlorophyll content should be selected.

3.4.3 Retrieval of Moisture Content

The plant moisture content is a crucial variable for understanding the water stress in vegetation during periods of drought. It also reflects the status of dryness which helps in monitoring vegetation during the dry season due to their vulnerability to wildfire (Ceccato et al. 2001). Besides, this parameter is of utmost importance for understanding the process of progress in biomass burning which can be effectively monitored through RS. Satellite RS provides the most objective, repetitive, and cost-effective methods to monitor vegetation, specifically in remote areas where regular basis ground measurements are not possible. Different satellite sensors working on different parts of the electromagnetic spectrum (EM) for the monitoring of vegetation water content can be grouped into three broad categories: (i) Visible to shortwave infrared (SWIR) spectrum between 0.4 and 2.5 μm, providing valuable spectral information on crop biophysical parameters (Tucker 1980). (ii) Thermal infrared (TIR) spectrum between 6.0 and 15.0 μm, delivering crucial information on thermal dynamics, evapotranspiration, and water stress of crop vegetation (Moran et al. 1994). (iii) Microwave spectrum between 0.1 and 100 cm, giving information on the dielectric constant linked to vegetation water content (Moghaddam and Saatchi 1999).

The results obtained from physical-based studies show that the SWIR region of the EM spectrum (1.4–2.5 μm) is highly influenced by the plant tissue water (Tucker 1980; Gausman 1985). The wavelength at 1530 and 1720 nm seem to be most suitable for vegetation water assessment (Faurtyot and Baret 1997).

Several physical or semiempirical models especially RTMs have been used to simulate the effect of water content on spectral reflectance (Jacquemoud et al. 1994; Faurtyot and Baret 1997). Ceccato et al. (2001) used reflectance values at 1600 nm to estimate moisture content from a dataset of 37 species with a varying moisture content, which was expressed as equivalent water thickness (EWT having unit gm/cm^2). They have reported a logarithmic relationship between reflectance and EWT. At low EWT (vegetation is losing water or under stress), reflectance value is more sensitive to EWT variations. As the EWT increases, the sensitivity of reflectance to EWT diminishes and reflectance values saturate at higher EWT. Using the single band reflectance, the logarithmic model could explain about 77% variation in the observed EWT across 37 species (i.e. $R^2 = 0.773$). When a simple ratio of two bands (R1600/R820) was used in the same type of logarithmic equation, it could explain about 92% variations in the EWT (Ceccato et al. 2001). Further Atzberger (2004) has used ANN-based inversion of SAILH+PROSPECT canopy reflectance

model to retrieve EWT. The study employed an object-based model inversion to retrieve EWT with a coefficient of determination of 0.92 and RMSE (%) of 10.6. Pasqualotto et al. (2018) have shown that hyperspectral RS–based water absorption area index (WAAI) and depth water index (DWI) could capture the variations in water content in a much better way compared to the traditional indices for a heterogeneous landscape (R^2 of 0.8 and 0.7 and RMSE of 290 and 400 g/m^{-2} respectively for WAAI and DWI). Apart from optical RS, SAR datasets have also been used for retrieving the crop water content. Chauhan et al. (2018) used hybrid-polarized RISAT-1 SAR data for retrieving the plant water content of wheat. They found a high coefficient of determination values between the observed and the RS-estimated plant water content (R^2 from 0.82 to 0.87) with low RMSE (0.17–0.38 kg m^{-2}).

However, many studies as mentioned above reported accurate retrieval of EWT, but Vohland et al. (2010) and Sehgal et al. (2016) have reported poor retrieval of the same parameter. The poor retrieval in these studies was due to the low range of EWT in the experimental datasets barring the proper model development. Hence, the application of retrieval techniques for plant moisture content should be selected based on the purpose. The accuracy may vary depending on the range of real variations of plant moisture in the training dataset. The various methods and RS datasets used for crop moisture retrieval is presented in Table 3.5.

3.4.4 Retrieval of Fraction of Absorbed Photosynthetically Active Radiation

The energy utilization ability of crop canopy is significantly characterized by the fAPAR, which describes both energy exchange processes and vegetation structure. fAPAR is prominently a basic crop biophysical parameter which is generally used to estimate NPP using RS methods and considered as ECVs that helps in assessing carbon and energy balance on global scale (D'Odorico et al. 2014). Many land-surface models including NPP models, crop growth models, ecological models, climate models, and water and carbon cycle models use fAPAR as critical input (Liu et al. 1997; Scurlock et al. 1999; Liang 2004). fAPAR can be defined as the solar radiation absorbed by crop vegetation within the spectral range of 400 nm to 700 nm, which is given by the following equation by Gobron et al. (2006):

$$\begin{aligned}\text{fAPAR} = &\big[(\text{incoming solar flux}) - (\text{flux to the ground}) \\ &+ (\text{flux from the ground}) - (\text{outgoing solar flux})\big]/(\text{incoming solar flux})\end{aligned} \tag{3.1}$$

When the crop area is close to 0 (pure soil), that is, the incoming solar flux is equal to the flux to the ground and the reflected flux from the ground is equal to the outgoing radiation flux, then the fAPAR will be 0. fAPAR can be measured as

Table 3.5 Methods and remote sensing datasets used for moisture retrieval

Methods/ models	Crop/ plant	Remote sensing data used	Specific band (s)/indices	Accuracy	References
Parametric regression	Various species of trees, crops, and plants	In situ datasets of LOPEX93 and PANAMA with simulated dataset of PROSPECT	Spectral similarity water indices with SAC effective metric for leaf water thickness	RMSE of 4.08% ($R^2 = 0.98$), 3.63% ($R^2 = 0.95$), and 8.11% ($R^2 = 0.80$) for PROSPECT, LOPEX93, and PANAMA, respectively	Fang and Liang (2005)
Parametric regression	Corn and soybean	Landsat Operational Land Imager and MODIS	NDWI	The RMSE of corn and soybean field plant VWC is 0.1 kg/plant and 0.02 kg/plant, the RMSE of corn and soybean field canopy VWC is 1.31 kg/m2 and 0.94 kg/m2, respectively;	Xu et al. (2020)
Semiempirical WCM and NN models	Wheat	RISAT-1 SAR data (hybrid polarization)	C-band with frequency of 5.35 GHz	RMSE of 0.38 kg m^{-2} to 0.17 kg m^{-2}	Chauhan et al. (2018)
PROSAIL + hyperspectral Indices	Corn, potato, garlic, onion, sugar beet, lucerne	HyMap	WAAI (971 and 1271 nm), DWI (970 and 1200 nm)	R^2=0.7 to 0.8	Pasqualotto et al. (2018)
Physical model (PROSPECT-D + PROSAIL)	Wheat and corn	Hyperspectral (PROSPECT and PROSAIL LUT)	Spectral range of 930–1060 nm with 970 nm as water absorption band	Relative RMSE (rRMSE) of 26% for wheat and 23% for corn	Wocher et al. (2018)
Radiative transfer model POROSAIL	Wheat	MODIS, Landsat TM, and IRS LISS-3 and field-based hyperspectral data	All broadbands of multispectral data and hyperspectral data (400–2500 nm)	0.003–0.009 g cm^{-2}	Mridha et al. (2014)
LUT-inversion	Wheat	IRS LISS-3	All board band	0.005 cm	Sehgal et al. (2016)

NB: *DWI* Depth water index, *WAAI* Water absorption area index, *LUT* Lookup table, *NN* Neural network, *WCM* Water cloud model, *SAC* Spectral angle cosine, *NDW*; Normalized difference water index, *MODIS* Moderate-Resolution Imaging Spectrometer, *Landsat TM* Land Satellite Thematic Mapper

instantaneous at any specific moment or as daily by integrating instantaneous fAPAR over the cosine of the solar zenith angle. As direct field measurement of APAR is very difficult, it is indirectly estimated by measuring PAR using Quantum sensor. fAPAR can be retrieved through different ways, using empirical methods based on LAI or VIs or using RTMs. As fAPAR is positively correlated with LAI, it is computed as a function of the extinction coefficient and LAI and used in biogeochemical process models (Ruimy et al. 1999). Dong et al. (2015) estimated fAPAR using field spectra simulated to Sentinel-2 reflectance which indicated that VIs developed using the red-edge and NIR reflectance [red-edge normalized difference vegetation index (ND705), modified simple ratio-2 (mSR2), MERIS terrestrial chlorophyll index (MTCI), red-edge simple ratio (SR705), and revised optimized soil-adjusted vegetation index ($OSAVI_{[705,\ 750]}$)] linearly correlated to fAPAR with high biomass. Zhang et al. (2014) reported an increased fAPAR in vegetative stage which persisted relatively constant at the reproduction stage followed by a decreased fAPAR during the senescence stage. They additionally proposed $fAPAR_{green}$ which shows visible seasonal trends than fAPAR.

$$fAPAR_{green} = fAPAR \times (\text{green LAI}/\text{green LAI}_{max}) \tag{3.2}$$

They found that $fAPAR_{green}$ is significantly correlated to the red-edge NDVI, and red-edge position (REP) derived from hyperspectral data correspond to Sentinel-2 bands throughout the crop growth period. The comparative study of the predictive performance of vegetation indices for the entire growing season showed that REP outperformed among all and can be recommended for monitoring seasonal dynamics of fAPAR in a maize canopy. The various methods and RS datasets used for fAPAR retrieval is presented in Table 3.6.

Computation of APAR through linear or nonlinear correlation with NDVI is very common in many RS studies (Prince and Goward 1995). At the same time, it is widely accepted to estimate the GPP and NPP using the NDVI–fAPAR and the LAI–fAPAR correlations over different spatial scales (Running et al. 1989; Field et al. 1995). Yuan et al. (2015) used a physically based RTMs (invertible forest reflectance model, INFORM) combined with ANN as an inversion algorithm for retrieval of fAPAR in forests from multispectral Landsat-8 data. They have developed predictive models through ANN between Landsat-8 reflectance and fAPAR and calibration of INFORM were done followed by validation with 42 forest stands. The study reported that there was a good agreement between the INFORM simulated spectra and forest canopy reflectance correspond to Landsat bands. The INFORM model performed well in terms of fAPAR retrieval using NN as an inversion algorithm with acceptable accuracy ($R^2 = 0.47$, RMSE = 0.11) and the accuracy keeps increasing when pixels at steep terrain are excluded. The AVHRR and MODIS global LAI/fAPAR are the most popular products available nowadays. These products have generated data using RTMs with the empirical alternative algorithms. The Canadian remote sensing center also developed a vegetation index–based fAPAR model and produced a national fAPAR map at 10 days temporal and 1 km spatial

Table 3.6 Methods and remote sensing datasets used for fAPAR retrieval

Methods/models	Crops/plants	Remote sensing data used	Specific band(s)/ indices	Accuracy	References
Parametric regression	Summer wheat, winter barley	Non-imaging hyperspectral data	WDVI and SAVI	Wheat: 0.031–0.105; barley: 0.032–0.118	Kneubühler Mathias Naef and Itten Klaus (2000)
Parametric regression	Boreal forest	Landsat 7 and Landsat 8 surface reflectance	18 possible Ratio and normalized vegetation indices	RMSE∼0.14	Majasalmia et al. (2017)
Both parametric and non-parametric regression	Sugarcane	Landsat-8 Operational Land Imager data	All bands (various spectral indices)	RMSE∼7.72–16.84	Muller et al. (2020)
Radiative transfer model with ANN	Cereal crops, broadleaf crops, grasses, forests, etc.	ENVISAT-MERIS	11 spectral bands	RMSE: 0.09	Bacour et al. (2006)
Physical model, (PROSPECT+SAIL) trained with neuronal network algorithm on Sentinel-2 reflectance data	Mixed-coniferous, boreal-deciduous, and tropical dry forest	Sentinel-2 and ground based fAPAR (10 min interval) using Wireless Sensor Networks	Sentinel-2 fAPAR products and ground fAPAR using two flux fAPAR equation	Huge discrepancies in accuracy of the product and ground observation with systematic underestimation up to 25%	Putzenlechner et al. (2019)
Hybrid geometric optical-RT model	VALERI, (WWW4) and AmeriFlux (WWW5) sites distributed over different land types covering forest, crop, grassland, and shrubland	MODIS, MISR, Landsat TM, ETM	Spectral range of 400 nm to 700 nm	RMSE varies from 0.085 to 0.224	Tao et al. (2016)
PROSAIL with (machine learning) Random Forest Tree Bagger (RFTB)	Wheat	Sentinel-2	Band 3 to 7, 8a, 11, and 12	RMSE: 0.10	Upreti et al. (2019)

NB: *ANN* Artificial neural network, *SAVI* Soil-adjusted vegetation index, *WDVI* Weighted-difference vegetation index, *MODIS* Moderate-Resolution Imaging Spectrometer, *MERIS* Medium-Resolution Imaging Spectrometer, *MISR* Multiangle Imaging Spectroradiometer

resolution using AVHRR data (Chen 1996). The European Commission Joint Research Center developed a JRC–fAPAR product using the RTM-based algorithms with a spatial resolution of 10 km for the globe and 2 km for Europe. The empirical retrieval algorithms can be successfully used for generating such fAPAR products, but its applications are limited. The retrieval method based on physical models seems to be more universal and useful as it accurately describes canopy multilayer scattering using radiative transfer principles.

3.5 Conclusions

A comprehensive summary focusing on retrieval of crop biophysical parameters namely LAI, leaf chlorophyll, and moisture content and fAPAR using RS is illustrated in this chapter. Various retrieval techniques such as vegetation index–based regression models, semiempirical models, and physically based models are discussed for estimations of aforementioned biophysical parameters. In order to retrieve different biophysical parameters, most spectral indices can be used to obtain some general regression equations for potential applications. But it may be limited by sensitivity to types of leaves, canopy architecture, background, and locations. On the other hand, as physical models consider the physical interaction processes, generally outperformed over the regression model, particularly in terms of the scale of application. But it is also constrained by the complexity of canopy radiation interaction processes and the invertibility and computational efficiency of selected inversion techniques. Depending on the different nature of data, a variety of cost functions should be selected for a specific application. Future research goals in this aspect may increase in accuracy and practicality of biophysical parameters retrieval from hyperspectral data considering data redundancy. Obtaining seamless calibrated/corrected images must be the prerequisite for parameter retrieval from physically based models as the retrieval is significantly impacted by system error. As most fAPAR retrieval algorithms do not separate direct and diffuse solar radiation and consequently lead to underestimation, the physically based retrieval models effectively consider this fact using the radiative transfer mechanism among multiple canopy scattering and, thus, these are more universal and useful. Future research works should ponder upon more and more toward refining the estimated retrieval accuracy and the appropriateness of practical requirements.

3.6 Limitation and Future Perspectives

RTM inversion methods are basically iterative minimization calculations applied to every pixel in the image to retrieve the input variable values fed to the RTMs. Though in principle, it is possible to map all state variables, its success is associated with the number of variables and their cross-relationship across the spectral domain

(Mousivand et al. 2014). It is also reported that inversion routine optimized for a single variable performs slightly better as compared to generic multiple output inversion algorithms (Rivera et al. 2014; Verrelst et al. 2014). To date, very few biophysical parameters are mapped routinely on a global scale over a longer period of time. For example, LAI datasets are being retrieved and mapped from MODIS and CYCLOPES products for more than a decade now with gradual refinement over time leading to more accurate estimates. RS data has the potential to help us retrieve various biophysical parameters characterizing various agroecosystems, but there are multiple challenges to upscale these parameters for wider application. The most important factor limiting its application is the spectral, spatial, and temporal resolution of present operational sensors. Vannier et al. (2011) reported that spectral resolution is as significant as its spatial resolution and therefore maps with lower spatial but higher spectral resolution can provide us with more meaningful ecological information. Typically, sensors can only record information pertaining to the defined scale (Wu and Li 2009), hence upscaling is another important issue limiting the application of RS data for parameter retrieval. According to Li et al. (2014), spatial resolution of the sensor is another important factor to be considered for retrieval of biophysical parameters for crops. Higher spatial resolution can minimize uncertainly with respect to surface heterogeneity, but it can again lead to the problem of mixed pixels. Still, a higher spatial resolution of sensors is not always the best solution for RS-based studies of crop systems. The temporal resolution of the RS system also plays an important role in vegetation monitoring. Retrieval models – both empirical and physical – are developed and calibrated at small scales on homogeneous surfaces. These models do not explicitly describe the scale and its effect. Therefore, scale-specific calibration and parameterization is required to be used for different agroecosystems.

The retrieval of crop biophysical parameters from different satellite sensors can be significantly impacted due to data measurement uncertainties. The satellite data requires advanced algorithms for calibration and atmospheric–radiometric–geometric corrections for improved surface reflectance products. In the case of global retrievals of biophysical products, the main challenge is the spatial heterogeneity of different biomes and the classification accuracy of land cover maps use for representing the biomes. Inaccurate biome representation can contribute significant errors in the LAI retrieval process, specifically over the regions undergoing dynamic land cover change. The radiative transfer approach for retrieval is generally preferred over the empirical approach due to its appropriate representation of physical processes but it is inherently complex and limited to high computational efficiency for inversion. Retrieval of biophysical parameters from hyperspectral images suffers major drawbacks and inappropriate model development due to data redundancy which can be substantiated by selecting optimum numbers of spectral bands.

Potential areas for future research are as follows:

- Increase in the accuracy and practicality of biophysical parameters retrieval from hyperspectral RS data considering data redundancy.

- Evaluation of robustness of minimization criteria and their performance can very well be done using various cost functions with LUTs under skewed error distribution and with large outliers.
- A statistical loss function may be designed based on penalized approximation through a framework of parametric or nonparametric data.
- Improvement of accuracy and data continuity and the spatial and temporal stability of existing LAI products which is critical to ensuring user requirement effectively
- More use of artificial intelligence or advanced machine learning algorithms along with cloud data for estimation of biophysical parameters over a larger scale.
- More investigations are required to explore the ambiguity induced by source and viewing geometry, optical properties of leaf and soil, and atmospheric components for retrieval of biophysical parameters using various information for different crops under diverse agricultural scenarios.

Advancement of sensor designing and retrieval algorithms may be more emphasized

- To better describe and reduce the actual ambiguities that are needed for the execution of new land surface data assimilation systems.
- Future research on fAPAR retrieval needs to focus on modeling direct and diffuse radiation separately (as under cloudy condition diffused radiation increases significantly) for improving retrieval accuracy.

References

Adam E, Mutanga O, Abdel-Rahman EM, Ismail R (2014) Estimating standing biomass in papyrus (Cyperus papyrus L.) swamp: exploratory of in situ hyperspectral indices and random forest regression. Int J Remote Sens 35(2):693–714

Atzberger C (2004) Object-based retrieval of biophysical canopy variables using artificial neural nets and radiative transfer models. Remote Sens Environ 93(1–2):53–67

Atzberger C, Jarmer T, Schlerf M, Koetz B, Werner W (2003) Retrieval of wheat bio-physical attributes from hyperspectral data and SAILH + PROSPECT radiative transfer model. In: Proceedings of the Third EARSeL Workshop on Imaging Spectroscopy Herrsching, Germany

Bacour C, Jacquemoud S, Leroy M, Hautecœur O, Weiss M, Prévot L, Bruguier N, Chauki H (2002a) Reliability of the estimation of vegetation characteristics by inversion of three canopy reflectance models on airborne POLDER data. Agronomie 22(6):555–565

Bacour C, Jacquemoud S, Tourbier Y, Dechambre M, Frangi JP (2002b) Design and analysis of numerical experiments to compare four canopy reflectance models. Remote Sens Environ 79 (1):72–83

Bacour C, Baret F, Béal D, Weiss M, Pavageau K (2006) Neural network estimation of LAI, fAPAR, fCover and LAI× Cab, from top of canopy MERIS reflectance data: principles and validation. Remote Sens Environ 105(4):313–325

Baranoski G, Rokne J (2005) A practical approach for estimating the red edge position of plant leaf reflectance. Int J Remote Sens 26(3):503–521

Baret F (1991) Vegetation canopy reflectance: factors of variation and application for agriculture. In: Remote sensing and geographical information systems for resource management in developing countries. Springer Netherlands, Dordrecht, pp 145–167

Baret F, Buis S (2008) Estimating canopy characteristics from remote sensing observations: Review of methods and associated problems. In: Advances in land remote Sensing. Springer, Dordrecht, pp 173–201

Baret F, Fourty T (1997) Radiometric estimates of nitrogen status in crops. In: Lemaire G (ed) Diagnosis of the nitrogen status in crops. Springer Verlag, New York, pp 201–227

Baret F, Clevers J, Steven M (1995) The robustness of canopy gap fraction estimates from red and near-infrared reflectances: a comparison of approaches. Remote Sens Environ 54:141–151

Baret F, Bacour C, Béal D, Weiss M, Berthelot B, Regner P (2006a) Algorithm theoretical basis document for MERIS top of canopy land products (TOC_VEG). Contract. 2006 Mar:1–25

Baret F, Pavageau K, Béal D, Weiss M, Berthelot B, Regner P (2006b) Algorithm theoretical basis document for MERIS top of atmosphere land products (TOA_VEG). INRA-CSE, Avignon, France

Baret F, Weiss M, Lacaze R, Camacho F, Makhmara H, Pacholcyzk P, Smets B (2013) GEOV1: LAI and FAPAR essential climate variables and FCOVER global time series capitalizing over existing products. Part1: principles of development and production. Remote Sens Environ 137:299–309

Bartholomeus H, Schaepman-Strub G, Blok D, Sofronov R, Udaltsov S (2012) Spectral estimation of soil properties in siberian tundra soils and relations with plant species composition. Appl Environ Soil Sci 2012:1–12

Becker-Reshef I, Justice C, Sullivan M, Vermote E, Tucker C, Anyamba A, Small J, Pak E, Masuoka E, Schmaltz J, Hansen M (2010) Monitoring global croplands with coarse resolution earth observations: The Global Agriculture Monitoring (GLAM) project. Remote Sens 2 (6):1589–1609

Bélanger G, Richards JE (1995) Growth analysis of timothy cultivars differing in maturity. Can J Plant Sci 75:643–648

Birth G, McVey G (1968) Measuring the color of growing turf with a reflectance spectrophotometer. Agron J 60(1968):640–643

Bonan GB (1993) Importance of leaf area index and forest type when estimating photosynthesis in boreal forests. Remote Sens Environ 43(3):303–314

Brede B, Verrelst J, Gastellu-Etchegorry JP, Clevers JG, Goudzwaard L, den Ouden J, Verbesselt J, Herold M (2020) Assessment of workflow feature selection on forest LAI prediction with sentinel-2A MSI, landsat 7 ETM+ and Landsat 8 OLI. Remote Sens 12(6):915

Breiman L (2001) Random forests. Mach Learn 45(1):5–32

Broge NH, Leblanc E (2000) Comparing prediction power and stability of broadband and hyperspectral vegetation indices for estimation of green leaf area index and canopy chlorophyll density. Remote Sens Environ 76:156–172

Broge N, Leblanc E (2001) Comparing prediction power and stability of broadband and hyperspectral vegetation indices for estimation of green leaf area index and canopy chlorophyll density. Remote Sens Environ 76(2):156–172

Broge NH, Mortensen JV (2002) Deriving green crop area index and canopy chlorophyll density of winter wheat from spectral reflectance data. Remote Sens Environ 81(1):45–57

Campos-Taberner M, García-Haro FJ, Camps-Valls G, Grau-Muedra G, Nutini F, Crema A, Boschetti M (2016) Multitemporal and multiresolution leaf area index retrieval for operational local rice crop monitoring. Remote Sens Environ 187:102–118

Camps-Valls G, Bruzzone L (eds) (2009) Kernel methods for remote sensing data analysis. Wiley, Chichester

Ceccato P, Flasse S, Tarantola S, Jacquemoud S, Grégoire JM (2001) Detecting vegetation leaf water content using reflectance in the optical domain. Remote Sens Environ 77(1):22–33

Chakraborty D, Sehgal VK, Sahoo RN, Pradhan S, Gupta VK (2015) Study of the anisotropic reflectance behaviour of wheat canopy to evaluate the performance of radiative transfer model PROSAIL5B. J Indian Soc Remote Sens 43(2):297–310

Chauhan S, Srivastava HS, Patel P (2018) Wheat crop biophysical parameters retrieval using hybrid-polarized RISAT-1 SAR data. Remote Sens Environ 216:28–43

Chen JM (1996) Canopy architecture and remote sensing of the fraction of photosynthetically active radiation in boreal conifer stands. IEEE Trans Geosci Remote Sens 34:1353–1368
Chen JM, Black TA (1992) Defining leaf area index for non-flat leaves. Plant Cell Environ 15 (4):421–429
Chen JM, Leblanc SG (1997) A four-scale bidirectional reflectance model based on canopy architecture. IEEE Trans Geosci Remote Sens 35(5):1316–1337
Cho M, Skidmore A, Corsi F, van Wieren S, Sobhan I (2007) Estimation of green grass/herb biomass from airborne hyperspectral imagery using spectral indice and partial least squares regression. Int J Appl Earth Obs Geoinf 9(4):414–424
Clark R, Roush T (1984) Reflectance spectroscopy: quantitative analysis techniques for remote sensing applications. J Geophys Res 89(B7):6329–6340
Clevers JG (2014) Beyond NDVI: extraction of biophysical variables from remote sensing imagery. In: Land use and land cover mapping in Europe 2014. Springer, Dordrecht, pp 363–381
Clevers JGPW, Kooistra L (2012) Using hyperspectral remote sensing data for retrieving canopy chlorophyll and nitrogen content. IEEE J Sel Top Appl Earth Obs Remote Sens 5:574–583
Clevers JG, Kooistra L, Van den Brande MM (2017) Using Sentinel-2 data for retrieving LAI and leaf and canopy chlorophyll content of a potato crop. Remote Sens 9(5):405
Colombo R, Bellingeri D, Fasolini D, Marino CM (2003) Retrieval of leaf area index in different vegetation types using high resolution satellite data. Remote Sens Environ 86(1):120–131
Combal B, Baret F, Weiss M, Trubuil A, Mace D, Pragne`re A, Myneni R, Knyazikhin Y, Wang L (2002) Retrieval of canopy biophysical variables from bidirectional reflectance using prior information to solve the ill-posed inverse problem. Remote Sens Environ 84:1–15
Cooper GF, Herskovits E (1992) A Bayesian method for the induction of probabilistic networks from data. Mach Learn 9(4):309–347
Coops NC, Smith ML, Martin M, Ollinger SV (2003) Prediction of eucalypt foliage nitrogen content from satellite-derived hyperspectral data. IEEE Trans Geosci Remote Sens 41 (6):1338–1346
Cornelissen JH, Lavorel S, Garnier E, Diaz S, Buchmann N, Gurvich DE, Reich PB, Ter Steege H, Morgan HD, Van Der Heijden MG, Pausas JG (2003) A handbook of protocols for standardised and easy measurement of plant functional traits worldwide. Aust J Bot 51(4):335–380
Croft H, Chen JM, Luo X, Bartlett P, Chen B, Staebler RM (2017) Leaf chlorophyll content as a proxy for leaf photosynthetic capacity. Glob Chang Biol 23(9):3513–3524
Cui S, Zhou K (2017) A comparison of the predictive potential of various vegetation indices for leaf chlorophyll content. Earth Sci Inf 10(2):169–181
Curran P, Windham W, Gholz H (1995) Exploring the relationship between reflectance red edge and chlorophyll concentration in Slash Pine Leaves. Tree Physiol 15:203–206
Darvishzadeh R, Skidmore A, Schlerf M, Atzberger C (2008) Inversion of a radiative transfer model for estimating vegetation LAI and chlorophyll in a heterogeneous grassland. Remote Sens Environ 112(5):2592–2604
Darvishzadeh R, Skidmore A, Abdullah H, Cherenet E, Ali A, Wang T, Nieuwenhuis W, Heurich M, Vrieling A, O'Connor B, Paganini M (2019a) Mapping leaf chlorophyll content from Sentinel-2 and RapidEye data in spruce stands using the invertible forest reflectance model. Int J Appl Earth Obs Geoinf 79:58–70
Darvishzadeh R, Wang T, Skidmore A, Vrieling A, O'Connor B, Gara TW, Ens BJ, Paganini M (2019b) Analysis of Sentinel-2 and RapidEye for retrieval of leaf area index in a saltmarsh using a radiative transfer model. Remote Sens 11(6):671
Daughtry C (2001) Discriminating crop residues from soil by short-wave infrared reflectance. Agron J 93(2001):125–131
Daughtry CS, Walthall CL, Kim MS, De Colstoun EB, McMurtrey Iii JE (2002) Estimating corn leaf chlorophyll concentration from leaf and canopy reflectance. Remote Sens Environ 74 (2):229–239
de Wit AJW (1999) The application of a genetic algorithm for crop model steering using NOAA-AVHRR data. In: Bellingham W (ed) Remote sensing for earth science, ocean, and sea ice

applications, SPIE Proceedings, Society of Photo-Optical Instrumentation Engineers (SPIE), Florence, Italy. Bellingham, Washington, DC

Delegido J, Alonso L, González G, Moreno J (2010) Estimating chlorophyl content of crops from hyperspectral data using a normalized area over reflectance curve (NAOC). Int J Appl Earth Obs Geoinf 12(3):165–174

Delegido J, Verrelst J, Meza CM, River JP, Alonso L, Moreno J (2013) A red-edge spectral index for remote sensing estimation of green LAI over agroecosystems. Eur J Agron 46:45–52

Delegido J, Van Wittenberghe S, Verrelst J, Ortiz V, Veroustraete F, Valcke R, Samson R, Rivera JP, Tenjo C, Moreno J (2014) Chlorophyll content mapping of urban vegetation in the city of Valencia based on the hyperspectral NAOC index. Ecol Indic 40:34–42

Djamai N, Fernandes R, Weiss M, McNairn H, Goïta K Validation and comparison of cropland leaf area index retrievals from Sentinel-2/MSI Data Using Sl2P Processor and vegetation indices models. In IGARSS 2019-2019 IEEE International Geoscience and Remote Sensing Symposium 2019 Jul 28 (pp 4595–4598). IEEE

D'Odorico P, Gonsamo A, Pinty B, Gobron N, Schaepman M, Coops NC, Mendez E (2014) Intercomparison of fraction of absorbed photosynthetically active radiation products derived from satellite data over Europe. Remote Sens Environ 142:141–154

Dong T, Meng J, Shang J, Liu J, Wu B (2015) Evaluation of chlorophyll-related vegetation indices using simulated sentinel-2 data for estimation of crop fraction of absorbed photosynthetically active radiation. IEEE J Sel Top Appl Earth Obs Remote Sens 8:4049–4059

Dorigo WA, Zurita-Milla R, de Wit AJW, Brazile J, Singh R, Schaepman ME (2007) A review on reflective remote sensing and data assimilation techniques for enhanced agroecosystem modeling. Int J Appl Earth Obs Geoinf 9(2):165–193

Durbha SS, King RL, Younan NH (2007) Support vector machines regression for retrieval of leaf area index from multiangle imaging spectroradiometer. Remote Sens Environ 107 (1–2):348–361

Eklundh L, Hall K, Eriksson H, Ardö J, Pilesjö P (2003) Investigating the use of Landsat thematic mapper data for estimation of forest leaf area index in southern Sweden. Can J Remote Sens 29:349–362

Fang H, Liang S (2005) A hybrid inversion method for mapping leaf area index from MODIS data: experiments and application to broadleaf and needleleaf canopies. Remote Sens Environ 94 (3):405–424

Fang H, Liang S, Kuusk A (2003) Retrieving leaf area index using a genetic algorithm with a canopy radiative transfer model. Remote Sens Environ 85(3):257–270

Faurtyot T, Baret F (1997) Vegetation water and dry matter contents estimated from top-of-the-atmosphere reflectance data: a simulation study. Remote Sens Environ 61(1):34–45

Féret JB, Gitelson AA, Noble SD, Jacquemoud S (2017) PROSPECT-D towards modeling leaf optical properties through a complete lifecycle. Remote Sens Environ 193:204–215

Field CB, Randerson JT, Malmstrom CM (1995) Global net primary production: combining ecology and remote sensing. Remote Sens Environ 51(1):75–88

Fukshansky L, Fukshansky-Kazarinova N, Martinez V, Remisowsky A (1991) Estimation of optical parameters in a living tissue by solving the inverse problem to the multiflux radiative transfer. Appl Opt 30(22):3145–3153

Gallego FJ, Kussul N, Skakun S, Kravchenko O, Shelestov A, Kussul O (2014) Efficiency assessment of using satellite data for crop area estimation in Ukraine. Int J Appl Earth Obs Geoinf 29:22–30

Gamon J, Serrano L, Surfus J (1997) The photochemical reflectance index: an optical indicator of photosynthetic radiation use efficiency across species, functional types and nutrient levels. Oecologia 112:492–501

Garnier E, Lavorel S, Ansquer P, Castro H, Cruz P, Dolezal J, Eriksson O, Fortunel C, Freitas H, Golodets C, Grigulis K (2007) Assessing the effects of land-use change on plant traits, communities and ecosystem functioning in grasslands: a standardized methodology and lessons from an application to 11 European sites. Ann Bot 99(5):967–985

Gausman HW (1985) Plant leaf optical properties in visible and nearinfrared light, Graduate Studies, Texas Tech University (No. 29). Texas Tech Press, Lubbock, Texas, p 78
Gitelson A, Merzlyak M (1994) Spectral reflectance changes associated with autumn senescence of Aesculus Hippocastanum L. and Acer Platanoides L. leaves. J Plant Physiol 143(1994):286–292
Gitelson A, Merzlyak M (1998) Remote sensing of chlorophyll concentration in higher plant leaves. Adv Space Res 22(1998):689–692
Gitelson A, Gritz Y, Merzlyak M (2003) Relationships between leaf chlorophyll content and spectral reflectance and algorithms for non-destructive chlorophyll assessment in higher plant leaves. J Plant Physiol 160:271–282
Gitelson AA, Keydan GP, Merzlyak MN (2006) Three-band model for noninvasive estimation of chlorophyll, carotenoids, and anthocyanin contents in higher plant leaves. Geophys Res Lett 33 (L11402):1–5. https://doi.org/10.1029/2006GL026457
Glenn EP, Huete AR, Nagler PL, Nelson SG (2008) Relationship between remotely-sensed vegetation indices, canopy attributes and plant physiological processes: what vegetation indices can and cannot tell us about the landscape. Sensors 8(4):2136–2160
Gobron N, Pinty B, Taberner M et al (2006) Monitoring the photosynthetic activity of vegetation from remote sensing data. Adv Space Res 38(10):2196–2202
Goel NS, Grier T (1988) Estimation of canopy parameters for inhomogeneous vegetation canopies from reflectance data: III. Trim: a model for radiative transfer in heterogeneous threedimensional canopies. Remote Sens Environ 25(3):255–293
Govaerts YM, Jacquemoud S, Verstraete MM, Ustin SL (1996) Three-dimensional radiation transfer modeling in a dicotyledon leaf. Appl Opt 35(33):6585–6598
Goward SN, Williams DL (1997) Landsat and earth systems science: development of terrestrial monitoring. Photogramm Eng Remote Sens 63(7):887–900
Gowda PH, Oommen T, Misra D, Schwartz RC, Howell TA, Wagle P (2015) Retrieving leaf area index from remotely sensed data using advanced statistical approaches. J Remote Sens GIS 5:156
Haboudane D, Miller JR, Pattey E, Zarco-Tejada PJ, Strachan IB (2004) Hyperspectral vegetation indices and novel algorithms for predicting green LAI of crop canopies: modeling and validation in the context of precision agriculture. Remote Sens Environ 90(3):337–352
Hall FG, Townshend JR, Engman ET (1995) Status of remote sensing algorithms for estimation of land surface state parameters. Remote Sens Environ 51(1):138–156
Hilker T, Lepine L, Coops NC, Jassal RS, Black TA, Wulder MA, Ollinger S, Tsui O, Day M (2012) Assessing the impact of N-fertilization on biochemical composition and biomass of a Douglas-fir canopy—a remote sensing approach. Agric For Meteorol 153:124–133
Homolova L, Malenovský Z, Clevers JG, García-Santos G, Schaepman ME (2013) Review of optical-based remote sensing for plant trait mapping. Ecol Complex 15:1–6
Houborg R, Boegh E (2008) Mapping leaf chlorophyll and leaf area index using inverse and forward canopy reflectance modeling and SPOT reflectance data. Remote Sens Environ 112 (1):186–202
Houborg R, Soegaard H, Boegh E (2007) Combining vegetation index and model inversion methods for the extraction of key vegetation biophysical parameters using Terra and Aqua MODIS reflectance data. Remote Sens Environ 106(1):39–58
Houborg R, McCabe M, Cescatti A, Gao F, Schull M, Gitelson A (2015) Joint leaf chlorophyll content and leaf area index retrieval from Landsat data using a regularized model inversion system (REGFLEC). Remote Sens Environ 159:203–221
Huang ZC, Turner B, Dury S, Wallis I, Foley W (2004) Estimating foliage nitrogen concentration from HyMap data using continuum removal analysis. Remote Sens Environ 93(1–2):18–29
Huemmrich KF (2001) The GeoSail model: a simple addition to the SAIL model to describe discontinuous canopy reflectance. Remote Sens Environ 75(3):423–431
Huete A (1988) A Soil-Adjusted Vegetation Index (SAVI). Remote Sens Environ 25 (1988):295–309

Huete A, Didan K, Miura T, Rodriguez EP, Gao X, Ferreira LG (2002) Overview of the radiometric and biophysical performance of the MODIS vegetation indices. Remote Sens Environ 83 (1–2):195–213

Im J, Jensen J, Coleman M, Nelson E (2009) Hyperspectral remote sensing analysis of short rotation woody crops grown with controlled nutrient and irrigation treatments. Geocarto Int 24 (4):293–312

Inoue Y, Guérif M, Baret F, Skidmore A, Gitelson A, Schlerf M, Darvishzadeh R, Olioso A (2016) Simple and robust methods for remote sensing of canopy chlorophyll content: a comparative analysis of hyperspectral data for different types of vegetation. Plant Cell Environ 39 (12):2609–2623

Jacquemoud S, Baret F (1990) PROSPECT: a model of leaf optical properties spectra. Remote Sens Environ 34(2):75–91

Jacquemoud S, Ustin SL (2001) Leaf optical properties: a state of the art. In: Proceedings of the Eighth International Symposium Physical Measurements & Signatures in Remote Sensing, CNES, Aussois, France

Jacquemoud S, Verdebout J, Schmuck G, Andreoli G, Hosgood B, Carrere V (1994) Estimation of leaf water content by inversion of the PROSPECT model. Comparison with spectral indices. Trans Am Geophys Union 75(44):206

Jacquemoud S, Baret F, Andrieu B, Danson FM, Jaggard K (1995) Extraction of vegetation biophysical parameters by inversion of the PROSPECT + SAIL models on sugar beet canopy reflectance data. Application to TM and AVIRIS sensors. Remote Sens Environ 52(3):163–172

Jacquemoud S, Bacour C, Poilve H, Frangi JP (2000) Comparison of four radiative transfer models to simulate plant canopies reflectance: direct and inverse mode. Remote Sens Environ 74 (3):471–481

Jensen R, Hardin P, Hardin A (2012) Estimating urban leaf area index (LAI) of individual trees with hyperspectral data. Photogramm Eng Remote Sens 78(5):495–504

Jin YQ, Liu C (1997) Biomass retrieval from high-dimensional active/passive remote sensing data by using artificial neural networks. Int J Remote Sens 18(4):971–979

Jones CL, Maness NO, Stone ML, Jayasekara R (2007) Chlorophyll estimation using multispectral reflectance and height sensing. Trans ASABE 50(5):1867–1872

Kalacska M, Sanchez-Azofeifa G, Caelli T, Rivard B, Boerlage B (2005) Estimating leaf area index from satellite imagery using bayesian networks. IEEE Trans Geosci Remote Sens 43 (8):1866–1873

Karimi Y, Prasher S, Madani A, Kim S (2008) Application of support vector machine technology for the estimation of crop biophysical parameters using aerial hyperspectral observations. Can Biosyst Eng/Le Genie des biosystems au Canada 50:7.13–7.20

Karnieli A (2003) Natural vegetation phenology assessment by ground spectral measurements in two semi-arid environments. Int J Biometeorol 47:179–187

Khanna S, Palacios-Orueta A, Whiting ML, Ustin SL, Riaño D, Litago J (2007) Development of angle indexes for soil moisture estimation, dry matter detection and land-cover discrimination. Remote Sens Environ 109:154–165

Kimes DS, Nelson RF, Manry MT, Fung AK (1998) Attributes of neural networks for extracting continuous vegetation variables from optical and radar measurements. Int J Remote Sens 19 (14):2639–2662

Kimes D, Nelson R, Salas W, Skole D (1999) Mapping secondary tropical forest and forest age from SPOT HRV data. Int J Remote Sens 20(18):3625–3640

Kira O, Nguy-Robertson AL, Arkebauer TJ, Linker R, Gitelson AA (2016) Informative spectral bands for remote green LAI estimation in C3 and C4 crops. Agric For Meteorol 218–219:243–249

Kneubühler Mathias Naef C, Itten Klaus I (2000) Assessment of crop vitality through analysis of combined field and laboratory measurements of biophysical and biochemical parameters. In: 2th EARsel workshop on Imaging Spectroscopy, Enschede, Netherlands, 11 July 2000 – 13 July 2000, n/

Knyazikhin Y, Glassy J, Privette JL, Tian Y, Lotsch A, Zhang Y, Wang Y, Morisette JT, Votava T, Myneni RB, Nemani RR, Running SW (1999) MODIS leaf area index (LAI) and fraction of photosynthetically active radiation absorbed by vegetation (FPAR) product (MOD15), algorithm theoretical basis document (ATBD), Version 4.0. http://eospso.gsfc.nasa.gov/atbd/modistables.html

Kogan F, Kussul N, Adamenko T, Skakun S, Kravchenko O, Kryvobok O, Shelestov A, Kolotii A, Kussul O, Lavrenyuk A (2013) Winter wheat yield forecasting in Ukraine based on Earth observation, meteorological data and biophysical models. Int J Appl Earth Obs Geoinf 23:192–203

Kolotii A, Kussul N, Shelestov A, Skakun S, Yailymov B, Basarab R, Lavreniuk M, Oliinyk T, Ostapenko V (2015) Comparison of biophysical and satellite predictors for wheat yield forecasting in Ukraine. In: International archives of the photogrammetry, remote sensing & spatial information sciences, 36th international symposium on remote sensing of environment, vol XL-7/W3. Germany, Berlin

Kravchenko AN (2009) Neural network method to solve inverse problems for canopy radiative transfer models. Cybern Syst Anal 45(3):477–488

Kuusk A (1998) Monitoring of vegetation parameters on large areas by the inversion of a canopy reflectance model. Int J Remote Sens 19(15):2893–2905

Lavorel S, Grigulis K, Lamarque P, Colace MP, Garden D, Girel J, Pellet G, Douzet R (2011) Using plant functional traits to understand the landscape distribution of multiple ecosystem services. J Ecol 99(1):135–147

Le Maire G, François C, Dufrène E (2004) Towards universal broad leaf chlorophyll indices using PROSPECT simulated database and hyperspectral reflectance measurements. Remote Sens Environ 89(1):1–28

Le Maire G, Marsden C, Nouvellon Y, Grinand C, Hakamada R, Stape JL, Laclau JP (2011) MODIS NDVI time-series allow the monitoring of Eucalyptus plantation biomass. Remote Sens Environ 115(10):2613–2625

Li X, Liu X, Liu M, Wu L (2014) Random forest algorithm and regional applications of spectral inversion model for estimating canopy nitrogen concentration in rice. J Remote Sens 18 (4):934–945

Liang NS (2004) Estimation of land surface biophysical variables. In: Kong GA (ed) Qualitative remote sensing of land surfaces, Wiley series in remote sensing. Wiley, New York, pp 246–309

Liang S (2007) Recent developments in estimating land surface bio-geophysical variables from optical remote sensing. Prog Phys Geogr 31(5):501–516

Liang L, Qin Z, Zhao S, Di L, Zhang C, Deng M, Lin H, Zhang L, Wang L, Liu Z (2016) Estimating crop chlorophyll content with hyperspectral vegetation indices and the hybrid inversion method. Int J Remote Sens 37(13):2923–2949

Lichtenthaler HK, Buschmann C (2001) Chlorophylls and carotenoids: measurement and characterization by UV-VIS spectroscopy. Curr Protocol Food Anal Chem 1(1):F4–F3

Liu J, Chen JM, Cihlar J et al (1997) A process based boreal ecosystem productivity simulator using remote sensing inputs. Remote Sens Environ 62:158–175

Liu J, Pattey E, Jégo G (2012) Assessment of vegetation indices for regional crop green LAI estimation from Landsat images over multiple growing seasons. Remote Sens Environ 123:347–358

Luther JE, Carroll AL (1999) Development of an index of balsam fir vigor by foliar spectral reflectance. Remote Sens Environ 69(3):241–252

Maier SW, Ludeker W, Gunther KP (1999) SLOP: a revised version of the stochastic model for leaf optical properties. Remote Sens Environ 68(3):273–280

Majasalmia T, Stenberga P, Rautiainenb M (2017) Comparison of ground and satellite-based methods for estimatingstand-level fPAR in a boreal forest. Agric For Meteorol 232:422–432

Malenovský Z, Ufer C, Lhotakova Z, Clevers JGPW, Schaepman ME, Albrechtova J, Cudlin P (2006) A new hyperspectral index for chlorophyll estimation of a forest canopy: area under curve normalised to maximal band depth between 650–725 nm. EARSeL eProc 5(2):161–172

Mariotto I, Thenkabail P, Huete A, Slonecker E, Platonov A (2013) Hyperspectral versus multispectral crop-productivity modeling and type discrimination for the HyspIRI mission. Remote Sens Environ 139:291–305

Meena RS, Mitran T, Kumar S, Yadav G, Bohra JS, Datta R (2018) Application of remote sensing for sustainable agriculture and forest management. Inf Process Agric 5:295–297

Meena RS, Kumar V, Yadav GS, Mitran T (2018a) Response and interaction of *Bradyrhizobium japonicum* and Arbuscular mycorrhizal fungi in the soybean rhizosphere: a review. Plant Growth Regul 84:207–223

Meroni M, Colombo R, Panigada C (2004) Inversion of a radiative transfer model with hyperspectral observations for LAI mapping in poplar plantations. Remote Sens Environ 92 (2):195–206

Miphokasap P, Honda K, Vaiphasa C, Souris M, Nagai M (2012) Estimating canopy nitrogen concentration in sugarcane using field imaging spectroscopy. Remote Sens 4(6):1651–1670

Mitchell J, Glenn N, Sankey T, Derryberry D, Germino M (2012) Remote sensing of sagebrush canopy nitrogen. Remote Sens Environ 124:217–223

Moghaddam M, Saatchi SS (1999) Monitoring tree moisture using an estimation algorithm applied to SAR data from BOREAS. IEEE Trans Geosci Remote Sens 37(2):901–916

Moran MS, Clarke TR, Inoue Y, Vidal A (1994) Estimating crop water deficit using the relation between surface-air temperature and spectral vegetation index. Remote Sens Environ 49 (3):246–263

Moran MS, Inoue Y, Barnes EM (1997) Opportunities and limitations for image-based remote sensing in precision crop management. Remote Sens Environ 61(3):319–346

Mousivand A, Menenti M, Gorte B, Verhoef W (2014) Global sensitivity analysis of the spectral radiance of a soil–vegetation system. Remote Sens Environ 145:131–144

Mridha NI, Sahoo RN, Kumar DN, Sehgal V, Krishna GO, Pradhan S, Gupta V (2014) Genetic algorithm based inversion modelling of PROSAIL for retrieval of wheat biophysical parameters from bi-directional reflectance data. J Agric Phys 14:87–95

Muller SJ, Sithole P, Singels A, Niekerka AV (2020) Assessing the fidelity of landsat-based fapar models in two diverse sugarcane growing regions. Comput Electron Agric 170:105248

Mustafa Y, Van Laake P, Stein A (2011) Bayesian network modeling for improving forest growth estimates. IEEE Trans Geosci Remote Sens 49(2):639–649

Mustafa Y, Stein A, Tolpekin V, van Laake P (2012) Improving forest growth estimates using a Bayesian network approach. Photogramm Eng Remote Sens 78(1):45

Mutanga O, Skidmore A, Kumar L, Ferwerda J (2005) Estimating tropical pasture quality at canopy level using band depth analysis with continuum removal in the visible domain. Int J Remote Sens 26(6):1093–1108

Mutanga O, Adam E, Cho MA (2012) High density biomass estimation for wetland vegetation using worldview-2 imagery and random forest regression algorithm. Int J Appl Earth Obs Geoinf 18(1):399–406

Navarro-Cerrillo RM, Trujillo J, de la Orden MS, Hernández-Clemente R (2014) Hyperspectral and multispectral satellite sensors for mapping chlorophyll content in a Mediterranean Pinus sylvestris L. plantation. Int J Appl Earth Obs Geoinf 26:88–96

Paruelo J, Tomasel F (1997) Prediction of functional characteristics of ecosystems: a comparison of artificial neural networks and regression models. Ecol Model 98(2–3):173–186

Pasqualotto N, Delegido J, Van Wittenberghe S, Verrelst J, Rivera JP, Moreno J (2018) Retrieval of canopy water content of different crop types with two new hyperspectral indices: water absorption area index and depth water index. Int J Appl Earth Obs Geoinf 67:69–78

Peñuelas J, Gamon JA, Fredeen AL, Merino J, Field CB (1994) Reflectance indices associated with physiological changes in nitrogen-and water-limited sunflower leaves. Remote Sens Environ 48 (2):135–146

Pisek J, Chen JM, Nilson T (2011) Estimation of vegetation clumping index using MODIS BRDF data. Int J Remote Sens 32(9):2645–2657

Prince SD, Goward SN (1995) Global primary production: a remote sensing approach. J Biogeogr 22:815–835

Pu R, Cheng J (2015) Mapping forest leaf area index using reflectance and texturalinformation derived from WorldView-2 imagery in a mixed natural forest area inFlorida, US. Int J Appl Earth Obs Geoinf 42:11–23

Pu R, Gong P, Biging GS, Larrieu MR (2003) Extraction of red edge optical parameters from Hyperion data for estimation of forest leaf area index. IEEE Trans Geosci Remote Sens 41:916–921

Putzenlechner B, Castro S, Kiese R, Ludwig R, Marzahn P, Sharp I, Sanchez-Azofeifa A (2019) Validation of sentinel-2 fapar products using ground observations across three forest ecosystems. Remote Sens Environ 232:111310

Ramoelo A, Skidmore A, Schlerf M, Mathieu R, Heitkönig I (2011) Waterremoved spectra increase the retrieval accuracy when estimating savanna grass nitrogen an phosphorus concentrations. ISPRS J Photogramm Remote Sens 66(4):408–417

Rasmussen MS (1997) Operational yield forecast using AVHRR NDVI data: reduction of environmental and inter-annual variability. Int J Remote Sens 18(5):1059–1077

Richter T, Fukshansky L (1996) Optics of a bifacial leaf. 1: a novel combined procedure for deriving the optical parameters. J Photochem Photobiol 63:507–516

Richter K, Atzberger C, Vuolo F, Weihs P, D'Urso G (2009) Experimental assessment of the Sentinel-2 band setting for RTM-based LAI retrieval of sugar beet and maize. Can J Remote Sens 35(3):230–247

Rivera JP, Verrelst J, Delegido J, Veroustraete F, Moreno J (2014) On the semiautomatic retrieval of biophysical parameters based on spectral index optimization. Remote Sens 6(6):4924–4951

Román MO, Gatebe CK, Schaaf CB, Poudyal R, Wang Z, King MD (2011) Variability in surface BRDF at different spatial scales (30 m–500 m) over a mixed agricultural landscape as retrieved from airborne and satellite spectral measurements. Remote Sens Environ 115(9):2184–2203

Rondeaux G, Steven M, Baret F (1996) Optimization of soil-adjusted vegetation indices. Remote Sens Environ 55:95–107

Rouse JW, Haas RH, Schell JA, Deering DW (1974) Monitoring vegetation systems in the Great Plains with ERTS. NASA Spec Publ 351:309–317

Ruimy A, Kergoat L, Bondeau A and potsdam NPP model intercomparison participants (1999) Comparing global NPP models of terrestrial net primary productivity (NPP): analysis of differences in light absorption and light-use efficiency, Glob Chang Biol 5(Suppl. 1):56–64

Running SW, Nemani RR, Peterson DL, Band LE, Potts DF, Pierce LL, Spanner MA (1989) Mapping regional forest evapotranspiration and photosynthesis by coupling satellite data with ecosystem simulation. Ecology 70(4):1090–1101

Satapathy S, Dadhwal VK (2005) Principal component inversion technique for the retrieval of leaf area index. J Indian Soc Remote Sens 33(2):323–330

Schlerf M, Atzberger C (2006) Inversion of a forest reflectance model to estimate structural canopy variables from hyperspectral remote sensing data. Remote Sens Environ 100(3):281–294

Schlerf M, Atzberger C, Hill J, Buddenbaum H, Werner W, Schuller G (2010) Retrieval of chlorophyll and nitrogen in Norway spruce (Picea abies L. Karst.) using imaging spectroscopy. Int J Appl Earth Obs Geoinf 12(1):17–26

Scurlock JMO, Cramer W, Olson RJ et al (1999) Terrestrial NPP: toward a consistent data set for global model evaluation. Ecol Appl 9(3):913–919

Sehgal VK, Chakraborty D, Sahoo RN, Pradhan S (2013) Canopy radiative transfer models and their inversion for the quantification of vegetation biophysical parameters from remote sensing. In: Soam SK, Sreekant PD, Rao NH (eds) Geospatial technologies for natural resources management, 1st edn. ; Chapter: 12. New India Publishing Agency, New Delhi

Sehgal VK, Chakraborty D, Sahoo RN (2016) Inversion of radiative transfer model for retrieval of wheat biophysical parameters from broadband reflectance measurements. Inf Process Agric 3 (2):107–118

Shelestov A, Kolotii A, Skakun S, Baruth B, Lozano RL, Yailymov B (2017) Biophysical parameters mapping within the SPOT-5 take 5 initiative. Eur J Remote Sens 50(1):300–309
Singhal G, Bansod B, Mathew L, Goswami J, Choudhury BU, Raju PL (2019) Estimation of leaf chlorophyll concentration in turmeric (Curcuma longa) using high-resolution unmanned aerial vehicle imagery based on Kernel ridge regression. J Indian Soc Remote Sens 47(7):1111–1122
Skidmore AK, Pettorelli N, Coops NC, Geller GN, Hansen M, Lucas R, Mücher CA, O'Connor B, Paganini M, Pereira HM, Schaepman ME (2015) Environmental science: agree on biodiversity metrics to track from space. Nature 523(7561):403–405
Souza AA, Galvão LS, Santos JR (2010) Relationships between Hyperion-derived vegetation indices, biophysical parameters, and elevation data in a Brazilian savannah environment. Remote Sens Lett 1(1):55–64
Stimson H, Breshears D, Ustin S, Kefauver S (2005) Spectral sensing of foliar water conditions in two co-occurring conifer species: Pinus edulis and Juniperus monosperma. Remote Sens Environ 96(1):108–118
Sun Y, Qin Q, Ren H, Zhang T, Chen S (2020) Red-edge band vegetation indices for leaf area index estimation from sentinel-2/MSI imagery. IEEE Trans Geosci Remote Sens 58(2):826–840
Tao X, Liang S, He T, Jin H (2016) Estimation of fraction of absorbed photosynthetically active radiation from multiple satellite data: model development and validation. Remote Sens Environ 184:539–557
Thenkabail PS, Smith RB, De Pauw E (2002) Hyperspectral vegetation indices and their relationships with agricultural crop characteristics. Remote Sens Environ 71(2):158–182
Tillack A, Clasen A, Kleinschmit B, Förster M (2014) Estimation of the seasonal leaf area index in an alluvial forest using high-resolution satellite-based vegetation indices. Remote Sens Environ 141:52–63
Trombetti M, Riaño D, Rubio M, Cheng Y, Ustin S (2008) Multi-temporal vegetation canopy water content retrieval and interpretation using artificial neural networks for the continental USA. Remote Sens Environ 112(1):203–215
Tucker C (1979) Red and photographic infrared linear combinations for monitoring vegetation. Remote Sens Environ 8:127–115
Tucker CJ (1980) Remote sensing of leaf water content in the near infrared. Remote Sens Environ 10(1):23–32
Tuia D, Verrelst J, Alonso L, Pérez-Cruz F, Camps-Valls G (2011) Multioutput support vector regression for remote sensing biophysical parameter estimation. IEEE Geosci Remote Sens Lett 8(4):804–808
Upreti D, Huang W, Kong W, Pascucci S, Pignatti S, Zhou X, Ye H, Casa R (2019) A comparison of hybrid machine learning algorithms for the retrieval of wheat biophysical variables from sentinel-2. Remote Sens 11(5):481
Ustin SL, Roberts DA, Gamon JA, Asner GP, Green RO (2004) Using imaging spectroscopy to study ecosystem processes and properties. Bioscience 54(6):523–534
Vannier C, Vasseur C, Hubert-Moy L, Baudry J (2011) Multiscale ecological assessment of remote sensing images. Landsc Ecol 26(8):1053–1069
Verger A, Baret F, Camacho F (2011) Optimal modalities for radiative transfer-neural network estimation of canopy biophysical characteristics: evaluation over an agricultural area with CHRIS/PROBA observations. Remote Sens Environ 115(2):415–426
Verhoef W, Bach H (2003) Simulation of hyperspectral and directional radiance images using coupled biophysical and atmospheric radiative transfer models. Remote Sens Environ 87 (1):23–41
Verrelst J, Schaepman M, Koetz B, Kneubühler M (2008) Angular sensitivity analysis of vegetation indices derived from CHRIS/PROBA data. Remote Sens Environ 112(5):2341–2353
Verrelst J, Schaepman ME, Malenovsky Z, Clevers JGPW (2010) Effects of woody elements on simulated canopy reflectance: implications for forest chlorophyll content retrieval. Remote Sens Environ 114(3):647–656

Verrelst J, Muñoz J, Alonso L, Delegido J, Rivera J, Camps-Valls G, Moreno J (2012) Machine learning regression algorithms for biophysical parameter retrieval: opportunities for Sentinel-2 and -3. Remote Sens Environ 118:127–139

Verrelst J, Camps-Valls G, Muñoz-Marí J, Rivera JP, Veroustraete F, Clevers JG, Moreno J (2015a) Optical remote sensing and the retrieval of terrestrial vegetation bio-geophysical properties–a review. ISPRS J Photogramm Remote Sens 108:273–290

Verrelst J, Rivera J, Veroustraete F, Muñoz-Marí J, Clevers JGPW, Camps-Valls G, Moreno J (2015b) Experimental sentinel-2 LAI estimation using parametric, non-parametric and physical retrieval methods – a comparison. ISPRS J Photogramm Remote Sens 108:260–272. https://doi.org/10.1016/j.isprsjprs.2015.04.013

Verrelst J, Rivera J, Leonenko G, Alonso L, Moreno J (2014) Optimizing LUT based RTM inversion for semiautomatic mapping of crop biophysical parameters from sentinel-2 and -3 data: role of cost functions. IEEE Trans Geosci Rem Sens 52:257–269

Verrelst J, Dethier S, Rivera JP, Munoz-Mari J, Camps-Valls G, Moreno J (2016) Active learning methods for efficient hybrid biophysical variable retrieval. IEEE Geosci Remote Sens Lett 13 (7):1012–1016

Vohland M, Mader S, Dorigo W (2010) Applying different inversion techniques to retrieve stand variables of summer barley with PROSPECT+ SAIL. Int J Appl Earth Obs Geoinf 12(2):71–80

Vuolo F, Atzberger C, Richter K, D'Urso G, Dash J (2010) Retrieval of biophysical vegetation products from rapideye imagery. In: Wagner W, Székely B (eds) ISPRS TC VII symposium – 100 years ISPRS, IAPRS, Vienna, Austria, Vol XXXVIII. Part 7A, 281–286

Vuolo F, Neugebauer N, Bolognesi SF, Atzberger C, D'Urso G (2013) Estimation of leaf area index using DEIMOS-1 data: application and transferability of a semi-empirical relationship between two agricultural areas. Remote Sens 5(3):1274–1291

Walthall C, Dulaney W, Anderson M, Norman J, Fang H, Liang S (2004) A comparison of empirical and neural network approaches for estimating corn and soybean leaf area index from Landsat ETM+ imagery. Remote Sens Environ 92(4):465–474

Weiss M, Baret F (1999) Evaluation of canopy biophysical variable retrieval performances from the accumulation of large swath satellite data. Remote Sens Environ 70(3):293–306

Wocher M, Berger K, Danner M, Mauser W, Hank T (2018) Physically-based retrieval of canopy equivalent water thickness using hyperspectral data. Remote Sens 10:1924

Wu H, Li ZL (2009) Scale issues in remote sensing: a review on analysis. Process Model Sens 9:1768–1793

Xin J, Zhenrong Y, van Leeuwenb L, Driessen PM (2002) Mapping crop key phenological stages in the North China plain using NOAA time series images. Int J Appl Earth Obs Geoinf 4:109–117

Xu C, Qu JJ, Hao X, Cosh MH, Zhu Z, Gutenberg L (2020) Monitoring crop water content for corn and soybean fields through data fusion of MODIS and landsat measurements in Iowa. Agric Water Manag 227:105844

Yang P, Wu WB, Tang HJ, Zhou QB, Zou JQ, Zhang L (2007) Mapping spatial and temporal variations of leaf area index for winter wheat in North China. Agric Sci China 6:1437–1443

Yang F, Sun J, Fang H, Zc Y, Zhang J, Zhu Y, Song K, Wang Z, Hu M (2012) Comparison of different methods for corn LAI estimation over northeastern china. Int J Appl Earth Obs Geoinf 18(1):462–471

Yao Y, Liu Q, Liu Q, Li X (2008) LAI retrieval and uncertainty evaluations for typical row-planted crops at different growth stages. Remote Sens Environ 112(1):94–106

Yuan H, Ma R, Atzberger C, Li F, Loiselle S, Luo J (2015) Estimating forest fAPAR from multispectral landsat-8 data using the invertible forest reflectance model inform. Remote Sens 7:7425–7446

Zarco-Tejada P, Miller J, Noland T, Mohamme G, Sampson P (2001) Scaling-up and model inversion methods with narrow- band optical indices for chlorophyll content estimation in closed forest canopies with hyperspectral data. IEEE Trans Geosci Remote Sens 39 (7):1491–1507

Zarco-Tejada P, Miller J, Mohammed G, Noland T, Sampson P (2002) Vegetation stress detection through chlorophyll a + b estimation and fluorescence effects on hyperspectral imagery. J Environ Qual 31(5):1433–1441

Zarco-Tejada PJ, Berjón A, López-Lozano R, Miller JR, Martín P, Cachorro V, González MR, De Frutos A (2005) Assessing vineyard condition with hyperspectral indices: leaf and canopy reflectance simulation in a rowstructured discontinuous canopy. Remote Sens Environ 99 (3):271–287

Zhang Q, Xiao X, Braswell B, Linder E, Baret F, Ill BM (2005) Estimating light absorption by chlorophyll, leaf and canopy in a deciduous forest using MODIS data and a radiative transfer model. Remote Sens Environ 99(3):357–371

Zhang F, Zhou G, Nilsson C (2014) Remote estimation of the fraction of absorbed photosynthetically active radiation for a maize canopy in Northeast China. J Plant Ecol 8(4):429–435

Chapter 4
Spatialization of Crop Growth Simulation Model Using Remote Sensing

Anima Biswal, Abhishek Chakraborty, and C. S. Murthy

Contents

Abstract Process-based crop growth simulation models (CGSMs) have been proven as a potential tool for analysing crop behaviour and yield prediction in various spatial and temporal scales. Since the early 1960s, the crop growth models (CGMs) have been used broadly: (1) as a tool for the policymakers to make an informed decision for sustainable land management; (2) as a research tool supporting the interdisciplinary studies covering agronomy, plant physiology, agrometeorology, plant breeding, soil science, climate change, market intelligence,

A. Biswal (✉) · A. Chakraborty
Agroecosystem and Modeling Division, Agricultural Sciences and Applications Group, National Remote Sensing Centre, Department of Space, ISRO, Hyderabad, Telangana, India
e-mail: biswal_a@nrsc.gov.in; abhishek_c@nrsc.gov.in

C. S. Murthy
Agricultural Sciences and Applications Group, National Remote Sensing Centre, Department of Space, ISRO, Hyderabad, Telengana, India
e-mail: murthy_cs@nrsc.gov.in

T. Mitran et al. (eds.), *Geospatial Technologies for Crops and Soils*,
https://doi.org/10.1007/978-981-15-6864-0_4

etc.; and (3) as a support tool for education and technology transfer. These models are developed as point-based models to simulate the crop growth and development for a homogeneous unit as a function of crop genotype, management practices, soil physico-chemical properties, and weather variables. The point-based applications of this model are best suited to the need of field experimentation, predicting, and analysing the crop behaviour under different environmental scenarios. But this approach is associated with limited applications at a regional scale under a heterogeneous real-world situation. In this context, satellite remote sensing (RS) techniques could supplement the crop growth modelling particularly by generating "the missing spatial information" for the unit of simulation. Though these two technologies developed independently, today, both of them can be used synergistically under various spatial and temporal scales for overall agriculture development under different socio-economic and climate change scenarios. The present chapter will provide a brief introduction of the CGSM, its scope, and development across the time epochs. It would further elaborate on the framework, methodology, and issues to run the CGSMs at the spatial domain. The role of remote sensing technique to retrieve crop biophysical parameters and its assimilation into CGSMs are also discussed along with future scope and challenges.

Keywords Crop growth model · Data assimilation · Remote sensing · Simulation · Biophysical parameters

Abbreviations

CGM	Crop Growth Model
CGSM	Crop Growth Simulation Model
3DVAR	Three-dimensional Variational Data Assimilation
4DVAR	Four-dimensional Variational Data Assimilation
AGB	Above-ground Biomass
AMIS	Agricultural Market Information System
ANN	Artificial Neural Network
ASTER	Advanced Spaceborne Thermal Emission and Refelectance Radiometer
BRDF	Bidirectional Refelectance Distribution Function
BRF	Bidirectional Reflectance Factor
CGKF	Constant Gain Kalman Filter
DA	Data Assimilation
EnKF	Ensemble Kalman filter
fAPAR	Fractional Absorbed Photosynthetically Active Radiation
GIS	Geographic Information System
GWD	Gridded Weather Data
HBM	Hierarchical Bayesian method
IDW	Inverse Distance Weighting
KF	Kalman Filter
LAI	Leaf Area Index
LUE	Light Use Efficiency

MCMC	Markov Chain Monte Carlo
MODIS	Moderate Resolution Imaging Spectroradiometer
N	Nitrogen
NASA	National Aeronautics and Space Administration
NDVI	Normalized Difference Vegetation Index
NOAA	National Oceanic and Atmospheric Administration
pdf	Probability Density Function
PF	Particle Filter
PTFs	Pedo-transfer Functions
RS	Remote Sensing
RTM	Radiative Transfer Model
SOC	Soil Organic Carbon
UAV	Unmanned Aerial Vehicle
VI	Vegetation Index

4.1 Introduction

CGMs simulate crop yield as a function of environment, crop genotype, and crop management factors mostly at a daily time step. Crop yield and production-related information are very crucial in determining various agronomic as well as socio-economic policy decisions that could affect the livelihood of a large section of the human population (Kasampalis et al. 2018). These crop models also called crop yield models or agriculture system models are just simplified depictions of the real world (Van Ittersum and Donatelli 2003) represented by a set of mathematical equations used to model the processes of the system (Oteng-Darko et al. 2013). Explanatory process-based CGSMs comprise quantitative descriptions of the processes that control the behaviour of a system (Penning de Vries et al. 1989; Dadhwal 2003) and simulate the diurnal effects of environmental factors on the crop growth and development processes. The process-based crop growth model simulates crop growth processes at a daily timescale starting with the sowing of the crop to the final crop harvestable maturity along with the quantitative information about the crop growth and development at each time step. The equation used in the crop model mathematically represents the elementary process of the "soil-plant-atmosphere" system. Three main modules of the crop model could, therefore, be identified. The soil module describes the processes of water and nutrient transport within the soil profile. The mathematical equations for processes like infiltration, drainage, redistribution, and nutrient transport particularly of nitrate are included in this module (Brisson et al. 1998). The plant module controls two mechanisms: (i) crop growth (biomass production-based on interception and assimilation of photosynthetically active solar radiation and finally limited by senescence) and (ii) crop development that simulates the phenology and drives growth by regulating source and sink (Brisson et al. 1998).

These process-based models are very much input data-intensive, hence posing a challenge to create an input database with reasonable accuracy at a desirable scale to run on an operational basis (Wallach et al. 2001). Hence, the application of these models on a regional scale involves lots of assumptions and uncertainties. RS data could be used that provide spatial information on weather, soil, crop type, crop phenology, and crop condition information on a regional scale. This information is assimilated into to crop growth model after proper validation, thus reducing the uncertainty (Dorigo et al. 2007; Jin et al. 2018). The latest developments in geospatial technology such as mobile phone-based position services and geographical information system (GIS) can also be linked to crop growth models to optimize farm management practices, crop stress, and extreme weather events. These models are also used to test the adaptability of new crop variety under different locations, develop breeding strategies, and predict in-season yield. Boote et al. (1996) carried out a detailed review to find out the potential applications and limitations of CGMs and suggested that a particular model is applicable for a given situation and the same can be replicated to alternate environmental setup with proper calibration. The model prediction accuracy is highly dependent on the limitation of input data which in turn restricts its scalability (Clevers et al. 2002). Nevertheless, CGMs can simulate the impact of economic decisions in terms of crop management factors and weather effects (Batchelor et al. 2002) and thus enable informed decisions making. To summarize, the major limitations in the application of CGMs at a regional scale are the generation of necessary high-quality and accurate input data (Bhatia 2014) which may be cost-intensive and time-consuming.

4.1.1 Crop Growth Models: Scope and Development

Agricultural system modelling started long back in the late 1950s and specific crop modelling activities started a decade later. Since the 1960s, a new era in agriculture sciences started with the modelling of photosynthetic rates of crop canopies leading to the development of Elementary CRop growth Simulator (ELCROS) and BAsic CRop growth Simulator (BACROS) by de Wit (1965). In the 1970s, crop models received significant attention (Pinter et al. 2003) with the first attempt to combine the surveillance capacities of RS data with the predictive feature of crop models under the Large Area Crop Inventory Experiment (LACIE) funded by National Aeronautics and Space Administration (NASA) and National Oceanic and Atmospheric Administration (NOAA). Such experiments were carried out to estimate wheat production by combining RS data and crop models. They have developed a method of estimating worldwide wheat production using LANDSAT data (Erickson 1984). In the 1980s, the United States Department of Agriculture (USDA) had developed a model for the tropical environment after a thorough understanding of the system and its components (Jones et al. 2003; Roubtsova 2014) under International Benchmark Sites Network for Agrotechnology Transfer (IBSNAT) program. This leads to the development of a Decision Support System for Agrotechnology Transfer (DSSAT)

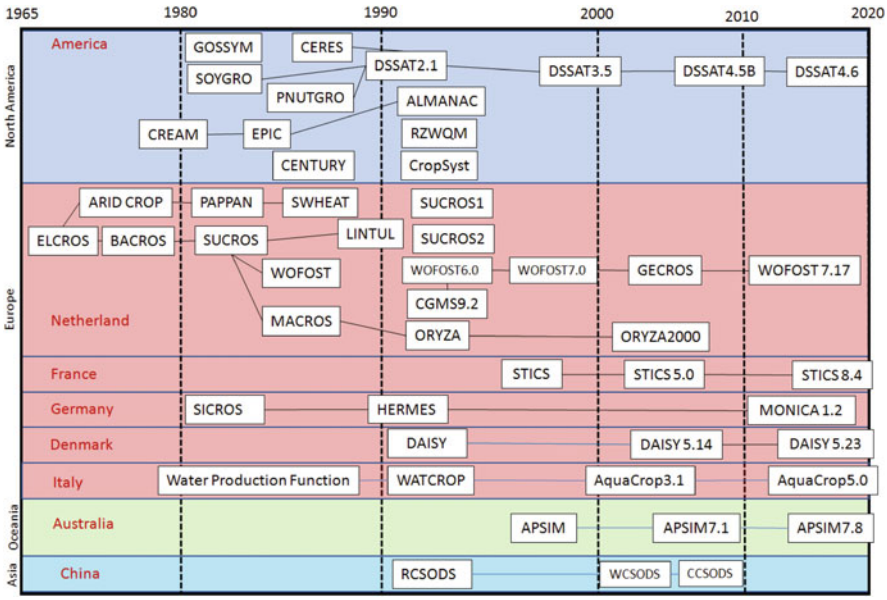

Fig. 4.1 Crop model developments over time. (Modified, Jin et al. 2018)

(Johnson et al. 2003). A schematic representation of the development of these process-based CGSMs over time is shown in Fig. 4.1. Process-based CGMs are descriptive and dynamic, simulating the process of crop growth and development through time in a phased manner using different sets of equations. These models are equipped with modular functions defining various physiological and soil processes as a function of driving variables like weather and crop management at each time step (Wallach et al. 2014). Such models are more input data-intensive than empirical or statistical models (Di Paola et al. 2016). Empirical or statistical models describe the crop growth and yield response over sites where historical data are available and mostly fail over different environmental conditions (Jones et al. 2017). This is the most important limitation of empirical models for studying the implication of climate change scenarios on crop growth and development. For example, location-specific crop management practices may evolve to increase the crop adaptive capacity for the future climate change scenarios, but these management practices were not considered in the limited data used to develop a particular empirical model (Jones et al. 2017). In this context, process-based CGMs are used as a potential tool not only for analysing the impact of climate change but also for selecting best management practices by optimizing all input resources to increase crop adaptability.

4.1.2 Minimum Data Requirement and Applications

Agriculture system operates at several spatial scales such as field, farm, regional, or global along with diverse temporal scales like hours, days, seasonal, and annual (Ewert et al. 2011). Many crop models require a large number of input data. For example, World Food Studies (WOFOST) used by the European Union Joint Resources Centre Monitoring Agricultural Resources (MARS) Unit Mission requires data for about 40 input parameters. However, the Food and Agriculture Organization (FAO) has developed the AquaCrop model that requires comparatively a smaller number of parameters (Mkhabela and Bullock 2012). The information related to weather, soil, crop management, phasic development of the crop, growing degree days, etc. are required for all crop growth model (Monteith and Moss 1977). According to Nix (1983), these input datasets may range in timescale between hours, daily, or weekly basis. For the first time, Hunt and Boote (1998) defined a minimum input data needed for operating crop growth model. The input required for a crop growth model can be categorized into a minimum and optimum/desirable for specific applications along with initial parameters (Ritchie and Alagarswamy 2002) as presented in Table 4.1. Weather is a driving force for CGSMs; hence, it needs maximum and minimum temperature, rainfall, solar radiation, etc. on a daily or weekly timescale depending on the defined time step of the model in a prescribed format. Several curve-fitting approaches like extrapolation function and interpolation are being followed over weather data for filling spatial and temporal data gaps in the model operation. Similarly, most of the commonly used models take layer-wise soil input data which includes various soil physico-chemical properties like bulk density (BD), soil texture, soil organic carbon (SOC), water content at field capacity and wilting point, initial nitrogen (N) content, and pH. Feeding the crop model with the crop management information is the most challenging task particularly when a simulation is carried out on a regional scale. The details of these data requirements are discussed in the subsequent section along with the scale and resolution issues involved in spatializing the CGSMs.

The economic outputs like grain yield, fruit yield, and biomass can be predicted through crop models (Murthy 2003). The management applications of crop simulation models can be categorized as follows:

Strategic application: To run the model before planting.

Practical application: To run the model before and during crop growth.

Forecasting application: To predict yield both before and during crop growth.

Besides the impact of climate change on crop growth and yield, crop vulnerability and adaptability analysis can be assessed through crop growth simulation modelling (Rosenzweig et al. 2014). These models are also useful to analyse the difference between actual and attainable crop yield, i.e. yield gap analysis (Lobell et al. 2009; van Ittersum et al. 2013). A list of popular CGSMs used worldwide along with their special uses is presented in Table 4.2.

However, most of these models are not able to generate integrated information on global climate change (greenhouse gas emission) and its impact on soil C and N

Table 4.1 Minimum data requirement for a crop growth simulation model

Input category	Weather	Soil	Crop management
Minimum	**Daily**, min and max temperature, precipitation Solar radiation	Water content at lower limit and field capacity (at10–20 cm soil depth) Crop root depth Hydraulic conductivity at depths of soil which restrict water flow	Characteristics of crops Date and depth of planting Density of plant population Date, amount, and depth of irrigation Date, amount, and types of fertilizers Date, amount, and quality of manure, crop residues, etc.
Optional/desirable for specific application	**Daily**, dew point temperature, wind profile, net radiation Rainfall intensity	Water retention curves and hydraulic conductivity (at 10–20 cm depth) Curve number of run-off Surface albedo Soil pH (10–20 cm depth) SOC at upper depths Soil textural information (at 10–20 cm depths) Surface water ponding capacity Soil BD (at 10–20 cm depths) Depth of groundwater and bypass flow fraction	Row direction and spacing Pesticide inputs Date of harvesting
Initial condition		Water contents (at 10–20 cm depths) Soil nitrate and ammonium content (at 10–20 cm depths) Soil extractable phosphorus (if P subroutine is run) at 10–20 cm depths Amounts and depth of manure/fresh plant residue incorporation	

Modified, Ritchie and Alagarswamy (2002)

dynamics. They are strong either in environmental impact assessment or in crop growth and soil component. Most of these models are not able to simulate the yield loss due to weed, pest, and disease infestation and damage due to extreme weather events like a hail storm and high wind.

Table 4.2 List of most popular crop growth simulation models, their usage and source

Crop model	Specific usages	Sources	References
ALMANAC	Plant community dynamics, nutrient cycling, and pesticide fate	https://www.ars.usda.gov/plains-area/temple-tx/grassland-soil-and-water-research-laboratory	Xie et al. (2003)
APSIM	To address the issues related to long-term resource management in farming systems	Apsim Initiative http://www.apsim.info	McCown et al. (1996)
AgrometShell	It can facilitate the integrated assessment of ground and satellite (coarse)-based information under a common interface	http://www.hoefsloot.com/agrometshell.htm	Di Paola et al. (2016)
AquaCrop	Studies yield response to water, soil water, and salt balances	http://www.fao.org/aquacrop	Steduto et al. (2009)
CENTURY	Simulation of carbon and nutrient dynamics over the different types of ecosystems	https://www.nrel.colostate.edu/PROGRAMS/MODELING/CENTURY/CENTURY.html	Gilmanov et al. (1997)
CERES-wheat	Decision-supporting tool for the design of crop management	http://nowlin.css.msu.edu/wheat_book	Lobell and Burke (2010)
COUP	To model moisture, heat, carbon, and nitrogen flows in the soil-plant-atmosphere continuum	https://www.coupmodel.com	Jansson and karlberg (2004) and Jansson and Karlberg (2010)
CROPGRO	Computes canopy level photosynthesis at hourly basis using photosynthetic parameters at leaf level and canopy light interception	http://ecobas.org/www-server/rem/mdb/cropgro.html	Batchelor et al. (2002)
CropSyst	Study of cropping system, simulation of multicrop on a daily basis over multiple years.	http://modeling.bsyse.wsu.edu/CS_Suite_4/CropSyst/index.html	Stöckle et al. (2003)
CROPWAT	Planning and management of irrigation	http://www.fao.org/land-water/databases-and-software/cropwat/en/	Desta et al. (2017)
DAISY	Dynamics of water, N, C, and pesticides in the bioactive zone near the soil surface	https://soil modeling.org/resources-links/model-portal/daisy	Abrahamsen and Hansen (2000) and Palosuo et al. (2011)
DSSAT	It consists of crop simulation models for more than 42 crops	http://dssat.net	Jones et al. (2003)
EPIC	It is a cropping system model that estimate soil productivity as affected by erosion	https://epicapex.tamu.edu	Di Paola et al. (2016)

(continued)

Table 4.2 (continued)

Crop model	Specific usages	Sources	References
FarmSim	Evaluates a baseline and an alternative farming technology for a representative farm using Monte Carlo simulation model	http://models.pps.wur.nl/node/961	Di Paola et al. (2016)
Fasset	Focuses on the estimation of farm management effects on carbon and nitrogen dynamics, particularly of emissions of reactive N species	http://www.fasset.dk	Olesen et al. (2004)
GLAM	GLAM is a regional-scale crop model that was designed to operate on the grid of global and regional climate models	http://www.see.leeds.ac.uk/see-research/icas/climate_change/glam/download_glam.html	Challinor et al. (2004)
GOSSYM	Irrigation and fertilizer management (N) and for PGR application	–	Gertsis and Whisler (1997)
HERMES	Plant growth, water, and N dynamics in the soil-plant system	http://www.zalf.de/de/forschung_lehre/software_downloads/Seiten/default.aspx	Palosuo et al. (2011)
INFOCROP	Simulate the climate change impacts on crop yield under different scenarios; effects of major pests on crop yield; C and N dynamics	https://www.iari.res.in	Aggarwal et al. (2006)
DNDC	Simulation of carbon and nitrogen biogeochemistry over the agroecosystems	http://www.dndc.sr.unh.edu/	Li et al. (2000)
LINTUL	Simulate crop growth model under both potential and rainfed conditions	–	Spitters (1990) and Spitters and Schapendonk (1990)
MONICA	Transport and biochemical turnover of C, N, and water in agroecosystems	–	Nendel et al. 2011
ORYZAv3	Simulate rice crop growth and N dynamics	https://sites.google.com/a/irri.org/oryza2000/about-oryza-version-3	Li et al. (2000, 2017) and Bouman and van Laar (2006)
RothC	Turnover of SOC in non-waterlogged topsoil	–	Diels et al. (2004)
RZWQM	Simulation of the effects of agricultural management practices on physical, chemical, and biological processes such as the movement of water, nutrients, and pesticides, and surface energy balance	https://www.ars.usda.gov/research/software/download/	Chen et al. (2019)

(continued)

Table 4.2 (continued)

Crop model	Specific usages	Sources	References
SALUS	Continuous monitoring of crop and soil parameters under different management practices over the years	–	Liu and Basso (2020)
STICS	It is able to model intercropping systems and crop rotation cycles	http://www.inra.fr/en/Scientists-Students/Agriculturalsystems/All-reports/Modelling-and-agrosystems/STICS-an-agronomy-dynamo	Brisson et al. (1998)
SUCROS	Simulates both potential and water-limited growth of a crop	http://models.pps.wur.nl/node/966	Bouman (1992)
SWAP	Simulation of the flow and transport processes at field level, during growing seasons and for long-term time series	http://www.swap.alterra.nl	Huang et al. (2015)
WOFOST	Recognizes three levels of crop production: potential, attainable (limited), and actual (reduced) production.	http://www.wageningenur.nl/en/Expertise-Services/Research-Institutes/alterra/Facilities-Products/Software-and-models/WOFOST.htm	Van Diepen et al. (1989)

C carbon, *N* nitrogen, *P* phosphorus, *PGR* plant growth regulators

4.2 Spatialization of Crop Growth Simulation Models

CGMs assume the simulated unit to be homogeneous for soil type, weather variables, crop management, irrigation, fertilization, variety, sowing, etc. The "extent" of CGMs is the entire region of interest, which could be a watershed or a big command area or an administrative boundary like district or state. This "extent" may consist of a finite number of smaller homogeneous areas called "support unit" or "unit of simulation". In reality, the region is often characterized by significant spatial variability, which is difficult to account fully. The application of CGMs on a larger area, than that for which it has been designed, is called the "spatialization" of the CGM. This is the application of crop models on a regional scale with inherent large heterogeneities in the soil, weather, and crop management factors between the units of simulation. Thus, spatialization leads to an analysis of the use of CGMs on units or scales outside the defined domain of validity of the hypotheses and the dedicated scale of the original model. A crop growth model is characterized by a spatial and temporal scale. But this review is confined to the spatial aspects since the focus of this chapter is on the spatialization of the crop growth model. The change of scale here pertains to the transition from a smaller unit of simulation to a bigger region.

According to Robert et al., change in the scale of the model involves alteration of the scale of input-output data, validation, and the framework structure of the model. To put it in the proper perspective, the water flow model in hydrodynamics is governed by Navier-Stokes equations at a finer scale of soil pores. It is further generalized by Darcy's law at the scale of a soil column. The CGMs further upscale it with generalized equations of the flow of water at a plot size of 1 m^2 or even under the controlled laboratory condition. In practice, the model parameters are fixed by calibrating the model by experimentation on the scale of an agriculture field. The models can be upscaled by (i) collecting input data for each unit of simulation under the region of interest, (ii) considering the interaction between these simulation units, and (iii) evaluating the performance of the output. All these three levels are linked with the availability of spatial data, scale changes, and associated issues. All these aspects of spatialization are discussed in detail in the following sections.

4.2.1 Issues and Methods Involved in Spatialization

The spatialization of a CGM involves space-time variation of the soil-plant-atmosphere system. It could be addressed in two ways: firstly, by characterizing the environmental variables like soil and weather and their interaction with the biological system, and, secondly, by taking care of the diverse human-induced crop management factors. The environmental data required for running a crop growth model includes the weather variables like maximum and minimum temperatures, precipitation, solar radiation, humidity, and wind speed, along with soil physico-chemical properties. In reality, these data are not available everywhere at a desirable scale; hence, they are usually measured or estimated for a given spatial unit (meteorological station and soil profile) for a limited number of locations within the region of interest. To run crop models on a regional scale, it is, therefore, necessary to estimate these parameters at the required scale for each unit of simulation. This involves a spatial approximation, broadly categorized into three groups of approaches. The first approach includes traditional choropleth mapping without taking random components into consideration. Classical soil mapping techniques (Legros 1996) comes under this approach. Thiessen polygons, trend analysis, or arbitrary weighted averaging of data also belong to this traditional mapping category (Laslett et al. 1987). The second category is based on statistical modelling considering the spatial variability, also termed as geostatistical techniques (Webster and Oliver 1990; Goovaerts 1997). The most popular geostatistical method is kriging or several modified forms of kriging to deal with different types of point-based, continuous, and categorical variables, using normal, log-normal, or other probability density functions. The geostatistical approach involves spatial interpolation to estimate the missing values at a point in space based on known values at neighbouring points. There are different types of spatial interpolation such as gridding, area averaging, and the estimation of missing data from neighbouring stations. These methods vary in their complexity, constraints on inputs, and computation

procedures. Various methods like kriging and co-kriging, inverse distance weighting (IDW), and thin-plate splines, etc. are popular in regional soil, weather, and crop analysis (Phillips et al. 1992; Hudson and Wackernagel 1994). IDW and simple kriging are pure geostatistical techniques of spatial interpolation whereas co-kriging takes advantage of additional knowledge obtained from external variables. Geostatistical approaches are most suitable for variables exhibiting stationarity and continuous spatial variations (Voltz and Webster 1990). Hence, it performs better for soil and climatic variables such as mapping of rainfall, temperature (Voltz and Webster 1990), soil texture, and soil pH (Creutin and Obled 1982; Van Meirvenne et al. 1994). The third category of methods is known as mesoscale modelling where the physics of the phenomenon is used to model its spatial behaviour (Takle 1995). Here, the spatial estimation of a variable is made based on the simulation of the processes that control the variable. For example, the prediction of the actual spatial variability of soil physico-chemical properties can be done based on the simulation of soil formation on a landscape scale (Minasny and McBratney 2001). But this kind of process-based approach is being developed to be augmented with the crop models on an operational basis.

As discussed above, the first approach is adopted by the EUMARS project, where the model is made to run on gridded input data as reported by Dallemand and Vossen (1995) and Rijks et al. (1998). An alternative approach was implemented by FAO (Gommes et al. 1998) where the model was made to run on actual available data and the yield output is subsequently interpolated using external variables like normalized difference vegetation index (NDVI) to guide the interpolation. Similarly, satellite enhanced data interpolation (SEDI) method is used for assisted interpolation taking advantage of the correlation between the variables to be interpolated and the environmental drivers (such as crop yield and NDVI/biomass). Hoefsloot (1996) described this concept of interpolation along with the technique of software implementation. This technique is applicable to any parameter of interest having spatial correlation and well distribution over the desirable extent of interpolation.

When the measured values of soil properties at each field are available, one generally relies on soil surveys in order to proceed for the spatialization of the crop growth model. These soil surveys provide information about the intrinsic spatial variability of soil physico-chemical properties. Voltz and Webster (1990) found that when soil properties vary abruptly classification is a better approach than standard kriging method. Thus, soil maps available on different scales can serve as a base for obtaining soil properties at the simulation unit. But in general, CGMs don't take soil types or soil textural classes as direct input. It requires quantitative measurements of properties like soil depth, percentage of sand silt and clay, bulk density, water-holding capacity, and hydraulic conductivity. Hence, quantitative maps of soil properties need to be created from the existing soil map keeping the scale factor in mind (Leenhardt et al. 1994). Soil maps at finer scales (i.e. 1:10000 or 1:25000) would provide better spatial variability of intrinsic soil properties than the coarser soil maps of 1:100000. In this context, pedo-transfer functions (PTFs) have been developed to derive soil properties difficult to measure from the widely available basic soil properties (Bouma 1989). For example, soil hydraulic property

is usually derived from soil textural information using PTFs. Several large soil database such as World Inventory of Soil Emission Potential (WISE) (Batjes 1996), USDA Natural Resources Conservation Service (NRCS) pedon database (NRCS, USDA 1994), UNSODA (Leij et al. 1996, 1997), and Hydraulic Properties of European Soils (HYPRES) (Lilly et al. 1999) have been widely used for the development of PTFs. In India, the National Bureau of Soil Survey and Land Use Planning (NBSSLUP) soil maps available at 250k and 50k are used in PTFs to generate quantitative soil properties and assimilate them to simulate CGMs at a regional scale.

For the spatialization of crop model, two main approaches are used to generate weather inputs, namely, zoning and interpolation (Leenhardt et al. 2006). In the zoning approach, the weather data of a meteorological station available in a specified zone is considered as the representative weather for the entire zone. Another alternative approach is the interpolation of the point weather data using nearest neighbour, arithmetic mean, optimal interpolation, spline function, kriging, etc. to generate spatial weather layers (Creutin and Obled 1982). The lack of observed daily weather data at the required scale is the most challenging constraint to simulate the effects of weather on crop growth and yields (Van Wart et al. 2013, 2015; Grassini et al. 2015). Currently, gridded weather data (GWD) are generated at a regional and global scale on an operational basis and regularly used in CGMs for decision supports (Miner et al. 2013; Mourtzinis et al. 2016). GWD is usually generated from satellite-derived weather information and/or interpolation of weather data from available meteorological stations using stringent empirical algorithms at defined spatial and temporal resolution. Influences of these gridded weather data on the simulation of CGMs are studied by various authors (Angulo et al. 2013; Zhao et al. 2015; Rezaei et al. 2015). These studies are mostly based on GWD at a very coarse spatial resolution like 50–100 km such as NASA-POWER (http:// power.larc.nasa.gov/), NCEP (National Centre for Climate Prediction http://www.esrl.noaa.gov/psd/data/gridded/data.ncep.reanalysis2.html), and CRU (Climate Research Unit; http://badc.nerc.ac.uk/data/cru/). However, there is a lack of robust assessment of most recently developed GWD with a higher spatial resolution (<20 km2), with respect to their potential usage particularly in the application of crop growth simulation models. The Prediction of Worldwide Energy Resources dataset from NASA (NASA-POWER) has been widely used as weather inputs in various crop models throughout the world. This is a weather database having daily weather attributes including solar radiation and maximum and minimum temperature, for 100×100 km raster of the entire globe starting from 1983 to date. These data are derived from satellite observations coupled with Goddard Earth Observing System climate model to obtain complete terrestrial coverage on a daily timescale. The quality evaluation of this NASA-POWER as input to the CGSMs has been carried out with mixed results (White et al. 2008; Bai et al. 2010, Biswal et al. 2014).

A major issue of mapping soil and weather input data is the problem of change in scale. Most often, the measurement units of weather data are smaller than the simulation units; hence, the problem lies in upscaling of the measured or mapped input data. This requires a thorough understanding and knowledge of the variable

across space and its aggregation over the simulation unit. In some cases, the change of scale could also be the other way round and requires downscaling of the weather data to suit the simulation unit. For example, Priya and Shibasaki (2001) estimated the required local information from meteorological stations of a national network and digital terrain model with a large scale using a purely statistical approach. In the context of spatial input data generation for CGMs, limited analysis has been done on the sources of error and their propagation. Crosetto et al. (2000) and Tarantola et al. (2000) presented a comprehensive approach to analysing uncertainty and sensitivity through GIS-based models for accurate and precise results, but this study is generic without specific application to CGMs. Poor-quality input data resulting from measurement errors or poor spatial aggregation or disaggregation are often the main source of errors in CGMs. Geographic information system (GIS) along with spatial data analysis plays an important role in integrating the crop model output into a larger geographic area (Delécolle et al. 1992; Ewert et al. 2011). Several researchers have demonstrated the linkage between crop model, GIS, and RS technology for regional crop forecasting (de Wit et al. 2010; Ma et al. 2013); precision agriculture (Seelan et al. 2003); yield gap analysis (Sibley et al. 2014); agro-ecological zoning (Ismail 2012); and crop suitability assessments (Mustafa et al. 2011; Mustak et al. 2015). Leitão et al. (2018) reported that broad-scale RS facilitates cost-efficient fast and periodic monitoring of the ecosystem in a larger area but is less useful for local scale applications (Leitao et al. 2018). With the advancement in RS technology, particularly the development of multispectral and hyperspectral sensors, RS has been proving its potential for upscaling vegetation parameters. But the trade-off among various sensor resolutions, viz. spatial, temporal, spectral, and radiometric, is the major limitation in the application of this technology. Further, it is a nearly impossible task to measure plant parameters in situ across the simulation unit, but we can always follow the empirical or physically based approach for biophysical parameter retrieval using RS technique. Upscaling in environmental research involves a combination of data generated at different temporal and spatial scales (Finke et al. 2002). It is important to consider the "observation scale" (spatial and temporal resolution of the measured data), "modelling scale" (temporal and spatial scale at which model operates), "operational scale" (scale time and space where the process operates), and finally the "geographic scale" (area of interest or target area of the research) in the upscaling protocol (Wu and Li 2009). Understanding the complexity of scale is essential as the mechanism of a model can be different at different scales. Models optimized for a particular scale become ill-performing at another scale without re-optimization (Wu and Li 2009). Heterogeneity is the intrinsic characteristic of the earth's surface which is a mosaic of different patches of vegetation type, soil, and land use. Even when a landscape looks homogeneous at a particular scale, the possibility of having inhomogeneity increases with the increase in the spatial resolution (Wu et al. 2000). Hence, in the RS domain, heterogeneity is a relative concept which is highly linked with the sensor spatial resolution (Li et al. 2014). Besides heterogeneity, another issue is the "linearity" or "non-linearity" involved in the scaling between the RS measurement and the biophysical parameter of interest (Wu and Li 2009). Besides the issues of spatial resolution, the issues of temporal

resolution of the sensors also need to be addressed. Li et al. (2014) demonstrated that in agroecosystem studies, some parameters could be retrieved from sensors with high spatial and low temporal resolution, whereas others need lower spatial and higher temporal resolution. The scale of the system to be modelled always depends on the objective of the study, and thus, identification of suitable scale for monitoring a particular system is the most important factor (Chemin and Alexandridis 2006; Alexandridis et al. 2008), along with different issues of aggregation and disaggregation of RS-derived information with minimal uncertainty (Alexandridis et al. 2010). RS satellites with higher spatial resolution such as SPOT, IKONOS, and Quickbird have a lower temporal resolution and narrow swath. On the other hand, satellites with a lower spatial resolution (coarser than 300 m) such as Terra/Aqua MODIS, NOAA, and AVHRR have daily global coverage. For crop modelling studies, these coarse-resolution satellites are preferred as they can generate a time series of information during the crop season. It should be noted that crop models are not expected to provide spatial information per se; rather, they require spatial information to operate. Thus, the combined use of RS data with crop models provides significant advantages by generating the "missing spatial information" expanding their coverage in two-dimensional spaces (Launay and Guerif 2005). This spatial information is crucial for the varied application of crop models starting from precision farming to regional yield prediction (Azzari et al. 2017). Furthermore, in-season monitoring of crops and providing preharvest yield estimation at various spatial and temporal scales are important for decision-making in trading, logistics, and insurance. This aspect of spatial data generation for running CGSMs is discussed in detail under Sect. 4.3 of this chapter.

4.2.2 Establishment of Spatial Framework

GIS tool enables the point-based crop model to simulate regional crop growth development and yield. Depending on the types of linkages of the model to GIS, three types of interfaces are identified: (i) linking, (ii) combining, and (iii) integrating (Hartkamp et al. 1999). The selection of interface is highly dependent on the factors like the objective of the research and expertise of the user along with the available computational framework. Simple linkage strategies employ GIS for spatially displaying the model outputs using interpolation techniques. In this approach, communication between GIS and the model takes place through unique identifiers of grid cells or polygons existing in input-output files and transferring the data back and forth in ASCII or binary format (Dadhwal 2003). The linkage of WOFOST model to ARC/INFO illustrates this aspect well (van Laanen et al. 1992) though in this approach, the full potential of GIS is not exploited. In combining strategy, the model is configured with interactive tools of GIS enabling automatic data exchange along with displaying model results (Burrough 1996). This approach usually involves complex programming and data management than the "linkage" approach. An illustration of this technique is presented by Engel et al. (1997) in the

Agricultural and Environmental GIS (AEGIS) with ArcView. Integration is still more complex than the above-mentioned approaches and involves the incorporation of one system into the other. The application of GIS interfacing in modelling had been initiated in the mid-1980s particularly in the field of hydrological modelling. The GIS-enabled applications of crop models have been demonstrated by various researchers worldwide, such as regional/global crop yield calculation and productivity analysis (Calixte et al. 1992), precision farming, climate change, and agro-ecological zonation (Aggarwal 1993). Lal et al. (1993) had carried out regional productivity analysis using DSSAT-BEANGROW and AEGIS. Han et al. (1995) studied potato yield and N leaching distribution for site-specific crop management by developing an interface between PC ARC/INFO GIS and SIMPOTATO simulation model at South Central Washington state. Aggarwal (1998) suggested a land-use option for Haryana state in India by integrated simulation modeling, expert knowledge, and GIS optimization techniques. In this study, agro-ecological land units were delineated by overlapping maps for soil attributes and climatic normal rainfall in GIS-IDRISI. Similarly, Sehgal (2000) developed a protocol of near-real-time crop monitoring system for crop condition assessment and yield forecasting for the Haryana region of India linking WTGROWS with GIS assimilating RS-derived biophysical parameters. Ines et al. (2002) studied water use efficiency of rice, maize, and groundnut at basin scale for the Laoag River basin in the Philippines using a GIS-enabled crop growth model. Junguo Liu (2009) presented "GEPIC", a GIS-based model to estimate crop water productivity regionally with a spatial resolution of 30 arc-minutes. Cedrez and Hijmans (2018) computed the potential yield (Yp) of crops for the entire world using WOFOST and LINTUL model.

4.3 Remote-Sensing-Based Retrieval of Crop Biophysical Parameters

Process-based CGSMs can incorporate physiological as well as biological knowledge of plants and are also capable to model the interaction between plants and their environment. In these models, vegetation state variables, such as developmental phase, leaf area index (LAI), above-ground biomass (AGB) are linked to driving variables like nutrient availability, weather conditions, and management factors. The final output of these models is the crop yield or accumulated biomass (Dele'colle et al. 1992). Hence, the information related to the crop canopy state variables such as LAI and AGB is a prerequisite to simulate the CGMs. Several techniques have been used to retrieve canopy state variables from reflective RS observations (400–2500 nm) by many researchers. Moulin et al. (1998) had proposed the use of sensors to parameterize CGMs based on the measurement of actual crop status. Several authors carried out studies related to the potential use of sensors including in situ, proximal sensing, and RS sensors to enhance prediction of CGM (Hoefsloot et al. 2012; Bai et al. 2012). However, the estimation of biophysical attributes in situ

is a laborious and time-consuming task (Weiss et al. 2004) even with the help of automation systems. Hence, satellite-based RS data is the only source of information to retrieve biophysical parameters at regional scales (Camacho et al. 2013; Kolotii et al. 2015; Shelestov et al. 2015). Retrieval of biophysical parameters using various spatial and temporal RS data has been an active area of research for the past several decades (Wiegand et al. 1992; Chen et al. 2002; Walthall et al. 2004; Ganguly et al. 2012; Li et al. 2015a, b).

The existing biophysical parameter retrieval methods are empirical or physical in nature. Physically based models simulate spectral response based on input such as leaf constituents, canopy architecture, sun-viewing geometry, background soil (Ganguly et al. 2012; Li et al. 2015a, b), and inverted back using observed spectral response and limited known input parameters. Different techniques like lookup tables (Ganguly et al. 2012), numerical optimization, and machine learning (Walthall et al. 2004; Verrelst et al. 2012, 2013) techniques are successfully used for inversion of the model. The empirical models basically linked biophysical attributes with various RS-based spectral indices (Turner et al. 1999; Fensholt et al. 2004; Verrelst et al. 2012). These models are quite easier to implement, site-specific, and data-driven. Hence, its scalability is limited. The selection of the most sensitive and informative spectral features is important in the empirical approach. The addition of all possible spectral features increases the complexity and dimensionality and required optimization to make the empirical model simple for regional applications. The details of these approaches and methods are discussed in Chap. 3 of this book.

4.3.1 Importance of Remotely Sensed Crop Biophysical Parameters

LAI is the most important crop biophysical parameter and a vital component of the process-based CGMs. It's a dimensionless quantity representing a one-sided leaf area per unit ground surface area. Spatially explicit measurements and retrieval of LAI from RS data are indispensable to model for simulation of ecological variables and processes at regional scales (Green et al. 1997). Recent studies have successfully demonstrated the retrieval of LAI using different parametric and nonparametric regression as well as physically based models (Cho et al. 2007; Im et al. 2009; Liu et al. 2018; Xie et al. 2019; Upreti et al. 2019). The RS data is also used to retrieve fractional absorbed photosynthetically active radiation (fAPAR) as it is highly related to dry matter production of a crop (Dong et al. 2013). Hilker et al. (2008) had conducted an experiment to retrieve fAPAR using spaceborne RS data for modelling plant dry matter production. They concluded that NDVI and enhanced vegetation index (EVI) are most promising for retrieval of fAPAR. Upreti et al. (2019) retrieved fAPAR through a hybrid approach using a neural network to train PROSAIL canopy reflectance model. Similarly, LUE is one of the key biophysical

parameters require to calculate potential plant production. Hilker et al. (2010) have used the photochemical reflectance index (PRI) using narrow bands of 531 and 570 nm to retrieve LUE. However, it is difficult to upscale this retrieval process to canopy level at a regional scale (Rahman et al. 2001; Hilker et al. 2008).

Biomass production estimation is one of the main areas of research in modelling of vegetation growth and development. However, most of the RS satellites can measure AGB, as not able to observe below-ground biomass (Lee 1978). Several kinds of research have demonstrated successful biomass retrieval using RS data (Claverie et al. 2009; Jin et al. 2015a, b).

Water stress is one of the critical limiting factors for the growth and development of crops which leads to a yield gap between actual and potential production. Hence, information regarding plant or crop moisture content is important for crop growth and yield modelling. Many researchers across the globe have used various RS-based indices, spectral information along with climate data to retrieve crop moisture stress. Lee et al. (2010) reported the use of thermal infrared (3–12 μm) for crop water estimation. Jackson et al. (1981) used the crop water stress index (CWSI) to measure crop moisture. Govender et al. (2009) reported the use of middle- and shortwave infrared bands for plant water stress measurement. Two most popular spectral indices, namely, normalized difference water index (NDWI) by Gao (1996) and water band index (WBI) by Penuelas et al. (1993), are being used to measure crop moisture content. Djamai et al. (2019) carried out studies on the retrieval of canopy water content using Sentinel-2 and Landsat-8 data.

Plant nitrogen content (N) is one of the most important biochemical constituents of leaf chlorophyll content and therefore strongly correlated to plant photosynthetic activity (Diacono et al. 2013). Several researchers have found strong correlations between spectral indices and plant chlorophyll content. Yao et al. used NDVI to retrieve chlorophyll in wheat crops. Bagheri et al. (2012) employed soil adjusted vegetation index (SAVI), modified soil adjusted vegetation index (MSAVI), and optimized soil adjusted vegetation index (OSAVI) for leaf chlorophyll retrieval of corn. Jain et al. (2007) used several red-edge bands to retrieve chlorophyll content in potato. Clevers and Gitelson (2012) estimated plant N and chlorophyll content using MERIS and Sentinel-2 data using an empirical approach. Similarly, Miphokasap et al. (2012) used ground-based hyperspectral data for retrieval of canopy N content using the empirical method.

4.3.2 Scale Issues in Remote-Sensing-Based Parameter Retrieval

The retrieval of parameters by inverting models does not express the characteristics of scale explicitly; they may be suitable for homogeneous surface or point measurement (Raffy 1992). Chehbouni et al. 2000 stated that it is not appropriate to use the locally calibrated relationships, between the modelled and observed variables, at a

regional scale simply by scaling the parameter. As a result, they need to be reparameterized to adapt to the new circumstances since the driving forces or mechanisms may be totally different at different scales. Hence, a model designed and calibrated at the leaf scale may not hold good at the canopy level. Consequently, the models or algorithms developed at one scale need to be revised for its application to other scales, and the impact of scale on the mechanism of the model or algorithms is to be investigated prior to changing the scale. Scale applicability of basic laws of physics such as Lambert's law (Li and Strahler 1985), Beer's law (Albers et al. 1990), and Planck's law (Li et al. 1999) at the pixel level is being discussed by various researchers. Their results suggested that the scale applicability needs to be considered carefully for retrieval of the model at different scales. Besides this, the heterogeneity of land surface and the linearity or non-linearity of retrieved parameters are also highly related to scale. In reality, heterogeneity is a surface property varying over scenes (Garrigues et al. 2006) and is a relative concept highly dependent on the sensor resolution. As the spatial resolution of the sensor becomes finer, the possibility of pixel heterogeneity increases. The surface heterogeneity greatly affects the parameter retrieval strategy using RS data (Chen 1999). Garrigues et al. (2006) suggested two strategies to minimize the errors in scale change; the first one is to quantify the intra-pixel heterogeneity, and the second is to define proper pixel size to capture the variability and minimizing the intra-pixel variability. There is no arbitrary conclusion about the effect of linearity or non-linearity of retrieval models on scale change. When the retrieval models for different cover types are quite different, the linear retrieval models could also be affected highly by scale effect (Chen 1999). At the same time, when the medium is homogeneous, non-linear retrieval models also cause no scale effect as demonstrated by the Taylor series expansion (Hu and Islam 1997; Garrigues et al. 2006). Chen (1999) suggested that scaling error is more when a non-linear algorithm is applied to mixed pixels with different land cover types. Various authors proposed different techniques to minimize the scale effect in RS-based retrieval of biophysical parameters (Verhoef 1984; Jacquemoud and Baret 1990; Raffy 1992; Tian et al. 2003). Hu and Islam (1997) demonstrated that different parameterization and assumptions in retrieval models can lead to a different conclusion for the same physical process. There are conflicting conclusions in the literature describing whether the products are scale-dependent or scale-free. There is relevant literature addressing these scale-change issues, such as bidirectional reflectance distribution function(BRDF) and albedo (Liang et al. 2002), temperature (Liu et al. 2006), emissivity (Zhang et al. 2004), carbon flux (Thorgeirsson and Soegaard 1999; Sasai et al. 2007), soil moisture (Hu et al. 1997; Oldak, et al. 2002; Manfreda et al. 2007; Das and Mohanty 2008), NDVI and vegetation fraction (Jiang et al. 2006; Tarnavsky et al. 2008), LAI (Hu and Islam 1997; Chen 1999; Fernandes et al. 2004; Garrigues et al. 2006; Jin et al. 2007; Hufkens et al. 2008), net primary production (NPP), and gross primary production (GPP) (Simic et al. 2004; Turner et al. 2004). It can be concluded that we need to change the scale of the retrieval models through appropriate assumptions and approximation. Furthermore, there should be a clear separation of system errors from the errors arising from retrieval models due to scale changes.

4.4 Assimilation of Parameters into the Process-Based Crop Growth Simulation Model

The objective of the spatialization of a crop growth model is to simulate the crop growth and development on a regional scale, where significant spatial variability in soil, weather, and crop state variables exists along with the large uncertainties (Hansen and Jones 2000). These uncertainties result in large errors in crop growth simulation and yield estimation. In this context, RS technology plays an important role by facilitating input data generation for CGMs particularly generating the "missing spatial information" and thereby reducing the uncertainty in the spatialization of CGMs and yield estimation. The recent development in RS technology helps us to generate accurate, reliable, and quantitative information on soil, weather, and crop parameters at the regional scale. Many researchers have retrieved canopy state variables, soil, and weather parameters using different techniques and RS data. A detailed list of some of these studies that are relevant from the crop modelling point of view is presented in Chap. 3 of this book. Several researchers have used RS to retrieve crop state variables or soil properties over large areas, such as fAPAR (Sakowska et al. 2016; Upreti et al. 2019), LAI (Fang et al. 2008; Jiang et al. 2014; Liu et al. 2018; Pasqualotto et al. 2019), fraction of vegetation cover (fCover) (Djamai et al. 2019), biomass (Claverie et al. 2009; Jin et al. 2015a, b), leaf N content (Huang et al. 2013), evapotranspiration (Huang et al. 2015), and soil properties (Dente et al. 2008; Ines et al. 2013; Chakrabarti et al. 2014).

These retrieved biophysical parameters of soil, weather, or crop canopy states need to be integrated with CGMs. In recent years, rapid and parallel development in CGMs as well as in RS and information technology (IT) leads to the development of their combined applications. The availability of higher spatial resolution sensors such as Sentinel-2, SPOT-6, Landsat-8, Rapid Eye, World View-2, and GeoEye-1 with high temporal frequency combined with wide spatial coverage and low operating cost facilitates operational crop growth monitoring and assessment in regional scale. Similarly, there has been rapid development in IT leading to robust computational infrastructures, algorithms, and techniques for processing huge RS data and generating relevant information for improving the predictive capability of CGMs both in temporal and spatial scales (Launay and Gue'rif 2005). In this context, various data assimilation (DA) techniques have been developed allowing a formal and well-understood way to combine the predictions of simulation models with RS or ground-based observations. In this process, the model predictions are matched with the observed data limiting the errors due to poor local parameterization. Further fine-tuning could be done by retrieving the local parameters using RS techniques (Xi et al. 2019). In the context of DA, one needs to first distinguish observed variables (RS or ground-based), state variables (crop model system generated), model parameters (establishing relationships between observed and state variable), and output variables (crop yield in most of the DA) (Delécolle et al.1992). Several algorithms and techniques have been developed worldwide to facilitate DA through the combined use of crop models with RS data (Mass 1988; Guerif and Duke 2000;

Dente et al. 2008; Curnel et al. 2011; Wang et al. 2013; Huang et al. 2015) to improve the accuracy of CGMs and in turn estimation accuracy of crop yield in regional scale. Various DA methods usually optimize the difference between the measured evidence (RS observation) and modelled prediction by using Bayes' rule (Huang et al. 2019a, b). Many techniques have been developed to carry out this Bayesian update, and their relative advantage is based on the assumption made to solve for the posteriori analysis for probability density function (pdf) of the parameter or state variable.

The schematic flow diagram of a typical DA system involving crop model and RS-derived biophysical parameters is presented in Fig. 4.3. A point-based crop growth simulation model is to be calibrated and validated on a field scale, and the most sensitive parameters of the model need to be fixed along with the smart assumption of the less sensitive and difficult to measure parameters in the study region. The calibrated model will then be able to simulate crop growth and development. Then, the calculated uncertainties in the calibrated parameters propagate through the model to account for the limitations in the process of calibration and parameterization. After the calibration, the model is ready to simulate the crop growth by providing local predictions of a large number of biophysical variables such as development state (DVS), LAI, AGB, evapotranspiration (ET), and soil moisture. At the same time, satellite-based RS has the potential to provide an independent estimate of these parameters over large areas. Then the DA methods will seek to update the uncertain model simulations of LAI, AGB, SM, etc. to match the certain observations obtained through earth observation (EO) systems so that pdf is consistent with both the model and observation. The model with the embedded DA process can run in the forward direction towards the harvest to simulate crop growth and yield using the short-term as well as seasonal weather forecasts.

4.4.1 Methods of Remote Sensing Data Assimilation

Extensive reviews on the assimilation of RS-derived biophysical parameters into CGMs have been carried out previously by several authors (Maas 1988; Delecolle et al. 1992; Liang 2005; Dorigo et al. 2007; Lewis et al. 2012; Kasampalis et al. 2018; Jin et al. 2018). Similarly, various techniques have been developed to integrate RS observations in the agroecosystem models. In general, three different strategies are applied which are described by researchers worldwide (Dele'colle et al. 1992; Moulin et al. 1998; Olioso et al. 1999; Makowski et al. 2002; Bach and Mauser 2003). Three broad methods of DA, i.e. calibration, forcing, and updating techniques, have been used globally and are discussed in the following section.

4.4.1.1 Calibration Method

The main aim of the calibration method is to minimize the differences between the RS data and the simulated data of the crop model using an optimization algorithm. The initial parameters of crop models are adjusted to optimally match with the simulated state variables of the crop model with the RS data (Fig. 4.2a). While calibrating the sensitivity, uncertainty analysis of crop models is carried out manually or automatically running the model using a set of realistic parameters within range. Several studies have been carried out using RS DA into crop models using the calibration method. The main disadvantage of the calibration method is to parameterize the complex relation existing among the model variables. The popular algorithms are mentioned as below:

(a) Maximum likelihood solution (MLS) (Dente et al. 2008)
(b) Simplex search algorithm (SSA) (Launay and Guerif 2005; Ma et al. 2008; Claverie et al. 2009; Ma et al. 2013)
(c) Least squares method (LSM) (Zhao et al. 2013)
(d) Powell's conjugate direction method (PCDM) (Fang et al. 2008, 2011)
(e) Shuffled complex evolution (SCE-UA) (Shen et al. 2009; Ren et al. 2009, 2011; Jin et al. 2010; Ma et al. 2013; Wang et al. 2014; Huang et al. 2015)
(f) Very fast annealing algorithm (VFSA) (Dong et al. 2013)

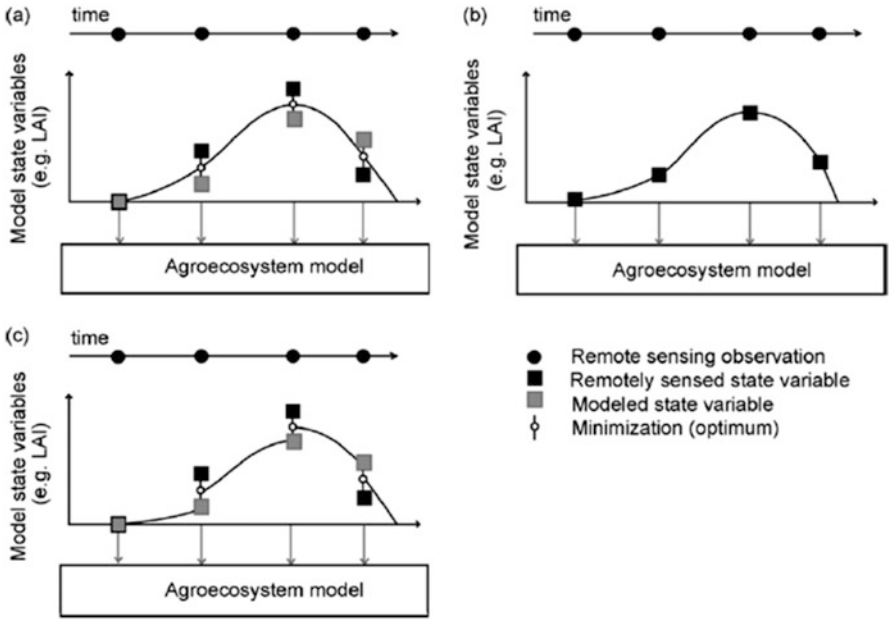

Fig. 4.2 Schematic representation of different methods for the assimilation of remotely sensed model state variables in agroecosystem models: (**a**) calibration, (**b**) forcing, and (**c**) updating. (Adopted, Dele'colle et al. 1992)

(g) Particle swarm optimization algorithm (PSO) (Wang et al. 2014; Liu et al. 2014; Jin et al. 2015a)

4.4.1.2 Forcing Method

Forcing methods use the RS data to replace the crop model simulation data (Fig. 4.2b) at each time step. The time step may be daily, weekly, or monthly which may not match with the temporal resolution of satellite data in most of the cases. Under normal circumstances, the temporal resolution of a satellite is less than the time step of the crop model. RS observations are available at a predefined temporal resolution of the satellite observations and generally less frequent than the model time step. Hence, various interpolation techniques like wavelet approaches, linear interpolation, and fast Fourier transformations (Roerink et al. 2000) have been used to fill the gaps between two observations. It helps to derive state variables as per the required time steps of the model. LAI data retrieved from RS images are most often used as an input parameter and state variable into a crop growth model. Huang et al. (2001), Clevers et al. (2002), Schneider (2003), Abou-Ismail (2004), Hadria et al. (2006), Thorp et al. (2010), Tripathy et al. (2013), and Yao et al. (2015) have retrieved LAI using different RS data. The simulated results of crop models were directly replaced by the retrieved LAI to improve the simulated LAI, AGB, and yield of crop models. Morel et al. (2012) used the estimated interception efficiency index (ε) and fAPAR as input into the MOSICAS model for estimating the yield of sugar beet and sugarcane, respectively. DA of RS data into the crop model is easy to operate using the forcing method. During this process, the simulated state variables were only replaced by the retrieved state variables derived from RS data.

4.4.1.3 Updating Methods

The updating method deals with continuous updating of model state variables with RS-based variables as per the availability (Fig. 4.2c). This method is based on the assumption that an updated state variable at each time step better simulates the state variable. It improves the accuracy of the simulated state variable at a succeeding time step. It is also referred to as sequential DA and many algorithms have been developed for this assimilation technique (McLaughlin 2002). These methods provide more flexibility in terms of data availability, but accounts for the errors in both observed and modelled state variables may affect the final output.

4.4.2 Issues in Data Assimilation

The assimilation of RS-derived biophysical and biochemical state variables into CGSMs can improve its predictive performance at a regional scale (Launay and

Gue'rif 2005). However, RS-derived state variables may contain some observational error (Bastiaanssen et al. 1998). In forcing method, the model follows the observed state variable and may include observation errors. However, the "calibration" and "updating" methods offer more flexibility in the assimilation of RS-based state variables and their associated errors in the model. Nouvellon et al. (2001) reported that the calibration method could generate more representative parameters based on the simplified physical description of the underlying processes and thus improves model prediction. But it's only applicable if there are a sufficient number of observations, and the observation error is also small. As it needs more computation time for the optimization process to assimilate RS data, the calibration method finds limited applications. However, this problem can be overcome by testing more robust and less time-consuming procedures such as methods based on extended and non-linear Kalman filtering (KF) (Nouvellon et al. 2001). The updating method has significantly reduced the computational times as compared to the calibration method as it requires a single run. Besides, in updating methods, the model state variables need to be adjusted during the model run itself and often intervene in the model structure and processing loops to a large extent. Walker et al. (2001) concluded that KF is a superior over the forcing method using a synthetic case. It has been successfully demonstrated that RS-derived biophysical variables can be utilized to calibrate parameters and initialize variables such as initial LAI and sowing date (Maas 1988; Guerif and Duke 2000). It can also be used to adjust or replace a state variable (LAI and fAPAR) in agroecosystem models (Bach and Mauser 2003; Launay and Gue'rif 2005). Most of these studies were carried out at subregional to local scales. However, these models can still be operated at the individual field level with high-resolution satellite data such as SPOT, Landsat TM, and Sentinel. Further, at these scales, the spatial and temporal resolution of RS images becomes a critical factor (Dele'colle et al. 1992; Launay and Gue'rif 2005).

4.4.3 Data Assimilation Algorithms

The currently used DA algorithms include KF, ensemble Kalman filter (EnKF), particle filter (PF), hierarchical Bayesian method (HBM), three-dimensional variational data assimilation (3DVAR), and four-dimensional variational data assimilation (4DVAR). All these algorithms are discussed in detail in the following section under the broad categories of the variational approach, KF and Bayesian Monte Carlo approaches. The variational approach can optimize a given criterion such as the minimization of a cost function, hence solving the assimilation problem. It is observed that in a wide range of functions, optimizers are used to solve a generic cost function problem for DA into a crop growth model. 3DVAR can assimilate observations without considering temporal dependency (Lorenc 1986). It can use the complex observation operator, hence making it easier to assimilate for state variables of non-director-related non-linear observations. However, 3DVAR model is limited in practical applications because of higher computational cost. Hence, 4DVAR was

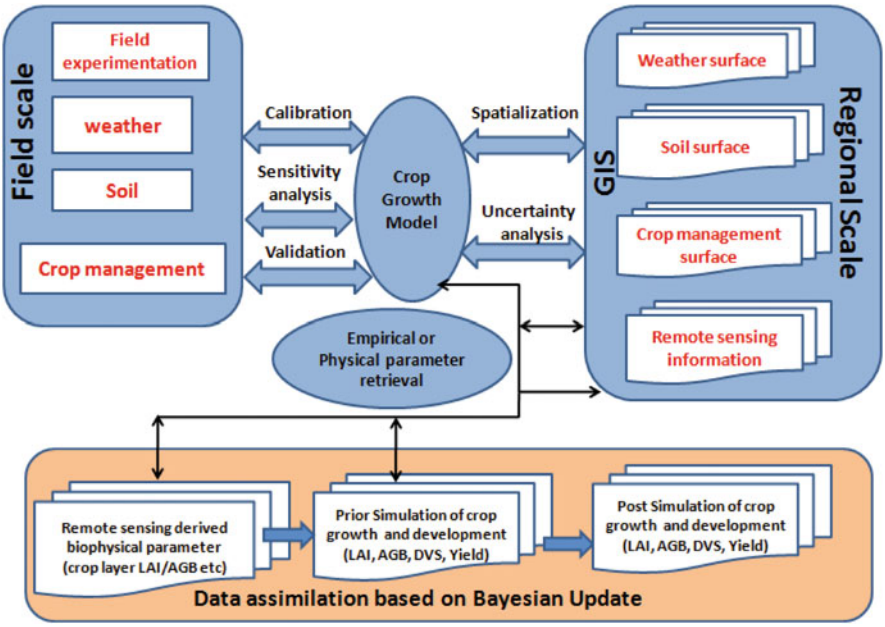

Fig.4.3 A schematic framework of spatialized crop growth simulation model with EO data assimilation

developed using 3DVAR algorithm to overcome such problems. 4DVAR integrates the solution over time (Le Dimet and Talagrand 1986). LAI or FAPAR is the mostly used linking variables between satellite observations and models. This is probably due to their straight forward representation or the connecting point within the crop growth simulation model and the wider availability of satellite-derived LAI and/or FAPAR products (Fig. 4.3).

Many researchers have explored the empirical relationship between various vegetation indices (VIs) with LAI and fAPAR or using radiative transfer models (RTMs) to convert LAI to reflectance. However, it is important to understand the limitations of the observation operators, in both cases. The assimilation of fAPAR is not necessarily the same as assimilating VIs. KF method cannot be used to address high-dimensional data. Hence, it is often difficult to generate inputs for crop canopy state variables, structure, and model uncertainty. To overcome these problems, Evensen (1994) developed the EnKF. Many studies have demonstrated that the EnKF method is very helpful for DA between crop models and RS data (Crow and Wood 2003; Hadria et al. 2006; De Wit and Van Diepen 2007; Bolten et al. 2009; Nearing et al. 2012). The KF equations hold good only with linear CGMs and linear observation operators and assume all the statistical functions as Gaussian. However, dynamic crop models are often not linear, as the growth process is affected by many factors, such as solar radiation, temperature, moisture, and other crop management factors. These interactions cannot be simulated adequately by linear

models. Hence, a standard KF cannot be employed directly for carrying out the assimilation process.

If direct RS-based measurements such as backscatter coefficients, radiance, and reflectance are to be assimilated, the local linear approximation needs to be feasible. If these approximations are available by using emulators (Gómez-Dans et al. 2016), then EKF might be an efficient alternative to the EnKF (Evensen 2009). RS-derived products can give direct, uncertainty-quantified measurement of state vector components like LAI. It can be directly connected to the model predictions. KF will be a good choice if the error related to the data product follows Gaussian distribution. It is a sequential approach to measure state vector at different points of time by considering the probability distribution of the variables for each time frame. It uses a series of measurements related to statistical noise; other errors are observed over time. Hence, the estimation of an unknown variable using such approaches tends to be more accurate than those based on a single measurement alone. However, the use of EnKF is an alternative approach to assimilate such products as most of the CGMs are non-linear.

The filtering approaches are casual as compared to the variational approach due to the only use of past information to assimilate a current observation. The variation approaches need information from the whole assimilation temporal window, resulting in a more constrained problem compared to filters (Huang et al. 2019a). Besides, filtering approaches facilitate near real-time operation with an on-line updating facility. The similarity between KF and 4DVAR is the fact that both follow the Gaussian assumption and Bayes' rule. However, in CGMs and non-linear observation operators, the uncertainties in the model don't follow Gaussian distribution, assuming normality in the posterior might be a poor choice. Rather, sampling-based methods like Markov chain Monte Carlo (MCMC) (Gilks and Roberts 1996) is a good choice. It uses the Markov chain to produce samples from the posterior pdf that will work for any problem, provided that the chain is allowed to run for a sufficient number of iterations. Again, a convergence of the chain is hard to diagnose. Hence, many thumb rules (R^ indicator) are usually employed (Cowles and Carlin 1996; Gelman et al. 2013). MCMC methods are more appropriate where the dimensionality of the problem is not very high. These methods become slow when the dimensionality is very high; hence, it is difficult to achieve convergence in the desired timescales. The functional equivalents of MCMC are sequential Monte Carlo methods, such as particle filters (PF). PF facilitates the propagation of non-Gaussian distributions through complicated CGMs. PF shows some potential for DA to integrate RS-derived biophysical parameters with a crop model as compared to widely used EnKF (Jiang et al. 2014; Machwitz et al. 2014; Chen and Cournède 2014). An important consideration for PF is that a large number of particles may be required to reliably describe the posterior pdf, particularly when the dimensionality of the problem increases. The approach appears to be promising for non-linear CGMs. Several researchers have demonstrated the applications of PF for crop model parameterization and uncertainty analysis (Makowski et al. 2002; Iizumi et al. 2009; Dumont et al. 2014). A detailed list of various algorithms and their usages along with crop models and RS data is presented in Table 4.3.

4.5 Future Scopes and Challenges

The spatial crop growth model can simulate regional crop growth development and yield using GIS and RS data. Studies conducted worldwide reported high simulation accuracies of the model on a coarser scale. But there is a scope to further improve upon the existing models to operate at a finer simulation unit like village or Gram Panchayat level without losing the accuracy. The crop models used today have their intrinsic limitations. Most of the crop models do not have the modules to simulate the impact of diseases, pest infestation, and climatic disasters such as flooding, hail, strong winds, and high temperature. The genetic coefficients of crop varieties in the crop models are fixed by field trials or from literature, and it is not possible to generate such coefficients on a regional scale by carrying out a large number of field experiments. Similarly, feeding the crop models with spatially divergence crop management information like input for irrigation, fertilization, sowing, etc. is furthermore challenging. Difficulties are also encountered to accommodate high spatiotemporal variations of the soil and weather parameters. Hence, the error is also high in parameterizing the soil properties such as soil moisture, soil texture, soil nutrients, carbon, and nitrogen content and daily weather inputs like maximum, minimum temperature, rainfall, and solar radiation. Low accuracy in the input data results in poor prediction of the model simulation. Most of the models assume uniform field growth situations (like the potential and water-limited production conditions), but in reality, several limiting factors can occur in the field. Hence, the actual field conditions are beyond the defined boundary conditions of the model range. These errors introduced through parameterization of crop model, hence influencing the accuracy of biomass, LAI, and yield estimates both at regional and global scales. To reduce the above-mentioned error, the following general issues need to be addressed:

What are the sensitive input parameters for the model?
Which of these parameters can be retrieved accurately through RS technique and how?
Which are the most suitable assimilation techniques for incorporating RS data into the model?
What is the effect of assimilation on simulated output?
What is the effect of spatial and temporal resolution on the predictive power of the model?

At the same time, some of the specific methods have been followed to reduce the uncertainty in simulation such as (1) the addition of modules for simulating the impact of diseases, insect/pest infestation, and climatic disasters and (2) combination of global sensitivity analysis such as Morris, extended Fourier amplitude sensitivity test (EFAST), intelligent optimization algorithms (IOA), MCMC, GA, general likelihood uncertainty estimation (GLUE) for parameter optimization and model accuracy improvement. Hence, the development of IOA for carrying out sensitivity

Table 4.3 Previous research on the assimilation of remote sensing parameter in the crop model

RS data	Crop model	Variables	Algorithm	References
AMSR-E, MODIS	WOFOST	LAI, SM	EnKF	Ines et al. (2013)
ASD	CERES-Wheat	NDVI	EnKF	Li et al. (2011)
ASD	RiceGrow	LAI, LNA	PSO	Zhu et al. (2010)
ASD	DSSAT	LAI, CNA	PSO	Li et al. (2015a,b)
ASD	RiceGrow	LAI, LNA	PSO and EnSRF	Wang et al. (2012)
ASD HJ TM	WheatGrow	LAI, LNA	SCE-UA	Huang et al. (2011)
ASD spectral data	WOFOST	VI	PSO	Wu et al. (2013)
ENVISAT ASAR	ORYZA2000 + CLOUD	Back scatter coefficient	SCE-UA	Shen et al. (2009)
ENVISAT/ASAR, MERIS	CERES-Wheat	LAI	Variational assimilation	Dente et al. (2008)
ERS, EUMETSAT	WOFOST	SM	EnKF	de Wit and van Diepen (2007)
GF-1	WOFOST+PROSAIL	FAPAR	PSO	Zhou et al. (2017)
Ground radiometry	CERES-Wheat	LAI	Updating and forcing	Thorp et al. (2010)
Handheld radiometer	SUCROS	Reflectance	FSEOPT	Guerif and Duke (1998)
HJ-1A/B	WOFOST	LAI	EnKF	Ma et al. (2013) and Cheng et al. (2018)
HJ-1A/B	WOFOST	LAI	SCE-UA	Chen et al. (2010)
HJ-1A/B	WOFOST	LAI	PSO	
HJ-1A/B CCD	CERES-Wheat	LAI	POD4DVAR	Jiang et al. (2014)
HJ-1A/B, Landsat TM	WheatGrow	LAI, LNA	EnSRF	Huang et al. (2013)
HJ-1A/B, Landsat-8	SAFY	LAI	EnKF	Silvestro et al. (2017)
HJ-1A/B, Landsat-8	AquaCrop	CC	PSO	Silvestro et al. (2017)
HJ-1A/B, RADARSAT-2	AquaCrop	AGB, CC	PSO	Jin et al. (2017)
IRS LISS-III	WTGROWS	LAI	Modified corrective approach	Sehgal et al. (2005)
IRTS-P3 infrared radiative thermometer	SVAT	Surface radiometric temperature	SCE-UA	Crow et al. (2008)

Landsat ETM+	WOFOST	LAI	EnKF	Li et al. (2014)
Landsat ETM+	SWAP	ET	GA	Ines et al. (2006)
Landsat TM	DSSAT+PROSAIL	NDVI	AA	Dong et al. (2013)
Landsat TM, ETM+ and OLI	DSSAT	LAI, VTCI	EnKF	Xie et al. (2017)
Landsat5 TM	SWAP	ET	PEST	Droogers et al. (2010)
Landsat-8	WOFOST	LAI	PSO	Jin et al. (2015a,b)
MODIS	WOFOST	LAI	EnKF	Wu et al. (2011), Zhao et al. (2013) and Zhu et al. (2013)
MODIS	SWAP	LAI	Powell	He et al. (2014)
MODIS	DSSAT+MCRM	NDVI, LAI, EVI	Powell	Fang et al. (2011)
MODIS	DSSAT	LAI	Powell	Fang et al. (2008)
MODIS	WOFOST	LAI	Powell, SCE-UA	Tian et al. (2013)
MODIS	SWAP	LAI, ET	SCE-UA	Huang et al. (2015)
MODIS	SWAP	LAI	SCE-UA	Xu et al. (2011)
MODIS	WOFOST	LAI	SCE-UA	Ma et al. (2013)
MODIS	EPIC	LAI	SCE-UA	Ren et al. (2011)
MODIS	COSIM	LAI	SCE-UA and SA	Zhao et al. (2005)
MODIS	DSSAT	LAI	AA	Jin et al. (2016)
MODIS	WOFOST	LAI, ET	FSEOPT software	Zhang et al. (2007)
MODIS	WOFOST	LAI	FSEOPT software	Ma et al. (2008)
MODIS	WOFOST	SAVI	FSEOPT	Ma et al. (2008)
MODIS	CERES-Wheat	LAI	Cost function	Wang et al. (2011)
MODIS	SWAP	LAI, ET	Constant gain Kalman filter	Vazifedoust et al. (2009)
MODIS (LAI GPP)	WOFOST-HYDRUS	LAI	EnKF	
MODIS HJ CCD	WOFOST	SAVI	PSO	Wu et al. (2012)
MODIS L1B	SWAP	ET	GA	Irmak and Kamble (2009)
MODIS L1B	SWAP	ET, LAI	GA	Charoenhirunyingyos et al. (2011)

(continued)

Table 4.3 (continued)

RS data	Crop model	Variables	Algorithm	References
MODIS LAI	CERES-Wheat	LAI	SCE-UA	Yan et al. (2006)
MODIS LAI GPP	WOFOST	LAI GPP	SA, SCE-UA	Wang (2013)
MODIS(LAI)	Py WOFOST	LAI	EnKF	Zhao et al. (2013)
MODIS, Landsat TM	WOFOST	LAI	EnKF	Huang et al. (2016)
MODIS, Landsat TM	WOFOST	LAI	SCE-UA	Huang et al. (2015)
MODIS, SMOS	DSSAT	LAI, SM	EnKF	Nearing et al. (2012)
PROBA/CHRIS	WOFOST	LAI	EnKF	Wang et al. (2013)
SAR	WOFOST	Biomass	Cost function	Tan et al. (2011)
SMOS	WOFOST	SM	EnKF	Chakrabarti et al. (2014)
SMOS	SWAP	SM	EnSRF	Singh and Panda (2015)
SPOT, airborne images	SUCROS	TSAVI	Numerical optimization	Guerif and Duke (2000)
SPOT, airborne images	SUCROS	TSAVI	Numerical optimization	Launay and Guerif (2005)
SPOT, ERS, Radarsat	WOFOST	LAI	EnKF	Curnel et al. (2011)
SPOT, ERS, Radarsat	WOFOST	LAI	ULM	Curnel et al. (2011)
SPOT, UAV	SUCROS+SAIL	TSAVI	SA	Launay and Guerif (2005)
Synthetic data	WOFOST	LAI, SM	EnKF	Pauwels et al. (2007)
Virtual reflectance	SUCROS+SAIL	Reflectance	SA	Guerif and Duke (2000)

CGKF constant gain Kalman filter, *EnKF* ensemble Kalman filter, *EnSRF* ensemble square root filter, *VTCI* vegetation temperature condition index, *SCE-UA* shuffled complex evolution method developed at the University of Arizona, *PSO* particle swarm optimization, *MLS* maximum likelihood solution, *SA* simple algorithm, *AA* annealing algorithm, *GA* genetic algorithm, *ULM* unconstrained Levenberg–Marquardt algorithm, *TSAVI* transformed soil adjusted vegetation index, *NDVI* normalized difference vegetation index, *EVI* enhanced vegetation index, ρ backscatter coefficient, λ band reflectance, *LNA* leaf nitrogen accumulation, *CC* canopy cover, *CAN* canopy nitrogen accumulation

analysis, calibration, and validation of crop models along with RS data retrieval and assimilation will be a demanding area of research in the future.

The prediction accuracy of crop models is improved through the assimilation of RS data. However, the RS data mainly obtained using various optical sensors may also contain some errors in a regional domain (Huang et al. 2001; Duchemin et al. 2003; Hadria et al. 2006; Thorp et al. 2010; Yao et al. 2015). Currently, the VIs derived from RS data is difficult to satisfy the requirement of crop models both temporally and spatially. Further, RS has challenges such as directional problem, scale effect and scale transformation, and retrieval techniques and method. These factors impact the retrieval accuracy of canopy state variables using RS data and at the DA chain (X. Jin et al. 2018). Crop area delineation is the foremost prerequisite of spatialization of CGMs, and towards this end, object-oriented image analysis (Blaschke 2010; Qi et al. 2012; Gu et al. 2017) could provide better representative crop maps for the models. Object-oriented classification enables the acquisition of a variety of spatial and textural features from multi-temporal RS images and carries out segmentation followed by crop area delineation. Improved algorithms based on machine learning techniques (Skakun et al. 2015; Guo et al. 2016) are very much useful for pixel-level classification and analysis of multispectral and multi-temporal RS data. Currently, the key problem of many RS-based parameter retrieval is due to the ill-posed issues during the inversion process (Li et al. 2015a,b). Though there is no definitive solution to the inversion problem, the introduction of the prior knowledge could provide better convergence. The uncertainty introduced by DA could be improved by combining different DA algorithms (such as a combination of EnKF and 4DVAR) (Dong et al. 2013). Development in the area of hyperspectral RS data can further improve the estimation accuracy of canopy state variables and soil properties at the field scale based on a combination of spectral shapes and spectral indices (Frels et al. 2018). With the fast development of versatile, lightweight, and low-cost portable sensors on the unmanned aerial vehicle (UAV) platform, newer avenue of RS data generation with the high spatial and temporal resolution is evolving (Bendig et al. 2015; Adao et al. 2017). Though this UAV technology is best suited to acquire high spatial and temporal RS data at the field scale, it does not provide regional-scale data promptly because of the small spatial coverage of UAV. To improve the stress detection and crop monitoring activities through RS, fluorescence-based sensors have been developed recently. In this context, Fluorescence Explorer (FLEX) of the European Space Agency is expected to monitor the photosynthetic activity of vegetation through chlorophyll fluorescence on a global scale. Fluorescence is considered to be a more accurate and earlier indicator of plant growth and stress than other biophysical parameters used (LAI, fAPAR), but the fluorescence data product would at a coarser scale account for its weak signal. Hence, lots of research is required on this fluorescence data retrieval and assimilation into the crop model. The recent trend in the development of constellations of nanosatellites (mass $<$ 10 kg) is another area of research in satellite RS. An operational example is the constellation of Planet Lab's "Doves", which are designed to cover the globe daily at 3–5 m spatial resolution. Development of intelligent algorithm to handle big data generated through multiple sensors on

different platforms and assimilating these data into process-based CGSMs at the required scale and resolution will become key research directions in the future.

4.6 Conclusions

Crop models and RS had parallel development courses, and both the technology complement each other. At the same time, the spatialization of CGMs demands the synergistic use of both. The combined use of various RS datasets and crop models using new DA methods could improve the retrieval accuracy of crop canopy state variables, soil properties, etc. The major challenge in the spatialization of CGMs is to address various issues and limitations of both techniques. In this chapter, a detailed discussion is carried out on the evolution, scope, and limitation of popular process-based crop growth simulation models at the beginning. The techniques and issues involved in the spatialization of crop models particularly the development of a spatial framework on the GIS environment and addressing the availability of data at various scales are discussed with emphasis on soil, weather, and retrieved crop biophysical parameters. Spatialization involves a change of scales in input, processes, and output. Various limitations of scale change are addressed in this chapter under various sections. The retrieval of biophysical parameters from RS data and its subsequent assimilation into the model is the central theme around which the entire concept of spatialization of the crop growth model revolves around. Different techniques for retrieval of crop biophysical parameters from RS data such as empirical, physical, and hybrid approaches are presented along with some of their recent application. This section also covers scale effect, optimal scale, and pixel heterogeneity and related issues involved in the retrieval process. The concept of RS DA into a crop growth model is discussed along with various algorithms. A list of recent studies on RS DA is presented. An attempt is made to cover all recent development and future scope for research in the area of spatialization of crop growth models.

References

Abou-Ismail O, Huang JF, Wang RC (2004) Rice yield estimation by integrating remote sensing with rice growth simulation model. Pedosphere 14(4):519–526

Abrahamsen P, Hansen S (2000) Daisy: an open soil-crop-atmosphere system model. Environ Model Softw 15(3):313–330

Adão T, Hruška J, Pádua L, Bessa J, Peres E, Morais R, Sousa JJ (2017) Hyperspectral imaging: a review on UAV-based sensors, data processing and applications for agriculture and forestry. Remote Sens 9(11):1110

Aggarwal PK (1993) Agro-ecological zoning using crop growth simulation models: characterization of wheat environments of India. In: Systems approaches for agricultural development. Springer, Dordrecht, pp 97–109

Aggarwal PK (1998) Exchange of methodologies in land use planning. In: Roetter R et al (eds) . IRRI, Los Baños, pp 59–65

Aggarwal PK, Kalra N, Chander S, Pathak H (2006) InfoCrop: a dynamic simulation model for the assessment of crop yields, losses due to pests, and environmental impact of agro-ecosystems in tropical environments. I. Model description. Agric Syst 89(1):1–25

Albers BJ, Strahler AH, Li X, Liang S, Clarke KC (1990) Radiometric measurements of gap probability in conifer tree canopies. Int J Remote Sens 34(3):179–192

Alexandridis TK, Gitas IZ, Silleos NG (2008) An estimation of the optimum temporal resolution for monitoring vegetation condition on a nationwide scale using MODIS/Terra data. Int J Remote Sens 29(12):3589–3607

Alexandridis TK, Katagis T, Gitas IZ, Silleos NG, Eskridge KM, Gritzas G (2010) Investigation of aggregation effects in vegetation condition monitoring at a national scale. Int J Geogr Inf Sci 24 (4):507–521

Angulo C, Rötter R, Trnka M, Pirttioja N, Gaiser T, Hlavinka P, Ewert F (2013) Characteristic 'fingerprints' of crop model responses to weather input data at different spatial resolutions. Eur J Agron 49:104–114

Azzari G, Jain M, Lobell DB (2017) Towards fine resolution global maps of crop yields: testing multiple methods and satellites in three countries. Remote Sens Environ 202:129–141

Bach H, Mauser W (2003) Methods and examples for remote sensing data assimilation in land surface process modeling. IEEE Trans Geosci Remote Sens 41(7):1629–1637

Bagheri N, Ahmadi H, Alavipanah S, Omid M (2012) Soil-line vegetation indices for corn nitrogen content prediction. Int Agrophys 26(2):103

Bai J, Chen X, Dobermann A, Yang H, Cassman KG, Zhang F (2010) Evaluation of NASA satellite-and model-derived weather data for simulation of maize yield potential in China. Agron J 102(1):9–16

Bai ZG, Conijn JG, Bindraban PS, Rutgerts B (2012) Global changes of remotely sensed greenness and simulated biomass production since 1981; Towards mapping global soil degradation. ISRIC-World Soil Information, Wageningen

Bastiaanssen WG, Menenti M, Feddes RA, Holtslag AA (1998) A remote sensing surface energy balance algorithm for land (SEBAL). 1. Formulation. J Hydrol 212:198–212

Batchelor WD, Basso B, Paz JO (2002) Examples of strategies to analyze spatial and temporal yield variability using crop models. Eur J Agron 18(1–2):141–158

Batjes NH (1996) Development of a world data set of soil water retention properties using pedotransfer rules. Geoderma 71(1–2):31–52

Bendig J, Yu K, Aasen H, Bolten A, Bennertz S, Broscheit J, Gnyp ML, Bareth G (2015) Combining UAV-based plant height from crop surface models, visible, and near infrared vegetation indices for biomass monitoring in barley. Int J Appl Earth Obs Geoinf 39:79–87

Bhatia AK (2014) Modelling and simulation of diffusive processes: methods and applications. In: Basu SK, Kumar N (eds) . Springer, Cham, pp 315–332

Biswal A, Sai MS, Rao SK (2014) Assessment of satellite and model derived long term solar radiation for spatial crop models: a case study using DSSAT in Andhra Pradesh. Comput Ecol Softw 4(3):205

Blaschke T (2010) Object based image analysis for remote sensing. ISPRS J Photogramm Remote Sens 65(1):2–16

Bolten JD, Crow WT, Zhan X, Jackson TJ, Reynolds CA (2009) Evaluating the utility of remotely sensed soil moisture retrievals for operational agricultural drought monitoring. IEEE J Sel Top Appl Earth Obs Remote Sens 3(1):57–66

Boote KJ, Jones JW, Pickering NB (1996) Potential uses and limitations of crop models. Agron J 88 (5):704–716

Bouma J (1989) Land qualities in space and time. In: Bouma J and Bregt AK (eds) In: Proceeding of the ISSS Symposium on land qualities in space and time, Wageningen, the Netherlands.22–26 Aug. 1988. Pudoc. Wageningen, pp 3–13

Bouman BA (1992) Linking physical remote sensing models with crop growth simulation models, applied for sugar beet. Int J Remote Sens 13(14):2565–2581
Bouman BA, Van Laar HH (2006) Description and evaluation of the rice growth model ORYZA 2000 under nitrogen-limited conditions. Agric Syst 87(3):249–273
Brisson N, Mary B, Ripoche D, Jeuffroy MH, Ruget F, Nicoullaud B, Gate P, Devienne-Barret F, Antonioletti R, Durr C, Richard G (1998) STICS: a generic model for the simulation of crops and their water and nitrogen balances. I. Theory and parameterization applied to wheat and corn. Agronomie 18:311–346
Burrough PA (1996) In: Models in action, quantitative approaches in Sys. Analysis no. 6. Stein A et al. (ed), The Netherlands. pp 56–59
Calixte JP, Beinroth FH, Jones JW, Lal H (1992) Linking DSSAT to a GIS. Agrotechnol Transfer 15:1–7
Camacho F, Cernicharo J, Lacaze R, Baret F, Weiss M (2013) GEOV1: LAI, FAPAR essential climate variables and FCOVER global time series capitalizing over existing products. Part 2: validation and intercomparison with reference products. Remote Sens Environ 137:310–329
Cedrez CB, Hijmans RJ (2018) Methods for spatial prediction of crop yield potential. Agron J 110 (6):2322–2330
Chakrabarti S, Bongiovanni T, Judge J, Zotarelli L, Bayer C (2014) Assimilation of SMOS soil moisture for quantifying drought impacts on crop yield in agricultural regions. IEEE J Sel Top Appl Earth Obs Remote Sens 7(9):3867–3879
Challinor AJ, Wheeler TR, Craufurd PQ, Slingo JM, Grimes DI (2004) Design and optimisation of a large-area process-based model for annual crops. Agric For Meteorol 124(1–2):99–120
Charoenhirunyingyos S, Honda K, Kamthonkiat D, Ines AV (2011) Soil hydraulic parameters estimated from satellite information through data assimilation. Int J Remote Sens 32 (23):8033–8051
Chehbouni A, Watts C, Kerr YH, Dedieu G, Rodriguez JC, Santiago F, Cayrol P, Boulet G, Goodrich DC (2000) Methods to aggregate turbulent fluxes over heterogeneous surfaces: application to SALSA data set in Mexico. Agric For Meteorol 105(1–3):133–144
Chemin Y, Alexandridis T (2006) Water productivity at different geographical scales in Zhanghe Irrigation District, China. Int J Geoinform 2:9–19
Chen JM (1999) Spatial scaling of a remotely sensed surface parameter by contexture. Int J Remote Sens 69(1):30–42
Chen Y, Cournède PH (2014) Data assimilation to reduce uncertainty of crop model prediction with convolution particle filtering. Ecol Model 290:165–177
Chen JM, Pavlic G, Brown L, Cihlar J, Leblanc SG, White HP, Hall RJ, Peddle DR, King DJ, Trofymow JA, Swift E (2002) Derivation and validation of Canada-wide coarse-resolution leaf area index maps using high-resolution satellite imagery and ground measurements. Remote Sens Environ 80(1):165–184
Chen J, Huang J, Lin H, Pei Z (2010) Rice yield estimation by assimilation remote sensing into crop growth model. Sci China 40:173–183
Chen X, Qi Z, Gui D, Gu Z, Ma L, Zeng F, Li L, Sima MW (2019) A model-based real-time decision support system for irrigation scheduling to improve water productivity. Agronomy 9 (11):686
Cheng Z, Meng J, Qiao Y, Wang Y, Dong W, Han Y (2018) Preliminary study of soil available nutrient simulation using a modified WOFOST model and time-series remote sensing observations. Remote Sens 10(1):64
Cho M, Skidmore A, Corsi F, van Wieren S, Sobhan I (2007) Estimation of green grass/herb biomass from airborne hyperspectral imagery using spectral indices and partial least squares regression. Int J Appl Earth Obs Geoinf 9(4):414–424
Claverie M, Demarez V, Duchemin B, Hagolle O, Keravec P, Marciel B, Ceschia E, Dejoux JF, Dedieu G (2009) Spatialization of crop leaf area index and biomass by combining a simple crop model SAFY and high spatial and temporal resolutions remote sensing data. In: 2009 IEEE International Geoscience and Remote Sensing Symposium (Vol. 3, pp. III-478)

Clevers JG, Gitelson AA (2012) Using the red-edge bands on Sentinel-2 for retrieving canopy chlorophyll and nitrogen content. In: Proceedings of the First Sentinel-2 Preparatory Symposium

Clevers J, Vonder O, Jongschaap R, Desprats JF, King C, Prévot L, Bruguier N (2002) Using SPOT data for calibrating a wheat growth model under mediterranean conditions. Agronomie 22:687–694

Cowles MK, Carlin BP (1996) Markov chain Monte Carlo convergence diagnostics: a comparative review. J Am Stat Assoc 91(434):883–904

Creutin JD, Obled C (1982) Objective analyses and mapping techniques for rainfall fields: an objective comparison. Water Resour Res 18(2):413–431

Crosetto M, Tarantola S, Saltelli A (2000) Sensitivity and uncertainty analysis in spatial modelling based on GIS. Agric Ecosyst Environ 81(1):71–79

Crow WT, Wood EF (2003) The assimilation of remotely sensed soil brightness temperature imagery into a land surface model using ensemble Kalman filtering: a case study based on ESTAR measurements during SGP97. Adv Water Resour 26(2):137–149

Crow WT, Kustas WP, Prueger JH (2008) Monitoring root-zone soil moisture through the assimilation of a thermal remote sensing-based soil moisture proxy into a water balance model. Remote Sens Environ 112(4):1268–1281

Curnel Y, de Wit AJW, Duveiller G, Defourny P (2011) Potential performances of remotely sensed LAI assimilation in WOFOST model based on an OSS experiment. Agric For Meteorol 151 (12):1843–1855

Dadhwal VK Crop growth and productivity monitoring and simulation using remote sensing and GIS. In: Sivakumar MVK, Roy PS, Harmsen K, Saha SK (eds) Satellite remote sensing and GIS applications in agricultural meteorology, Proceedings of the Training Workshop, Dehra Dun, India, 7–11 July 2003; World Meteorological Organization: Geneva, Switzerland, 2003 pp 263–290

Dallemand JF, Vossen P (1995) Agrometeorological models, theory and applications in the MARS project. In: Proceedings of the workshop for central and eastern Europe on agrometeorological models, theory and applications in the MARS project. Ispra, Italy, 21–25 Nov. 1994. Office for official publications of the EC, EUR 16008, Luxembourg. 246 pp

Das NN, Mohanty BP (2008) Temporal dynamics of PSR-based soil moisture across spatial scales in an agricultural landscape during SMEX02: a wavelet approach. Remote Sens Environ 112 (2):522–534

de Vries P, Jansen FWT, ten Berge DM, Bakema HFM (1989) A Simulation of Ecophysiological Processes of Growth in Several Annual Crops. Centre for Agricultural Publishing and Documentation (Pudoc), Wageningen

de Wit CT (1965) Photosynthesis of Leaf Canopies Agric Res Rep. Centre for Agricultural Publication and Documentation (PUDOC), Wageningen

de Wit AD, Van Diepen CA (2007) Crop model data assimilation with the ensemble Kalman filter for improving regional crop yield forecasts. Agric For Meteorol 146(1–2):38–56

de Wit A, Baruth B, Boogaard H, van Diepen K, van Kraalingen D, Micale F, te Roller J, Supit I, van den Wijngaart R (2010) Using ERA-INTERIM for regional crop yield forecasting in Europe. Clim Res 44(1):41–53

Delécolle R, Maas SJ, Guérif M, Baret F (1992) Remote sensing and crop production models: present trends. ISPRS J Photo Remote Sens 47(2–3):145–161

Dente L, Satalino G, Mattia F, Rinaldi M (2008) Assimilation of leaf area index derived from ASAR and MERIS data into CERES-wheat model to map wheat yield. Remote Sens Environ 112(4):1395–1407

Desta FY, Abera K, Eshetu M, Koech R, Alemu MM (2017) Irrigation water planning for crops in the central highlands of Ethiopia, aided by FAO CROP WAT MODEL. Afri J Agric Res 12 (28):2329–2335

Di Paola A, Valentini R, Santini M (2016) An overview of available crop growth and yield models for studies and assessments in agriculture. J Sci Food Agr 96(3):709–714

Diacono M, Rubino P, Montemurro F (2013) Precision nitrogen management of wheat. A review. Agron Sustain Dev 33(1):219–241

Diels J, Vanlauwe B, Van der Meersch MK, Sanginga N, Merckx R (2004) Long-term soil organic carbon dynamics in a subhumid tropical climate: 13C data in mixed C3/C4 cropping and modeling with ROTHC. Soil Biol Biochem 36(11):1739–1750

Djamai N, Fernandes R, Weiss M, McNairn H, Goïta K (2019) Validation of the sentinel simplified level 2 product prototype processor (SL2P) for mapping cropland biophysical variables using Sentinel-2/MSI and Landsat-8/OLI data. Int J Remote Sens 225:416–430

Dong Y, Zhao C, Yang G, Chen L, Wang J, Feng H (2013) Integrating a very fast simulated annealing optimization algorithm for crop leaf area index variational assimilation. Math Comput Model 58(3–4):877–885

Dorigo WA, Zurita-Milla R, de Wit AJ, Brazile J, Singh R, Schaepman ME (2007) A review on reflective remote sensing and data assimilation techniques for enhanced agroecosystem modeling. Int J Appl Earth Obs Geoinf 9(2):165–193

Droogers P, Immerzeel WW, Lorite IJ (2010) Estimating actual irrigation application by remotely sensed evapotranspiration observations. Agric Water Manag 97(9):1351–1359

Duchemin B, Hadria R, Rodriguez JC, Lahrouni A, Khabba S, Boulet G, Mougenot B, Maisongrande P, Watts C (2003). Spatialisation of a crop model using phenology derived from remote sensing data. In: IGARSS 2003. In: 2003 IEEE International Geoscience and Remote Sensing Symposium. Proceedings (IEEE Cat.No. 03CH37477) 2003 Jul 21 (Vol. 4, pp. 2200–2202)

Dumont B, Leemans V, Mansouri M, Bodson B, Destain JP, Destain MF (2014) Parameter identification of the STICS crop model, using an accelerated formal MCMC approach. Environ Model Softw 52:121–135

Engel T, Hoogenboom G, Jones JW, Wilkens PW (1997) AEGIS/WIN: a computer program for the application of crop simulation models across geographic areas. Agron J 89(6):919–928

Erickson JD (1984) The LACIE experiment in satellite aided monitoring of global crop production. In the role of terrestrial vegetation in the global carbon cycle. Meas Remote Sens 23:191–217

Evensen G (1994) Sequential data assimilation with a nonlinear quasi geostrophic model using Monte Carlo methods to forecast error statistics. J Geophys Res Oceans 99(C5):10143–10162

Evensen G (2009) The ensemble Kalman filter for combined state and parameter estimation. IEEE Control Syst Mag 29(3):83–104

Ewert F, van Ittersum MK, Heckelei T, Therond O, Bezlepkina I, Andersen E (2011) Scale changes and model linking methods for integrated assessment of agri-environmental systems. Agric Ecosyst Environ 142(1–2):6–17

Fang H, Liang S, Hoogenboom G, Teasdale J, Cavigelli M (2008) Corn-yield estimation through assimilation of remotely sensed data into the CSM-CERES-maize model. Int J Remote Sens 29 (10):3011–3032

Fang H, Liang S, Hoogenboom G (2011) Integration of MODIS LAI and vegetation index products with the CSM–CERES–maize model for corn yield estimation. Int J Remote Sens 32 (4):1039–1065

Fensholt R, Sandholt I, Rasmussen MS (2004) Evaluation of MODIS LAI, fAPAR and the relation between fAPAR and NDVI in a semi-arid environment using in situ measurements. Int J Remote Sens 91(3–4):490–507

Fernandes RA, Miller JR, Chen JM, Rubinstein IG (2004) Evaluating image-based estimates of leaf area index in boreal conifer stands over a range of scales using high-resolution CASI imagery. Remote Sens Environ 89(2):200–216

Finke PA, Bierkens MF, de Willigen PE (2002) Choosing appropriate upscaling and downscaling methods for environmental research. Int Asso Hydrol Sci Publ 273:405–409

Frels K, Guttieri M, Joyce B, Leavitt B, Baenziger PS (2018) Evaluating canopy spectral reflectance vegetation indices to estimate nitrogen use traits in hard winter wheat. Field Crop Res 217:82–92

Ganguly S, Nemani RR, Zhang G, Hashimoto H, Milesi C, Michaelis A, Wang W, Votava P, Samanta A, Melton F, Dungan JL (2012) Generating global leaf area index from Landsat: algorithm formulation and demonstration. Int J Remote Sens 122:185–202

Gao BC (1996) NDWI-normalized difference water index for remote sensing of vegetation liquid water from space. Int J Remote Sens 58(3):257–266

Garrigues S, Allard D, Baret F, Weiss M (2006) Quantifying spatial heterogeneity at the landscape scale using variogram models. Int J Remote Sens 103(1):81–96

Gelman A, Carlin JB, Stern HS, Dunson DB, Vehtari A, Rubin DB (2013) Bayesian data analysis. CRC press, Boca Raton

Gertsis AC, Whisler FD (1997) GOSSYM: a cotton crop simulation model as a tool for the farmer. In: International Symposium on Applications of Modelling as Innovative Technique in the Agri-Food Chain. MODEL-IT 476 pp 213–218

Gilks WR, Roberts GO (1996) Strategies for improving MCMC. Markov chain Monte Carlo Pract 6:89–114

Gilmanov TG, Parton WJ, Ojima DS (1997) Testing the 'CENTURY' ecosystem level model on data sets from eight grassland sites in the former USSR representing a wide climatic/soil gradient. Ecol Model 96(1–3):191–210

Gómez-Dans JL, Lewis PE, Disney M (2016) Efficient emulation of radiative transfer codes using Gaussian processes and application to land surface parameter inferences. Remote Sens 8(2):119

Gommes R, Snijders FL, Rijks JQ (1998) The FAO crop forecasting philosophy in national food security warning systems. In: Rijks D, Terres JM and Vossen P (eds). pp 123–130

Goovaerts P (1997) Geostatistics for natural resources evaluation. Oxford University Press on Demand

Govender M, Govender PJ, Weiersbye IM, Witkowski ET, Ahmed F (2009) Review of commonly used remote sensing and ground-based technologies to measure plant water stress. Water SA 35 (5):741–752

Grassini P, van Bussel LG, Van Wart J, Wolf J, Claessens L, Yang H, Boogaard H, de Groot H, van Ittersum MK, Cassman KG (2015) How good is good enough? Data requirements for reliable crop yield simulations and yield-gap analysis. Field Crop Res 177:49–63

Green EP, Mumby PJ, Edwards AJ, Clark CD, Ellis AC (1997) Estimating leaf area index of mangroves from satellite data. Aquat Bot 58(1):11–19

Gu H, Li H, Yan L, Liu Z, Blaschke T, Soergel U (2017) An object-based semantic classification method for high resolution remote sensing imagery using ontology. Remote Sens 9(4):329

Guérif M, Duke C (1998) Calibration of the SUCROS emergence and early growth module for sugar beet using optical remote sensing data assimilation. Eur J Agron 9:127–136

Guerif M, Duke CL (2000) Adjustment procedures of a crop model to the site specific characteristics of soil and crop using remote sensing data assimilation. Agric Ecosyst Environ 81 (1):57–69

Guo X, Huang X, Zhang L, Zhang L, Plaza A, Benediktsson JA (2016) Support tensor machines for classification of hyperspectral remote sensing imagery. IEEE Trans Geosci Remote Sens 54 (6):3248–3264

Hadria R, Duchemin B, Lahrouni A, Khabba S, ErRaki S, Dedieu G, Chehbouni AG, Olioso § A (2006) Monitoring of irrigated wheat in a semiarid climate using crop modelling and remote sensing data: impact of satellite revisit time frequency. Int J Remote Sens 27(6):1093–1117

Han S, Evans RG, Hodges T, Rawlins SL (1995) Linking a geographic information system with a potato simulation model for site-specific crop management. J Environ Qual 24(4):772–777

Hansen JW, Jones JW (2000) Scaling-up crop models for climate variability applications. Agric Syst 65(1):43–72

Hartkamp AD, White JW, Hoogenboom G (1999) Interfacing geographic information systems with agronomic modeling: a review. Agron J 91(5):761–772

He B, Li X, Quan X, Qiu S (2014) Estimating the aboveground dry biomass of grass by assimilation of retrieved LAI into a crop growth model. IEEE J Sel Top Appl Earth Obs Remote Sens 8 (2):550–561

Hilker T, Coops NC, Wulder MA, Black TA, Guy RD (2008) The use of remote sensing in light use efficiency based models of gross primary production: a review of current status and future requirements. Sci Total Environ 404(2–3):411–423

Hilker T, Hall FG, Coops NC, Lyapustin A, Wang Y, Nesic Z, Grant N, Black TA, Wulder MA, Kljun N, Hopkinson C (2010) Remote sensing of photosynthetic light-use efficiency across two forested biomes: spatial scaling. Int J Remote Sens 114(12):2863–2874

Hoefsloot P, Ines AV, Dam JC, Duveiller G, Kayitakire F, Hansen J (2012) Combining crop models and remote sensing for yield prediction: Concepts, applications and challenges for heterogeneous smallholder environments

HoefslootP (1996) IGT manual, Ver. 1.10. Working paper series N. 5. SADC/FAO, GCPS/RAF/296/NET, Harare, 53 pp. Programme and manual are retrievable from FTP://FTP.FAO.ORG/SDRN/IGT

Hu Z, Islam S (1997) A framework for analyzing and designing scale invariant remote sensing algorithms. IEEE Trans Geosci Remote Sens 35(3):747–755

Hu Z, Islam S, Cheng Y (1997) Statistical characterization of remotely sensed soil moisture images. Int J Remote Sens 61(2):310–318

Huang J, Tang S, Ousama AI, Wang R (2001) Integration of remote sensing data and simulation model to estimate rice yield, info-tech and info-net, 2001. In: Proceedings, ICII 2001-Beijing.2001 International Conferences on, IEEE. pp. 101–107

Huang Y, Zhu Y, Wang H, Yao X, Cao W, Hannaway DB, Tian Y (2011) Predicting winter wheat growth based on integrating remote sensing and crop growth modeling techniques. Acta Ecol Sin 31(4):1073–1084

Huang Y, Zhu Y, Li W, Cao W, Tian Y (2013) Assimilating remotely sensed information with the wheatgrow model based on the ensemble square root filter for improving regional wheat yield forecasts. Plant Prod Sci 16(4):352–364

Huang J, Ma H, Su W, Zhang X, Huang Y, Fan J, Wu W (2015) Jointly assimilating MODIS LAI and ET products into the SWAP model for winter wheat yield estimation. IEEE J Sel Top Appl Earth Obs Remote Sens 8(8):4060–4071

Huang J, Sedano F, Huang Y, Ma H, Li X, Liang S, Tian L, Zhang X, Fan J, Wu W (2016) Assimilating a synthetic Kalman filter leaf area index series into the WOFOST model to improve regional winter wheat yield estimation. Agric For Meteorol 216:188–202

Huang J, Gómez-Dans JL, Huang H, Ma H, Wu Q, Lewis PE, Liang S, Chen Z, Xue JH, Wu Y, Zhao F (2019a) Assimilation of remote sensing into crop growth models: current status and perspectives. Agric For Meteorol 276:107609

Huang J, Ma H, Sedano F, Lewis P, Liang S, Wu Q, Su W, Zhang X, Zhu D (2019b) Evaluation of regional estimates of winter wheat yield by assimilating three remotely sensed reflectance datasets into the coupled WOFOST–PROSAIL model. Eur J Agron 102:1–3

Hudson G, Wackernagel H (1994) Mapping temperature using kriging with external drift: theory and an example from Scotland. Int J Climatol 14(1):77–91

Hufkens K, Bogaert J, Dong QH, Lu L, Huang CL, Ma MG, Che T, Li X, Veroustraete F, Ceulemans R (2008) Impacts and uncertainties of upscaling of remote-sensing data validation for a semi-arid woodland. J Arid Environ 72(8):1490–1505

Hunt LA, Boote KJ (1998) Data for model operation, calibration, and evaluation. In: Understanding options for agricultural production. Springer, Dordrecht, pp 9–39

Iizumi T, Yokozawa M, Nishimori M (2009) Parameter estimation and uncertainty analysis of a large-scale crop model for paddy rice: application of a Bayesian approach. Agric For Meteorol 149(2):333–348

Im J, Jensen J, Coleman M, Nelson E (2009) Hyperspectral remote sensing analysis of short rotation woody crops grown with controlled nutrient and irrigation treatments. Geocarto Int 24 (4):293–312

Ines AV, Gupta AD, Loof R (2002) Application of GIS and crop growth models in estimating water productivity. Agric Water Manag 54(3):205–225

Ines AV, Honda K, Gupta AD, Droogers P, Clemente RS (2006) Combining remote sensing-simulation modeling and genetic algorithm optimization to explore water management options in irrigated agriculture. Agric Water Manag 83(3):221–232

Ines AV, Das NN, Hansen JW, Njoku EG (2013) Assimilation of remotely sensed soil moisture and vegetation with a crop simulation model for maize yield prediction. Remote Sens Environ 138:149–164

Irmak A, Kamble B (2009) Evapotranspiration data assimilation with genetic algorithms and SWAP model for on-demand irrigation. Irrig Sci 28(1):101–112

Ismail M (2012) Using remote sensing and GIS application in agro-ecological zoning of Egypt. Int J Environ Sci 1:85–94

Jackson RD, Idso SB, Reginato RJ, Pinter PJ Jr (1981) Canopy temperature as a crop water stress indicator. Water Resour Res 17(4):1133–1138

Jacquemoud S, Baret F (1990) PROSPECT: a model of leaf optical properties spectra. Int J Remote Sens 34(2):75–91

Jain N, Ray SS, Singh JP, Panigrahy S (2007) Use of hyperspectral data to assess the effects of different nitrogen applications on a potato crop. Precis Agric 8(4–5):225–239

Jansson PE, Karlberg L (2004) COUP model–coupled heat and mass transfer model for soil-plant-atmosphere system. Trita-LWR Rep 3087

Jansson PE, Karlberg L (2010) Coupled heat and mass transfer model for soil-plant-atmosphere systems. Royal Institute of Technology, Stockholm, p 484

Jiang Z, Huete AR, Chen J, Chen Y, Li J, Yan G, Zhang X (2006) Analysis of NDVI and scaled difference vegetation index retrievals of vegetation fraction. Remote Sens Environ 101 (3):366–378

Jiang Z, Chen Z, Chen J, Liu J, Ren J, Li Z, Sun L, Li H (2014) Application of crop model data assimilation with a particle filter for estimating regional winter wheat yields. IEEE J Sel Top Appl Earth Obs Remote Sens 7(11):4422–4431

Jin Z, Tian Q, Chen JM, Chen M (2007) Spatial scaling between leaf area index maps of different resolutions. J Environ Manag 85(3):628–637

Jin H, Wang J, Bo Y, Chen G, Xue H (2010) Data assimilation of MODIS and TM observations into CERES-Maize model to estimate regional maize yield. In: Remote sensing and modeling of ecosystems for sustainability VII, vol 7809. Int Soc Opt Photon, 780908

Jin M, Liu X, Wu L, Liu M (2015a) An improved assimilation method with stress factors incorporated in the WOFOST model for the efficient assessment of heavy metal stress levels in rice. Int J Appl Earth Obs Geoinf 41:118–129

Jin X, Yang G, Xu X, Yang H, Feng H, Li Z, Shen J, Lan Y, Zhao C (2015b) Combined multi-temporal optical and radar parameters for estimating LAI and biomass in winter wheat using HJ and RADARSAR-2 data. Remote Sens 7(10):13251–13272

Jin H, Li A, Wang J, Bo Y (2016) Improvement of spatially and temporally continuous crop leaf area index by integration of CERES-Maize model and MODIS data. Eur J Agron 78:1–2

Jin X, Li Z, Yang G, Yang H, Feng H, Xu X, Wang J, Li X, Luo J (2017) Winter wheat yield estimation based on multi-source medium resolution optical and radar imaging data and the aqua crop model using the particle swarm optimization algorithm. ISPRS J Photogramm Remote Sens 126:24–37

Jin X, Kumar L, Li Z, Feng H, Xu X, Yang G, Wang J (2018) A review of data assimilation of remote sensing and crop models. Euro J Agron 92:141–152

Johnson LF, Roczen DE, Youkhana SK, Nemani RR, Bosch DF (2003) Mapping vineyard leaf area with multispectral satellite imagery. Comput Electron Agric 38(1):33–44

Jones JW, Hoogenboom G, Porter CH, Boote KJ, Batchelor WD, Hunt LA, Wilkens PW, Singh U, Gijsman AJ, Ritchie JT (2003) The DSSAT cropping system model. Eur J Agron 18 (3–4):235–265

Jones JW, Antle JM, Basso B, Boote KJ, Conant RT, Foster I, Godfray HC, Herrero M, Howitt RE, Janssen S, Keating BA (2017) Brief history of agricultural systems modeling. Agric Syst 155:240–254

Kasampalis DA, Alexandridis TK, Deva C, Challinor A, Moshou D, Zalidis G (2018) Contribution of remote sensing on crop models: a review. J Imaging 4(4):52

Kolotii A, Kussul N, Shelestov A, Skakun S, Yailymov B, Basarab R, Lavreniuk M, Oliinyk T, Ostapenko V (2015) Comparison of biophysical and satellite predictors for wheat yield forecasting in ukraine. Int Arch Photo Remote Sens Spatial Infor Sci

Lal H, Hoogenboom G, Calixte JP, Jones JW, Beinroth FH (1993) Using crop simulation models and GIS for regional productivity analysis. Trans ASAE 36(1):175–184

Laslett GM, McBratney AB, Pahl PJ, Hutchinson F (1987) Comparison of several spatial prediction methods for soil pH. J Soil Sci 38:325–341

Launay M, Guerif M (2005) Assimilating remote sensing data into a crop model to improve predictive performance for spatial applications. Agric Ecosyst Environ 111(1–4):321–339

Le Dimet FX, Talagrand O (1986) Variational algorithms for analysis and assimilation of meteorological observations: theoretical aspects. Tellus Ser A Dyn Meteorol Oceanogr 38(2):97–110

Lee R (1978) Forest microclimatology. Columbia University Press, New York

Lee WS, Alchanatis V, Yang C, Hirafuji M, Moshou D, Li C (2010) Sensing technologies for precision specialty crop production. Comput Electron Agric 74(1):2–33

Leenhardt D, Voltz M, Bornand M, Webster R (1994) Evaluating soil maps for prediction of soil water properties. Euro J Soil Sci 45(3):293–301

Leenhardt D, Wallach D, Le Moigne P, Guérif M, Bruand A, Casterad MA (2006) Using crop models for multiple fields. Working with crop models, Elsevier. 2006 May 10:209–248

Legros JP, Cartographie des sols (1996) De l'analysespatiale à la gestion des territoires, Coll. Gérerl'environnement, Presses polytechniquesetuniversitairesromandes

Leij F, Alves WJ, van Genuchten MT, Williams JR (1996) The UNSODA UnsaturatedSoil hydraulic database, User's manual version 1.0. EPA/600/R-96/095. NationalRisk Management laboratory, Office of Research and Development, Cincinnati

Leij FJ, Alves WJ, van Genuchten MTh, Williams JR (1997) The UNSODA unsaturatedsoil hydraulic database. In: M.Th. van Genuchten and F.J. Leij (eds.) Characterization and measurement of the hydraulic properties of unsaturated porous media. Proceedings of the International Workshop, Riverside, California, October 22–24, 1997, pp 1269–1281

Leitão PJ, Schwieder M, Pötzschner F, Pinto JR, Teixeira AM, Pedroni F, Sanchez M, Rogass C, van der Linden S, Bustamante MM, Hostert P (2018) From sample to pixel: multi-scale remote sensing data for upscaling aboveground carbon data in heterogeneous landscapes. Ecosphere 9 (8):02298

Lewis P, Gómez-Dans J, Kaminski T, Settle J, Quaife T, Gobron N, Styles J, Berger M (2012) An earth observation land data assimilation system (EO-LDAS). Remote Sens Environ 120:219–235

Li X, Strahler AH (1985) Geometric-optical modeling of a conifer forest canopy. IEEE Trans Geosci Remote Sens 5:705–721

Li X, Strahler AH, Friedl MA (1999) A conceptual model for effective directional emissivity from non isothermal surfaces. IEEE Trans Geosci Remote Sens 37(5):2508–2517

Li C, Aber J, Stange F, Butterbach Bahl K, Papen H (2000) A process oriented model of N_2O and NO emissions from forest soils: 1. Model development. J Geophys Res Atmos 105 (D4):4369–4384

Li R, Li CJ, Dong YY, Liu F, Wang JH, Yang XD, Pan YC (2011) Assimilation of remote sensing and crop model for LAI estimation based on ensemble kalman filter. Agric Sci in China 10 (10):1595–1602

Li Z, Xu D, Guo X (2014) Remote sensing of ecosystem health: opportunities, challenges, and future perspectives. Sensors 14(11):21117–21139

Li Z, Jin X, Wang J, Yang G, Nie C, Xu X, Feng H (2015a) Estimating winter wheat (Triticumaestivum) LAI and leaf chlorophyll content from canopy reflectance data by integrating agronomic prior knowledge with the PROSAIL model. Int J Remote Sens 36 (10):2634–2653

Li Z, Wang J, Xu X, Zhao C, Jin X, Yang G, Feng H (2015b) Assimilation of two variables derived from hyperspectral data into the DSSAT-CERES model for grain yield and quality estimation. Remote Sens 7(9):12400–12418

Li T, Angeles O, Marcaida M III, Manalo E, Manalili MP, Radanielson A, Mohanty S (2017) From ORYZA2000 to ORYZA (v3): an improved simulation model for rice in drought and nitrogen-deficient environments. Agric For Meteorol 237:246–256

Liang S (2005 Mar 11) Quantitative remote sensing of land surfaces. John Wiley & Sons, Hoboken

Liang S, Fang H, Chen M, Shuey CJ, Walthall C, Daughtry C, Morisette J, Schaaf C, Strahler A (2002) Validating MODIS land surface reflectance and albedo products: methods and preliminary results. Int J Remote Sens 83(1–2):149–162

Lilly A, Wösten JHM, Nemes A, Le Bas C (1999) The development and use of the HYPRES database in Europe. In: van Genuchten M Th and Leij F J (eds.) Characterization and Measurement of the Hydraulic Properties of Unsaturated Porous Media. Proceedings of the International Workshop, Riverside, California, October 22–24, 1283–1204

Liu J (2009) A GIS-based tool for modelling large-scale crop-water relations. Environ Model Softw 24(3):411–422

Liu L, Basso B (2020) Linking field survey with crop modeling to forecast maize yield in smallholder farmers' fields in Tanzania. Food Sec 5:1–2

Liu Y, Hiyama T, Yamaguchi Y (2006) Scaling of land surface temperature using satellite data: a case examination on ASTER and MODIS products over a heterogeneous terrain area. Int J Remote Sens 105(2):115–128

Liu F, Liu X, Zhao L, Ding C, Jiang J, Wu L (2014) The dynamic assessment model for monitoring cadmium stress levels in rice based on the assimilation of remote sensing and the WOFOST model. IEEE J Sel Top Appl Earth Obs Remote Sens 8(3):1330–1338

Liu Y, Xiao J, Ju W, Zhu G, Wu X, Fan W, Li D, Zhou Y (2018) Satellite-derived LAI products exhibit large discrepancies and can lead to substantial uncertainty in simulated carbon and water fluxes. Remote Sens Environ 206:174–188

Lobell DB, Burke MB (2010) On the use of statistical models to predict crop yield responses to climate change. Agric For Meteorl 150(11):1443–1452

Lobell DB, Cassman KG, Field CB (2009) Crop yield gaps: their importance, magnitudes, and causes. Annu Rev Environ Resour 34:179–204

Lorenc AC (1986) Analysis methods for numerical weather prediction. Q J Royal Meteorol Soc 112 (474):1177–1194

Ma YP, Wang SL, Zhang L, Hou YY, Zhuang LW, He YB, Wang FT (2008) Monitoring winter wheat growth in North China by combining a crop model and remote sensing data. Int J Appl Earth Obs 10:426–437

Ma H, Huang J, Zhu D, Liu J, Su W, Zhang C, Fan J (2013) Estimating regional winter wheat yield by assimilation of time series of HJ-1 CCD NDVI into WOFOST–ACRM model with ensemble Kalman filter. Math Comp Model 58(3–4):759–770

Maas SJ (1988) Use of remotely-sensed information in agricultural crop growth models. Ecol Model 41(3–4):247–268

Machwitz M, Giustarini L, Bossung C, Frantz D, Schlerf M, Lilienthal H, Wandera L, Matgen P, Hoffmann L, Udelhoven T (2014) Enhanced biomass prediction by assimilating satellite data into a crop growth model. Environ Model Softw 62:437–453

Makowski D, Wallach D, Tremblay M (2002) Using a Bayesian approach to parameter estimation; comparison of the GLUE and MCMC methods. Agronomie 22(2):191–203

Manfreda S, McCabe MF, Fiorentino M, Rodríguez-Iturbe I, Wood EF (2007) Scaling characteristics of spatial patterns of soil moisture from distributed modelling. Adv Water Resour 30 (10):2145–2150

McCown RL, Hammer GL, Hargreaves JN, Holzworth DP, Freebairn DM (1996) APSIM: a novel software system for model development, model testing and simulation in agricultural systems research. Agric Syst 50(3):255–272

McLaughlin D (2002) An integrated approach to hydrologic data assimilation: interpolation, smoothing, and filtering. Adv Water Resour 25(8–12):1275–1286
Minasny B, McBratney AB (2001) A rudimentary mechanistic model for soil formation and landscape development: II. A two-dimensional model incorporating chemical weathering. Geoderma 103(1–2):161–179
Miner GL, Hansen NC, Inman D, Sherrod LA, Peterson GA (2013) Constraints of no-till dryland agroecosystems as bioenergy production systems. Agron J 105(2):364–376
Miphokasap P, Honda K, Vaiphasa C, Souris M, Nagai M (2012) Estimating canopy nitrogen concentration in sugarcane using field imaging spectroscopy. Remote Sens 4(6):1651–1670
Mkhabela MS, Bullock PR (2012) Performance of the FAO AquaCrop model for wheat grain yield and soil moisture simulation in Western Canada. Agric Water Manage 110:16–24
Monteith JL, Moss CJ (1977) Climate and the efficiency of crop production in Britain [and discussion]. Philos T Roy Soc B 281:277–294
Morel J, Martiné JF, Bégué A, Todoroff P, Petit M (2012) A comparison of two coupling methods for improving a sugarcane model yield estimation with a NDVI-derived variable. In: Remote sensing for agriculture, ecosystems, and hydrology XIV (Vol. 8531, p. 85310E). International Society for Optics and Photonics
Moulin S, Bondeau A, Delecolle R (1998) Combining agricultural crop models and satellite observations: from field to regional scales. Int J Remote Sens 19(6):1021–1036
Mourtzinis S, Ortiz BV, Damianidis D (2016) Climate change and ENSO effects on southeastern US climate patterns and maize yield. Sci Rep 6(1):1–7
Murthy VRK (2003) Crop growth modeling and its applications in agricultural meteorology. In: Proceedings of the Satellite Remote Sensing and GIS Applications in Agricultural Meteorology, Dehra Dun, India, 7–11 July 2003; World Meteorological Organisation: Dehra Dun, India. pp 235–261
Mustafa AA, Singh M, Sahoo RN, Ahmed N, Khanna M, Sarangi A, Mishra AK (2011) Land suitability analysis for different crops: a multi criteria decision making approach using remote sensing and GIS. Researcher 3(12):61–84
Mustak SK, Baghmar NK, Singh SK (2015) Land suitability modeling for gram crop using remote sensing and GIS: a case study of Seonath basin, India. Bull Environ Sci Res 4:6–17
Nearing GS, Crow WT, Thorp KR, Moran MS, Reichle RH, Gupta HV (2012) Assimilating remote sensing observations of leaf area index and soil moisture for wheat yield estimates: an observing system simulation experiment. Water Resour Res 48(5)
Nendel C, Berg M, Kersebaum KC, Mirschel W, Specka X, Wegehenkel M, Wenkel KO, Wieland R (2011) The MONICA model: testing predictability for crop growth, soil moisture and nitrogen dynamics. Ecol Model 1222(9):1614–1625
Nix HA (1983) Minimum Data Sets for Agrotechnology Transfer. In: Proceedings of the International Symposium on Minimum Data Sets for Agrotechnology Transfer, ICRISAT Center, Patancheru, India, 21–26 March 1983; ICRISAT Center: Patancheru, India. pp 181–188
Nouvellon Y, Moran MS, Seen DL, Bryant R, Rambal S, Ni W, Bégué A, Chehbouni A, Emmerich WE, Heilman P, Qi J (2001) Coupling a grassland ecosystem model with Landsat imagery for a 10-year simulation of carbon and water budgets. Remote Sens Environ 78(1–2):131–149
Oldak A, Pachepsky Y, Jackson TJ, Rawls WJ (2002) Statistical properties of soil moisture images revisited. J Hydrol 255(1–4):12–24
Olesen JE, Hansen PK, Berntsen J, Christensen S (2004) Simulation of above-ground suppression of competing species and competition tolerance in winter wheat varieties. Field Crops Res 89 (2–3):263–280
Olioso A, Chauki H, Courault D, Wigneron JP (1999) Estimation of evapotranspiration and photosynthesis by assimilation of remote sensing data into SVAT models. Remote Sens Environ 68(3):341–356
Oteng-Darko P, Yeboah S, Addy SN, Amponsah S, Danquah EO (2013) Crop modeling: a tool for agricultural research–A. J Agric Res Develop 2(1):1–6

Palosuo T, Kersebaum KC, Angulo C, Hlavinka P, Moriondo M, Olesen JE, Patil RH, Ruget F, Rumbaur C, Takáč J, Trnka M (2011) Simulation of winter wheat yield and its variability in different climates of Europe: a comparison of eight crop growth models. Eur J Agron 5 (3):103–114

Pasqualotto N, Delegido J, Van Wittenberghe S, Rinaldi M, Moreno J (2019) Multi-crop green LAI estimation with a new simple Sentinel-2 LAI index (SeLI). Sensors 19(4):904

Pauwels VR, Verhoest NE, De Lannoy GJ, Guissard V, Lucau C, Defourny P (2007) Optimization of a coupled hydrology–crop growth model through the assimilation of observed soil moisture and leaf area index values using an ensemble Kalman filter. Water Resour Res 43(4)

Peñuelas J, Filella I, Biel C, Serrano L, Save R (1993) The reflectance at the 950–970 nm region as an indicator of plant water status. Int J Remote Sens 14(10):1887–1905

Phillips DL, Dolph J, Marks D (1992) A comparison of geostatistical procedures for spatial analysis of precipitation in mountainous terrain. Agric For Meteorol 58(1–2):119–141

Pinter PJ Jr, Hatfield JL, Schepers JS, Barnes EM, Moran MS, Daughtry CS, Upchurch DR (2003) Remote sensing for crop management. Photogramm Eng Remote Sens 169(6):647–664

Priya S, Shibasaki R (2001) National spatial crop yield simulation using GIS-based crop production model. Ecol Model 136(2–3):113–129

Qi Z, Yeh AG, Li X, Lin Z (2012) A novel algorithm for land use and land cover classification using RADARSAT-2 polarimetric SAR data. Remote Sens Environ 118:21–39

Raffy M (1992) Change of scale in models of remote sensing: a general method for spatialization of models. Int J Remote Sens 40(2):101–112

Rahman AF, Gamon JA, Fuentes DA, Roberts DA, Prentiss D (2001) Modeling spatially distributed ecosystem flux of boreal forest using hyperspectral indices from AVIRIS imagery. J Geophys Res Atmos 27(106):33579–33591

Ren J, Yu F, Du Y, Qin J, Chen Z (2009) Assimilation of field measured LAI into crop growth model based on SCE-UA optimization algorithm. In: 2009 IEEE International Geoscience and Remote Sensing Symposium (Vol. 3, pp. III-573)

Ren J, Chen Z, Tang H, Zhou Q, Qin J (2011) Regional crop yield simulation based on crop growth model and remote sensing data. Trans Chinese Soc Agric Eng 27(8):257–264

Rezaei EE, Siebert S, Ewert F (2015) Impact of data resolution on heat and drought stress simulated for winter wheat in Germany. Eur J Agron 65:69–82

Rijks D, Terres JM, Vossen P (1998)Agrometeorological applications for regional crop monitoring and production assessment, Official Publications of the EU, EUR17735, Luxembourg. 516 pp

Ritchie JT, Alagarswamy G (2002) Overview of crop models for assessment of crop production. In: Effects of climate change and variability on agricultural production systems. Springer, Boston, pp 43–68

Roerink GJ, Menenti M, Verhoef W (2000) Reconstructing cloud free NDVI composites using Fourier analysis of time series. Int J Remote Sens 21(9):1911–1917

Rosenzweig C, Elliott J, Deryng D, Ruane AC, Müller C, Arneth A (2014) Assessing agricultural risks of climate change in the 21st century in a global gridded crop model inter comparison. P Natl Acad Sci 111:3268–3273

Roubtsova E (2014) Modelling and simulation of diffusive processes methods and applications. Springer, London

Sakowska K, Juszczak R, Gianelle D (2016) Remote sensing of grassland biophysical parameters in the context of the Sentinel-2 satellite mission. J Sensors:1–16. https://doi.org/10.1155/2016/4612809

Sasai T, Okamoto K, Hiyama T, Yamaguchi Y (2007) Comparing terrestrial carbon fluxes from the scale of a flux tower to the global scale. Ecol Model 208(2–4):135–144

Schneider K (2003) Assimilating remote sensing data into a land-surface process model. Int J Remote Sens 24(14):2959–2980

Seelan SK, Laguette S, Casady GM, Seielstad GA (2003) Remote sensing applications for precision agriculture: a learning community approach. Remote Sens Environ 88(1–2):157–169

Sehgal VK (2000) Ph.D Thesis, IARI, New Delhi

Sehgal VK, Sastri CV, Kalra N, Dadhwal VK (2005) Farm-level yield mapping for precision crop management by linking remote sensing inputs and a crop simulation model. J Indian Soc Remote Sens 33(1):131–136

Shelestov A, Kolotii A, Camacho F, Skakun S, Kussul O, Lavreniuk M, Kostetsky O (2015) Mapping of biophysical parameters based on high resolution EO imagery for JECAM test site in Ukraine. In: IEEE International Geosci and Remote Sens Symposium (IGARSS) 2015 Jul 26, pp. 1733–1736

Shen S, Yang S, Li B, Tan B, Li Z, Le Toan T (2009) A scheme for regional rice yield estimation using ENVISAT ASAR data. Sci China Ser D Earth Sci 52(8):1183–1194

Sibley AM, Grassini P, Thomas NE, Cassman KG, Lobell DB (2014) Testing remote sensing approaches for assessing yield variability among maize fields. Agron J 106(1):24–32

Silvestro PC, Pignatti S, Pascucci S, Yang H, Li Z, Yang G, Huang W, Casa R (2017) Estimating wheat yield in China at the field and district scale from the assimilation of satellite data into the Aquacrop and simple algorithm for yield (SAFY) models. Remote Sens 9(5):509

Simic A, Chen JM, Liu J, Csillag F (2004) Spatial scaling of net primary productivity using sub-pixel information. Remote Sens Environ 93(1–2):246–258

Singh G, Panda R (2015) Modelling and assimilation of root-zone soil moisture using near-surface observations from soil moisture ocean salinity (SMOS) satellite. In: ASABE 1st climate change symposium: adaptation and mitigation conference proceedings 2015. American Society of Agricultural and Biological Engineers, pp. 1–1

Skakun S, Kussul N, Shelestov AY, Lavreniuk M, Kussul O (2015) Efficiency assessment of multitemporal C-band Radarsat-2 intensity and Landsat-8 surface reflectance satellite imagery for crop classification in Ukraine. IEEE J Sel Top Appl Earth Obs Remote Sens 9(8):3712–3719

Spitters CJT (1990) Crop growth models: their usefulness and limitations. Acta Hortic (267):349–368

Spitters CJT, Schapendonk AHCM (1990) Evaluation of breeding strategies for drought tolerance in potato by means of crop growth simulation. Plant Soil 123:193–203

Steduto P, Hsiao TC, Raes D, Fereres E (2009) AquaCrop—the FAO crop model to simulate yield response to water: I. concepts and underlying principles. Agron J 101(3):426–437

Stöckle CO, Donatelli M, Nelson R (2003) CropSyst, a cropping systems simulation model. Eur J Agron 18(3–4):289–307

Takle ES (1995) Use of physically based meteorological models for enhancing agro climatic databases. FAO Agrometeorology Series Working Paper (FAO)

Tan Z, Liu XN, Zhang XQ, Wu L (2011) Simulation of dynamics of crop biomass by assimilation SAR data into crop growth model. Chinese Agric Sci Bull 27(27):161–167

Tarantola S, Giglioli N, Saltelli A, Jesinghaus J (2000) Global sensitivity analysis for the quality assessment of GIS-based models. In: Heuvelink GBM, Lemmens MJPM (eds), Accuracy 2000, Proceedings of the 4th International Symposium on Spatial Accuracy Assessment in Natural Resources and Environmental Sciences. Amsterdam, pp 637–641

Tarnavsky E, Garrigues S, Brown ME (2008) Multi scale geostatistical analysis of AVHRR, SPOT-VGT, and MODIS global NDVI products. Remote Sens Environ 112(2):535–549

Thorgeirsson H, Soegaard H (1999) Simulated carbon dioxide exchange of leaves of barley scaled to the canopy and compared to measured fluxes. Agric For 98:479–489

Thorp KR, Hunsaker DJ, French AN (2010) Assimilating leaf area index estimates from remote sensing into the simulations of a cropping systems model. Trans ASABE 53(1):251–262

Tian Y, Wang Y, Zhang Y, Knyazikhin Y, Bogaert J, Myneni RB (2003) Radiative transfer based scaling of LAI retrievals from reflectance data of different resolutions. Int J Remote Sens 84 (1):143–159

Tian L, Li Z, Huang J, Wang L, Su W, Zhang C, Liu J (2013) Comparison of two optimization algorithms for estimating regional winter wheat yield by integrating MODIS leaf area index and world food studies model. Sens Lett 11(6–7):1261–1268

Tripathy R, Chaudhari KN, Mukherjee J, Ray SS, Patel NK, Panigrahy S, Parihar JS (2013) Forecasting wheat yield in Punjab state of India by combining crop simulation model WOFOST and remotely sensed inputs. Remote Sens Lett 4(1):19–28

Turner DP, Cohen WB, Kennedy RE, Fassnacht KS, Briggs JM (1999) Relationships between leaf area index and Landsat TM spectral vegetation indices across three temperate zone sites. Int J Remote Sens 70(1):52–68

Turner DP, Ollinger S, Smith ML, Krankina O, Gregory M (2004) Scaling net primary production to a MODIS footprint in support of earth observing system product validation. Int J Remote Sens 25(10):1961–1979

Upreti D, Huang W, Kong W, Pascucci S, Pignatti S, Zhou X, Ye H, Casa R (2019) A comparison of hybrid machine learning algorithms for the retrieval of wheat biophysical variables from sentinel-2. Remote Sens 11(5):481

USDA Natural Resource Conservation Service (1994) National Soil Pedon Database, Lincoln, NE

Van Diepen CV, Wolf J, Van Keulen H, Rappoldt C (1989) WOFOST: a simulation model of crop production. Soil Use Manag 5(1):16–24

Van Ittersum MK, Donatelli M (2003) Modelling cropping systems: highlights of the symposium and preface to the special issues. Eur J Agron 18(3–4):187–197

Van Ittersum MK, Cassman KG, Grassini P, Wolf J, Tittonell P, Hochman Z (2013) Yield gap analysis with local to global relevance—a review. Field Crop Res 143:4–17

Van Lanen HA, Van Diepen CA, Reinds GJ, De Koning GH, Bulens JD, Bregt AK (1992) Physical land evaluation methods and GIS to explore the crop growth potential and its effects within the European Communities. Agric Syst 39(3):307–328

Van Wart J, Grassini P, Cassman KG (2013) Impact of derived global weather data on simulated crop yields. Glob Chang Biol 19(12):3822–3834

Van Wart J, Grassini P, Yang H, Claessens L, Jarvis A, Cassman KG (2015) Creating long-term weather data from thin air for crop simulation modeling. Agric For Meteorol 209:49–58

Vazifedoust M, Van Dam JC, Bastiaanssen WG, Feddes RA (2009) Assimilation of satellite data into agrohydrological models to improve crop yield forecasts. Int J Remote Sens 30 (10):2523–2545

Verhoef W (1984) Light scattering by leaf layers with application to canopy reflectance modeling: the SAIL model. Int J Remote Sens 16(2):125–141

Verrelst J, Muñoz J, Alonso L, Delegido J, Rivera JP, Camps-Valls G, Moreno J (2012) Machine learning regression algorithms for biophysical parameter retrieval: opportunities for Sentinel-2 and-3. Int J Remote Sens 118:127–139

Verrelst J, Rivera JP, Moreno J, Camps-Valls G (2013) Gaussian processes uncertainty estimates in experimental Sentinel-2 LAI and leaf chlorophyll content retrieval. ISPRS J Photo Remote Sens 86:157–167

Voltz M, Webster R (1990) A comparison of kriging, cubic splines and classification for predicting soil properties from sample information. J Soil Sci 41(3):473–490

Walker JP, Willgoose GR, Kalma JD (2001) One-dimensional soil moisture profile retrieval by assimilation of near-surface observations: a comparison of retrieval algorithms. Adv Water Resour 24(6):631–650

Wallach D, Goffinet B, Bergez JE, Debaeke P, Leenhardt D, Aubertot JN (2001) Parameter estimation for crop models. Agron J 93(4):757–766

Wallach D, Makowski D, Jones JW, Brun F, Jones JW (2014) Working with dynamic crop models. Academic Press, Cambridge, MA, pp 407–436

Walthall C, Dulaney W, Anderson M, Norman J, Fang H, Liang S (2004) A comparison of empirical and neural network approaches for estimating corn and soybean leaf area index from Landsat ETM+ imagery. Int J Remote Sens 92(4):465–474

Wang PJ, Sun R, Zhang JH, Zhou YY, Xie DH, Zhu QJ (2011) Yield estimation of winter wheat in the North China plain using the remote-sensing–photosynthesis–yield estimation for crops (RS-P-YEC) model. Int J Remote Sens 32(21):6335–6348

Wang H, Zhu Y, Ma ML, Li WL, Gu KJ, Cao WX, Tian YC (2012) Coupling remotely sensed information with a rice growth model by combining updating and assimilation strategies. Acta Ecol Sin 32(14):4505–4515

Wang J, Li X, Lu L, Fang F (2013) Estimating near future regional corn yields by integrating multi-source observations into a crop growth model. Euro J Agron 49:126–140

Wang H, Zhu Y, Li W, Cao W, Tian Y (2014) Integrating remotely sensed leaf area index and leaf nitrogen accumulation with Rice grow model based on particle swarm optimization algorithm for rice grain yield assessment. J Appl Remote Sens 8(1):083674

Webster R, Oliver MA (1990) Statistical methods in soil and land resource survey. Oxford University Press (OUP)

Weiss M, Baret F, Smith GJ, Jonckheere I, Coppin P (2004) Review of methods for in situ leaf area index (LAI) determination: part II. Estimation of LAI, errors and sampling. Agric For Meteorol 121(1–2):37–53

White JW, Hoogenboom G, Stackhouse PW, Hoell JM (2008) Evaluation of NASA satellite- and assimilation model-derived long term daily temperature data over the continental US. Agric For Meteorol 148:1574–1584

Wiegand CL, Maas SJ, Aase JK, Hatfield JL, Pinter PJ Jr, Jackson RD, Kanemasu ET, Lapitan RL (1992) Multisite analyses of spectral-biophysical data for wheat. Remote Sens Environ 42 (1):1–21

Wu H, Li ZL (2009) Scale issues in remote sensing: a review on analysis, processing and modeling. Sensors 9(3):1768–1793

Wu J, Jelinski DE, Luck M, Tueller PT (2000) Multiscale analysis of landscape heterogeneity: scale variance and pattern metrics. Geogr Inf Sci 6(1):6–19

Wu S, Huang J, Liu X, Fan J, Ma G, Zou J (2011 Oct 29) Assimilating MODIS-LAI into crop growth model with EnKF to predict regional crop yield. In: International conference on computer and computing Technologies in Agriculture. Springer, Berlin, pp 410–418

Wu L, Liu X, Zhou B, Li L, Tan Z (2012) Spatial-time continuous changes simulation of crop growth parameters with multi-source remote sensing data and crop growth model. J Remote Sens 16(6):1173–1191

Wu L, Liu X, Wang P, Zhou B, Liu M, Li X (2013) The assimilation of spectral sensing and the WOFOST model for the dynamic simulation of cadmium accumulation in rice tissues. Int J Appl Earth Obs Geoinf 25:66–75

Xie Y, Kiniry JR, Williams JR (2003) The ALMANAC model's sensitivity to input variables. Agric Syst 78(1):1–6

Xie Y, Wang P, Bai X, Khan J, Zhang S, Li L, Wang L (2017) Assimilation of the leaf area index and vegetation temperature condition index for winter wheat yield estimation using Landsat imagery and the CERES-Wheat model. Agric Meteorol 246:194–206

Xie Q, Dash J, Huete A, Jiang A, Yin G, Ding Y, Peng D, Hall CC, Brown L, Shi Y, Ye H (2019) Retrieval of crop biophysical parameters from Sentinel-2 remote sensing imagery. Int J Appl Ear Obs Geoinf 80:187–195

Xu W, Jiang H, Huang J (2011) Regional crop yield assessment by combination of a crop growth model and phenology information derived from MODIS. Sens Lett 9(3):981–989

Yan Y, Liu Q, Liu Q, Li J, Chen L (2006) Methodolagy of winter wheat yield prediction based on assimilation of remote sensing data with crop growth model. J Remote Sens Beijing 10(5):804

Yao F, Tang Y, Wang P, Zhang J (2015) Estimation of maize yield by using a process-based model and remote sensing data in the Northeast China plain. Phys Chem Earth Parts A/B/C 87:142–152

Zhang RH, Li ZL, Tang XZ, Sun XM, Su HB, Zhu C, Zhu ZL (2004) Study of emissivity scaling and relativity of homogeneity of surface temperature. Int J Remote Sens 25(1):245–259

Zhang L, Wang SL, He YB, Ma YP, Zhuang LW, Hou YY (2007) Winter wheat growth simulation under water stress by remote sensing in North China. Acta Agron Sin 33(3):401–410

Zhou G, Liu X, Zhao S, Liu M, Wu L (2017) Estimating FAPAR of rice growth period using radiation transfer model coupled with the WOFOST model for analyzing heavy metal stress. Remote Sens 9(5):424

Zhao Y, Qin J, Zhou X (2005) Study on combinations of remote sensing and cotton model to retrieve initial inputs and parameters. Cotton Sci 17(5):280–284

Zhao Y, Chen S, Shen S (2013) Assimilating remote sensing information with crop model using ensemble Kalman filter for improving LAI monitoring and yield estimation. Ecol Model 270:30–42

Zhao G, Siebert S, Enders A, Rezaei EE, Yan C, Ewert F (2015) Demand for multi-scale weather data for regional crop modeling. Agric For Meteorol 200:156–171

Zhu Y, Zhu Y, Huang Y, Yao X, Liu L, Cao W, Tian Y (2010) Assimilation technique of remote sensing information and rice growth model based on particle swarm optimization. J Remote Sens 14(6):1226–1240

Zhu X, Zhao Y, Feng X (2013) A methodology for estimating leaf area index by assimilating remote sensing data into crop model based on temporal and spatial knowledge. Chin Geogr Sci 23(5):550–561

Chapter 5
Crop Monitoring Using Microwave Remote Sensing

P Srikanth, Abhishek Chakraborty, and C S Murthy

Contents

P. Srikanth (✉)
Crop Assessment Division, Agricultural Sciences and Applications Group, National Remote Sensing Center, Department of Space, ISRO, Hyderabad, Telengana, India
e-mail: srikanth_p@nrsc.gov.in

A. Chakraborty
Agroecosystem and Modeling Division Agricultural Sciences and Applications Group, National Remote Sensing Centre Department of Space, ISRO, Hyderabad, Telangana, India
e-mail: abhishek_c@nrsc.gov.in

C. S. Murthy
Agricultural Sciences and Applications Group, National Remote Sensing Centre, Department of Space, ISRO, Hyderabad, Telangana, India
e-mail: murthy_cs@nrsc.gov.in

T. Mitran et al. (eds.), *Geospatial Technologies for Crops and Soils*,
https://doi.org/10.1007/978-981-15-6864-0_5

Abstract Satellite-based preharvest estimates of agricultural output are an essential requirement of agriculture management and policy. Optical remote sensing is limited by the cloudy and obscure weather conditions during monsoon season. Microwave signal can penetrate cloud, haze, and fog making it suitable for mapping and monitoring of crops in all weather conditions. The interaction of the microwave with the crop canopy is greatly influenced by the senor characteristics such as wavelength, angle of incidence, and polarization and also the target properties such as surface roughness, crop geometry, and soil and vegetation water content. Synthetic aperture radar (SAR) data has been successfully used for mapping of flooded rice crop. Limited success has also been received for wheat, corn, and soybean crops with reasonable accuracies. Crop biophysical parameters such as leaf area index (LAI) and crop biomass can also be retrieved with limited uncertainty using different wavelength, polarization, and incident angle of SAR data. Synergistic use of SAR and optical data showed promising results in the assessment of crop parameters and condition at regional level. This chapter provides a brief introduction to microwave remote sensing (MRS) and its interaction with crop canopy at different wavelength and polarization followed by few case studies showcasing successful utilization of SAR date for agricultural crop monitoring.

Keywords Biomass · Crops · Leaf area index · Microwave · Polarization · Synthetic Aperture Radar

Abbreviations

EM	Electromagnetic
FIR	Far Infrared
LAI	Leaf Area Index
MIR	Middle Infrared
MRS	Microwave Remote Sensing
NDVI	Normalized Difference Vegetation Index
NIR	Near Infrared
RADAR	Radio Detection and Ranging
RS	Remote Sensing
SAR	Synthetic Aperture Radar
SWIR	Short-wave Infrared
UV	Ultraviolet
WCM	Water Cloud Model

5.1 Introduction

Agriculture is the backbone of a nation as it ensures food security and social stability. It is the mainstay of the economy in many developing countries. The Sustainable Development Goal 2 (SDG2) addresses “End hunger, achieve food security and

improved nutrition, and promote sustainable agriculture". It requires seamless interconnected activities to support sustainable agriculture, empowerment of small and marginal farmers, promotion of gender equality, eradication of rural poverty, ensuring healthy lifestyles, combating climate change, etc. Geospatial technology plays a very vital role in agroecosystem services to achieve SDG2 goals (Mitran et al. 2018; Meena et al. 2020). Regular mapping and monitoring of crop growth and preharvest production estimates is an essential requirement of agriculture management and policy decisions. Satellite-based remotely sensed data offer near-real-time mapping of crop area, crop condition and growth, crop damage, and production estimate at the regional/national level. Visible, near-infrared (NIR), and short-wave infrared (SWIR) regions of the electromagnetic (EM) spectrum have been extensively used successfully to derive the agriculture outputs. But these regions have some inherent limitations for different weather conditions. The availability of analysis-ready optical data is limited during the cloudy and obscure weather conditions as it is affected by cloud, haze, fog, and other atmospheric constituents like aerosols, water vapour, and dust. Some of the adverse impacts of the atmosphere on the optical data can be corrected, while the effect of cloud, haze, and fog remains unresolved as optical wavelengths cannot penetrate them. These challenging weather conditions cause great difficulties in the establishment of crop mapping procedures, area and production estimations, and retrieval of biophysical parameters, particularly during *kharif*/monsoon season. The microwave region of the EM spectrum, having higher wavelengths, can penetrate cloud, haze, and fog. Thus, it provides valuable data at all weather conditions. It can also operate during night-time in contrast to the optical sensors. The microwave wavelengths are sensitive to surface geometry and dielectric properties. They can penetrate soil and crop canopy depending on the operating wavelength or frequency and incident angle. So, it is capable to provide subsurface or below canopy information in selected situations. Depending on the configuration of the microwave sensor such as wavelength, polarization, phase, incidence angles, a wealth of information about the target object can be obtained. These characteristic properties of the microwave sensors have potential applications in the field of agriculture monitoring and assessment. This book chapter deals with some of the basic principles of MRS (passive and active), the interaction of the microwaves with agriculture crops, identification and mapping of selected crops, and retrieval of crop biophysical parameters with some limited case studies.

5.2 Basics of Microwave Remote Sensing

The EM spectrum has been divided into different regions, namely, gamma rays, X-ray, ultraviolet (UV), visible, NIR, middle infrared (MIR), far infrared (FIR), microwave, and radio wave based on increasing wavelength and decreasing frequencies (Fig. 5.1). The optical wavelengths can be focused with lenses and range between 0.3 and 15 micrometres (basically the reflective and emissive portion of the EM spectrum). This region is most widely used for remote sensing (RS) purpose followed by the MIR and FIR. The microwave region in the EM spectrum ranges

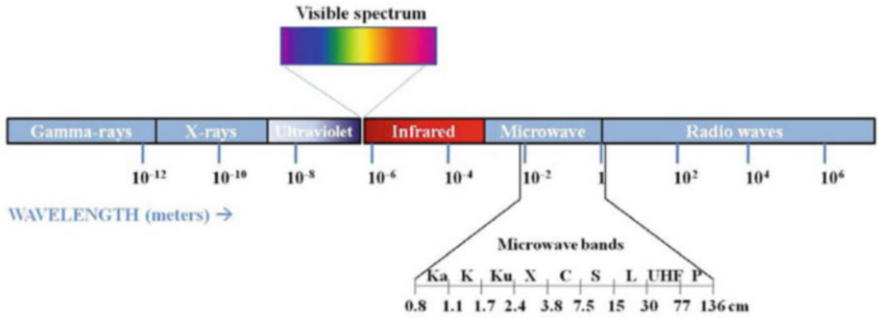

Fig. 5.1 Electromagnetic spectrum with different spectral regions in the increasing order of the wavelength

approximately from 1 cm to 1 m wavelength represented by different bands as shown in Fig. 5.1. Microwave wavelengths are relatively longer than optical wavelengths in the visible and infrared regions and hence got special characteristics which are important for RS. Longer wavelengths have the capability to penetrate clouds, haze, dust, fog, and moderate rainfall, and also, the microwave radiation is almost transparent to atmospheric constituents compared to the optical wavelengths. These special properties of the microwave wavelengths make it possible to sense the microwave energy in almost all-weather conditions, and also, microwave sensors can be operated in daytime and night-time. RS in the microwave region can be either active or passive.

5.2.1 Passive Microwave Remote Sensing

A passive microwave sensor detects the naturally emitted microwave energy within its field of view. This emitted energy depends on the various properties of the surface or emitting objects such as moisture (dielectric properties) and temperature. An example of typical passive microwave sensors is scanners or radiometers. Basically, an antenna is employed to detect and record microwave energy. Because of the longer wavelengths, the energy available to the detector or antenna is quite small compared to optical wavelengths. Thus, a larger field of view is required to detect enough energy to record a signal. This is the reason why the spatial resolution of the data acquired by most of the passive microwave sensors is relatively coarser. One of the important applications of passive MRS in agriculture is the surface soil moisture estimation. A series of operational passive microwave satellites have been providing such information, i.e. Scanning Multichannel Microwave Radiometer (SMMR) (1978–1987), Special Sensor Microwave Imager (SSM/I) of Defence Meteorological Satellite Program since 1987, the microwave imager from the Tropical Rainfall Measuring Mission (TRMM) since 1997, Advanced Microwave Scanning Radiometer–Earth Observing System (AMSR-E) on-board of NASA EOS Aqua satellite since 2002, Soil Moisture and Ocean Salinity (SMOS) since 2009, and

recently Advanced Microwave Scanning Radiometer-2 of JAXA's Global Change Observation Mission first Water (GCOM-W1) since 2012.

5.2.2 *Active Microwave Remote Sensing*

Active microwave sensors use their own source of microwave energy to illuminate the target. These sensors are either imaging or non-imaging. Radio detection and ranging (RADAR) is the most important active microwave sensor. It can operate any time during day or night and has the major advantages to penetrate through the moderate rain, cloud, haze, etc. The examples of active microwave sensors are radar altimeters, scatterometers, synthetic aperture radar (SAR), etc. SAR is most widely used for earth observation applications and natural resources assessment. Some of the past, present, and future SAR satellite missions are presented in Table 5.1.

Table 5.1 List of some of the past, present, and future SAR satellites

Sl. no.	SAR satellites	Frequency band	Active period	Operator
1	ERS-1	C	1991–2000	ESA
2	ERS-2	C	1995–2011	ESA
3	Envisat	C	2002–2012	ESA
4	Sentinel-1	C	2014-present	ESA
5	JERS-1	L	1992–1998	JAXA
6	ALOS-1	L	2006–2011	JAXA
7	ALOS-2	L	2014-present	JAXA
8	Radarsat-1	C	1995–2013	CSA
9	Radarsat-2	C	2007–present	CSA
10	Radarsat constellation	C	2019–present	CSA
11	TerraSAR-X	X	2007–present	DLR
12	TanDEM-X	X	2010–present	DLR
13	RISAT-1	C	2012–2017	ISRO
14	NISAR	L and S	Future	NASA and ISRO
15	COSMO-SkyMed	X	2007–present	ASI
16	PAZ	X	2018–present	INTA
17	KOMPSat-5	X	2013–present	KARI

ERS European Remote Sensing Satellite, *Envisat* Environmental Satellite, *JERS* Japanese Earth Resources Satellite, *ALOS* Advanced Land Observing Satellite, *Radarsat* Radar Satellite, *RISAT* Radar Imaging Satellite, *NISAR* NASA-ISRO Synthetic Aperture, *KOMPSat* Korea Multiple-purpose Satellite, *ESA* European Space Agency, *JAXA* Japan Aerospace Exploration Agency, *CSA* Canadian Space Agency, *DLR* Deutsches Zentrum für Luft- und Raumfahrt E.V, *ISRO* Indian Space Research Organization, *NASA* National Aeronautics and Space Administration, *ASI* Italian Space Agency (ASI), *INTA* Instituto Nacional de Técnica Aeroespacial, *KARI* Korea Aerospace Research Institute

5.3 Microwave Interaction with the Agriculture Crops

The interaction of the microwave with the target is greatly influenced by the sensor characteristics and also by some of the target properties. The operating wavelength, polarization, and incidence angle are important parameters of the SAR sensor that control the microwave interaction with crops/soils.

5.3.1 Wavelength/Frequency

EM waves including RADAR signals are categorized according to their frequency or, equivalently, according to their wavelength. Wavelength is the distance between successive crests or trough of waves (Fig. 5.2). Agricultural crop/soil components that have the dimensions comparable to or larger than the incident wavelengths tend to cause larger reflections/scattering when the polarization alignment is in agreement with the structural alignment of the surface components (McNairn and Brisco 2004).

Longer wavelengths can penetrate more into the crop canopy and hence enable us to get the information about the underlying soil compared to shorter wavelengths (Ulaby et al. 1986). The microwave portion of the EM spectrum is quite wide, relative to the visible and infrared. There are many bands commonly used and given code letters such as Ka (0.8–1.1 cm), K (1.1–1.7 cm), Ku (1.7–2.4 cm), X (2.4–3.8 cm), C (3.8–7.5 cm), S (7.5–15 cm), L (15–30 cm), and P (77–136 cm) in the increasing order of their wavelengths. Most commonly used wavelength bands for agriculture applications are X, C, and L bands. The microwave signal interacts with the objects based on its geometric dimension/orientation and dielectric properties. L band being higher in wavelength (15–30 cm) interacts less with the crop canopy elements and can penetration more to get the under-canopy features, whereas C and X bands interact more with the crop leaves/branches and provide information related to the crop canopy. The shorter radar wavelengths will tend to interact more

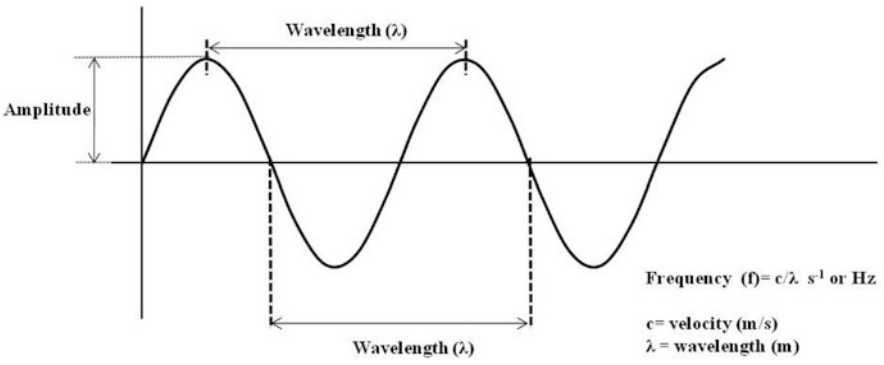

Fig. 5.2 Wavelength and frequency

with the canopy elements and saturate early by the upper part of the canopy. As wavelength increases, the signal goes deeper into the crop canopy, and the saturation effect is less comparatively. Thus, the X band with around 3 cm wavelength will see the upper part of dense crops, whereas L band with 15–30 cm wavelength could provide information on the soil or bottom portion of the crop. C band was found to be suitable for crops with low biomass, whereas L band performs better for high biomass crops (McNairn et al. 2009). The interaction of X, C, and L bands with crop canopy varies with the type of crop, canopy architecture, canopy moisture, biomass, and soil background. Hence, a suitable microwave band needs to be selected based on the purpose and type of applications.

5.3.2 Polarization

An EM wave (satellite signal) consists of a coupled oscillating electric and magnetic field which are orthogonal to each other and also to the direction of travel (Fig. 5.3). Conventionally, polarization refers to the orientation of the electric field vector of the EM wave. When the electric field oscillates in a single direction, it is called linearly polarized. In the case of circular or elliptical polarization, the electric field rotates at a constant rate in a plane as it travels. Based on the rotational direction of the electrical field to the direction of travel, it is further classified as right or left circular polarization. In the field of RS, horizontal and/or vertical polarization terms are widely used. If the electric field vector of the EM wave is parallel to the object plane or the earth, it is called horizontal polarization. Likewise, in the case of vertical polarization, the electric field vector is perpendicular to the earth or object plane.

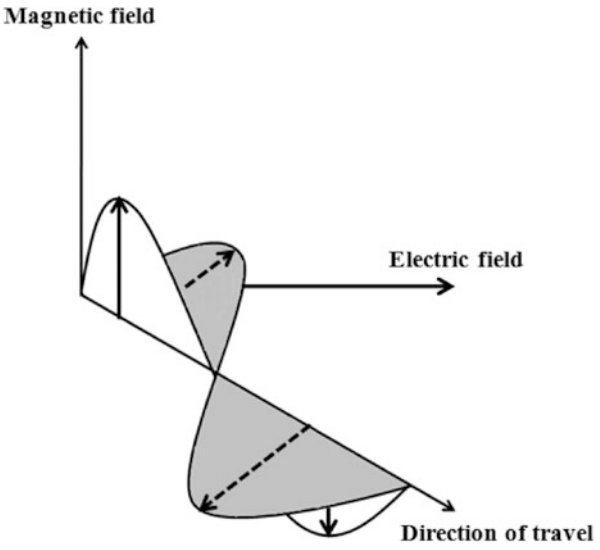

Fig. 5.3 Orientation of magnetic and electric field vector of an EM wave. The polarization of the wave is the same as the electric field, and in this case, it is horizontal

Most of the SAR sensors are designed to transmit microwave signals either in horizontally (H) or vertically polarized (V). Similarly, the antenna receives the signal either in horizontally or vertically polarized backscattered energy. Some radar can transmit H and V simultaneously and receive both simultaneously. These two polarization states of the microwave signal are conventionally designated by the letter "H" for horizontal and "V", for vertical. Thus, we can have four combinations of the polarizations: HH (horizontal transmit and receive), HV (horizontal transmit and vertical receive), VH (vertical transmit and horizontal receive), and VV (vertical transmit and receive). The first letter denotes the transmitted polarization and a second letter for received polarization. HH and VV are termed as co-polarizations or like polarizations. HV (or VH) is the depolarization component and found to be positively correlated with the vegetation volume. Dual polarization SAR systems can provide the images in two polarization combinations (HH + HV or VV + VH). Some SAR sensors are capable of acquiring the data in all linear polarization combinations (HH + HV + VV + VH) and termed as a quad-pol system. Polarimetric SAR systems are capable of acquiring the data in all four polarizations by conserving a coherent phase between transmitted and received polarizations. Different polarization components should be selected based on the type of crop, its growth stage, canopy architecture, spacing, and soil/water background. For example, HH polarization was found to have more penetration compared to VV polarization for small grain cereal crops like rice and wheat with vertically oriented canopy. The VV polarization gets attenuated with vertically oriented stems/leaves, whereas HH can go deeper into the canopy and provide better information thereof (McNairn and Brisco 2004). SAR sensors with single-polarization configuration (HH or VV) provide one-dimensional datasets and hence require multi-date coverage for meaningful information on crop type. In contrast, multi-polarization single date data can provide much better information on the crop-type due to the increased dimensionality (McNairn and Brisco 2004). Some SAR sensors can also transmit circular polarization and receive circular polarization (LL, left circular transmit and left circular receive; RR, right circular transmit and right circular receive), whereas some can transmit in circular polarization and receive in linear (RH, right circular transmit and horizontal receive; RV, right circular transmit and vertical receive) (Misra et al. 2013). Circular polarization is mostly required for geological and interplanetary applications. However, recent research shows its potential to assess land resources.

5.3.3 Incidence Angle

The incident angle (θ) refers to the angle between the incident radar beam and the direction perpendicular to the ground surface (Fig. 5.4). It is further modified as a local incident angle (θi) considering the surface normal to the local slope. Incidence angle at which the SAR image is acquired also influences the interaction of the radar energy. In crops, low (or steep) incidence angles can penetrate the crop canopy. The

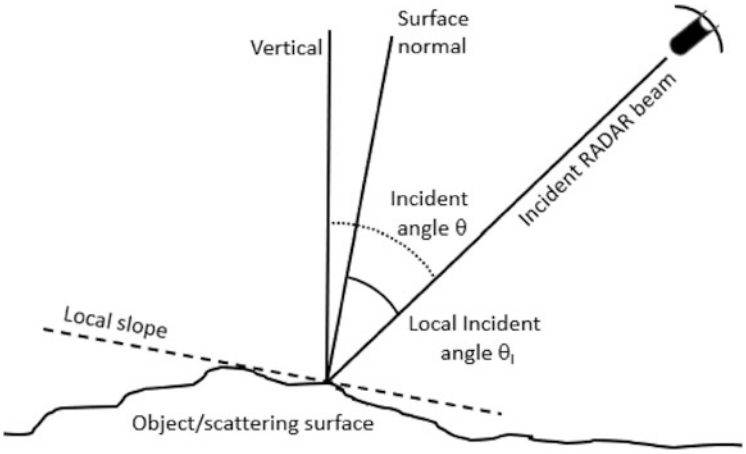

Fig. 5.4 Reference geometry showing incident and local incident angle

radar waves travel more vertically at steeper incidence angles, so the scattering of RADAR wave at these incidence angles is less influenced crop canopy and can provide information about the soil properties. The radar waves travel longer paths and interact more through the vegetation canopy at wide (or high) incident angles (Valcarce-Diñeiro et al. 2018). Hence, the wide incidence angle has less penetration into the crop canopy, especially for crops with large biomass. This resulted in the saturation of the radar backscatter of a wide incident angle at a lower leaf area index (LAI) (Jiao et al. 2011). The horizontally polarized microwaves can penetrate the canopy to a greater extent as compared to vertically polarized waves at steep angles, and hence, the more information about the underlying soil can be obtained from HH polarization (McNairn and Brisco 2004). However, it was reported by some researchers (Lopez-Sanchez et al. 2011; Ramana et al. 2017) that RADAR return from crop canopy does not vary significantly with change in incidence angle during the early vegetative (low biomass and LAI) and late vegetative stages (high biomass and LAI).

5.3.4 Target Parameters

Scattering of microwave radiation from a natural land surface depends on the geometrical properties of the surface element (soil surface roughness height and correlation length, vegetation canopy shape, dimensions, the orientation of stems, leaves, ears, etc.) and its electrical properties or dielectric constant mainly govern by the moisture content (Weeks et al. 1996; Della Vecchia et al. 2006). The variations of the backscattering coefficient from different (roughness) surfaces with the change in the incident angle are presented in Fig. 5.5. The relatively smooth or slightly rough surface cause near specular scattering (directional). Hence, the backscattering

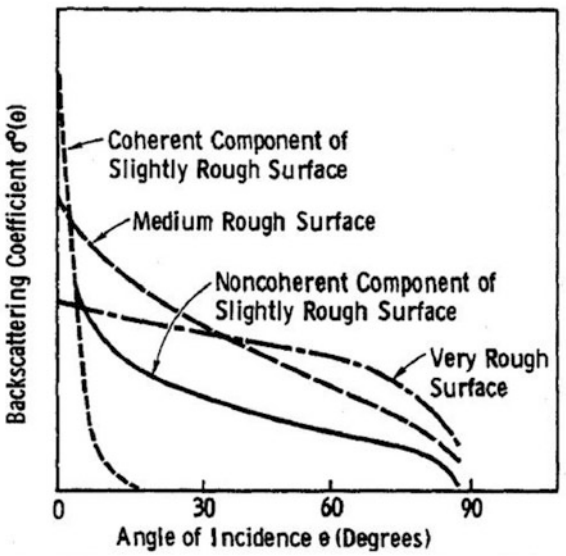

Fig. 5.5 Backscatter variations with surface roughness and incidence angle. (Adopted, Ulaby et al. 1982)

coefficient is found to be high at a steep incidence angle due to specular (directional) scattering towards the antenna. As the incidence angle increases, the scattered signal bounces away from the antenna, and the backscattering coefficient sharply declines. In contrast, rough surfaces cause diffused scattering (random directions). The backscattering coefficient at steep incidence angles is found to be low for a rough surface in comparison to a smoother one. But a decrease in the backscattering coefficient with the increase in the incident angle is found to be less in rough surface than that of a smoother one. It is apt to note here that the backscattering ratio of high and low incident angles can act as a good proxy for surface roughness. The crop canopy above the ground further competes with the interactions. In simple terms, the crop canopy adds to the surface roughness by increasing the number of scattering elements in terms of stems, leaves, branches, etc. and enhances the volume scattering. Initially, the backscatter is found to be low when the crop is at the germination or early vegetative stage. It is observed to be increased gradually with the increase in crop biomass.

The backscatter also influenced by the dielectric properties of the target object. In RADAR RS, the dielectric property is mainly governed by the soil and vegetation water content. Free water causes specular scattering, hence producing a low return for a side-looking antenna. Bound water (as in the case of soil moisture and plant water content) causes more RADAR return. Hence, dry soil looks darker in the SAR image, and moist soil will produce a brighter appearance. Above-ground crop canopy also adds to the equivalent water thickness of the object plane and causes more backscattering.

5.4 Crop Type Identification and Mapping

Geospatial map of a crop showing its spatial distribution is one of the basic and essential requirements for many applications such as drought, in-season crop condition, crop parameter retrieval, crop damage due to flood-pest-disease, and preharvest production estimate (Chang-an et al. 2019). RS technology has been used extensively, for decades, in inventorying and mapping of some of the major food grain crops of the world. Rice is one of the main staple food crops particularly in South East Asia (He et al. 2018, ricepedia.org and worldatlas.com; Nelson et al. 2014). Monitoring the rice and its seasonal fluctuations is a critical task because more than half of the world's population consumes rice daily. Timely and reliable information on the area under the rice crop and its preharvest production are of immense use in many of these countries (Setiyono et al. 2017). Monsoon season is the main rice-growing season in South East Asia, though rice is also grown in the dry season with assured irrigation conditions. Due to some agronomic advantages, rice saplings are transplanted in the puddled field under flooded conditions. It is further grown under standing water throughout the season except during maturity. This unique practice of rice cultivation provides the basis for monitoring rice crops using SAR data during the monsoon period. There is substantial literature on the use of SAR data for rice crop mapping with well-established procedures over different regions of the world (Le Toan et al. 1997; Kurosu et al. 1997; Chakraborty and Panigrahy 2000; Choudhury and Chakraborty 2006; Bouvet et al. 2009; Parihar et al. 2012; Nelson et al. 2014; Setiyono et al. 2017; Nguyen and Wagner 2017; Minh et al. 2019; Hassan et al. 2019). The SAR backscattering coefficient (also termed as sigma nought) is found to be very low due to specular reflection by the standing water in the rice fields during the puddling (a tillage practice) or transplantation stage of the crop. The backscatter gradually increases with an increase in the number of tillers and stems and attains its peak during the maximum vegetative growth stage of the crop. It remains in plateau during the reproductive phase of the crop as there is no further increase in above-ground biomass, and the crop goes through flowering, grain formation, grain filling, grain hardening stages, etc. The backscatter marginally decreases as the crop starts senescing and reaches its harvesting stage. The typical temporal backscattering coefficients of HH polarized C-band SAR data over rice crop are presented in Figs. 5.6 and 5.7. This sudden dip of backscatter return due to puddling and transplanting of the rice crop is unique, unlike other crops. Hence, it forms the basis for the identification of a pixel as rice or non-rice based on the continuous monitoring of the pixel using a multi-temporal backscatter signature. The approach not only classifies the rice crop but also could provide the probable date of transplantation.

The rice cropped area thus generated can further be used for different value additions. One of such examples is to assess flood-affected rice area due to cyclonic heavy rainfall. Microwave scattering at the transplanting stage is dominated by specular reflection which results in low returned HH and very low HV signal (Le Toan et al. 1997). Rice backscatter at the heading stage is much higher than

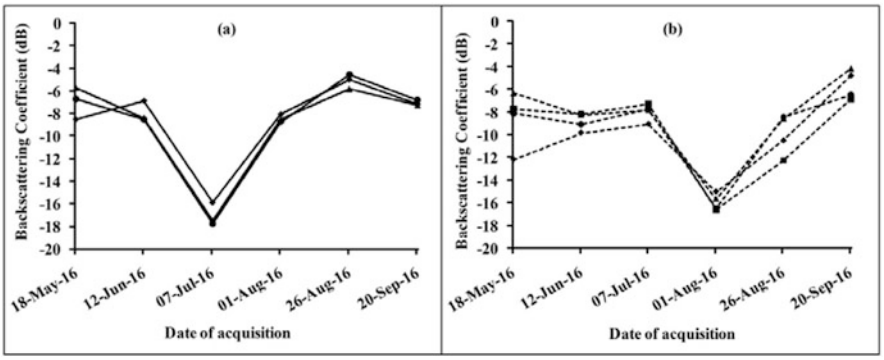

Fig. 5.6 Temporal backscatter profile of rice crop in HH-polarization C-band RISAT-1 SAR data: Dip in the backscatter represents the transplantation stage of the crop ((**a**) July transplanted rice crop, (**b**) August transplanted rice crop)

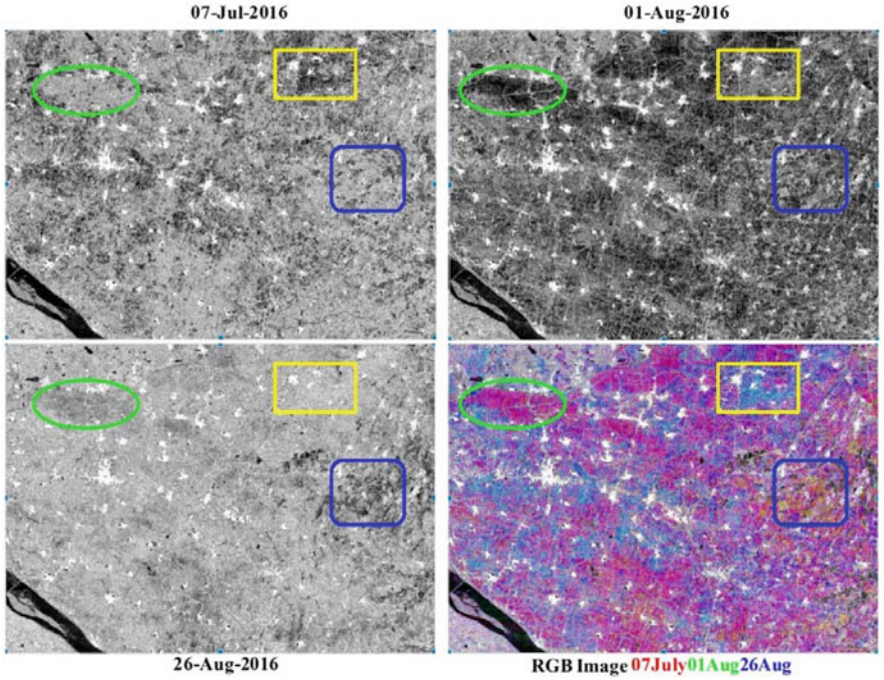

Fig. 5.7 Manifestation of rice crop in HH-polarization RISAT-1 SAR images at different time frame: Yellow rectangular box indicates rice crop transplanted in the first week of July, green oval indicates rice crop transplanted in the first week of August, and blue square box indicates the rice crop transplanted in the last week of August; the bottom right image is the RGB combination of 07 Jul, 01 Aug and 26 Aug images

that at the transplantation stage due to double-bounce scattering between rice and ground surface and volume scattering from leaves and stems (Zhang et al. 2011). Different classification approaches such as decision rule-based classification, supervised classification, and machine learning techniques (random forest, support vector machine) are used by many researchers for rice crop area mapping based on temporal backscatter signatures of SAR data (Chakraborty et al. 1997; Nelson et al. 2014; Onojeghuo et al. 2018; Hassan et al. 2019; Minh et al. 2019; Phung et al. 2020). The separability of the rice crop and other land covers can be enhanced using amplitude ratio and arithmetic product of HH and HV dual-polarized SAR images (Zhang et al. 2011). Further, Mansaray et al. (2017) reported higher overall classification accuracies by combining the multi-date backscatter coefficients generated from Sentinel-1A SAR data and optical indices derived from the LANDSAT data. This study also concluded that temporal backscatter from VH polarization is the optimal one for rice crop mapping due to its consistent increase with the growth of the crop.

MRS has been successfully used for mapping of flooded rice crop in many countries. Apart from rice crops, limited success has also been made for other crops like wheat, corn, and soybeans. Wheat crop leaf orientation is erectophyle in nature meaning its canopy elements are near-vertically oriented. As a result, HH polarized backscatter is found to be more than VV polarized (Mattia et al. 2003; Brown et al. 2003). This differential response of HH and VV polarized backscatter is further enhanced with the increase in incidence angle from 20° to 40° (Brown et al. 2003). Hence, a simple rule-based approach using the HH/VV backscatter ratio is found to be useful for discriminating the wheat from non-wheat classes (Satalino et al. 2009). The classification accuracy of the wheat crop can further be improved by combining SAR coherence and texture information along with the linear dual (VV and VH) polarizations (Zhou et al. 2017). Hence, multi-temporal C-band SAR images with different polarization combinations can reliably map winter wheat operationally (Skakun et al. 2015). However, the best results for wheat crop classification can be obtained by combining optical and SAR data (Skakun et al. 2015; Zhou et al. 2017). In addition to the mapping of the wheat crop, its key phenological parameters, namely, germination, heading, and soft dough stage, also can be mapped with reasonable accuracies using the time series VV, VH dual-polarization SAR data (Nasrallah et al. 2019). Similarly, SAR data can also be used for crops with spreading types of canopies (planophyle) such as corn or maize. The C-band SAR backscatter is found to increase sharply in the initial growth stages of maize crop as it grows very fast in terms of crop height, leaf area, and attains canopy closure. Further, the rate of increase of backscatter slows down as there is no addition of canopy elements rather an accumulation of biomass of existing canopy structures (Wiseman et al. 2014). This typical behaviour of SAR backscatter can be used to classify maize (corn) crops with an accuracy of more than 90% (Skakun et al. 2015).

5.4.1 *Mapping of Rice Cropped Area and Delineating the Date of Transplantation from the Temporal Sentinel-1A SAR Data: A Case Study*

5.4.1.1 Study Area

The study was conducted in parts of Bhadrak district (20.99° N, 86.60°E), in the Odisha state of India.

5.4.1.2 Data Used

Multi-date Sentinel-1A VV-polarization data was used to delineate the date of transplantation and mapping of rice cropped area. It is available at 10 m pixel spacing with 12-day temporal resolution. A total 18 number of scenes (available from 7 June to 23 September 2017) were used in the present study.

5.4.1.3 Method of Approach

The schematic diagram of the methodology followed to delineate the rice cropped area is presented in Fig. 5.8. The Sentinel-1A data was first radiometrically corrected, and speckle was suppressed using a suitable filter. The digital number (DN) values were converted into a backscattering coefficient and corrected for local terrain undulation using the digital elevation model. This terrain corrected backscatter images were layer stacked, and the statistics of backscattering coefficient over the rice training sites (using field data) were extracted. Temporal backscatter profiles of the selected training sites of rice crops are plotted and presented in Fig. 5.9. The decision rules were formulated based on the temporal backscatter response to classify rice crops. These rule sets were also used to delineate the rice cropped pixels. Further, the date of transplantation of rice crop has been retrieved and mapped.

5.4.1.4 Salient Findings

The temporal backscatter profiles as presented in Fig. 5.9 showed the typical dip (−21 to −16 dB) of the backscattering coefficient over the rice area of Bhadrak district of Odisha during the puddling and transplanting activities as discussed earlier. But there were variations in the intensity and position of the dips. Based on the position and extent of dip, various types of profiles were identified over the rice area in the study site. These different types of profiles represent different dates of rice transplantation and could provide insight into the spatial patterns of staggered sowing of rice crops. The total rice cropped area in the study site found to be

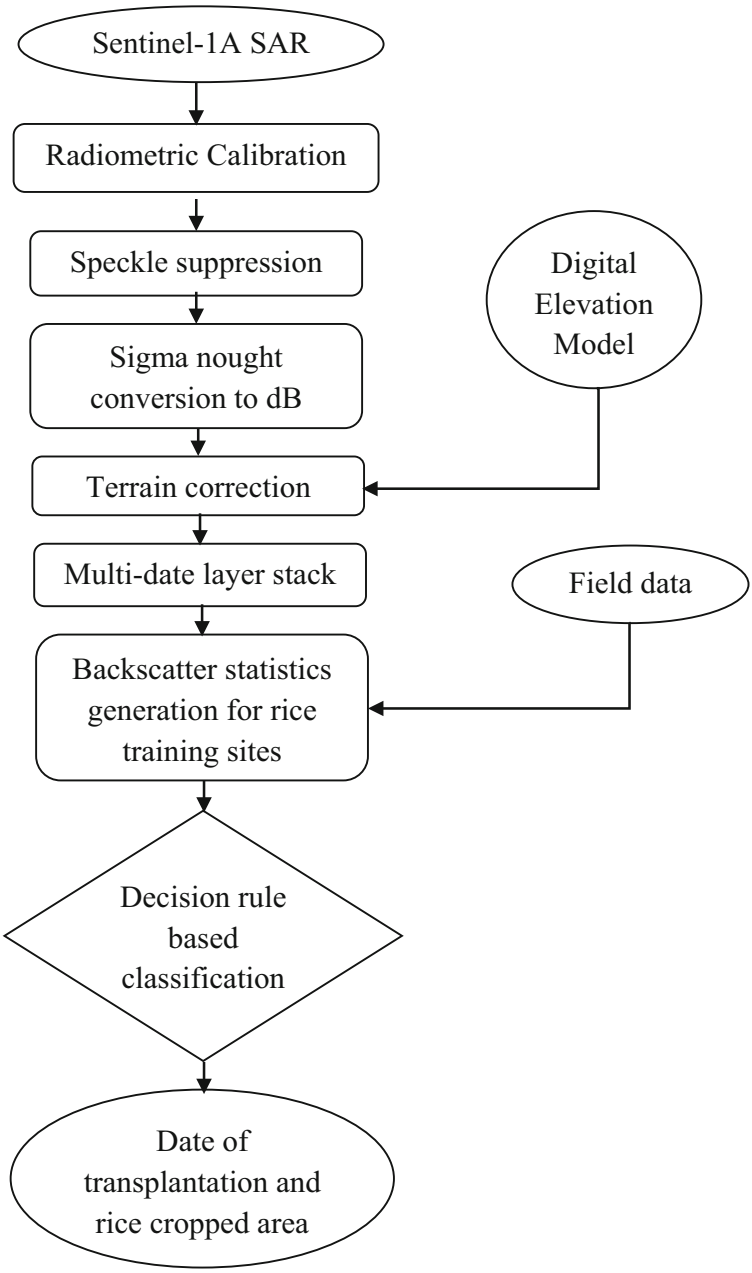

Fig. 5.8 Schematic diagram of the methodology followed to delineate rice crops using Sentinel-1A SAR data

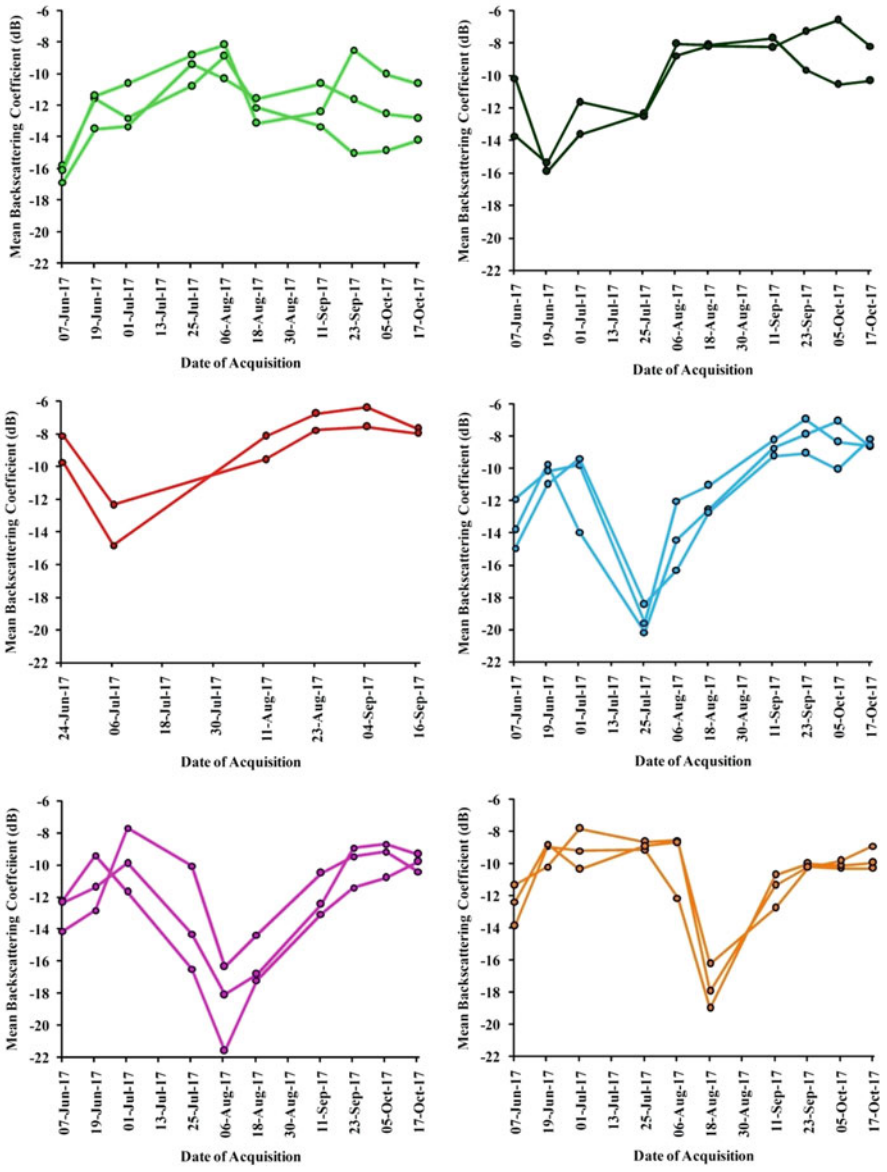

Fig. 5.9 Temporal backscatter profiles of rice crop in Bhadrak district

114 thousand ha during *kharif* (monsoon) in 2017. The RGB of the temporal SAR and the classified rice map are presented in Fig. 5.10a and 5.10b, respectively. There are at least six different transplantation dates that were identified from June to September of 2017 within the total rice area. The staggering in the sowing/transplantation of the rice crop was also mapped and spatially depicted in Fig. 5.11. The area under each transplantation date was assessed and presented in Fig. 5.11.

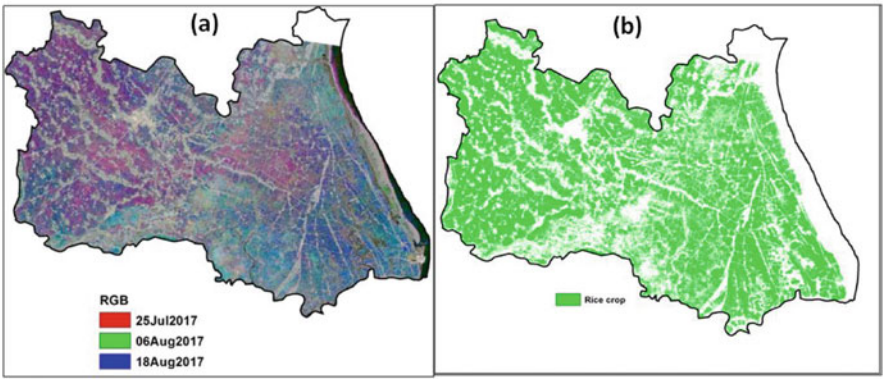

Fig. 5.10 (**a**) RGB of the Sentinel-1A SAR data, (**b**) classified map of rice crop

The results of the study show that the rice cropped area could be successfully mapped at 10 m spatial resolution using Sentinel-1A multi-date data. The date of transplantation of rice crop also could be mapped with 12 days interval at 10 m pixel resolution. The derived information is one of the important inputs to the crop simulation models for the rice crop yield estimation.

5.4.2 Assessment of Flood-Affected Rice Cropped Area by Integrating Synthetic Aperture Radar and Optical Data: A Case Study

5.4.2.1 Study Area

A cyclone referred to as "*Titli*" caused havoc rainfall and damage on the east coast of India during the second week of October 2018. This study aims to assess the affected rice cropped area in the Srikakulam district (18.53° N; 83.98°E) of Andhra Pradesh state of India.

5.4.2.2 Data Used

Multi-temporal Sentinel-1 SAR and maximum composites of normalized difference vegetation index (NDVI) of Sentinel-2 multispectral data corresponding to pre- and post-cyclone were used in the study.

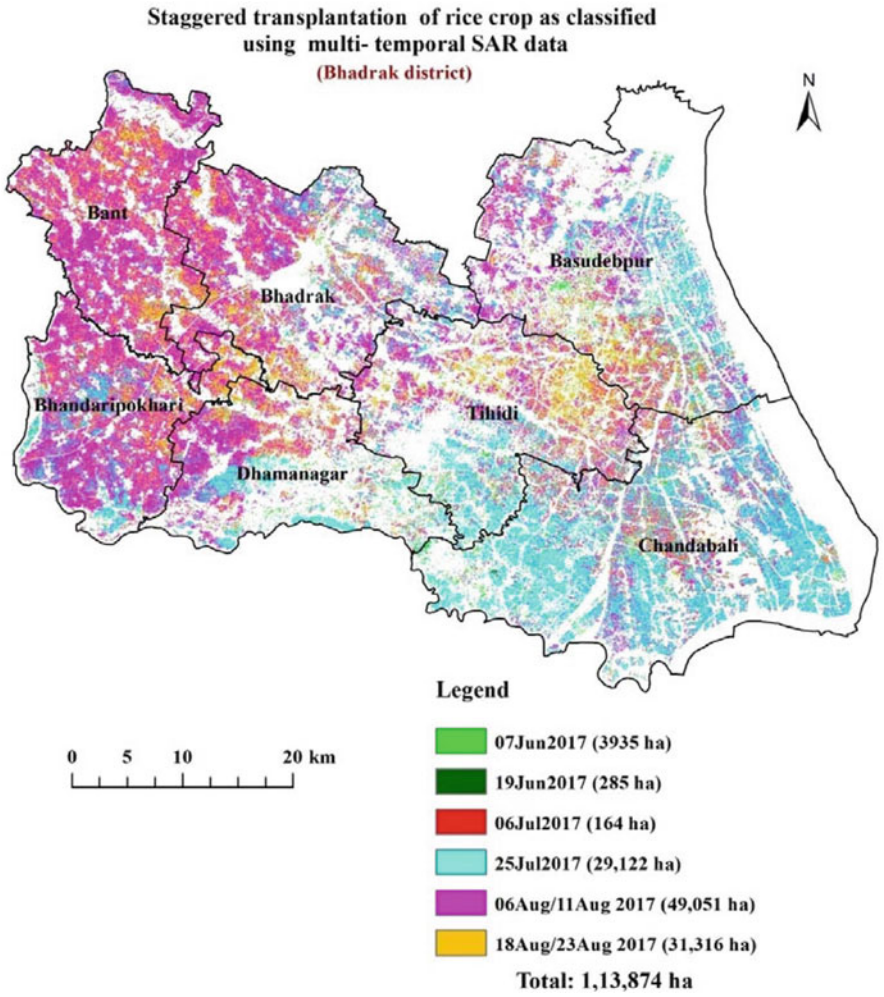

Fig. 5.11 Dates of transplantation of rice crop as mapped from the temporal Sentinel-1 data

5.4.2.3 Method of Approach

The in-season rice cropped areas were derived from the temporal SAR data following the methodology presented in Fig. 5.8. A decision rule-based classification approach of the temporal backscatter was employed to delineate the rice cropped area. Flood inundation map generated by the Disaster Management Support Group of National Remote Sensing Centre was also used in this study. This flood layer was generated using multiple near real-time and pre- and post-event optical and SAR satellite data. It mainly accounts for the flood inundation under fully submerged conditions. But from satellite images, it was observed that there were some areas

adjacent to the flood layer which were partially submerged. To account for this, a 500 m buffer around the flood layer was generated and used in this study. Pre-event (1 September to 13 October 2018) and post-event (13 October to 31 October 2018), maximum value composite of NDVI ($NDVI_{max}$) images of the rice cropped area were derived from Sentinel 2 data. Flood inundation layer and buffer layer were intersected with the rice crop layer to extract the rice crop area under inundation. Further, NDVI deviation classes were computed and classified the total rice crop area under inundation into different severity classes based on the reduction in the NDVI from pre- to post-event.

5.4.2.4 Salient Findings

$NDVI_{max}$ corresponding to the pre- and post-cyclonic event are presented in Fig. 5.12. The result shows that there is a significant reduction in the NDVI in post-cyclonic event. To find out the rice cropped area affected due to *Titli* cyclone, the flood layer has been intersected with the rice cropped area. The rice cropped area under the flood layer was found to be 18,610 ha. The deviation of the NDVI of rice crop from pre-cyclone to post-cyclone was computed and classified into four classes (very severe, severe, moderate, and slight) based on the percent reduction in the NDVI. In addition to the flood layer, some rice areas surrounding the flood layer got

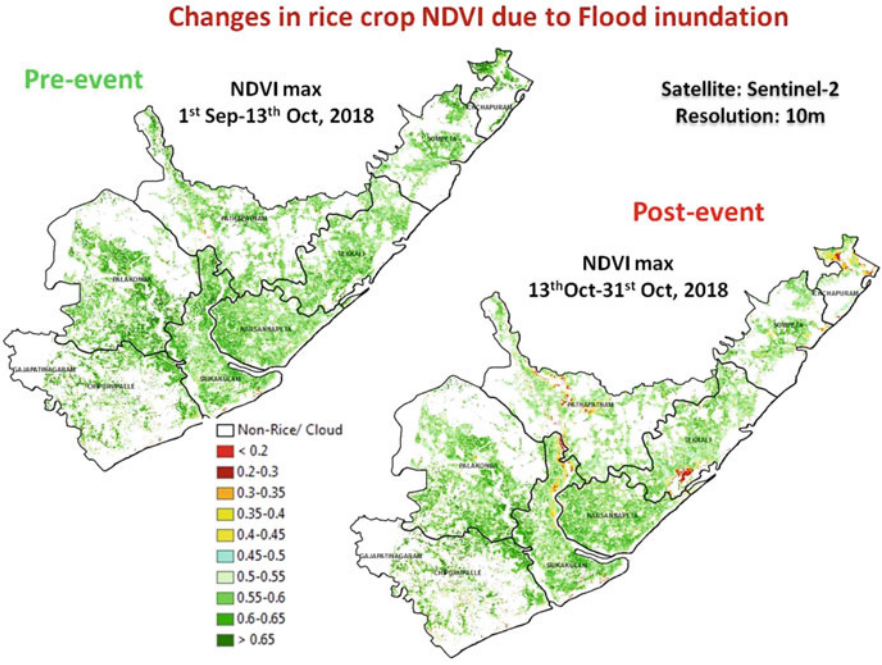

Fig. 5.12 NDVI maximum composite images corresponding to pre- and post-*Titli* cyclone

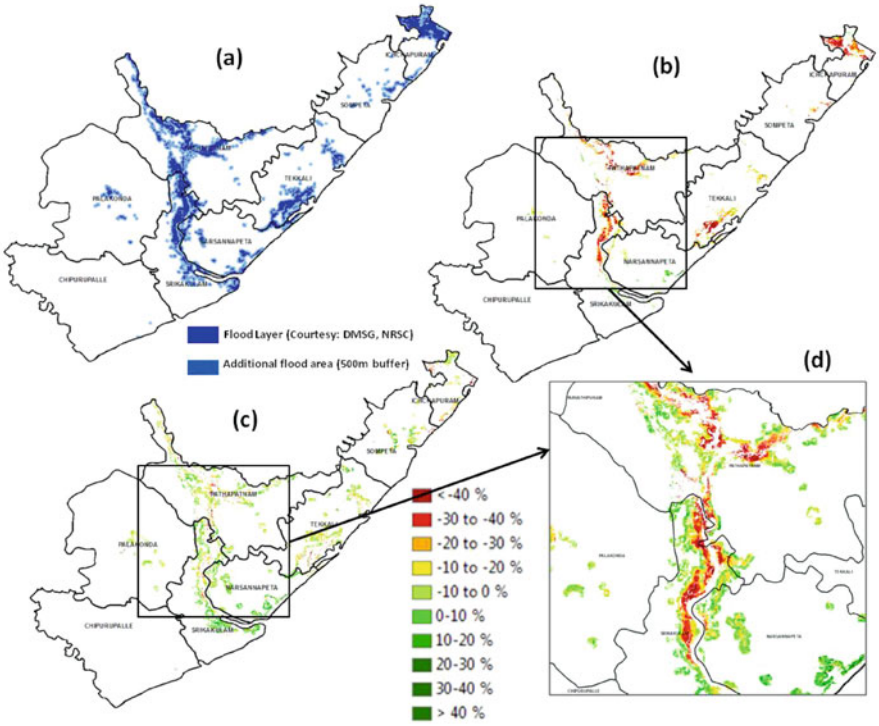

Fig. 5.13 (**a**) Flood inundation layer and additional flood area under 500 m buffer. (**b**) Affected rice cropped area under flood layer. (**c**) Additional affected rice cropped area surrounding the flood layer under 500 m buffer. (**d**) Zoomed view of the NDVI reduction classes of rice crop in and around flood inundated area

affected by the cyclone which showed a higher reduction in NDVI values. To account for the affected rice cropped area surrounding the flooded layer, a 500 m buffer area around the flood area was generated, and the total rice cropped area affected due to cyclone in and around the flooded regions was computed (Fig. 5.13). The severity class wise statistics are provided in Table 5.2. The results of the study show that the flood-affected rice cropped area could be successfully mapped by the synergistic use of SAR and optical data. The derived information is one of the important inputs to the farmers and government to settle the insurance claim.

5.5 Retrieval of Crop Parameters Using Microwave Data

Crop biophysical parameters such as LAI, crop height, and biomass are descriptors of plant growth and can serve as vital inputs to yield forecasting models (Betbeder et al. 2016). LAI is defined as a one-sided leaf area per unit ground area. LAI is an

Table 5.2 Affected rice cropped area due to flood inundation during Titli cyclone

Class	Affected area under flood layer (ha)	Additional affected area around the flood layer (ha)	Total affected area (ha)
$< -40\%$ (very severe)	4089	955	5044
-30 to -40% (severe)	3520	1070	4590
-20 to -30% (moderate)	3492	2244	5736
-10 to -20% (slight)	3437	5429	8866
Total	14,538	9698	24,236

important crop biophysical parameter as it determines the fractional absorbed photosynthetically active radiation (fAPAR) and the intern controls the photosynthetic processes (Jonckheere et al. 2004). Similarly, crop biomass is related to carbon accumulated over the crop growing season. Crop biophysical parameters are primarily monitored through two approaches: field measurements by surveyors and retrievals through appropriate models using remotely sensed data. The field measurements are time-consuming, expensive, and difficult to upscale. Hence, it is not suitable for regional-, national-, and global-level applications (Weiss et al. 2004; Boote et al. 1996). RS-based approach offers several advantages for estimating the crop growth parameters at regional, national, and global scales. Several studies have demonstrated the estimation of crop biophysical parameters using the multispectral and hyperspectral data in VNIR region of the EM spectrum (Broge and Leblanc 2001; Fang and Liang 2005; Pandya et al. 2006; Wang et al. 2007; Wang et al. 2011; Richter et al. 2010; Dong et al. 2012; Thorp et al. 2012; Shelestov et al. 2017; Sun et al. 2018; Xie et al. 2018). However, such measurements are sometimes affected by the cloudy weather conditions, thus leading to the uncertainty in the parameter estimation. In this context, SAR data has great potential for assessing these parameters due to its all-weather observation capability.

Many scattering models have been developed, including empirical, semi-empirical, and physical models to relate SAR backscatter to crop parameters (Clevers and van Leeuwen 1996; Ferrazzoli et al. 1999; McNairn et al. 2002; Chakraborty et al. 2005; Dabrowska-Zielinska et al. 2007; Chen et al. 2007; Inoue et al. 2014; Zhang et al. 2014). Among these, the empirical models are the simplest ones to estimate the crop parameters; however, these empirical models are site-specific (Graham and Harris 2003; Shelestov et al. 2017). The physical model generally describes the interaction between radar signals vs. targets and mainly consists of complicated equations. However, the practical implementation of such models is limited as these models require a lot of input parameters resulting in uncertainty (Dong et al. 2012; Inoue et al. 2014). Considering the physical background and the simplicity, semi-empirical models can be a good compromise between the empirical and physical models.

5.5.1 Crop LAI Estimation Using Microwave Data

LAI is an excellent indicator of crop health and development and hence used as an input parameter for several crop growth and yield forecasting models (Kross et al. 2015; Pandya et al. 2006). The spatiotemporal information of LAI is often used in agricultural monitoring, ecological modelling, climate change studies and global circulation models to compute energy and water fluxes (Chase et al. 1996). Many researchers studied the sensitivity of SAR backscatter to crop LAI using empirical and semi-empirical methods. Empirical methods use statistical regression between the SAR backscatter and LAI. Satalino et al. (2006) reported that the co-polarization ratio of HH and VV at an incidence angle of 40° correlated well with LAI of wheat crop. Lin et al. (2009) reported that the cross-polarization ratio of HV and HH is having the highest correlation with the LAI of sugarcane crops. Significant correlations were observed for C-band linear (HH/HV/VV/VH) and circular (LL/RR) backscatter coefficients at 25° incidence angle for both corn and soybeans, while the correlations were lower at 39° incident angle as penetration of the wide angles into the crop canopy is limited for large-biomass crops (Jiao et al. 2011). As discussed at the beginning of this section, empirical models are site-specific and have limited scope for expanding it to a larger area. Recently, the water cloud model (WCM) has been the most popular and widely used semi-empirical model for estimating the LAI using SAR data. The crop parameter retrieval using WCM is carried out in two steps: the first step is the calibration of the model, and the second one is the inversion of the parameters. The WCM was initially proposed by Attema and Ulaby (1978), and the vegetation cover/layer was assumed as a homogeneous anisotropic scatterer to ignore the multiple scattering effects between vegetation and soil (Ulaby et al. 1984). Later, many researchers have modified this model to make it more simplified. Kweon and Oh (2014) modified the WCM by incorporating leaf angle distribution of canopy to accurately estimate the backscattering coefficients. Various scattering layers of the crop at different phenological stages were incorporated by Yang et al. (2016) to estimate the rice biophysical parameters using modified WCM. Tao et al. (2016) introduced the modified version of WCM by incorporating the vegetation fraction and integral equation model to retrieve the LAI based on C-band SAR and optical data. C-band polarimetric SAR data has been used by Beriaux et al. (2015) for retrieving LAI in maize fields using WCM and Bayesian fusion technique. It is observed that cross-polarization is sensitive for high LAI values and VV polarization is suitable for LAI <2. Hosseini et al. (2015) retrieved LAI of corn and soybean crops with reasonable accuracy using C- and L-band SAR data. A new LAI estimation approach was developed by them through the coupling of WCM and soil moisture model by Ulaby et al. (1978) (soil moisture model for bare soil). Yang et al. (2016) proposed a modified WCM (MWCM) to estimate the rice crop LAI and dry/wet biomass.

5.5.2 *Crop Biomass Estimation Using Microwave Data*

Crop biomass represents the carbon accumulation by the crop over some time and has a direct relationship with agricultural crop yield/production. Previous research showed that the SAR backscattering coefficient is sensitive to crop biomass and hence affected by the shape geometry and dimensions of plant constituents such as leaves, branches, and stems (Ulaby et al. 1984; Baronti et al. 1995; Ferrazzoli et al. 1997). Therefore, crops with the same biomass may have different values of the backscattering coefficient. L band is the suitable wavelength (frequency) band for studying the contribution from crops characterized by relatively broad leaves, while the use of C band is suitable for investigating narrow-leaf crops (Macelloni et al. 2001). Chen et al. (2007) found a significant empirical relationship between the backscattering coefficients of ENVISAT ASAR alternating polarization HH/HV data and the rice biomass. Mattia et al. (2003) reported that at a wide incidence angle (40°) C-band like-polarization ratio (HH/VV) was closely correlated to wheat biomass, whereas, at steep angles (23°), the ratio was positively related to wheat biomass up to the heading stage and dropped by 2 dB thereafter. Wiseman et al. (2014) demonstrated that dry biomass of corn, canola, and soybeans has significant correlations with Radarsat-2 C-band SAR backscatter and polarimetric parameters. Dry biomass of corn and canola was found to have strong correlations with SAR entropy. In the case of soybeans crop, the HV was found to be most sensitive to biomass. Gao et al. (2013) used both optical and radar data (Huan Jing-1 and RA DARSAT-2, respectively) for estimating structural parameters of maize, including LAI, height, and biomass. Hosseini et al. (2019) successfully used optical and SAR data to model corn biomass (both wet and dry) with reasonable accuracy in agricultural lands in Canada. Recently, Reisi-Gahrouei et al. (2019) developed multiple linear regression and artificial neural network-based models to estimate the biomass of different crops using time series of L-band polarimetric data from Uninhabited Aerial Vehicle Synthetic Aperture Radar (UAVSAR). The results indicated that an artificial neural network provides more accurate biomass estimates compared to multiple linear regressions. Mandal et al. (2019) have used the multi-target random forest regression method to estimate plant area index and wet biomass of wheat crop.

5.6 Conclusions

SAR datasets have been widely used to map some of the word's important crops such as rice, wheat, and corn. Each crop, because of its package of practices and canopy architecture, is sensitive to different radar frequencies (X or C or L), polarization, and incidence angle. C-band SAR data was found to be suitable for the low biomass crops, whereas longer wavelengths (L band) were found to be suitable for assessing the large biomass crops. Multi-temporal, multi-frequency, and multi-polarized SAR datasets were found to provide more information on crops

compared to single-dimensional data. However, single-date polarimetric data acquired in suitable bio-window of the crop may give comparable crop classification accuracies as that of optical data. SAR and optical data complement each other, and the synergistic use of both data will result in better crop classification. SAR data was also found to be suitable for assessing the crop biophysical parameters such as LAI and biomass. Several researchers have established a site-specific empirical relationship between the SAR backscatter and crop biophysical parameters. Semi-empirical models based on physical and experimental data were found to be easier to optimize and hence were widely used by many researchers. WCM is one of the most widely used semi-empirical models, because of its simplicity in parameterization and inversion. LAI and biomass were estimated by many researchers using various modified versions of this model with relatively low uncertainty. Recent studies used machine learning approaches for the parameterization of these models. SAR data could provide assured and reasonably accurate estimation of crop parameters as it is less affected by adverse weather conditions; hence, it can be used in crop simulation models for better yield forecasts in the future. SAR data is an essential requirement during the natural disasters like cyclones, floods, and typhoons to map the inundation extent as well as to assess the impact of such events on the crops that are affected during this period.

References

Attema EP, Ulaby FT (1978) Vegetation modeled as a water cloud. Radio Sci 13(2):357–364

Baronti S, Del Frate F, Ferrazzoli P, Paloscia S, Pampaloni P, Schiavon G (1995) SAR polarimetric features of agricultural areas. Int J Remote Sens 16(14):2639–2656

Beriaux E, Waldner F, Collienne F, Bogaert P, Defourny P (2015) Maize leaf area index retrieval from synthetic quad pol SAR time series using the water cloud model. Remote Sens 7 (12):16204–16225

Betbeder J, Fieuzal R, Baup F (2016) Assimilation of LAI and dry biomass data from optical and SAR images into an agro-meteorological model to estimate soybean yield. IEEE J Sel Top Appl Earth Obs Remote Sens 9(6):2540–2553

Boote K, Jones J, Pickering N (1996) Potential uses and limitations of crop models. Agron J 88:704–716

Bouvet A, Le Toan T, Lam-Dao N (2009) Monitoring of the rice cropping system in the Mekong delta using ENVISAT /ASAR dual polarization data. IEEE Trans Geosci Remote Sens 47:517–526

Broge NH, Leblanc E (2001) Comparing prediction power and stability of broadband and hyperspectral vegetation indices for estimation of green leaf area index and canopy chlorophyll density. Remote Sens Environ 76(2):156–172

Brown SC, Quegan S, Morrison K, Bennett JC, Cookmartin G (2003) High-resolution measurements of scattering in wheat canopies-implications for crop parameter retrieval. IEEE Trans Geosci Remote Sens 41(7):1602–1610

Chakraborty M, Manjunath K, Panigrahy S, Kundu N, Parihar J (2005) Rice crop parameter retrieval using multi-temporal, multi-incidence angle Radarsat SAR data. ISPRS J Photogramm Remote Sens 59:310–322

Chakraborty M, Panigrahy S (2000) A processing and software system for rice crop inventory using multi-date RADARSAT ScanSAR data. ISPRS J Photogramm Remote Sens 55(2):119–128

Chakraborty M, Panigrahy S, Sharma SA (1997) Discrimination of rice crop grown under different cultural practices using temporal ERS-1 SAR data. ISPRS J Photogramm Remote Sens 52:183–191

Chang-an L, Zhong-xin C, Yun S, Jin-song C, Hasi T, Hai-zhu P (2019) Research advances of SAR remote sensing for agriculture applications: a review. J Integr Agric 18(3):506–525

Chase TN, Pielke RA, Kittel TG, Nemani R, Running SW (1996) Sensitivity of a general circulation model to global changes in leaf area index. J Geophys Res 101(D3):7393–7408

Chen J, Lin H, Pei Z (2007) Application of ENVISAT ASAR data in mapping rice crop growth in Southern China. IEEE Geosci Remote Sens Lett 4(3):431–435

Choudhury I, Chakraborty M (2006) SAR signature investigation of rice crop using RADARSAT data. Int J Remote Sens 27(3):519–534

Clevers JGPW, van Leeuwen HJC (1996) Combined use of optical and microwave remote sensing data for crop growth monitoring. Remote Sens Environ 56(1):42–51

Dabrowska-Zielinska K, Inoue Y, Kowalik W, Gruszczynska M (2007) Inferring the effect of plant and soil variables on C- and L-band SAR backscatter over agricultural fields, based on model analysis. Adv Space Res 39(1):139–148

Della Vecchia A, Ferrazzoli P, Guerriero L, Blaes X, Defourny P, Dente L, Mattia F, Satalino G, Strozzi T, Wegmuller U (2006) Influence of geometrical factors on crop backscattering at C-band. IEEE Trans Geosci Remote Sens 44(4):778–790

Dong Y, Wang J, Li C, Yang G, Wang Q, Liu F, Zhao J, Wang H, Huang W (2012) Comparison and analysis of data assimilation algorithms for predicting the leaf area index of crop canopies. IEEE J Sel Top Appl Earth Obs Remote Sens 6(1):188–201

Fang H, Liang S (2005) A hybrid inversion method for mapping leaf area index from MODIS data: experiments and application to broadleaf and needle leaf canopies. Remote Sens Environ 94 (3):405–424

Ferrazzoli P, Guerriero L, Quesney A, Taconet O, Wigneron JP (1999) Investigating the capability of C-band radar to monitor wheat characteristics. In: IGARSS 1999: proceedings of the International Geoscience and Remote Sensing Symposium, pp 723–725

Ferrazzoli P, Paloscia S, Pampaloni P, Schiavon G, Sigismondi S, Solimini D (1997) The potential of multi frequency polarimetric SAR in assessing agricultural and arboreous biomass. IEEE Trans Geosci Remote Sens 35(1):5–17

Gao S, Niu Z, Huang N, Hou X (2013) Estimating the leaf area index, height and biomass of maize using HJ-1 and RADARSAT-2. Int J Appl Earth Obs Geoinf 24(1):1–8

Graham AJ, Harris R (2003) Extracting biophysical parameters from remotely sensed radar data: a review of the water cloud model. Prog Phys Geogr 27:217–229

Hassan B, Nicolas B, Mohammad EH, Mehrez Z, Dinh HTM, Emile N, Dominique C, Hatem B (2019) Mapping paddy rice using Sentinel-1 SAR time series in Camargue, France. Remote Sens 11:887

He Z, Li S, Wang Y, Dai L, Lin S (2018) Monitoring rice phenology based on backscattering characteristics of multi-temporal RADARSAT-2 datasets. Remote Sens 10(2):340

Hosseini M, McNairn H, Merzouki A, Pacheco A (2015) Estimation of Leaf Area Index (LAI) in corn and soybeans using multi-polarization C-and L-band radar data. Remote Sens Environ 170:77–89

Hosseini M, McNairn H, Mitchell S, Robertson LD, Davidson A, Homayouni S (2019) Synthetic aperture radar and optical satellite data for estimating the biomass of corn. Int J Appl Earth Obs Geoinf 83:101933

https://www.worldatlas.com/

Inoue Y, Sakaiya E, Wang C (2014) Capability of C-band backscattering coefficients from high-resolution satellite SAR sensors to assess biophysical variables in paddy rice. Remote Sens Environ 140:257–266

Jiao X, McNairn H, Shang J, Pattey E, Liu J, Champagne C (2011) The sensitivity of RADARSAT-2 polarimetric SAR data to corn and soybean leaf area index. Canadian J Remote Sens 37 (1):69–81

Jonckheere I, Fleck S, Nackaerts K, Muys B, Coppin P, Weiss M, Baret F (2004) Review of methods for in situ leaf area index determination: Part I. Theories, sensors and hemispherical photography. Agric Forest Meteorol 121(1–2):19–35

Kross A, McNairn H, Lapen D, Sunohara M, Champagne C (2015) Assessment of RapidEye vegetation indices for estimation of leaf area index and biomass in corn and soybean crops. Int J Appl Earth Obs Geoinf 34:235–248

Kurosu T, Fujita M, Chiba K (1997) The identification of rice fields using multi-temporal ERS-1 C band SAR data. Int J Remote Sens 18(14):2953–2965

Kweon SK, Oh Y (2014) A modified water-cloud model with leaf angle parameters for microwave backscattering from agricultural fields. IEEE Trans Geosci Remote Sens 53(5):2802–2809

Le Toan T, Ribbes F, Wang LF, Floury N, Ding KH, Kong JA, Fujita M, Kurosu T (1997) Rice crop mapping and monitoring using ERS-1 data based on experiment and modeling results. IEEE Trans Geosci Remote Sens 35(1):41–56

Lin H, Chen J, Pei Z, Zhang S, Hu X (2009) Monitoring sugarcane growth using ENVISAT ASAR data. IEEE Trans Geosci Remote Sens 47(8):2572–2580

Lopez-Sanchez JM, Cloude SR, Ballester-Berman JD (2011) Rice phenology monitoring by means of SAR polarimetry at X-band. IEEE Trans Geosci Remote Sens 50(7):2695–2709

Macelloni G, Paloscia S, Pampaloni P, Marliani F, Gai M (2001) The relationship between the backscattering coefficient and the biomass of narrow and broad leaf crops. IEEE Trans Geosci Remote Sens 39(4):873–884

Mandal D, Kumar V, Mcnairn H, Bhattacharya A, Rao YS (2019) Joint estimation of Plant Area Index (PAI) and wet biomass in wheat and soybean from C-band polarimetric SAR data. Int J Appl Earth Obs Geoinf 79:24–34

Mansaray LR, Zhang D, Zhou Z, Huang J (2017) Evaluating the potential of temporal Sentinel-1A data for paddy rice discrimination at local scales. Remote Sens Lett 8(10):967–976

Mattia F, Le Toan T, Picard G, Posa FI, D'Alessio A, Notarnicola C, Gatti AM, Rinaldi M, Satalino G, Pasquariello G (2003) Multitemporal C-band radar measurements on wheat fields. IEEE Trans Geosci Remote Sens 41(7):1551–1560

McNairn H, Brisco B (2004) The application of C-band polarimetric SAR for agriculture: a review. Canadian J Remote Sens 30(3):525–542

McNairn H, Ellis J, Van Der Sanden JJ, Hirose T, Brown RJ (2002) Providing crop information using RADARSAT-1 and satellite optical imagery. Int J Remote Sens 23(5):851–870

McNairn H, Shang J, Jiao X, Champagne C (2009) The contribution of ALOS PALSAR multipolarization and polarimetric data to crop classification. IEEE Trans Geosci Remote Sens 47(12):3981–3992

Meena RS, Lal R, Yadav GS (2020) Long term impacts of topsoil depthand amendments on soil physical and hydrological properties of anAlfisol in Central Ohio, USA. Geoderma 363:1141164

Minh HV, Avtar R, Mohan G, Misra P, Kurasaki M (2019) Monitoring and mapping of rice cropping pattern in flooding area in the Vietnamese Mekong Delta using Sentinel-1A data: a case of an Giang Province. ISPRS Int J Geoinf 8(5):211

Misra T, Rana SS, Desai NM, Dave DB, Rajeevjyoti ARK, Rao CV, Bakori BV, Neelakantan R, Vachchani JG (2013) Synthetic aperture radar payload on-board RISAT-1: configuration, technology and performance. Curr Sci 104(4):446–461

Mitran T, Lal R, Mishra U, Meena RS, Ravisankar T, Sreenivas K (2018) Climate change impact on soil carbon stocks in India. In: Lal R, Stewart BA (eds) Advances in soil science, Soil and climate, pp 291–308

Nasrallah A, Baghdadi N, El Hajj M, Darwish T, Belhouchette H, Faour G, Darwich S, Mhawej M (2019) Sentinel-1 data for winter wheat phenology monitoring and mapping. Remote Sens 11 (19):2228

Nelson A, Setiyono T, Rala AB, Quicho ED, Raviz JV, Abonete PJ, Maunahan AA, Garcia CA, Bhatti HZ, Villano LS, Thongbai P (2014) Towards an operational SAR-based rice monitoring

system in Asia: examples from 13 demonstration sites across Asia in the RIICE project. Remote Sens 6(11):10773–10812
Nguyen DB, Wagner W (2017) European rice cropland mapping with Sentinel-1 data: the Mediterranean region case study. Water 9(6):392
Onojeghuo AO, Blackburn GA, Wang Q, Atkinson PM, Kindred D, Miao Y (2018) Mapping paddy rice fields by applying machine learning algorithms to multi-temporal Sentinel-1A and Landsat data. Int J Remote Sens 39(4):1042–1067
Pandya MR, Singh RP, Chaudhari KN, Bairagi GD, Sharma R, Dadhwal VK, Parihar JS (2006) Leaf area index retrieval using IRS LISS-III sensor data and validation of the MODIS LAI product over Central India. IEEE Trans Geosci Remote Sens 44(7):1858–1865
Parihar J, Panigrahy S, Chakraborty M, Manjunath R, Sharma SA (2012) Rice crop assessment and monitoring using SAR data: Indian experience and its extendibility to Asian region, 33rd Asian Conference on Remote Sensing. 1:602–615
Phung HP, Nguyen LD, Thong NH, Thuy LT, Akan AA (2020) Monitoring rice growth status in the Mekong Delta, Vietnam using multitemporal Sentinel-1 data. J Appl Remote Sens 14 (1):014518
Ramana KV, Srikanth P, Sesha Sai MVR, Annapurna G, Das PK, Ramani AV, Aparna N, Diwakar PG, Dadhwal VK, Singh KRP (2017) Multi-incidence angle RISAT-1 Hybrid Polarimetric SAR data for large area mapping of maize crop – a case study in Khagaria district, Bihar, India. Int J Remote Sens 38(20):5487–5501
Reisi-Gahrouei O, Homayouni S, McNairn H, Hosseini M, Safari A (2019) Crop biomass estimation using multi regression analysis and neural networks from multitemporal L-band polarimetric synthetic aperture radar data. Int J Remote Sens 40(17):6822–6840
Ricepedia.org
Richter K, Atzberger C, Vuolo F, D'Urso G (2010) Evaluation of sentinel-2 spectral sampling for radiative transfer model based LAI estimation of wheat, sugar beet, and maize. IEEE J Sel Top Appl Earth Obs Remote Sens 4(2):458–464
Satalino G, Dente L, Mattia F (2006) Integration of MERIS and ASAR data for LAI estimation of wheat fields. In: 2006 IEEE international symposium on geoscience and remote sensing 2006 July 31, pp 2255–2258. IEEE
Satalino G, Mattia F, Le Toan T, Rinaldi M (2009) Wheat crop mapping by using ASAR AP data. IEEE Trans Geosci Remote Sens 47(2):527–530
Setiyono TD, Holecz F, Khan NI, Barbieri M, Quicho E, Collivignarelli F, Maunahan A, Gatti L, Romuga GC (2017) Synthetic Aperture Radar (SAR)-based paddy rice monitoring system: development and application in key rice producing areas in tropical Asia. In: IOP conference series: earth and environmental science 2017 Jan. Vol 54, No. 1, p 012015. IOP Publishing
Shelestov A, Kolotii A, Skakun S, Baruth B, Lozano RL, Yailymov B (2017) Biophysical parameters mapping within the SPOT-5 take 5 initiative. Eur J Remote Sens 50(1):300–309
Skakun S, Kussul N, Shelestov AY, Lavreniuk M, Kussul O (2015) Efficiency assessment of multitemporal C-band Radarsat-2 intensity and Landsat-8 surface reflectance satellite imagery for crop classification in Ukraine. IEEE J Sel Top Appl Earth Obs Remote Sens 9(8):3712–3719
Sun Y, Ren H, Zhang T, Zhang C, Qin Q (2018) Crop leaf area index retrieval based on inverted difference vegetation index and NDVI. IEEE Geosci Remote Sens Lett 15(11):1662–1666
Tao L, Li J, Jiang J, Chen X (2016) Leaf area index inversion of winter wheat using modified water-cloud model. IEEE Geosci Remote Sens Letters 13(6):816–820
Thorp KR, Wang G, West AL, Moran MS, Bronson KF, White JW, Mon J (2012) Estimating crop biophysical properties from remote sensing data by inverting linked radiative transfer and ecophysiological models. Remote Sens Environ 124:224–233
Ulaby FT, Allen CT, Eger G, Kanemasu E (1984) Relating the microwave backscattering coefficient to leaf area index. Remote Sens Environ 14:113–133
Ulaby FT, Batlivala PP, Dobson MC (1978) Microwave backscatter dependence on surface roughness, soil moisture and soil texture. Part I-Bare soil. IEEE Trans Geosci Remote Sens 17:33–40

Ulaby FT, Moore RK, Fung AK (1982) Microwave remote sensing, vol 2. House, Artech
Ulaby FT, Moore RK, Fung AK (1986) Microwave remote sensing: active and passive, Volume scattering and emission theory, advanced systems and applications, vol III. Artech House, Dedham, pp 1797–1848
Valcarce-Diñeiro R, Lopez-Sanchez JM, Sánchez N, Arias-Pérez B, Martínez-Fernández J (2018) Influence of incidence angle in the correlation of C-band polarimetric parameters with biophysical variables of rain-fed crops. Canadian J Remote Sens 44(6):643–659
Wang FM, Huang JF, Lou ZH (2011) A comparison of three methods for estimating leaf area index of paddy rice from optimal hyperspectral bands. Precis Agric 12(3):439–447
Wang FM, Huang JF, Tang YL, Wang XZ (2007) New vegetation index and its application in estimating leaf area index of rice. Chin J Rice Sci 21(2):159–166
Weeks RJ, Smith M, Pak K, Li WH, Gillespie A, Gustafson B (1996) Surface roughness, radar backscatter, and visible and near-infrared reflectance in Death Valley, California. J Geophys Res Planets 101(E10):23077–23090
Weiss M, Baret F, Smith GJ, Jonckheere I, Coppin P (2004) Review of methods for in situ leaf area index (LAI) determination: Part II. Estimation of LAI, errors and sampling. Agric Forest Meteorol 121(1–2):37–53
Wiseman G, McNairn H, Homayouni S, Shang J (2014) RADARSAT-2 polarimetric SAR response to crop biomass for agricultural production monitoring. IEEE J Sel Top Appl Earth Obs Remote Sens 7(11):4461–4471
Xie Q, Dash J, Huang W, Peng D, Qin Q, Mortimer H, Casa R, Pignatti S, Laneve G, Pascucci S, Dong Y (2018) Vegetation indices combining the red and red-edge spectral information for leaf area index retrieval. IEEE J Sel Top Appl Earth Obs Remote Sens 11(5):1482–1493
Yang Z, Li K, Shao Y, Brisco B, Liu L (2016) Estimation of paddy rice variables with a modified water cloud model and improved polarimetric decomposition using multi-temporal RADARS AT-2 images. Remote Sens 8(10):878
Zhang Y, Liu X, Su S, Wang C (2014) Retrieving canopy height and density of paddy rice from Radarsat-2 images with a canopy scattering model. Int J Appl Earth Obs Geoinf 28:170–180
Zhang Y, Wang C, Zhang Q (2011) Identifying paddy fields with dual-polarization ALOS/PALS AR data. Can J Remote Sens 37(1):103–111
Zhou T, Pan J, Zhang P, Wei S, Han T (2017) Mapping winter wheat with multi-temporal SAR and optical images in an urban agricultural region. Sensors 17(6):1210

Chapter 6
Crop Production Estimation Using Remote Sensing

Dibyendu Deb, Subhadeep Mandal, Shovik Deb, Ashok Choudhury, and Satyajit Hembram

Contents

Abstract The ever-increasing global population demands a steep increase in food grain production. To cope up with this demand and maintain a steady supply, proper crop monitoring and production forecasting systems are some of the major requirements. Advance estimation of crop yield is useful for different stakeholders to plan standard agronomical practices, procurement, determine storage availability, transportation, price fixation, and marketing of agricultural products. This estimation can be done by statistical analysis using traditional ground-based study or by using remotely sensed data. The developments in the field of satellite and sensor technologies in the last few decades have established the second method as the most trusted and efficient tool to forecast crop production. Its time and cost-effectiveness with precise estimation capacity ascertain its competence. This chapter presents an exhaustive discussion on the role of these methods (particularly satellite remote sensing) in crop yield estimation. Analysis and transformation of space data to process different vegetation indices and their use in crop production estimation

D. Deb
Indian Grassland and Fodder Research Institute, Jhansi, India

S. Mandal · S. Deb (✉) · A. Choudhury · S. Hembram
Uttar Banga Krishi Viswavidyalaya, Cooch Behar, West Bengal, India
e-mail: shovik@ubkv.ac.in

T. Mitran et al. (eds.), *Geospatial Technologies for Crops and Soils*,
https://doi.org/10.1007/978-981-15-6864-0_6

have been detailed. These vegetation indices are generally used as an explanatory variable in different traditional and advanced statistical models. Further, recent advancements in modeling techniques have introduced applications like machine learning, artificial intelligence, pattern recognition, mobile computing, etc., and thus opened a new dimension in production forecasting processes. This chapter also tried to focus on these rapidly evolving sectors and their possible contribution to the crop yield estimation.

Keywords Machine learning · Space data · Statistical modelling · Vegetation indices · Yield estimation

Abbreviations

AgRISTARS	Aerospace Remote Sensing
ANN	Artificial Neural Networks
APSIM	Agricultural Production Systems sIMulator
AVHRR	Advanced Very High Resolution Radiometer
CAPE	Crop Acreage and Production Estimation
CCE	Crop Cutting Experiments
CHAMAN	Coordinated Programme on Horticulture Assessment and Management Using Geoinformatics
CI-TARS	Crop Identification Technology Assessment for Remote Sensing
CropSyst	Cropping Systems Simulation Model
DSSAT	Decision Support System for Agrotechnology Transfer
EMR	Electromagnetic Radiation
ESA	European Space Agency
EVI	Enhanced Vegetation Index
FASAL	Forecasting Agricultural Output Using Space, Agrometeorology and Land-Based Observations
GCES	General Crop Estimation Surveys
GVI	Green Vegetation Index
IRS	Indian Remote Sensing
ISRO	Indian Space Research Organisation
LACIE	Large Area Crop Inventory Experiment
LISS	Linear Imaging Self-Scanning
MODIS	Moderate-Resolution Imaging Spectroradiometer
MSAVI	Modified Soil-Adjusted Vegetative Index
MSG-SEVIRI	Meteosat Second Generation-Spinning Enhanced Visible and Infrared Imager
NDVI	Normalized Difference Vegetation Index
NIR	Near-Infrared
NOAA	National Oceanic and Atmospheric Administration
NRSC	National Remote Sensing Centre
NSSO	National Sample Survey Office (NSSO)

OSAVI	Optimized Soil-Adjusted Vegetation Index
RDVI	Renormalized Difference Vegetation Index
RS	Remote Sensing
SAR	Synthetic Aperture Radar
SAVI	Soil-Adjusted Vegetation Index
SIMRIW	Simulation Model for Rice–Weather Relations
SPOT	Système Pour l'Observation de la Terre
SUFALAM	Space Technology Utilization for Food Security, Agricultural Assessment and Monitoring
SVM	Support Vector Machines
VNIR	Visible and Near-Infrared

6.1 Introduction

Maximizing crop yield to meet the demand of the increasing population is a major challenge for scientists and policymakers of twenty-first century. To feed the future world population, an estimated overall rise of 70% food production between 2005 to 2050 is required (Alexandratos and Bruinsma 2012). However, we are far behind to achieve targeted yield potential even after maintaining today's best management practices. To match this demand, maybe a new green revolution is required. Along with sustainable advanced technologies and integrated management practices, mathematical modeling for precise crop production estimation will be one of the major pillars for this.

The initial crop simulation models were developed for direct yield estimation only. Those models were made to simulate an idealized planting condition with no sensitivity towards abiotic stresses and long-term predictive ability. Besides, field experiments and trials were primarily concentrated on the goal of increasing production by eliminating yield-reducing factors. With passage of time, a comprehensive monitoring system was developed at the regional and national levels. The United States and European countries started to generate forecasting data for regions of interest. This led the foundation of several country-based empirical models trained with in situ yield data.

The use of satellite remote sensing (RS) in agriculture and especially for crop production estimation is a comparatively newer approach (Deb and Chakraborty 2018). RS is capable of providing spatially explicit and efficient crop yield prediction as it can capture information at wide ranges of spatial and temporal scales with wall-to-wall coverage. Any area of interest can be revisited frequently with a backup of huge archived historical data. In countries like India, where the economy largely depends on agriculture, an early forecast of agricultural production is of utmost importance for making a national budget, contingency planning, and anticipating the market demands. Satellite RS has been proved worthy in this context in the last few decades and increasingly getting popular as an evolving technology by providing

standardized, cheaper, and faster crop yield estimation (Bauman 1992). The precision of crop production modeling using space or air data get sophisticated with the advancement of satellite or aerial sensors and ways of image processing. The following sections have detailed the continuous line of developments in this context.

6.2 Traditional Ways for Crop Yield Estimation: Global and Indian Perspective

Over the years, several global approaches were tested to select suitable crop yield forecasting systems. The initiative was started in western countries but later expended worldwide. It is difficult to draw a chronology of the estimation techniques due to their interdependency and interconnectivity. However, field survey-based estimation was the first one to start. Initially, previous year's yield data along with detailed field surveys and farmer-level interviews were used to forecast yield of next year. Crop reporters' opinions and meteorological phenomena were the two main methods for yield forecasting up to 1929 throughout the world (Irwin 1938; Meena et al. 2018).

In India, using statistical tools for crop yield estimation is not new. Even ancient books like Kautilya's *Arthashastra* mentioned different statistical processes for crop yield estimation. As far as the use of modern crop statistics is concerned, it was first used in 1884 in India for estimation and forecasting of wheat yield (Dadhwal et al. 2002). In 1940, Professor P. C. Mahalanobis of Indian Statistical Institute and P. V Sukhatme of Indian Council of Agricultural Research first initialized Crop Cutting Experiments (CCE) in India to estimate crop yield. The method was very straightforward and used the dry weight of the production. Later, to carry out General Crop Estimation Surveys (GCES), Stratified Multistage Random Sampling design was used. Professor Mahalanobis also rejuvenated the large-scale sample survey technique (Mahalanobis 1952). The advantage of a sample survey is that it deals with only a part of a huge number of variables with a smaller scale of operation. Under the guidance of Professor Mahalanobis, National Sample Survey Office (NSSO) was established in 1970 from the modification of the National Sample Survey Unit of the Indian Statistical Institute (ISI). The NSSO started to analyze, interpret, and compile big data with the aim of yield forecasting. Since 1999, it started acting under the Ministry of Statistics and Programme Implementation.

From the initial day, the Ministry of Agriculture used to prepare the crop production estimation based on land revenue systems for different listed crops. Till today, the yield forecast for Kharif crop is usually prepared during July–August every year (depending on the commencement of southwest monsoon) and the result is reviewed during December–January. For Rabi crop, the advance estimate is given during December–January, and the result is reviewed during April after information for the respective crop production is available (Singh 2012). This forecasting technique is not foolproof and suffers from several shortcomings like delay in

reporting, several non-sampling errors, etc. Even noncompletion of enumeration was reported up to the tune of 20% for sample villages from 1982–83 to 1984–85. These traditional methods involve high-end statistical techniques with complex stratified multistage sampling designs and extensive field data surveys.

The traditional approach for crop yield estimation is generally precise for an area as large as a district. However, when the need is to estimate crop statistics with accuracy for a comparatively smaller area like for a block or tehsil, the number of crop cutting experiments are needed to be much higher, making this method a very costly affair. On the other hand, for a very large spatial scale like a state or country, massive human resource involvement is required with huge cost and time. In this regard, RS and modeling-based cost production estimation can be a very effective alternative tool. This less labor-intensive and highly precise technique has advantages over traditional crop yield estimation methods in terms of its geographical coverage as well as spatial and temporal resolution (Satir and Berberoglu 2016).

6.3 Crop Yield Modeling and Use of Remotely Sensed Data

Application of RS in the civilian domain was first started in the United States around 1960. Since its inception, one of its main application focuses was in agriculture and especially for crop area estimation. After the launch of first Landsat with Multispectral Scanner (sensor) in 1972, its digitally processed output images came into use for crop yield forecasting. Projects like Crop Identification Technology Assessment for Remote Sensing (CI-TARS), Large Area Crop Inventory Experiment (LACIE), and Agriculture and Resources Inventory Surveys through Aerospace Remote Sensing (AgRISTARS) were started. The CI-TARS program was the first full-phase demonstration to show the capabilities of RS to monitor crop (corn and soybean) inventory in the United States. The LACIE and AgRISTARS programs were initiated for implementing Landsat-based agricultural applications and were financially supported by multiple agencies. The National Oceanic and Atmospheric Administration (NOAA) started to perform large-scale crop monitoring as well as yield forecasting since 1980 using Advanced Very High Resolution Radiometer (AVHRR) (Bolton and Friedl 2013; Roy et al. 2014). However, all of these or any other remotely sensed data-based programs for yield estimation need some kind of mathematical modeling. The following sections detailed the different approaches for that.

6.3.1 Use of Vegetation Indices as Input Variable for Model

The response of vegetation cover to different spectral bands varies, depending on the change in physical and biological properties of the vegetation canopies of different crops (Datta and Deb 2012). If there are gross differences in biomass canopies, the

reflectance captured by multispectral scanners (mounted in satellite or airplane) can distinguish them. However, the vegetation canopy reflectance usually gets influenced by background brightness like reflectance from soil or other components exposed within canopy covers. In general, vegetation pigments can be identified by the optical region of the electromagnetic radiation (EMR) while vegetation geometry and dielectric property (of vegetation biomass water) can be recognized by the microwave region of EMR (Dadhwal et al. 2002). Several studies have established that reflectance from blue, green, and red bands has a high correlation with green vegetation health and thus RS using these EMR bands remains highly successful for estimating crop yield. In addition to these visible bands, the reflectance of healthy vegetation in near-infrared (NIR) region is very high. The strong absorption of red band and high reflectance of NIR from healthy vegetation canopies has been used to generate indicative mathematical vegetation indices.

One of the most common vegetation indexes is the Normalized Difference Vegetation Index (NDVI) and has been in use since the 1980s in crop yield forecasting. The NDVI is a fast, effective, and promising complement for conventional survey-based crop health monitoring and production estimation and adopted by scientists worldwide. It is calculated as the ratio of red and NIR bands of any pixel and the expression for calculation of NDVI is as below:

$$\mathrm{NDVI} = \frac{\rho_{\mathrm{NIR}} - \rho_{\mathrm{R}}}{\rho_{\mathrm{NIR}} + \rho_{\mathrm{R}}} \tag{6.1}$$

Here, ρ_{NIR} and ρ_{R} represent spectral reflectance from NIR and red wavelengths respectively.

To use NDVI for crop production estimation, ground-observed crop data of a location should be mathematically compared with the NDVI value of a pixel of the satellite image, covering that location. A large set of data can serve as a good input variable for model building. For example, Fig. 6.1 shows a continuous NDVI map of an area of the Bundelkhand region of India, and then compares the ground-observed biomass with pixel NDVI values.

Although NDVI is the most widely used vegetation index for crop production and yield forecasting, there are several other indices suitable for application in various conditions and can be optimized to serve required purposes.

Renormalized Difference Vegetation Index (RDVI) is one of them. RDVI has been proved to have the capability to establish a relationship with vegetation biophysical parameters. It can be calculated as follows:

$$\mathrm{RDVI} = (\rho_{\mathrm{NIR}} - \rho_{\mathrm{R}}) + \sqrt{\rho_{\mathrm{NIR}} + \rho_{\mathrm{R}}} \tag{6.2}$$

An important concern in any vegetation index is the interference caused by soil background. For instance, the reflectance value of an area (pixel), 50% covered by soil, and rest by crop canopy cannot be properly represented by NDVI. To address this issue, indices have been developed considering a factor, which minimizes soil brightness by calibration. Soil Adjusted Vegetation Index (SAVI) is an example,

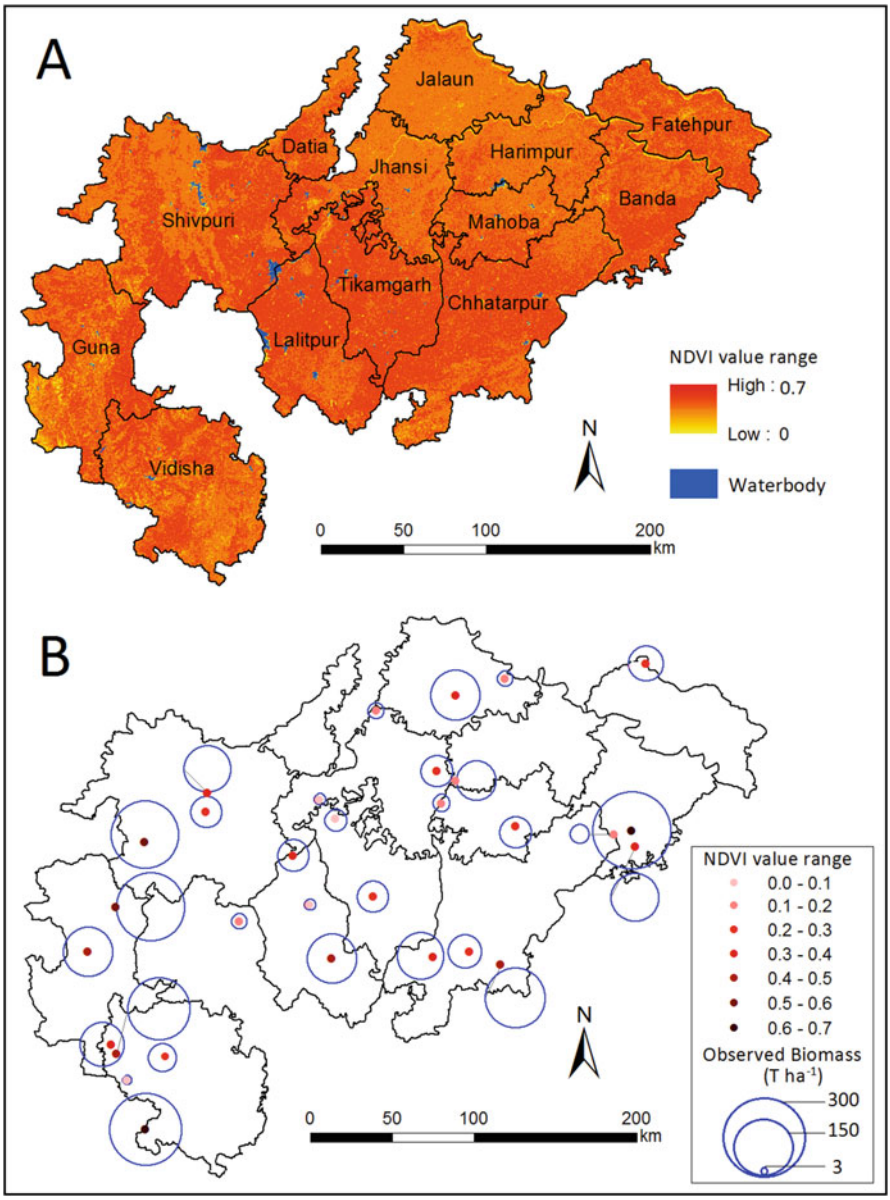

Fig. 6.1 (**a**) Satellite data–derived NDVI map of the area of Bundelkhand, India, and (**b**) comparison of ground-observed vegetation biomass of some locations with respective NDVI values. (Adopted, Deb et al. 2017)

which has been developed by adding soil brightness adjustment factor in NDVI equation.

$$\mathrm{SAVI} = \left[\frac{\rho_{\mathrm{NIR}} - \rho_{\mathrm{R}}}{\rho_{\mathrm{NIR}} - \rho_{\mathrm{R}} + \mathrm{L}}\right] \times (1 + \mathrm{L}) \tag{6.3}$$

Here L is the adjustment factor, L = 0.25 in case of high vegetation, L = 0.5 for intermediate vegetation density, and L = 1.0 for low vegetation density. The SAVI has further been revised to develop Modified Soil-Adjusted Vegetative Index (MSAVI) as per the Eq. 6.4.

$$\mathrm{MSAVI} = \frac{1}{2}\left[2\rho_{\mathrm{NIR}} + 1 - \sqrt{(\rho_{\mathrm{NIR}} + 1)^2 - 8(\rho_{\mathrm{NIR}} - \rho_{\mathrm{R}})}\right] \tag{6.4}$$

Another soil-adjusted vegetative index is Optimized Soil-Adjusted Vegetation Index (OSAVI), which reduces the soil background reflectance in both low and high vegetation cover.

$$\mathrm{OSAVI} = \frac{(1 + 0.16)\,(\rho_{\mathrm{NIR}} - \rho_{\mathrm{R}})}{\rho_{\mathrm{NIR}} - \rho_{\mathrm{R}} + 0.16} \tag{6.5}$$

There are also some indices, which use additional optical bands than red and NIR. Green Vegetation Index (GVI) uses reflectance from green (ρ_{G}) and NIR bands. Enhanced Vegetation Index (EVI) considers blue band (ρ_{B}) along with red and NIR bands.

$$\mathrm{GVI} = (\rho_{\mathrm{NIR}} - \rho_{\mathrm{G}})/(\rho_{\mathrm{NIR}} + \rho_{\mathrm{G}}) \tag{6.6}$$

$$\mathrm{EVI} = 2.5 \times \left[\frac{\rho_{\mathrm{NIR}} - \rho_{\mathrm{R}}}{\rho_{\mathrm{NIR}} + 6 \times \rho_{\mathrm{R}} - 7.5 \times \rho_{\mathrm{B}} + 1}\right] \tag{6.7}$$

These indices are particularly good under certain land cover conditions. For example, EVI performs well where land is covered by thick vegetation and it (EVI) can reduce the background and atmospheric noises. All these indices have proved as excellent input variable in models for crop production forecasting, as detailed below.

6.3.2 Traditional Statistical Models

Crop yield depends largely on the fluctuation of weather and climate changes. Researchers generally use conceptual or numerical models to anticipate how crop production will respond to all these changes. These numerical models are developed based on years of researches on crop physiology and reproduction so that these models can emulate the crop production system. One class of such models is trained with extensive plant physiology (like evapotranspiration data, photosynthesis) and meteorological input data, which are the main factors affecting crop production.

These models predict crop performances in field conditions, which are subjects to unpredictable weather fluctuations causing difficulty calibrating the models.

In another class of models, the yield is simulated using space-borne data. Different vegetation indices, as the derivatives of remotely sensed data, are used as model input parameters. This class of models has been popularly used for the last three decades for agricultural applications across the world (Ren et al. 2008; Deb et al. 2017). In one of the established methods, satellite images are used to capture the completion of the vegetation stage of a crop in a specific area. The vegetation indices, derived from the satellite data for that/those exact pixel/s, are then correlated with ground crop yield for prediction. In India, National Remote Sensing Centre (NRSC) is involved in yield prediction of few major crops like rice, wheat, sorghum, etc. at the district level through Crop Acreage and Production Estimation (CAPE) project. Markov Chain Model is another regularly used simulation for crop yield estimation (Deb et al. 2018). For the crop production model, Kogan et al. (2012) used vegetation health indices (vegetation condition index and temperature condition index), derived from AVHRR data for 21 years (1985–2005). In studies, where the variation in yield for such a long period has to be taken into consideration, time-series models are generally used for forecasting crop production.

Traditional regression models have limitations as the relationship between vegetation physiology and RS data–derived vegetation indices is complex and often not just simple linear. Thus, in the last decades, nonlinear models and multiple linear regression became popular among researchers. Nonlinear models are found to demonstrate a good correlation between vegetation properties and spectral reflectance. Again, at times modeling crop yield also requires consideration of multiple variables (Bendig et al. 2015; Deb et al. 2017). Figure 6.2 depicts a predicted yield map of three crops in an area of Mediterranean Turkey. A stepwise linear regression model was used here for yield estimation, using vegetation indices as explanatory variables (Satir and Berberoglu 2016).

6.3.3 Simulation Models

These models simulate crop growth and its yield using independent variables like weather conditions, soil conditions, and crop management. However, remotely sensed data can also be used as input in these models for larger spatial coverage, better perception about leaf area index, a light interception by the crop canopy. Multispectral and especially hyperspectral remote sensing can reveal important spectral properties of crop canopy and thus has the potential to provide precise information on plant biophysical properties. Some popular crop simulation models are Cropping Systems Simulation Model (CropSyst), Agricultural Production Systems sIMulator (APSIM), Decision Support System for Agrotechnology Transfer (DSSAT), etc. The CropSyst model was developed by the Department of Biological Systems Engineering of Washington State University and can develop a multi-crop, multiyear simulation model. The APSIM model is a very advanced simulation model

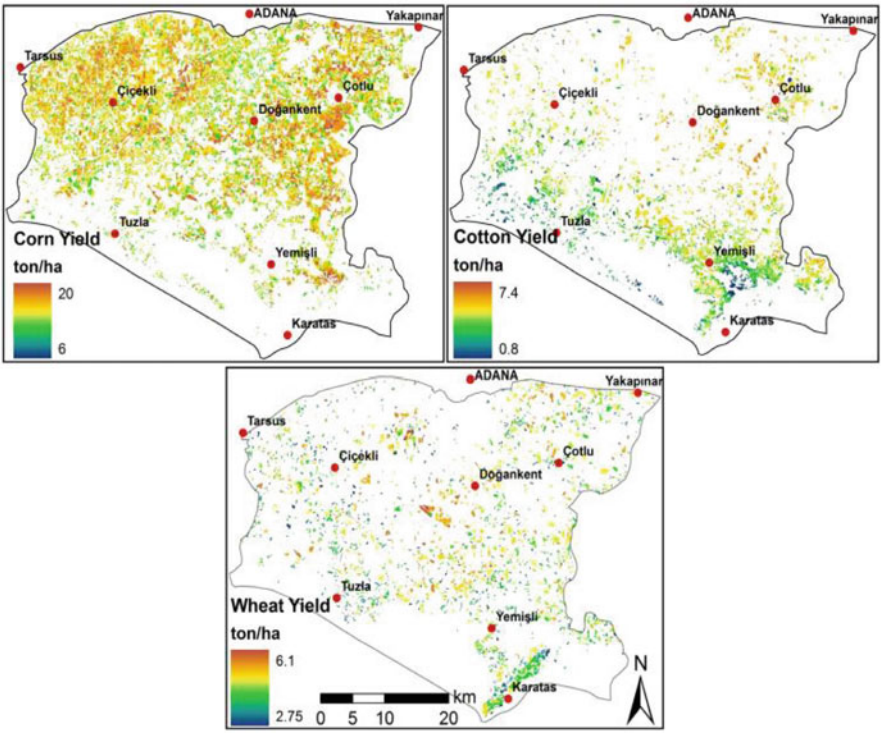

Fig. 6.2 Yield prediction map of corn, cotton, and wheat by stepwise linear regression using vegetation indices as input variables. The study area is at Çukurova plane, Turkey. (Adopted, Satir and Berberoglu 2016)

for agricultural production and stands for Agricultural Production Systems Simulator. It was developed by the Commonwealth Scientific and Industrial Research Organisation (CSIRO). The DSSAT is a simulation model that can predict for more than 25 crops (Jame and Cutforth 1996). This model can predict the growth and yield of the crops, soil nitrogen and carbon balances, soil, and plant water. In the DSSAT model, the incorporation of remotely sensed data has enabled better crop yield estimation potential in a single-season time scale (Kasampalis et al. 2018). On the other hand, Synthetic Aperture Radar (SAR) remote sensing data is used to improve the accuracy of rice yield in regional scale through the SIMRIW (Simulation Model for Rice–Weather Relations) crop model (Maki et al. 2017).

6.3.4 Use of Machine Learning and Artificial Intelligence

Another option is the use of advanced modeling techniques like Machine Learning. The advantage of machine learning in crop production modeling is its capacity to

mimic any real ecological process. There are several machine learning techniques like Artificial Neural Networks (ANN), Support Vector Machines (SVM), Decision Tree, Genetic Programming, Random Forests, etc. These models have appeared as a better substitute due to their advantages like nonlinearity, input–output mapping, adaptivity, generalization, and fault tolerance (Mountrakis et al. 2011; Lu et al. 2014). At the time of estimating crop yield using machine learning, the use of RS data as an input variable is a common practice. Predominantly these models are built by comparing vegetation indices with original ground yield data. After validation of the model on a small scale, it can be applied over a larger area. Machine learning, in a true sense, is a multivariate application and can involve thousands of variables. The working principle of machine learning algorithms is called universal approximation, which means no prior knowledge about the existing relationship between the dataset is required. It learns the underlying pattern from a training set of data. The use of machine learning techniques in combination with RS data results in precise crop yield estimation for a larger area. Among machine learning, the two most popular choices for precise crop yield forecasting are ANN and SVM. However, these are considered black-box models as they come up with predicted values only but not with the prediction equation. This issue can be dealt with models like Genetic Programming. Figure 6.3 depicts a comprehensive procedure to estimate crop production using various mathematical models and RS derived vegetation indices as an input variable.

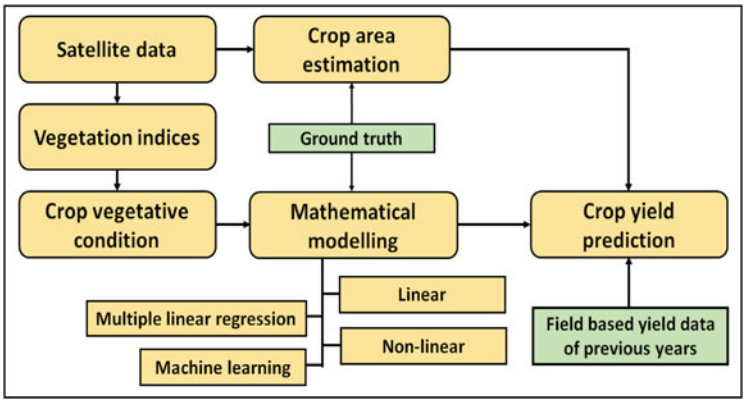

Fig. 6.3 Flowchart describing crop yield estimation process using satellite data and mathematical models

6.4 Present Operational Programs and Its Success

In recent years, spaceborne RS has seen a lot of improvements in respect to both radiometric calibration and spatial and spectral resolution. One big step was the launch of the Moderate Resolution Imaging Spectroradiometer (MODIS) by NOAA. The frequency of observations for both AVHRR and MODIS are satisfactory and widely available across the world with a few processed themes. However, coarse spatial resolution is an issue for both of them. For MODIS these are 250 m (bands 1 and 2), 500 m (bands 3–7), and 1000 m (bands 8–36) while for AVHRR it is 1.1 km for local area coverage and 4 km for global coverage. The development in the front of spatial resolution saw huge progress after the launch of the Landsat satellite series by United States and with free access to the data. While the Multispectral Scanner (mounted on Landsat 1–5) has a spatial resolution of 68 m × 83 m, it is even finer for the Thematic Mapper (Landsat 4–5), Enhanced Thematic Mapper+ (Landsat 7), and Operational Land Imager (Landsat 8) (30 m). However, the accessibility of a major amount of this medium-resolution data is very limited on a regional scale (Bolton ad Friedl 2013). Another problem with Landsat data is its less temporal repetition. For example, Landsat 7 and 8 has 16-day repetition period. It throws a huge challenge for agricultural farm applications, which require more frequent data for monitoring and assessment of crop growth stages. To overcome this challenge, an innovative way has been found out by the researchers through which high-resolution images obtained from Landsat can be merged with higher frequency data like MODIS or AVHRR data.

The path shown by the United States about the use of RS data in crop yield estimation was followed by many other countries from Asia and Europe. In Europe, monitoring agriculture through space data commenced to provide technical support to the European Agricultural Guidance and Guarantee Fund and to apply RS technology for the agricultural monitoring in the member states. This project helped to formulate effective and efficient Common Agricultural Policy for the European countries. The use of RS data in crop yield estimation got further established by some multinational space programs like SPOT-vegetation, Meteosat Second Generation-Spinning Enhanced Visible and Infrared Imager (MSG-SEVIRI), and MODIS-Terra. The precise and timely forecast of crop yield by these remotely sensed data-based projects got backed-up by a defined sampling approach, crop identification, and monitoring on more than one date and rigorous field survey. At present, the European Space Agency (ESA) has satellites like SPOT 7 with a spatial resolution of 1.5 m only (panchromatic) and 6 m (multispectral). Even Sentinel-2 data of up to 10 m resolution have been made free by ESA.

In the space race and space-data application, India also holds a major global role. Indian Space Research Organisation (ISRO) started to use RS in crop yield studies with the launching of the Indian Remote Sensing (IRS) program in 1988. Space Application Centre and NRSC (earlier known as National Remote Sensing Agency) took the lead role here in collaboration with other Indian institutes. A national project named Large Area Crop Acreage was launched by the Ministry of Agriculture for

yield forecasting for few major crops like rice, wheat, groundnut, sorghum, mustard, sugarcane, and cotton. Later this project got renamed CAPE. Use of high-resolution RS data, advanced modeling, and subsequent precise yield forecasting made this program a huge success for preparation of national crop inventory. The CAPE project was also proved to be a good source of knowledge about crop yield and spectral relationship, factors affecting crop area discrimination, and the importance of timely information for accurate crop yield forecasting. Operational success of CAPE encouraged another updated program named Forecasting Agricultural Output Using Space, Agrometeorology and Land-Based Observations (FASAL). It was initiated with extensive goal of nationwide multi-crop forecasting with consideration of Indian monsoon data, national economic data, and ground data, recorded at different stages of crop growth. Following the success of FASAL, an umbrella program named SUFALAM (Space Technology Utilization for Food Security, Agricultural Assessment and Monitoring) has been initiated by ISRO with multiple objectives like yield forecasting for selected crops, promotion of precision farming, crop insurance, upgradation of agro-advisory-based services, etc. A similar program was launched for monitoring horticultural crops like onion, potato, and mango under the name Coordinated Programme on Horticulture Assessment and Management Using Geoinformatics (CHAMAN). Mahalanobis National Crop Forecast Centre took a major role here.

In Indian RS history, IRS 1A and 1B mounted sensor Linear Imaging Self-Scanner−1 (LISS-I) was a milestone. It was widely used as the major data source for crop yield modeling during the late 1980s and the early 1990s. The LISS-II data from the same satellites were preferred to model multiple crops when grown simultaneously. These data had a spatial resolution of 72.5 m (LISS-I) and 36.25 m (LISS-II). With continuous upgradation of space technology, India achieved multispectral sensors with a finer spatial resolution like LISS-III (23.5 m) (mounted on IRS 1C, 1D, Resoursesat 1, 2, 2a) and LISS-IV (5.8 m) (mounted on Resoursesat 2, 2a). Further, panchromatic data up to 0.25 m are available now from Cartosat 3, 3a, and 3b. At present, a combination of these multispectral and panchromatic data can lead to precise estimation of crop yield up to the village or even farm level.

Besides the government-controlled initiatives, private commercial RS industry has made a big leap toward a variety of applications in recent years. It includes crop monitoring–based crop insurance, food security, resource management planning, etc. Several factors are responsible for this boom in technical business, such as easy availability of location identification technology (like Global Positioning System); massive development in telecommunications; huge innovation in robotics, machine, and deep learning; drone technology; etc. Widespread development in free and open-source software is also helping the small firms to invest in this sector. In this front, several startups companies are now working by introducing artificial intelligence and computer vision in aerial and satellite imagery analysis. They are enabling farmers to make better decisions to improve crop health and yield. They have also been proved helpful in bridging the gap between first mile and last mile, that is, benefit of using

high-end technology like RS for farmers and the planning of their farming operations.

6.5 Conclusion and Future Perspective

In our present capacity, the basic limitation in crop production estimation is proper identification of "maximum yield potential." Although, RS made the data interpretation easier with improved accuracy, it does not mean that the future trajectories of yield potential can be estimated without hassle (Chen et al. 2018). Besides, environmental variation does not follow any known equation. With the present knowledge, it is hard to take account of uncertain factors like global warming or soil health degradation and their impact on crop production. Researches in coming years should concentrate on these grounds. Another future direction should be wider use of SAR data as it provides information on crop physical structure and moisture status in addition to biological properties. Use of SAR data also outperforms optical data due to its cloud-free, all-weather, day–night sensing capability (Zhang et al. 2014). On the contrary, inclusion of hyperspectral data along with multispectral data can minimize overfitting problem arises from co-linearity between multispectral wavebands.

No modelling or classification algorithm is full proof. They have their own advantages and limitations. Therefore, more research should be carried out on mixed classification approaches that utilize both visual and quantitative analytics. Modern classification systems sometimes suffer from overfitting of data as well as spatial mis-interpolation (Yang et al. 2019). Future research should wave off this uncertainty by stronger integration of data, at process level or output level. Finally, regional-level crop production models should be a major focus in coming years as regional risk in agriculture, management practices, and local weather–mediated variability cannot be estimated from large area survey. Hopefully, the fast development in RS and modelling technology will finetune these aspects of crop production estimation in the near future.

References

Alexandratos N, Bruinsma J (2012) World Agriculture towards 2030/2050. The 2012 Revision. Agricultural Development Economics Division, ESA working paper number 12–03. Food and Agriculture Organization of the United Nations

Bauman BAM (1992) Linking physical remote sensing models with crop growth simulation models applied for sugar beet. Int J Remote Sens 14:2565–2581

Bendig J, Yu K, Aasen H, Bolten A, Bennertz S, Broscheit J, Gnyp ML, Bareth G (2015) Combining UAV-based plant height from crop surface models, visible, and near infrared vegetation indices for biomass monitoring in barley. Int J Appl Earth Obs Geoinf 39:79–87

Bolton DK, Friedl MA (2013) Forecasting crop yield using remotely sensed vegetation indices and crop phenology metrics. Agric For Meteorol 173:74–84
Chen Y, Zhang Z, Tao F (2018) Improving regional winter wheat yield estimation through assimilation of phenology and leaf area index from remote sensing data. Eur J Agron 101:163–173
Dadhwal VK, Singh RP, Dutta S, Parihar JS (2002) Remote sensing based crop inventory: a review of Indian experience. Trop Ecol 43:107–122
Datta D, Deb S (2012) Analysis of coastal land use/land cover changes in the Indian Sunderbans using remotely sensed data. Geo Spat Inf Sci 15:241–250
Deb S, Chakraborty S (2018) Digital soil science for identification of problem soil characteristics. In: Rakshit A, Sarkar B, Abhilash PC (eds) Soil amendments for sustainability: challenges and perspectives. CRC Press, Boca Raton, pp 51–56
Deb D, Singh JP, Deb S, Datta D, Ghosh A, Chaurasia RS (2017) An alternative approach for estimating above ground biomass using Resourcesat-2 satellite data and artificial neural network in Bundelkhand region of India. Environ Monit Assess 189:576
Deb S, Debnath MK, Chakraborty S, Weindorf DC, Kumar D, Deb D, Choudhury A (2018) Anthropogenic impacts on forest land use and land cover change: modelling future possibilities in the Himalayan Terai. Anthropocene 21:32–41
Irwin JO (1938) Crop estimation and its relation to agricultural meteorology. Suppl J R Stat Soc 5:1–45
Jame YW, Cutforth HW (1996) Crop growth models for decision support systems. Plant Sci 76:9–19
Kasampalis DA, Alexandridis TK, Deva C, Challinor A, Moshou D, Zalidis G (2018) Contribution of remote sensing on crop models: a review. J Imaging 4:52
Kogan F, Salazar L, Roytman L (2012) Forecasting crop production using satellite-based vegetation health indices in Kansas, USA. Int J Remote Sens 33:2798–2814
Lu D, Chen Q, Wang G, Liu L, Li G, Moran E (2014) A survey of remote sensing-based aboveground biomass estimation methods in forest ecosystems. Int J Digit Earth 9:63–105
Mahalanobis PC (1952) Some aspects of the design of sample surveys. Sankhyā: Indian J Stat 12:1–7
Maki M, Sekiguchi K, Homma K, Hirooka Y, Oki K (2017) Estimation of rice yield by simriw-rs, a model that integrates remote sensing data into a crop growth model. J Agric Meteorol 73:2–8
Meena RS, Mitran T, Kumar S, Yadav G, Bohra JS, Datta R (2018) Application of remote sensing for sustainable agriculture and forest management. Inf Process Agric 5:295–297
Mountrakis G, Im J, Ogole C (2011) Support vector machines in remote sensing: a review. ISPRS J Photogramm Remote Sens 66:247–259
Ren J, Chen Z, Zhou Q, Tang H (2008) Regional yield estimation for winter wheat with MODIS-NDVI data in Shandong China. Int J Appl Earth Obs Geoinf 10:403–413
Roy DP, Wulder MA, Loveland TR, Woodcock CE, Allen RG, Anderson MC, Helder D, Irons JR, Johnson DM, Kennedy R, Scambos TA (2014) Landsat-8: science and product vision for terrestrial global change research. Remote Sens Environ 145:154–172
Satir O, Berberoglu S (2016) Crop yield prediction under soil salinity using satellite derived vegetation indices. Field Crop Res 192:134–143
Singh R (2012) Crop yield estimation and forecasting using remote sensing. In: Singh KN, Kumar A, Chandra H (eds) Forecasting techniques in agriculture. Indian Agricultural Statistics Research Institute, New Delhi, pp 201–215
Yang Q, Shi L, Han J, Zha Y, Zhu P (2019) Deep convolutional neural networks for rice grain yield estimation at the ripening stage using UAV-based remotely sensed images. Field Crop Res 235:142–153
Zhang Y, Zhang H, Lin H (2014) Improving the impervious surface estimation with combined use of optical and SAR remote sensing images. Remote Sens Environ 141:155–167

Chapter 7
Concepts and Applications of Chlorophyll Fluorescence: A Remote Sensing Perspective

Karun Kumar Choudhary, Abhishek Chakraborty, and Mamta Kumari

Contents

Abstract Light energy absorbed by plant chlorophyll pigments is principally utilized for photosynthesis. The surplus energy is dissipated as heat or re-emitted as chlorophyll fluorescence (CF). The CF is wavelength specific and directly linked to the efficiency of the photosystems I and II. Hence, it is one of the few direct

K. K. Choudhary (✉)
Crop Assessment Division, Agricultural Sciences and Applications Group, Remote Sensing Applications Area, National Remote Sensing Centre, Hyderabad, Telangana, India
e-mail: karunkumar_choudhary@nrsc.gov.in

A. Chakraborty · M. Kumari
Agroecosystem and Modeling Division, Agricultural Sciences and Applications Group, National Remote Sensing Centre, Department of Space, ISRO, Hyderabad, Telangana, India
e-mail: abhishek_c@nrsc.gov.in; mamta_kumari@nrsc.gov.in

T. Mitran et al. (eds.), *Geospatial Technologies for Crops and Soils*,
https://doi.org/10.1007/978-981-15-6864-0_7

assessments of vegetation condition, growth processes, and productivity. The active CF retrievals are computationally simple but lack scalability; hence, passive measurement in terms of solar-induced chlorophyll fluorescence (SIF) from ground-based, airborne, and space-borne instruments is popular for regional or global monitoring of vegetation condition. The retrieval of SIF from upwelling radiance from vegetation canopy, though complex, is one of the promising developments in the field of remote sensing. Significant research works have been done on the instrumentation, measurement, retrieval, and application of CF for crop/vegetation monitoring and assessment. The present book chapter reviews the basic concepts of chlorophyll fluorescence, its measurement, major SIF retrieval techniques and its applications along with future challenges.

Keywords Chlorophyll fluorescence · Crop condition · Crop stress · Fraunhofer line depth · Gross primary productivity · Pulse-amplitude modulation · Photosynthetic efficiency · Sun-induced chlorophyll fluorescence

Abbreviations

C_{ab}	Chlorophyll a and b Content
CF	Chlorophyll Fluorescence
CFIS	Chlorophyll Fluorescence Imaging Spectrometer
ESA	European Space Agency
FAPAR	Fraction of Absorbed Photosynthetically Active Radiation
Fd	Ferrodoxin
FL	Fraunhofer Line
FLD	Fraunhofer Line Depth
FLEX	Fluorescence Explorer
FWHM	Full Width Half Maxima
GOME-2	Global Ozone Monitoring Experiment-2
GOSAT	Greenhouse Gases Observing Satellite
GPP	Gross Primary Productivity
LUE	Light Use Efficiency
MERIS	Medium Resolution Imaging Spectrometer
MetOp-A, -B	Meteorological Operational Satellite A or B
MODIS	Moderate Resolution Imaging Spectroradiometer
MODTRAN	Moderate Resolution Atmospheric Transmission
NADP	Nicotinamide adenine Dinucleotide Phosphate
NPP	Net Primary Productivity
NPQ	Non-photochemical Quenching
OCO	Orbiting Carbon Observatory
PAM	Pulse-amplitude Modulation
PAR	Photosynthetically Active Radiation
PCA	Principal Component Analysis
PQ	Photochemical Quenching

PRI	Photochemical Reflectance Index
PROSPECT	PROpriétésSPECTrales
PSI	Photosystem I
PSII	Photosystem II
RTM	Radiative Transfer Model
S-5P	Sentinel-5 Precursor
SCIAMACHY	Scanning Imaging Absorption Spectrometer for Atmospheric Chartography
SCOPE	Soil-Canopy-Observation of Photosynthesis and Energy Fluxes
SEN2FLEX	Sentinel-2 and Fluorescence Experiment
SFM	Spectral fitting methods
SIF	Sun-induced Chlorophyll Fluorescence
SNR	Signal-to-noise Ratio
SR	Spectral Resolution
SVD	Singular Value Decomposition
TANSO-FTS	Thermal and Near-Infrared Sensor for Carbon Observation Fourier Transform Spectrometer
TROPOMI	Tropospheric Monitoring Instrument

7.1 Introduction

When a substance is irradiated by some energy (generally light), it absorbs part of it and occasionally re-emits at a higher wavelength as fluorescence. This phenomenon is found in the plant system as chlorophyll fluorescence. Living plant cells capture solar energy through the "photosynthesis" process and convert it into chemical energy as food. In doing so, part of the absorbed solar energy is re-emitted as chlorophyll fluorescence (CF). In recent decades, analysis of CF has emerged as an excellent method to check the performance of photosynthetic machinery in the plant as it is directly linked with the functional status of photosystem II present in the thylakoid of the chloroplast. Since its first discovery by Sir David Brewster in 1834 (Brewster 1834) and subsequently pioneer investigations by Kautsky and Hirsh (1931), McAlister and Mayer (1940), Duysens and Sweers (1963), Govindjee (1995), and others, today, we have made significant progress to assess the CF signal from leaf to regional level, from laboratory to in-situ conditions, and from actual measurement to radiative transfer modelling. CF can be analysed through active instruments based on pulse-amplitude modulation (PAM), and fluorescence yield parameters could be generated to link it to the photosynthetic efficiencies. On the other hand, passive measurement of CF as sun-induced chlorophyll fluorescence (SIF) has gained attention during the recent years as its estimation using remote sensing techniques at specific narrow bandwidths has widespread applications in regional productivity monitoring, early stress detection, plant biophysical parameter retrieval, etc. With the progress of electro-optics technology, it is now possible to

sense the weak SIF signal in a very narrow spectral range through remote sensors. Successful SIF retrieval is being carried out from ground-based (Liu et al. 2015a, b), airborne (Zarco-Tejada et al. 2009), and satellite sensors (Guanter et al. 2007; Frankenberg et al. 2011a, b). SIF consists of the emission in the red and far-red regions of the electromagnetic spectrum with two broad peaks at 690 and 740 nm. Passive measurement of SIF in this narrow spectral region and assessing the photosynthetic machinery of vegetation is the challenge of remote sensing community. SIF retrieval technique developments were mostly made by ground-based/airborne sensors and are being scaled up at satellite platform. Till now, no satellite is launched dedicatedly for SIF measurement, but attempts have been made to retrieve SIF from suitable narrow-band observations available on different atmospheric satellites like GOSAT, MetOp-GOME, OCO2, and Sentinel-5P. Hence, satellite-based estimation of chlorophyll fluorescence opens up a plethora of new and innovative applications of remote sensing data for regional crop monitoring. This chapter aims to concisely review the basics of chlorophyll fluorescence, its origin, active and passive retrieval techniques, and the applications of SIF from remote sensing point of view.

7.2 Basics of Chlorophyll Fluorescence

7.2.1 Photosynthesis and Emission of Chlorophyll Fluorescence

Photosynthesis is the primary process to harvest solar energy and the basis of life for almost all living creature on the planet earth. Photosynthesis is mainly a three-step process composed of carbon dioxide (CO_2) diffusion to the chloroplast, light absorption by pigment system, and reduction of CO_2 into sugars (Govindjee 2004). Two chlorophyll-protein complexes, namely, photosystem II (PS-II) and photosystem I (PS-I), residing in the thylakoid membrane of the chloroplast, participate in the light-driven transfer of an electron to reduce the NADP+ (Whitmarsh and Govindjee 2002). Splitting of water occurs at PS-II which absorb the light energy at 680 nm and transfer the electron to plastoquinone (Pq). Pq in turn carries the electron to a series of protein complexes (cytochrome-bf, plastocyanin) before reaching to PS-I. PS-I absorb light at 700 nm and further reduce another protein complex known as ferredoxin (Fd) in the stroma of the chloroplast. Fd, in conjunction with Fd–$NADP^+$ reductase (FNR) enzyme, reduces $NADP^+$ to NADPH and releases the ATP to reduce the CO_2 into sugar through a series of dark reactions in Calvin-Benson cycle (Bendall and Manasse 1995). The schematic diagram presents a simplistic representation of the linear electron transfer pathway of the photosynthesis process (Fig. 7.1).

Light-harvesting pigments are mostly chlorophyll-a (Chl-a), chlorophyll-b (Chl-b), and carotenoids, residing in the antenna complexes of the PS-I and PS-II.

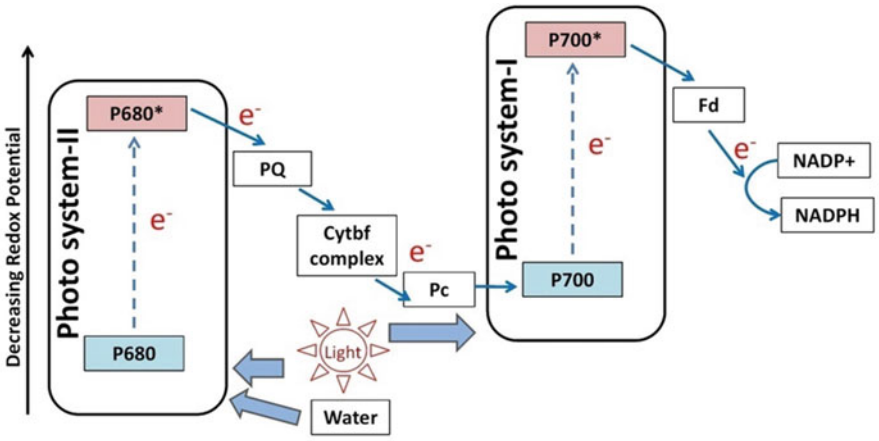

Fig. 7.1 Electron transport pathway in light reaction of photosynthesis

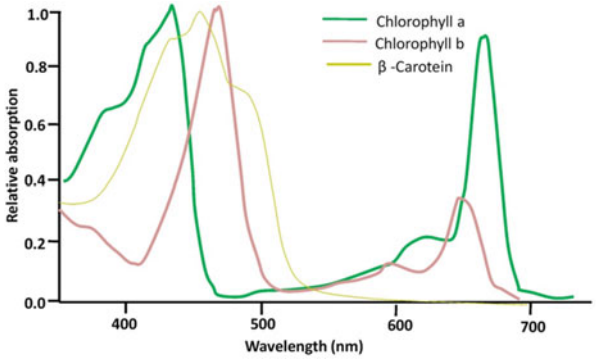

Fig. 7.2 Absorption spectra of chlorophyll and carotenoid pigments. (Modified, Johnson 2016)

The absorption spectra of these pigments are shown in Fig. 7.2 (Johnson 2016). Chl-a and Chl-b have their absorption peaks in blue and red regions, while the carotenoids absorb light in the blue region only. Hence, leaves appear as yellow/red in the case of chlorophyll disintegration. Chl-a molecules, present in PS-I and PS-II, absorb a certain quantity of energy and reach to an excited state (marked as * in Fig. 7.1). This excitation energy of Chl-a molecules gets quenched by various ways to bring the Chl-a into the ground state. There can be three modes of the release of this energy (Fig. 7.3): (1) through a photochemical method to reduce the CO_2 into sugar as explained in Sect. 7.1 also known as photochemical quenching (PQ); (2) non-photochemical quenching (NPQ), i.e. thermal dissipation; and (3) re-emission at a relatively higher wavelength as chlorophyll fluorescence (CF). Both the photosystems involve in CF but show spectral and intensity differences among each other (Fig. 7.3). PS-I absorbs the light in the infrared region of 700 nm and emits CF in an infrared region of 740 nm, also known as CF_{740} or far-red CF,

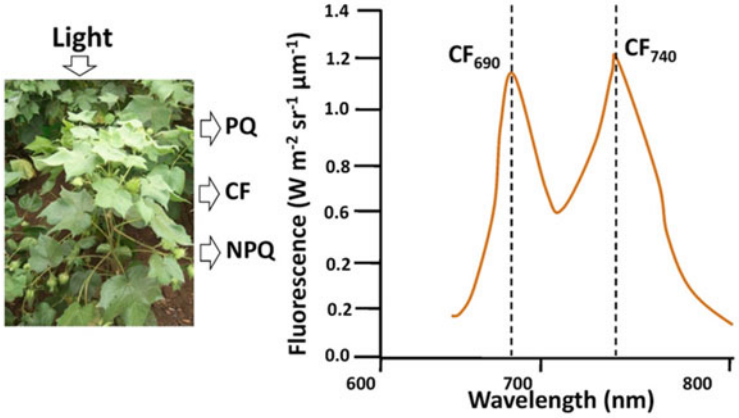

Fig. 7.3 Fate of absorbed light by chlorophyll and typical chlorophyll fluorescence emission spectra between 600 and 800 nm

whereas the PS-II absorbs at a red wavelength (680 nm) and emits at a relatively higher wavelength of the red region, i.e. 690 nm (CF_{690} known as red CF).

Although both PS-I and PS-II emit CF, PS-I CF remains invariant with the plant stress or photosynthetic mechanism, whereas PS-II CF shows significant sensitivity and measurable changes toward the level of plant stress, the functional efficiency of the photosystem, photoprotective mechanism, heat dissipation mechanism, etc. Hence, PS-II CF is more important to assess the photosynthetic mechanism, electron transport rate, and CO_2 assimilation in the plant.

7.2.2 Quenching Mechanisms and Analysis

7.2.2.1 Active Measurement with Kautsky Fluorometer

One of the earliest observations of CF was made by Kautsky and Hirsh in 1931. They measured the rate of increase in the yield of chlorophyll fluorescence after exposing the leaf extract from dark to light. This typical change in the intensity of CF with time after illuminating a dark-adapted chlorophyll pigment to continuous light is popularly known as the *Kautsky effect*, and the curves generated with these observations are called *Kautsky curve*. A typical *Kautsky curve* is shown in Fig. 7.4. It can be observed that initially, the CF intensity increases with the time range (in the order of microseconds) and achieves its peak called maximum CF (F_m). The CF intensity further decreases and reaches a steady-state level called steady-state CF (F_t). The initial rise in CF is caused by the activation of all reaction centres of PS-II leading to an increase in the photochemical quenching (PQ). It achieves F_m when all the reaction centres get saturated. The later slowdown of CF is caused by

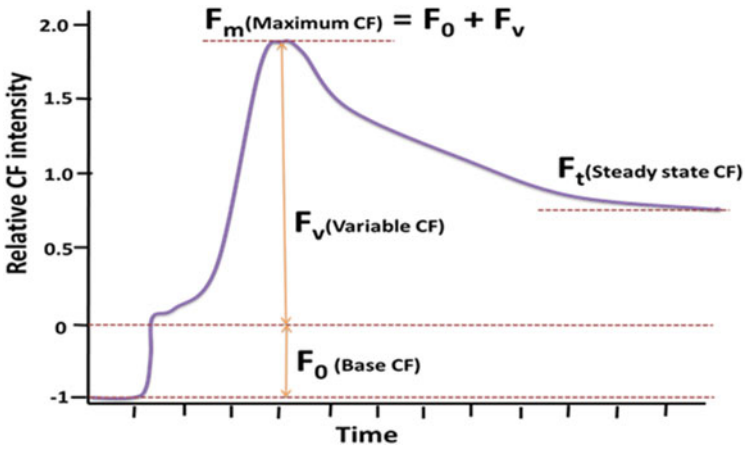

Fig. 7.4 A typical Kautsky curve of a green leaf. (Adopted, Ritchie 2006)

non-photochemical quenching (NPQ), i.e. the protective mechanism of dissipating heat. In a healthy plant cell, the time to reach a steady-state CF level is around 15–30 min with the significant variations between the plant species (Johnson et al. 1990).

7.2.2.2 Active Measurement with Pulse-Amplitude Modulation Fluorescence

PAM is another technique for quenching analysis and active measurement of CF parameters. In this technique, instead of continuous light, a high-intensity light pulse is used to measure the CF emission, and it is a more efficient and popular technique to measure CF in the presence of background measuring light (Schreiber 2004). PAM-fluorometer-based observations are mostly taken in two modes, i.e. dark-adapted and light-adapted. The leaf needs to be put in dark for 20–60 min before the dark adapted measurement. Dark-adapted measurement allows the determination of the maximum potential quantum efficiency of PS-II also represented as F_v/F_m. F_v/F_m is also known as "intrinsic quantum yield" (Kitajimaand Butler 1975). F_v/F_m has both photochemical and non-photochemical components (Baker 2008). Fv/Fm measurement is very fast which takes only 1–2 s. The base or ground fluorescence (F_0) is measured first with a weak modulating light (ML) beam; then, a saturation pulse (SP) is applied at a higher wavelength to saturate the receptors at PS-I. The application of SP raises the fluorescence to a maximum value, F_m. Figure 7.5 shows different measured parameters in the dark-adapted and light-adapted phase through a typical PAM fluorescence curve. F_v/F_m does not measure photosynthetic efficiency while photosynthesis is taking place.

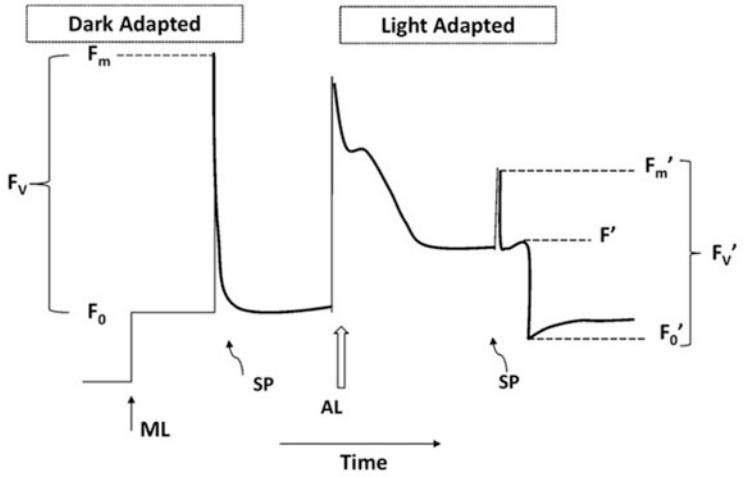

Fig. 7.5 A typical PAM fluorescence curve: modulating light (ML), actinic light (AL), saturation light (SP) (Adopted, Misra et al. 2012)

In PAM fluorometry, mostly three types of light pulses are used, i.e. measuring/modulating light (ML) which does not affect PS-II, actinic light (AL) which opens the reaction centre of the PS-II, and saturation light/pulse (SP) which closes the PS-II.

In the light-adapted measurements, the leaf surface is directly illuminated with AL, and SP is turned on and off repeatedly. This process induces the fluorescence to reach a maximum value (Fm'). The initial increase of Fm' with few pulses is known as "photochemical quenching" which is related to the electron transport rate in the light reaction of photosynthesis (Edwards and Baker 1993). Subsequent pulses of saturating light lead to a decline in fluorescence intensity due to "non-photochemical quenching", i.e. NPQ (Oxbrough and Baker 1997). PAM instruments measure CF at a definite wavelength only, i.e. the wavelength of ML, while the signal produced by SP and AL is not detected by the instruments. SP and AL only change the redox potential of PS-II and not generate the CF. The measured CF at different redox potentials of PS-II helps in studying the health status of PS-II (Guo and Tan 2015). A list of commonly used fluorescence quenching parameters is given in Table 7.1.

Yield (Y-II, $\Delta F/F_m'$, or $F_m' - F_s/F_m'$) indicates the ratio of the amount of light used in photochemistry in PS-II to the amount of light absorbed by chlorophyll associated with PS-II. (Genty et al. 1989; Maxwell and Johnson 2000). Y-II also represents the achieved efficiency of PS-II under the current light condition and steady-state photosynthetic rate. Y-II is related linearly with carbon assimilation for C_3 plants and curvilinear for C_4 plants due to photorespiration and pseudo-cyclic electron transport in C_4 plants (Genty et al. 1989, 1990).

Table 7.1 List of commonly used quenching parameters

Parameter	Formula	Description	Significance	References
F	–	CF emission from dark-adapted leaves	Not directly used for assessing the photosynthetic performance as these are affected environmental factors	Baker and Rosenqvist (2004)
F′or F_s'	–	CF emission from light-adapted leaves also known as "steady-state CF"		
F_0	–	Minimum CF from dark-adapted leaf	CF level when reaction centres of PS-II are open	
F_0'	–	Minimum CF from light-adapted leaf		
F_m	–	Maximal CF from dark-adapted leaf	CF level when reaction centres of PS-II are open	
F_m'	–	Maximal CF from light-adapted leaf		
F_v	–	Variable fluorescence from dark-adapted leaf	Represents the ability of PS-II to perform photosynthesis	
F_v'	–	Variable fluorescence from light-adapted leaf		
F_q'	$(F_m'-F')$	Difference in fluorescence between F_m' and F′	Photochemical quenching (PQ) due to open PS-II centres	Maxwell and Johnson (2000)
F_v/F_m	$(F_m-F_o)/F_m$	Maximum photosynthetic efficiency of PS-II	Maximum efficiency at which light is absorbed by antennae of PS-II	
F_q'/F_m'	$(F_m'-F')/F_m'$	PS-II operating efficiency	Estimates the efficiency at which light absorbed by PS-II antennae is used for photochemistry Also represented as YII or $\Delta F/F_m'$	
F_v'/F_m'	$(F_m'-F_o')/F_m'$	Maximum efficiency PS-II	Gives an estimate of operating efficiency if all the PS-II centres were open	
F_q'/F_v'	$(F_m'-F')/(F_m'-F_o')$	PS-II efficiency factor	Relates the PS-II maximum efficiency to the PS-II operating efficiency, known as the coefficient of photochemical quenching (qP)	
ETR	$PPFD \times 0.84 \times 0.5 \times (\Delta F/F_m')$	Electron transport rate	Electron transport rate through PS-II	
NPQ	$(F_m-F_m')/F_m'$	Non-photochemical quenching	Relates with the rate constant for heat loss from PS-II	

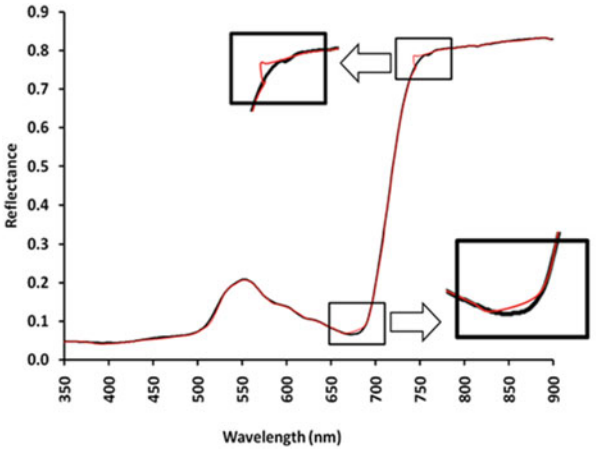

Fig. 7.6 Schematic representation of actual reflectance curve (black line) and CF- contaminated apparent reflectance curve (red line) of a groundnut crop

7.3 Sun-Induced Chlorophyll Fluorescence and Its Retrieval

Sun-induced chlorophyll fluorescence (SIF) is another synonymous term used for CF measured between red and far-red region (650–850 nm) under natural sunlight condition. SIF is commonly used term for remote estimation of CF using the reflected radiance upwelling from the plant canopy. SIF contribution to the reflected radiance is of the order of 2–5%, hence making it challenging to decouple the SIF signal from the reflected radiance (Maxwell and Johnson 2000). Figure 7.6 shows a representative illustration of the apparent reflectance hyperspectral curve measured with a field spectroradiometer (red line) overlaid on fluorescence-filtered actual reflectance hyperspectral curve (black line). Two peaks in the apparent reflectance can be observed at 690 and 740 nm showing feeble CF signals.

A number of techniques have been proposed to retrieve the SIF from the radiance data and have been explained in details in various reviews by Meroni et al. (2009), Liu et al. (2015a, b), Frankenberg and Berry (2018), Mohammed et al. (2019), Cendrero-Mateo et al. (2019), Ni et al. (2019), etc.

7.3.1 Fraunhofer Line Depth-Based Retrieval

To separate the SIF part from the reflected radiance, the principle of Fraunhofer line depth (FLD) is popularly utilized (Plascyk 1975; Plascyk and Gabriel 1975). FLD principle makes use of filling of the solar Fraunhofer lines (Hα: 656.4 nm, Fe: 758.8 nm and KI: 770.1 nm) or telluric oxygen absorption bands (O2-B: 687 nm,

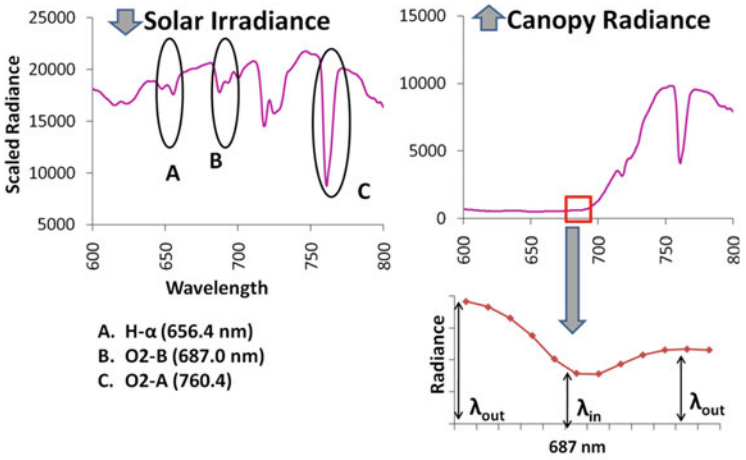

Fig. 7.7 Irradiance and radiance curve measured through ASD Fieldspec3 on the groundnut canopy and representation of 3-FLD principle

O2-A: 760 nm) to retrieve the SIF signal. FLD principle assumes that the reflectance and SIF are wavelength-independent within the narrow absorption bands and make use of radiance observations at two separate wavelengths: one within the absorption band and the other outside the absorption band (λ_{in} and λ_{out} in Fig. 7.7).

Since the upwelling radiance (L (λ)) from the canopy contains two components, i.e. reflected radiance and SIF, it can be mathematically expressed as

$$L(\lambda) = \frac{R(\lambda).E(\lambda)}{\pi} + F(\lambda) \tag{7.1}$$

where λ is the wavelength, R is actual reflectance (in fraction), E (λ) is the downwelling irradiance from the sun at λ wavelength, and F is the upwelling SIF from the canopy. Since L (λ) is directional in nature; hence, E (λ) is divided by π. The apparent reflectance from the canopy (R*(λ)) is computed as

$$R^*(\lambda) = \frac{\pi.L(\lambda)}{E(\lambda)} = R(\lambda) + \frac{\pi.F(\lambda)}{E(\lambda)} \tag{7.2}$$

SIF is retrieved through solving Eqs. 7.1 and 7.2 using the E and L observations inside (λ_{in}) and outside (λ_{out}) the absorption feature, i.e.

$$L(\lambda_{in}) = \left[R(\lambda_{in}).\frac{E(\lambda_{in})}{\pi}\right] + F(\lambda_{in}) \tag{7.3}$$

$$L\left(\lambda_{out}\right) = \left[R(\lambda_{out}).\frac{E(\lambda_{out})}{\pi}\right] + F\left(\lambda_{out}\right) \tag{7.4}$$

FLD principle is based on the assumption that the R (λ_{in}) ≅ R (λ_{out}), which dose not hold good for broad bandwidths. Hence, several modifications of FLD methods are suggested by various researchers. Maier et al. 2003 suggested a 3-FLD method that uses two λ_{out} and one λ_{in}. The 3-FLD method assumes a linear relation between R (λ_{in}) and R (λ_{out}). Another approach was presented by Gomez-Chova et al. (2006) and Moya et al. (2006) as cFLD, where they introduced two coefficients to account for changes in R and F at λ_{in} and λ_{out}. The iFLD method as suggested by Alonso et al. (2008) uses hyperspectral data to generate the correction factors for changes in R and F. The extended FLD (eFLD) method was demonstrated by Mazzoni et al. (2007). All the FLD methods exploit the radiance data and compute the SIF in its physical unit, i.e. $Wm^{-2}sr^{-1}\mu m^{-1}$.

Mohammed et al. (2019) have categorized the Fraunhofer line methods into two categories: (1) a physical based model applied at specified Fraunhofer line as utilized in GOSAT, OCO-2, and Sentinel-5P, and (2) a data-driven statistical approach using principal component analysis (PCA) or singular value decomposition (SVD) as in GOME-2-derived SIF. SIF retrieval using solar Fraunhofer lines requires high spectral resolution (better than 0.1 nm), high radiometric resolution, and very high signal-to-noise ratio (SNR), while the retrieval of SIF using telluric oxygen absorption features can be possible with the relatively coarser spectral resolution and relatively lower SNR.

7.3.2 Spectral Fitting Methods Based Retrieval

Spectral fitting method (SFM) is an improvement over FLD method for SIF retrieval where all available hyperspectral bands are utilized for R and F estimation at each wavelength through spectral curve fitting (Zhao et al. 2018; Cogliati et al. 2019). The SFM methods include fluorescence spectrum reconstruction (FSR) by Zhao et al. 2014, the full-spectrum spectral fitting (F-SFM) by Liu et al. (2015a, b), and the advanced FSR (aFSR) by Zhao et al. (2018). Different fitting functions are utilized for fluorescence spectrum reconstruction. A linear fitting function was applied by Meroni and Colombo 2006, quadratic function by Mazzoni et al. 2008, and n-degree polynomial by Guanter et al. 2009. To apply various SFM, a model named SpecFit was developed by Cogliati et al. (2015a, b) to construct full spectrum SIF using cubic spline fitting method.

7.3.3 *Reflectance-Based Retrieval*

Reflectance-based methods exploit the apparent reflectance measured at a specific wavelength in the range of 650–800 nm and convert it into an index to qualitatively express SIF information. The reflectance-based approach cannot estimate SIF in its physical unit. Spectral indices can be generated either using reflectance data (Zarco-Tejada et al. 2000a, b) or derivatives of the reflectance data (Zarco-Tejada et al. 2003). Most of the reflectance-based indices use the reflectance value at two-wavelength, one affected by SIF (near 685 and 740 nm) and other less or not affected by SIF.

Laboratory studies conducted by Zarco-Tejada et al. 2000a, b showed the sensitivity of few reflectance-based indices (eg. R_{680}/R_{630}, R_{685}/R_{630}, R_{687}/R_{630} and R_{690}/R_{630}) towards the maximum photosynthetic efficiency of PS-II (F_v/F_m). These indices showed a significant correlation with the diurnal changes in the F_v/F_m. In the same study, the red-edge-based derivative indices (e.g. D_{730}/D_{706} and DP21 (Dλp/D703), where D is the derivative of reflectance and λp is the inflection point of the reflectance spectrum in the red-edge spectral region) were also tested and related with the chlorophyll a and b content (C_{ab}) of the leaves. The red-edge region between 685 and 740 nm is most widely used to generate reflectance-based indices to utilize the double-peak feature of reflectance derivatives (Zarco-Tejada et al. 2000b, 2003; Das et al. 2014) in 690–710 nm region. The typical double-peak feature appears due to the combined effect of SIF emission and low C_{ab} content. A comprehensive list of reflectance-based indices used for the retrieval of SIF is listed in the review paper by Meroni et al. 2009. The reflectance-based indices are best suited for SIF retrieval in laboratory conditions where there is a lack of natural sunlight.

7.3.4 *Sun-Induced Chlorophyll Fluorescence Retrieval Using Radiative Transfer Models*

The recent approach for SIF retrieval is based on solving the process-based radiative transfer models (RTM) or energy balance models where the reflection and CF emission behaviour of leaf/canopy is simulated using biophysical and biochemical properties, bidirectional radiative distribution function (BRDF) of the plant. SIF emission from leaf/canopy is a complex response to environmental and physiological factors. To model the SIF emission, several RTM have been evolved in the last few decades; these include leaf-level models based on PROSPECT like FluorMODleaf (Pedrós et al. 2010) and Fluspect (Vilfan et al. 2016) and canopy-level models like FLSAIL model (Rosema et al. 1991), FluorSAIL (Miller et al. 2005), FluorFLIM model (Zarco-Tejada et al. 2013), SCOPE model (Vander Tol et al. 2009), and mSCOPE (Yang et al. 2017).

Table 7.2 List of parameters used in FluorMOD leaf (Pedros et al. 2010)

Symbol	Parameter name
N	Number of elementary plates, leaf structural parameter
C_{ab}	Total chlorophyll content
C_{cx}	Total carotenoid content
C_w	Equivalent water thickness
C_m	Dry matter content
σ_{II}/σ_I	Relative absorption cross section of PS-I and PS-II
τ_I and τ_{II}	Fluorescence quantum efficiency of PS-I and PS-II

7.3.4.1 FluorMOD-Based Retrieval

One of the widely used model at leaf-level SIF estimation is FluorMOD which is based on a hemispherical radiative transfer model, MODTRAN4, and an extension of leaf model PROSPECT-5 (Feret et al. 2008). The FluorMOD simulates the SIF of a fresh leaf between 640 and 840 nm for any excitation light of the visible spectrum (Pedros et al. 2010). The parameters used for FluorMOD are listed in Table 7.2.

FluorMOD also considers the reabsorption of emitted light within the leaf and estimate the upward and downward SIF between 400 and 700 nm. Further, a canopy level SIF model was developed by Verhoef (2005) as FluorSAIL. The FluorMODleaf and the FluorSAIL models were linked into a FluorMOD graphical user interface (GUI) by Zarco-Tejada et al. 2006 (Fig. 7.8). FluorMOD-GUI facilitates the simulation of SIF through varying the leaf and canopy attributes and is widely used for model calibration/validation.

7.3.4.2 Soil-Canopy Observation of Photosynthesis and Energy Flux-Based Retrieval

SCOPE model by Van der Tol et al. (2009) is a combination of energy balance, radiative transfer model and leaf biochemical model. The model simulates the radiation transport in a multilayer canopy as a function of solar zenith angle and leaf orientation to estimate the SIF in the view direction. Table 7.3 provides the lists of input parameters required by the SCOPE model for estimating the SIF.

SCOPE model is widely used recently to invert the vegetation functional properties like LAI, vegetation water content, and GPP using the satellite estimated SIF data (Zhang et al. 2014; Bayat et al. 2018; Hu et al. 2018; Pacheco-Labrador et al. 2019; Dutta et al. 2019). Celesti et al. (2018) have proposed a new method to retrieve the biophysical parameters from the canopy-level high-resolution apparent reflectance data using numerical inversion of the SCOPE model. In this model, a full spectrum of SIF is retrieved through computing the residual between the modelled and measured reflectance data.

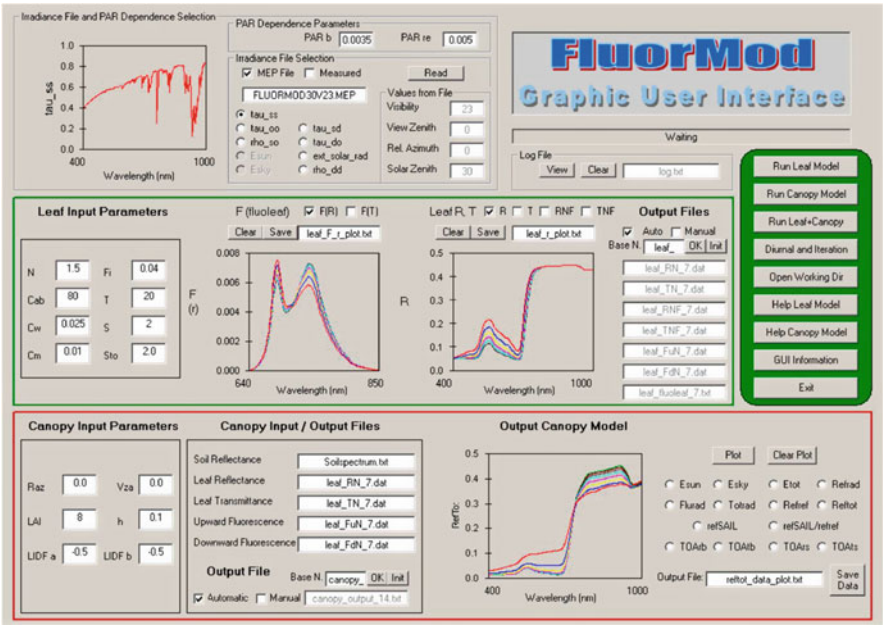

Fig. 7.8 GUI-based FluorMOD software. (Zarco-Tejada et al. 2006)

Table 7.3 The input parameters used for SCOPE simulations (Zhang et al. 2014)

Symbol	Parameters
C_{ab}	Chlorophyll a + b content
C_{dm}	Dry matter content
C_w	Leaf equivalent water thickness
C_s	Senescent material
N	Leaf structural parameters
$LIDF_{a,\ b}$	Leaf angle distribution parameter a and b
w	Leaf width
m	Ball-Berry stomatal conductance parameter
R_d	Dark respiration rate at 25 °C as fraction of V_{cmax}
λ_c	Cowan's water use efficiency parameter
ρ	Leaf thermal reflectance
τ	Leaf thermal transmittance
ρ_s	Soil thermal reflectance
LAI	Leaf area index
h_c	Canopy height

7.4 Ground and Airborne Instrumentation for Sun-Induced Chlorophyll Fluorescence Retrieval

Field instrumentation helps in understanding the SIF retrieval mechanism and its relationships with biophysical properties of the plant and facilitate upscaling from the canopy to the landscape levels (Porcar-Castell et al. 2014a, b). SIF retrieval at the canopy and regional scale is entirely based on the spectroscopic measurements. Since the SIF signal contributes a very small part of the reflected radiance, a highly specialized spectroradiometer with fine (FWHM 1–5 nm) or ultrafine (FWHM $<$1 nm) spectral resolution (SR) is required to capture the irradiance/radiance signal and to apply different FL-based or other retrieval techniques. Methods used for SIF retrieval depend on the SR and dynamic range of spectroradiometer; e.g. SFM and statistical-based retrieval methods require radiance/reflectance data with ultrafine resolution (Meroni et al. 2010; Guanter et al. 2013), while FLD-based retrieval using O2-A and O2-B bands may be possible with fine-resolution spectra (Plascyk 1975; Damm et al. 2011).

Although there is no instrument which directly provides the SIF value at the different wavelength the researcher customizes different models of spectroradiometer for indirect retrieval at canopy level based on its SR, sampling interval, noise equivalent delta radiance (nEΔL, signal to noise ratio), the field of view, etc. Table 7.4 lists some of the most widely used spectroradiometers for SIF retrieval at field scale.

Julitta et al. (2016) have compared four different spectroradiometers and concluded that for accurate far-red (740 nm) SIF retrieval, an SR less than 1.0 nm is required, while red SIF (690 nm) retrieval requires better than 0.5 nm SR. A detailed review about the instrument setup, protocols, and sensor characteristics for SIF retrieval is presented in Pacheco-Labrador et al. (2019), Aasen et al. (2019), and Cendrero-Mateo et al. (2019). Liu et al. (2015a, b) have presented the effect of SR and SNR on the canopy-level SIF retrieved using FLD methods. Ground-based spectrometers/radiometers are mostly customized as per the requirement for SIF estimation.

There are various customized SIF measuring systems which are being used for field-based applications or validation of the satellite-derived SIF. Most of them are customization of Ocean Optics sensors. Ocean Optics HR2000-based systems include TriFLEX used by CRNS France (Daumard et al. 2012) and FluoSpec by Brown University (Yang et al. 2015). Ocean Optics HR4000-based systems are S-FLUO box by JRC and JB Hyperspectral, Germany (Julitta et al. 2016); Multiplexer Radiometer Irradiometer (MRI) by University of Milan-Bicocca, Milan, Italy (Cogliati et al. 2015a, b); etc. Ocean Optics QE Pro-based systems are FluoSpec2 by the University of Virginia (Yang et al. 2018a, b); FloX by JB Hyperspectral, Germany (Wohlfahrt et al. 2018); and PICCOLO-DOPPIO, University of Edinburgh, Scotland (Mac Arthur et al. 2014).

Recently, a tower-based permanent mounted radiometer is becoming popular for simultaneously measuring the SIF, carbon, and water fluxes from agroecosystems or

Table 7.4 List of commonly used spectroradiometers for estimation of SIF

Instrument	Spectral range (nm)	FWHM (nm)	Sampling interval (nm)	SNR	Imaging/non-imaging
Ocean Optics HR4000 narrow range	670–857	0.2	0.05	250	Non-imaging
Ocean Optics MAYA	650–803	0.44	0.08	450	Non-imaging
Ocean Optics QE Pro	645–810	0.5	0.17	1080	Non-imaging
Ocean optics HR4000 full range	197–1115	1.0	0.3	590	Non-imaging
ASD FieldSpec Pro	350–2500	3.0	1.4	4000	Non-imaging
Spectra Vista GER 1500	350–1050	3.2	1.0	4000	Non-imaging
Headwall photonics Hyperspec	670–780	0.25	0.05	680	Imagine
HySpex Mjolnir VS-620	400–1000	3.0	1.0	180	Imagine
ROSIS	430–860	7.0	4.0	–	Imagine
CASI	350–2500	2.2	1.4	480	Imagine
APEX	380–2500	5.7	1.75	625	Imagine
HyPlant	670–780	0.25	0.11	210	Imagine
NASA/JPL CFIS	737–772	<0.1	0.05	–	Imagine

ROSIS Reflective Optics System Imaging Spectrometer, *CASI* Compact Airborne Spectrographic Imager, *APEX* Airborne Prism Experiment

forest ecosystems. FUSION is one such prototype developed by Goddard's Space Flight Center, NASA, by assembling two ocean optics spectrometers USB 4000 and HR 4000 (Julitta et al. 2016). Other tower-mounted SIF measuring systems are AutoSIF (Xu et al. 2018), PhotoSpec (Grossmann et al. 2018), etc.

Hyperspectral imagers are being used for UAV and airborne observations. Most of the hyperspectral imagers are coarser in SR, and the SIF estimations are mostly based on the reflectance derived indices or radiative transfer modelling. The list of the few airborne sensors used for SIF studies is in Table 7.4. HyPlant, CFIS, and Hyperspec are few airborne sensors that have been dedicatedly made for full-range SIF retrieval for satellite-derived SIF data validation. A detailed review of various instruments and systems for SIF measurements can be found in Bandopadhyay et al. (2020).

7.5 Satellite-Based Sun-Induced Chlorophyll Fluorescence Retrieval and Products

The first dedicated SIF measuring satellite Fluorescence Explorer (FLEX) is planned for launch in 2022 by European Space Agency (ESA). FLEX along with the tandem mission of Sentinel-3 (S-3) will focus on the measurement of SIF along with reflectance and surface temperature so that the SIF signal can be interpreted precisely

at regional scales (Mohammed et al. 2014). The FLEX mission will consist of two imaging spectroradiometer, i.e. FLORIS-HR and FLORIS-LR. The FLORIS-HR will be operating in red (O2-B, 677–697 nm) and far-red (O2-A, 740–780 nm) region separately and will produce the spectral data with 0.3 nm SR. While FLORIS-LR will collect the data in 500–780 nm range with SR of 2 nm. The Swath of FLEX mission will be 150 km with a ground sampling of 300 m and repetitivity of less than 27 days (Vicent et al. 2016).

Till now, the SIF retrieval is being carried out using the high-resolution radiance data from the atmospheric satellites meant for measuring atmospheric trace gas concentrations. The first attempt for SIF retrieval for the land surface was done by Guanter et al. (2007) using Medium Resolution Imaging Spectrometer (MERIS) sensor onboard Envisat-1 satellite. The first global coverage of far-red SIF data was produced using TANSO-FTS sensor on GOSAT satellite with the independent efforts by Frankenberg et al. (2011a, b), Joiner et al. (2012), and Guanter et al. (2012). SIF retrieval algorithms were further applied on Scanning Imaging Absorption spectrometer for Atmospheric Chartography (SCIAMACHY) sensor onboard Envisat (Joiner et al. 2012; Wolanin et al. 2015; Köhler et al. 2015; Khosravi et al. 2015), on Global Ozone Monitoring Experiment 2 (GOME-2) sensor onboard MetOP satellite (Joiner et al. 2013), on high-resolution Orbiting Carbon Observatory 2 (OCO-2) satellite data (Frankenberg et al. 2014), on Atmospheric Carbon dioxide Grating Spectroradiometer (AGCS) onboard TanSat satellite (Du et al. 2018), and TROPOspheric Monitoring Instrument (TROPOMI) onboard Sentinel-5P (Kohler et al. 2018). Currently, global SIF data from GOME-2, OCO-2, and TROPOMI are freely available for scientific communities to perform regional vegetation studies. The specifications of SIF products from the current sensors are listed in Table 7.5.

Table 7.5 Current SIF products from satellite

Sensors (Satellite)	Ground footprint (km × km)	Temporal resolution (days)	FWHM (nm)	Retrieval method
TANSO-FTS (GOSAT)	10 * 10	3	0.025	FLD at KI band (769.9–770.25 nm)
GOME-2 (MetOp)	40 * 40	29	0.5	Filling-in of the O2-A band (principal component approach)
OCO-2	1.3 * 2.2	16	0.04	Radiative transfer model using O2-A band
TROPOMI (Sentinel-5P)	7*7	16	0.5	Filling-in of the O2-A band (principal component approach)
ACGS (TanSat)	2 * 2	16	0.04	Statistical method (singular vector decomposition, SVD)

7.6 Applications of Chlorophyll Fluorescence

Chlorophyll fluorescence parameters provide a deep insight into the photosynthesis machinery especially photosystem-II; hence, it is a very useful tool to study the vegetation response to radiation (Falkowski and Raven 2013). CF has a wide range of applications from estimation of chlorophyll concentration to regional-level productivity assessment, from aquatic to land vegetations, from varietal screening to stress adaptation studies, etc. (Baker and Rosenqvist 2004; Guo and Tan 2015). There are vast applications of CF on oceanic phytoplankton, aquatic plants, and forest vegetation; however, this section is emphasized on the agricultural applications. Both the active (PAM-based CF) and passive (SIF) measurement methods provide the information on photosynthesis mechanism, but their measurement protocols are different in terms of physical units, intensity, and wavelength. PAM-based instruments can measure the CF parameters (e.g. F_v/F_m, F_v'/F_m', ETR, NPQ) and have vast applications at leaf and molecular level. On the other hand, the SIF-based instruments cannot measure the CF parameters but has added advantages to measure CF at different wavelengths and at canopy or field level. Figure 7.9 depicts various applications of CF in plant/crop related studies and researches. For the sake of simplicity, the applications of CF in agriculture are discussed in following three subsections.

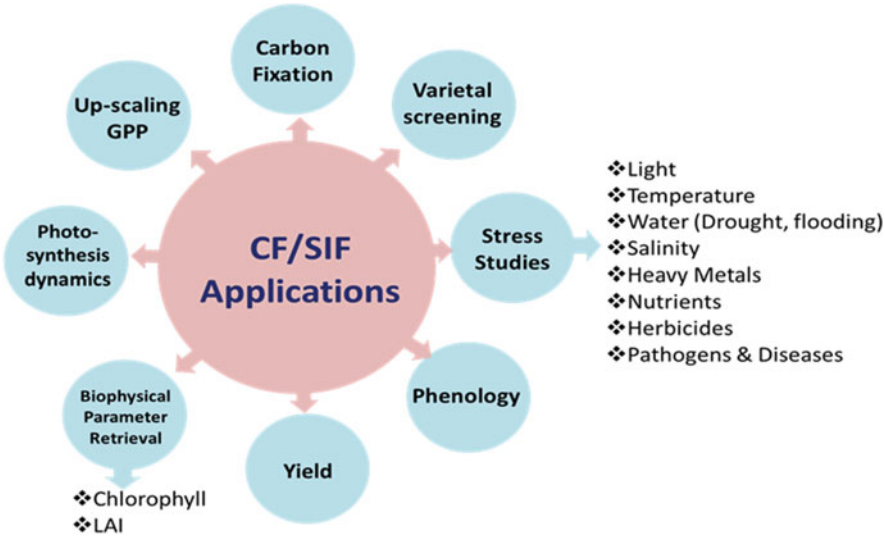

Fig. 7.9 Applications of CF in crop-related studies

7.6.1 Applications of Pulse-Amplitude Modulation-Based Chlorophyll Fluorescence

Active measurement of CF through PAM instruments provides a rapid, reliable, non-destructive, and cost-effective method for monitoring the health condition of vegetation. PAM instruments can measure a number of quenching parameters under various protocols (dark-adapted, light-adapted, continuous quenching analysis) which can be related to the leaf biophysical/biochemical properties, gaseous exchanges, and photochemistry. PAM-derived CF indices are used in many of the studies for assessing the PS-II status under drought stress (Fracheboud and Leipner 2003; Woo et al. 2008; Mishra et al. 2012), flooding stress (Ezin et al. 2010; Caudle and Maricle 2012), light stress (Critchley and Smillie 1981; Van Kooten and Snel 1990; Lichtenthaler and Burkart 1999), chilling stress (Zhang et al. 2010; Kalaji et al. 2016), heat stress (Wu et al. 2014; Azam et al. 2015), salinity stress (Dkhil and Denden 2012), nutrient stress (Afzal et al. 2014), heavy metal toxicity (Paunov et al. 2018), herbicidal stress (Liu et al. 2013; Guo and Tan 2015), and pathogens and diseases (Ivanov and Bernards 2016).

Abiotic stress like drought changes the photosynthetic activity which intern is reflected in the chlorophyll-a concentration of leaves. CF parameters like dark-adapted F_v/F_m and light-adapted F_v'/F_m' help in understanding the structure and function of PS-II (Longenberger et al. 2009). It is now proven that a permanent decrease in F_v/F_m and F_v'/F_m' is a reliable indicator of low efficiency of PS-II because of photoinhibition. Figure 7.10 shows the effect of imposed water stress on the fluorescence parameters, viz. photochemical efficiency and photosynthetic yield of a cotton cultivar which were highly correlated with the measured leaf properties like chlorophyll content index, stomatal conductance, and leaf temperature (Choudhary et al. 2013).

Figure 7.11 depicts the spectral reflectance curve and fluorescence parameters, viz. F′, Fm′, and Y (II) of different irrigation treatments on groundnut crop. It can be observed that at the optimum irrigation level, i.e. irrigation water to cumulative pan evaporation (IW:CPE ratio) of 0.8, the CF parameters were at its maximum, while they decrease on either side because of the lack of or excess of water (Choudhary et al. 2014). Spectral properties can further be correlated with the CF parameters.

Nutrient deficiency also affects the structure and function of PS-II, but in this case, the F_v/F_m is not so sensitive parameter. CF-based parameters like performance index using observations on the multiple leaves were found to be highly correlated with the nutrient deficiencies (Živčák et al. 2014). For the plants under salinity stress, the F_v/F_0 ratio and ETR decrease significantly (Pereira et al. 2000). Likewise, with the quenching parameters, it is possible to differentiate between different crop stresses, and hence, CF is considered to be an important tool for screening varieties of crops for different stress (Narina et al. 2014).

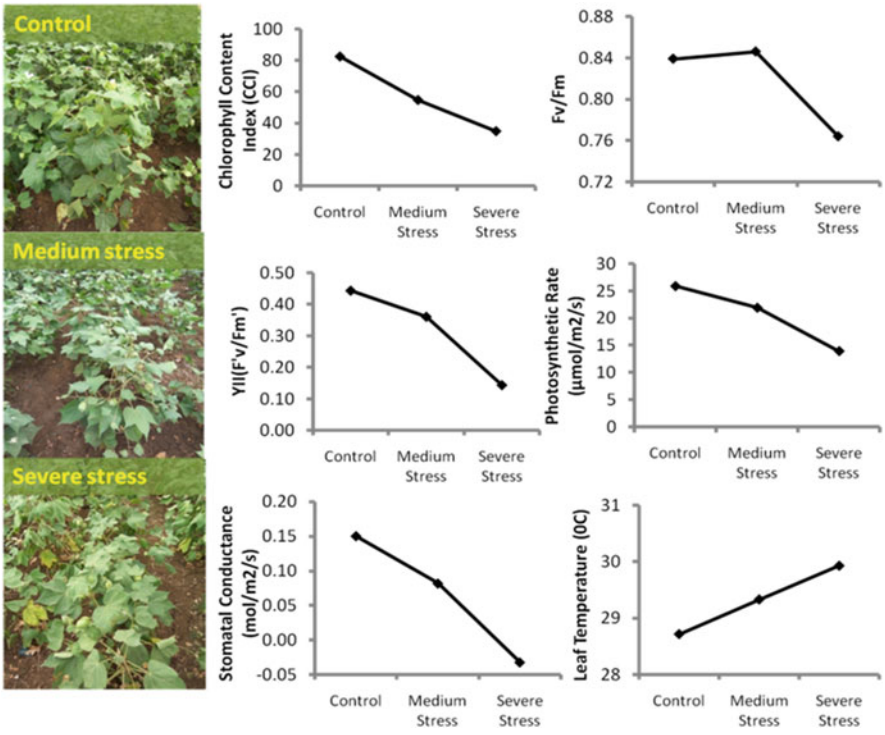

Fig. 7.10 Effect of water stress on the PAM fluorescence parameters and leaf properties of a cotton cultivar GIHV218

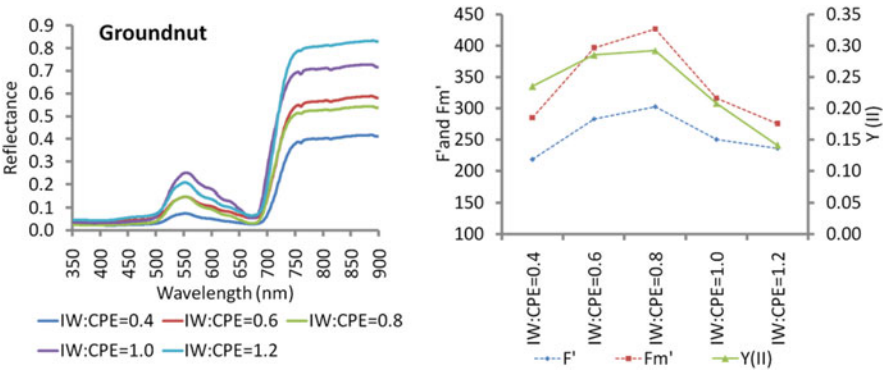

Fig. 7.11 Effect of different irrigation treatments on the PAM fluorescence parameters and leaf spectral properties of a groundnut cultivar

7.6.2 *Applications of Sun-Induced Chlorophyll Fluorescence*

Remote sensing of CF is based on the retrieval of SIF and its applications to understanding the dynamic changes in the photosynthetic machinery. Unlike PAM-based CF measurements, SIF is measured in a very narrow spectral range and is highly sensitive to the ambient light conditions. Most of the SIF applications are linked to the seasonal dynamic of photosynthesis measured from permanent towers, airborne platform, or satellites (Rascher et al. 2009). Successful SIF retrieval from the tower and its applications are presented by Rossini et al. (2010a, b, 2016) and Drolet et al. (2014). Zarco-Tejada and co-workers have made significant progress in the airborne SIF for its applications from stress detection to parameter retrieval (Zarco-Tejada et al. 2009, 2013). Satellite-based SIF applications for regional productivity assessment, stress detection, etc. were demonstrated by Damm et al. (2010), Zhang et al. (2016), Wagle et al. (2016), and Wei et al. (2018). Some of the reviewed applications of the SIF are summarized below:

7.6.2.1 Sun-Induced Chlorophyll Fluorescence for Water Stress Monitoring

GOME-2-derived SIF were correlated with tower-based GPP to assess and monitor the drought of 2012 in Great Plains by Wang et al. 2016. They found a significant correlation between SIF and palmer drought severity index. They concluded that the SIF is more sensitive than NDVI for drought assessment during peak growing season. Leaf-level early water stress was detected by Ni 2016 using SIF derived from FLD method and SCOPE-based modelling. Hsiao et al. (2010) suggested a dynamic fluorescence index (DFI), derived from LED-based fluorescence imaging, to detect the seedling water stress.

7.6.2.2 Sun-Induced Chlorophyll Fluorescence for Productivity Assessment

Numerous work has been carried out on SIF-GPP relationship at canopy level from spectroradiometer data and at regional level from satellite-derived SIF data, and it was concluded that the far-red SIF is significantly correlated with the fAPAR and GPP (Rossini et al. 2010a, b; Yang et al. 2015). Figure 7.12 shows the monthly average SIF data derived from GOME-2 sensor for the Indian subcontinent and its relationship with flux-tower measured GPP.

Regional net primary production (NPP) was correlated with the GOME-2 SIF for consecutive 3 years by Patel et al. 2018 and found a better agreement than the integrated NDVI. High-resolution SIF (1.35 km $\times$ 2.25 km) from OCO-2 satellite showed a significant correlation with flux tower-based GPP for midday and daily time scale (Li et al. 2018). Duveiller and Cescatti (2016) downscale the GOME-2

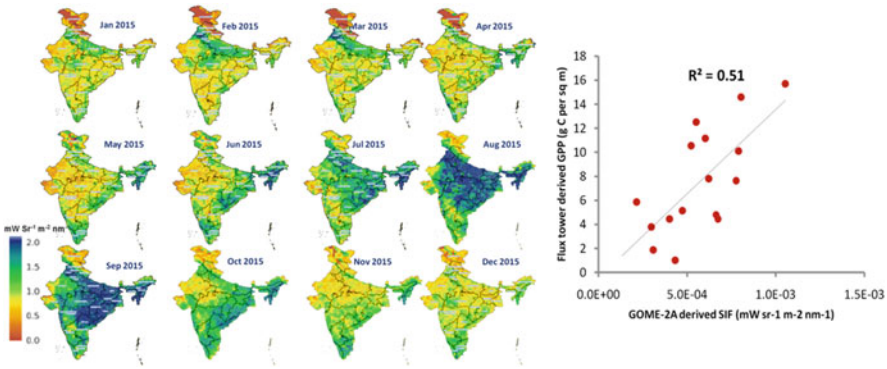

Fig. 7.12 Monthly averaged GOME 2A SIF data and its relationship with flux tower (located rice crop at Maruteru, Andhra Pradesh, India)-derived monthly average GPP (Unpublished work)

data from 0.50 to 0.05 and showed its agreement with the GPP at a smaller scale. Smith et al. 2018 analysed GOME-2 SIF, OCO-2 SIF, and flux tower-based GPP data and concluded that the SIF can successfully capture seasonal and inter-annual GPP dynamics. Scale issues between SIF and GPP have been addressed by Wood et al. 2017. Wei et al. 2019 used OCO-2 SIF at 757 and 771 nm for predicting autumn crop production in China. In this study, SIF outperformed the MODIS-derived indices. Recently Peng et al. (2020) have gone one step ahead and applied OCO-2, TROPOMI, and GOME-2 SIF data along with broadband vegetation indices for crop-specific yield assessment of soybean and maize.

7.6.2.3 Sun-Induced Chlorophyll Fluorescence for Nutrient Stress Studies

Subhash and Mohanan (1997) used laser-induced SIF intensity ratio, i.e. F_{690}/F_{730} to identify nutrient stress in sunflower. They used curve fitting method (Gaussian spectral function) to derive fluorescence intensity from laser-induced fluorescence spectra. Cendrero Mateo in his PhD thesis (Cendrero Mateo 2013) has concluded that daily SIF dynamics is able to differentiate the water and nitrogen stress in wheat crop. Belanger et al. 2007 used different fluorescence ratios to the detection of nitrogen stress in potato. Photosynthetic activities under cadmium stress on tomato crop were studied by Cherif et al. (2011) using red and far-red SIF retrieved from Ocean Optics USB 4000 spectrometer.

7.7 Challenges in Sun-Induced Chlorophyll Fluorescence Retrieval

Detangling SIF signal from reflected radiance data is the major core area of research in SIF spectrometry. The current SIF products rely on one wavelength or a narrow bandwidth; future challenge lies in estimating the full range SIF, i.e. from 670 to 760 nm. Satellite-derived SIFs are mainly concentrated to the far-red SIF, while the red SIF is even more important for plant research as it is linked with the PS-II. There is a need to standardize and harmonize the SIF retrieval method as each method (e.g. FLD, SFM, RTM) has its pros and cons (Frankenberg and Berry 2018). Better atmospheric correction to reduce the bias in SIF estimate is the next requirement. SIF retrieved from the radiative transfer modelling requires canopy parameters to build a sound reflectance model; hence, further research is needed to quantify these canopy parameters. SIF-based product validation depends on the ground instrumentation networks which are sparse. The SR and SNR need to be further improved for accurate ground-based SIF retrieval.

7.8 Conclusions

Chlorophyll fluorescence is a mechanism to dissipate the excess energy absorbed by the photosynthetic machinery in plant leaves at some higher wavelength than the absorbed one. Quenching analysis helps in finding the proportion of light participating in photochemical (photosynthesis) processes, non-photochemical processes, and fluorescence. Chlorophyll fluorescence emits in the range of 670–760 nm with two peaks, one at 690 nm (red SIF) and other 740 nm (far-red SIF). As the SIF contributes only 2–5% of the reflected radiance, its retrieval is challenging. Various retrieval techniques have been proposed in which the FLD-based retrieval is the most popular, while RTM-based retrieval is more process-oriented. Instrumentation specifications are being tuned for SIF retrieval and have been demonstrated in recent studies from the ground and aerial platforms for successful SIF retrieval. Satellite-based SIF retrieval techniques have been successfully demonstrated for few atmospheric satellites like GOSAT-TANSOFTS, MetOp-GOME-2, OCO-2, and Sentinel 5P- TROPOMI . These SIF products were applied for the regional estimation of productivity, stress detection, and phenological studies. The future of vegetation remote sensing lies in the successful retrieval of SIF signals at a more disaggregated level. ESA-FLEX mission of 2022 is one step toward this effort.

Acknowledgements We would like to acknowledge Dr. CS Murthy (Group Director, ASAG), Dr. KV Ramana (GD, PPEG), Deputy Director (RSA), and Director (NRSC) for facilitating data collection and analysis and their constant encouragements to write this review.

References

Aasen H, Van Wittenberghe S, Sabater Medina N, Damm A, Goulas Y, Wieneke S, Hueni A, Malenovský Z, Alonso L, Pacheco-Labrador J, Cendrero-Mateo MP (2019) Sun-induced chlorophyll fluorescence II: review of passive measurement setups, protocols, and their application at the leaf to canopy level. Remote Sens 11(8):927

Afzal A, Gulzar I, Shahbaz M, Ashraf M (2014) Water deficit-induced regulation of growth, gas exchange, chlorophyll fluorescence, inorganic nutrient accumulation and antioxidative defense mechanism in mungbean [*Vigna radiata* (L.) Wilczek]. J Appl Bot Food Qual 8:87

Alonso L, Gomez-Chova L, Vila-Frances J, Amoros-Lopez J, Guanter L, Calpe J, Moreno J (2008) Improved Fraunhofer line discrimination method for vegetation fluorescence quantification. IEEE Geosci Remote Sens Lett 5(4):620–624

Azam F, Chang X, Jing R (2015) Mapping QTL for chlorophyll fluorescence kinetics parameters at seedling stage as indicators of heat tolerance in wheat. Euphytica 202(2):245–258

Baker NR (2008) Chlorophyll fluorescence: a probe of photosynthesis in vivo. Annu Rev Plant Biol 2(59):89–113

Baker NR, Rosenqvist E (2004) Applications of chlorophyll fluorescence can improve crop production strategies: an examination of future possibilities. J Exp Bot 55(403):1607–1621

Bandopadhyay S, Rastogi A, Juszczak R (2020) Review of top-of-canopy sun-induced fluorescence (SIF) studies from ground, UAV, airborne to spaceborne observations. Sensors 20(4):1144

Bayat B, van der Tol C, Verhoef W (2018) Integrating satellite optical and thermal infrared observations for improving daily ecosystem functioning estimations during a drought episode. Remote Sens Environ 209:375–394

Bélanger MC, Viau AA, Samson G, Chamberland M (2007) Comparison of reflectance and fluorescence spectroscopy for the detection of nitrogen deficiency in potato plants. Can J Remote Sens 33(2):69–80

Bendall DS, Manasse RS (1995) Cyclic photophosphorylation and electron transport. Biochimica et Biophysica Acta (BBA)-Bioenergetics 1229(1):23–38

Brewster D (1834) Observations on the lines of the solar Spectrum, and on those produced by the Earth's Atmosphere, and by the action of Nitrous Acid Gas. Earth Environ Sci Trans R Soc Edinb 12(2):519–530

Caudle KL, Maricle BR (2012) Effects of flooding on photosynthesis, chlorophyll fluorescence, and oxygen stress in plants of varying flooding tolerance. Trans Kans Acad Sci 115(1/2):5–18

Celesti M, van der Tol C, Cogliati S, Panigada C, Yang P, Pinto F, Rascher U, Miglietta F, Colombo R, Rossini M (2018) Exploring the physiological information of Sun-induced chlorophyll fluorescence through radiative transfer model inversion. Remote Sens Environ 15 (215):97–108

Cendrero Mateo MP (2013) Chlorophyll fluorescence response to water and nitrogen deficit, PhD thesis, Graduate College, The University of Arizona

Cendrero-Mateo MP, Wieneke S, Damm A, Alonso L, Pinto F, Moreno J, Guanter L, Celesti M, Rossini M, Sabater N, Cogliati S (2019) Sun-induced chlorophyll fluorescence III: benchmarking retrieval methods and sensor characteristics for proximal sensing. Remote Sens 11(8):962

Cherif J, Derbel N, Nakkach M, Mediouni C, Von Bergmann H, Jemal F, Ben Lakhdar Z (2011) Detection of photosynthetic activity under cadmium stress by measurement of the red and far-red chlorophyll fluorescence. Int J Remote Sens 10(32):4233–4248

Choudhary KK, Ramana KV, Sesha Sai MVR (2013) Chlorophyll Fluorescence as Crop Stress Indicator Pixel2people 5(1): 5

Choudhary KK, Srikanth P, Ramana KV, Sesha Sai MVR, Kameshwara Rao SVC (2014) Retrieval of steady state chlorophyll fluorescence in groundnut and safflower using ground based hyperspectral data, poster presented at ISPRS TC VIII midterm technical symposium at Hyderabad, India

Cogliati S, Rossini M, Julitta T, Meroni M, Schickling A, Burkart A, Pinto F, Rascher U, Colombo R (2015a) Continuous and long-term measurements of reflectance and sun-induced chlorophyll fluorescence by using novel automated field spectroscopy systems. Remote Sens Environ 164:270–281

Cogliati S, Verhoef W, Kraft S, Sabater N, Alonso L, Vicent J, Moreno J, Drusch M, Colombo R (2015b) Retrieval of sun-induced fluorescence using advanced spectral fitting methods. Remote Sens Environ 169:344–357

Cogliati S, Celesti M, Cesana I, Miglietta F, Genesio L, Julitta T, Schuettemeyer D, Drusch M, Rascher U, Jurado P, Colombo R (2019) A spectral fitting algorithm to retrieve the fluorescence Spectrum from canopy radiance. Remote Sens 11(16):1840

Critchley C, Smillie RM (1981) Leaf chlorophyll fluorescence as an indicator of high light stress (photoinhibition) in Cucumis sativus L. Funct Plant Biol 8(2):133–141

Damm A, Elbers JA, Erler A, Gioli B, Hamdi K, Hutjes R, Kosvancova M, Meroni M, Miglietta F, Moersch A, Moreno J (2010) Remote sensing of sun-induced fluorescence to improve modeling of diurnal courses of gross primary production (GPP). Global Chang Biol l16(1):171–186

Damm A, Erler A, Hillen W, Meroni M, Schaepman ME, Verhoef W, Rascher U (2011) Modeling the impact of spectral sensor configurations on the FLD retrieval accuracy of sun-induced chlorophyll fluorescence. Remote Sens Environ 115(8):1882–1892

Das PK, Choudhary KK, Laxman B, Kameswara Rao SV, Seshasai MV (2014) A modified linear extrapolation approach towards red edge position detection and stress monitoring of wheat crop using hyperspectral data. Int J Remote Sens 35(4):1432–1449

Daumard F, Goulas Y, Champagne S, Fournier A, Ounis A, Olioso A, Moya I (2012) Continuous monitoring of canopy level sun-induced chlorophyll fluorescence during the growth of a sorghum field. IEEE Trans Geosci Remote Sens 50(11):4292–4300

Dkhil BB, Denden M (2012) Effect of salt stress on growth, anthocyanins, membrane permeability and chlorophyll fluorescence of Okra (Abelmoschusesculentus L.) seedlings. Am J Plant Physiol 7(4):174–183

Drolet G, Wade T, Nichol CJ, MacLellan C, Levula J, Porcar-Castell A, Nikinmaa E, Vesala T (2014) A temperature-controlled spectrometer system for continuous and unattended measurements of canopy spectral radiance and reflectance. Int J Remote Sens 35(5):1769–1785

Du S, Liu L, Liu X, Zhang X, Zhang X, Bi Y, Zhang L (2018) Retrieval of global terrestrial solar-induced chlorophyll fluorescence from Tan Sat satellite. Sci Bull 63(22):1502–1512

Dutta D, Schimel DS, Sun Y, van der Tol C, Frankenberg C (2019) Optimal inverse estimation of ecosystem parameters from observations of carbon and energy fluxes. Biogeosciences 16 (1):77–103

Duveiller G, Cescatti A (2016) Spatially downscaling sun-induced chlorophyll fluorescence leads to an improved temporal correlation with gross primary productivity. Remote Sens Environ 182:72–89

Duysens LN, Sweers HE (1963) In: Japanese society of plant physiologists (ed) Studies on microalgae and photosynthetic bacteria. University of Tokyo Press, Tokyo 353–372

Edwards GE, Baker NR (1993) Can CO2 assimilation in maize leaves be predicted accurately from chlorophyll fluorescence analysis? Photosynth Res 37:89–102

Ezin V, Pena RD, Ahanchede A (2010) Flooding tolerance of tomato genotypes during vegetative and reproductive stages. Braz J Plant Physiol 22(2):131–142

Falkowski PG, Raven JA (2013) Aquatic photosynthesis. Princeton University Press, Oxford

Feret JB, François C, Asner GP, Gitelson AA, Martin RE, Bidel LP, Ustin SL, Le Maire G, Jacquemoud S (2008) PROSPECT-4 and 5: advances in the leaf optical properties model separating photosynthetic pigments. Remote Sens Environ 16(112/6):3030–3043

Fracheboud Y, Leipner J (2003) The application of chlorophyll fluorescence to study light, temperature, and drought stress. In: Practical applications of chlorophyll fluorescence in plant biology. Springer, Boston, pp 125–150

Frankenberg C, Berry J (2018) Solar induced chlorophyll fluorescence: origins, relation to photosynthesis and retrieval. In: Reference module in earth systems and environmental sciences, Elsevier Inc

Frankenberg C, Butz A, Toon GC (2011a) Disentangling chlorophyll fluorescence from atmospheric scattering effects in O2 A-band spectra of reflected sun-light. Geophys Res Lett 38(3): L03801

Frankenberg C, Fisher JB, Worden J, Badgley G, Saatchi SS, Lee JE, Toon GC, Butz A, Jung M, Kuze A, Yokota T (2011b) New global observations of the terrestrial carbon cycle from GOSAT: patterns of plant fluorescence with gross primary productivity. Geophys Res Lett 38 (17)

Frankenberg C, O'Dell C, Berry J, Guanter L, Joiner J, Köhler P, Pollock R, Taylor TE (2014) Prospects for chlorophyll fluorescence remote sensing from the Orbiting Carbon Observatory-2. Remote Sens Environ 5:147):1–147):2

Genty B, Briantais JM, Baker NR (1989) The relationship between the quantum yield of photosynthetic electron transport and quenching of chlorophyll fluorescence. Biochim Biophys Acta 990:87–92

Genty B, Wonders J, Baker NR (1990) Non-photochemical quenching of F0 in leaves is emission wavelength dependent: consequences for quenching analysis and its interpretation. Photosynth Res 26:133–139

Gomez-Chova L, Alonso-Chorda L, Amoros-Lopez J, Vila-Frances J, Del Valle-Tascon S, Calpe J, Moreno J (2006) Solar induced fluorescence measurements using a field spectroradiometer. AIP Conf Proc 852:274–281

Govindjee (1995) Sixty-three years since Kautsky: chlorophylla fluorescence. Aust J Plant Physiol 22:131–160

Govindjee G (2004) Chlorophyll a fluorescence: a bit of basics and history. Chlorophyll a fluorescence: a signature of photosynthesis. Springer, Dordrecht, pp 1–42

Grossmann K, Frankenberg C, Magney TS, Hurlock SC, Seibt U, Stutz J (2018) Photo spec: a new instrument to measure spatially distributed red and far-red solar-induced chlorophyll fluorescence. Remote Sens Environ 216:311–327

Guanter L, Alonso L, Gómez-Chova L, Amorós-López J, Vila J, Moreno J (2007) Estimation of solar-induced vegetation fluorescence from space measurements. Geophys Res Lett 34(8): L08401

Guanter L, Segl K, Kaufmann H, Verhoef W, Gomez-Chova L, Alonso L (2009) Atmospheric corrections for fluorescence signal retrieval. Final Report ESA— ESTEC Contract 20882/07/NL/LvH

Guanter L, Frankenberg C, Dudhia A, Lewis PE, Gómez-Dans J, Kuze A, Suto H, Grainger RG (2012) Retrieval and global assessment of terrestrial chlorophyll fluorescence from GOSAT space measurements. Remote Sens Environ 1(121):236–251

Guanter L, Rossini M, Colombo R, Meroni M, Frankenberg C, Lee JE, Joiner J (2013) Using field spectroscopy to assess the potential of statistical approaches for the retrieval of sun-induced chlorophyll fluorescence from ground and space. Remote Sens Environ 15(133):52–61

Guo Y, Tan J (2015) Recent advances in the application of chlorophyll a fluorescence from photosystem II. Photochem Photobiol 91(1):1–4

Hsiao SC, Chen S, Yang IC, Chen CT, Tsai CY, Chuang YK, Wang FJ, Chen YL, Lin TS, Lo YM (2010) Evaluation of plant seedling water stress using dynamic fluorescence index with blue LED-based fluorescence imaging. Comput Electron Agric 72(2):127–133

Hu L, Fan W, Ren H, Liu S, Cui Y, Zhao P (2018) Spatiotemporal dynamics in vegetation GPP over the great khingan mountains using GLASS products from 1982 to 2015. Remote Sens 10(3):488

Ivanov DA, Bernards MA (2016) Chlorophyll fluorescence imaging as a tool to monitor the progress of a root pathogen in a perennial plant. Planta 243(1):263–279

Johnson MP (2016) Photosynthesis. Essays Biochem 60:255–273

Johnson WM, Barlow EA, Brucker GG (1990) Inventors; Schneider USA Inc, assignee. Hemostasis Valve United States Patent US 4(932):633

Joiner J, Yoshida Y, Vasilkov AP, Middleton EM, Campbell PKE, Yoshida Y, Kuze A, Corp LA (2012) Filling-in of near-infrared solar lines by terrestrial fluorescence and other geophysical effects: simulations and space-based observations from SCIAMACHY and GOSAT. Atmos Meas Tech 5:809–829

Joiner J, Guanter L, Lindstrot R, Voigt M, Vasilkov AP, Middleton EM, Huemmrich KF, Yoshida Y, Frankenberg C (2013) Global monitoring of terrestrial chlorophyll fluorescence from moderate spectral resolution near-infrared satellite measurements: methodology, simulations, and application to GOME-2. Atmos Meas Tech 6:2803–2823

Julitta T, Corp LA, Rossini M, Burkart A, Cogliati S, Davies N, Hom M, Arthur AM, Middleton EM, Rascher U (2016) Comparison of sun-induced chlorophyll fluorescence estimates obtained from four portable field spectroradiometers. Remote Sens 8:122

Kalaji HM, Jajoo A, Oukarroum A, Brestic M, Zivcak M, Samborska IA, Cetner MD, Łukasik I, Goltsev V, Ladle RJ (2016) Chlorophyll a fluorescence as a tool to monitor physiological status of plants under abiotic stress conditions. Acta Physiol Planta 38(4):102

Kautsky H, Hirsh A (1931) Chlorophyllfluoreszenz und kohlensäuereassimilation. Naturwissen 48:964

Khosravi N, Vountas M, Rozanov VV, Bracher A, Wolanin A, Burrows JP (2015) Retrieval of terrestrial plant fluorescence based on the in-filling of far-red fraunhofer lines using SCIAMA CHY observations. Front Environ Sci 17(3):78

Kitajima MB, Butler WL (1975) Quenching of chlorophyll fluorescence and primary photochemistry in chloroplasts by dibromothymoquinone. Biochimica et Biophysica Acta (BBA)-Bioenergetics 376(1):105–115

Köhler P, Guanter L, Joiner J (2015) A linear method for the retrieval of sun-induced chlorophyll fluorescence from GOME-2 and SCIAMACHY data. Atmos Meas Tech 8:2589–2608

Köhler P, Frankenberg C, Magney TS, Guanter L, Joiner J, Landgraf J (2018) Global retrievals of solar-induced chlorophyll fluorescence with TROPOMI: first results and intersensor comparison to OCO-2. Geophys Res Lett 45(19):10–456

Li X, Xiao J, He B (2018) Chlorophyll fluorescence observed by OCO-2 is strongly related to gross primary productivity estimated from flux towers in temperate forests. Remote Sens Environ 204:659–671

Lichtenthaler HK, Burkart S (1999) Photosynthesis and high light stress. Bulg J Plant Physiol 25 (3–4):3–16

Liu L, Zhao J, Guan L (2013) Tracking photosynthetic injury of Paraquat-treated crop using chlorophyll fluorescence from hyperspectral data. Eur J Remote Sens 46(1):459–473

Liu L, Liu X, Hu J (2015a) Effects of spectral resolution and SNR on the vegetation solar-induced fluorescence retrieval using FLD-based methods at canopy level. Eur J Remote Sens 48:743

Liu X, Liu L, Zhang S, Zhou X (2015b) New spectral fitting method for full-Spectrum solar-induced chlorophyll fluorescence retrieval based on principal components analysis. Remote Sens 7:10626–10645

Longenberger PS, Smith CW, Duke SE, McMichael BL (2009) Evaluation of chlorophyll fluorescence as a tool for the identification of drought tolerance in upland cotton. Euphytica 166(1):25

MacArthur A, Robinson I, Rossini M, Davis N, MacDonald K (2014) A dual-field-of-view spectrometer system for reflectance and fluorescence measurements (Piccolo Doppio) and correction of etaloning. In: Proceedings of the 5th International Workshop on Remote Sensing of Vegetation Fluorescence, Paris, France 2014 Apr, pp 22–24

Maier SW, Gunther KP, Stellmes M (2003) Sun-induced fluorescence: a new tool for precision farming. In: Schepers J, Van Toai T (eds) Digital imaging and spectral techniques: applications to precision agriculture and crop physiology, ASA Special Publications, vol 66. ASA, CSSA, and SSSA, Madison, pp 209–222

Maxwell K, Johnson GN (2000) Chlorophyll fluorescence—a practical guide. J Exp Bot 51 (345):659–668

Mazzoni M, Agati G, Del Bianco S, Cecchi G, Mazzinghi P (2007) High resolution measurements of solar induced chlorophyll fluorescence in the Fraunhofer Ha and in the atmospheric oxygen

lines. In: Proceedings of the 3rd international workshop on remote sensing of vegetation Fluorescences, Florence, 7–9 February 2007
Mazzoni M, Falorni P, Del Bianco S (2008) Sun-induced leaf fluorescence retrieval in the O2-B atmospheric absorption band. Opt Express 16:7014–7022
McAlister ED, Myers J (1940) Time course of photosynthesis and fluorescence. Science 92:241–243
Meroni M, Colombo R (2006) Leaf level detection of solar induced chlorophyll fluorescence by means of a subnanometer resolution spectroradiometer. Remote Sens Environ 103(4):438–448
Meroni M, Rossini M, Guanter L, Alonso L, Rascher U, Colombo R, Moreno J (2009) Remote sensing of solar-induced chlorophyll fluorescence: review of methods and applications. Remote Sens Environ 113(10):2037–2051
Meroni M, Busetto L, Colombo R, Guanter L, Moreno J, Verhoef W (2010) Performance of spectral fitting methods for vegetation fluorescence quantification. Remote Sens Environ 114:363–374
Miller J, Berger M, Goulas Y, Jacquemoud S, Louis J, Mohammed G, Noise N, Moreno J, Moya I, Pedros R, Verhoef W, Zarco-Tejada P (2005) Development of a Vegetation Fluorescence Canopy Model, Final Report. ESA/ESTEC Contract No.16365/02/NL/FF. (138 p)
Mishra KB, Iannacone R, Petrozza A, Mishra A, Armentano N, La Vecchia G, Trtílek M, Cellini F, Nedbal L (2012) Engineered drought tolerance in tomato plants is reflected in chlorophyll fluorescence emission. Plant Sci 182:79–86
Misra AN, Misra M, Singh R (2012) Chlorophyll fluorescence in plant biology, In book: biophysics, chapter: 7, Publisher: In Tech, pp 171–192
Mohammed GH, Goulas Y, Magnani F, Moreno J, Olejničkova J, Rascher U, Vander Tol C, Verhoef W, Daumard F, Galle A, Malenovsky Z, Pernokis D, Rivera JP, Verrelst, J, Drusch M (2014) FLEX/Sentinel-3 Tandem Mission Photosynthesis Study, Final Report. ESA/ESTEC Contract No. 4000106396/12/NL/AF p159
Mohammed GH, Colombo R, Middleton EM, Rascher U, van der Tol C, Nedbal L, Goulas Y, Pérez-Priego O, Damm A, Meroni M, Joiner J (2019) Remote sensing of solar-induced chlorophyll fluorescence (SIF) in vegetation: 50 years of progress. Remote Sens Environ 231:111177
Moya I, Daumard F, Moise N, Ounis A, Goulas Y (2006) First airborne multiwavelength passive chlorophyll fluorescence measurements over La Mancha (Spain) fields. Second Recent Adv Quantitative Remote Sens 25:820–825
Narina SS, Pathak SC, Bhardwaj HL (2014) Chlorophyll fluorescence to evaluate pigeon pea breeding lines and mung bean for drought tolerance. J Agril Sci 6(11):238
Ni Z (2016) Chlorophyll fluorescence retrieval method and its application on detecting the early water stress (Doctoral dissertation)
Ni Z, Huo H, Tang S, Li ZL, Liu Z, Xu S, Chen B (2019) Assessing the response of satellite sun-induced chlorophyll fluorescence and MODIS vegetation products to soil moisture from 2010 to 2017: a case in Yunnan Province of China. Int J Remote Sens 40(5–6):2278–2295
Oxborough K, Baker NR (1997) Resolving chlorophyll a fluorescence images of photosynthetic efficiency into photochemical and non-photochemical components: calculation of qP and Fv'/Fm' without measuring Fo. Photosynth Res 54:135–142
Pacheco-Labrador J, Perez-Priego O, El-Madany TS, Julitta T, Rossini M, Guan J, Moreno G, Carvalhais N, Martín MP, Gonzalez-Cascon R, Kolle O (2019) Multiple-constraint inversion of SCOPE. Evaluating the potential of GPP and SIF for the retrieval of plant functional traits. Remote Sens Environ 234:111362
Patel NR, Padalia H, Devadas R, Huete A, Senthil Kumar A, Krishna Murthy YV (2018) Estimating net primary productivity of croplands in indo-Gangetic Plains using GOME-2 sun-induced fluorescence and MODIS NDVI. Curr Sci 111(6):133–1337
Paunov M, Koleva L, Vassilev A, Vangronsveld J, Goltsev V (2018) Effects of different metals on photosynthesis: cadmium and zinc affect chlorophyll fluorescence in durum wheat. Int J Mol Sci 19(3):787

Pedrós R, Goulas Y, Jacquemoud S, Louis J, Moya I (2010) Fluor MODleaf: a new leaf fluorescence emission model based on the PROSPECT model. Remote Sens Environ 114(1):155–167
Peng B, Guan K, Zhou W, Jiang C, Frankenberg C, Sun Y, He L, Köhler P (2020) Assessing the benefit of satellite-based solar-induced chlorophyll fluorescence in crop yield prediction. Int J Appl Earth Obs Geoinf 90:102–126
Pereira WE, de Siqueira DL, Martínez CA, Puiatti M (2000) Gas exchange and chlorophyll fluorescence in four citrus rootstocks under aluminium stress. J Plant Physio 157(5):513–520
Plascyk JA (1975) The MK II Fraunhofer line discriminator (FLD-II) for airborne and orbital remote sensing of solar-stimulated luminescence. Opt Eng 14(4):339–346
Plascyk JA, Gabriel FC (1975) The Fraunhofer line discriminator MKII-an airborne instrument for precise and standardized ecological luminescence measurement. IEEE Trans Instrum Meas 24 (4):306–313
Porcar-Castell A, Tyystjärvi E, Atherton J, Van der Tol C, Flexas J, Pfündel EE, Moreno J, Frankenberg C, Berry JA (2014a) Linking chlorophyll a fluorescence to photosynthesis for remote sensing applications: mechanisms and challenges. J Exp Botany 65(15):4065–4095
Porcar-Castell A, Tyystjärvi E, Atherton J, van der Tol C, Flexas J, Pfündel EE, Moreno J, Frankenberg C, Berry JA (2014b) Linking chlorophyll a fluorescence to photosynthesis for remote sensing applications: mechanisms and challenges. J Exp Bot 65:4065–4095
Rascher U, Agati G, Alonso L, Cecchi G, Champagne S, Colombo R, Damm A, Daumard F, De Miguel E, Fernandez G, Franch B (2009) CEFLES2: the remote sensing component to quantify photosynthetic efficiency from the leaf to the region by measuring sun-induced fluorescence in the oxygen absorption bands. Biogeosciences 6(7):1181–1198
Ritchie RJ (2006) Consistent sets of spectrophotometric chlorophyll equations for acetone, methanol and ethanol solvents. Photosyn Res 89(1):27–41
Rosema A, Verhoef W, Schroote J, Snel JF (1991) Simulating fluorescence light-canopy interaction in support of laser-induced fluorescence measurements. Remote Sens Environ 37(2):117–130
Rossini M, Meroni M, Migliavacca M, Manca G, Cogliati S, Busetto L, Picchi V, Cescatti A, Seufert G, Colombo R (2010a) High resolution field spectroscopy measurements for estimating gross ecosystem production in a rice field. Agric For Meteorol 150(9):1283–1296
Rossini M, Meroni M, Migliavacca M, Manca G, Cogliati S, Busetto L, Picchi V, Cescatti A, Seufert G, Colombo R (2010b) High resolution field spectroscopy measurements for estimating gross ecosystem production in a rice field. Agric For Meteorol 150(9):1283–1296
Rossini M, Meroni M, Celesti M, Cogliati S, Julitta T, Panigada C, Rascher U, Van der Tol C, Colombo R (2016) Analysis of red and far-red sun-induced chlorophyll fluorescence and their ratio in different canopies based on observed and modeled data. Remote Sens 8(5):412
Schreiber U (2004) Pulse-amplitude-modulation (PAM) fluorometry and saturation pulse method: an overview. In: Papageorgiou GC, Govindjee (eds) Chlorophyll a Fluorescence: a signature of Photosynthesis. Springer, Dordrecht, pp 279–319
Smith WK, Biederman JA, Scott RL, Moore DJP, He M, Kimball JS, Litvak ME (2018) Chlorophyll fluorescence better captures seasonal and interannual gross primary productivity dynamics across dryland ecosystems of Southwestern North America. Geophys Res Lett 45:748–757
Subhash N, Mohanan CN (1997) Curve-fit analysis of chlorophyll fluorescence spectra: application to nutrient stress detection in sunflower. Remote Sens Environ 60(3):347–356
Van der Tol C, Verhoef W, Rosema A (2009) A model for chlorophyll fluorescence and photosynthesis at leaf scale. Agric For Meteorol 149(1):96–105
Van Kooten O, Snel JF (1990) The use of chlorophyll fluorescence nomenclature in plant stress physiology. Photosynth Res 25(3):147–150
Verhoef W (2005) FluorMOD: extension of SAIL to model solar-induced canopy fluorescence spectra. In: 2nd international workshop on remote sensing of vegetation fluorescence 17–-19 November 2004. CD-ROM, Montreal
Vicent J, Sabater N, Tenjo C, Acarreta JR, Manzano M, Rivera JP, Jurado P, Franco R, Alonso L, Verrelst J, Moreno J (2016) FLEX end-to-end mission performancesimulator. IEEE Trans Geosci Remote Sens 54:4215–4223

Vilfan N, Van der Tol C, Muller O, Rascher U, Verhoef W (2016) Fluspect-B: a model for leaf fluorescence, reflectance and transmittance spectra. Remote Sens Environ 186:596–615

Wagle P, Zhang Y, Jin C, Xiao X (2016) Comparison of solar-induced chlorophyll fluorescence, light-use efficiency, and process-based GPP models in maize. Ecol Appl 26(4):1211–1222

Wang S, Huang C, Zhang L, Lin Y, Cen Y, Wu T (2016) Monitoring and assessing the 2012 drought in the great plains: Analyzing satellite-retrieved solar-induced chlorophyll fluorescence, drought indices, and gross primary production. Remote Sens 8(2):61

Wei X, Wang X, Wei W, Wan W (2018) Use of sun-induced chlorophyll fluorescence obtained by OCO-2 and GOME-2 for GPP estimates of the Heihe River basin, China. Remote Sens 10 (12):2039

Wei J, Tang X, Gu Q, Wang M, Ma M, Han X (2019) Using solar-induced chlorophyll fluorescence observed by OCO-2 to predict autumn crop production in China. Remote Sens 14:1715

Whitmarsh J, Govindjee (2002) Photosystem II. Encyclopedia of the life sciences. Macmillan Publishers Ltd/Nature Publishing Group, London, pp 1–13

Wohlfahrt G, Gerdel K, Migliavacca M, Rotenberg E, Tatarinov F, Müller J, Hammerle A, Julitta T, Spielmann FM, Yakir D (2018) Sun-induced fluorescence and gross primary productivity during a heat wave. Sci Rep 8(1):1–9

Wolanin A, Rozanov VV, Dinter T, Noël S, Vountas M, Burrows JP, Bracher A (2015) Global retrieval of marine and terrestrial chlorophyll fluorescence at its red peak using hyperspectral top of atmosphere radiance measurements: feasibility study and first results. Remote Sens Environ 166:243–261

Woo NS, Badger MR, Pogson BJ (2008) A rapid, non-invasive procedure for quantitative assessment of drought survival using chlorophyll fluorescence. Plant Methods 4(1):27

Wood JD, Griffis TJ, Baker JM, Frankenberg C, Verma Yuen MK (2017) Multiscale analyses of solar-induced florescence and gross primary production. Geophys Res Lett 44:533–541

Wu T, Weaver DB, Locy RD, McElroy S, van Santen E (2014) Identification of vegetative heat-tolerant upland cotton (Gossypium hirsutum L.) germplasm utilizing chlorophyll fluorescence measurement during heat stress. Plant Breed 133(2):250–255

Xu S, Liu Z, Zhao L, Zhao H, Ren S (2018) Diurnal response of sun-induced fluorescence and PRI to water stress in maize using a near-surface remote sensing platform. Remote Sens 10(10):1510

Yang X, Tang J, Mustard JF, Lee JE, Rossini M, Joiner J, Munger JW, Kornfeld A, Richardson AD (2015) Solar-induced chlorophyll fluorescence that correlates with canopy photosynthesis on diurnal and seasonal scales in a temperate deciduous forest. Geophys Res Lett 42(8):2977–2987

Yang P, Verhoef W, van der Tol C (2017) The mSCOPE model: a simple adaptation to the SCOPE model to describe reflectance, fluorescence and photosynthesis of vertically heterogeneous canopies. Remote Sens Environ 201:1–1

Yang K, Ryu Y, Dechant B, Berry JA, Hwang Y, Jiang C, Kang M, Kim J, Kimm H, Kornfeld A, Yang X (2018a) Sun-induced chlorophyll fluorescence is more strongly related to absorbed light than to photosynthesis at half-hourly resolution in a rice paddy. Remote Sens Environ 216:658–673

Yang X, Shi H, Stovall A, Guan K, Miao G, Zhang Y, Zhang Y, Xiao X, Ryu Y, Lee JE (2018b) Fluo spec 2: an automated field spectroscopy system to monitor canopy solar-induced fluorescence. Sensors 18:2063

Zarco-Tejada PJ, Miller JR, Mohammed GH, Noland TL (2000a) Chlorophyll fluorescence effects on vegetation apparent reflectance: I. leaf-level measurements and model simulation. Remote Sens Environ 74(3):582–595

Zarco-Tejada PJ, Miller JR, Mohammed GH, Noland TL, Sampson PH (2000b) Chlorophyll fluorescence effects on vegetation apparent reflectance: II. Laboratory and airborne canopy-level measurements with hyperspectral data. Remote Sens Environ 74(3):596–608

Zarco-Tejada PJ, Pushnik JC, Dobrowski S, Ustin SL (2003) Steady-state chlorophyll a fluorescence detection from canopy derivative reflectance and double-peak red-edge effects. Remote Sens Environ 84(2):283–294

Zarco-Tejada PJ, Miller JR, Pedrós R, Verhoef W, Berger M (2006) FluorMODgui V3. 0: a graphic user interface for the spectral simulation of leaf and canopy chlorophyll fluorescence. Comput Geosci 32(5):577–591

Zarco-Tejada PJ, Berni JA, Suárez L, Sepulcre-Cantó G, Morales F, Miller JR (2009) Imaging chlorophyll fluorescence with an airborne narrow-band multispectral camera for vegetation stress detection. Remote Sens Environ 113(6):1262–1275

Zarco-Tejada PJ, Suárez L, González-Dugo V (2013) Spatial resolution effects on chlorophyll fluorescence retrieval in a heterogeneous canopy using hyperspectral imagery and radiative transfer simulation. IEEE Geosci Remote Sens Lett 10(4):937–941

Zhang YH, Chen LJ, He JL, Qian LS, Wu LQ, Wang RF (2010) Characteristics of chlorophyll fluorescence and antioxidative system in super-hybrid rice and its parental cultivars under chilling stress. Biol Plant 54(1):164–168

Zhang Y, Guanter L, Berry JA, Joiner J, Van der Tol C, Huete A, Gitelson A, Voigt M, Kohler P (2014) Estimation of vegetation photosynthetic capacity from space-based measurements of chlorophyll fluorescence for terrestrial biosphere models. Glob Chang Biol 20:3727–3742

Zhang Y, Xiao X, Jin C, Dong J, Zhou S, Wagle P, Joiner J, Guanter L, Zhang Y, Zhang G, Qin Y (2016) Consistency between sun-induced chlorophyll fluorescence and gross primary production of vegetation in North America. Remote Sens Environ 183:154–169

Zhao F, Guo Y, Verhoef W, Gu X, Liu L, Yang G (2014) A method to reconstruct the solar-induced canopy fluorescence spectrum from hyperspectral measurements. Remote Sens 6 (10):10171–10192

Zhao F, Li R, Verhoef W, Cogliati S, Liu X, Huang Y, Guo Y, Huang J (2018) Reconstruction of the full spectrum of solar-induced chlorophyll fluorescence: Intercomparison study for a novel method. Remote Sens Environ 219:233–246

Živčák M, Olšovská K, Slamka P, Galambošová J, Rataj V, Shao H, Kalaji HM, Brestič M (2014) Measurements of chlorophyll fluorescence in different leaf positions may detect nitrogen deficiency in wheat. Zemdirbyste-Agriculture 101(4):437–444

Chapter 8
Point and Imaging Spectroscopy in Geospatial Analysis of Soils

Rodnei Rizzo, Wanderson de Souza Mendes, Nélida Elizabet Quiñonez Silvero, Fabricio da Silva Terra, André C. Dotto, Natasha V. dos Santos, Benito R. Bonfatti, Raul R. Poppiel, and José A. M. Demattê

Contents

R. Rizzo · W. de Souza Mendes · N. E. Q. Silvero · A. C. Dotto · N. V. dos Santos · B. R. Bonfatti · R. R. Poppiel · J. A. M. Demattê (✉)
Department of Soil Science, "Luiz de Queiroz" College of Agriculture, University of São Paulo, Piracicaba, SP, Brazil
e-mail: rodnei.rizzo@usp.com; wandersonsm@usp.br; neli.silvero@usp.br; andrecd@usp.br; natasha.valadares.santos@usp.br; benito.bonfatti@usp.br; jamdemat@usp.br; https://esalqgeocis.wixsite.com/geocis

F. da Silva Terra
Institute of Agricultural Sciences, Federal University of Jequitinhonha and Mucuri Valleys, Unaí, MG, Brazil
e-mail: fabricio.terra@ufvjm.edu.br

T. Mitran et al. (eds.), *Geospatial Technologies for Crops and Soils*,
https://doi.org/10.1007/978-981-15-6864-0_8

Abstract The regular monitoring of soil physical, chemical, and biological properties is very essential, due to its role in soil ecosystem functions. A cost-effective alternative for soil monitoring corresponds to spectral sensing techniques. Soil spectral sensing techniques can support decision-making in agricultural systems at both time and spatial scales, maximizing food production while preserving an adequate soil condition. Due to the large number of ground, airborne, and orbital spectral sensors operating today, this technology has been increasingly assimilated by soil scientists. However, it is important to have an adequate comprehension about the technique principles and limitations. This chapter provides a wide perspective about the soil spectral sensing in the visible (vis: 350–700 nm), near-infrared (NIR: 700–1000 nm), and shortwave infrared (SWIR: 1000–2500 nm), considering reflectance data at different acquisition levels. Here, it is discussed how soil constituents interact with EMR and the resulting soil spectral behaviors. We describe the predictive potential of vis-NIR-SWIR data for quantitative assessment of soil and which soil attributes have been reliably estimated and the most commonly used vis-NIR-SWIR equipment, as well as their advantages and limitations. Finally, we discuss the current application in soil science and future perspectives.

Keywords Applicability of soil sensing · Hyperspectral sensors · Proximal and remote sensing · Soil predictive potential · Spectral libraries

Abbreviations

ACORN	Atmospheric CORrection Now
ANN	Artificial Neural Network
ATCOR	ATmospheric CORrection
ATREM	ATmospheric REMoval algorithm
AVIRIS	Airborne Visible/Infrared Imaging Spectrometer
CIE	Commission internationale de l'éclairage
CHRIS	Compact High-Resolution Imaging Spectrometer
DS	Direct Standardization
EMR	Electromagnetic Radiation
EnMAP	Environmental Mapping and Analysis Program
EPO	External Parameter Organization
FAO	Food and Agriculture Organization
FLAASH	Fast Line-of-sight Atmospheric Analysis of Spectral Hypercubes
FOV	Field of View
FS	Field Spectroscopy
GPS	Global Positioning System
HATCH	High-accuracy ATmosphere Correction for Hyperspectral data
HISUI	Hyperspectral Imager Suite
HyspIRI	Hyperspectral InfraRed Imager
IS	Imaging Spectroscopy
ISDAS	Imaging Spectrometer Data Analysis System

LS	Laboratory Spectroscopy
MESMA	Multiple Endmember Spectral Mixture Analysis
ML	Machine Learning
MSC	Multiplicative Scatter Correction
NIR	Near-infrared
OSC	Orthogonal Signal Correction
PA	Precision Agriculture
PLSR	Partial Least Square Regression
PRISMA	Hyperspectral Precursor of the Application Mission
PS	Proximal Sensing
PSp	Point Spectroscopy
QUAC	Quick Atmospheric Correction
RF	Random Forest
RMS	Root Mean Square
RMSE	Root Mean Square Error
RPD	Ratio of Performence to Deviation
RPIQ	Ratio of Performence to Interquartile
RS	Remote Sensing
SHALOM	Spaceborne Hyperspectral Applicative Land and Ocean Mission
SM	Soil moisture
SNR	Signal-to-Noise Ratio
SNV	Standard Normal Variate
SOC	Soil Organic Carbon
SOM	Soil Organic Matter
SS	Soil Spectroscopy
SSLs	Soil Spectral Libraries
SSS	Soil Spectral Sensing
SVM	Support Vector Machine
SWIR	Shortwave Infrared
VNIR	Visible and Near-Infrared

8.1 Introduction

Soil is an extremely important component of the earth's biosphere, influencing the ecosystems functioning and the maintenance of environmental quality at local and global scales (Glanz 1995). Soil condition is influenced by numerous management practices, including cultivation, irrigation, fertilization, and clearing of natural vegetation (Doran 2002). An important step in the evaluation of land management suitability is to assess the soil condition (Karlen et al. 1997; Doran and Zeiss 2000). Thus, regular monitoring of soil physical, chemical, and biological properties is very essential, for its role in soil ecosystem functions (Bouma and Montanarella 2016). A cost-effective alternative for soil monitoring corresponds to spectral

sensing techniques. Soil spectral sensing (SSS) has been recognized by the Global Soil Partnership from the Food and Agriculture Organization (FAO 2019) as a key method for the improvement of governance and promoting sustainable management of soils. The diversity, concentration, and size of inorganic and organic components in soils result in specific behaviors of the reflected electromagnetic radiation (EMR). The method requires no chemicals and is able to detect various soil properties simultaneously (Nocita et al. 2015). Besides that, SSS techniques can support management decision-making in agricultural systems at both time and spatial scales, maximizing yields while preserving an adequate soil condition (Aitkenhead et al. 2017). Due to a large number of ground, airborne, and orbital spectral sensors operating today, this technology has been increasingly assimilated by soil scientists (Ben-Dor et al. 2009). However, it is still important to have an adequate comprehension of their principles and limitations. This chapter provides a wide perspective about the SSS in the visible (vis: 350–700 nm), near-infrared (NIR: 700–1000 nm), and shortwave infrared (SWIR: 1000–2500 nm), considering reflectance data at different acquisition levels. Here, it is discussed how soil constituents interact with EMR and the resulting soil spectral behaviors. We describe the predictive potential of vis-NIR-SWIR data for quantitative assessment of soil and which soil attributes have been reliably estimated and the most commonly used vis-NIR-SWIR equipment, as well as their advantages and limitations. Finally, we discuss the current application in soil science and future perspectives.

8.2 Definitions in Soil Sensing

Many definitions have been proposed to describe the study of soils by its reflectance data, which are often related or even synonymous (Fig. 8.1). Here we discuss some of the most common definitions, including SSS, remote sensing (RS), proximal sensing (PS), soil spectroscopy (SS), point and imaging spectroscopy (PSp and IS), as well as laboratory and field spectroscopy (LS and FS).

Soil spectral sensing is probably one of the broadest terms concerning the acquisition of EMR with no direct contact with the targeted object. According to Demattê et al. (2015), such a definition removes the relativity from terms like proximal and remote. This is an advantage, especially when dealing with multi-sensor monitoring systems, where spectral data are acquired from ground, air− or spaceborne sensors. Usually, the term remote sensing is applied to define a concept similar to SSS, where it is considered as the acquisition of information about an object without touching it (Fussel et al. 1986). According to Francis and Reeves (1977), a more adequate definition considers RS as "the noncontact recording of information from the ultraviolet, visible, infrared, and microwave regions of the electromagnetic spectrum by means of instruments such as scanners and cameras located on mobile platforms, such as aircraft or spacecraft, and the analysis of acquired information by means of photo interpretive techniques, image interpretation, and state-of-the-art image processing system." Some authors also discriminate

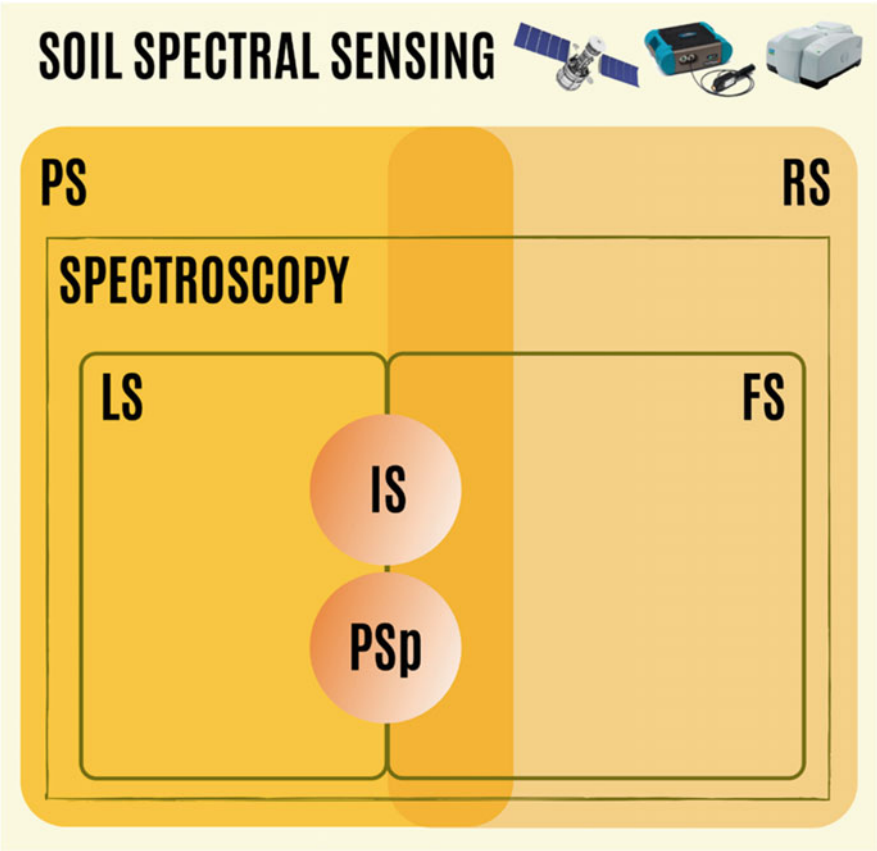

Fig. 8.1 Diagram representing the relation among terms

RS by the spectral range evaluated, where optical (ultraviolet, visible, and infrared ranges) and radar/microwave (microwave range) remote sensing are usually employed (Joshi et al. 2016; Notarnicola et al. 2006). Fussel et al. (1986) indicate that the word "remote," from Latin *remotus*, means not only distant but also indirect, acting upon something indirectly, not arising from a primary or proximate action, not immediately present to the senses, and controlled indirectly or from a distance. Over time, this ambiguity has resulted in eventual miscommunication, as well as many attempts by researchers to propose alternate definitions.

Soil scientists who work with information measured at shorter ranges have been using the expression proximal sensing (Rossel et al. 2011), which not only recognizes small distances between the sensor and sensed object but indirectly assumes that the term "remote" should be considered as a reference of distance. Although recently adopted in soil science, the term has been mentioned in literature for a considerable time, such as in Price (1986), which describes PS as the acquisition of

information from a ground-based platform that is in close proximity to the target or object of interest. This concept focuses on the detection of information about an object in a short distance, primarily in the field, using not only spectral sensors but also any measurement device (Rossel et al. 2011). Three commonly used synonyms for the term proximal sensing include in situ sensing, close-range sensing, and field spectroscopy.

Another expression commonly observed in literature and directly related to the abovementioned terms is spectroscopy. According to Ben-Dor et al. (2018), a spectrum is a collection of discrete energies covering a wide spectral range of photons that travel along with the energy source, surface, and sensor pathways, after removing the atmospheric and source effects. Therefore, spectroscopy is concerned with the absorption, emission, or reflection of EMR by atoms or molecules (Hollas 2005). Information retrieved by soil spectra can be discriminated by both point and image spectroscopy, which can be obtained in the laboratory, field, or from air and space domains. Soil reflectance at point scale (i.e., point spectroscopy) can be performed at short distances and under controlled conditions, preferably using standard protocols, being described as laboratory spectroscopy (Escribano et al. 2017). Alternatively, portable spectroradiometer can be used at field conditions (field spectroscopy), also acquiring information at short distances, but under noncontrolled conditions. Intrinsic characteristics of field measurements are variations in viewing angle, illumination conditions, as well as soil roughness, moisture, management, and sealing (Ben-Dor and Banin 1995). In general, FS gives less accurate results than LS, mainly due to the uncontrolled natural conditions in the field. On the other hand, FS information is retrieved over larger areas, and it can also provide a fairly good indication of spatial variability of soil properties (Escribano et al. 2017).

While PS has a good but limited potential to provide spatially explicit information, imaging spectroscopy is defined by Goetz et al. (1985) as the image acquisition in hundreds of contiguous and registered spectral bands from which reflectance spectra can be derived. IS can be employed at a short distance, where measurements can be retrieved at laboratory or field conditions. Although IS sensors are an excellent option at a short distance, Ben-Dor et al. (2009) see a bigger potential at airborne and space domains. According to these authors, the IS is a new and invaluable resource, which improves the RS by expanding point spectroscopy into a spatial domain and under field conditions.

8.3 Hyperspectral Sensors

The first soil spectroscopy studies were conducted between the 1960s and 1970s, and although the method gained visibility, technology was not advanced enough for an adequate implementation (Bowers and Hanks 1971; Goetz 2009). In the last decades, the computational advances and the miniaturization of important electronic components allowed the development of better hyperspectral sensors and data

processing techniques. Such a fact resulted in the increased availability of spectral and spatial information for environmental studies. A hyperspectral sensor measures contiguous wavelengths (bands), and no gaps occur through which important information might not be detected (Goetz 2009). The necessity to adequately describe spectral features results in sensors with hundreds of contiguous and narrower bands (usually >100 bands).

A great number of soil spectroscopy studies perform laboratory measurements using benchtop or portable equipment. Generally, these spectroradiometers provide readings every 1 or 3 nm, resulting in excellent information for the soil's characterization and properties predictions (Lagacherie et al. 2008). FS readings can be retrieved by static or on-the-go methods. Static measurements are performed by holding a spectroradiometer fore-optic on a soil surface, eventually by a penetrometer mounting (Bricklemyer and Brown 2010). This method has been applied to exposed pit walls (Ben-Dor et al. 2008), exterior walls of soil core holes (Ben-Dor et al. 2008), or the surface of intact soil cores (Waiser et al. 2007; Morgan et al. 2009).

Another option is to perform on-the-go measurements, which usually require a spectroradiometer enclosed within or connected to an implement that is inserted into the soil and pulled by a tractor (Bricklemyer and Brown 2010; Kweon et al. 2013) (Fig. 8.2). Mouazen et al. (2007) developed a spectrometer attached to a subsoiler to perform carbon and moisture measurements. Kodaira and Shibusawa (2013) developed a real-time soil sensor mounted on a tractor and equipped with one micro-CCD camera and two spectrometers to investigate soil. Christy (2008) proposed an on-the-go system for collecting vis-NIR-SWIR spectra. Recently, on-the-go sensors have gained significant importance over imaging sensors (air- and spaceborne), mainly due to the limitations imposed by crop residue and consequently soil surface coverage (Adamchuk et al. (2004). On the other hand, performing spectral readings with a sensor moving through the soil can cause inconsistent soil presentation and smearing. Furthermore, spectral data averaged over some traveling distance can provide different behaviors depending on the acquisition time and velocity and consequently degrade the accurate vis-NIR-SWIR predictions (Waiser et al. 2007; Morgan et al. 2009).

The growing demand for large-scale investigations related to environmental issues has required the development of air- and spaceborne IS. Imaging sensors measure surface reflectance with a given spatial resolution, covering an area instead of a single point (Gerighausen et al. 2012) and providing spectral information at high spatial density (Franceschini et al. 2015). Currently, airborne sensors predominate over spaceborne IS (Table 8.1) (Transon et al. 2018). Airborne sensors such as AVIRIS and APEX have excellent potential for IS (Rast and Painter 2019). These sensors were developed to facilitate the study of terrestrial targets, having a high spectral and spatial resolution and flexible revisit time and providing measurements of atmospheric properties from the ground to altitudes of 20 km (Gholizadeh et al. 2018; Schumann et al. 2013). Besides that, the possibility of maneuvering the sensors' platform (aircraft) allows users to measure the same target from different

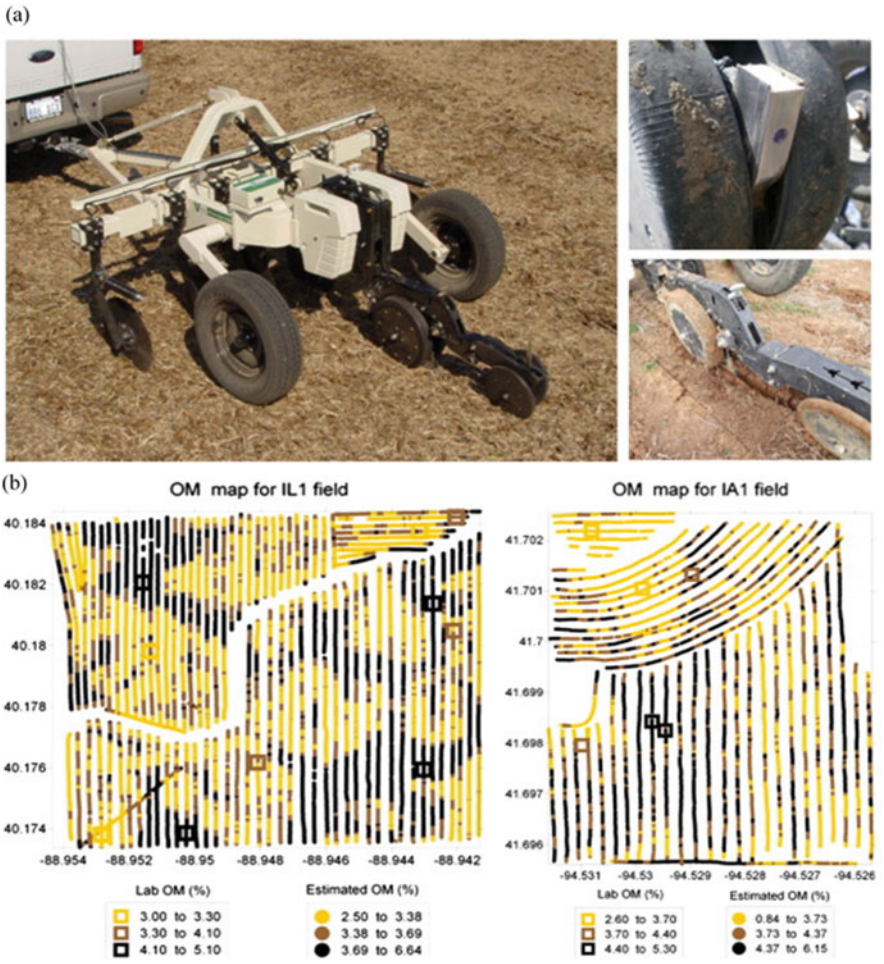

Fig. 8.2 Veris Optic Mapper with soil electrical conductivity and optical sensors (**a**), and the estimated soil organic matter (SOM) maps and conventionally measured SOM (colored squares) of two agricultural fields (**b**) in the USA. (Adopted, Kweon et al. (2013))

angles. Besides that, some of the airborne sensors have been used as a pre-simulation for studies of upcoming satellite sensors (e.g., HySpex, APEX, and AVIRIS).

Differently from airborne sensors, the spaceborne ones have the advantage of covering even larger areas and having lower costs for the users, therefore enabling large-scale environmental monitoring and assessments. There are few spaceborne hyperspectral sensors, even when considering the upcoming launches (Transon et al. 2018). Some of the most relevant spaceborne sensors are the Hyperion and the Compact High-Resolution Imaging Spectrometer (CHRIS). Hyperion, onboard of the EO-1 platform, was a NASA satellite mission that operated for 17 years

Table 8.1 Description of some airborne hyperspectral sensors, including characteristics such as signal-to-noise ratio (SNR) and field of view (FOV)

Sensor	Spectral range (nm)	Spectral resolution (nm)	Spatial resolution (m)	Number of bands	Technology	SNR	FOV	Operation
AVIRIS	380–2500	10	20	224	Whisk broom	1000	30°	1987
AAHIS	440–880	3		288			40°	1994
AHS160	430–2540		2–7	63			90°	2005
AISA Eagle	400–1000	1.56–9.36	3	>488	Pushbroom		21°	1993
AISA Hawk	1000–2400	8.5	6	254	Pushbroom		17.8°–35.5°	1993
AISA DUAL	400–2500	3.3–12		>500	Pushbroom		24°–37.7°	1993
AISA OWL	7600–12,300	100		>96	Pushbroom		24° or 32.3°	1993
APEX	400–2500	1–7	1–5					2011
CASI-2 CASI-1500	400–1000 380–1050	1.8		288	Pushbroom	420	37.8°	1990
DAIS-7915	400–2450 3000–12,600	15–45 200–900	3–20	72 7	Whisk broom	80–150	64–78°	1994
DAIS-16115	400–2500 3000–5000 8000–12,000	8–25 333 333	3–20	140 6 12	Whisk broom	80–200	78°	1994
HySpex	416–992 968–2498	3.5–6.0 5.6–7.0		160 256	Pushbroom	>330	16°	1995
HYDICE	400–2500	3, 10–20	3–20	210	Pushbroom	50–280	8.94°	1995
HyMap	450–2480 8000–12,000	15–20 100–200	2–10	128	Whisk broom	>500	61.3°	1996
MIVIS	400–2478 8200–12,700	10 400–500	8–50	102 10	Whisk broom	>400–700	70°	1993
SASI-600	960–2440	15		100				

(2000–2017). CHRIS on the European Space Agency's PROBA platform orbits the Earth since 2001 and records spectra in the vis-NIR-SWIR region. Although very useful for several soil and environmental applications, the main disadvantage of these sensors is the low signal-to-noise ratio (Castaldi et al. 2016), which provided inaccurate results.

Upcoming spaceborne sensors, from several countries, are planned for launch in the next years and are very promising for environmental studies (Table 8.2). They provide high revisit time (from 3 to 5 days), higher spatial resolution and demonstrate high feasibility for predicting several soil properties (Castaldi et al. 2016, 2019). The upcoming sensors here described are the Environmental Mapping and Analysis Program (EnMAP) from German Space Agency (Guanter et al. 2015); Hyperspectral Precursor of the Application Mission (PRISMA) from Italian Space Agency (Pignatti et al. 2013); Hyperspectral InfraRed Imager (HyspIRI) from NASA mission (Lee et al. 2015); Hyperspectral Imager Suite (HISUI), developed by the Japanese Ministry of Economy, Trade, and Industry; HYPXIM developed by a French ad hoc group of science and defense users (Briottet et al. 2011); and Spaceborne Hyperspectral Applicative Land and Ocean Mission (SHALOM), co-found and managed by the Italian and Israeli Space Agency (Natale et al. 2013).

8.4 Interactions Between EMR and Soil

The soil spectrum is a cumulative property resulting from interactions between EMR and each soil component (Bowers and Hanks 1971), where changes in soil composition can affect the resulting soil spectral behavior (Fig. 8.3). Such components partially absorb or reflect the incoming EMR, depending on the macroscopic and microscopic interactions with the soil system.

Ben-Dor et al. (1999) named the physical or chemical parameters that significantly affect the nature and shape of a soil spectrum as chromophores. They are divided into two categories, chemical or physical. In soils, chemical chromophores can be discriminated as minerals (clay, iron oxide, primary minerals – feldspar – salt, and hard-to-dissolve substances such as carbonates, phosphates), SOM, and water (Ben-Dor et al. 1999). Physical chromophores are properties that affect the whole spectral region and waveband positions, but they do not directly relate to the chemical functional group (Ben-Dor et al. 1999). Some examples of physical chromophores are particle size variation and refraction indexes of a material. A comprehensive review of each chemical and physical chromophore in soils is given in Ben-Dor et al. (1999, 2002), Clark (1999), and Ben-Dor (2002).

While Ben-Dor et al. (1999) adopted the term chromophores, Stenberg et al. (2010) simply divided soil attributes into two groups, the spectrally active and non-active attributes. Terra et al. (2021) proposed other classification, first- and second-order spectral relations. First-order soil properties directly affect soil spectra,

Table 8.2 Description of some spaceborne hyperspectral sensors, including characteristics such as signal-to-noise ratio (SNR) and field of view (FOV)

Sensor	Spectral range (nm)	Spectral resolution (nm)	Spatial resolution (m)	Number of bands	Temporal resolution (days)	Technology	SNR	FOV	Altitude	Operation
EO1-HYPERION	422–2395	10	30	244	16	Pushbroom	40–161	6°	700	2000
HJ-A/HSI	450–950	5	100	110–128						2008
EnMAP*	420–2450	5–20	30	262	4	Pushbroom	>150–500	1.3°	643	After 2019
Proba-1 CHRIS	410–1010	1.25–11	18–36	63	7	Pushbroom	>200	1.3°	550–670	2001
PRISMA*	400–1010 920–2500	10	30	66 171	7–14	Pushbroom	>200–600 >200–400	2.7°	615	After 2019
HyspIRI*	380–2500 3000–12,000	10 80–520	30 60	214 7	16 5	Pushbroom	236–560	5.67°	700	After 2019
HISUI*	400–970 970–2500	60–110 10–12.5	5 30	4 185	2–60	Pushbroom	>450–620 300–2100	1.5°	410	After 2019
SHALOM*	400–1010 920–2500	10	10	275	4	Pushbroom	>200–600 >100–400		640	After 2019
HYPXIM*	400–700 700–1100 100–2500 400–800 8000–12,000	10 10 10 400 100/200	8	210	3–5	Pushbroom	>250 >200 >100 >90 >100		660	After 2019

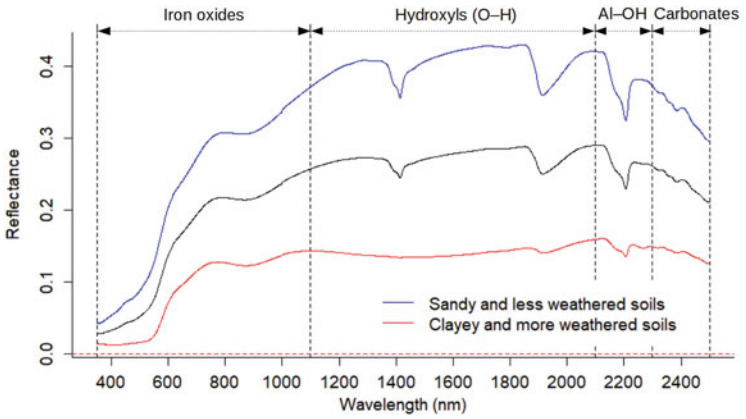

Fig. 8.3 The vis-NIR-SWIR spectral behavior of dry mineral soils highlighting changes in reflectance intensities and absorption features with their causes due to different mineral and organic compositions. (Adopted, Terra et al. 2021)

modifying their overall reflectance intensities and absorption features due to macroscopic and microscopic interactions. Second-order soil properties do not directly affect soil spectra, where they do not produce absorption features or change reflectance intensities. However, these properties are generally adsorbed or depend on functional groups of minerals and organic compounds.

Regardless of the term, the most important aspect here is to understand that soil spectroscopy is a promising tool, but it has some restrictions. When employing such information, the user must be aware of the soil attributes that can actually be inferred from the spectrum, as well as the interrelations between the attributes in soil system.

8.4.1 Macroscopic and Microscopic Interactions

Interactions at macroscopic level are directly related to EMR diffraction and scattering phenomena, which result from soil physical and textural properties. Depending on particle size distribution, structure, and compaction, soils will have different reflectance intensities (albedo). In fact, compaction has an important role in spectral measurements, once it affects the surface roughness (microrelief). In rougher surfaces, diffuse (scattered) reflectance and shading increases, resulting in attenuation of spectra's intensity (Adams and Filice 1967; Townsend 1987). On the other hand, smoother surfaces present higher directional (specular) reflectance and increased intensity. High reflectance intensities are also related to the presence of transparent minerals, such as quartz in sand fraction, which do not absorb energy. In general, soil minerals are trans-opaques, simultaneously reflecting and absorbing radiance in different spectral ranges. Other soil attributes, such as SOM and

moisture, produce an overall attenuation of the soil reflectance intensity, due to the absorption of electromagnetic energy through all spectral range (Terra et al. 2018).

Differently from macroscopic interactions, the microscopic phenomena are responsible for absorption features (negative peaks) in soil spectrum, being dependent on soil mineral and organic composition (Fig. 8.3). These interactions occur in the first 10 to 50 μm of soil surface and are related to the EMR absorption by atoms and molecules (functional groups) of organic and mineral compounds (Baumgardner et al. 1986). The main soil organic functional groups are aromatics (C-H), amines (N-H), alkyls (C-H), carboxyls (C=O), amides (C=O), aliphatics (C-H), methyls (C-H), phenolics (C-OH), polysaccharides (C-O), and carbohydrates (C-O). The main inorganic functional group is hydroxyl (-OH), which is exposed on the outer surface of phyllosilicate and oxidic clay minerals (silanol, Si]-OH; aluminol, Al]-OH; and ferrol, Fe]-OH) (Sparks 2002), being also observed in water molecules.

8.4.2 Spectral Features and Soil Attributes

The features observed in the vis-NIR spectrum (350–1000 nm) are mostly related to interactions between radiation and ions in the minerals crystalline structure of iron oxidic minerals. Such interactions take place at electronic level and result in rearrangement of valence electrons due to charge-transfer and crystal-field effects (Sherman and Waite 1985). In soils, these electronic transitions occur mostly in iron oxides, since Fe is a transition metal and the ferric ion (Fe^{3+}) is present in hematite (Fe_2O_3) and goethite (FeOOH) (Fig. 8.4). In the visible range, these absorptions with different intensities explain the reddish and yellowish colors that hematite and goethite give to soils, respectively (Fig. 8.4). Magnetite ($FeO.Fe_2O_3$) and ilmenite ($FeTiO_3$) are also iron oxides; both are opaque minerals with reflectance spectra presenting very low albedo ($< 5\%$) and no clear absorption features between 350 and 1100 nm. Their absorbed radiance is related to ionic and intra-ionic charge-transfer (Hunt 1977).

In the SWIR (1000–2500 nm), microscopic interactions occur due to non-fundamental molecular vibrations (Hunt 1977). In soils, these vibrations are basically related to stretching overtone of OH bond at 1400 nm, bending-stretching combination of molecular H_2O at 1900 nm, and bending-stretching combination of aluminum-hydroxyl bond (Al-OH) at 2200 nm (Hunt and Salisbury 1971a) (Fig. 8.3). Hydroxyl molecules and molecular H_2O are found in the structures of phyllosilicate clay minerals. These minerals are formed by a combination of silicon tetrahedral sheets (O^{2-} groups coordinated around Si^{4+}) and one alumina octahedral sheet (OH^- groups coordinated around Al^{3+}). They are discriminated into 1:1 (Si-tetrahedron + Al-octahedron) and 2:1 (Si-tetrahedron + Al-octahedron + Si-tetrahedron) clay minerals, corresponding to kaolinite (1:1) and mica or smectite (2:1) groups (Hunt and Salisbury 1971b), respectively. Once different phyllosilicates share the same absorption features (i.e., 1400 nm, 1900 nm, and 2200 nm), their distinction is only possible by the shape, width, and intensity of such features.

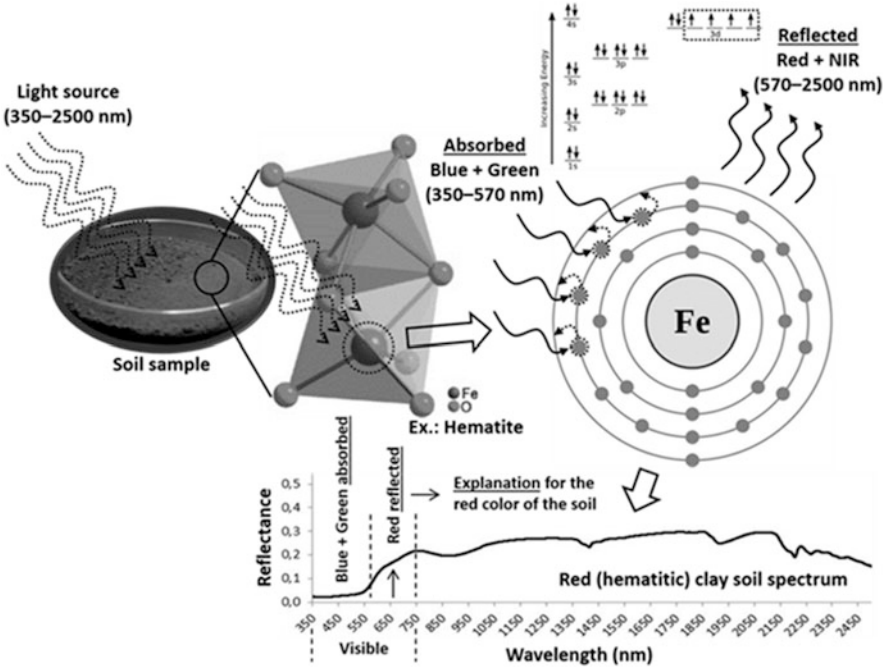

Fig. 8.4 Electronic transitions of iron ions in the hematite and the spectral behavior of hematitic soils, indicating why some soils are red colored. (Adopted, Terra et al. 2021)

Kaolinite presents a dissymmetry at 2205 nm toward higher wavelengths and relatively weak features at the three features. Once 2:1 clay minerals present water molecules strongly adsorbed on the interlayer surfaces, absorption features at 1400 nm and 1900 nm are quite strong (Demattê and da Silva Terra 2014). In cases where high water contents are observed, these two bands become deeper and broader with their maximum absorptions shifted to 1450 nm and 1940 nm. This process is followed by a general decrease of the soil albedo, resulting from macroscopic interaction (Bowers and Hanks 1971). At soil saturation conditions, typical absorptions of liquid water at 760 nm, 970 nm, and 1190 nm can also be observed, mainly in spectra of quartz sandy soils with low organic matter content (Tian and Philpot 2015).

Other features strongly influenced by soil attributes are positioned at 2260 nm and 2350 nm (Fig. 8.2). The first one is related to gibbsite [Al $(OH)^3$], which is the main aluminum oxide observed in heavily weathered soils. In this case, the feature results from the bending-stretching combination of aluminum-hydroxyl bond (Al-OH). In incipient soils or areas with regular liming, i.e., systems with high content of carbonate minerals (calcite $CaCO_3$; dolomite [$CaMg\ (CO_3)_2$]), the soil spectrum presents a characteristic feature at 2350 nm. This spectral behavior is produced by a third stretching overtone of C-O bonds (Hunt and Salisbury 1971b).

Besides all the inorganic compounds here described, spectral features might be influenced by SOM. Even in spectra of "mineral soils," where organic carbon contents are generally lower than 12% (IUSS Working Group WRB 2015), it might be possible to detect absorptions across NIR-SWIR ranges, which are assigned to stretching overtones in more than ten organic compounds (Rossel and Behrens 2010; Terra et al. 2015; Rossel and Hicks 2015). However, organic carbon peaks are easily masked by stronger absorptions of oxide and phyllosilicate clay minerals and water.

8.5 Soil Modeling by Point and Imaging Spectroscopy

Since the soil spectral behavior is directly related to the concentrations of organic and mineral components, as well as elements absorbed on their surfaces, soil properties predictions can be reliably acquired by coupling spectroscopic and chemometric tools. PSp and IS have been used in spatio-temporal analysis of soils, both providing satisfactory-good predictions (Ben-Dor et al. 2009; Chabrillat et al. 2013; Demattê et al. 2015). The difference between them is related to the fact that point data, usually acquired at laboratory conditions, allow the user to perform sample preparation and have little or no influence of external factors (e.g., atmospheric conditions), differently from aerial and orbital platforms. Terra et al. (2021), Demattê et al. (2015), and Rossel et al. (2006) provide a comprehensive discussion about the potential of vis-NIR-SWIR reflectance in the soil evaluation.

8.5.1 Influence of Sample and Environment Conditions in Soil Spectroscopy

Soil sample preparation is extremely common when performing laboratorial measurements and might have considerable influence in soil predictions. Usually, samples are oven-dried at 45 °C for 48 h and later sieved to <2 mm, in order to reduce the particle size effect in spectral measurements (Ben-Dor and Banin 1995). Miltz and Don (2012) investigated the impact of sample preparation on spectra and found that drying (oven-dried vs. air-dried) and grinding (grinding vs. crushing and sieving) decreased the error for organic carbon predictions. In this case, grinding was the most influent factor accounting for 35% of the error. It has also been reported that grinding (or ball milling) has great effect on clay content prediction performances. Soil particles grinding has a substantial effect on spectra increasing overall reflectance, especially in soils with high clay content, as aggregates are crushed (Stenberg et al. 2010). Drying of samples also increases the total reflectance, but in addition the absorption bands at 1400 and 1900 nm are attenuated (Krishnan et al. 1980). Chakraborty et al. (2019) indicated that moisture, from non-dried samples, can

increase measurement errors up to 29%. Recently, protocols have been established for spectral acquisition geometries and soil preparation, in order to standardize LS measurements and enable spectral data sharing and intercomparison of predictions from different laboratories (Ben Dor et al. 2015; Rossel et al. 2016).

While external factors are adequately controlled in laboratory, field and aero/orbital spectroscopy are largely influenced by soil surface roughness, covering (e.g., green vegetation, crop residues, litter and soil crusts) and moisture. These environmental factors are extremely variable in both space and time, and the combined effects that they have on a spectrum are still not well understood (Escribano et al. 2017). Irregularities in soil surfaces produce shadow areas, where light do not directly reach the surface. Reflectance of rougher surfaces is lower than energy reflected from directly illuminated soil fragments (Chabrillat et al. 2019). Although their shape is quite similar, the spectrum of ploughed soils (rough surface) has overall reflectance lower than that related to sunlit fragments (Cierniewski and Gulinski 2010). According to Matthias et al. (2000), the surface of a sandy soil had a decrease of 25% in reflectance after ploughed. Potter et al. (1987) found the opposite effect in sandy soils, but in this case, authors indicated a combined effect of ploughing and subsequent wetting (rainfall) and drying of surface, which resulted in soil crust. Soil crust corresponds to a thin and platy layer at the soil surface that is exposed to solar radiation and consequently can be detected by remote sensors (Agassi et al. 1981). In this case, reflectance of crust-covered soils is higher than the ones without a crust (Goldshleger et al. 2009). Therefore, the influence of soil roughness on spectral reflectance is variable, especially after tillage treatments.

The development of soil crust is not only controlled by mechanic forces but also biogenic/organic process (Chabrillat et al. 2019). In arid regions it is possible to observe surfaces with a biogenic crust (Pinker and Karnieli 2007). The biogenic crust corresponds to lower and nonvascular (microphytic) plants, which covers a thin layer of the soil upper surface (Rogers and Lange 1972). O'neill (1994) indicated that soil spectral features around 2080–2100 nm are influenced by cellulose and consequently by microphytic crust. Karnieli and Tsoar (1995) indicated a decrease in the soil's albedo due to the microphytic crust, which resulted in the false identification of anomalies in soils.

In general, it is very unlikely to find bare soils at the field. Usually, the soil surface is partially or completely covered by vegetation and organic and inorganic debris. Bartholomeus et al. (2007) indicated that a vegetation cover of more than 20% prevents accurate soil properties estimation. In other cases, only a few percent fractional vegetation cover were sufficient to dramatically decrease the accuracy of SOC and clay predictions (Bartholomeus et al. 2011). The soil spectral region most strongly affected by green vegetation is between 680 nm and 1300 nm, due to the steep rise in reflectance that it causes (e.g., Ammer et al. 1991). Dry vegetation has great influence on the albedo of the vis-NIR region and in absorption features of the SWIR region, due to cellulose, lignin, and water (Ben-Dor et al. 2018). According to Murphy and Wadge (1994), in soil-vegetation mixtures, crop residues (dead vegetative tissue) have greater impact on soil spectra than green vegetation, especially on the 2200 nm absorption feature.

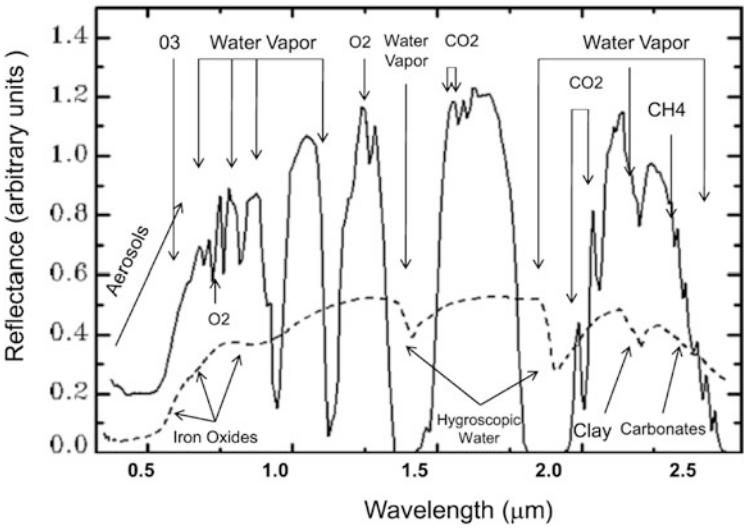

Fig. 8.5 Simulated AVIRIS soil spectrum and the major gas absorption features which overlap with soil features. (Adopted, Ben-Dor et al. 2018)

If soil spectra are measured with air- or spaceborne sensors, not only the conditions of surface will influence the data but also the atmospheric gases and aerosols between the measured surface and the sensor. The vis region is influenced by absorption of ozone (around 600 nm), aerosol scattering (monotonous decay from 400 to 800 nm), oxygen (760 nm), and water vapor (730 nm and 820 nm) (Fig. 8.5). NIR and SWIR are affected by absorption of water vapor (940, 1140, 1380, and 1880 nm), oxygen (around 1300 nm), carbon dioxides (around 1560, 2010, and 2080 nm), and methane (2350 nm) (Ben-Dor et al. 2018) (Fig. 8.5). Therefore, users should be aware of the possible issues with the dataset before employing predictive models to soil reflectance spectra of air- and spaceborne sensors.

8.5.2 Spectra Preprocessing

Once soil spectra have been measured, it is usually applied a preprocessing technique to the raw data to remove irrelevant information, which could affect the potential of predictive models (Gholizadeh et al. 2013). These techniques aim to decrease the noise and enhance possible spectral features related to the predicted soil property. One of the most common preprocessing methods is the log-transform from reflectance (R) into absorbance (A = log (1/R)), which preserves a linear correlation between radiance and concentrations. The Kubelka-Munk function, multiplicative scatter correction (MSC), and standard normal variate (SNV) are interesting options to deal with scattering effects (Terra et al. 2021). Among the functions used for noise

effects removal, the most common are the averaging spectra, Savitzky-Golay transformation (Savitzky and Golay 1964), and moving average filters. To highlight absorption peaks, it is recommended techniques such as continuum removal (Clark and Roush 1984), baseline correction, first- and second-derivative processing, and wavelet transform (Ricker 1953).

With the development of portable sensors and the increasing use of FS, different methodologies have been employed to reduce effects from environmental factors on the field spectra, consequently enhancing the model's predictive performance. Minasny et al. (2011) implemented the external parameter orthogonalization (EPO; Roger et al. 2003) to remove the effects of moisture in spectra of rewetted soil, improving predictions of soil carbon. The EPO-processed spectra from samples with highest moisture content had an $R^2 = 0.87$, while the same spectra without EPO preprocessing presented R^2 of 0.56 and higher bias value. Ackerson et al. (2015) used the EPO to remove effects of soil water content, roughness, aggregation, and temperature variations from field measurements. The EPO-processed data provided much better prediction capabilities, with an improvement in RMSE and R^2 of 418 g kg^{-1} to 98 g kg^{-1} and 0.59 to 0.82, respectively. Another method employed to remove the influence of in situ factors is the direct standardization (DS) algorithm. Ji et al. (2015) used DS to reduce the effects of environmental factors on field spectra, aiming to improve the performance of OC models. Franceschini et al. (2018) tested the EPO, DS, and orthogonal signal correction (OSC), to remove the effects of in situ factors from on-the-go data acquired with a vis-NIR-SWIR spectrometer. In this case, OSC had the best overall performance for the evaluated soil properties.

When dealing with data from remote sensors, the pretreatment process requires a few more steps. Images acquired by these sensors need geometric and radiometric corrections. Geometric correction is concerned with placing the measurements or derivative products in their proper planimetric (map) location (Jensen and Jensen 2013). Radiometric correction aims to improve the accuracy of surface spectral reflectance, emittance, or back-scattered measurements, acquired with RS systems (Johannsen and Daughtry 2009; Jensen 2005). The most important external variables that can cause remote sensor data to exhibit radiometric and geometric error are the terrain elevation, slope, aspect, and atmosphere (Jensen 2005). Among these variables, correction of the atmospheric effects is one of most discussed, and several algorithms have been proposed to correct RS data.

The first algorithms corresponded to empirical methods such as internal average reflectance approach (Kruse, Raines, and Watson 1985) and flat field approach (Roberts, Yamaguchi, and Lyon 1986). Conel et al. (1987) developed the empirical line (EL) method, which requires field measurements (spectra) of distinct targets for the correction. Later, Bernstein et al. (2005) proposed the quick atmospheric correction (QUAC), a semiempirical correction method that determines atmospheric compensation parameters from the information contained within the image such as pixel endmember spectra (i.e., pure, unmixed pixels in the scene). This approach allows the retrieval of reasonably accurate reflectance data even when a sensor has no proper radiometric or wavelength calibration or the solar illumination intensity is unknown (Jensen 2005).

Once empirical approaches are fairly restrictive, depending on image statistics and field reflectance measurements, many researchers have developed theoretical modeling techniques. Such techniques simulate absorption and scattering effects of atmospheric components using a radiative transfer model (Minu et al. 2016). Some of the modeling techniques described in literature corresponds to ATmospheric REMoval algorithm (ATREM) (Gao et al. 1993), ATmospheric CORrection (ATCOR) (Richter 1993), Imaging Spectrometer Data Analysis System (ISDAS) (Staenz et al. 1998), Fast Line-of-sight Atmospheric Analysis of Spectral Hypercubes (FLAASH) (Adler-Golden et al. 1998), High-accuracy ATmosphere Correction for Hyperspectral data (HATCH) (Qu et al. 2001), and Atmospheric CORrection Now (ACORN) (ACORN 2002). Even though these are robust models, the resulting spectra still present residual atmospheric absorptions and scattering effects (Clark et al. 2002).

8.5.3 Soil Predictive Potential by Different Acquisition Levels

To perform robust predictive models, soil spectra must be associated with multiple linear or nonlinear regression techniques based on machine learning (ML) algorithms, such as support vector machines (SVM), artificial neural networks (ANN), boosted trees, random forest (RF), partial least squares regression (PLSR), and deep learning (Padarian et al. 2019a, b). The performances of prediction models depend on the size and spectral variability of soil datasets (local, regional, country, or global) and generally are assessed by the R^2 (coefficient of determination), RMSE (root mean square error), RPD (ratio of performance to deviation), and RPIQ (ratio of performance to interquartile) (Bellon-Maurel et al. 2010; Ramirez-Lopez et al. 2013a, b). Currently there are several studies in literature performing an intercomparison among the most common multivariate calibration models, in order to define the best methods for soil attributes prediction (e.g., Padarian et al. 2019a, b; Reda et al. 2019; Yang et al. 2019).

8.5.3.1 First-Order Attributes

The model's robustness tends to be related to the soil attributes evaluated, where the first-order ones have greater chance of being adequately predicted (Terra et al. 2021). In literature, these are usually the attributes with highest coefficient of determination and lowest error (Fig. 8.6). Generally, these properties are strongly correlated with reflectance or absorbance data, and their concentrations are better quantified by ML algorithms (Terra et al. 2015). The most commonly predicted attribute is clay content, where spectroscopic predictions started in the mid-1990s (Ben-Dor and Banin 1995; Janik and Skjemstad 1995; Janik et al. 1998) and adequate performances have been described since then ($R^2 \geq 0.75$). Sand and clay spectral modeling are usually more efficient than other soil properties; therefore they are considered the

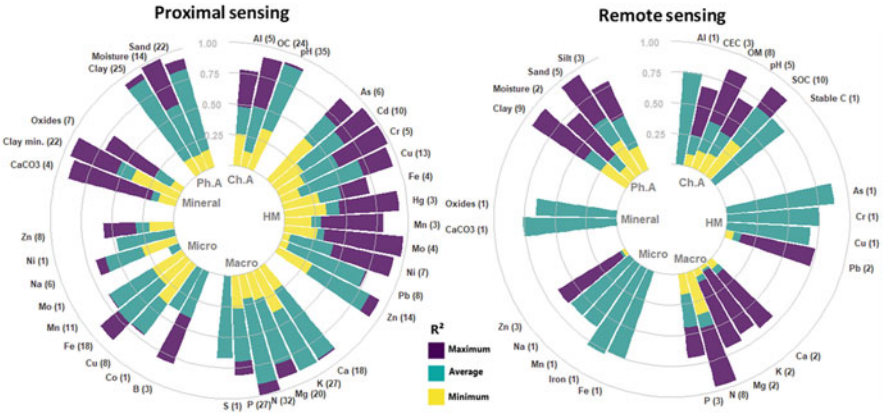

Fig. 8.6 R^2 of prediction models described in literature. Values inside parenthesis represent the total number of predictions. Proximal sensing R^2 were retrieved from Terra et al. (2021), and the remote sensing ones from literature review (Anne et al. 2014; Bartholomeus et al. 2011; Ben-Dor et al. 2002; Casa et al. 2013; Castaldi et al. 2014; Choe et al. 2008; DeTar et al. 2008; Gerighausen et al. 2012; Gomez et al. 2012, 2008; Guo et al. 2019; Hbirkou et al. 2012; Hively et al. 2011; Lu et al. 2013; Peón et al. 2017; Qi et al. 2018; Selige et al. 2006; Steinberg et al. 2016; Tan et al. 2020; Vohland et al. 2017; Wang et al. 2010; Yang et al. 2016; Zhang et al. 2013). Coefficients are grouped in physical (Ph.A) and chemical attributes (Ch.A), heavy metals (HM), macro- (Macro) and micronutrients (Micro), and mineralogy (Mineral)

most relevant ones. Spectroscopy is also promising for total organic carbon predictions, being successfully applied in several cases (Bellon-Maurel et al. 2010; Terra et al. 2015; Xu et al. 2018). Fractions of soil organic carbon (SOC), such as particulate, humic, and resistant fractions, and SOM composition, such as carbohydrate, protein, lignin, lipid, and black carbon, have been accurately modeled by reflectance spectroscopy (Cécillo et al. 2012; Rossel and Hicks 2015). Although carbon is a first-order attribute, the models' performances are still variable (Rossel et al. 2016).

Another attribute significantly correlated to reflectance is soil moisture; consequently modeling of water content at soil field capacity (by laboratory vis-NIR-SWIR spectroscopy) presents good performance ($R^2 > 0.80$) (Fig. 8.6) (Ben-Dor et al. 2008; Demattê et al. 2006). Similarly, abundances of phyllosilicates and oxides have been successfully quantified by reflectance spectroscopy based on different techniques (Terra et al. 2015). Oxides extracted by acid digestion suggesting mineralogical compositions such as SiO_2, Fe_2O_3, Al_2O_3, TiO_2, and MnO have also been accurately predicted (Ben-Dor and Banin 1995; Terra et al. 2015). Concentrations of calcium carbonates ranging from 10% to 75% were satisfactorily estimated by Ben-Dor and Banin (1995) with standard errors of 5.9% and 7.9% for calibration and prediction models, respectively.

8.5.3.2 Second-Order Attributes

Even though second-order properties do not affect soil spectra, there is a great interest in employing reflectance spectroscopy analysis to predict plant nutrients in soils, in particular macro- and micronutrients (Terra et al. 2019). Quantifying the concentration of elements in the soil solution, corresponding to the fraction available for plant absorption, will probably not provide robust models (Janik et al. 1998). Attempts to predict soil nutrients based on reflectance spectroscopy indicated highly variable R^2 values in vis-NIR-SWIR range for calcium (0.01–0.9), magnesium (0.12–0.90), potassium (0–0.9), phosphorus (0.02–0.92), and nitrogen (0.09–0.9) (Fig. 8.6). Among these elements, nitrogen has presented better results with mean $R^2 > 0.70$ (Fig. 8.6).

This same issue is observed for predictions of micronutrients, but due to the lowest natural concentration of those nutrients, they would not be detected by the technique even if they had specific spectral absorptions in the vis-NIR-SWIR range (Soriano-Disla et al. 2014). The most common micronutrients evaluated by soil spectroscopy are Cu, Mn, Fe, and Zn (Fig. 8.6). As expected, performances of the models are highly variable, and their mean R^2 values are usually low-satisfactory for B (R^2 ranging between 0.4 and 0.74), Cu (0.01–0.71), Fe (0.19–0.9), Mn (0.01–0.7), Na (0.08–0.68), and Zn (0.26–0.57).

Although heavy metals are second-order attributes, they are generally adsorbed or depend on functional groups of minerals and organic compounds, which in turn are spectrally active attributes. Therefore, their concentrations may be indirectly modeled by reflectance spectroscopy. Some researchers have described good fitting between conventional wet analyses and vis-NIR-SWIR predictions, where the performance of these models is related to a local covariation between the predicted element and first-order property (Sarathjith et al. 2014). Researchers are mostly focused in arsenic (As), cadmium (Cd), copper (Cu), nickel (Ni), lead (Pb), and zinc (Zn), although predictions of mercury (Hg) and chrome (Cr) are also reported (Fig. 8.6). The R^2 for vis-NIR-SWIR models are also highly variable, and their mean values are usually satisfactory for Cd (R^2 ranging between 0.3 and 0.97), Cr (0.44–0.98), Cu (0.25–0.95), Mo (0.64–0.97), and Ni (0.5–0.92) (Fig. 8.6). In general, spectroscopic models for predictions of other heavy metals (As, Fe, Mn, Pb, and Zn) have presented unsatisfactory mean R^2.

The different laboratory methods used to define the standard values, as well as the different fractions assessed (e.g., extractable, exchangeable, and total), probably contribute to the large variation described here (Chang et al. 2001). Furthermore, fractions most related to concentration of the element in solution, rather than to the chemistry of the soil matrix, will probably be poorly predicted (Soriano-Disla et al. 2014). The good predictions of soil macronutrients are related to covariations between element assessed and first-order soil attributes. Ca, Mg, and K are usually predicted based on the covariation with mineralogical properties (Chang et al. 2001). N is highly correlated with SOM and carbon concentrations, mostly because of the amide groups. Accurate spectral predictions of phosphorus concentration in soils are

related to its covariation with clay mineralogy and organic matter content (Iznaga et al. 2014; Sarathjith et al. 2014; La et al. 2016).

8.5.3.3 Comparing Proximal and Remote Sensors

Due to the limited availability of hyperspectral data from air- and spaceborne sensors, the number of researches quantifying soil properties from RS is significantly reduced when compared to the proximal sensors (Fig. 8.6). In both cases, the attributes most evaluated are clay and sand content, as well as SOM and carbon (Fig. 8.6). The predictive potential of proximal and RS is slightly different, and proximal sensors have a higher potential, which is related to the lower influence of the external factors. Such factors attenuate the data signal and impact in soil reflectance measured with RS. Remotely sensed data is affected by many external factors, including atmospheric conditions (Anderson et al. 1994; Richter and Schläpfer 2002; Mulder et al. 2011), structural effects, sensors spectral resolutions, geometric distortions, and spectral mixture of features (Kriebel 1978; Richter and Schläpfer 2002; Mulder et al. 2011). Since PS and RS have different field of view, differences can also be related to the measurement scale. In this case, the spectrum from a satellite pixel usually averaged out more signal than punctual ground measurements.

The inherent trade-off between fully covering the study site with RS data of lower detail and accuracy, or having a more proximal and detailed set of punctual (or spatial) measurements is a non-solvable problem. It demonstrates a basic dilemma in environmental sensing studies, not only related to the quality/coverage of measurements but also to the cost and time required by surveys and data acquisition systems (Lopez and Frohn 2017). This trade-off is the reason why the synergistic use of remotely and proximally sensed data is a key element needed to solve questions at multi-scale research (Demattê et al. 2015). Besides that, it is important to perform a careful selection of the sensing techniques for a particular soil study, which will result in the most suitable dataset and scale for the desired application.

8.6 Soil Spectral Libraries

One of the major gaps in the effective monitoring of soils with vis-NIR-SWIR data is the calibration of robust spectroscopic models, which must be able to assess attributes from a wide range of soil types (Cécillon et al. 2009). Researchers have suggested that the development of large soil spectral databases could facilitate the use of spectroscopy, reducing the number of calibration samples required for local and regional applications, as well as facilitating soil monitoring from spectroscopy (McCarty et al. 2002; Shepherd and Walsh 2002; Brown 2007). These large databases are defined by Brown et al. (2006) as soil spectral libraries (SSLs). The SSLs

are discriminated as local, regional, or global, according to their geographical extent and the represented soil variability. Local libraries refer to field-scale datasets, while the regional SSLs represent a greater geographic extent, such as physio-climatic zones. The global libraries consist of the world's major soil taxa, being built from samples of multiple continents (Brown et al. 2006). SSLs are intended for two purposes mainly: (a) to be used in RS procedures as in situ measurements for calibration and/or endmembers selection in data processing or (b) for modeling of soil properties by reflectance spectroscopy (Brown 2007; Brodský et al. 2011a; Selige et al. 2006; Rossel et al. 2006).

There are a considerable number of vis-NIR-SWIR SSLs spread around the world for national and continental uses, with significant amounts of soil samples (> 1000) per library, such as in Africa (Shepherd and Walsh 2002; Stevens et al. 2013), the USA (Brown et al. 2006), Europe (Stevens et al. 2013), Czech Republic (Brodský et al. 2011b), Belgium (Genot et al. 2011), Denmark (Knadel et al. 2012), China (Li et al. 2015), Brazil (Demattê et al. 2019), and Australia (Rossel and Webster 2012). At world scale, Brown et al. (2006) measured and analyzed the spectra of 4184 soil samples with great compositional diversity from across the Americas, Africa, and Asia. Recently, the combined effort of several researchers allowed the creation of a global soil spectral library with more than 23,600 samples (Rossel et al. 2016).

Many studies in the literature describe how to develop and use SSLs (Shepherd and Walsh 2002; Guerrero et al. 2016; Rossel et al. 2016), but basically it is important to consider (a) the number of samples that are needed to adequately describe the soil variability at the targeted site; (b) the methods used to sample, handle, prepare, store, and scan soils; and (c) the reference analytical methods used (Rossel et al. 2008). Even if the libraries are built following rigorous procedures, it might not contain enough diversity to allow prediction of soil properties (Guerrero et al. 2010). On the other hand, the accuracy of spectroscopic models usually decreases when the SSLs contain an extremely heterogeneous set of samples (Wetterlind and Stenberg 2010; Ramirez-Lopez et al. 2013a, b; Shi et al. 2015), consequently presenting limited performance at local and regional scales.

There are many attempts to enhance the accuracy of regional/global SSL's models, aiming to predict soil properties at local scale. One of them is the addition of new local samples to an established SSL, process also known as "spiking" (Brown 2007; Wetterlind and Stenberg 2010). Some studies report improvements in soil predictions when combining SSLs, local samples, and spiking techniques (Brown 2007; Guerrero et al. 2010). There are also methods which perform local statistical modeling, such as locally weighted regression (Igne et al. 2010), LOCAL (Gogé et al. 2012), and fast Fourier transform local-weighted regression (Gogé et al. 2014). These methodologies optimize the calibration process by subsetting or weighting SSL's samples, according to their degree of spectral similarity with the targeted soils. In this specific case, the term "local" describes a set of samples with similar spectral features, irrespective of their spatial proximity (Shi et al. 2015). Another strategy corresponds to the spatially constrained models, which basically define SSL subsets according to geospatial data, e.g., agrogeological zones, agricultural fields, or soil

types (Stevens et al. 2010; Vasques et al. 2010; Wetterlind and Stenberg 2010; McDowell et al. 2012; Shi et al. 2015).

Recently, studies are also exploring approaches that combine soil spectral libraries and other georeferenced information (Shepherd and Walsh 2002), such as from digital terrain models, field observations, and multi- and hyperspectral RS imagery (e.g., Vågen et al. 2006; Viscarra Rossel 2011; Vasques et al. 2015; Rizzo et al. 2016). Using the Australian SSL, Rossel et al. (2011) performed maps of kaolinite, illite, and smectite for the whole country at two depths (0–20 cm, 60–80 cm). Rizzo et al. (2016) produced a digital soil map using as training set vis-NIR-SWIR spectra from local soil samples, a regional spectral library, and terrain attributes. The authors indicated the potential of combining local reflectance measurements and a regional SSL to improve soil mapping campaigns. Demattê et al. (2018) used a regional SSL to validate a multispectral satellite composite image of bare soils. Later, the authors used such image to define high-resolution soil attributes maps. Mendes et al. (2019) employed an SSL to calibrate spectral transfer functions which were capable of predicting the spectral reflectance from subsurface soil, based on the surface soil reflectance. These functions were combined to satellite images to map the soil spectral behavior at soil subsurface layers.

Although a promising tool for soil monitoring, some issues must be addressed before employing a SSL. A matter of great concern when developing large spectral libraries is the involvement of multiple personnel, laboratories, and instruments (Brown et al. 2006; Croft et al. 2012). Such aspects can increase uncertainties in measurements of both reflectance and soil properties. The vis-NIR-SWIR spectra present subtle variations even when obtained on supposedly identical equipment. Therefore, a model calibrated with spectra from a specific instrument could not perform adequately when employing information from another spectroradiometer (Cécillon et al. 2009; Croft et al. 2012). Efforts must focus on increasing the quality of the analytical data and the impact of global datasets to predict local data (Cambule et al. 2012).

8.7 Applications of vis-NIR-SWIR Data

8.7.1 Soil Organic Carbon Stock

A relevant mechanism for climate change mitigation is to reduce the carbon dioxide in the atmosphere by soil carbon assimilation (Lal 2014). In this process, it is extremely important to define the carbon pools and evaluate stocks changes, but an adequate assessment of SOC stocks requires extensive sampling and soil analyses (Goidts et al. 2009). Several studies describe the capacity of vis-NIR-SWIR data to predict SOC content (Wetterlind and Stenberg 2010; Nocita et al. 2015). While such studies frequently report predictions of gravimetric SOC (SOC_g) on a mass basis, carbon accounting requires volumetric SOC (Roudier et al. 2015). According

to Bellon-Maurel and McBratney (2011), the prediction of volumetric SOC (SOC_v) by vis-NIR-SWIR spectroscopy can be performed indirectly or directly. The first one, respectively, estimates SOC_g and bulk density (ρ_b) independently and later calculates stocks based on such predictions. The other option is to predict SOC_v directly from the vis-NIR-SWIR spectra, employing a model calibrated with conventional SOC_y measurements. The direct prediction is considered the best one, once it reduces uncertainty propagation in predictions (Bellon-Maurel & McBratney 2011).

The potential of direct predictions is described by Cambou et al. (2016), which estimated SOC stock from partially disturbed cores (sampled with a manual auger) and indicated that vis-NIR-SWIR spectroscopy had reasonable performance ($R^2_{val} = 0.70$, SEPc = 2.0 g C dm^{-3}). Rodier et al. (2015) measured vis-NIR-SWIR spectra from intact soil cores (at field conditions) and later tested both direct and indirect prediction methods to detect vertical changes in SOC stocks. The authors found no statistical difference in accuracy between these approaches and suggested that the direct prediction of SOC_v is the most feasible option. Lobsey and Rossel et al. (2016) developed a technique that uses gamma-ray attenuation and vis-NIR-SWIR spectroscopy to measure ex situ the bulk density of wet soil cores and later perform indirect predictions of SOC stocks. It provided accurate and verifiable predictions, allowing stocks to be reliably predicted by indirect means. Later, Rossel et al. (2017) developed the Soil Condition Analysis System. It integrates an automated soil core sensing system with statistical analytics and modeling to characterize soil at fine depth resolutions. It includes a γ-ray attenuation densitometer to measure bulk density and a vis-NIR-SWIR spectroradiometer. The system is capable of providing spatially explicit estimates of total SOC, particulate, humus, and resistant organic.

Priori et al. (2016) combined laboratory vis-NIR-SWIR and passive gamma-ray data to directly map C stocks of the topsoil (0–30 cm) in agricultural fields. Predictions were interpolated using geographically weighted multiple regression, elevation, and gamma-ray maps. The prediction model had a R^2 of 0.77 and RMSE of 0.67 kg m^{-2}, indicating the model's potential for monitoring the effects of management and erosion on soil carbon. Guo et al. (2019) described the potential of SOC stocks being mapped by laboratory and airborne vis-NIR-SWIR spectroscopy. They indicated that differences between laboratory ($R^2 = 0.66$, RPIQ = 2.39) and airborne spectral ($R^2 = 0.42$, RPIQ = 1.84) predictions are mostly related to atmospheric and soil surface conditions. The authors also describe airborne data as very useful for digital soil mapping and dynamic monitoring of carbon pools.

According to the literature, both direct and indirect predictions can provide adequate stock prediction, and although good results are observed, there is still room for improvement. The main issue of field sensors is to simultaneously predict the bulk density and SOC_g or even to directly measure the SOC_y. This is considered by Bellon-Maurel and McBratney (2011) a great challenge. Furthermore, there are few studies like Guo et al. (2019), which evaluate the potential of hyperspectral soil RS. With the launching of new spaceborne sensors, it is essential to develop studies

combining point and image spectroscopy to improve the predictive potential and generate highly detailed maps of SOC stocks.

8.7.2 Soil Moisture

Soil moisture (SM) affects several processes in soil system, having a direct relationship with global climate and weather and influencing in several hydrometeorological processes (Petropoulos et al. 2015), such as evapotranspiration and precipitation. For those reasons, spatiotemporal monitoring of SM is highly desirable (Lobell and Asner 2002). Soil SM strongly affects the albedo and features in NIR region (Lobell and Asner 2002; Ben-Dor et al. 2009). Predictions of SM in laboratory and field generally provide good-excellent results (Fig. 8.6). Dalal and Henry (1986), for example, used NIR spectroscopy and regression analysis and found an R^2 of 0.9.

Attempts have been made to spatially predict SM content by on-the-go sensors (at field conditions), and some had good performance. Christy (2008) calibrated an on-the-go hyperspectral sensor for SM prediction, using the spectral ranges at 350–1050 and 900–1700 nm. They found R^2 ranging from 0.79 to 0.82. Kodaira and Shibusawa (2013) used a real-time vis-NIR-SWIR soil sensor to measure several soil properties in field. The authors found a good performance for SM ($R^2 = 0.95$) when they employed the 500–1600 nm spectral range and second derivative as pretreatment. Although a reasonable option, Franceschini et al. (2018) indicated that on-the-go sensors present higher predictions error compared with laboratory measurements.

The number of studies predicting SM from air- and spaceborne sensors is still limited; nevertheless, they are promising. Bach and Mauser (1994) combined a model for internal reflectance with absorption coefficients into Beer's law (Palmer and Williams 1974; Lekner and Dorf 1988). Later, the authors applied the process in the prediction of water contents with an AVIRIS image of an irrigated field in Germany. Ben-Dor et al. (2002) used DAIS-7915 hyperspectral airborne sensor to measure saturated and field moisture in clayey soils and found that airborne sensors are feasible for providing reliable predictions for SM, with $R^2 > 0.65$. Whiting et al. (2004) isolated the influence of the fundamental water band from soil samples with different gravimetric moisture contents. They fitted an inverted Gaussian function centered on the assigned fundamental water absorption region at 2800 nm, over the logarithmic soil spectra continuum. Based on this method and an AVIRIS image, they were able to map the soil surface moisture content in two fields located in the USA and Spain. Haubrock (2008) and Haubrock et al. (2004, 2008) developed a model for predicting gravimetric SM based on RS techniques. The method combined point and IS (especially reflectance at 1800 nm and 2119 nm) and hydrological measurements. Such technique was applied to HyMap airborne images to map soil surface moisture at a field in Germany (Fig. 8.7; Haubrock et al. 2008). In this case, RS data was highly correlated with the field moisture content measured at the time of the overflight. Finally, Finn et al. (2011) used HIS hyperspectral airborne sensor to

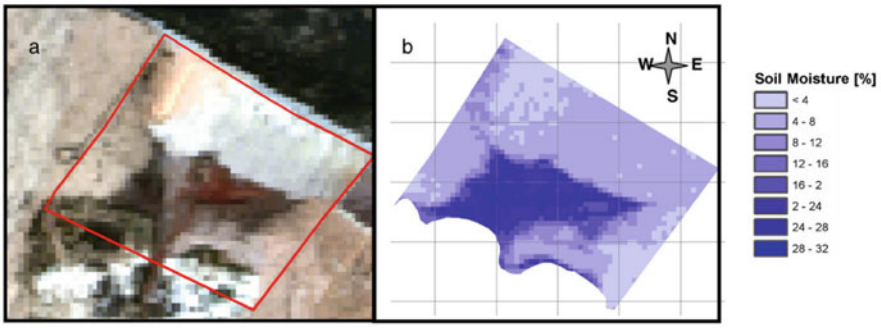

Fig. 8.7 HyMap airborne image (**a**) and the corresponding soil surface moisture map (**b**) at a field in Germany. (Modified, Ben-Dor et al. (2009) and Haubrock et al. (2008))

correlate the SWIR bands with SM measured in situ. These authors not only indicated the potential of HIS sensor to detect SM but also described the bands between 1300 and 1670 nm as highly correlated with SM ($r > 0.70$).

8.7.3 Precision Agriculture

Agricultural fields are heterogeneous in terms of soil conditions, varying in space and time (Ge et al. 2011). Conventional soil fertility recommendations are based in elaborated sampling procedures, which provide "average" soil fertility values from a given field. Such procedure usually results in either too much or too little fertilizer locally applied (Stoorvogel et al. 2015). The advent of global positioning systems (GPS) led to the development of the precision agriculture (PA) concept. PA aims to improve the efficiency of resources use by employing variable rate applications (Stenberg et al. 2010). Information needed by PA include high-resolution (<10 m) maps of soil properties. The sampling density used to develop these maps is often defined without background information regarding the soil variability (Franzen and Peck 1995). Furthermore, sustainable agriculture practices are hindered by the costs associated with the high sampling density required by PA (Ramirez-Lopez et al. 2019).

Soil vis-NIR-SWIR spectroscopy can provide detailed spatial sampling over a site, generating a good continuous description of soil variability (Demattê et al. 2015). Using only vis-NIR-SWIR laboratory spectra, Ramirez-Lopez et al. (2019) defined the optimal set size and the best samples with which to calibrate vis-NIR models. Later, robust block kriging was used to predict particle size fractions and calcium content maps. The results indicated that samples selection based on vis-NIR-SWIR spectra considerably decreased the need for soil sampling and conventional chemical analysis. Rizzo et al. (2016) spatialized the soil vis-NIR-SWIR spectral behavior at farm scale and used this information along with fuzzy

c-means clustering to define soil mapping units. Based on fuzzy centroids, the authors defined representative samples to each mapping unit. Christy (2008) employed an on-the-go vis-NIR-SWIR spectroradiometer in eight fields in central Kansas, USA. For each field, a clustering k-mean algorithm was used to select 15 sample locations that best represented the spectral data space. He evaluated the potential of the system not only to define sampling locations but also to perform real-time spatial prediction of soil attributes. In fact, acquiring spatial explicit data at high density and measuring soil surface at adjustable depth are the main advantages of on-the-go reflectance measurements (Franceschini et al. 2018).

Soil spectroscopy data can be also employed to aid in management practices. Rossel et al. (2010), for example, developed a soil fertility index for sugarcane production and mapped it using laboratorial vis-NIR-SWIR spectra and terrain attributes. Tekin et al. (2013) produced lime recommendation maps using online vis-NIR measurements, with $R^2 = 0.81$ and RMSEP = 0.20. Maleki et al. (2007) carried out on-the-go measurements of soil spectra in two fields located in Belgium. They used such information to optimize the variable rate application of elemental P. In this case, P was calculated from vis-NIR-SWIR spectra, and subsequently the required elemental P was determined. The authors described herein and many others in literature (e.g., Schirrmann et al. 2011; Kweon et al. 2013; Franceschini et al. 2018) indicated laboratorial and FS as useful tools to describe the spatial variability of soil fertility or quality. Air- and spaceborne hyperspectral sensors can also be used in PA (Bajwa and Tian 2005; Stamatiadis et al. 2013), but in this case retrieving soil spectral data is fairly difficult due to crop residues covering the fields surface (Franceschini et al. 2018).

8.7.4 Soil Degradation by Erosion

Inappropriate human activities and land exposure to adverse climatic conditions can result in soil quality loss and degradation (Tóth et al. 2008). This is of great concern, once degraded soils do not adequately provide ecosystem services as it originally could. Soil degradation is affected by many processes, but one of most important is the erosion. There is a global loss of 75 million tons of soils every year, which costs approximately $400 billion (Eswaran et al. 2001; Ben-Dor et al. 2009). Eroded soils usually present significant alteration on physical and chemical properties, such as color, pH, SOM, texture, structure, consistence, coarse fragments, free iron oxides, $CaCO_3$, and/or clay minerals (De Alba 2003; Escribano et al. 2017). These attributes are considered excellent indicators when evaluating changes in soil conditions.

Spectroscopy can provide all the required information for an adequate assessment and monitoring of soil degradation processes (Shoshany et al. 2013). In this case, the degradation is detected by evaluating spatiotemporal alterations in soil indicators. Most of these indicators are spectrally active and consequently can be monitored by hyperspectral data acquired with ground or airborne sensors.

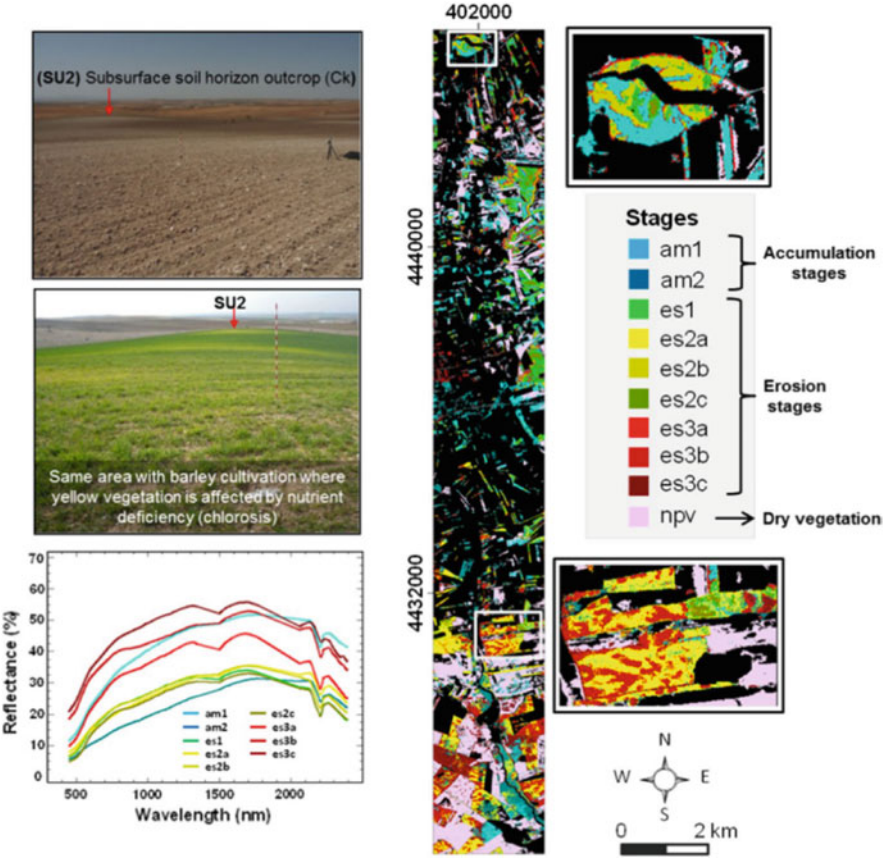

Fig. 8.8 Soil erosion and degradation mapping from AISA sensors hyperspectral images. (Modified, Chabrillat et al. (2019); Schmid et al. (2016))

Many studies on soil properties and conditions have been carried out to define the spatial variability of soil properties and erosion processes on local and regional scales (Hill and Schütt 2000; Ben-Dor et al. 2006; Vrieling 2006; Corbane et al. 2008; Escribano et al. 2017). Jarmer et al. (2007) developed regression functions built on CIE (*Commission internationale de l'éclairage*) color coordinates and specific absorption features from HyMap imagery, to design a degradation assessment and monitoring system over southeastern Spain. Schmid et al. (2016) acquired soil hyperspectral data from AISA sensors and combined them to morphological and physicochemical ground data to map classes of soil erosion and accumulation stages. According to the authors, it was possible to detect different soil horizons at surface due to different intensity of erosion processes, which in turn have distinct soil properties. They calibrated a support vector machine algorithm to extrapolate the erosion and accumulation stages to the whole region (Fig. 8.8). Žížala et al. (2017) used soil properties maps (SOC stock, sand, silt, clay, Fe, and $CaCO_3$) derived from

hyperspectral data of CASI1500 and SASI600 sensors, along with digital elevation models and fuzzy classification, to define soil erosion classes in farms of Czech Republic. Rossel et al. (2017) accessed soil degradation by analyzing soil organic C stocks and condition with vis-NIR-SWIR proximal sensing. Bracken et al. (2019) applied the Multiple Endmember Spectral Mixture Analysis (MESMA) to data from sensors AISA Eagle and Hawk and detected soil erosion in a semiarid Mediterranean environment. In this case, the authors found an overall accuracy of 70.3% when using the unmixing fraction maps and terrain derivatives.

The results described herein indicate that when modeling erosion processes, point and image spectroscopy can monitor important variables, which have currently been poorly or not detected by other methods (Haubrock et al. 2004, 2008). On the other hand, most of the modeling processes proposed till now cannot provide information about areas that are prone to erosion, but not yet affected (Ben-Dor et al. 2009). One of the few studies trying to address such problem was developed by Makisara et al. (1995). The authors used an airborne AISA sensor, in southern Israel to detect problematic areas in the image and define locations with plowing priority, in order to increase the water infiltration rate and consequently reduce the chance of erosion. With the development and launching of new hyperspectral sensors, it is important that researchers keep expanding the capabilities of spectroscopy to detect and prevent soil erosion process.

8.8 Conclusions and Future Perspectives

In this brief review, we discussed the advances in point and IS and how it has been supporting scientists in the spatiotemporal characterization of soils. Although the methodology has limitations concerning which attributes can truly be monitored by vis-NIR-SWIR spectral range, spectroscopy is definitely an important data source in different topics of soil science. The technique is already capable of describing soil condition/quality and providing real-time information. With the development of public datasets (e.g., soil spectral libraries) and low-cost portable sensors or free aerial/orbital images, the technique will be even more accessible and consequently easily employed to help farmers and decision-makers. The SSLs stored on the cloud and combined to machine learning algorithms will be able to deploy robust prediction models at farm scale, reducing the need for conventional soil analysis. The soil assessment process will be faster and therefore the decision-making will become more assertive.

Although the technology is currently restricted by issues in miniaturization, in the medium term, sensors will become even more accessible (e.g., hyperspectral imaging based on smartphones cameras), leading to the increased use of IS in the upcoming decades (Stuart et al. 2019). Furthermore, the Unmanned Aerial Vehicle platforms will provide greater flexibility than more conventional sensing strategies, allowing the user to define important parameters such as survey size and flight altitude, resulting in better data sources for the application. In parallel, the upcoming

high signal-to-noise ratio satellite imaging will provide spectroscopy data for the next 5 years (EnMAP, SHALOM, PRISMA), resulting in a major step toward the operational quantitative monitoring of soil surfaces at large scales (Escribano et al. 2017).

Finally, the integration of proximal and remote soil spectral sensors (covering different spectral ranges and platforms) provides the ability to improve the prediction accuracy of individual soil properties. Apparently, the combination of multiple sensors has been the best alternative for the assessment of soil properties at real time, and future work should focus in the design and evaluation of such strategy.

References

Ackerson JP, Demattê JA, Morgan CL (2015) Predicting clay content on field-moist intact tropical soils using a dried, ground VisNIR library with external parameter orthogonalization. Geoderma 259:196–204

ACORN (2002) ACORN 4.0, User's guide, analytical imaging and geophysics. LLC, Boulder

Adams JB, Filice AL (1967) Spectral reflectance 0.4 to 2.0 microns of silicate rock powders. J Geophys Res 72(22):5705–15 Res. https://doi.org/10.1029/jz072i022p0570

Adamchuk VI, Hummel JW, Morgan MT, Upadhyaya SK (2004) On-the-go soil sensors for precision agriculture. Comput Electron Agric 44(1):71–91

Adler-Golden S, Berk A, Bernstein LS, Richtsmeier S, Acharya PK, Matthew MW, Anderson GP, Allred CL, Jeong LS, Chetwynd JH (1998) FLAASH, a MODTRAN4 atmospheric correction package for hyperspectral data retrievals and simulations. In: Summaries of the seventh JPL Airborne Earth Science Workshop 1998 Dec 12 (vol 1, pp 9–14). JPL Pub

Agassi M, Shainberg I, Morin J (1981) Effect of electrolyte concentration and soil sodicity on infiltration rate and crust formation 1. Soil Sci Soc Am J 45(5):848–851. https://doi.org/10.2136/sssaj1981.03615995004500050004x

Aitkenhead MJ, Gaskin GJ, Lafouge N, Hawes C (2017) Phylis: a low-cost portable visible range spectrometer for soil and plants. Sensors 17(1):99. https://doi.org/10.3390/s17010099

Ammer U, Koch B, Schneider T, Wittmeier H (1991) High resolution spectral measurements of vegetation and soil in field and laboratory. Proceedings of the 5th international Colloquium, physical measurements and signatories in remote sensing, Courchevel, France. I: pp 213–218

Anderson GP, Wang J, Hoke ML, Kneizys FX, Chetwynd JH, Rothman LS, Kimball LM, McClatchey RA, Shettle EP, Clough ST, Gallery WO, Abreu LW, Selby JEA (1994) History of one family of atmospheric radiative transfer codes, Proc. SPIE 2309, passive infrared remote sensing of clouds and the atmosphere II. https://doi.org/10.1117/12.196674

Anne NJ, Abd-Elrahman AH, Lewis DB, Hewitt NA (2014) Modeling soil parameters using hyperspectral image reflectance in subtropical coastal wetlands. Int J Appl Earth Obs Geoinf 33:47–56. https://doi.org/10.1016/j.jag.2014.04.007

Bach H, Mauser W (1994) Modelling and model verification of the spectral reflectance of soils under varying moisture conditions. In: International Geoscience and Remote Sensing Symposium (IGARSS). https://doi.org/10.1109/igarss.1994.399735

Bajwa SG, Tian LF (2005) Soil fertility characterization in agricultural fields using hyperspectral remote sensing. Trans ASAE 48(6):2399–2406. https://doi.org/10.13031/2013.20079

Bartholomeus H, Epema G, Schaepman M (2007) Determining iron content in Mediterranean soils in partly vegetated areas, using spectral reflectance and imaging spectroscopy. Int J Appl Earth Obs Geoinf 9(2):194–203

Bartholomeus H, Kooistra L, Stevens A, van Leeuwen M, van Wesemael B, Ben-Dor E, Tychon B (2011) Soil organic carbon mapping of partially vegetated agricultural fields with imaging spectroscopy. Int J Appl Earth Obs Geoinf 13(1):81–88

Baumgardner MF, Silva LF, Biehl LL, Stoner ER (1986) Reflectance properties of soils. In: Advances in agronomy, vol 38. Academic, New York, pp 1–44

Bellon-Maurel V, Fernandez-Ahumada E, Palagos B, Roger JM, McBratney A (2010) Critical review of chemometric indicators commonly used for assessing the quality of the prediction of soil attributes by NIR spectroscopy. TrAC Trends Anal Chem 29(9):1073–1081

Bellon-Maurel V, McBratney A (2011) Near-infrared (NIR) and mid-infrared (MIR) spectroscopic techniques for assessing the amount of carbon stock in soils - Critical review and research perspectives. Soil Biol Biochem https://doi.org/10.1016/j.soilbio.2011.02.019

Ben-Dor E (2002) Quantitative remote sensing of soil properties. Adv Agron 75:173–244

Ben-Dor E, Banin A (1995) Near-infrared analysis as a rapid method to simultaneously evaluate several soil properties. Soil Sci Soc Am J 59(2):364–372

Ben-Dor E, Irons JR, Epema GF (1999) Soil reflectance. In: Rencz AN (ed) Remote sensing for the earth sciences: manual of remote sensing, vol 3. Wiley, New York, pp 111–188

Ben-Dor E, Patkin K, Banin A, Karnieli A (2002) Mapping of several soil properties using DAIS-7915 hyperspectral scanner data-a case study over clayey soils in Israel. Int J Remote Sens 23 (6):1043–1062

Ben-Dor E, Levin N, Singer A, Karnieli A, Braun O, Kidron GJ (2006) Quantitative mapping of the soil rubification process on sand dunes using an airborne hyperspectral sensor. Geoderma 131 (1–2):1–21

Ben-Dor E, Heller D, Chudnovsky A (2008) A novel method of classifying soil profiles in the field using optical means. Soil Sci Soc Am J 72(4):1113–1123

Ben-Dor E, Chabrillat S, Demattê JA, Taylor GR, Hill J, Whiting ML, Sommer S (2009) Using imaging spectroscopy to study soil properties. Remote Sens Environ 113:38–55

Bernstein LS, Adler-Golden SM, Sundberg RL, Levine RY, Perkins TC, Berk A, Ratkowski AJ, Felde G, Hoke ML (2005) A new method for atmospheric correction and aerosol optical property retrieval for VIS-SWIR multi-and hyperspectral imaging sensors: QUAC (QUick atmospheric correction). Spectral Sciences Inc Burlington MA; 2005 Jan.

Ben-Dor E, Sabine C, Demattê J (2018) Characterization of soil properties using reflectance spectroscopy. In: Thenkabail P, Lyon S, John G, Huete A (eds) Fundamentals, sensor systems, spectral libraries, and data mining for vegetation. https://doi.org/10.1201/9781315164151-8

Bouma J, Montanarella L (2016) Facing policy challenges with inter- and transdisciplinary soil research focused on the UN sustainable development goals. Soil 2(2):135–145

Bowers SA, Hanks RJ (1971) Reflection of radiant energy from soils. (Doctoral dissertation, Kansas State University)

Bracken A, Coburn C, Staenz K, Rochdi N, Segl K, Chabrillat S, Schmid T (2019) Detecting soil erosion in semi-arid Mediterranean environments using simulated EnMAP data. Geoderma 340:164–174

Bricklemyer RS, Brown DJ (2010) On-the-go VisNIR: potential and limitations for mapping soil clay and organic carbon. Comput Electron Agric 70(1):209–216

Briottet X, Marion R, Carrere V, Jacquemoud S, Chevrel S, Prastault P, D'oria M, Gilouppe P, Hosford S, Lubac B, Bourguignon A (2011) HYPXIM: a new hyperspectral sensor combining science/defence applications. In: 3rd workshop on hyperspectral image and signal processing: evolution in remote sensing (WHISPERS). IEEE, Lisbon, pp 1–4. https://doi.org/10.1109/WHISPERS.2011.6080957

Brodský L, Klement A, Penížek V, Kodešová R, Borůvka L (2011a) Building soil spectral library of the Czech soils for quantitative digital soil mapping. Soil Water Res 26(4):165–172

Brodský L, Klement A, Penížek V, Kodešová R, Boruvka L (2011b) Building soil spectral library of the czech soils for quantitative digital soil mapping. Soil Water Res 6(4):165–172

Brown DJ (2007) Using a global VNIR soil-spectral library for local soil characterization and landscape modeling in a 2nd-order Uganda watershed. Geoderma 140(4):444–453

Brown DJ, Shepherd KD, Walsh MG, Dewayne Mays M, Reinsch TG (2006) Global soil characterization with VNIR diffuse reflectance spectroscopy. Geoderma 132(3–4):273–290

Casa R, Castaldi F, Pascucci S, Basso B, Pignatti S (2013) Geophysical and hyperspectral data fusion techniques for in-field estimation of soil properties. Vadose Zone J 12(4):vzj2012.0201

Cambou A, Cardinael R, Kouakoua E, Villeneuve M, Durand C, Barthès BG (2016) Prediction of soil organic carbon stock using visible and near infrared reflectance spectroscopy (VNIRS) in the field. Geoderma 261:151–159

Cambule AH, Rossiter DG, Stoorvogel JJ, Smaling EMA (2012) Building a near infrared spectral library for soil organic carbon estimation in the Limpopo National Park, Mozambique. Geoderma 183–184:41–48

Castaldi F, Casa R, Castrignanò A, Pascucci S, Palombo A, Pignatti S (2014) Estimation of soil properties at the field scale from satellite data: a comparison between spatial and non-spatial techniques. Eur J Soil Sci 65(6):842–851

Castaldi F, Palombo A, Santini F, Pascucci S, Pignatti S, Casa R (2016) Evaluation of the potential of the current and forthcoming multispectral and hyperspectral imagers to estimate soil texture and organic carbon. Remote Sens Environ 179:54–65

Castaldi F, Chabrillat S, Van Wesemael B (2019) Sampling strategies for soil property mapping using multispectral sentinel-2 and hyperspectral EnMAP satellite data. Remote Sens 11(3):309

Cécillon L, Barthès BG, Gomez C, Ertlen D, Génot V, Hedde M, Stevens A, Brun JJ (2009) Assessment and monitoring of soil quality using near-infrared reflectance spectroscopy (NIRS). Eur J Soil Sci 60(5):770–784

Chabrillat S, Ben-Dor E, Rossel RA, Demattê JA (2013) Quantitative soil spectroscopy. Appl Environ Soil Sci 2013:616578

Chabrillat S, Ben-Dor E, Cierniewski J, Gomez C, Schmid T, van Wesemael B (2019) Imaging spectroscopy for soil mapping and monitoring. Surv Geophys 40(3):361–399

Chakraborty S, Li B, Weindorf DC, Morgan CL (2019) External parameter orthogonalisation of eastern European VisNIR-DRS soil spectra. Geoderma 337:65–75

Chang C, Laird D, Mausbach MJ (2001) Near-infrared reflectance spectroscopy – principal components regression analyses of soil properties. Soil Sci Soc Am J 65:480–490

Choe E, van der Meer F, van Ruitenbeek F, van der Werff H, de Smeth B, Kim K-W (2008) Mapping of heavy metal pollution in stream sediments using combined geochemistry, field spectroscopy, and hyperspectral remote sensing: a case study of the Rodalquilar mining area, SE Spain. Remote Sens Environ 112(7):3222–3233

Christy CD (2008) Real-time measurement of soil attributes using on-the-go near infrared reflectance spectroscopy. Comput Electron Agric 61(1):10–19

Cierniewski J, Gulinski M (2010) Furrow microrelief influence on the directional hyperspectral reflectance of soil at various illumination and observation conditions. IEEE Trans Geosci Remote Sens 48(11):4143–4148

Clark RN (1999) Spectroscopy of rocks and minerals, and principles of spectroscopy. Manual Remote Sens 3:3–58

Clark RN, Roush TL (1984) Reflectance spectroscopy: quantitative analysis techniques for remote sensing applications. J Geophys Res Solid Earth 89(B7):6329–6340

Clark RN, Swayze GA, Livo KE, Kokaly RF, King TVV, Dalton JB, Vance JS, Rockwell BW, Hoefen T, McDougal RR (2002) Surface reflectance calibration of terrestrial imaging spectroscopy data: a tutorial using AVIRIS. In: Proceedings of the 10th airborne earth science workshop. JPL publication, Pasadena, CA. http://speclab.cr.usgs.gov/PAPERS.calibration.tu

Conel JE, Green RO, Vane G, Bruegge CJ, Alley RE (1987) AIS-2 radiometry and comparison of methods for the recovery of ground reflectance. In: Vane G (ed) Proceedings of the 3rd airborne imaging spectrometer data analysis workshop vol 87(30), JPL Publication, Pasadena, CA, pp 18–47

Corbane C, Raclot D, Jacob F, Albergel J, Andrieux P (2008) Remote sensing of soil surface characteristics from a multiscale classification approach. Catena 75(3):308–318

Croft H, Kuhn NJ, Anderson K (2012) On the use of remote sensing techniques for monitoring spatio-temporal soil organic carbon dynamics in agricultural systems. Catena 94:64–74
Dalal RC, Henry RJ (1986) Simultaneous determination of moisture, organic carbon, and total nitrogen by near infrared reflectance spectrophotometry. Soile Sci Soc Am J 50(1):120–123
De Alba S (2003) Simulating long-term soil redistribution generated by different patterns of mouldboard ploughing in landscapes of complex topography. Soil Till Res 71(1):71–86
Demattê JA, da Silva Terra F (2014) Spectral pedology: a new perspective on evaluation of soils along pedogenetic alterations. Geoderma 217:190–200
Demattê JA, Sousa AA, Alves MC, Nanni MR, Fiorio PR, Campos RC (2006) Determining soil water status and other soil characteristics by spectral proximal sensing. Geoderma 135:179–195
Demattê JA, Morgan CL, Chabrillat S, Rizzo R, Franceschini MH, Vasques GM, Wetterlind J, Thenkabail PS (2015) Spectral sensing from ground to space in soil science: state of the art, applications, potential and perspectives. In: Land resources monitoring, modeling, and mapping with remote sensing. CRC Press, pp 661–732
Demattê JA, Fongaro CT, Rizzo R, Safanelli JL (2018) Geospatial soil sensing system (GEOS3): a powerful data mining procedure to retrieve soil spectral reflectance from satellite images. Remote Sens Environ 212:161–175
Demattê JA, Dotto AC, Paiva AF, Sato MV, Dalmolin RS, Maria do Socorro B, da Silva EB, Nanni MR, ten Caten A, Noronha NC, Lacerda MP (2019) The Brazilian soil spectral library (BSSL): a general view, application and challenges. Geoderma 354:113793
DeTar WR, Chesson JH, Penner JV, Ojala JC (2008) Detection of soil properties with airborne hyperspectral measurements of bare fields. Trans ASABE 51(2):463–470
Dor EB, Ong C, Lau IC (2015) Reflectance measurements of soils in the laboratory: standards and protocols. Geoderma 245:112–124
Doran JW (2002) Soil health and global sustainability: translating science into practice. Agric Ecosyst Environ 88(2):119–127
Doran JW, Zeiss MR (2000) Soil health and sustainability: managing the biotic component of soil quality. Appl Soil Ecol 15(1):3–11. https://doi.org/10.1016/S0929-1393(00)00067-6
Escribano P, Schmid T, Chabrilla, S, Rodríguez-Caballero E, García M (2017) Optical remote sensing for soil mapping and monitoring. Soil mapping and process modeling for sustainable land use management, 87–125. https://doi.org/10.1016/b978-0-12-805200-6.00004-9
Eswaran H, Lal R, Reich PF (2001) Land degradation: an overview. In: Bridges EM, Hannam ID, Oldeman LR, de Vries FWTP, Scherr SJ, Sompatpanit S (eds) Responses to land degradation. Proceedings 2nd. International conference on land degradation and desertification, Khon Kaen, Thailand. New Delhi, Oxford Press
FAO (2019) Global soil partnership. http://www.fao.org/global-soil-partnership/en/
Finn MP, Lewis M, Bosch DD, Giraldo M, Yamamoto K, Sullivan DG, Kincaid R, Luna R, Allam GK, Kvien C, Williams MS (2011) Remote sensing of soil moisture using airborne hyperspectral data. GISci Remote Sen 48(4):522–540
Franceschini MHD, Demattê JAM, da Silva Terra F, Vicente LE, Bartholomeus H, de Souza Filho CR (2015) Prediction of soil properties using imaging spectroscopy: considering fractional vegetation cover to improve accuracy. Int J Appl Earth Obs Geoinf 38:358–370
Franceschini MH, Demattê JA, Kooistra L, Bartholomeus H, Rizzo R, Fongaro CT, Molin JP (2018) Effects of external factors on soil reflectance measured on-the-go and assessment of potential spectral correction through orthogonalisation and standardisation procedures. Soil Till Res 177:19–36
Francis RE, Reeves RG (1977) Manual of remote sensing. J Range Manag
Franzen DW, Peck TR (1995) Field soil sampling density for variable rate fertilization. J Prod Agric 8(4):568–574
Fussel J, Rundquist D, Harrington JA (1986) On defining remote sensing. Photogramm Eng Remote Sens 52(9):1507–1511
Gao BC, Heidebrecht KB, Goetz AF (1993) Derivation of scaled surface reflectances from AVIRIS data. Remote Sens Environ 44(2–3):165–178

Ge Y, Thomasson JA, Sui R (2011) Remote sensing of soil properties in precision agriculture: a review. Front Earth Sci 5(3):229–238

Genot V, Colinet G, Bock L, Vanvyve D, Reusen Y, Dardenne P (2011) Near infrared reflectance spectroscopy for estimating soil characteristics valuable in the diagnosis of soil fertility. J Near Infrared Spectrosc 19(2):117–138

Gerighausen H, Menz G, Kaufmann H (2012) Spatially explicit estimation of clay and organic carbon content in agricultural soils using multi-annual imaging spectroscopy data. Appl Environ Soil Sci 2012:1–23

Gholizadeh A, Borůvka L, Saberioon M, Vašát R (2013) Visible, near-infrared, and mid-infrared spectroscopy applications for soil assessment with emphasis on soil organic matter content and quality: state-of-the-art and key issues. Appl Spectrosc 67(12):1349–1362

Gholizadeh A, Saberioon M, Ben-Dor E, Borůvka L (2018) Monitoring of selected soil contaminants using proximal and remote sensing techniques: background, state-of-the-art and future perspectives. Crit Rev Environ Sci Technol 48(3):243–278

Glanz JT (1995) Saving our soil: solutions for sustaining earth's vital resource. Johnson Books, Boulder, CO

Goetz AFH (2009) Three decades of hyperspectral remote sensing of the Earth: a personal view. Remote Sens Environ 113:S5–S16

Goetz AFH, Vane G, Solomon JE, Rock BN (1985) Imaging spectrometry for earth remote sensing. Science 228(4704):1147–1153

Gogé F, Joffre R, Jolivet C, Ross I, Ranjard L (2012) Optimization criteria in sample selection step of local regression for quantitative analysis of large soil NIRS database. Chemom Intell Lab Syst 110(1):168–176

Gogé F, Gomez C, Jolivet C, Joffre R (2014) Which strategy is best to predict soil properties of a local site from a national Vis-NIR database? Geoderma 213:1–9

Goidts E, Van Wesemael B, Crucifix M (2009) Magnitude and sources of uncertainties in soil organic carbon (SOC) stock assessments at various scales. Eur J Soil Sci 60(5):723–739

Goldshleger N, Ben-Dor E, Chudnovsky A, Agassi M (2009) Soil reflectance as a generic tool for assessing infiltration rate induced by structural crust for heterogeneous soils. Eur J Soil Sci 60 (6):1038–1051

Gomez C, Raphael A, Rossel V, McBratney AB (2008) Soil organic carbon prediction by hyperspectral remote sensing and field vis-NIR spectroscopy: an Australian case study. Geoderma 146(3-4):403–411

Gomez C, Lagacherie P, Coulouma G (2012) Regional predictions of eight common soil properties and their spatial structures from hyperspectral Vis–NIR data. Geoderma 189-190:176–185

Guanter L, Kaufmann H, Segl K, Foerster S, Rogass C, Chabrillat S, Kuester T, Hollstein A, Rossner G, Chlebek C, Straif C (2015) The EnMAP spaceborne imaging spectroscopy mission for earth observation. Remote Sens 7(7):8830–8857

Guerrero C, Zornoza R, Gómez I, Mataix-Beneyto J (2010) Spiking of NIR regional models using samples from target sites: effect of model size on prediction accuracy. Geoderma 158 (1–2):66–77

Guerrero C, Wetterlind J, Stenberg B, Mouazen AM, Gabarrón-Galeote MA, Ruiz-Sinoga JD, Zornoza R, Rossel RA (2016) Do we really need large spectral libraries for local scale SOC assessment with NIR spectroscopy? Soil Tillage Res 155:501–509

Guo L, Zhang H, Shi T, Chen Y, Jiang Q, Linderman M (2019) Prediction of soil organic carbon stock by laboratory spectral data and airborne hyperspectral images. Geoderma 337:32–41

Haubrock S-N (2008) Surface soil moisture quantification and validation based on hyperspectral data and field measurements. J Appl Remote Sens 2(1):023552

Haubrock S, Chabrillat S, Kaufmann H (2004) Application of hyperspectral imaging and laser scanning for the monitoring and assessment of soil erosion in a recultivation mining area. In: Erasmi Cyffka B, Kappas M (eds) Remote Sens GIS Environ Stud Appl Geogr Goltze

Haubrock SN, Chabrillat S, Lemmnitz C, Kaufmann H (2008) Surface soil moisture quantification models from reflectance data under field conditions. Int J Remote Sen 29(1):3–29

Hill J, Schütt B (2000) Mapping complex patterns of erosion and stability in dry Mediterranean ecosystems. Remote Sens Environ 74(3):557–569
Hbirkou C, Pätzold S, Mahlein A-K, Welp G (2012) Airborne hyperspectral imaging of spatial soil organic carbon heterogeneity at the field-scale. Geoderma 175-176:21–28
Hollas JM (2005) Modern spectroscopy, 4th edn. Wiley, Chichester
Hunt GR (1977) Spectral signatures of particulate minerals in the visible and near infrared. Geophysics 42(3):501–513
Hunt GR, Salisbury JW (1971a) Visible and near-infrared spectra of mineral and rocks: I. silicate minerals. Moderns Geology 1:283–300
Hunt GR, Salisbury JW (1971b) Visible and near-infrared spectra of mineral and rocks: II. carbonates. Moderns Geology 2:23–30
Igne B, Reeves JB, McCarty G, Hively WD, Lund E, Hurburgh CR (2010) Evaluation of spectral pretreatments, partial least squares, least squares support vector machines and locally weighted regression for quantitative spectroscopic analysis of soils. J Near Infrared Spectrosc 18 (3):167–176
IUSS Working Group WRB (2015) World reference base for soil resources 2014, update 2015. International soil classification system for naming soils and creating legends for soil maps. World soil resources reports no. 106. FAO, Rome
Iznaga AC, Orozco MR, Alcantara EA, Pairol MC, Sicilia YE, De Baerdemaeke J, Saeys W (2014) Vis/NIR spectroscopic measurement of selected soil fertility parameters of Cuban agricultural Cambisols. Biosyst Eng 125:105–121
Janik L, Skjemstad J (1995) Characterization and analysis of soils using mid-infrared partial least-squares.2. Correlations with some laboratory data. Aust J Soil Res 33:637
Janik LJ, Merry RH, Skjemstad JO (1998) Can mid infrared diffuse reflectance analysis replace soil extractions? Aust J Exp Agric 38(7):681–696
Jarmer T, Hill J, Mader S (2007) The use of hyperspectral remote sensing data for the assessment of chemical properties of dryland soils in SE-Spain. In: Reusen I, Cools J (eds) Proceedings of the 5th EARSeL workshop imaging spectroscopy: innovation in environmental research, 23–25 April 2007. Bruges, Belgium. On CD-ROM
Jensen JR (2005) Introductory digital image processing: a remote sensing perspective (4th edn), Keith CC (ed), Prentice Hall Ser Geogr Inf, Sci Saddle River
Jensen JR, Jensen RR (2013) Introductory geographic information systems. Pearson, Boston, 400 p
Ji W, Viscarra Rossel RA, Shi Z (2015) Accounting for the effects of water and the environment on proximally sensed Vis–NIR soil spectra and their calibrations. Eur J Soil Sci 66(3):555–565
Johannsen CJ, Daughtry CST (2009) Chapter 17: Surface reference data collection. In: Warner TA, Nellis MD, Foody GM (eds) The handbook of remote sensing. Sage Publications, Los Angeles, pp 244–256
Joshi N, Baumann M, Ehammer A, Fensholt R, Grogan K, Hostert P, Jepsen MR, Kuemmerle T, Meyfroidt P, Mitchard ET, Reiche J (2016) A review of the application of optical and radar remote sensing data fusion to land use mapping and monitoring. Remote Sens 8(1):70
Karnieli A, Tsoar H (1995) Spectral reflectance of biogenic crust developed on desert dune sand along the Israel-Egypt border. Remote Sens 16(2):369–374
Karlen DL, Mausbach MJ, Doran JW, Cline RG, Harris RF, Schuman GE (1997) Soil quality: a concept, definition, and framework for evaluation (A guest editorial). Soil Sci Soc Am J 61 (1):4–10
Knadel M, Deng F, Thomsen A, Greve MH (2012) Development of a Danish national Vis-NIR soil spectral library for soil organic carbon determination. Digit Soil Assess Beyond
Kodaira M, Shibusawa S (2013) Using a mobile real-time soil visible-near infrared sensor for high resolution soil property mapping. Geoderma 199:64–79
Kriebel KT (1978) Average variability of the radiation reflected by vegetated surfaces due to differing irradiations. Remote Sens Environ 7(1):81–83
Krishnan P, Alexander JD, Butler BJ, Hummel JW (1980) Reflectance technique for predicting soil organic matter 1. Soil Sci Soc Am J 44(6):1282–1285

Kruse FA, Raines GI, Watson K (1985) Analytical techniques for extracting geologic information from multichannel airborne spectroradiometer and airborne imaging spectrometer data. In: Proceedings of the 4th thematic conference on remote sensing for exploration geology. 1–4 April, 1985, 309–324, California

Kweon G, Lund E, Maxton C (2013) Soil organic matter and cation-exchange capacity sensing with on-the-go electrical conductivity and optical sensors. Geoderma 199:80–89

La WJ, Sudduth KA, Kim HJ, Chung SO (2016) Fusion of spectral and electrochemical sensor data for estimating soil macronutrients. Trans ASABE 59(4):787–794

Lagacherie P, Baret F, Feret J-B, Netto JM, Robbez-Masson JM (2008) Estimation of soil clay and calcium carbonate using laboratory, field and airborne hyperspectral measurements. Remote Sens Environ 112(3):825–835

Lal R (2014) Societal value of soil carbon. J Soil Water Conserv 69(6):186A–192A

Lee CM, Cable ML, Hook SJ, Green RO, Ustin SL, Mandl DJ, Middleton EM (2015) An introduction to the NASA hyperspectral InfraRed imager (HyspIRI) mission and preparatory activities. Remote Sens Environ 167:6–19

Lekner J, Dorf MC (1988) Why some things are darker when wet. Appl Opt 27(7):1278–1280

Li S, Ji W, Chen S, Peng J, Zhou Y, Shi Z (2015) Potential of VIS-NIR-SWIR spectroscopy from the Chinese soil spectral library for assessment of nitrogen fertilization rates in the paddy-rice region, China. Remote Sens 7(6):7029–7043

Lobell DB, Asner GP (2002) Moisture effects on soil reflectance. Soil Sci Soc Am J 66(3):722–727

Lobsey CR, Viscarra Rossel RA (2016) Sensing of soil bulk density for more accurate carbon accounting. Eur J Soil Sci 67(4):504–513

Lopez RD, Frohn RC (2017) Remote sensing for landscape ecology: New metric indicators. CRC Press, Boca Raton. 2017 Aug 9

Lu P, Wang L, Zheng N, Li L, Zhang W (2013) Prediction of soil properties using laboratory VIS–NIR spectroscopy and hyperion imagery. J Geochem Explor 132:26–33

Makisara KM, Meinander M, Rantasuo M, Okkonen J, Aikio M, Sipola K, Pylkko P, Braam B (1995) Airborne imaging spectrometer for applications (ASIA). In: Proceedings international geosciences and remote sensing symposium, Digest, pp 479–481

Maleki MR, Mouazen AM, Ramon H, De Baerdemaeker J (2007) Optimisation of soil VIS–NIR sensor-based variable rate application system of soil phosphorus. Soil Till Res 94(1):239–250

Mendes WDS, Medeiros Neto LG, Demattê JAM, Gallo BC, Rizzo R, Safanelli JL, Fongaro CT (2019) Is it possible to map subsurface soil attributes by satellite spectral transfer models? Geoderma 343:269–279

Matthias AD, Fimbres A, Sano EE, Post DF, Accioly L, Batchily AK, Ferreira LG (2000) Surface roughness effects on soil albedo. Soil Sci Soc Am J 64(3):1035–1041

McCarty GW, Reeves JB, Reeves VB, Follett RF, Kimble JM (2002) Mid-infrared and near-infrared diffuse reflectance spectroscopy for soil carbon measurement. Soil Sci Soc Am J 66 (2):640–646

McDowell ML, Bruland GL, Deenik JL, Grunwald S (2012) Effects of subsetting by carbon content, soil order, and spectral classification on prediction of soil total carbon with diffuse reflectance spectroscopy. Appl Environ Soil Sci 2012

Miltz J, Don A (2012) Optimizing sample preparation and near infrared spectra measurements of soil samples to calibrate organic carbon and total nitrogen content. J Near Infrared Spectrosc 20 (6):695–706

Minasny B, McBratney AB, Bellon-Maurel V, Roger JM, Gobrecht A, Ferrand L, Joalland S (2011) Removing the effect of soil moisture from NIR diffuse reflectance spectra for the prediction of soil organic carbon. Geoderma 167:118–124

Minu S, Shetty A, Gopal B (2016) Review of preprocessing techniques used in soil property prediction from hyperspectral data. Cogent Geosci 2(1):1–7

Morgan CLS, Waiser TH, Brown DJ, Tom Hallmark C (2009) Simulated in situ characterization of soil organic and inorganic carbon with visible near-infrared diffuse reflectance spectroscopy. Geoderma 151(3-4):249–256

Mouazen AM, Maleki MR, De Baerdemaeker J, Ramon H (2007) On-line measurement of some selected soil properties using a VIS–NIR sensor. Soil Tillage Res 93(1):13–27
Mulder VL, De Bruin S, Schaepman ME, Mayr TR (2011) The use of remote sensing in soil and terrain mapping—a review. Geoderma 162(1–2):1–9
Murphy RJ, Wadge G (1994) The effects of vegetation on the ability to map soils using imaging spectrometer data. Remote Sens 15(1):63–86
Natale VG et al (2013) SHALOM—Space-borne hyperspectral applicative land and ocean mission, 2013 5th Workshop on hyperspectral image and signal processing: evolution in remote sensing (WHISPERS). Gainesville, FL, pp 1–4. https://doi.org/10.1109/WHISPERS.2013.8080667
Nocita M, Stevens A, van Wesemael B, Aitkenhead M, Bachmann M, Barthès B, Dor EB, Brown DJ, Clairotte M, Csorba A, Dardenne P (2015) Soil spectroscopy: an alternative to wet chemistry for soil monitoring. In: Advances in agronomy, vol 132. Academic Press, pp 139–159
Notarnicola C, Angiulli M, Posa F (2006) Use of radar and optical remotely sensed data for soil moisture retrieval over vegetated areas. IEEE Trans Geosci Remote Sens 44(4):925–935
O'neill AL (1994) Reflectance spectra of microphytic soil crusts in semi-arid Australia. Remote Sens 15(3):675–681
Padarian J, Minasny B, McBratney AB (2019a) Machine learning and soil sciences: a review aided by machine learning tools. SOIL discussions 2019 Sept 3:1–29
Padarian J, Minasny B, McBratney AB (2019b) Using deep learning to predict soil properties from regional spectral data. Geoderma Reg 16:e00198
Palmer KF, Williams D (1974) Optical properties of water in the near infrared. J Opt Soc Am 64 (8):1107–1110
Peón J, Recondo C, Fernández S, Calleja JF, De Miguel E, Carretero L (2017) Prediction of topsoil organic carbon using airborne and satellite hyperspectral imagery. Remote Sens 9(12):1211
Petropoulos GP, Ireland G, Barrett B (2015) Surface soil moisture retrievals from remote sensing: current status, products & future trends. Phys Chem Earth A/B/C 83:36–56
Pinker RT, Karnieli A (2007) Characteristic spectral reflectance of a semi-arid environment. Int J Remote Sens 16(7):1341–1363
Pignatti S, Palombo A, Pascucci S, Romano F, Santini F, Simoniello T, Umberto A, Vincenzo C, Acito N, Diani M, Matteoli S (2013) The PRISMA hyperspectral mission: Science activities and opportunities for agriculture and land monitoring. In: 2013 IEEE International Geoscience and Remote Sensing Symposium-IGARSS 2013 Jul 21 (pp 4558–4561). IEEE
Potter KN, Horton R, Cruse RM (1987) Soil surface roughness effects on radiation reflectance and soil heat flux. Soil Sci Soc Am J 51(4):855–860
Price M (1986) The analysis of vegetation change by remote sensing. Prog phys geogr earth environt 10(4):473–491
Priori S, Fantappiè M, Bianconi N, Ferrigno G, Pellegrini S, Costantini EA (2016) Field-scale mapping of soil carbon stock with limited sampling by coupling gamma-ray and Vis-NIR spectroscopy. Soil Sci Soc Am J 80(4):954–964
Qi H, Paz-Kagan T, Karnieli A, Jin X, Li S (2018) Evaluating calibration methods for predicting soil available nutrients using hyperspectral VNIR data. Soil Tillage Res 175:267–275
Qu Z, Goetz AFH, Heidbrecht KB (2001) High accuracy atmosphere correction for hyperspectral data (HATCH). In: Proceedings of the ninth JPL airborne earth science workshop, 00-18. JPL Publication, Pasadena, CA, pp 373–381
Ramirez-Lopez L, Behrens T, Schmidt K, Rossel RV, Demattê JA, Scholten T (2013a) Distance and similarity-search metrics for use with soil Vis–NIR spectra. Geoderma 199:43–53
Ramirez-Lopez L, Behrens T, Schmidt K, Stevens A, Demattê JAM, Scholten T (2013b) The spectrum-based learner: a new local approach for modeling soil Vis-NIR spectra of complex datasets. Geoderma 195–196:268–279
Ramirez-Lopez L, Wadoux AC, Franceschini MH, Terra FS, Marques KP, Sayão VM, Demattê JA (2019) Robust soil mapping at the farm scale with Vis–NIR spectroscopy. Eur J Soil Sci 70 (2):378–393

Rast M, Painter TH (2019) Earth observation imaging spectroscopy for terrestrial systems: an overview of its history, techniques, and applications of its missions. Surv Geophys 40 (3):303–331

Reda R, Saffaj T, Ilham B, Saidi O, Issam K, Brahim L (2019) A comparative study between a new method and other machine learning algorithms for soil organic carbon and total nitrogen prediction using near infrared spectroscopy. Chemom Intell Lab Syst 195:103873

Richter R, Schläpfer D (2002) Geo-atmospheric processing of airborne imaging spectrometry data. Part 2: atmospheric/topographic correction. Int J Remote Sens 23(13):2631–2649

Ricker N (1953) The form and laws of propagation of seismic wavelets. Geophysics 18(1):10–40

Rizzo R, Demattê JA, Lepsch IF, Gallo BC, Fongaro CT (2016) Digital soil mapping at local scale using a multi-depth Vis–NIR spectral library and terrain attributes. Geoderma 274:18–27

Roberts DA, Y Yamaguchi, R Lyon (1986) Comparison of various techniques for calibration of AIS data Proceedings of the 2nd airborne imaging spectrometer data analysis workshop 86:35, JPL Publication, Pasadena, CA, pp 21–30

Roger JM, Chauchard F, Bellon-Maurel V (2003) EPO–PLS external parameter orthogonalisation of PLS application to temperature-independent measurement of sugar content of intact fruits. Chemom Intell Lab Syst 66(2):191–204

Rogers RW, Lange RT (1972) Soil surface lichens in arid and subarid South-Eastern Australia. I. Introduction and floristics. Aust J Botany 20(2):197–213

Rossel VA (2011) Fine-resolution multiscale mapping of clay minerals in Australian soils measured with near infrared spectra. J Geophys Res Earth 116:F4

Rossel RV, Behrens T (2010) Using data mining to model and interpret soil diffuse reflectance spectra. Geoderma 158(1–2):46–54

Rossel VA, Hicks WS (2015) Soil organic carbon and its fractions estimated by visible–near infrared transfer functions. Eur J Soil Sci 66(3):438–450

Rossel RAV, Webster R (2012) Predicting soil properties from the Australian soil visible-near infrared spectroscopic database. Eur J Soil Sci 63(6):848–860

Rossel RV, Walvoort DJ, McBratney AB, Janik LJ, Skjemstad JO (2006) Visible, near infrared, mid infrared or combined diffuse reflectance spectroscopy for simultaneous assessment of various soil properties. Geoderma 131(1–2):59–75

Rossel RAV, Jeon YS, Odeh IOA, McBratney AB (2008) Using a legacy soil sample to develop a mid-IR spectral library. Aust J Soil Res 46(1):1–16

Rossel VR, Rizzo R, Demattê JA, Behrens T (2010) Spatial modeling of a soil fertility index using visible–near-infrared spectra and terrain attributes. Soil Sci Soc Am J 74(4):1293–1300

Rossel RV, Adamchuk VI, Sudduth KA, McKenzie NJ, Lobsey C (2011) Proximal soil sensing: an effective approach for soil measurements in space and time. In: Advances in agronomy, vol 113. Academic Press, pp 243–291

Rossel RV, Behrens T, Ben-Dor E, Brown DJ, Demattê JA, Shepherd KD, Shi Z, Stenberg B, Stevens A, Adamchuk V, Aïchi H (2016) A global spectral library to characterize the world's soil. Earth Sci Rev 155:198–230

Rossel VA, Lobsey CR, Sharman C, Flick P, McLachlan G (2017) Novel proximal sensing for monitoring soil organic C stocks and condition. Environ Sci Technol 51(10):5630–5641

Roudier P, Hedley CB, Ross CW (2015) Prediction of volumetric soil organic carbon from field-moist intact soil cores. Eur J Soil Sci 66(4):651–660

Sarathjith MC, Das BS, Wani SP, Sahrawat KL (2014) Dependency measures for assessing the covariation of spectrally active and inactive soil properties in diffuse reflectance spectroscopy. Soil Sci Soc Am J 78(5):1522–1530

Savitzky A, Golay MJ (1964) Smoothing and differentiation of data by simplified least squares procedures. Anal Chem 36(8):1627–1639

Schirrmann M, Gebbers R, Kramer E, Seidel J (2011) Soil pH mapping with an on-the-go sensor. Sensors 11(1):573–598

Schmid T, Rodriguez-Rastrero M, Escribano P, Palacios-Orueta A, Ben-Dor E, Plaza A, Milewski R, Huesca M, Bracken A, Cicuendez V, Pelayo M, Chabrillat S (2016)

Characterization of soil erosion indicators using hyperspectral data from a Mediterranean rainfed cultivated region. IEEE J Sel Top Appl Earth Obs Remote Sens https://doi.org/10.1109/JSTARS.2015.2462125

Schumann U, Fahey DW, Wendisch M, Brenguier JL (2013) Introduction to airborne measurements of the earth atmosphere and surface, in: airborne measurements for environmental research: methods and instruments. https://doi.org/10.1002/9783527653218.ch1

Selige T, Böhner J, Schmidhalter U (2006) High resolution topsoil mapping using hyperspectral image and field data in multivariate regression modeling procedures. Geoderma 136 (1–2):235–244

Shepherd KD, Walsh MG (2002) Development of reflectance spectral libraries for characterization of soil properties. Soil Sci Soc Am J 66(3):988–998

Sherman DM, Waite TD (1985) Electronic spectra of Fe^{3+} oxides and oxide hydroxides in the near IR to near UV. Am Mineral 70(11–12):1262–1269

Shi Z, Ji W, Viscarra Rossel RA, Chen S, Zhou Y (2015) Prediction of soil organic matter using a spatially constrained local partial least squares regression and the Chinese Vis-NIR spectral library. Eur J Soil Sci 66(4):679–687

Shoshany M, Goldshleger N, Chudnovsky A (2013) Monitoring of agricultural soil degradation by remote-sensing methods: a review. Int J Remote Sens 34(17):6152–6181

Soriano-Disla JM, Janik LJ, Viscarra Rossel RA, MacDonald LM, McLaughlin MJ (2014) The performance of visible, near-, and mid-infrared reflectance spectroscopy for prediction of soil physical, chemical, and biological properties. Appl Spectrosc Rev 49(2):139–186

Sparks DL (2002) Environmental soil chemistry, 2nd edn. Academic Press, San Diego, 352p

Staenz K, Szeredi T, Schwarz J (1998) ISDAS–A System for processing/analysing hyperspectral data: technical note. Can J Remote Sens 24:99–113. https://doi.org/10.1080/07038992.10855

Stamatiadis S, Evangelou L, Blanta A, Tsadilas C, Tsitouras A, Chroni C, Christophides C, Tsantila E, Samaras V, Dalezios N, Dimogiannis D (2013) Satellite visible–near infrared reflectance correlates to soil nitrogen and carbon content in three fields of the Thessaly plain (Greece). Commun Soil Sci Plant Anal 44(1–4):28–37

Steinberg A, Chabrillat S, Stevens A, Segl K, Foerster S (2016) Prediction of common surface soil properties based on Vis-NIR airborne and simulated EnMAP imaging spectroscopy data: prediction accuracy and influence of spatial resolution. Remote Sens 8(7):613

Stenberg B, Rossel RA, Mouazen AM, Wetterlind J (2010) Visible and near infrared spectroscopy in soil science. In: Advances in agronomy, vol 107. Academic, Burlington, pp 163–215

Stevens A, Udelhoven T, Denis A, Tychon B, Lioy R, Hoffmann L, Van Wesemael B (2010) Measuring soil organic carbon in croplands at regional scale using airborne imaging spectroscopy. Geoderma 158(1–2):32–45

Stevens A, Nocita M, Tóth G, Montanarella L, van Wesemael B (2013) Prediction of soil organic carbon at the European scale by visible and near infrared reflectance spectroscopy. PLoS One 8 (6)

Stoorvogel JJ, Kooistra L, Bouma J (2015) Managing soil variability at different spatial scales as a basis for precision agriculture. In: Lal R, Stewart BA, (eds). Soil-specific farming: precision agriculture. 1:37–72

Stuart MB, McGonigle AJ, Willmott JR (2019) Hyperspectral imaging in environmental monitoring: a review of recent developments and technological advances in compact field deployable systems. Sensors 19(14):3071

Tan K, Wang H, Chen L, Qian D, Peijun D, Pan C (2020) Estimation of the spatial distribution of heavy metal in agricultural soils using airborne hyperspectral imaging and random forest. J Hazard Mater 382:120987

Tekin Y, Kuang B, Mouazen AM (2013) Potential of on-line visible and near infrared spectroscopy for measurement of pH for deriving variable rate lime recommendations. Sensors 13 (8):10177–10190

Terra FS, Demattê JAM, Viscarra Rossel RA (2015) Spectral libraries for quantitative analyses of tropical Brazilian soils: comparing Vis-NIR and mid-IR reflectance data. Geoderma 255:81–93

Terra FS, Demattê JA, Rossel RA (2018) Proximal spectral sensing in pedological assessments: Vis–NIR spectra for soil classification based on weathering and pedogenesis. Geoderma 318:123–136

Terra FS, Rizzo R, Ben Dor E, Demattê JAM (2021) Chapter 41 – Soil sensing by visible and IR radiation. In: Ciurczak EW, Igne B, Workman J, Burns DA (eds) Handbook of near-infrared analysis, vol 1, 4th edn. CRC Press Taylor & Francis Group, Boca Raton, pp 479–519

Tian J, Philpot WD (2015) Relationship between surface soil water content, evaporation rate, and water absorption band depths in SWIR reflectance spectra. Remote Sens Environ 169:280–289

Tóth G, Montanarella L, Rusco E (2008) Threats to soil quality in Europe. Institute Environment Sustainability, Ispra

Townsend TE (1987) Discrimination of iron alteration minerals in visible and near-infrared reflectance data. J Geophys Res Solid Earth 92(B2):1441–1454

Vågen T-G, Shepherd KD, Walsh MG (2006) Sensing landscape level change in soil fertility following deforestation and conversion in the highlands of Madagascar using Vis-NIR spectroscopy. Geoderma 133(3–4):281–294

Vasques GM, Grunwald S, Harris WG (2010) Spectroscopic models of soil organic carbon in Florida, USA. J Environ Qual 39(3):923–934

Vasques GM, Demattê JA, Viscarra Rossel RA, Ramírez López L, Terra FD, Rizzo R, De Souza Filho CR (2015) Integrating geospatial and multi-depth laboratory spectral data for mapping soil classes in a geologically complex area in southeastern Brazil. Eur J Soil Sci 66(4):767–779

Vohland M, Ludwig M, Thiele-Bruhn S, Ludwig B (2017) Quantification of soil properties with hyperspectral data: selecting spectral variables with different methods to improve accuracies and analyze prediction mechanisms. Remote Sens 9(11):1103

Vrieling A (2006) Satellite remote sensing for water erosion assessment: a review. Catena 65 (1):2–18

Waiser TH, Morgan CLS, Brown DJ, Hallmark CT (2007) In situ characterization of soil clay content with visible near-infrared diffuse reflectance spectroscopy. Soil Sci Soc Am J 71 (2):389–396

Wang J, He T, Lv C, Chen Y, Wu J (2010) Mapping soil organic matter based on land degradation spectral response units using Hyperion images. Int J Appl Earth Obs Geoinf 12:S171–S180

Wetterlind J, Stenberg B (2010) Near-infrared spectroscopy for within-field soil characterization: small local calibrations compared with national libraries spiked with local samples. Eur J Soil Sci 61(6):823–843

Whiting ML, Li L, Ustin SL (2004) Predicting water content using gaussian model on soil spectra. Remote Sens Environ 89(4):535–552

Xu S, Zhao Y, Wang M, Shi X (2018) Comparison of multivariate methods for estimating selected soil properties from intact soil cores of paddy fields by Vis–NIR spectroscopy. Geoderma 310:29–43

Yang LY, Gao XH, Zhang W, Shi FF, He LH, Jia W (2016) Estimating heavy metal concentrations in topsoil from vegetation reflectance spectra of Hyperion images: a case study of Yushu county, Qinghai, China. Chinese J Appl Ecol. https://doi.org/10.13287/j.1001-9332.201606.030

Yang M, Xu D, Chen S, Li H, Shi Z (2019) Evaluation of machine learning approaches to predict soil organic matter and pH using Vis-NIR spectra. Sensors 19(2):263

Zhang T, Lin L, Zheng B (2013) Estimation of agricultural soil properties with imaging and laboratory spectroscopy. J Appl Remote Sens 7(1):073587

Žížala D, Zádorová T, Kapička J (2017) Assessment of soil degradation by erosion based on analysis of soil properties using aerial hyperspectral images and ancillary data, Czech Republic. Remote Sens 9(1):28

Chapter 9
Digital Soil Mapping: The Future Need of Sustainable Soil Management

Priyabrata Santra, Mahesh Kumar, N. R. Panwar, and R. S. Yadav

Contents

Abstract Digital soil mapping (DSM) involves in development of a statistical or mathematical model to estimate soil class or properties at unsampled locations using information on spatial variation of soil properties and different covariates affecting soil formation process. There are three main approaches followed in DSM, and these are geostatistical approach, state-factor (clorpt) approach, and pedotransfer function (PTF) approach. In the geostatistical approach, spatial variation parameters (nugget, sill, and range) are identified from a spatial soil database using semivariogram followed by making unbiased estimate of soil properties at unsampled location through kriging. In the state-factor (clorpt) approach, the soil formation theory is the backbone. In this approach soil is considered to be influenced by five major

P. Santra (✉) · M. Kumar · N. R. Panwar · R. S. Yadav
ICAR-Central Arid Zone Research Institute, Jodhpur, Rajasthan, India

T. Mitran et al. (eds.), *Geospatial Technologies for Crops and Soils*,
https://doi.org/10.1007/978-981-15-6864-0_9

factors: climate (cl), organism (o), relief (r), parent material (p), and time (t). Therefore, abundantly available information on these factors in different digital platforms are exploited to develop model to estimate soil properties at unsampled location. The PTF approach is used to develop digital soil maps of complex soil properties and difficult to measure soil properties. In this approach digital soil map of basic soil properties is first developed using the first two approaches, which are then combined to map of complex soil properties through PTF model. All these three approaches of DSM are discussed in detail along with assessment of its accuracy and uncertainty. Through the DSM approaches, available legacy soil data may be converted to digital products for its better accessibility and utility, e.g., through development of soil information system.

Keywords Digital soil mapping · Geostatistical modeling · Hyperspectral soil signatures · Machine learning · Pedotransfer functions · Soil information systems

Abbreviations

DEM	Digital Elevation Model
DSM	Digital Soil Mapping
DSMM	Digital Soil Mapping and Modeling
ANN	Artificial Neural Network
AWI	Arid Western India
IK	Indicator Kriging
KED	Kriging with External Drift
k-NN	k-nearest neighborhood
LCCC	Lin's Concordance Correlation Coefficient
LK	Lognormal Kriging
MLR	Multiple Liner Regression
OK	Ordinary Kriging
PK	Probability Kriging
PTF	Pedotransfer Function
RF	Random Forest
RK	Regression Kriging
SVM	Support Vector Machine
SVR	Support Vector Regression
UK	Universal Kriging
VIS-NIR-SWIR	Visible-Near-Infrared-Shortwave-Infrared

9.1 Introduction

Mapping soil properties has been conventionally done through surveying efforts followed by laboratory analysis. Soil maps developed by the conventional approach are generally hard copy maps and therefore are not easily accessible to end users. Moreover, mapping units of these maps are delineated based on soil profile data and surveyor's field experience. These mapping units sometimes represent quite a large area in the field, and thus soil properties of interest vary considerably within a unit. With the advancement of geostatistics and abundant availability of digital information on earth features, there is a possibility to map soil properties utilizing available soil data and auxiliary information on earth features and environmental variables. Through this approach, available legacy soil data may be converted to digital products for its better accessibility and utility. Moreover, in the context of digital India and soil health missions, it is timely and apt to prepare the digital soil maps for different regions of the country.

In a conventional approach, mapping of soil is done by expert surveyor based on his field observations and few auxiliary information, e.g., aerial photographs, remote sensing imageries, geological maps, vegetation pattern maps, etc. Information on different soil properties is attached to each polygon or mapping unit of the map. These labeled polygon maps are often called digital soil maps since the late 1970s. However, in a true sense, these maps cannot be called as digital soil maps; rather it can be called as digitized soil maps. In the DSM methodology, a statistical or mathematical model is developed to estimate soil class or properties at unsampled locations using the information on spatial variation of soil properties and different covariates affecting the soil formation process. DSM have recently gained importance in different parts of the world (McBratney et al. 2003; Lagacherie et al. 2006; Behrens and Scholten 2006; Grunwald 2009; Sanchez et al. 2009; Minasny and McBratney 2016). To get quantitative answers on the role of soil in carbon sequestration and its impact on biomass production and human health, the GlobalSoilMap.net project has been implemented by FAO and UNESCO in the year 2006. World Soil Information Centre (ISRIC, Netherland) has been working on several projects on DSM, e.g., Global Soil Information Facilities (GSIF), Africa Soil Information Service (AfSIS), World Inventory of Soil Emission Potentials (WISE), Soil and Terrain Database (SOTER), etc. Apart from these international programs, several countries have initiated their DSM programs, e.g., DIGISOL in Europe, OzDSM in Australia, NCSS DSM program of the USA, etc. Some of the digital soil products available in the WebGIS version are soil map of Scotland (http://www.soilsscotland.gov.uk/data/soilsurvey25k.php), soil information systems of California (http://casoilresource.lawr.ucdavis.edu/soilwebapps/), etc. All these DSM programs were based on legacy soil data available from different surveying efforts; however rapidly measurable soil spectral signatures have potential to improve the accuracy of the developed map (Shepherd and Walsh 2002; Brown et al. 2006; BenDor et al. 2009; Rossel et al. 2016; Katuwal et al. 2018).

Quantifying the spatial variation of soil properties for mapping purpose has been studied in India long ago by Agarwal and Gupta (1998) and Dahiya et al. (1998) followed by several researchers (Das 2007; Santra et al. 2008, 2012a, b, 2017a, b, c; Kamble and Aggrawal 2011; Chatterjee et al. 2015, Singh et al. 2016). Recently, Santra et al. (2017a, b, c) made a comprehensive review of DSM in India. Scattered efforts have been made by several researchers in India for soil spectral library generation (NBSS&LUP 2005; Saxena et al. 2003; Srivastava et al. 2004; Singh et al. 2014). Reflectance spectra of soil have also been used for the rapid characterization of soil properties. For example, (i) Santra et al. (2009) characterized soil hydraulic properties using proximal spectral reflectance, (ii) Gulfo et al. (2012) assessed soil moisture content using hyperspectral reflectance, (iii) Divya et al. (2014) characterized soil texture using hyperspectral reflectance, (iv) Kaduputiya et al. (2010) assessed soil nutrient contents using diffused reflectance spectra, etc. Apart from these, reflectance spectroscopy has been recently applied to estimate several soil properties in West Bengal, Rajasthan, Karnataka, etc. (Sharathjith et al. 2014; Santra et al. 2015, Mohanty et al. 2016; Gupta et al. 2016; Chakraborty et al. 2017). A detailed review of hyperspectral signature-based soil resource assessment is available in Das et al. (2015).

9.2 Digital Soil Mapping Methodology

DSM is the digital way of mapping soil properties. The digital way indicates the application of several computation methods and modeling approaches in the mapping procedure and finally presenting the soil maps in digital format rather than hard copy. A big advantage of the digital format of the soil map is the easy accessibility of it to end users. There are three main approaches followed in DSM or digital soil mapping and modeling (DSMM) as depicted in Fig. 9.1. These are the geostatistical approach, state-factor (clorpt) approach, and PTF approach. In the geostatistical approach, spatial variation parameters (nugget, sill, and range) are identified from a spatial soil database using semivariogram followed by making an unbiased estimate of soil properties at an unsampled location through kriging. In the state-factor (clorpt) approach, the soil formation theory proposed by Dokuchaev (1883) and Jenny (1941) is the backbone. In this approach, soil is considered to be influenced by five major factors: climate (cl), organism (o), relief (r), parent material (p), and time (t). Therefore, abundantly available information on these factors in different digital platforms are exploited to develop a model to estimate soil properties at an unsampled location. Later on, the clorpt approach is slightly modified by McBratney et al. (2003) including soil itself and the spatial locations of samples as a factor in the soil formation process, which is termed as "scorpan" approach. The pedotransfer approach is used to develop digital soil maps of complex soil properties and difficult to measure soil properties. In this approach, a digital soil map of basic soil properties is first developed using the first two approaches, which are then combined to map of complex soil properties through the PTF model. The PTF models are typically the

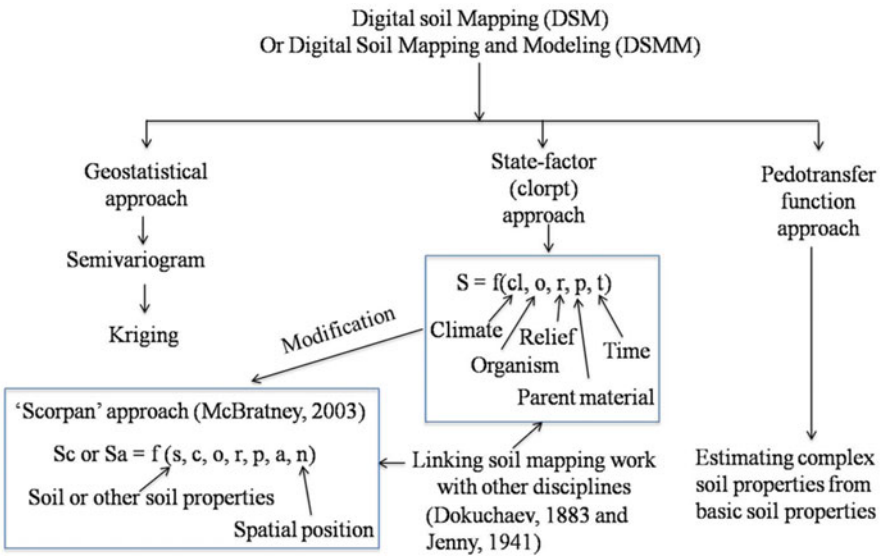

Fig. 9.1 Digital soil mapping approaches

regression-based models relating to complex soil properties with basic soil properties. Nowadays, PTFs are not only restricted to regression-based models; rather several advanced machine learning tools are applied.

9.3 Legacy Soil Data and Digital Soil Mapping

Surveying efforts during the past few decades have led to the development of large soil databases in different parts of the world but are often left as unused after achieving the primary goal of the survey. This large soil database is often called a legacy soil database. The legacy soil database of a country or a target ecosystem may be utilized to develop digital soil maps, which then can be reutilized by stakeholders in different land management decisions. However, these legacy soil data need to be harmonized both temporally and depth-wise. In the case of temporal harmonization, the time-dependent changes of soil properties, if any, are identified, and then soil properties at a particular time reference are computed. In the case of depth harmonization, the soil properties for standard soil depths are computed using the spline technique. Six standard soil depths as followed by FAO Global Soil Mapping protocol are 0–5, 5–15, 15–30, 30–60, 60–100, and 100–200 cm.

A schematic diagram to utilize legacy soil data in DSM is presented in Fig. 9.2. There are several sources of legacy soil data (e.g., soil series-level database, soil atlas, local soil archive, published soil data in journals, etc.), which may be collated together in a single platform. If the number of soil sampling points in the legacy soil

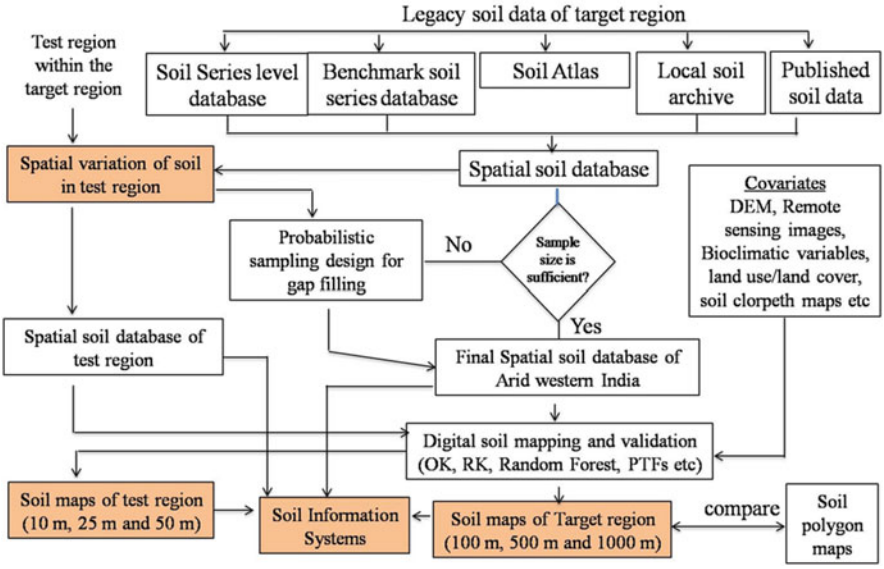

Fig. 9.2 A framework of DSM using legacy soil data

data is large enough to draw the semivariogram plot and to identify the spatial variation pattern, then we can straightway go for DSM using standard procedure. Otherwise, additional sampling effort may be required to fill the gap in sampling locations in order to compute the robust semivariogram model. For this purpose, a test region in the targeted spatial domain for DSM may be identified, and spatial variation pattern of the selected soil properties may be identified. Using this known spatial variation pattern, probabilistic sampling design may be formulated to increase the sampling density within the extent of the target area. Later on, information on several covariates may be used to develop accurate digital soil maps of the target area.

9.4 Scale Issue in DSM

Accuracy and uncertainty of digital soil maps largely depend on the scale of spatial data. The scale is defined by scale triplets (Blöschl and Sivapalan 1995), which are spacing, support, and extent (Fig. 9.3). The spacing is defined as the distance between a pair of sampling points, the extent is defined as the maximum distance between two sampling points in two-dimensional space of a spatial data, and the support is defined as the ground area from where the sample is collected and analyzed in the laboratory to represent it as a point data in a spatial database. These three scale triplets uniquely specify the scale of a spatial soil database and generally help to identify the pattern in the data. For example, the spatial extent of a

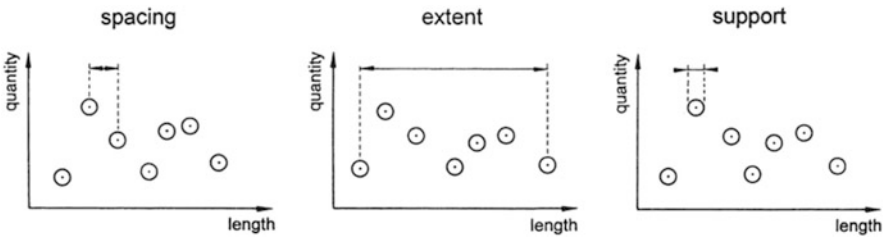

Fig. 9.3 The scale triplet (spacing, extent, and support). (Adopted, Blöschl and Sivapalan 1995)

spatial soil database in a farmer's field may be a maximum 100–200 m in India, whereas for a state-level spatial soil database, the extent is about 600–800 km. The support for measurement of bulk density in the field is about 5 cm, whereas if we take multiple samples from a field and then composting it to a single value for that field, then the support of that measurement will be total field block. Spacing is another important scale parameter in the DSM approach specifically in the geostatistical approach. If the minimum spacing between a sampling pair in the spatial database is large, then it will not be able to capture the spatial variation parameter. In the case of large spacing, the sampling density is low, whereas in closed spaced sampling points, the sampling density is high. It is always desirable to have large sampling density in the spatial database; however, the cost and time involved in achieving this optimistic sampling density is also needed to be looked into.

Therefore, the scale issue of a spatial soil database needs to be resolved first, and it depends on the soil properties on which we are interested to identify the spatial variation. The effect of the sampling scale on hydrological processes is beautifully depicted schematically by Blöschl and Sivapalan (1995), which is presented here in Fig. 9.4. This explanation for the hydrological process in the figure is also true for the spatial pattern of soil properties. In the figure, the solid line represents the natural variation of soil properties, whereas the small circles represent sampling locations. In general, it is not possible to collect soil samples from all possible locations to capture the full natural variability of the target soil property. Rather, we collect soil samples from a subset of all possible locations. For example, if we take soil samples following Fig. 9.4a, we fail to capture the microscale variation in the data because the spacing is too large to capture this small-scale variation. This type of spatial pattern may be observed for soil nutrient content which is highly influenced by specific land management practices followed in fragmented land units in an area. Under such a situation, the spacing between sampling pairs needs to be decreased or the sampling density needs to be increased, and this change in sampling scale is again to be optimized with sampling budget and time constraints. In another case, as shown in Fig. 9.4b, if the extent of the data is too small, then it will not capture the large-scale variability. Therefore, we need to increase our survey area to include large-scale variations of the soil property in the data. In this case, we may ignore excessive sampling with small separation distance; rather we may shift our focus to

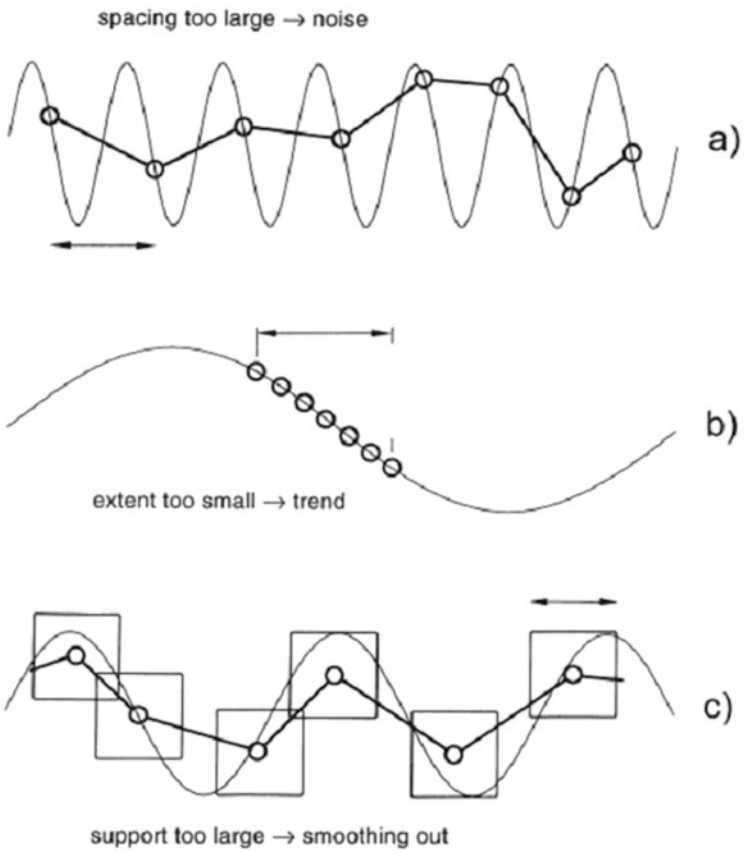

Fig. 9.4 The effect of measurement scale on capturing the "true" spatial pattern. The circles are the measurements, and the thin line is the "true" spatial pattern. (Adopted, Blöschl and Sivapalan 1995)

include sampling pairs with large separation distance. Such type of large-scale variation may be observed in soil properties which are more influenced by parent material, which has large spatial continuity. In the third case as depicted in Fig. 9.4c, if the support is quite large, then most of the variability in the data will be smoothed out. Measurement of soil properties is generally done based on samples collected from the field using an auger or sampling core with a cross-sectional area having 4–5 cm diameter. Therefore, support of measurements of soil properties is about 4–5 cm, which is often assumed as point support considering the large extent of the field as compared to the support. Sometimes, in situ measurement of soil properties is carried out with large support, e.g., about 20–40 cm for infiltration measurements, about 2–4 m for in situ measurement of soil water retention, etc. Often, we composite the soil samples from multiple locations in a field and in the process we increase the support of measurements to rule out the random variation in the field. In a regional-scale soil mapping, the support of measurements may be increased to 1 ha by making

multiple measurements in 1 ha field and then averaging it to a single value. However, in a field-scale soil mapping, such an increase in support is not desirable. From the above discussion, we understand that issue of sampling scale can be resolved after gathering knowledge on natural variation of soil properties. The question may be asked that "how we can know the natural variation of a soil property so that we can optimize the sampling strategy?" Natural variation of a soil property in an area may be approximated from previously identified spatial variation parameters of the target soil property from a nearby place. Otherwise, it may also be approximated from a preliminary survey. Later on, sampling efforts may be designed through probabilistic sampling theory with prior knowledge on spatial variation identified in the preliminary survey.

9.5 Geostatistical Approach of Digital Soil Mapping

In geostatistics, soil property at a particular location [$Z(x)$] is considered as a set of values following a probability distribution and not just a single value. Therefore, at each possible location x, a soil property, $Z(x)$, is considered as a random variable with a mean, μ, and a variance, σ^2. This description of random variable of $Z(x)$ applies to infinitely many locations in space. At each possible location in space (x_i, i=1, 2, 3...), it has its own probability distribution. Therefore, a range of possible values exists at a particular location following the probability distribution, and this is called an ensemble. One member from this ensemble for a particular location is called as realization of the property and is represented as $Z(x_i)$. A set of random variables or multiple realizations, $Z(x_1)$, $Z(x_2)$...$Z(x_i)$, is called as a random function, a random process, or a stochastic process. The set of true values of Z at each possible location that comprise the true realization of the random function is known as a regionalized variable.

Following the regionalized variable theory, values of the variables which are located near to each other are expected to be similar, whereas values of the variables which are separated from each other by a large distance are expected to be dissimilar. This relation of regionalized variables may be described by covariance. In classical statistics, covariance of two variables z_1 and z_2 for n pair of observations can be written as

$$C(z_1, z_2) = \frac{1}{n} \sum_{i=1}^{n} (z_{i,1} - \overline{z_1})(z_{i,2} - \overline{z_2}) \tag{9.1}$$

Likewise, in geostatistics, the covariance of a regionalized random variable, Z, for two locations (x_1 and x_2) can be written as

$$C(x_1, x_2) = E[\{z(x_1) - \mu(x_1)\}\{z(x_2) - \mu(x_2)\}] \tag{9.2}$$

However, we cannot simply calculate the covariance because we do not know exactly the value of $\mu(x_1)$ and $\mu(x_2)$. We have measured only one value at each location x_1 and x_2. To solve this problem, assumption of stationarity comes into picture.

The stationarity rule of geostatistics implies that the distribution of a random process has certain parameters that are stationary across all possible locations in two-dimensional space. The first-order stationarity states that the expected value of a regionalized variable at any location is constant for all x, which is mathematically written as $E[Z(x)]=\mu$. Assuming the first-order stationarity rule, we can replace mean of the regionalized variable at all possible location $[\mu(x_1), \mu(x_2),\ldots\mu(x_i)]$ by a single value μ. The value of μ can be estimated from arithmetic averaging of measured values at multiple locations. The second-order stationarity rule states that the squared deviation of the value from μ at all possible locations is also constant and equals to square of standard deviation. Mathematically, the second-order stationarity is written as $E\ [\{Z(x)\text{-}\mu\}^2]= \sigma^2$. Another rule of second-order stationarity defines the stationarity of covariance, which states that covariance of the regionalized variables located at two locations x_i and x_j depends only on their separation distance and not on their absolute positions. By applying this stationarity rule, it can be stated that for any pair of observation points x_i and x_j separated by a lag distance h, $E\ [\{Z(x_i)\text{-}\mu\}\{Z(x_j)\text{-}\mu\}] = C(x_i,x_j)$ and is constant for any given h. Therefore, the constancy of mean, variance, and covariance as discussed above are called as the second-order stationarity or weak stationarity.

After considering the stationarity rule, the auto-covariance function can be rewritten as

$$\begin{aligned} &COV[Z(x), Z(x+h)] \\ &= E[\{Z(x) - \mu\}\{Z(x+h) - \mu\}] \\ &= E\left[\{Z(x)\}\{Z(x+h)\} - \mu^2\right] \\ &= C(h) \end{aligned} \tag{9.3}$$

The above covariance is also called as auto-covariance since it represents the covariance of Z with itself but at different locations. To remove the dependence of auto-covariance on scale, i.e., h, it is often represented as dimensionless parameter autocorrelation, $\rho(h)$:

$$\rho(h) = \frac{C(h)}{C(0)} \tag{9.4}$$

where $C(0)$ is the covariance at lag 0, which is actually σ^2.

After assuming the stationarity rules, problem arises again to consider μ to be constant within the sampling domain. Generally, μ changes in field as we keep on increasing the extent of sampling domain, and variances also increase with increase

in area of interest. Here, Matheron (1965) identified the problem and proposed the intrinsic hypothesis, which states that for a short separation distance at least, the difference between $Z(x)$ and $Z(x+h)$ is zero and the term covariance is replaced by variance of the difference in $Z(x)$ and $Z(x+h)$. In mathematical formula, these two hypotheses are written as

$$E[Z(x) - Z(x+h)] = 0 \tag{9.5}$$

$$VAR[Z(x) - Z(x+h)] = E\left[\{Z(x) - Z(x+h)\}^2\right] = 2\gamma(h) \tag{9.6}$$

where $\gamma(h)$ refers to semivariance, which is obviously the half of the variance.

9.5.1 Semivariogram

Semivariance as a function of h is called the semivariogram. From field measurements of soil properties at multiple locations, experimental semivariograms $\widehat{\gamma}(h)$ for different lag distances h are calculated as follows (Goovaerts 1998):

$$\widehat{\gamma}(h) = \frac{1}{2N(h)} \sum_{i=1}^{N(h)} [Z(x_i) - Z(x_i + h)]^2 \tag{9.7}$$

where $N(h)$ is the number of data pairs within a given lag class, $Z(x_i)$ is the value of the variable at the location x_i, and $Z(x_i+h)$ is the value of the variable at a lag of h from the location x_i. Experimental semivariograms $[\widehat{\gamma}(h)]$ as obtained from Eq. (9.7) are generally fitted in standard models so as to obtain the spatial variation parameters: nugget (C_0), sill ($C + C_0$), and range (a). Weighted least square technique is generally followed in fitting procedure, and the weight to semivariogram value at each lag is assigned in such a way that it is inversely proportional to the number of pairs for that particular lag. Sometimes, the semivariogram values at smaller lags are assigned with higher weights than the semivariogram values at large lag distance. During semivariogram calculation, maximum lag distance is generally taken as half of the minimum extent of sampling area so as to minimize the border effect. We are not discussing here the isotropic and anisotropic semivariogram. For general purpose, omnidirectional or isotropic semivariogram is followed if there is no trend of direction on the data. However, if there is strong trend of x- and y-direction on the data, the anisotropic semivariogram may also be calculated. Best-fit semivariogram model is selected with the lowest value of fitting error. Four commonly used semivariogram models are spherical, exponential, Gaussian, and linear, and mathematical expressions of these models are given below:

$$\text{Spherical model}: \quad \gamma(h) = C_0 + C\left[1.5\frac{h}{a} - 0.5\left(\frac{h}{a}\right)^3\right] \text{ if } 0 \leq \text{h} \leq \text{a; otherwise } C_0 + C \tag{9.8}$$

$$\text{Exponential model}: \quad \gamma(h) = C_0 + C_1\left[1 - \exp\left\{-\frac{h}{a}\right\}\right] \quad \text{for } h \geq 0 \tag{9.9}$$

$$\text{Gaussian model}: \quad \gamma(h) = C_0 + C\left[1 - \exp\left\{\frac{-h^2}{a^2}\right\}\right] \text{ for } h \geq 0 \tag{9.10}$$

$$\text{Linear model}: \quad \gamma(h) = C_0 + C_1\left[\frac{h}{a}\right] \text{ if } h < \text{a; otherwise} = C_0 + C_1 \tag{9.11}$$

Apart from these four standard models, the Matern model is also quite often used. The parameter a in all these semivariogram models indicates range up to which spatial correlation between a pair of observation exists, beyond which a pair of observations is not spatially correlated. However, in case of exponential and Gaussian models, a represents the theoretical range, whereas practical range for these two semivariogram models is the lag distance at which semivariogram value reaches to 95% of sill. In all the above semivariogram models, nugget is expressed as C_0, which actually quantifies microscale variation and measurement error for the respective soil property, whereas partial sill (C) indicates the amount of variation which can be defined by spatial correlation structure.

All these semivariogram models as discussed above are called as bounded semivariogram models or authorized semivariogram models. Apart from bounded semivariograms, there are some unbounded semivariograms also. The major feature of unbounded semivariogram is continuous increase in semivariogram values with lag distance and is generally expressed by the formula $\gamma(h) = wh^{\alpha}$, where $\gamma(h)$ is the semivariogram for a lag distance h, w describes the intensity of variation, and α describes the curvature. For a value of α=1, the semivariogram is unbounded liner and w is simply the gradient. The parameter α has lower limit 0 and upper limit 2. In case of α<1, the semivariogram looks like convex upward, whereas for α>1, the semivariogram looks like concave upward. It is very strange to obtain unbounded variation or infinite variation of a feature on earth surface. However, often we observe infinite variation on this planet. This is so because we have been encountering more variation as long as we have been incorporating new regions into survey. This type of unbounded variation is observed if the environmental variables and parent material have influence on soil property. Thus, the unbounded variation is often neglected; rather a bounded semivariogram model is generally tried to fit in the experimental variograms. For this purpose, we generally detrend the influence of

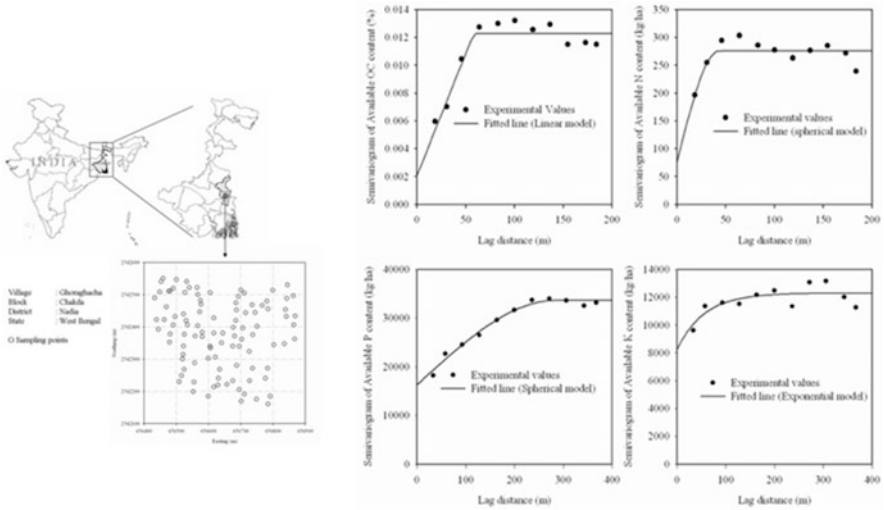

Fig. 9.5 Semivariogram of SOC and major soil nutrient contents (N, P, and K) in an intensively cultivated village in West Bengal, India. (Adopted, Chatterjee et al. 2015)

direction (*x*- and *y*-direction), environmental covariates, and other earth features on soil properties. After detrending, the residual value is again fitted in standard models.

Experimental and fitted semivariogram of soil organic carbon (SOC) and major nutrient (N, P, and K) contents in an intensively cultivated village at Gayeshpur, West Bengal, is presented in Fig. 9.5 (Chatterjee et al. 2015). From these semivariogram structures, it is observed that spatial variation pattern is different for different soil properties. Spherical semivariogram model was found best fitted for N and P content, whereas the linear model is best fitted for SOC content, and the exponential model is best fitted for K content. If we look at the range of spatial variation, it is higher in P content and less in N content. It indicates that spatial variation of P content shows more spatial continuity than other soil properties in this case. The variation of N content is highly random since it is highly influenced by external inputs of nitrogenous fertilizer. These semivariograms also show that how much the proportion of total sill is contributed by the nugget component. The more is the nugget component, the less is the spatial variation component and the more is the randomness. In a pure nugget model, the total variation is contributed by nugget and there is no spatial component.

9.5.2 Kriging

Once the semivariogram parameters are identified, it is possible to estimate the soil property at unsampled location through kriging approach, and ordinary kriging (OK) is mostly followed for this purpose. In OK, the unbiased estimates of soil

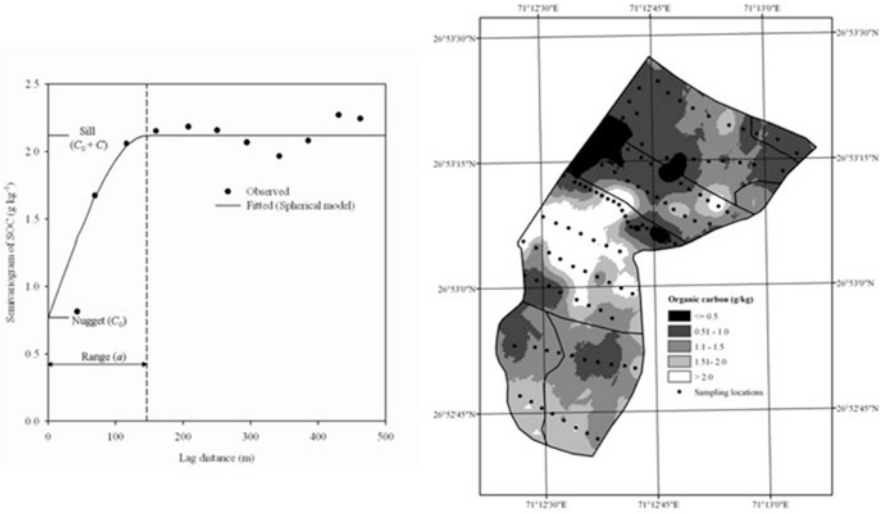

Fig. 9.6 Semivariogram and ordinary kriging map of SOC content in a farmer's field at Jaisalmer. (Adopted, Santra et al. 2012a, b)

properties at unsampled locations, $\widehat{z}(u)$, are computed through weighted linear combinations of measured soil attributes at neighbor points z (u_α) located within a neighborhood centered around u:

$$\widehat{z}(u) = \sum_{\alpha=1}^{n(u)} \lambda_\alpha z(u_\alpha) \tag{9.12}$$

where λ_α is the weight assigned to the measured data points $z(u_\alpha)$ located within a given neighborhood, $W(u)$ centered on u. Weights for n number of neighbor points are chosen in such a way so that error variance, $\sigma_E^2(u) = Var\{z*(u) - z(u)\}$, is minimized under the constraint of no bias of the estimator. Figure 9.6 shows a map of soil organic content in a farmer's field at Jaisalmer, Rajasthan, prepared through OK approach (Santra et al. 2012a). From Fig. 9.6, it may be noted that the range of SOC content is around 150 m, which indicates that soil sampling locations that are apart by 150 m or less are spatially correlated with each other beyond which it shows a random pattern. In the case of a random pattern, which is generally observed for the pure nugget model, the arithmetic average of all sampling points could be a simple approach to obtain an estimate. However, still we prefer nugget model semivariogram because in this case, we get an estimate at an unsampled location along with error variance, which helps to judge the reliability of the estimate. Later on, we will discuss the accuracy and uncertainty issue of a digital soil map. Such a digital soil map may be quite helpful for the management of organic manure applications in a farmer's field.

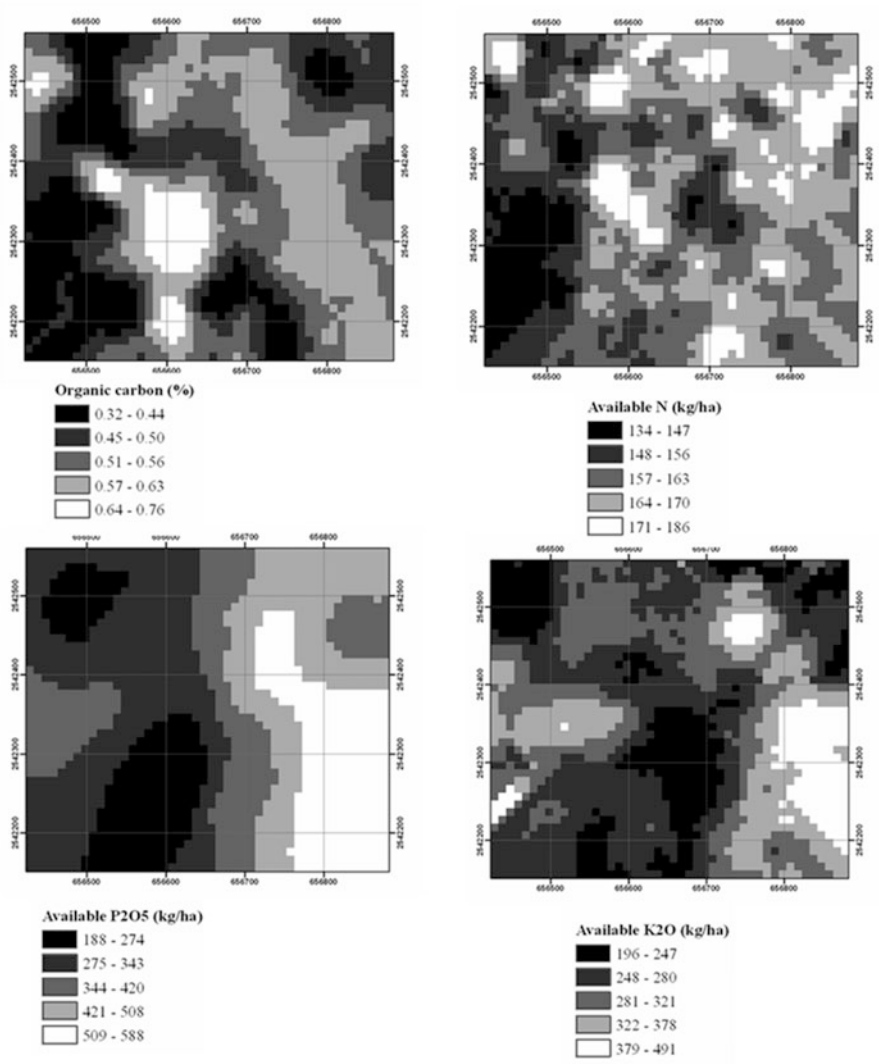

Fig. 9.7 Ordinary kriging map of SOC and major soil nutrient (N, P, and K) content in an intensively cultivated village in West Bengal, India. (Adopted, Chatterjee et al. 2015)

Apart from the SOC content map, digital maps of soil nutrient content prepared through the OK approach are depicted in Fig. 9.7. The spatial continuity in P content as we observed in the semivariogram of this property (Fig. 9.5) is also clearly visible on the map. The patchy variation in N content is quite understood from the short range in semivariogram. These maps of soil nutrient content will be quite helpful for nutrient management in the agricultural field. However, it is quite difficult to obtain a good spatial variation structure of nutrient content since it is largely influenced by

the application of fertilizer. Therefore, it is suggested to include the past history of fertilizer doses applied at different locations in the field to detrend the influence of external fertilizer application and then modeling the spatial variation using the standard semivariogram.

9.5.3 Co-kriging

Sometimes, the target soil property, which we want to estimate spatially, is very costly and time-consuming to measure at multiple locations in the field. In those cases, we use the information about surrogate soil properties, which have an influence on target soil properties. Co-kriging may be a suitable solution under such a situation. For applying co-kriging, the data on co-variables may be available at the same locations where the measured value of the target variable is available (co-located points) or may be available at other locations or both. Generally, co-kriging is most appropriate if the co-variables can be measured cheaply and therefore a denser sampling of co-variables than of target variable can be done. A detailed description of the co-kriging method can be found in Webster and Oliver (2007) and Rossiter (2018). Here, the co-kriging system is mentioned in brief to understand the theory behind it. Co-kriging is an extension of the theory of single regionalized variable used for OK. Similar to semivariogram, the cross-semivariogram between the target variable and co-variable is calculated as follows:

$$\widehat{\gamma}_{uv}(h) = \frac{1}{2m(h)} \sum_{i=1}^{m(h)} \{z_u(x_i) - z_u(x_i + h)\}\{z_v(x_i) - z_v(x_i + h)\} \tag{9.13}$$

where $\widehat{\gamma}_{uv}(h)$ is the cross-semivariogram between target variable, z_{u}, and co-variable, z_{v}, and $m(h)$ is the number of data pairs of target variable and co-variable with a lag distance of h. The co-kriging system estimates z_u at unknown location x_0 with the following expression:

$$z_u(x_0) = \sum_{l=1}^{V} \sum_{i=1}^{n_l} \lambda_{il} z_l(x_i) \tag{9.14}$$

where V is the number of variables and among these one is target variable and λ_{il} is the weight, which is assigned in such a way that

$$\sum_{i=1}^{n_l} \lambda_{il} = \begin{cases} 1 & l = u \\ 0 & l \neq u \end{cases} \tag{9.15}$$

An example of cross-semivariogram of SOC with pH and EC is depicted in Fig. 9.8. It is to be noted here that this cross-semivariogram is calculated because of

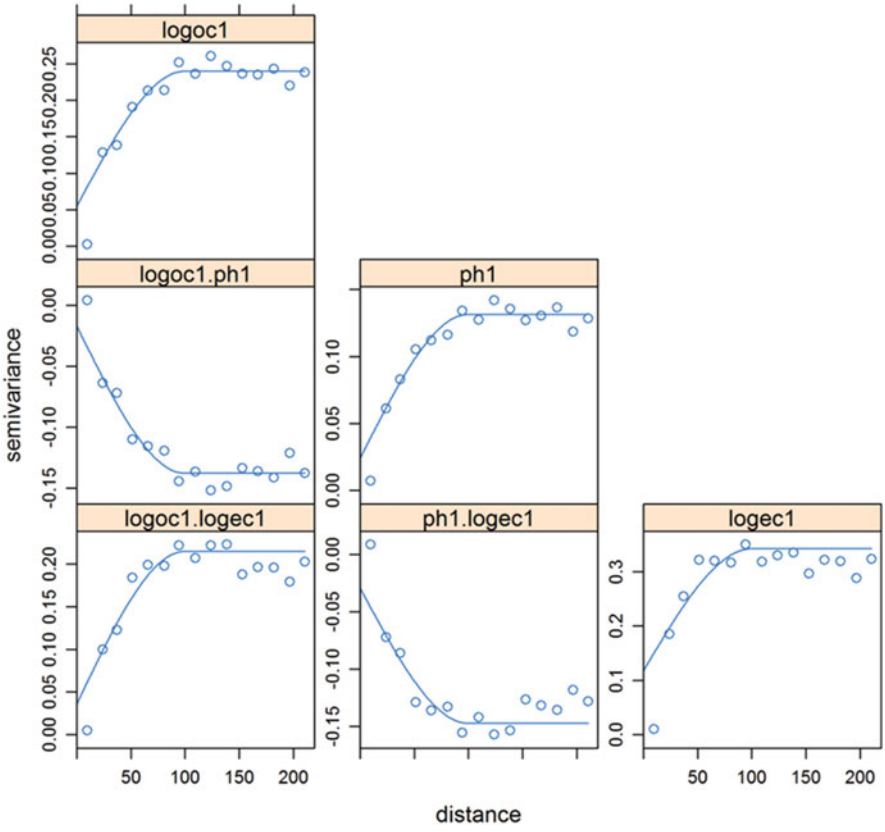

Fig. 9.8 Cross-variograms of SOC contents, pH, and electrical conductivity (EC)

significant correlation of SOC with pH and EC. From the cross-semivariogram, it is observed that range of target variable (OC) is almost similar with the co-variables (pH and EC) and this should be a major criterion to apply co-kriging.

If OK is compared with co-kriging, we generally observe that the prediction performance is improved in co-kriging. However, the uncertainty of prediction is higher in the case of co-kriging since multiple numbers of variables are employed in the prediction process. For example, the performance of OK and co-kriging in the prediction of SOC content in the above example is presented in Table 9.1. Mean error (ME) and root mean squared residual (RMSR) of predicted SOC are slightly lower in co-kriging than OK, and the performance is best when both the co-variables (pH and EC) are used in the co-kriging process. Such superior performance of co-kriging was also reported in literatures, e.g., Ersahin (2001), Carter et al. (2011), etc. However, the value of mean squared deviation ratio (MSDR), which generally quantifies the uncertainty, deviates from its desirable value of 1 in case of co-kriging. This suggests that co-kriging improves the prediction of the target variable but along with it also increases the uncertainty in predicted values;

Table 9.1 Cross-validation performances of ordinary kriging and co-kriging

Kriging method	Target variable	Covariates	Soil layer (cm)	ME	RMSR	MSDR
Ordinary kriging	Log[SOC]	-	0-15	0.0085	0.37	1.04
			15-30	0.0053	0.35	0.95
Co-kriging	Log[SOC]	pH	0-15	-0.0018	0.28	1.13
			15-30	0.0005	0.31	1.07
	Log[SOC]	Log [EC]	0-15	0.0018	0.30	1.12
			15-30	-0.0002	0.30	1.11
	Log [SOC (%)]	pH and Log [EC]	0-15	-0.0005	0.26	1.15
			15-30	-0.0006	0.28	1.14

therefore, it is strictly followed if only the target variable is very costly and time-consuming to measure in the field. Otherwise, it is always advisable to follow OK.

9.5.4 Other Variants of Kriging

The OK approach is mostly followed for providing a spatial estimate of soil property. When the OK approach provides the estimate for a point location, it is called punctual kriging. Otherwise, if the OK approach provides the estimate over block support, then it is called block kriging. Other than OK, simple kriging is also sometimes followed where the mean value of the target variable is known. Apart from OK and co-kriging, there are several variants of kriging approaches, e.g., regression kriging (RK), universal kriging (UK), kriging with external drifts (KED), probability kriging (PK), indicator kriging (IK), lognormal kriging (LK), etc. Regression kriging is followed if there is a presence of an external trend on data. Under such cases trend is predicted through regression model, and regression residual is predicted through OK, which is finally added to obtain RK prediction. RK is often confused with UK and KED since all these three kriging approaches model the trend (drift) in the data. However, there is little difference between RK and (UK and KED). In the case of RK, the trend and residuals are predicted separately, whereas in the case of UK and KED, trend and residual predictions are made simultaneously within the kriging system. In the case of UK, the trend of spatial coordinates is only considered, whereas in the case of KED, the trend of an external variable is modeled. The PK is able to provide an estimate with a probability to be near to a predefined threshold value and thus is often used to assess the risk associated with a target variable. The IK is a nonparametric and nonlinear approach of kriging where target variables are converted to a binary variable (indicator). In the case of LK, the target variable is first transformed logarithmically to fit it in a normal

distribution, and then OK is applied on the log-transformed variable. However, to understand better the prediction, it is to be back-transformed. The back-transformation of predicted log-transformed values needs to be done carefully following the standard procedure; otherwise, it will lead to wrong interpretation (Webster and Oliver 2007). Details of all these kriging approaches are available in Webster and Oliver (2007) and Santra et al. (2017b, c).

9.6 State-Factor (Clorpt) Approach of DSM

In the state-factor approach, statistical models are built between target soil property and the "clorpt" factors. The information on "clorpt" factor is now abundantly available in digital platforms, which are often called as covariates. Apart from the availability of data on covariates, several statistical and mathematical tools have been evolved in recent times, which have the capability to handle a huge amount of fine-resolution data on covariates and also are able to build model both linear and nonlinear relationship. Therefore, the state-factor approach of DSM methodologies has now been preferred over the other two approaches. In the following, we describe the data on covariates and the machine learning tools that are available to apply the DSM methodology.

9.6.1 Covariates on Terrain Attributes

Maps of terrain attributes provide information on the relief factor of the "clorpt" approach. Different terrain attributes can be calculated using the digital elevation model (DEM) of an area. Hydrology and spatial analysis tools of GIS software, e.g., ArcGIS, QGIS, SAGA, etc., may be used to determine these terrain attributes. For the processing of DEM of a targeted study area, the data acquired through Shuttle Radar Topography Mission (SRTM) with a spatial resolution of 90 m may be used which is available at http://srtm.csi.cgiar.org/ (Rabus et al. 2003). In Fig. 9.9, examples of terrain attributes determined from SRTM DEM of arid western India are presented. These terrain attributes are altitude, slope, elevation, above channel network, hillshade, profile curvature, plan curvature, terrain ruggedness index (TRI), and topographic wetness index (TWI).

A detailed description of such terrain properties may be found in Santra et al. (2017a). All these derived terrain attributes have significant relation with sand content in arid western India as observed through stepwise regression analysis.

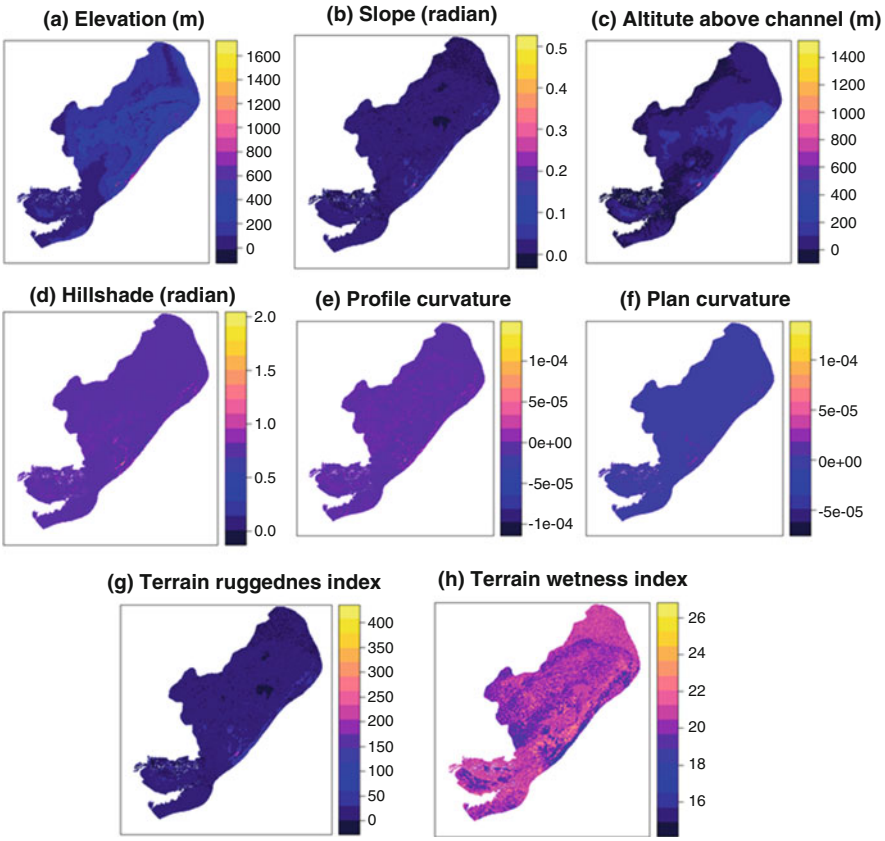

Fig. 9.9 Covariate maps of terrain attributes in arid western India. (Adopted, Santra et al. 2017a)

9.6.2 Covariates on Bioclimatic Variables

Bioclimatic variables provide information on the climate factor of the "clorpt" approach. The increasing availability of these bioclimatic variables in digital platforms makes it easy to apply these covariate data in the DSM approach. The raster data (30-second resolution) on bioclimatic variables can be downloaded from http://worldclim.org/current for its use in DSM. Hijmans et al. (2005) presented a detailed description of such bioclimatic variables. Examples of bioclimatic variables for arid western India, which were used in DSM of sand content by Santra et al. (2017a), are presented in Fig. 9.10.

These bioclimatic variables are annual mean temperature and precipitation, seasonality of temperature and precipitation, annual range of temperature, mean diurnal range of temperature, and precipitation during the wettest quarter of the year.

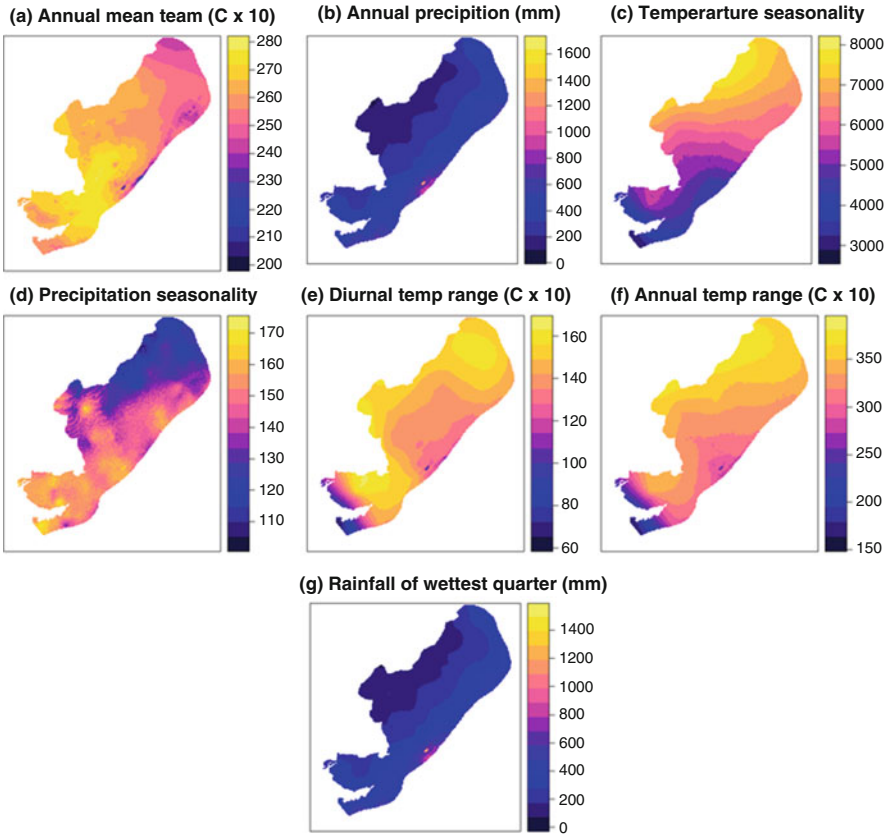

Fig. 9.10 Covariate maps of bioclimatic variables in arid western India. (Adopted, Santra et al. 2017a)

9.6.3 Machine Learning Algorithms in DSM

With the advancement of machine learning algorithms as a field of artificial intelligence, there is a possibility to build a model describing the relationship between soil parameters and the covariates affecting soil formation process (Murase 2000; Banerjee et al. 2018; Jha et al. 2019). The machine learning tools apply data mining techniques to identify the statistical relationship and then build the model. Different machine learning tools are now available to identify the relationship between soil properties and covariates. Few common machine learning tools are multiple linear regression (MLR), support vector machine/regression (SVM/SVR), random forest regression (RF), artificial neural network (ANN), k-nearest neighborhood (k-NN), cubist, etc. The machine learning tools are becoming popular since it requires less intervention of human brain and also learns input-output relationship in a better way. Increasing accessibility of high-level computer programming language, e.g., R,

Python, etc., makes it much easier to apply machine learning tools in DSM. Few commonly used machine learning tools in DSM are discussed below. However, a detailed description of these machine learning tools is available in Khaledian and Miller (2019).

The MLR approach builds the linear regression equations between soil properties and multiple covariates. It is the most simple and popular approach to machine learning tools. The coefficients of the regression equations are called the model parameters. A basic requirement of the MLR approach is that the covariates should not be correlated with each other, i.e., absence of collinearity in covariates. For this purpose, often stepwise regression analysis is carried out before building the MLR model to remove the collinearity in data. Several efforts have been made in the past to apply the MLR approach in DSM, e.g., Angelini et al. (2017), and are still widely used.

SVM/SVR is an ML algorithm that has gained popularity in recent times. The procedures adopted in SVR are complex in nature to understand; however, the outputs are very close to the real field situation. An SVM actually constructs a hyperplane or a set of hyperplanes in a high- or infinite-dimensional space, which are used for regression models. In the SVR approach, a margin of tolerance is defined for covariates using the observations (support vectors), and then data are separated and fitted linearly. The margin is actually the distance from the decision surface, which is maximally far from any observation. This decision surface ensures the high generalization ability of the algorithm and thus makes the results more applicable to the unseen data. In addition, the SVR approach applies kernel functions to map nonlinear vectors to a very high-dimensional space for solving nonlinear problems. The SVR algorithm requires the user to set the number of support vectors and the fraction of support vectors needed to maximize the margin, which is also called the hyperparameter of the algorithm. Application of SVR in the classification of soil types and estimation of soil properties may be found in Kovačević et al. (2010).

RF regression is a ML approach, which consists of an ensemble of randomized classification and regression trees (CART) (Breiman 2001). Predictions through RF regressions are made by generating numerous trees within the algorithm and finally aggregating them using the average of the individual tree outputs. There are three user-defined parameters on which RF regression is dependent, and these are the number of trees in the forest, the minimum number of data points in each terminal node, and the number of features tried at each node (mtry). A detailed description of the use of RF regression in DSM is available in Grimm et al. (2008). Here an example of preparing a sand content map by applying the RF regression algorithm is presented in Fig. 9.11. Covariates used in this example are soil category map, terrain attributes, and bioclimatic variables. A major advantage of RF regression-based digital soil maps is that the predicted data are available in the resolution of covariate maps. Therefore, the use of fine-resolution covariate maps results in digital soil maps with detailed information. Hence, the RF regression-based DSM is most suitable in case of sparsely available soil data, where it is difficult to build semivariogram models from limited data.

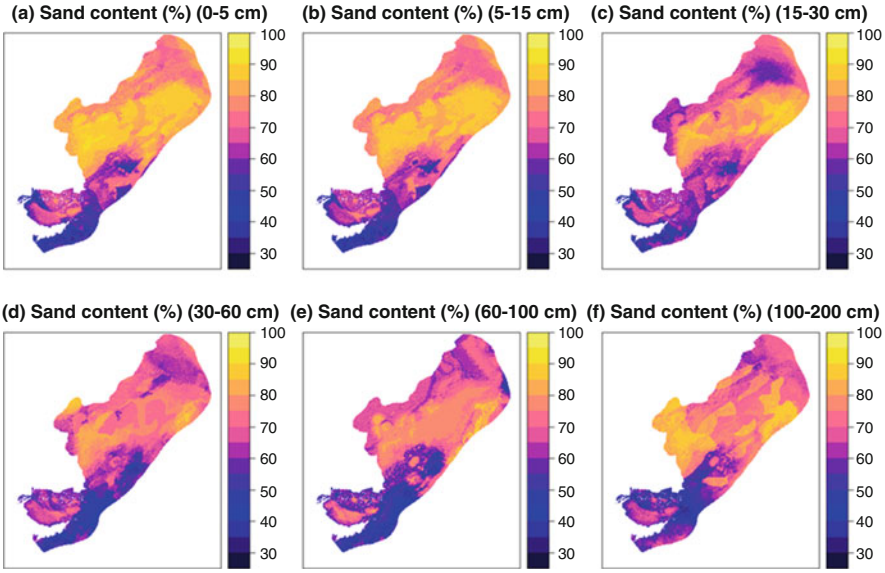

Fig. 9.11 Spatial maps of sand content in arid western India developed through random forest regression approach

ANNs are composed of artificial neurons that mimic biological neurons, which receive input, combine the input with their internal state, and produce output using an output function. The neurons are typically organized into multiple layers. Neurons of one layer are connected to neurons of nearby layers, which may be immediately preceding layer and immediately the following layer. The neuron layer that receives external data is called the input layer, whereas the layer that produces the output is called the output layer. In between the input and output layer, there may be hidden layers. Major hyperparameters of ANN are learning rate, the number of hidden layers, and batch size. Learning from the input data through ANN is done by adjusting the weights of the network so that the accuracy of the output is highest. The hyperparameter learning rate is defined as the number of the corrective steps to adjust for errors in each observation. A high learning rate shortens the training time, but with lower ultimate accuracy, whereas a lower learning rate takes longer time, but may lead to greater accuracy. Because of their ability to reproduce and model nonlinear processes, ANN has found applications in many disciplines. Details on the procedures of ANN application in DSM methodology may be found in Behrens et al. (2005).

k-NN algorithm applies a nonparametric method to provide an output based on the similarity concept, which assumes that similar things exist together in proximity. An estimate of soil property at an unknown location is obtained by averaging the values at k-nearest neighbors. Weights are assigned to each neighbor based on the distance; the higher is the distance of neighbor the lesser is the weight. The distance

metric is commonly calculated as Euclidean distance. Other distance metrices, e.g., Mahalanobis distance, Manhattan distance, Hamming distance, etc., are also used. The k-NN is an instance-based learning where the regression functions are approximated locally, and therefore a variety of regression curves are calculated based on the neighbors. The parameter k needs to identify optimally to obtain the best estimate of the target variable. An example of k-NN application in DSM may be found in Mansuy et al. (2014).

The cubist is a rule-based algorithm that is an extension of Quinlan's M5 model tree. Cubist generates a tree structure from a pool of covariates. The tree breaks through intermediate nodes to several final nodes using rules. A prediction is made using the linear regression model at the terminal node of the tree but is "smoothed" by taking into account the prediction from the linear model in the previous node of the tree. Besides, cubist as an ensemble model adds boosting to improve the prediction performance using two hyperparameters (i.e., committees and instances). Through the committee parameter, iterative model trees are created in sequence, and final prediction is obtained by simple averaging of the predictions from each model tree. The instance parameter adjusts the predictions from rule-based models (whether it is with a committee or without committee) using nearest neighbors. Thus, ensemble learning combines models produced by multiple repetitions of the same algorithm. This strategy usually obtains stronger predictive performance than results produced from any of the models individually. The application of the cubist model in DSM may be found in Akpa et al. (2016).

9.6.4 Application of Hyperspectral and Remote Sensing Signature in DSM

Quantifying the spectral reflectance of soil visible, near-infrared, and shortwave infrared (VIS-NIR-SWIR) region (350 to 2500 nm) and then relating it with soil properties has emerged as a rapid and noninvasive technique for estimation of soil properties (Ben-Dor et al. 2009). Hyperspectral signature of soil in 350–2500 nm region has been successfully used for estimating soil properties. A brief review of such applications of hyperspectral signature in estimating soil properties is available in Das et al. (2015) and Santra et al. (2015).

Figure 9.12 represents typical hyperspectral signatures in the VNIR region (350 to 2500 nm) for few arid soils of India. From the spectral curves, a wide range in spectral signatures is quite visible. The vibrational absorbance of the soil reflectance spectra is because of presence of various functional groups, namely, –OH in minerals and –OH, –CH, and –NH in soil organic matter (Rossel and McBratney 1998; Reeves et al. 1999). The soil reflectance spectra predominantly shows three absorption peaks at 1400, 1900, and 2200 nm as presented in Fig. 9.12. The absorption peaks at 1400 and 1900 nm correspond to water absorption (Leone and Sommer 2000), and 2200 nm indicates metal-hydroxyl stretching because of clay mineral (Chabrillat et al. 2002). The absorption features at 870 and 1000 nm and

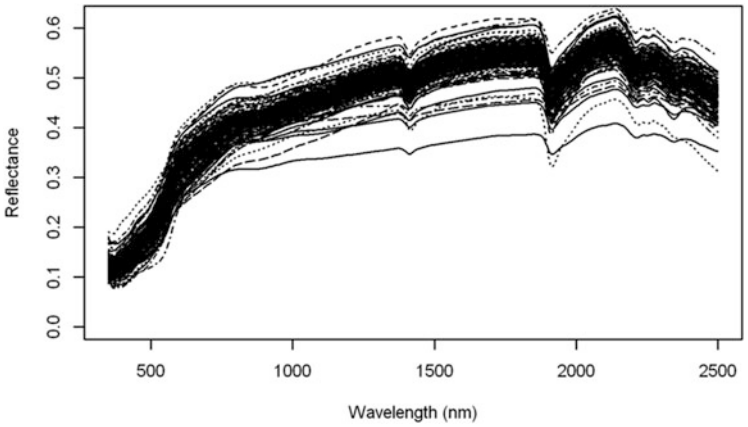

Fig. 9.12 Hyperspectral signature of soils from hot arid region of India

between 2200 and 2500 nm are mainly due to the presence of iron oxides and carbonates, respectively (Clark 1999; Chang and Laird 2002).

Soil properties and parameters influencing the reflectance at specific bands can be identified through the spectral data modeling approach. Band reflectance from these spectral data can be calculated to relate to soil properties. While calculating the band reflectance, it may also be kept in mind the bandwidth corresponds to the available spectral bands in operational or futuristic remote sensing satellites so that the algorithm can be translated to remote sensing platforms in the future. The overall brightness of spectra and the slope of the spectra at red to the near-infrared region can also be used to relate with soil properties. Spectral absorption features at specific wavelength region can also be analyzed in detail to capture the variation in spectral features so as to relate with content of a specific material in soil, which causes the absorption feature. Use of spectral signatures to estimate soil properties have been tried by different researchers throughout the world (Das et al. 2015). Here, an example of few spectral algorithms is presented in Table 9.2 from Santra et al. (2015).

Laboratory-based algorithms developed using relationship between soil properties and proximally measured spectral reflectance can be translated to the remote sensing platforms. However it depends on various factors like spectral resolution, spectral and spatial resolution, consistency of satellite images, atmospheric degradation of spectral behavior, land surface composition, soil moisture content, roughness of the surface, presence of gravels on surface, etc. An example of such demonstration is shown in Fig. 9.13, where sand content is estimated using the band reflectance of Landsat-8 data (path, 142; row, 49). The Landsat-8 data that corresponds to 19th of June 2013 was downloaded from the earth explorer website (http://earthexplorer.usgs.gov/). Finally, the reflectance-based models as shown in Table 9.2 were used to convert Landsat-8 data to map of sand content.

Table 9.2 Spectral algorithms soil properties estimation using principal components of soil reflectance spectra in VNIR-SWIR region, using Resourcesat-1 and Landsat-8 OLI band reflectance

Model type	Model equation	R^2
PCs of hyperspectral soil reflectance -based model	OC = 0.192 + -0.0008 × PC1 + 0.002 × PC2 + 0.002 × PC3	0.12
	Sand = 90.15 + 0.025 × PC1 – 0.537 × PC3	0.41
	Silt = 4.46 + 0.284 × PC3	0.27
	Clay = 5.40 – 0.017 × PC1 + 0.252 × PC3	0.43
[a]Derived IRS- P6 band reflectance-based model	OC = 1.11 +3.82 × B2 – 5.64 × B3	0.27
	Sand = 66.3 – 304.5 × B2 + 605.7 × B3 – 366.3 × B4 + 88.1 × B5	0.20
	Silt = 11.53 + 157.52 × B2 – 264.82 × B3 + 102.10 × B4	0.17
	Clay = 18.19 + 109.65 × B2 – 255.16 × B3 + 175.8 × B4 – 49.42 × B5	0.16
[b]Derived Landsat-8 OLI band reflectance-based model	OC = 1.12 + 3.72 × Band 3 – 5.56 × Band 4	0.27
	Sand = 52.8 – 168.5 × Band 3 + 316.1 Band 4 – 129.1 × Band 5 – 434.9 × Band 6 + 480.5 × Band 7	0.44
	Silt = 22.54 + 102.21 × Band 3 – 147.35 × Band 4 + 266.63 × Band 6 – 253.86 × Band 7	0.32
	Clay = 23.67 – 45.91 × Band 4 + 251.89 × Band 6 – 252.77 × Band 7	0.44

Adopted, Santra et al. (2015)
[a]Derived band reflectance corresponding to IRS-P6 bands of LISS-III, LISS-IV, and AWiFS camera: B2 = 520–590 nm, B3 = 620–680 nm, B4 = 770–860 nm, B5 = 1550–1700 nm
[b]Derived band reflectance to Landsat-8 OLI bands: Band 3 = 530–590 nm, Band 4 = 640–670 nm, Band 5 = 850–880 nm, Band 6 = 1570–1650 nm, Band 7 = 2110–2290 nm

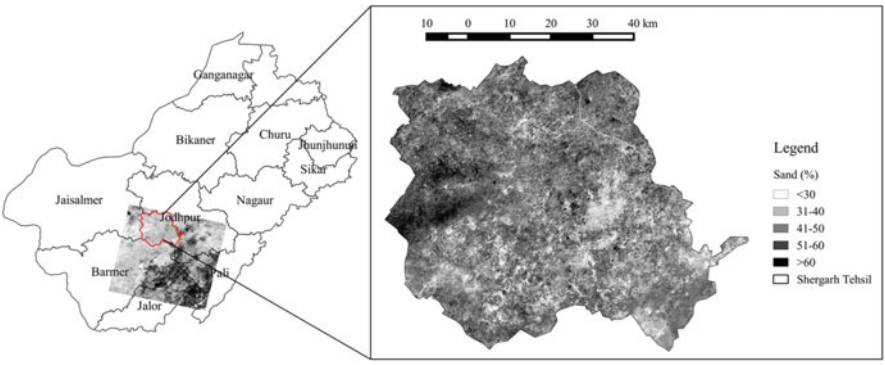

Fig. 9.13 Estimated sand content map of Shergarh Tehsil, Jodhpur, using spectral algorithm and Landsat data (OLI band)

9.7 Pedotransfer Function (PTF) Approach for Digital Soil Mapping

PTFs are models which help to estimate complex and difficult to measure soil properties using basic soil properties as input. Soil water retention behavior relating soil moisture content (θ) with pressure head (h) is generally tedious to measure at multiple locations in field and therefore is often estimated through PTF models (Santra and Das 2008; Santra et al. 2018). Soil physicochemical properties, e.g., cation exchange capacity (CEC), and soil thermal properties, e.g., specific heat capacity, conductivity, etc., have also been used as a target variable in PTF model. These established PTF models can be used to convert digital soil maps of basic soil properties to maps of complex soil properties. In the following, few examples on converting maps of basic soil properties to soil water retention behavior are given.

In the first example, spatial maps on water content at field capacity (FC) (θ_{FC}) and permanent wilting point (PWP) (θ_{PWP}) were prepared through linking soil maps on basic properties and PTFs (Santra et al. 2008). The PTFs for θ_{FC} and θ_{PWP} used in this example were developed from the available soil data in benchmark soils of India, and these PTF models are given below:

$$\theta_{FC}(\%, \mathrm{w/w}) = 21.931 - 0.20564 \times \mathrm{sand} + 0.175 \times \mathrm{clay} + 4.6737 \times \mathrm{OC} \left(R^2 = 0.89\right) \tag{9.16}$$

$$\theta_{PWP}(\%, \mathrm{w/w}) = 8.7255 - 0.092946 \times \mathrm{sand} + 0.15944 \times \mathrm{clay} \left(R^2 = 0.78\right) \tag{9.17}$$

where sand is the % sand content (0.05–2 mm), clay is the % clay content (<0.002 mm), and OC is the % OC content in the soils. Using OK approach, maps of sand content, clay content, and OC content were first prepared, and then these three maps were joined together using above mentioned PTF models. The developed maps of θ_{FC} and θ_{PWP} are presented in Fig. 9.14. Another possible way to generate these maps is to predict θ_{FC} and θ_{PWP} at each location, where basic soil properties were measured and then OK is applied on estimated θ_{FC} and θ_{PWP} to generate the final maps. In the first approach, the error of spatial prediction associated with each map of basic soil property and the error of PTF model will be added on to the final map of soil water retention behavior. Therefore, the reliability of final map highly depends on the accuracy of spatial prediction methods as well as on the accuracy of PTF models. In the second approach, the limitation is to obtain good spatial trend to apply geostatistical methods for preparation of maps of complex soil properties which therefore are not commonly used. Moreover, in the first approach, we obtain the digital map of basic soil properties along with target map of complex soil properties, which together help in several land management decisions. These maps of soil water retention at farm level may help in applying right amount of irrigation water at right time.

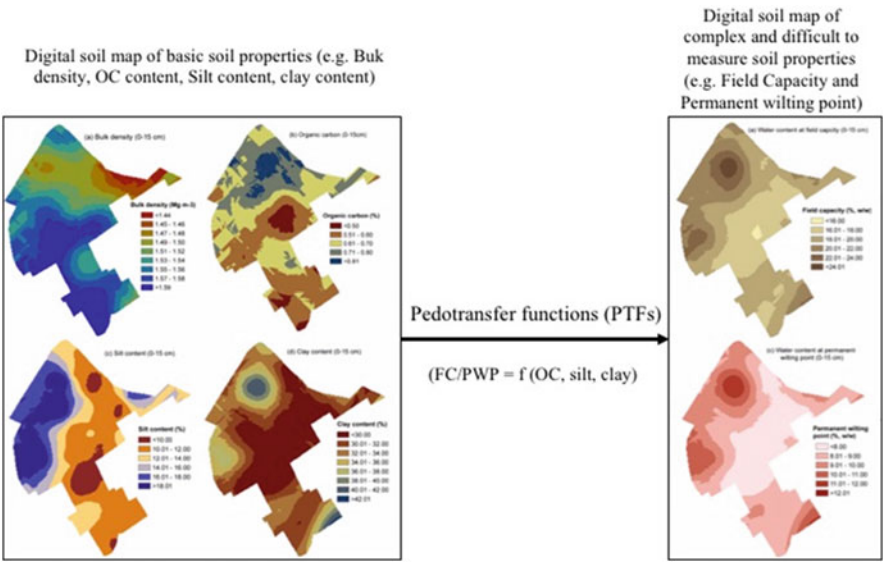

Fig. 9.14 Translating digital soil maps of basic soil properties to map of soil water retention using PTF model at experimental farm of ICAR-Indian Agricultural Research Institute, New Delhi. (Adopted, Santra et al. 2008)

Another example of converting maps of basic soil properties to maps of soil water retention at field capacity and the permanent wilting point is presented in Fig. 9.15. Here, maps of sand, silt, and clay content are converted to maps of FC and PWP content in the hot arid ecosystem of India. The PTFs used in this example are regression-based PTF models and are available in Santra et al. (2018). The developed maps of FC and PWP may be quite useful for the sustainable utilization of water resources in arid western India (AWI). From these maps, it is noted that soil water retention at FC was lowest (~10%) at the western part of the AWI, where sand dunes are dominant. The value of $\theta_{1/3bar}$ was around 25% for soils at coastal deltaic plain lying at the southern part of the AWI. The central and northern part of AWI, which covers a major portion of the region, has $\theta_{1/3bar}$ of 15%. Similarly, soil water retention at PWP was also very low (~4–6%) at the western and northern plain of the AWI and high (~8–10%) at the southern coastal plain of the AWI. Soil water retention at FC reaches 2–3 days after saturation, whereas to reach PWP it may require a long time to dry at which plants start to wilt. The amount of soil water available between these two critical soil moisture contents is called available water capacity (AWC), which is extracted by the plant for its growth and development. From the surface maps of $\theta_{1/3bar}$ and θ_{15bar}, it is found that the plant available water content is about 6–9% for western, central, and northern part of the AWI. Therefore, growing crops with high water requirement in this region may not be feasible since it will require frequent application of irrigation water to maintain sufficient soil moisture regime for plant growth. In such situation, surface map of $\theta_{1/3bar}$ and

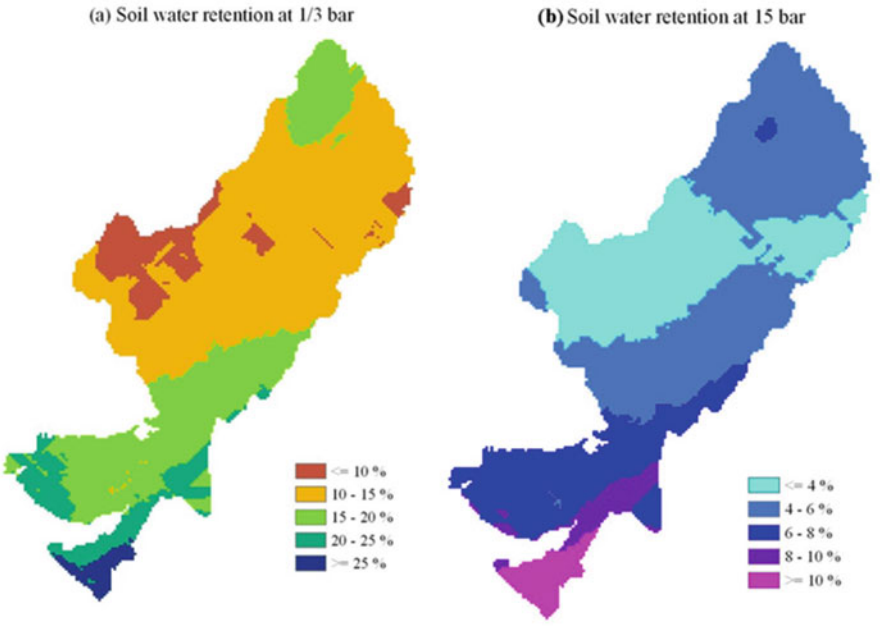

Fig. 9.15 Estimated surface map of soil water retention within the arid western India (AWI) for (a) 1/3bar ($\theta_{1/3bar}$) and 15 bar (θ_{15bar}) using PTF model

θ_{15bar} may help the end users for judicious use of water, which is very scarce in the region.

9.8 Accuracy and Uncertainty Analysis of Digital Soil Maps

Accuracy and uncertainty of digital soil maps play a key role in the reliability of digital products. Accuracy is generally defined as how close is the estimated value to the true value. The more close is the estimated value toward the measured value, the higher will be the accuracy. It is generally calculated as an error, which is the difference in observed and predicted value. Several error indices are used to quantify the magnitude and distribution of error. Uncertainty indicates the fluctuations of the estimated value from its mean. Otherwise, it can also be quantified as a confidence interval. The narrow is the range of confidence interval, the less is the uncertainty and vice versa. The uncertainty of digital soil products is often neglected. Because in most of the classical spatial prediction approaches, the error variance of the predicted values at a particular location is not calculated, rather a single predicted value is obtained in most cases. However, in geostatistical approaches, kriging variance of prediction is always calculated along with the mean predicted values. Therefore, confidence interval may be calculated either at 90% significance level ($\mu \pm$

1.645×σ) or 95% significance level (μ±1.96×σ). Otherwise, repetitive stochastic simulations, e.g., sequential Gaussian simulation, are carried on a particular location to obtain the mean and standard deviation of predicted values, which helps to quantify the uncertainty.

In DSM approaches, accuracy is generally quantified through cross-validation approach. k-fold cross validation is generally followed. In this approach, the total dataset is randomly divided into k sets of data. Then the (k-1) sets of data are used as training data for building the model, and then the developed model is tested on k^{th} fold dataset as validation data. The procedure is repeated till each set of data gets a chance to appear as validation data once in the total procedure. The k-fold cross-validation approach results into observed and predicted values of soil property at each measured location. These observed and predicted values are then used to calculate different cross-validation indices, few of which are given below:

$$\mathrm{r} = \frac{\sum_{i=1}^{n}\left[z(s_i) - \overline{z}_{obs}\right]\left[\widehat{z}(s_i) - \overline{z}_{pred}\right]}{\sqrt{\sum_{i=1}^{n}\left[z(s_i) - \overline{z}_{obs}\right]^2}\sqrt{\sum_{i=1}^{n}\left[\widehat{z}(s_i) - \overline{z}_{pred}\right]^2}} \tag{9.18}$$

$$\mathrm{LCCC} = \frac{2\rho\sigma_{obs}\sigma_{pred}}{\left(\overline{z}_{obs} - \overline{z}_{pred}\right) + \sigma_{obs}^2 + \sigma_{pred}^2} \tag{9.19}$$

$$\mathrm{RMSE} = \sqrt{\frac{1}{n}\sum_{i=1}^{n}\left[Z(s_i) - \widehat{Z}(s_i)\right]^2} \tag{9.20}$$

$$\mathrm{bias} = \frac{1}{n}\sum_{i=1}^{n}\left[Z(s_i) - \widehat{Z}(s_i)\right] \tag{9.21}$$

where $z(s_i)$ is the measured values of the variable at the location s_i,$\widehat{Z}(s_i)$ is the predicted values with variance σ^2 at the location s_i, and n is the number of sampling sites.

The R^2 indicates the precision of prediction, and it is actually measured as square of the Pearson correlation coefficient (r) between observed and predicted values. Both accuracy and precision of the prediction are evaluated by Lin's concordance correlation coefficient (LCCC) (Lin 1989). LCCC is calculated as the orthogonal distance of values from the 1:1 line of observed vs predicted values and it ranges from -1 to +1.

A zero LCCC value indicates no agreement between measured and predicted values. However, values equal to 1 and -1 indicate perfect positive and negative agreement, respectively. The accuracy of the prediction can be measured using RMSE statistics. The larger RMSE value shows less prediction accuracy. Similarly the mean error of prediction can be estimated using bias, and a value of zero indicates unbiasedness of the prediction.

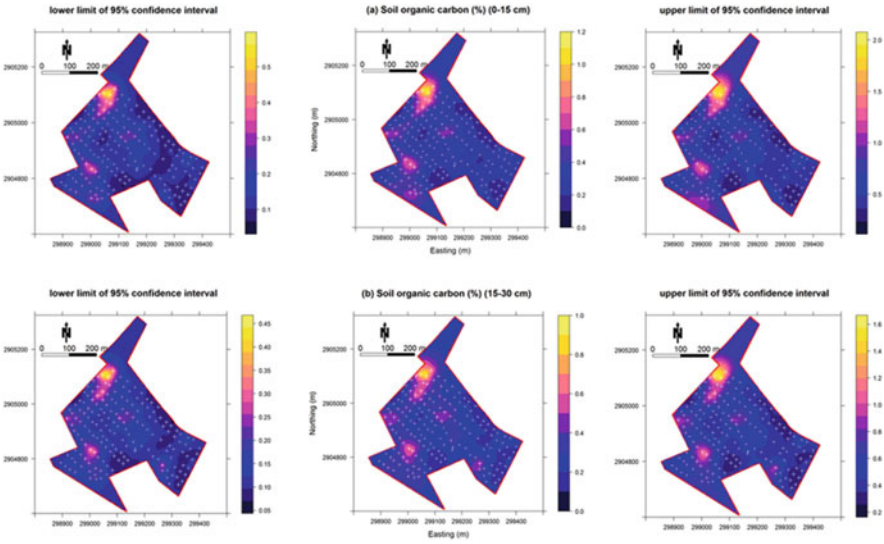

Fig. 9.16 Uncertainty of digital soil map of SOC content in horticultural orchard of ICAR-CAZRI, Jodhpur. (Adopted, Singh et al. 2016)

Apart from these indices, mean squared deviation ratio (MSDR) is also an important index to judge the goodness of fit in prediction (Bishop and Lark 2008), which is actually the transformation of G index and is calculated as follows:

$$MSDR = \frac{1}{n}\sum_{i=1}^{n}\left(\frac{\{z(x_i) - \widehat{z}(x_i)\}^2}{{\sigma_i}^2}\right) \tag{9.22}$$

If the correct semivariogram model is used, the *MSDR* values should be close to 1 (Lark 2000).

Most commonly used approach to quantify the uncertainty of prediction is the calculation of 95% confidence interval maps as follows:

$$\begin{aligned}\text{Upper limit} = {} & \text{kriged prediction map} + 1.96 \\ & \times \text{map of standard deviation of prediction}\end{aligned}$$

$$\begin{aligned}\text{Lower limit} = {} & \text{kriged prediction map} + 1.96 \\ & \times \text{map of standard deviation of prediction}\end{aligned}$$

An example of such confidence interval map of SOC in a horticultural orchard is presented in Fig. 9.16. The left-hand side maps of the figure show the lower limit, and right-hand side maps show the upper limit of 95% confidence interval, whereas the central map shows the mean predicted SOC content of the orchard. From these maps, it is clearly visible that if we ignore the confidence interval maps, we remain unaware of the fluctuation in predictions. The more is the fluctuations (the wider is

the range of confidence interval), the less is the reliability of the map. It is like the wild guess on soil properties for a particular location and judges how much correct is the guess. The wider is the interval, the higher will be chance of correctness of the guess. Supposing that if the confidence interval is more than standard deviation of measured values, the predicted map is of little use because under such cases we can rely more on the arithmetic mean as the most probable value of any unsampled location.

9.9 DSM Applications: Soil Information System

The ultimate goal of the DSM is to make available the unutilized soil data (legacy data) to end users at a spatial scale. This helps a wide variety of users for different purposes, e.g., farmers for nutrient and water management in an agricultural field, decision-makers for adopting different land management decisions, researchers for modeling landscape processes, etc. The development of the soil information system leads to achieving the ultimate goal of DSM. Several countries have developed the national-level soil information system throughout the world. Here, as an example, the soil information system "SoilGrids250m" developed by ISRIC-World Soil Information is discussed. Soil organic stock map of the world as a snapshot from "SoilGrids250m" is presented in Fig. 9.17.

The "SoilGrids250m" is developed based on soil profile data of 240,000 locations. Global-level predictions of organic carbon concentration, total nitrogen

Fig. 9.17 SoilGrids250m: An example of soil information system

content, pH_{water}, cation exchange capacity (measured at pH 7), soil texture (proportion of sand, silt, and clay), and volume of coarse fragments are available in the "SoilGrids250m." Predictions are available in six standard soil depths as specified by the Global Soil Map project (0–5 cm, 5–15 cm, 15–30 cm, 30–60 cm, 60–100 cm, and 100–200 cm). The major features of the "SoilGrids250m" are:

(a) Direct coupling with standardized soil profile (point) data provided by the ISRIC-World Soil Information Service (*WoSIS*)
(b) Use of the modern map projection like homolosine that minimizes angular and distance distortions simultaneously
(c) An improved selection of covariate layers using recursive feature elimination
(d) Adoption of an improved and more realistic cross-validation procedure
(e) Quantification of uncertainties in the soil predictions, using prediction intervals, through implementation of quantile regression forests

9.10 Conclusion

Soil plays a crucial role not only in the agricultural production system but also helps in taking many soil and land management decisions. For example, soil nutrients support plant growth and yield, soil hydraulic properties dictate partitioning rainfall into a runoff, soil water retention behavior governs soil moisture regime in an agricultural field, soil pollutants content helps in assessing the risk associated with handing polluted soils, etc. Therefore, soil survey or target-based soil sampling efforts have been done regularly to gather knowledge on soil properties to adopt suitable soil management practices. However, it is not always possible to collect soil samples from multiple locations from a target area. Therefore, estimates are tried at unsampled locations using the information at measured locations of the surveyed area. DSM provides the estimate of soil properties at unsampled locations in the most rational approach which includes geostatistics, state-factor (clorpt) approach, and PTF models. Here, we discussed, in brief, these three approaches with examples. Further, the accuracy and uncertainty of digital soil products help to judge the reliability of it to stakeholders, and thus the inclusion of this information in digital soil products should be an essential requirement. With the advancement of information technology (IT) applications, it will be more appropriate to make these digital soil products available in different IT platforms, e.g., android applications, WebGIS applications, spatial soil database management systems, etc., which together is called soil information system. Therefore, future efforts are required to apply DSM technology to available legacy soil data and to prepare soil maps and make it accessible to wide users as soil information systems.

References

Aggarwal P, Gupta RP (1998) Two dimensional Geosta-tistical analysis of soils. In: Gupta RP, Gnildyal BP (eds) Theory and practice in agrophysics measurements. Allied Publishers, Buffalo, pp 253–263

Akpa SI, Odeh IO, Bishop TF, Hartemink AE, Amapu IY (2016) Total soil organic carbon and carbon sequestration potential in Nigeria. Geoderma 271:202–215. https://doi.org/10.1016/j.geoderma.2016.02.021

Angelini ME, Heuvelink GBM, Kempen B (2017) Multivariate mapping of soil with structural equation modelling. Eur J Soil Sci 68(5):575–591. https://doi.org/10.1111/ejss.12446

Bannerjee G, Sarkar U, Das S, Ghosh I (2018) Artificial Intelligence in Agriculture: A Literature Survey. Int J Sci Res Comput Sci Appl Manage Stud 7(3):1–6

Behrens T, Scholten T (2006) Digital soil mapping in Germany-a review. J Plant Nutr Soil Sci 169:434–443

Behrens T, Förster H, Scholten T, Steinrücken U, Spies ED, Goldschmitt M (2005) Digital soil mapping using artificial neural networks. J Plant Nutr Soil Sci 168(1):21–33. https://doi.org/10.1002/jpln.200421414

Ben Dor E, Chabrillat S, Dematte JAM, Taylor GR, Hill J, Whiting ML, Sommer S (2009) Using imaging spectroscopy to study soil properties. Remote Sens Environ 113(1):S38–S55

Bishop TFA, Lark RM (2008) A comparison of parametric and non-parametric methods for modelling a coregionalization. Geoderma 148:13–24

Blöschl G, Sivapalan M (1995) Scale issues in hydrological modelling – a review. Hydrol Process 9:251–290

Breiman L (2001) Random forests. Mach Learn 45:5–32

Brown DJ, Shepherd KD, Walsh MG, Dewayne Mays M, Reinsch TG (2006) Global soil characterization with VNIR diffuse reflectance spectroscopy. Geoderma 132:273–290

Carter GP, Miskewitz RJ, Isukapalli S, Mun Y, Vyas V, Yoon S, Georgeopoulos P, Uchrin CG (2011) Comparison of kriging and cokriging for the geostatistical estimation of specific capacity in the Newark Basin (NJ) aquifer system. J Environ Sci Health A Tox Hazard Subst Environ Eng 46(4):371–377

Chabrillat S, Goetz AFH, Krosley S, Olsen HW (2002) Use of hyperspectral images in the identification and mapping of expansive clay soils and the role of spatial resolution. Remote Sens Environ 82:431–445

Chakraborty S, Li B, Deb S, Paul S, Weindorf DC, Das BS (2017) Predicting soil arsenic pools by visible near infrared diffuse reflectance spectroscopy. Geoderma 296:30–37

Chang CW, Laird DA (2002) Near-infrared reflectance spectroscopic analysis of soil C and N. Soil Sci 167:110–116

Chatterjee S, Santra P, Majumdar K, Ghosh D, Das I, Sanyal SK (2015) Geostatistical approach for management of soil nutrients with special emphasis on different forms of potassium considering their spatial variation in intensive cropping system of West Bengal, India. Environ Monit Assess 187(4):183

Clark RN (1999) Spectroscopy of rocks and minerals, and principles of spectrocopy. In: Rencz AN (ed) Remote sensing for the earth sciences: manual of remote sensing. American Society for Photogrammetry and Remote Sensing, New York, pp 3–58

Dahiya IS, Kalta B, Agrawal RP (1998) Kriging for interpolation through spatial variability analysis of data. In: Gupta RP, Ghildyal BP (eds) Theory and practice in agrophysics measurements. Allied Publishers, Buffalo, pp 242–252

Das M (2007) Spatial variability analysis of soil hydraulic conductivity in an irrigation command. J Indian Soc Soil Sci 55(1):10–13

Das BS, Sarathjith MC, Santra P, Sahoo RN, Srivastava R, Routray A, Ray SS (2015) Hyperspectral remote sensing: opportunities, status and challenges for rapid soil assessment in India. Curr Sci 10:860–868

Divya Y, Sanjeevi S, Ilamparuthi K (2014) Studies on textural and compositional characteristics of sand and clay mixtures using hyperspectral radiometry. J Indian Soc Remote Sens 42 (3):589–600
Dokuchaev VV (1883) The Russian chernozem report to the free economic society. Imperial University of St. Petersburg, St. Petersburg. in Russian
Ersahin S (2001) Comparing ordinary kriging and cokriging to estimate infiltration rate. Soil Sci Soc Am J 67(6):1848–1855
Goovaerts P (1998) Geostatistical tools for characterizing the spatial variability of microbiological and physico-chemical soil properties. Biol Fertil Soils 27:315–334
Grimm R, Behrens T, Märker M, Elsenbeer H (2008) Soil organic carbon concentrations and stocks on Barro Colorado Island—digital soil mapping using random forests analysis. Geoderma 146 (1–2):102–113. https://doi.org/10.1016/j.geoderma.2008.05.008
Grunwald S (2009) Multicriteria characterization of recent digital soil mapping and modelling approaches. Geoderma 152:195–207
Gulfo E, Sahoo RN, Sharma RK, Khanna M (2012) Soil moisture assessment using hyperspectral remote sensing. In: Proceedings of the second national workshop on challenges and opportunities of water resources management in Tana Basin, Upper Blue Nile Basin, Ethiopia. Blue Nile Water Institute, Bahir Dar University, Ethiopia 2012 Oct, pp 69–77
Gupta A, Das BS, Kumar A, Chakraborty P, Mohanty B (2016) Rapid and non-invasive assessment of Atterberg limits using diffuse reflectance spectroscopy. Soil Sci Soc Am J 80(5):1283–1295
Hijmans RJ, Cameron SE, Parra JL, Jones PG, Jarvis A (2005) Very high resolution interpolated climate surfaces for global land areas. Int J Climatol 25:1965–1978
http://casoilresource.lawr.ucdavis.edu/soilwebapps/
http://earthexplorer.usgs.gov/
http://earthexplorer.usgs.gov/
http://srtm.csi.cgiar.org/
http://worldclim.org/current
http://www.soilsscotland.gov.uk/data/soilsurvey25k.php
Jenny H (1941) Factors of soil formation, a system of quantitative pedology. McGraw-Hill, New York
Jha K, Doshi A, Patel P, Shah M (2019) A comprehensive review on automation in agriculture using artificial intelligence. Artif Intell Agric 2:1–12
Kadupitiya HK, Sahoo RN, Ray SS, Chakraborty D, Ahmed N (2010) Quantitative assessment of soil chemical properties using visible (VIS) and near-infrared (NIR) proximal hyperspectral data. Trop Agric 158:41–60
Kamble KH, Aggrawal P (2011) Geostatistical analyst for deciding optimal interpolation strategies for delineating compact zones. Int J Geosci 2(04):585
Katuwal S, Hermansen C, Knadel M, Moldrup P, Greve MH, de Jonge LW (2018) Combining X-ray computed tomography and visible near-infrared spectroscopy for prediction of soil structural properties. Vadose Zone J 17(1)
Khaledian Y, Miller BA (2019) Selecting appropriate machine learning methods for digital soil mapping. Appl Math Model. https://doi.org/10.1016/j.apm.2019.12.016
Kovačević M, Bajat B, Gajić B (2010) Soil type classification and estimation of soil properties using support vector machines. Geoderma 154(3–4):340–347. https://doi.org/10.1016/j.geoderma.2009.11.005
Lagacherie P, McBratney AB, Voltz M (2006) Digital soil mapping: an introductory perspective. Elsevier, Amsterdam
Lark RM (2000) A comparison of some robust estimators of the variogram for use in soil survey. Eur J Soil Sci 51:137–157
Leone AP, Sommer S (2000) Multivariate analysis of laboratory spectra for the assessment of soil development and soil degradation in the Southern Apennines (Italy). Remote Sens Environ 72:346–359

Lin LI (1989) A concordance correlation coefficient to evaluate reproducibility. Biometrics 45:255–268

Mansuy N, Thiffault E, Paré D, Bernier P, Guindon L, Villemaire P, Poirier V, Beaudoin A (2014) Digital mapping of soil properties in Canadian managed forests at 250 m of resolution using the k-nearest neighbor method. Geoderma 235:59–73. https://doi.org/10.1016/j.geoderma.2014.06.032

Matheron G (1965) Les variables régionalisées et leur estimation. Une application de la théorie des fonctions aléatoires aux sciences de la nature. Masson, Paris

McBratney AB, MendonçaSantos ML, Minasny B (2003) On digital soil mapping. Geoderma 117:3–52

Minasny B, McBratney AB (2016) Digital soil mapping: a brief history and some lessons. Geoderma. https://doi.org/10.1016/j.geoderma.2015.07.017

Mohanty B, Gupta A, Das BS (2016) Estimation of weathering indices using spectral reflectance over visible to mid-infrared region. Geoderma 266:111–119

Murase H (2000) Artificial intelligence in agriculture. Comput Electron Agric 29:1/2

NBSS & LUP (2005) Reflectance libraries for development of soil sensor for periodic assessment of state of soil resources. NATP project report (NBSS No. 835). National Bureau of Soil Survey/ Land Use Planning, Nagpur

Rabus B, Eineder M, Roth A, Bamler R (2003) The shuttle radar topography mission—a new class of digital elevation models acquired by spaceborne radar. ISPRS J Photogramm Remote Sens 57 (4):241–262

Reeves JB, McCarty GW, Meisenger JJ (1999) Near-infrared diffuse reflectance spectroscopy for the analysis of agricultural soil. J Near Infrared Spectrosc 7:179–193

Rossel RV, McBratney A (1998) Laboratory evaluation of a proximal sensing technique for simultaneous measurement of soil clay and water content. Geoderma 85:19–39

Rossel RV, Behrens T, Ben-Dor E, Brown DJ, Demattê JA, Shepherd KD, Shi Z, Stenberg B, Stevens A, Adamchuk V, Aïchi H (2016) A global spectral library to characterize the world's soil. Earth Sci Rev 155:198–230

Rossiter DG (2018) Technical note: co-kriging with the gstat package of the R environment for statistical computing. http://www.css.cornell.edu/faculty/dgr2/_static/files/R_PDF/CoKrigeR.pdf

Sanchez PA, Ahamed S, Carré F, Hartemink AE, Hempel JW, Huising J, Lagacherie P, McBratney AB, McKenzie NJ, Mendonça-Santos ML, Minasny B, Montanarella L, Okoth P, Palm CA, Sachs JD, Shepherd KD, Vagen TG, Vanlauwe B, Walsh MG, Winowiecki LA, Zhang GL (2009) Digital soil map of the world. Science 325(5941):680–681

Santra P, Das BS (2008) Pedo-transfer functions for soil hydraulic properties developed from a hilly watershed of Eastern India. Geoderma 146(3–4):439–448

Santra P, Chopra UK, Chakraborty D (2008) Spatial variability of soil properties and its application in predicting surface map of hydraulic parameters in an agricultural farm. Curr Sci 10:937–945

Santra P, Sahoo RN, Das BS, Samal RN, Pattanaik AK, Gupta VK (2009) Estimation of soil hydraulic properties using proximal spectral reflectance in visible, near-infrared, and shortwave-infrared (VIS–NIR–SWIR) region. Geoderma 152(3–4):338–349

Santra P, Kumawat RN, Mertia RS, Mahla HR, Sinha NK (2012a) Spatial variation of soil organic carbon stock in a typical agricultural farm of hot arid ecosystem of India. Curr Sci 10:1303–1309

Santra P, Das BS, Chakravarty D (2012b) Spatial prediction of soil properties in a watershed scale through maximum likelihood approach. Environ Earth Sci 65(7):2051–2061

Santra P, Singh R, Sarathjith MC, Panwar NR, Varghese P, Das BS (2015) Reflectance spectroscopic approach for estimation of soil properties in hot arid western Rajasthan, India. Environ Earth Sci 74(5):4233–4245

Santra P, Kumar M, Panwar N (2017a) Digital soil mapping of sand content in arid western India through geostatistical approaches. Geoderma Reg 9:56–72

Santra P, Kumar M, Panwar NR, Das BS (2017b) Digital soil mapping and best management of soil resources. In: Rakshit A, Abhilash PC, Singh HB, Ghosh S (eds) Adaptive soil management: From theory to practice. Springer, Singapore, pp 3–38. https://doi.org/10.1007/978-981-10-3638-5_1

Santra P, Kumar M, Panwar NR, Pandey CB (2017c) Soil resources and its mapping through geostatistics using R and QGIS. New India Publishing Agency, New Delhi, p 340

Santra P, Kumar M, Kumawat RN, Painuli DK, Hati KM, Heuvelink G, Batjes N (2018) Pedotransfer functions to estimate soil water retention at field capacity and permanent wilting point in hot arid western India. J Earth Syst Sci 127:35. https://doi.org/10.1007/s12040-018-0937-0

Sarathjith MC, Das BS, Wani SP, Sahrawat KL (2014) Dependency measures for assessing the covariation of spectrally active and inactive soil properties in diffuse reflectance spectroscopy. Soil Sci Soc Am J 78(5):1522–1530

Saxena RK, Vermal KS, Srivastava RA, Av AK, Shiwalkar AA, Londhel SL (2003) Spectral reflectance properties of some dominant soils occurring on different altitudinal zones in Uttaranchal Himalayas. Agropedology 13(2):35–43

Shepherd KD, Walsh MG (2002) Development of reflectance spectral libraries for characterization of soil properties. Soil Sci Soc Am J 66:988–998

Singh M, Srivastava R, Sethi M, Sood A (2014) Development of spectral reflectance methods and low cost sensors for real-time application of variable rate inputs in precision farming (final report). National Agricultural Innovation Project (ICAR)/Punjab Agricultural University, Ludhiana

Singh A, Santra P, Kumar M, Panwar N, Meghwal PR (2016) Spatial assessment of soil organic carbon and physicochemical properties in a horticultural orchard at arid zone of India using geostatistical approaches. Environ Monit Assess 188(9):529

Srivastava RA, Prasad JA, Saxena R (2004) Spectral reflectance properties of some shrink-swell soils of Central India as influenced by soil properties. Agropedology 14:45–54

Webster R, Oliver MA (2007) Geostatistics for environmental scientists. Wiley, Chichester

Chapter 10
Soil Moisture Retrieval Techniques Using Satellite Remote Sensing

Anush Kumar K., Raj Setia, Dharmendra Kumar Pandey, Deepak Putrevu, Arundhati Misra, and Brijendra Pateriya

Contents

Abstract Soil moisture is required to understand the land surface processes, land-atmosphere interaction, drought forecasting, crop growth patterns, etc. It is a dynamic variable that changes significantly on different spatial and temporal scales even in a smaller area. Remote sensing (RS) techniques provide an alternative way to estimate the high spatial and temporal variability of soil moisture. This chapter includes the state of art and techniques used to retrieve soil moisture from satellite RS in different parts of the world. Several techniques have been developed to retrieve soil moisture either from optical/thermal/microwave sensors or fusion of these sensors, but microwave sensors either with a fine spatial resolution (and coarse temporal resolution) or with a coarse spatial resolution (and fine temporal resolution) seem promising than optical and thermal sensors depending on applications.

Anush Kumar K. · R. Setia (✉) · B. Pateriya
Punjab Remote Sensing Centre, Ludhiana, India
e-mail: rksetia@prsc.gov.in; director@prsc.gov.in

D. K. Pandey · D. Putrevu · A. Misra
Space Applications Centre, Ahmedabad, Gujarat, India
e-mail: dkp@sac.isro.gov.in; dputrevu@sac.isro.gov.in; arundhati@sac.isro.gov.in

T. Mitran et al. (eds.), *Geospatial Technologies for Crops and Soils*,
https://doi.org/10.1007/978-981-15-6864-0_10

However, microwave sensors have shown its high potential and capability for deriving global soil moisture information due to all weather capability and longer penetration depth. Many operational products of soil moisture have been developed using passive microwave sensors; however, coarse spatial resolution and penetration depth over vegetation-covered surfaces are the major factors that limit the utility of these soil moisture products for agricultural purposes. The major initiatives have been taken by various space agencies across the globe to develop the microwave sensors with L and/or S bands for its potential use in soil moisture besides other applications. Sentinel-1 synthetic aperture radar (SAR, active microwave sensor) data has opened up a new research area to develop high-spatial-resolution soil moisture products for agricultural applications. Several studies have shown the potentials of Sentinel-1 SAR data and high-resolution optical data along with operational products (like SMAP) to downscale the coarse soil moisture data to retrieve high spatial soil moisture at a regular interval over vegetation-covered surfaces. However, future sensors are required to estimate soil moisture from depth up to 0.7–1 m (microwave sensors with P band) over sparse vegetation areas and varying surface roughness using active and passive microwave sensors.

Keywords Microwave · Remote sensing · Retrieval · Synthetic aperture radar · Soil moisture content · Thermal emission

Abbreviation

AMSR-E	Advanced Microwave Scanning Radiometer-Earth Observing System
ANN	Artificial Neural Network
ASTER	Advanced Spaceborne Thermal Emission and Reflection Radiometer
ATI	Apparent Thermal Inertia
DEM	Digital Elevation Model
DWT	Discrete Wavelength Transform
EF	Evaporative Fraction
ESTAR	Electronically Scanned Thinned Array Radiometer
ETM+	Enhanced Thematic Mapper Plus
EVI	Enhanced Vegetation Index
HWSD	Harmonized World Soil Database
LSMEM	Land Surface Microwave Emission model
LST	Land Surface Temperature
MIRAS	Microwave Imaging Radiometer with Aperture Synthesis
MODIS	Moderate Resolution Imaging Spectroradiometer
MOSDAC	Meteorological & Oceanographic Satellite Data Archival Centre
MPDI	Microwave Polarization Difference Indices
NDVI	Normalized Difference Vegetation Index
NIR	Near Infrared
NISAR	NASA-ISRO Synthetic Aperture Radar
PALS	Passive and Active L- and S-band Sensor
RS	Remote Sensing

SAR	Synthetic Aperture Radar
SMAP	Soil Moisture Active Passive
SMOS	Soil Moisture and Ocean Salinity
SWIR	Shortwave Infrared
TM	Thematic Mapper
TVDI	Temperature Vegetation Dryness Index
VEDAS	Visualization of Earth Observation Data and Archival System
VI	Vegetation Index
VNIR	Visible and Near Infrared
VOD	Vegetation Optical Depth
WDI	Water Deficit Index

10.1 Introduction

The rapid acquisition of spatial and temporal variability of soil moisture remains vital for agricultural, hydrological, climatological, and other environmental studies (Aubert et al. 2003). Soil moisture plays an important role in characterizing earth's climate; hence, it is included in the list of essential climate variables (ECVs) (GCOS 2010). One of the key drivers for the partitioning of precipitation between infiltration and runoff is soil water which drives soil erosion and sedimentation. The growth of plants is mainly controlled by soil moisture, which is required for photosynthesis. Moreover, soil moisture regulates the rate of plant transpiration and evaporation which in turn affect near-surface temperature, humidity, and atmospheric water vapor (Cavanaugh et al. 2011). It plays a significant role in the interaction between the atmosphere and the land surface (Findell and Eltahir 2003). Therefore, accurate information about soil moisture is required for understanding the land surface processes, land-atmosphere interaction, drought forecasting, crop growth patterns, etc. (Legates et al. 2011). Besides this, soil moisture is used as one of the inputs in climate models, crop growth and yield models, process-based models for nutrient dynamics in soils and hydrological models, etc.

Traditionally, soil moisture is measured using a gravimetric technique; however, soil probes are now used for point measurement of soil moisture as indirect measurement, and this may be representative for a smaller area. However, soil moisture is a dynamic variable that changes significantly on different spatial and temporal scales even in a smaller area. Remote sensing (RS) techniques provide an alternative way to measure high spatial and temporal variability of soil moisture while replacing costly, time-consuming, and labour-intensive methods for measuring soil moisture in larger areas. The recent advancement in remote RS technologies such as optical, thermal, and microwave techniques have created tremendous potential in soil moisture assessment and estimation (Barrett and Petropoulos 2013). Previous studies have shown that optical RS datasets can be used for assessing soil moisture in bare surfaces only (Notarnicola et al. 2006). In vegetation-covered soils, optical satellite data is not useful because it barely reaches the surface (penetrate the surface up to

5 mm only). However, the penetration of solar radiation into the soil, sand, vegetation, and building surfaces is usually limited to at most 1 or 2 mm (Sørensen 1991). The penetration may reach 1–2 cm for large size grain, specifically for the wavelengths above 0.5 μm (Sørensen 1991). However, cloud cover is a common problem in optical RS, particularly during monsoon season, in which the solar radiations are mainly reflected by clouds and not by earth surface. There is a large difference between the dielectric constant of dry soil and water at microwave wavelength which varies between 4 and 40. The radar backscatter and thermal emissions from soils have strong dependency on moisture content. There is a strong dependence of the radar backscatter and thermal emission from the soil on its moisture content. Thermal infrared measurements depend on the diurnal range of land surface temperature (Tmax−Tmin) or measurement of the crop canopy-air temperature differential (Good 2015). The passive (radiometers) and active (radar) microwave sensors measure brightness temperature and backscatter coefficient from surfaces during all the weather conditions, respectively. In this chapter, the estimation of soil moisture using optical, thermal, and microwave RS techniques has been highlighted. The main objective of this chapter is to identify the key techniques used for estimating soil moisture using optical, thermal, and microwave RS techniques. This chapter also explores new initiatives taken for the estimation of soil moisture.

10.2 Optical, Thermal and Microwave Remote Sensing of Soil Moisture

In general, the soil moisture content is expressed in four different terms based on the depth up to which the electromagnetic wave penetrates the soil:

1. Skin or surface soil moisture is usually estimated by optical and thermal RS methods (Fig. 10.1). The estimation is closely confined to the water content in the upper thin layer of 1 mm thickness between the land and the atmosphere.
2. Near-surface soil moisture is estimated by using observations through microwave RS methods (X-, C-, and L- band). The water content within 1–10 cm of the soil layer is estimated (Fig. 10.1).
3. Root zone soil moisture (amount of water stored in the plant root zone) is estimated through P-band microwave sensors or various other methods.
4. Vadose zone soil moisture is estimated through deep penetrating airborne electromagnetic sensors.

Optical RS sensors operate within 400–2500 nm wavelength range and the change in soil reflectance associated with the change in soil color is measured to estimate the soil moisture content. Generally, soil moisture decreases the reflectance of solar radiations (i.e. lowers the albedo) of soil systems (Huan-Jun et al. 2009). However, a gradual increase in soil moisture results in increasing the dark color of soils up to field capacity. Beyond field capacity of soils, increasing soil moisture does not further darken the soils, instead, it results in building up of water sheet on

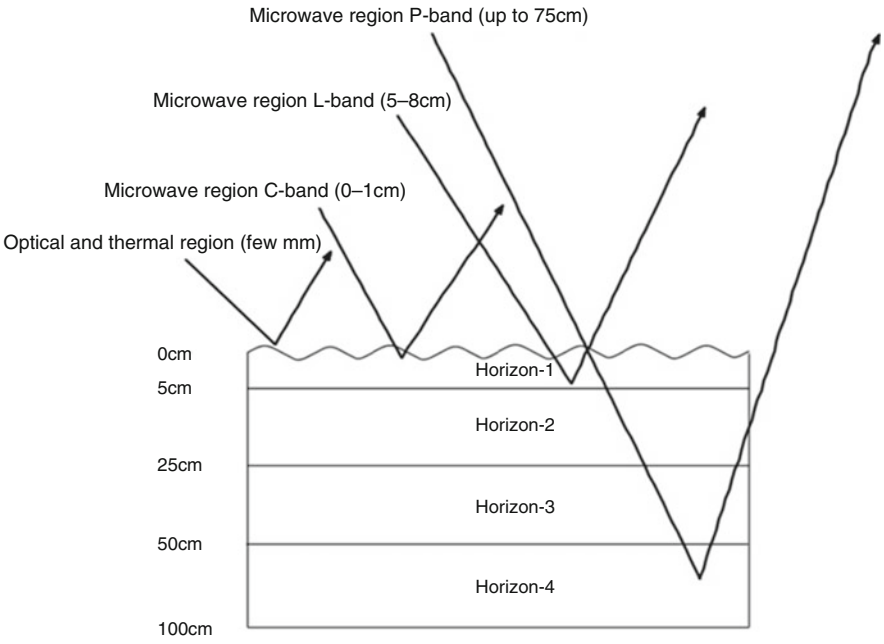

Fig. 10.1 Overview of optical, thermal and microwave remote sensing of soil moisture

the aggregate surfaces which in turn creates a shiny and better reflecting surface and thereby, increasing the reflectance (higher albedo). This phenomenon is one of the major reasons for differences in the reflectance of soils (Dobos 2014).

An increase in reflectance with decreasing soil moisture may not always be true, but it also depends on surface roughness, organic matter content, and mineralogical composition of soils (Lobell and Asner 2002). The smooth surfaces (like wet soil surface, plant leaves or water body, etc.) may have higher reflection than rough surfaces. In general, fine-textured and dry clayey soils (particle size less than 0.002 mm) have a smooth surface that produces high albedo (increased reflectance), but clayey soils are mostly wet, resulting in absorption of the incoming solar radiations and thereby, decrease in reflectance. Conversely, coarse-textured and dry sandy soils (particle size between 2 and 0.05 mm) reflect most of the incoming solar radiations and increases reflectance. These properties are useful for estimating soil moisture from bare surfaces only but single spectra or vegetation indices are used to estimate soil moisture for vegetation-covered soils using optical RS.

In the case of thermal infrared RS methods for soil moisture estimation, wavelength from 3500 to 14,000 nm is utilized. Primarily, thermal inertia or temperature index methods are used for estimating soil moisture using the thermal band. The microwave region of the electromagnetic (EM) spectrum ranges from 0.3 to 300 GHz (wavelength 1 m to 1 mm). It can be used in all weather conditions. The microwave interactions are majorly governed by the physical parameters of its targets rather than their spectral parameters. The microwave RS instruments are

mostly classified as passive and active: Passive sensors measure the thermal emission of the targets in their view and active imagers use their own source of illumination, hence eliminating the need for background sources such as the Sun. Passive microwave imagers measure the microwave energy radiated (by thermal emission) or reflected (from sun) from the target. The microwave energy emitted from the target primarily depends on the physical temperature and dielectric property of the target. The dielectric property is related to the composition of the target. Passive imaging measures some of the most important parameters, like, temperature, roughness, salinity, and moisture content. These parameters are difficult to measure in other parts of the EM spectrum due to atmospheric interactions and dependency on background sources like the Sun. Also, passive imagers have an advantage over active imagers when it comes to the cost and complexity of the system but lack when it comes to spatial resolution. Active microwave imager or the popular version of it called Synthetic Aperture Radar (SAR) is an active system that uses its own source of illumination and works in all-weather conditions suitable for day and night imaging. The microwave interaction with the surface is singular in nature, hence, the information obtained will be indicative of moisture content, salinity, and physical characteristics (orientation, size and shape) along with the reflectivity.

In optical RS, spectral bands are commonly defined using wavelength whereas, in microwave RS, they are defined using frequency. In general, microwave region of the EM spectrum is divided into several bands (P, L, S, C, X, Ku, K, Ka, Q, V and W bands) However, the bands of L, S, C, and X are the most common bands used in the current trend of microwave RS. There are many advantages of using microwave sensors but few disadvantages limit its usages. One of the main concerns is the antenna dimension due to the use of longer wavelengths. Even for data of coarse resolution (kilometers) about a meter or more long antennas are required which poses a challenge for deploying space-borne instruments. The coarser resolution is in the case of passive imaging but for finer or high-resolution imaging, active imaging is used specifically, SAR at the cost of complex and resource-hungry systems (large & heavy with high power consumption and high data-rates).

10.3 Techniques to Retrieve Soil Moisture

10.3.1 Optical Remote Sensing Techniques

In the optical region of the EM spectrum, soil moisture is correlated with the spectral reflectance. The relationship between soil moisture and reflectance for various soil types is well documented by Weidong et al. (2002) and Gao et al. (2013). Huan-Jun et al. (2009) developed a moisture adjusting method by estimating the quantitative relationship between the reflectance of soil and soil moisture particularly for black soils in northeast China. The changes in soil reflectance for soil samples ranging from air-dry to saturated soil moisture were depicted using a cubic equation with parameters reflectance and soil moisture content. The parameters like moisture

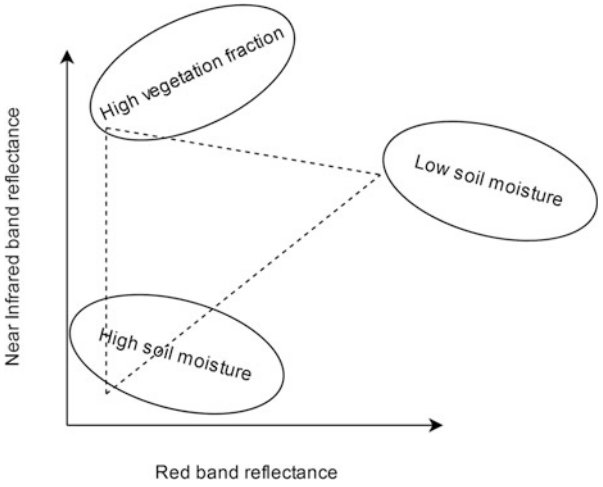

Fig. 10.2 Physical interpretation of Red/NIR bands feature space "scatterplot" (Modified, Gao et al. 2013)

threshold and moisture inflection of soil reflectance were determined from this equation. When the soil moisture measures below the moisture threshold, then soil reflectance was derived through simulation (with a linear model). For soils with different organic matter content, the parameters of the model will differ accordingly. To estimate the soil moisture over vegetated fields of Beijing, China using Landsat TM/ETM+ EO images (April 2009), the spectral feature space was plotted from reflectance of red and Near Infrared (NIR) bands by Gao et al. (2013). The plot formed a triangular shape and the bare soil pixels form a straight line if the soil texture is the same where the line is called soil line. In this triangular plot, the reflectance of the red band is low because of its absorption by chlorophyll, whereas NIR band reflectance is high because of strong reflection from vegetation (Fig. 10.2). The long-distance from pixel to soil line indicates higher vegetation fraction and biomass. The reflectance of bare soil increases with decreasing soil moisture, hence the longer the distance from the soil line to the red-NIR spectral feature origin, the lower the soil water content. Based on the linear decomposition of mixture pixel, the reflectance of red-NIR bands was derived by combining the soil line equation with a developed empirical relationship between vegetation canopy and mixture pixel and the results showed that the NIR band reflectance-based soil moisture was better than a red band.

Hyperspectral data has also potential to estimate soil moisture. Peng et al. (2013) used the discrete wavelet transform (DWT) method for soil moisture retrieval. They used the hyperspectral data (ASD Pro FR portable Spectroradiometer) along with a total of 78 observations of soil moisture (both in the field. They used 13 different mother wavelet and six decomposition levels (varied from 5 to 10) for hyperspectral data decomposition. Two feature extraction methods (band selection and DWT) were used to retrieve soil moisture. The wavelet transform method proved efficient for soil moisture measurements as it was successful in preserving the high- and low-frequency spectral information at different decomposition scales. Similarly,

Stamenkovic et al. (2013) used airborne hyperspectral imaging spectrometer (HyperSpecTIR) of April 2007 to estimate soil moisture from bare soils. They found that the non-linear data-driven method was effective in capturing the dependence between soil reflectance and topsoil moisture even though the penetration depth of the hyperspectral data is limited.

The reflectance-based methods for soil moisture retrieval have advantages of good spatial resolution, availability of multiple satellites and the capability of hyperspectral sensors for effective estimations through promising techniques, but the limitations of using reflectance are cloudy weather, no night-time image, poor temporal resolution and failure to establish the relationships with soil moisture content when the vegetation cover is high.

10.3.2 Thermal Infrared Remote SensingTechniques

The thermal infrared regions have been used to retrieve soil moisture. The basis of using thermal infrared data is the sensitivity of land surface temperature to surface soil water content due to its impact on the surface heating process under bare soil or sparse vegetation cover condition. Qin et al. (2013) developed an algorithm for upscaling the point scale measurement of soil moisture in-situ data to grid-scale (or foot print-scale) using the Moderate Resolution Imaging Spectroradiometer (MODIS) derived apparent thermal inertia (ATI). The relationship between MODIS derives ATI and the station averaged soil moisture was developed. The soil moisture time series at a certain spatial scale was calculated based on this relationship. Apparent thermal inertia can be used to improve the spatial resolution of soil moisture. Lei et al. (2014) developed a surface soil moisture model based on the heat conduction equation (for calculation of ATI) with improved spatial resolution, by integrating MODIS and TM/ETM+ derived mean surface temperature data. The enhanced ATI has a R^2 value of 0.789 with soil moisture content.

The soil moisture retrieval methods using thermal infrared data show promising results and the availability of multiple satellite datasets also makes it convenient. Similar to optical RS, the thermal infrared-based method also fails to perform under cloudy days, and the presence of sparse vegetation cover limits the relationship of soil moisture content and thermal inertia.

10.3.3 Fusion of Optical and Thermal Infrared Data

Many have used the visible and thermal infrared data together which showed the potential to derive soil moisture precisely than when used separately. Carlson (2007) developed a triangle approach to estimate soil surface wetness and evapotranspiration fraction from RS imageries. Normalized difference Vegetation Index (NDVI) and Radiant surface temperature were plotted on the x- and y-axis, respectively (Fig. 10.3). Two images from two different sites were used for plotting a triangle.

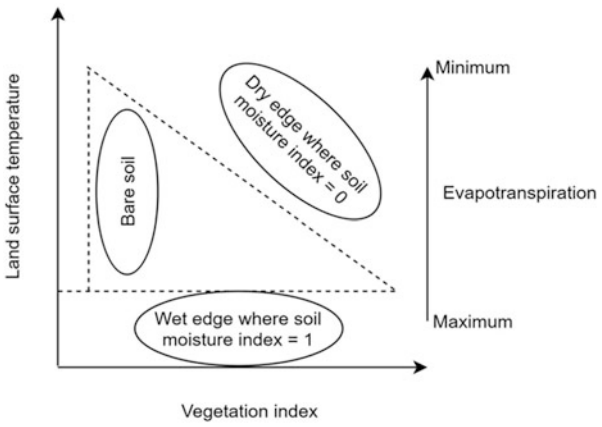

Fig. 10.3 Physical interpretation of Vegetation Index/Land surface temperature feature space "scatterplot" (Modified, Carlson 2007)

One image from AVHRR sensor over eastern Pennsylvania in the summertime and another from NASA NS001 radiometer (5 m surface resolution) over Walnut Gulch, Arizona in the summertime. The triangle method can be used for soil moisture estimation with large image data sets. The required parameters can be generated quickly with no requirement of atmospheric or surface data. The limitation of the triangle method is that there involves a matter of subjectivity while interpreting the triangle plot and also there is a requirement for high-resolution images.

Wang et al. (2007) used the MODIS NDVI (1 km) and LST data to establish the relationship between NDVI, LST, and ground-based soil moisture observation and they found a significant correlation between the datasets, irrespective of land cover and soil type. Mallick et al. (2009) estimated the volumetric surface soil moisture content in cropped areas at the field to landscape scales in parts of Punjab, Haryana, Odisha, and Karnataka from NDVI and surface temperature. Using ASTER data for field-scale and MODIS data for landscape scale, the soil wetness index was derived by plotting LST and NDVI in feature space (triangle method) from which the volumetric surface soil moisture content was further derived. The RMSE for field-scale using ASTER data was higher ($0.039 m^3/m^3$) than MODIS derived landscape scale ($0.033 m^3/m^3$) volumetric surface soil moisture content. Wang et al. (2011) estimated soil moisture using the trapezoidal relationship between land surface temperature (Ts) and vegetation index (VI). They used MODIS derived Ts and enhanced vegetation index (EVI). The algorithm approach was to plot Ts and EVI in x- and y-axis respectively and to find the trapezoidal vertices for each pixel by running the algorithm iteratively. Based on the trapezoid the water deficit index (WDI), they found that the retrieved soil moisture could capture the temporal variation but not the spatial variation for such a semi-arid region. Rahimzadeh-Bajgiran et al. (2013) developed a new soil moisture estimation method using optical/thermal infrared MODIS data based on the evaporative fraction (EF) for Canadian Prairies in parts of Saskatchewan and Alberta. The land surface temperature method of Wang et al. (2011) was modified by incorporating the North American Regional Reanalysis (NAAR) air temperature (Ta) data for soil moisture

estimation. The difference between MODIS Terra and Aqua derived two separate Ts data and NAAR derived Ta were used in combination. The estimated soil moisture was then compared with the in-situ soil moisture measurement and a significant correlation was found (R2varied between 0.42 and 0.77). Holzman et al. (2014) used the LST and EVI (Enhanced Vegetation Index) from MODIS to derive TVDI (Temperature Vegetation Dryness Index) which was used to derive soil moisture in Argentine pampas. TVDI was significantly positively correlated with soil moisture (R^2 between 0.61 and 0.83).

Sadeghi et al. (2017) proposed a novel OPticalTRApezoid Model (OPTRAM) advantageous over the previously used Thermal-Optical TRAapezoid Model (TOTRAM) which was based on the pixel distribution of the LST-VI space with two major limitations. One limitation was the requirement of thermal data and the second being the requirement for parameterization for each observation date. OPTRAM was based on the linear relationship between soil moisture and SWIR transformed reflectance (STR) and the parameterization was done on within the STR-VI space. They derived soil moisture using OPTRAM from Sentinel-2 and Landsat-8 data for the Walnut Gulch and Little Washita watersheds study area and the modelled soil moisture data were compared with in-situ data. Both model accuracies were found to be comparable where OPTRSM had a requirement for data from the optical EM domain. Vani et al. (2019) used the triangle method to estimate soil moisture from Landsat 8 images for years from 2007 to 2011 for a catchment in Southern New South Wales, Australia. Theoretical dry and wet edges were derived from the LST-VI space-based triangle method. The general soil moisture variation patterns were observed between the satellite-derived and in-situ soil moisture (from 20 agriculture stations) due to the background effects of soil properties on satellite-derived soil moisture.

The synergistic uses of optical and thermal results in the estimation of soil moisture with high spatial resolution. The major limitations for creating the operational products from the fused optical and thermal products are low temporal resolution, cloudy condition, no availability of data during night-time, and low penetration depth.

10.3.4 Microwave Remote Sensing Techniques

Optical and thermal RS data have many limitations mainly for its use in estimating soil moisture but active and passive microwave data is used to measure the soil moisture with good spatial and temporal resolution over large areas in different parts of the world (Crapolicchio and Lecomte 2005; Wagner et al. 2009; Njoku et al. 2002; Entekhabi et al. 2010). In a passive microwave system, brightness temperature is used to measure the soil moisture as decreasing brightness temperature indicates increasing soil moisture. In the active microwave system, higher backscatter will indicate higher content of soil moisture. An active microwave system like Synthetic Aperture Radar (SAR) has the potential to map the soil moisture in high resolution

(~10 m) but with low temporal resolution (12 to 36 days). In the case of a passive microwave system (like Radiometer), high temporal resolution can be achieved (~12 hrs) but with the constraint of low spatial resolution (20 to 50 km). The following parameters affect the microwave RS measurements and determine the efficacy of soil moisture retrieval:

- Frequency/wavelength: L band and C band are the most commonly used bands in microwave systems. L band penetrates most vegetation and successfully reaches the surface and subsurface. C band does not penetrate as much as L band but is still used for soil moisture measurements.
- As the incidence angle of a microwave sensor increases, the signal becomes attenuated (an electromagnetic wave inevitably loses energy when it travels through a dielectric medium. The energy loss is referred to as attenuation) due to several scatterers. For soil moisture application, low incidence angle data are suitable since the surface roughness and vegetation effects become minimum which in turn resulting in reducing errors.
- Polarization (a property of the EM wave which describes the direction in which the oscillations are taking place) also affects the retrieval of soil moisture. Active measurements have VV, VH, HH, and HV combinations, whereas passive measurements have either V or H. Different polarization has different effect on the target of interest; for example, HH polarization is most useful for soil moisture changes in C band, whereas VV polarization is most useful in crustal deformation and landslide applications for C-band.
- Surface roughness plays a major role in radar backscatter as the signal backscatters to the sensors based on the target's geometry. In SAR images, water bodies appear dark in tone due to low backscatter because the surface is smooth except where the water is disturbed by current or wind stress. This helps in differentiating land and water in times of flood damage assessment and coastal zone erosion mapping.
- Microwave signal backscatters are affected by dielectric constant (the ratio of the electric permeability of the material with respect to that of free space.). In the case of soil, dry soil has low dielectric constant, and wet soil has a high dielectric constant. This helps in measuring soil moisture content.
- Topography variations result in change in backscatter, as in slope facing the sensor would give high backscatter and surface facing away would give low or zero backscatter. This is true for active systems, whereas passive systems do not get affected by topography due to its large footprint.

Besides the above parameters, observation depth and vegetation characteristics also play an important role in estimating soil moisture. In passive microwave images, the microwaves emitted from the earth's surface are measured for various applications. From the passive microwave data, the brightness temperature measured from the satellite is extracted in order to derive or retrieve soil moisture using various models. The brightness temperature, T_B, of random volume over a surface is expressed as

$$\begin{aligned} T_B = &\text{(attenuated surface emission)} + \text{(direct volume emission)} \\ &+ \text{(scattered volume emission)} \end{aligned}$$

$$= T_{SURF}\Upsilon_v + T_V + T_V\Gamma\Upsilon_v \tag{10.1}$$

$$= \in_s T_s\Upsilon_v + T_V(1-a)(1-\Upsilon_v) + T_V(1-a)(1-\Upsilon_v)\Gamma\Upsilon_v \tag{10.2}$$

$$= \in_s T_s\Upsilon_v + T_V(1-a)(1-\Upsilon_v)(1+\Gamma\Upsilon_v) \tag{10.3}$$

For the above model, the surface layer is having physical temperature T_S and emissivity e_s lying beneath a sparse volume scattering layer with a brightness temperature of T_V and vertical opacity (t_v). The volume effects become threefold when the volume is sparse with low transmissivity (Υ_V). The volume effects are as follows:

- The surface emission signal attenuated by the factor, Υ_V, which gives (T_{SURF} Υ_V).
- A direct term of its own T_V.
- The term $T_V\Gamma$ shows the contribution of the part of the emission from the volume that goes downwards and scatters off the surface.

The surface emissivity and the volume transmissivity are dependent on the zenith angle, θ; then for a given zenith angle, θ, the observed brightness temperature is expressed as

$$T_B = \in_v T_S\left[cos\,\theta \exp\left(-\frac{\tau_v}{cos\theta}\right)\right] + T_V \tag{10.4}$$

The term $cos\theta$ accounts for the difference in path length when the measurement is not taken vertically. For active microwave images, the radar backscatter coefficient is derived from the signal that is transmitted and received by the radar.

Radar backscatter coefficient:

$$\sigma 0 = \frac{magnitude\ of\ received\ pulse}{magnitude\ of\ transmitted\ pulse} \tag{10.5}$$

Since σ_0 is unitless, it is converted to dB = $10\log_{10}$ (σ_0).

The σ_0 increases as surface roughness increases and also as dielectric constant increases. The backscatter coefficient depends on both system and target properties. System properties are wavelength/frequency, polarization, and the incidence angle. Target properties are dielectric constant, surface roughness, and feature orientation.

A number of techniques have been developed by scientific community to retrieve soil moisture from passive and active microwave images, and these techniques are described below:

10.3.4.1 Passive Microwave Remote Sensing Techniques

The radiative transfer equations have been used to retentive soil moisture from passive microwave images. Gao et al. (2004) proposed a land surface microwave emission model (LSMEM) using the radiative transfer equation (parameters like sensor viewing conditions and atmospheric parameters over a soil surface) developed by Kerr and Njoku (1990). The model was used to retrieve soil moisture from brightness temperature by airborne Electronically Scanned Thinned Array Radiometer (ESTAR) L-band radiometer during the 1999 Southern Great Plains Hydrology Experiment (SGP99). The estimated soil moisture was validated with an RMSE of 1.8%–2.8%. Chai et al. (2010) tested an artificial neural network (ANN) for deriving soil moisture at 1 km resolution on different dates using the training sample at the same site for a specific date. Combing the dual-polarized brightness temperature and an ANN architecture of a single hidden layer of 20 neurons as input, accuracy up to 3.7% v/v was achieved using the variability and subregion methodology.

Chen et al. (2012) used the Advanced Microwave Scanning Radiometer-Earth Observing System (AMSR-E) data to derive soil moisture (as an indicative of drought occurrence) using the inversion method. The brightness temperature (Tb) from the C band of AMSR-E was used to derive a modified surface roughness index for mapping the land surface roughness. The AMSR-E-derived Tb was combined with microwave polarization difference index (MPDI)-based vegetation cover classification to derive a semi-empirical model. This model was inverted to calculate surface soil moisture, and the coefficient of determination (R^2) was 0.87 for bare ground and flat areas, 0.85 for sparse vegetation and flat surface areas, and between 0.8 and 0.83 for dense vegetation areas. The time-series monitoring of surface soil moisture proved effective to detect initiation, duration, and recovery of the drought events. Li et al. (2014) also used the AMSR-E soil moisture product (derived from the X-band frequency brightness temperature using single-channel retrieval algorithm) coupled with in situ observation over three large climate regions in the United States. They found that AMSR-E soil moisture retrievals showed the smallest spatial variability among all the three data types. Pan et al. (2014) improved the existing LSMEM model to improve the accuracy of soil moisture because it was using only the H polarization of AMSR-E data for soil moisture retrieval which was introducing several errors to the system and also the model used a relatively large number of parameters. They found that the use of dual polarization (H and V) is much more effective than single polarization where the dual polarization addresses the problems of vegetation opacity and polarization mixing measured by the sensor. The existing LSMEM algorithm has revised by combining one roughness and two vegetation parameters into one effective vegetation optical depth (VOD) value and by providing the new algorithm that estimates VOD effectively from dual polarization resulting in the initial guess of soil moisture. The results were validated within the United States using in situ observations, and these were proven to be good and robust and were successful in reproducing the spatial and temporal dynamics of soil moisture.

Soil moisture estimated by passive microwave remote sensors is useful particularly over bare surfaces. This data is available in all weather conditions along with high temporal resolution. The major limitations are the coarse resolution of the radiometer data and its inefficiency to retrieve soil moisture over sparse vegetation areas and varying surface roughness.

10.3.4.2 Active Microwave Remote Sensing Techniques

Many active microwave images have been used in different parts of the world to map the soil moisture. Baghdadi et al. (2012) retrieved the bare soil moisture content from Terra SAR-X data using two cases where the first case was one image at either low or high incidence angle and the second where two images where one was at low incidence angle and another at high angle. Their results showed that Terra SAR-X images were capable enough to retrieve the soil moisture accurately with an RMSE of 3%. Nevertheless, the use of two incidence angles has no significance when it comes to soil moisture retrieval than using one incidence angle, but high incidence angle output was proven to be 1% better than low incidence angle output. Al-Bakri et al. (2014) studied the performances of empirical and semi-empirical models to predict soil moisture in the Yarmouk basin in Jordan using the backscatter coefficient of RADARSAT 2 C- band SAR data during May and June 2010. Soil moisture content was significantly positively correlated with horizontally polarized backscatter with R^2 of 0.64. From the empirical and semi-empirical regression model, the calculated RMSE for the SAR volumetric soil moisture content was 0.09 and 0.06 m3/m3, respectively. Due to non-inverted pixels in the soil moisture maps produced by the semi-empirical model, there were high differences in change in soil moisture content.

Panciera et al. (2013) compared the integral equation model (IEM) and Dubois and Oh models (surface scattering models) to predict backscatter for fully polarized L-band airborne observations. The Oh model was found to be most accurate before any site-specific calibration. The mean errors between the observed and simulated backscatter were −0.04 dB and 1.2 dB and for VV and HH polarizations, respectively. The IEM and Dubois model presented large errors of which IEM resulted in a maximum error of 4.5 dB for VV polarization. The error observed was primarily due to the surface roughness of the targets. A semi-empirical calibration of the surface roughness was applied to overcome the mismatch between the observed and simulated backscatter value. The IEM resulted in much less error of −0.3 dB and − 0.2 dB for HH and VV, respectively, outperforming the Oh model after the site-specific calibration. Baup et al. (2011) used the ENVISAT ASAR multi-angle C-band data to generate surface soil moisture maps in Sahelian rangelands. They generated a soil moisture map at 1 km resolution which was in good agreement with field data and ERS Wind Scatterometer surface soil moisture products.

Dave et al. (2019) used RISAT-1 C-band dual-polarization data for estimating surface soil moisture for winter wheat crop from the initial to maturity stage in the

Bhal region of Gujarat (India) using modified Dubois model developed by Rao et al. (2013). The modified Dubois model is defined as follows:

$$\sigma^{o}_{hh} = 10^{-2.75} \frac{cos^{2.5}\theta}{sin^{5}\theta} \times 10^{0.028 s\, tan\, \theta} (ks\, sin\, \theta)^{1.4} \lambda^{0.7} \tag{10.6}$$

Radar backscatter coefficient, σ^{o}_{hh}, is the function of incidence angle θ, dielectric constant ε, wavelength l, wave number k (2p/l), and root mean square height s, which is replaced by HV/HH ratio. Inverting the above equation, dielectric constant, ε, is given by

$$\varepsilon = \frac{\log\left(\sigma^{o}_{hh}\right) - \log\left(AC\right)}{B} \tag{10.7}$$

$$A = 10^{-2.75} \frac{cos^{1.5}\theta}{sin^{5}\theta}\ B = 0.028 tan\theta\ C = (kssin\theta)^{1.4} \lambda^{0.7} \quad \text{(where)}$$

From the above-defined dielectric constant, ε, soil moisture θ_v is derived as follows:

$$\theta_v = -5.3X10^{-2} + 2.92X10^{-2}\varepsilon - 5.5X10^{-4}\varepsilon^2 + 4.3X10^{-6}\varepsilon^3 \tag{10.8}$$

Dave et al. (2019) modified the above model to use only the backscatter from the HH polarization along with Topp's model to derive the soil moisture (Topp et al. 1980). Their results showed the correlation between measured and modelled value was 0.76 for the initial stage, 0.49 for maximum (peak) growth, and0.63 for the maturity stage. These results showed that vegetation affects the retrieval accuracy of soil moisture using radar data.

Active microwave RS-based soil moisture retrieval methods have advantages (like fine resolution soil moisture output and the capacity to provide data despite any clouds and time of the day), but temporal resolution, surface roughness, and amount of vegetation cover limit its use.

10.3.4.3 Active and Passive Microwave Data Fusion

Both active and passive microwave sensors data have their own advantages and disadvantages which can be used in complement with each other to downscale the coarse resolution passive radiometer data to obtain finer resolution soil moisture maps. Passive sensor data is less sensitive to surface roughness and provides soil moisture on a coarse resolution, whereas the active sensor data is highly sensitive to surface roughness and other parameters but provides soil moisture on a fine resolution. Several attempts have been done to obtain fine resolution soil moisture maps by downscaling approaches.

Zhan et al. (2006) analysed the data from the observation system simulation experiment (OSSE) as a performance check before NASA's Earth System Science Pathfinder Hydrospheric State (Hydros) mission which used L-band radiometer and radar systems. Soil moisture at scales 9 km and 3 km were derived using the 36 km radiometer data and 3 km radar data. The noisy fine-resolution radar data was compensated by the coarse resolution accurate radiometer data. Using the Bayesian merging method, the RMSE of low and high noise data sets were reduced by 0.5% vol/vol and 1.4% vol/vol, respectively, for the 9 km soil moisture product for the experimental data for consecutive 34 days. The 3 km scale soil moisture product also performed well using this compared with the direct inversion method.

Piles et al. (2009) developed a change detection algorithm to downscale the 36 km L- band radiometer data and 3 km radar data as preparation for the Soil Moisture Active Passive (SMAP) mission. For algorithm development, OSSE and field experiment Passive and active L- and S-band sensor (PALS) data were used. They used the 36 km radiometer brightness temperature and 3 km radar backscatter observation to derive 10 km soil moisture observation. They made three assumptions: (i) soil moisture and the log of backscatter are linearly related at 10 km scale, (ii) slope of the linear relation (between soil moisture and the log of the backscatter) and backscatter changes are uncorrelated, and (iii) variations on vegetation type occur principally at scales larger than the radiometer pixel area of 40 km. The algorithm had yielded an improved RMSE by 2% volumetric soil moisture content when four-month OSSE data were used. Magagi et al. (2012) experimented with Saskatchewan, Canada, for soil moisture retrieval using the Soil Moisture and Ocean Salinity (SMOS) satellite data (for data validation of the mission) and SMAP data (for pre-launch assessment of the mission). The data were collected using both airborne and spaceborne platforms along with ground measurements on soil properties such as roughness, soil moisture and temperature, and bulk density and vegetation parameters like biomass, vegetation height, and leaf area at the time of sensor acquisitions. Besides, continuous measurement of soil moisture and temperature profiles and meteorological conditions was acquired using two ground-based in situ networks. Two sites (33 km x 71 km), almost of two SMOS pixel size, were selected in agricultural and boreal forested areas to capture the contrasting soil and vegetation conditions. The airborne L-band brightness temperatures matched up well with the SMOS data over the agricultural area. The absolute soil moisture estimates could not meet the required accuracy for the SMOS mission, but the temporal evolution of the soil moisture of the SMOS mission was in good agreement with the ground data.

Piles et al. (2014) proposed a downscaling algorithm to obtain multi-resolution soil moisture estimates from the SMOS data using visible and infrared observations. Two years of SMOS and MODIS terra/aqua data were combined to produce a 1 km soil moisture map over the Iberian Peninsula. These soil moisture maps were compared to the 0–5 cm REMEDHUS ground-based measurement network. Downscaled maps captured the soil moisture dynamics of general land uses except for irrigated crops. Results indicate that the downscaled output improved the SMOS estimates maintaining temporal correlation and root mean squared differences with

ground-based measurements. Shi et al. (2014) proposed a new algorithm for downscaling the radiometer and radar data to produce high-resolution soil moisture maps. The algorithm was based on spectral downscaling combining the phase and amplitude information in the Fourier domain. The Fourier phase was estimated using the fine resolution radar data through a new proposed way. The algorithm was applied to the PALS data from the SMEX02 experiments for downscaling which proved to be better than the radiometer only inversion product. The RMSE of the downscaled brightness temperature for H and V polarization were found to be 3.26 K and 6.12 K, respectively. The RMSE for downscaled soil moisture was found to be 0.0459 m3/m3.

Akbar and Moghaddam (2015) developed a method for combining active and passive data to produce soil moisture maps using Monte Carlo numerical simulations and optimization. The algorithm was tested for corn, soybean, and grassland cover types for active-only, passive-only, and active-passive combined scenarios. The combined data output was found to be accurate compared to the other scenarios, especially in high vegetation water content values. Montazaka et al. (2016) used active and passive L-band data for producing downscaled soil moisture maps as a part of the SMAP validation program. They used this dataset to produce soil moisture using three different fusion algorithms: (i) use of passive sensor data and subsequent disaggregated active data to estimate the soil moisture, (ii) use of passive microwave backscatter data disaggregated by active backscatter data and further inverted to derive soil moisture and, and (iii) fusion of two single-source soil moisture products from active and passive data sets. The fusion of radiometer brightness temperatures and radar backscatters shows the best performance, with the same accuracy as single-source coarse-scale radiometer soil moisture retrieval but on a higher spatial resolution. Das et al. (2018) tested several soil moisture retrieval algorithms on the SMAP radar and radiometer data of 2.5 months until the failure of the radar part of the SMAP sensor. The acquired data till the failure of radar sensor coincided with the northern hemisphere's vegetation green-up and crop growth season. Various algorithms were tested on the data against in situ data from core calibration and validation sites and sparse networks to produce 3 km and 9 km high-resolution soil moisture maps. The baseline algorithm was proven best amongst the other algorithms. The unbiased RMSE was found close to 0.04 m3/m3for 9 km resolution data as per the SMAP requirement and 0.053 m3/m3 for 3 km resolution data. The results of this study showed that the product obtained by combining radar and radiometer data has the potential to provide high-resolution soil moisture with high accuracy on a global scale.

Das et al. (2019) combined the L-band SMAP radiometer data with the C-band Sentinel 1A/Sentinel 1B SAR data to produce high-resolution soil moisture of 3 km and 1 km resolution. Sentinel 1 Interferometric Wide (IW) data was found suitable as it has a similar orbit configuration that of SMAP. The major differences in Sentinel-1 and SMAP data set are:

I. Sentinel 1 data are of C-band, whereas SMAP data are of L-band.

II. Sentinel 1 images are acquired in multiple incidence angles, whereas SMAP data are acquired in single multiple angles.
III. The swath is 250 km for of Sentinel-1 and 1000 km of SMAP.

The original developed downscaling algorithm for SMAP mission is given as follows (Das et al.2013, 2018; Entekhabi et al. 2014):

$$T_{B_p}(M_j) = T_{B_p}(C) + \beta(C).\{[\sigma_{pp}(M_j) - \sigma_{pp}(C)] + \Gamma.[\sigma_{pq}(C) - \sigma_{pq}(M_j)] \tag{10.9}$$

where $T_{B_p}(C)$ is the coarse resolution (~36 km) brightness temperature in unit K and $\sigma_{pp}(C)$ and $\sigma_{pq}(C)$ are the co-pol and cross-pol radar backscatter aggregated for coarse resolution in units dB. $\sigma_{pp}(M_j)$ and $\sigma_{pq}(M_j)$ the co-pol and cross-pol radar backscatters at medium or desired resolution (3 or 1 km) in dB. $\beta(C)$ and Γ are algorithm parameters. Since the SMAP algorithm was optimized for daily coverage radar data, the authors modified it to incorporate the 12 days coverage radar data of Sentinel-1using the snapshot retrieval approach by Jagdhuber et al. (2018), and it is given as follows:

$$T_{B_p}(M_j) = \left[\frac{T_{B_p}(C)}{T_S} + \beta'(C).\{[\sigma_{pp}(M_j) - \sigma_{pp}(C)] + \Gamma.[\sigma_{pq}(C) - \sigma_{pq}(M_j)]\}\right].T_S \tag{10.10}$$

where T_S is the emission temperature of the surface soil in units K and β'(C) is the snapshot parameter which compensates the sparse time series data of Sentinel-1 12-day coverage. The produced high-resolution soil moisture maps showed a reasonable accuracy of $0.05 m^3/m^3$.

Toride et al. (2019) proposed a new downscaling algorithm named integrated passive and active downscaling or I-PAD to produce high-spatiotemporal-resolution data over regions without detailed soil data. The data used were AMSR-E and ALOS PALSAR. The data were combined through a dual-pass land data assimilation system to derive the 1 km soil moisture maps of Mongolia and the Little Washita basin. The analysis showed that I-PAD could capture the overall spatial trend of soil moisture proving that the algorithm can be applied over data-sparse regions.

The primary advantage of fusing active and passive microwave data is its ability to produce high-resolution soil moisture maps with high temporal resolution. The method lacks in validation part of the derived products and also use of multiple satellite results in different penetration depth for soil moisture content measurement.

10.3.5 Microwave and Optical/Thermal Infrared Data Fusion

As explained above, optical/thermal RS data produces soil moisture on a finer scale and at a fairly fine temporal resolution, whereas microwave RS data reacts differently to various biophysical and geophysical parameters related to land and can retrieve soil moisture for various ranges of vegetation characteristics. A key advantage in combining microwave and optical data is its capability to minimize the effects of vegetation biomass and surface roughness.

Using the passive microwave data from AMSR-E, visible wavelength data from MODIS and topographic attributes from the SRTM DEM, Temimi et al. (2010) presented a methodology for monitoring soil wetness index over Peace-Athabasca Delta (PAD) in the Mackenzie river basin (Canada). They proposed a new topography wetness index (TWI) using passive microwave data and vegetation parameters because the classic topography-based wetness index is unable to capture the temporal variability of soil moisture and also does not take into account the vegetation effect. AMSR-E data were used to assess the soil wetness regularly. MODIS data were used to develop a rating curve relationship between discharge observations and the extent of flooded areas. The proposed index proved efficient than the previous classic index. Piles et al. (2011) carried different downscaling experiments to improve the 40 km SMOS data using visible/infrared data from the Landsat image. The algorithm was based on the universal triangle concept using VIS/IR data parameters (like NDVI and LST) and relating these to the soil moisture status. The results matched well with the ground observations at 10 and 1 km spatial resolution without compromising the RMSE. Gao et al. (2017) used the time-series Sentinel-1 and Sentinel-2 data of almost 1.5 years over Urgell (Spain) to produce high-resolution 100 m soil moisture data. They used the following two methods to produce high-resolution soil moisture data:

(i) Change detection (changes in radar backscatter and NDVI during the study period) which was optimized to utilize the Sentinel-1 high repeat frequency through inversion using the following equation:

$$M_V(i,j,NDVI,d) = \frac{\Delta\sigma_{(i,j)}^{NDVI}}{f(NDVI)}(M_{V_{max}} - M_{V_{min}}) + M_{V_{min}}(i,j,d) \tag{10.11}$$

where $M_{V\ max}$ and $M_{V\ min}$ are the maximum and minimum soil moisture values calculated for the time period of the study using SMOS coarse-resolution data, $\Delta\sigma_{(i,j)}^{NDVI}$ is the radar backscatter difference of each pixel with its minimum value where the pixels are within the NDVI range of 0.1–0.8, and f (NDVI) is the slope between the radar backscatter difference and the NDVI values.

(ii) Computation of radar backscatter difference of two consecutive day Sentinel-1 data expressed as a function of NDVI optical index using the equation:

$$M_V(i,j,t_2) = M_V(i,j,t_1) + H(\delta\sigma(t_1,t_2))$$
$$M_V(i,j,t_3) = M_V(i,j,t_2) + H(\delta\sigma(t_2,t_3)) \quad (10.12)$$

For consecutive days t1, t2, t3, and so on, soil moisture is calculated iteratively. Here, the change in radar backscatter δσ is the difference between the radar backscatter of consecutive date Sentinel-1 images. These two approaches of Gao et al. (2017) are being used by authors to retrieve soil moisture from cropped areas of Indian Punjab. An overview of the approach is given in Fig.10.4.

Fang et al. (2018,) used the improved thermal inertia theory to downscale the SMAP radiometer data from 9 km to 1 km utilizing the NDVI and LST derived from NLDAS (North American Land Data Assimilation System), MODIS, and AVHRR data. The outputs were validated using the SMAPVEX15 experiment data, and the algorithm was found to be applicable in any site since the outputs were not site-specific.

10.4 Operational Products of Soil Moisture

The satellite-based soil moisture product became available since 2002 when the first global multiannual soil moisture dataset (1992–2000) derived from ERS-1 and ERS-2 SCAT observations was published (Wagner et al. 2003). Since then, scientists in different parts of the worlds have developed soil moisture products using different sensors and techniques. The list of operations soil moisture products is given in Table 10.1. The soil moisture product of AMSR-2, MIRAS, and SMAP over India has been given in Fig. 10.5, and all of these three soil moisture products are with coarse resolution. The high-resolution soil moisture of 3 km and 1 km resolution has been produced by combining the L-band SMAP radiometer data with the C-band Sentinel 1A/Sentinel 1B SAR data by Das et al. (2019), and the soil moisture of 1 km resolution over India has been given in Fig.10.5.

10.5 Soil Moisture Data Products: A Case Study from India

Soil wetness index (SWI) and soil moisture (SM) data products were developed by Space Applications Centre, Indian Space Research organisation using SMAP L-band radiometer data. The algorithm for soil wetness index (SWI) data products as a primary product was adopted from ASCAT soil moisture product (Wagner et al. 2013) based on change detection approach (time series methodology). From a mathematical point of view, the TU Wien change detection algorithm is less complex as compared to the semi-empirical modelling approaches build upon the cloud model (Wagner et al. 2013). This model can be inverted analytically; hence, direct soil moisture estimation is possible from the microwave measurement without

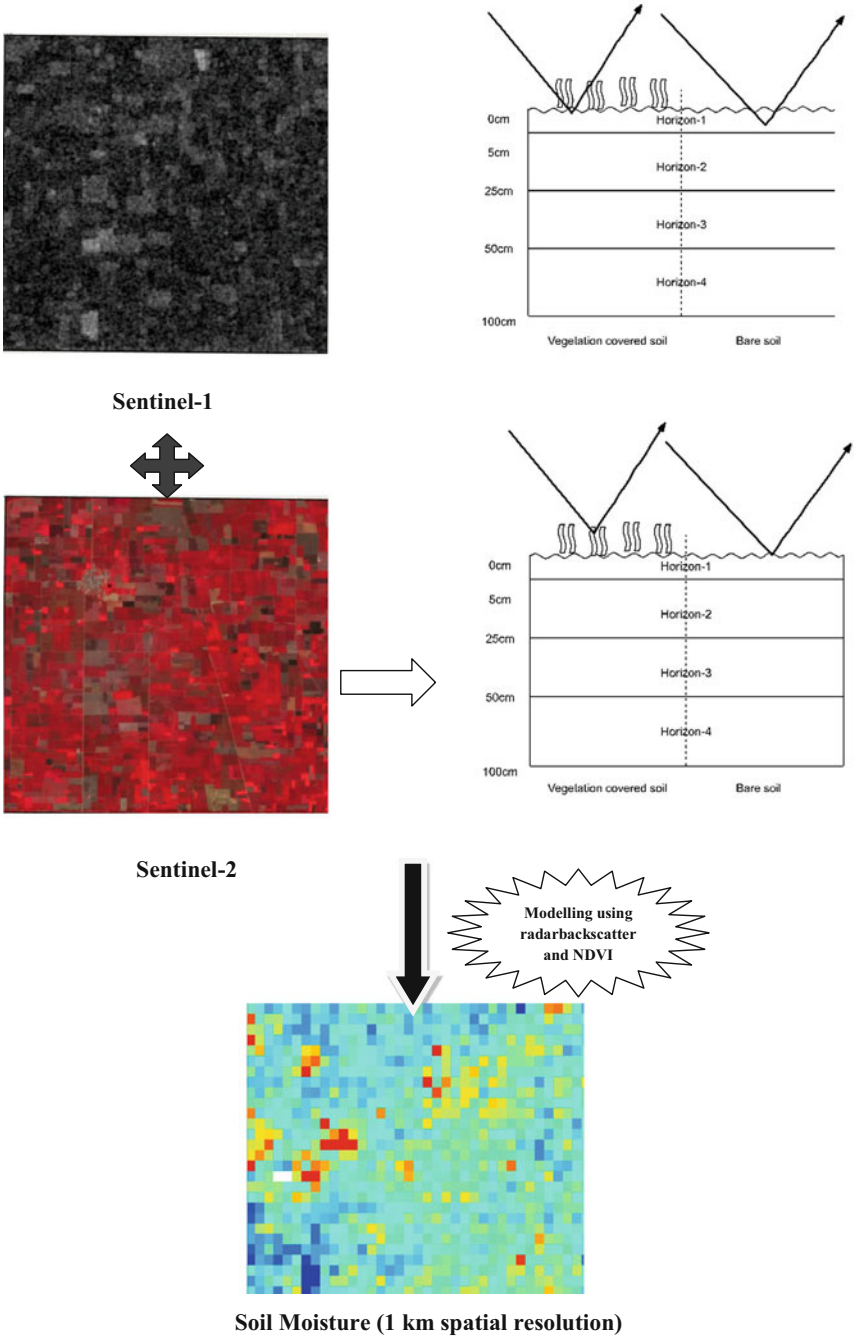

Fig. 10.4 Retrieval of soil moisture using the fusion of Sentinel-1 and Sentinel-2. (Modified, Gao et al. 2017)

Table 10.1 Operational soil moisture products derived using remote sensing

Sensor	Platform	Wavelength	Polarization	Swath (km)	Data availability	Spatial resolution (km)	Temporal resolution (days)
AMSR-E (Advanced Microwave Scanning Radiometer)	Aqua (NASA)	X/C band	H and V	1450	2002–2011	6–75	1
AMSR-2 (Advanced Microwave Scanning Radiometer 2)	GCOM-W1 (JAXA)	X/C band	H and V	1445	2012–ongoing	5–60	1
ASCAT (Advanced Scatterometer)	METOP (ESA)	L band	VV	2x550	2006–ongoing	25	1–2
MIRAS (radiometer) (Microwave Imaging Radiometer with Aperture Synthesis)	SMOS (ESA)	L band	H and V	1000	2010–ongoing	36	1–3
SMAP (*Soil Moisture Active Passive*) (radar (inactive) and radiometer)	SMAP (NASA)	L band	VV, HH, and VV/HH (radar) and H, V, and U (radiometer)	1000 for both radar and radiometer	January 2015 to July 2015 (Radar) and 2015–ongoing (radiometer)	3 for radar) and 36 for radiometer	1–3 for both radar and radiometer
Sentinel-1 (radar) (soil moisture product for Europe only)	Sentinel-1 (ESA)	C band	HH + HV and VV + VH	20–400	2014–ongoing	0.005–0.04	3–12

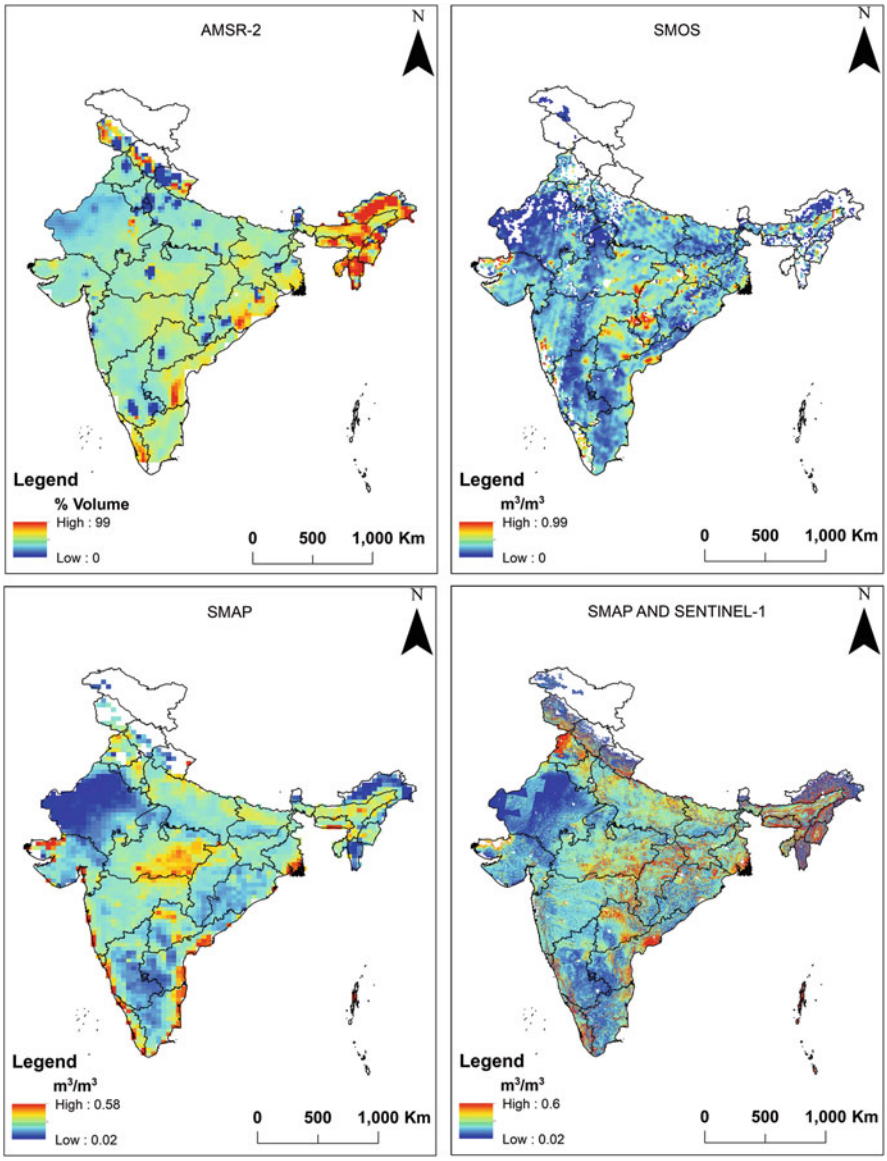

Fig. 10.5 Soil moisture products over India from different sensors (January 2020)

iterative adjustment processes. Because of this, it is also quite straight forward to perform an error propagation to estimate the retrieval error for each land surface pixel (Naeimi et al. 2009). With the above advantage of simplistic approach, less requirement of ancillary data and analytical solution to soil moisture inversion from time-series data, same algorithm was adopted and implemented using time series

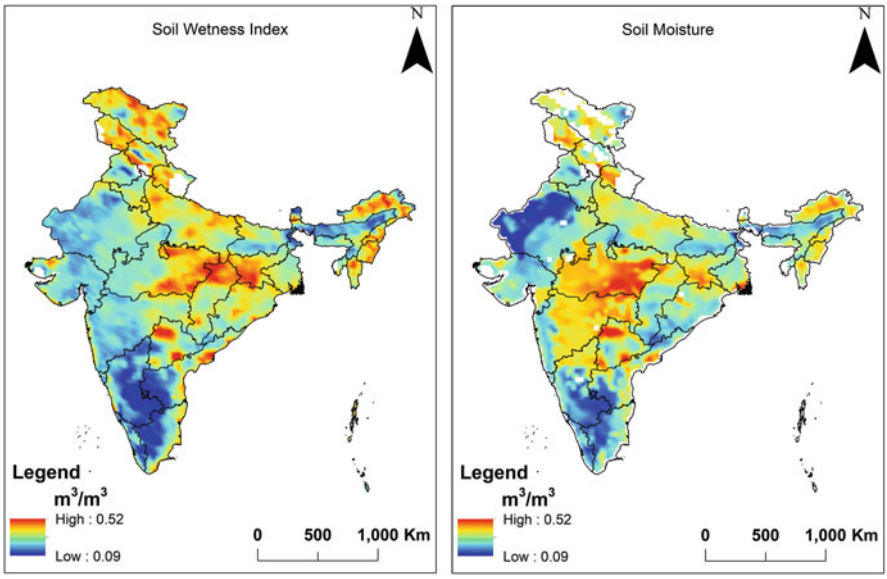

Fig. 10.6 Soil wetness index (SWI) and soil moisture (SM) daily operational data products over India during January 2020

SMAP L-band Tb data to derive large-scale soil moisture as a soil wetness index (SWI) whose value ranges from 0 to 1, showing driest to saturation condition (Pandey et al. 2016).

The absolute soil moisture W(t) at time can also be derived from soil wetness index (t) at time if the W_{min} and W_{max} corresponding to the minimum and maximum soil moisture values (gravimetric or volumetric) are available (Thapliyal et al. 2005; Chaurasia et al. 2012):

$$\boldsymbol{W(t) = W_{min} + SWI(t) * (W_{max} - W_{min})} \tag{10.13}$$

The W_{min} and W_{max} represent the permanent wilting point (PWP) and the field capacity (FC) of soil, which can be derived from soil texture information. Using above approach, soil moisture as a secondary product was derived using soil wetness index (SWI) data product and soil texture information from Harmonized World Soil Database (HWSD) whose value covers the top 5 cm of the soil column, ranges from 0 to 0.55 m^3/m^3 (Fig. 10.6).

Currently, soil wetness index (SWI) and soil moisture (SM) as primary and secondary products are generated as daily operational products over India which is available on https://www.mosdac.gov.in/swi/ in Meteorological & Oceanographic Satellite Data Archival Centre (MOSDAC) and Visualization of Earth Observation Data and Archival System (VEDAS) web portal of SAC (ISRO) for visualization and user interaction. The daily operational soil moisture maps over India are freely

available since April 2015 on https://mosdac.gov.in/opendata/soil_moisture/ (Pandey et al. 2016). The spatial resolution of both soil wetness and soil moisture products is 0.125 degree (~12.5 km).

10.6 Future Missions

The NASA-ISRO Synthetic Aperture Radar (NISAR) is one of the upcoming missions, having dual-frequency (L&S-band) SAR which will be utilized for major applications like agriculture, surface deformation, and disaster management. The NISAR mission will provide data in 10-meter spatial resolution with 12 days of temporal resolution. Since it is a radar, the coverage will be day/night during all-weather conditions. NISAR will work in both L-band ($\lambda = 24$ cm) and S-band ($\lambda = 10$ cm) wavelength (Rosen et al. 2016). Among other applications, the NISAR mission will provide high-resolution soil moisture maps at individual field level and will be helpful inefficient irrigation, water use, and fertilization.

10.7 Conclusions

Soil moisture is one of the important parameters for several applications in fields like hydrology and agriculture. The accurate retrieval of soil moisture becomes a top priority in hydrological modelling, crop modelling, atmospheric modelling, etc. RS techniques are efficient in retrieving soil moisture with high spatial and temporal resolution up to a depth of about 3–5 cm. Optical, thermal, and microwave regions of the EM spectrum have their own advantages and disadvantages in retrieving the soil moisture. Using optical, thermal, and microwave RS in synergy has proved to be more efficient and has now become the prospect for soil moisture retrieval. The current soil moisture products provide global coverage with almost-daily temporal resolution. The vegetation cover is a major challenge to retrieve soil moisture at places where the land is covered with thick vegetation and the current products prove accurate in low vegetated to bare soil-covered areas. Although the operational products are useful in many applications, there is a requirement for soil moisture products at depths around 10–15 cm. P-band microwave data could be the solution since it is of longer wavelength (~70 cm, corresponding to a lower frequency of typically 430 MHz), and the P-band is expected to have higher soil moisture retrieval accuracy since its sensitivity towards vegetation water content and surface roughness is minimal compared with other microwave bands. Existing Sentinel-1 SAR data has great potential to downscale the soil moisture of available operational products (like SMAP or SMOS) or with optical data to retrieve soil moisture at a finer spatial resolution over vegetation-covered surfaces.

References

Akbar R, Moghaddam M (2015) A combined active–passive soil moisture estimation algorithm with adaptive regularization in support of SMAP. IEEE Trans on Geosci Remote Sens 53 (6):3312–3324

Al-Bakri J, Suleiman A, Berg A (2014) A comparison of two models to predict soil moisture from remote sensing data of RADARSAT II. Arab J Geosci 7(11):4851–4860

Aubert D, Loumagne C, Oudin L (2003) Sequential assimilation of soil moisture and streamflow data in a conceptual rainfall–runoff model. J Hydrol 280(1–4):145–161

Baghdadi N, Cresson R, El Hajj M, Ludwig R, La Jeunesse I (2012) Estimation of soil parameters over bare agriculture areas from C-band polarimetric SAR data using neural networks

Barrett B, Petropoulos GP (2013) Satellite remote sensing of surface soil moisture. Remote sensing of energy fluxes and soil moisture content 85

Baup F, Mougin E, De Rosnay P, Hiernaux P, Frappart F, Frison P-L, Zribi M, Viarre J (2011) Mapping surface soil moisture over the Gourma mesoscale site (Mali) by using ENVISAT ASAR data

Carlson T (2007) An overview of the "triangle method" for estimating surface evapotranspiration and soil moisture from satellite imagery. Sensors 7(8):1612–1629

Cavanaugh ML, Kurc SA, Scott RL (2011) Evapotranspiration partitioning in semiarid shrubland ecosystems: a two-site evaluation of soil moisture control on transpiration. Ecohydrology 4 (5):671–681

Chai S-S, Walker JP, Makarynskyy O, Kuhn M, Veenendaal B, West G (2010) Use of soil moisture variability in artificial neural network retrieval of soil moisture. Remote Sens 2(1):166–190

Chaurasia S, Thapliyal PK, Pal PK (2012) Application of a time-series-based methodology for soil moisture estimation from AMSR-E observations over India. IEEE Geosci Remote Sens Letters 9(5):818–821

Chen X-Z, Chen S-S, Zhong R-F, Su Y-X, Liao J-S, Li D, Han L-S, Li Y, Li X (2012) A semi-empirical inversion model for assessing surface soil moisture using AMSR-E brightness temperatures. J Hydrol 456:1–11

Crapolicchio R, Lecomte P (2005) The ERS-2 scatterometer mission: events and long-loop instrument and data performances assessment. Envisat & ERS Symposium

Das NN, Entekhabi D, Njoku EG, Shi JJ, Johnson JT, Colliander A (2013) Tests of the SMAP combined radar and radiometer algorithm using airborne field campaign observations and simulated data. IEEE Trans Geosci Remote Sens 52(4):2018–2028

Das NN, Entekhabi D, Kim S, Jagdhuber T, Dunbar S, Yuehl S, O'Neill PE, Colliander A, Walker J, Jackson TJ (2018) High resolution soil moisture product based on Smap active-passive approach using Copernicus sentinel 1 data. In: IGARSS 2018–2018 IEEE international geoscience and remote sensing symposium, 2018. IEEE, pp 3768–3770

Das NN, Entekhabi D, Dunbar RS, Chaubell MJ, Colliander A, Yueh S, Jagdhuber T, Chen F, Crow W, O'Neill PE (2019) The SMAP and Copernicus sentinel 1A/B microwave active-passive high resolution surface soil moisture product. Remote Sens Environm 233:111380

Dave R, Kumar G, Kr. Pandey D, Khan A, Bhattacharya B (2019) Evaluation of modified Dubois model for estimating surface soil moisture using dual polarization RISAT-1 C-band SAR data. Geocarto Int:1–11

Dobos E (2014) Albedo. In: Encyclopedia of natural resources-land-volume I. CRC Press, pp 7–9

Entekhabi D, Njoku EG, O'Neill PE, Kellogg KH, Crow WT, Edelstein WN, Entin JK, Goodman SD, Jackson TJ, Johnson J (2010) The soil moisture active passive (SMAP) mission. Proc IEEE 98(5):704–716

Entekhabi D, Yueh S, O'Neill PE, Kellogg KH, Allen A, Bindlish R, Brown M, Chan S, Colliander A, Crow WT (2014) SMAP handbook–soil moisture active passive: Mapping soil moisture and freeze/thaw from space

Fang B, Lakshmi V, Bindlish R, Jackson TJ (2018) Downscaling of SMAP soil moisture using land surface temperature and vegetation data. Vadose Zone J 17(1)

Findell KL, Eltahir EA (2003) Atmospheric controls on soil moisture–boundary layer interactions. Part II: feedbacks within the continental United States. J Hydrometeorol 4(3):570–583

Gao H, Wood EF, Drusch M, Crow W, Jackson TJ (2004) Using a microwave emission model to estimate soil moisture from ESTAR observations during SGP99. J Hydrometeorol 5(1):49–63

Gao Z, Xu X, Wang J, Yang H, Huang W, Feng H (2013) A method of estimating soil moisture based on the linear decomposition of mixture pixels. Mathematical Comput Model 58 (3–4):606–613

Gao Q, Zribi M, Escorihuela MJ, Baghdadi N (2017) Synergetic use of Sentinel-1 and Sentinel-2 data for soil moisture mapping at 100 m resolution. Sensors 17(9):1966

GCOS Implementation plan for the global observing system for climate in support of the UNFCCC, GCOS-138 (2010). In: Proceedings of the conference of the parties (COP), Copenhagen, Denmark. Citeseer, pp 7–19

Good E (2015) Daily minimum and maximum surface air temperatures from geostationary satellite data. J Geophy Res Atmosp 120(6):2306–2324

Holzman ME, Rivas R, Piccolo MC (2014) Estimating soil moisture and the relationship with crop yield using surface temperature and vegetation index. Int J Appl Earth Observ Geoinform 28:181–192

Huan-Jun L, Zhang Y-Z, Zhang X-L, Zhang B, Kai-Shan S, Zong-Ming W, Na T (2009) Quantitative analysis of moisture effect on black soil reflectance. Pedosphere 19(4):532–540

Jagdhuber T, Entekhabi D, Das NN, Link M, Baur M, Akbar R, Montzka C, Kim S, Yueh S, Baris I (2018) Physics-based modeling of active-passive microwave Covariations for geophysical retrievals. In: IGARSS 2018–2018 IEEE Int Geosci remote sensing symposium. IEEE, pp 250–253

Kerr YH, Njoku EG (1990) A semiempirical model for interpreting microwave emission from semiarid land surfaces as seen from space. IEEE Trans Geosci Remote Sens 28(3):384–393

Legates DR, Mahmood R, Levia DF, DeLiberty TL, Quiring SM, Houser C, Nelson FE (2011) Soil moisture: a central and unifying theme in physical geography. Prog Phys Geogra 35(1):65–86

Lei S-G, Bian Z-F, Daniels JL, Liu D (2014) Improved spatial resolution in soil moisture retrieval at arid mining area using apparent thermal inertia. Trans Nonferrous Metals Soc China 24 (6):1866–1873

Lobell DB, Asner GP (2002) Moisture effects on soil reflectance. Soil Sci Soci America J 66 (3):722–727

Magagi R, Berg AA, Goïta K, Belair S, Jackson TJ, Toth B, Walker A, McNairn H, O'Neill PE, Moghaddam M (2012) Canadian experiment for soil moisture in 2010 (CanEx-SM10): overview and preliminary results. IEEE Trans Geosci Remote Sens 51(1):347–363

Mallick K, Bhattacharya BK, Patel N (2009) Estimating volumetric surface moisture content for cropped soils using a soil wetness index based on surface temperature and NDVI. Agricult Forest Meteorol 149(8):1327–1342

Montzka C, Jagdhuber T, Horn R, Bogena HR, Hajnsek I, Reigber A, Vereecken H (2016) Investigation of SMAP fusion algorithms with airborne active and passive L-band microwave remote sensing. IEEE Trans Geosci Remote Sens 54(7):3878–3889

Naeimi V, Scipal K, Bartalis Z, Hasenauer S, Wagner W (2009) An improved soil moisture retrieval algorithm for ERS and METOP scatterometer observations. IEEE Transa Geosci Remote Sens 47(7):1999–2013

Njoku EG, Wilson WJ, Yueh SH, Dinardo SJ, Li FK, Jackson TJ, Lakshmi V, Bolten J (2002) Observations of soil moisture using a passive and active low-frequency microwave airborne sensor during SGP99. IEEE Trans Geosci Remote Sens 40(12):2659–2673

Notarnicola C, Angiulli M, Posa F (2006) Use of radar and optical remotely sensed data for soil moisture retrieval over vegetated areas. IEEE Trans Geosci Remote Sens 44(4):925–935

Pan M, Sahoo AK, Wood EF (2014) Improving soil moisture retrievals from a physically-based radiative transfer model. Remote Sens Environ 140:130–140

Panciera R, Tanase MA, Lowell K, Walker JP (2013) Evaluation of IEM, Dubois, and Oh radar backscatter models using airborne L-band SAR. IEEE Trans Geosci Remote Sens 52 (8):4966–4979

Pandey D et al (2016) Development of a time series–based methodology for estimation of soil wetness using SMAP radiometer data: preliminary results. In: SAC/EPSA/GHCAG/MHTD/ TR/05/2016. Ahmedabad, India

Peng J, Shen H, Wu JS (2013) Soil moisture retrieving using hyperspectral data with the application of wavelet analysis. Environ Earth Sci 69(1):279–288

Piles M, Camps A, Vall-Llossera M, Corbella I, Panciera R, Rudiger C, Kerr YH, Walker J (2011) Downscaling SMOS-derived soil moisture using MODIS visible/infrared data. IEEE Trans Geosci Remote Sens 49(9):3156–3166

Piles M, Entekhabi D, Camps A (2009) A change detection algorithm for retrieving high-resolution soil moisture from SMAP radar and radiometer observations. IEEE Trans Geosci Remote Sens 47(12):4125–4131

Piles M, Sánchez N, Vall-llossera M, Camps A, Martínez-Fernández J, Martínez J, González-Gambau V (2014) A downscaling approach for SMOS land observations: evaluation of high-resolution soil moisture maps over the Iberian Peninsula. IEEE J Selected Topics Appl Earth Observ Remote Sens 7(9):3845–3857

Qin J, Yang K, Lu N, Chen Y, Zhao L, Han M (2013) Spatial upscaling of in-situ soil moisture measurements based on MODIS-derived apparent thermal inertia. Remote Sens Environ 138:1–9

Rahimzadeh-Bajgiran P, Berg AA, Champagne C, Omasa K (2013) Estimation of soil moisture using optical/thermal infrared remote sensing in the Canadian prairies. ISPRS J Photogram Remote sens 83:94–103

Rao SS, Das S, Nagaraju M, Venugopal M, Rajankar P, Laghate P, Reddy MS, Joshi A, Sharma J (2013) Modified Dubois model for estimating soil moisture with dual polarized SAR data. J Indian Soci Remote Sens 41(4):865–872

Rosen P, Hensley S, Shaffer S, Edelstein W, Kim Y, Kumar R, Misra T, Bhan R, Satish R, Sagi R (2016) An update on the NASA-ISRO dual-frequency DBF SAR (NISAR) mission. In: IEEE International Geoscience and Remote Sensing Symposium (IGARSS), 2016 IEEE, pp 2106–2108

Sadeghi M, Tabatabaeenejad A, Tuller M, Moghaddam M, Jones SB (2017) Advancing NASA's AirMOSS P-band radar root zone soil moisture retrieval algorithm via incorporation of Richards' equation. Remote Sens 9(1):17

Shi J, Guo P, Zhao T, Du J (2014) Soil moisture downscaling algorithm for combining radar and radiometer observations for SMAP mission. In: XXXIth URSI General Assembly and Scientific Symposium (URSI GASS), 2014. IEEE, pp 1–4

Sørensen B (1991) Renewable energy: a technical overview. Energy Policy 19(4):386–391

Stamenkovic J, Tuia D, De Morsier F, Borgeaud M, Thiran J-P (2013) Estimation of soil moisture from airborne hyperspectral imagery with support vector regression. In: 5th Workshop on Hyperspectral Image and Signal Processing: Evolution in Remote Sensing (WHISPERS), 2013. IEEE, pp 1–4

Temimi M, Leconte R, Chaouch N, Sukumal P, Khanbilvardi R, Brissette F (2010) A combination of remote sensing data and topographic attributes for the spatial and temporal monitoring of soil wetness. J Hydrol 388(1–2):28–40

Thapliyal P, Pal P, Narayanan M, Srinivasan J (2005) Development of a time series–based methodology for estimation of large-area soil wetness over India using IRS-P4 microwave radiometer data. J Appl Meteorol 44(1):127–143

Topp GC, Davis JL, Annan AP (1980) Electromagnetic determination of soil water content: measurements in coaxial transmission lines. Water Resou Res 16(3):574–582

Toride K, Sawada Y, Aida K, Koike T (2019) Toward high-resolution soil moisture monitoring by combining active-passive microwave and optical vegetation remote sensing products with land surface model. Sensors 19(18):3924

Vani V, Kumar KP, Ravibabu MV (2019) Temperature and vegetation indices based surface soil moisture estimation: a remote sensing data approach. In: Proceedings of international conference on remote sensing for disaster management, 2019. Springer, pp 281–289

Wagner W, Scipal K, Pathe C, Gerten D, Lucht W, Rudolf B (2003) Evaluation of the agreement between the first global remotely sensed soil moisture data with model and precipitation data. J Geophy Res Atmos 108(D19)

Wagner W, Sabel D, Doubkova M, Bartsch A, Pathe C (2009) The potential of Sentinel-1 for monitoring soil moisture with a high spatial resolution at global scale. In: Symposium of Earth Observation and Water Cycle Science, 2009

Wagner W, Hahn S, Kidd R, Melzer T, Bartalis Z, Hasenauer S, Figa-Saldaña J, de Rosnay P, Jann A, Schneider S (2013) The ASCAT soil moisture product: a review of its specifications, validation results, and emerging applications. Meteorol Z 22(1):5–33

Wang L, Qu J, Zhang S, Hao X, Dasgupta S (2007) Soil moisture estimation using MODIS and ground measurements in eastern China. Int J Remote Sens 28(6):1413–1418

Wang W, Huang D, Wang X-G, Liu Y-R, Zhou F (2011) Estimation of soil moisture using trapezoidal relationship between remotely sensed land surface temperature and vegetation index. Hydrol Earth System Sci 15(5):1699

Weidong L, Baret F, Xingfa G, Qingxi T, Lanfen Z, Bing Z (2002) Relating soil surface moisture to reflectance. Remote Sens Environ 81(2–3):238–246

Zhan X, Houser PR, Walker JP, Crow WT (2006) A method for retrieving high-resolution surface soil moisture from hydros L-band radiometer and radar observations. IEEE Trans Geosci Rem Sens 44(6):1534–1544

Chapter 11
Geospatial Modelling for Soil Quality Assessment

Suresh Kumar and Justin George Kalambukattu

Contents

Abstract Unsustainable use of land resources leads to degradation of soil resulting decline in soil functions such as crop productivity, regulation of the hydrological cycle, water quality, and soil quality. Soil quality is influenced by inherent and anthropogenic factors. It is used to evaluate soil resource functions as how well soil performs for all its functions at present and how these functions will be preserved for future use. It cannot be measured directly, so we evaluate indicators. Indicators are measurable properties of soil. Indicators can be physical, chemical, and biological properties or characteristics of soils. Soil quality indices are usually used for the

S. Kumar (✉) · J. G. Kalambukattu
Agriculture & Soils Department, Indian Institute of Remote Sensing, Dehradun, Uttarakhand, India
e-mail: suresh_kumar@iirs.gov.in; justin@iirs.gov.in

T. Mitran et al. (eds.), *Geospatial Technologies for Crops and Soils*,
https://doi.org/10.1007/978-981-15-6864-0_11

objective measurement of soil quality. These are useful tools for assessing the overall soil condition and response to management towards natural and anthropogenic factors. It helps to determine what conservation practices are needed to protect soil and water resources. The geospatial technique helps in providing spatial distribution of soils and representation of soil quality. Satellite remote sensing data and derived digital elevation models (DEMs) are used to map soils and landforms to evaluate soil quality. Soil quality assessment has been recognized as an important step towards understanding the long-term effects of various land management practices. It will help the land managers in preparing land use plans and management decisions for optimal use, hence assisting in sustainable land management. The chapter discusses various geospatial modelling methods in soil quality assessment.

Keywords Geographic information system · Remote sensing · Soil health · Soil quality · Soil quality indicators

Abbreviations

AHP	Analytical Hierarchy Process
AS	Aggregate Stability
ASI	Aggregate Stabillity Index
BD	Bulk Density
BG	b-Glucosidase
BS	Base Saturation
CEC	Cation Exchange Capacity
DEM	Digital Elevation Model
DHA	Dehydrogenase Activity
DSM	Digital Soil Mapping
DSSAT	Decision Support System for Agro-technology Transfer
EC	Electrical Conductivity
EPIC	Erosion Productivity Impact Calculator
FCC	Fertility Capability Soil Classification
FDAse	Fluorescein Diacetate Hydrolase
GIS	Geographic Information System
GMD	Geometric Mean Diameter
IQI	Integrated Quality Index
IDW	Inverse Distance Weighted
LISS	Linear Imaging Self Scanning
LULC	Land Use Land Cover
MBC	Microbial Biomass Carbon
MCDM	Multi-Criteria-Decision-Making
MDS	Minimum Dataset
MRS	Multiresolution Segmentation
MS	Moisture Saturation
MWD	Mean Weight Diameter

NDVI	Normalized Difference Vegetation Index
NIR	Near Infrared
NQI	Nemoro Quality Index
PAW	Plant Available Water
PCA	Principal Component Analysis
PLS-DA	Partial Least Squares-Discriminant Analysis
PLSR	Partial Least Squares Regression
PLU	Physiography Land Use
PMN	Potentially Mineralizable Nitrogen
qCO_2	Metabolic Quotient
RothC	Rothamsted Carbon Model
RS	Remote Sensing
RUSLE	Revised Universal Soil Loss Equation
SAR	Sodium Adsorption Ratio
SCI	Soil Condition Index
SHC	Saturated Hydraulic Conductivity
SMAF	Soil Management Assessment Framework
SOC	Soil Organic Carbon
SOM	Soil Organic Matter
SQI	Soil Quality Index
SSQI	Spectral Soil Quality Index
STIR	Soil Tillage Intensity Rating
TCS	Total Carbon Stocks
TNS	Total Nitrogen Stocks
TOC	Total Organic Carbon
TP	Total Porosity
TPI	Topographic Position Index
USLE	Universal Soil Loss Equation
VNIR	Visible and Near Infrared
WEPP	Water Erosion Prediction Project
WFPS	Water-filled Pore Space
WSA	Water-stable Aggregates

11.1 Introduction

The ever-growing world population leads to enormous pressure on land resources to produce almost 70% higher agricultural produce by 2050 compared to 2005 (Lal 2015). Overexploitation of land may lead to degradation, and at present, 33% of arable land suffers from various kinds of degradation processes. These land degradation processes may result in a decline in soil quality or soil health and a decrease in ecosystem goods and services. It may severely affect our chances of achieving the increased agricultural productivity necessary to nourish the expected global

population of 9.5 billion by 2050 (Lal 2015; Meena et al. 2018). Thus, sustainable land management practices to maintain or improve soil quality and achieve optimum agricultural production levels are extremely needed.

Soil quality refers to "the inherent capacity of a soil to function within natural or managed ecosystem boundaries to sustain biological productivity, maintain environmental quality and promote plant and animal health" (Doran and Parkin 1994; Meena et al. 2018a). A thorough understanding of soil quality or its parameters enables us to gain insight into the status of soil as a natural resource and also enables us to make necessary alterations in different soil parameters to improve the functioning of a particular soil (Herrick 2000). The various functions of soil or ecosystem services derived from it necessitate defining soil quality from other perspectives too. For example, the definition of soil quality from an environmental perspective states it as "the capacity of the soil to promote the growth of plants, protect watersheds by regulating the infiltration and partitioning of precipitation, and prevents water and air pollution by buffering potential pollutants such as agricultural chemicals, organic wastes, and industrial chemicals" (Sims et al. 1997). Thus, the definition of soil quality varies as per its functions and services derived from it.

Soil quality evaluation has widely been accepted as a vital step towards realizing the long-term consequences of various land management practices. Soil quality assessment is essential to show the influence of various agricultural management practices on soil productivity as well as environmental quality (NRC 1993). Several physical, chemical, and biological indicators are being used to assess soil quality from a crop production perspective. Among these indicators, biological indicators are considered most sensitive to changes compared to other physical/chemical indicators and could effectively describe the soil quality in an overall view. Several conceptual frameworks for monitoring soil quality have been proposed by various researchers (Andrews et al. 2004; Viscarra Rossel et al. 2006, Basak et al. 2016; Biswas et al. 2017). Selection of a minimum dataset (MDS) consisting of different physical, chemical, and biological properties vital in terms of soil functioning has been usually described as a common initial step in all these frameworks (Rezaei et al. 2006).

Geospatial techniques widely used for assessing soil quality and mapping involve visual interpretation of aerial photographs as well as satellite images to delineate soil physiographic units, which form the basis of soil survey and characterization. This technique helps to understand how the complex relationships among landforms, land use land cover (LULC), and the terrain will result in variations of soil properties on a spatial domain. Thus, the mapping of soil quality involves two steps: The first step involves the generation of the different soil property maps, while the second one involves the interpretation of the soil properties for a specific soil function or service of our interest, which will help to guide the decision-making process (Miller 2017). Li et al. (2005) used 13 soil quality indicators to generate soil quality map for sustainable agriculture management by integrating remote sensing (RS)-derived LULC maps and soil map along with soil information of the study area. They demonstrated the use of geospatial techniques and modelling for soil quality assessment and mapping with adequate as well as accurate soil properties data. Though the

soil quality tends to give an overview of the functional capacity of the soil, it is yet to be widely adopted as a land management indicator worldwide. Among the different limitations which tend to restrict its adoption, one of the main barriers is that most soil quality assessments provide information at small scale or point scales, while management of various ecosystems are majorly undertaken at landscape levels, thus necessitating the representation of soil quality over large spatial extends. This spatial representation of soil quality could help to bridge the gap between its current use and its potential use for land management (Jaenicke 1998). The localized nature of soil quality information can be expressed over a large spatial extent with the aid of various geospatial techniques through the amalgamation of remote sensing data and field generated soil information in a geographic information system (GIS) environment. The chapter discusses various soil quality indicators, their measurement and geospatial methods for assessing soil quality, and how they can be used for sustainable land (soil) management.

Geospatial techniques involving the use of RS, Global Positioning System (GPS) and GIS, provide new approaches for studying various soil quality aspects in different spatial as well as temporal domains (Schiewe 2003). It has been widely documented as a vital tool for soil/land resource inventory at different scales extending from local to regional and even up to global scales. Reliable and timely soil information regarding their extent, nature, spatial distribution, and limitations due to land degradation caused by water/wind erosion, soil salinity and/or alkalinity, soil compaction, wetness, etc. is necessary for soil health and quality assessment. The prime role RS plays in land resource management is providing information regarding soil, terrain, and LULC types and is the most effective tool for land resources monitoring. Availability of high-spatiotemporal-resolution RS datasets has facilitated the monitoring of various land resources regarding their diverse uses, soil health, wetlands, and land degradation status. Spaceborne RS data is widely being used for mapping soil resources. The main use of RS data is for the segmentation of landscape into more or less homogeneous soil-landscape units. Subsequently, soils occurring in each unit are characterized by dominant soil type (Dwivedi 2001). Digital soil mapping techniques, incorporating different secondary (non-soil) data sources into the mapping process, have been identified as potential means of soil mapping and can improve the detailing as well as geographic coverage of soil databases (Mulder et al. 2011). Various DEM-derived terrain parameters were found to be efficient in characterizing different soil-forming environments as well as delineating soil patterns at various scales. The integration of RS data (with high precision and synoptic coverage) with GIS will help in decreasing the cost and time as well as increasing the information content for effective soil quality estimation. The availability of remote sensing data ranging from coarser resolution to very high spatial resolutions will help in the preparation of soil/soil quality maps at diverse scales to meet the planning requirements at different levels. Advanced RS techniques such as hyperspectral remote sensing as well as microwave remote sensing have opened new vistas for soil mapping especially concerning the quantification of soil properties including nutrients, texture, and soil moisture status at varying resolutions.

11.2 Soil Quality Indicators and Measurement

11.2.1 Soil Quality Indicators

Assessing soil quality with respect to desired function or attribute involves the identification and subsequent quantification of certain sensitive parameters, referred to as soil quality indicators. Soil quality indicators, which reflect the changes due to land management practices, may include various chemical, physical, and biological soil properties. At any given point of time, a baseline or reference value of these soil quality indicators is essential to identify the impact of the different management practices (Bunemann et al. 2018). Indicators are identified as a soil property or attribute, which needs to be estimated for assessing soil quality pertaining to a given soil function. The measurement of many of these indicator properties is possible through routine laboratory analysis, while some require more sophisticated measurement techniques. Soil quality can be classified into (i) inherent and (ii) dynamic soil quality (USDA 2006). The inherent soil quality is constant and does not show much temporal variation. The various management practices have little or negligible influence on the inherent soil properties, and they do not change over a given timeframe. They are a direct derivation of the different soil-forming factors and include properties like soil texture, mineralogy, soil depth, pattern etc. On the other hand, the dynamic soil properties are easily influenced by anthropogenic activities or disturbances occurring in nature, and they are subject to change in a given time frame. These include various physical, chemical, and biological properties like bulk density, porosity, infiltration rate, soil organic carbon (SOC), available nutrients, soil pH, various soil enzyme activites etc. The dynamic soil quality is subject to changes depending on the management practices such as the quantity of soil organic matter (SOM), the soil structure, cation exchange capacity (CEC) etc. that change with the variation in the soil management practices. Soil quality research generally revolves around the concept of managing these dynamic parameters to improve the soil functions and maintain the fitness of soil resources (de La Rosa and Sobral 2008). In general, for efficient characterization of the different soil functions, a group of soil quality indicators is assessed which is referred to as the minimum dataset. This minimum dataset helps us to measure the capability of soil to execute a definite function and also capture the change in temporal scale. The minimum dataset should include such parameters, which will easily aid us to detect the changes brought about by different soil management practices. In most cases, minimum data sets are sensibly chosen by combining different soil properties, which would reflect the key soil function under consideration (Franzlubbers and Haney 2006; Meena et al. 2020). Soil Quality Institute (USDA 2006) has laid down the prerequisites for a minimum dataset for measuring soil quality. The most commonly used soil quality indicators forming components of the minimum dataset that includes different chemical, physical, and biological parameters are given in Fig. 11.1 (USDA 2006).

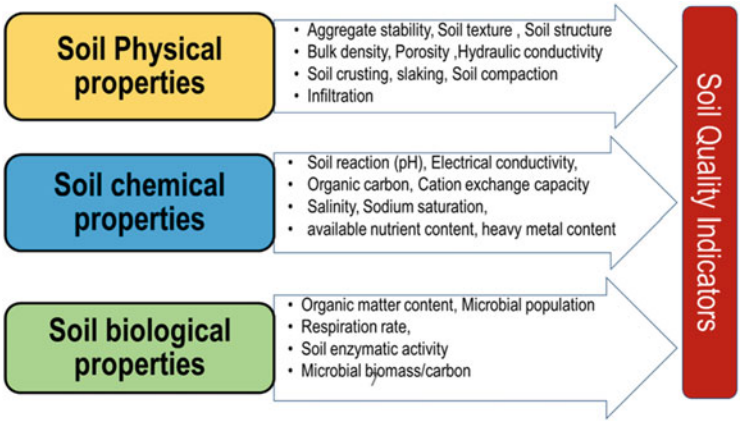

Fig. 11.1 Different soil quality indicators. (Adopted, USDA 2006)

11.2.2 Soil Quality Measurement

Though the concept of soil quality and its systematic measurement was introduced during the late twentieth century, the evaluation of soil and land existed much before in terms of fitness of a particular land unit for specific land use (FAO 1976). Measurement of the suitability of land or soil is to assess potentials or limitations of the land towards a particular use, whereas soil quality measurement gives us more quantifiable and detailed information regarding the current state of soil and helps to quantify the deviation of soil from the optimal functioning state.

Physical properties considered for soil quality measurement includes bulk density (BD), total porosity (TP), saturated hydraulic conductivity (SHC), moisture saturation (MS), aggregate stability (AS) larger than 2 mm, aggregates between 2 and 1 mm, and aggregate stability index (ASI). The chemical properties primarily used as soil quality indicators consist of pH, soil organic matter (SOM), CEC, exchangeable cations, available phosphorus (P), total nitrogen (N), and base saturation (BS). Whereas, the different biological properties are total organic carbon (TOC), total carbon stock (TCS), microbial biomass carbon (MBC), total organic N (TON), the metabolic quotient (qCO_2), total N stock (TNS), and C/N ratio. The Soil Management Assessment Framework (SMAF) has proposed interpretation algorithms for 13 soil properties to be used as soil quality indicators. Those properties include BD, plant available water (PAW), water-stable macroaggregation (WSA), water-filled pore space (WFPS), pH, electrical conductivity (EC), SOC, extractable P, sodium adsorption ratio (SAR), and extractable K in addition to potentially mineralizable N (PMN), MBC, and b-glucosidase (BG) activity (Andrews et al. 2004). The SMAF has been widely adopted in the United States and other similar countries abroad for evaluating near-surface (0–5 and 5–15 cm) soil properties and processes (Imaz et al. 2010; Stott et al. 2011). Ezeaku (2015) assessed soil quality based on various biological and physico-chemical soil quality indicators to study the sustainability

of various management and land-use systems. The most sensitive indicators observed in the study were soil pH, porosity, CEC, available P, BD, TOC, earthworm population, and plant available water holding capacity (PAWC). However, total N, exchangeable K, total P, and K were found to be moderately sensitive, and percentage base saturation was observed to be a weaker indicator. Mukherjee and Lal (2014) used various physical indicators, namely, potential AWC, soil penetration resistance, BD, mean weight diameter (MWD), aggregate size distributions, a fraction of water-stable aggregates (WSA), and geometric mean diameter (GMD) along with other chemical indicators for assessing soil quality. Sofi et al. (2016) used various SOC fractions as well as activities of different soil enzymes such as dehydrogenase, phosphatase, aryl sulphatase, and fluorescein diacetate hydrolase (FDAse) as biological indicators for soil quality assessment under diverse cropping systems in the northwestern Himalayas. Basak et al. (2016) and Biswas et al. (2017) assessed soil-quality indices for subtropical rice-based cropping systems in Eastern India. Luo et al. (2017) used different biological soil quality indicators comprising microbial biomass, microbial count, and activities of various soil enzymes (such as urease, catalase, invertase, alkaline phosphatase) along with different physical and chemical indicators as the minimum dataset for assessing the impact of long-term tillage systems on soil quality indicators, in Northwest China. Similarly, Bhaduri et al. (2017) have reported the effectiveness of biological indicators for soil quality assessment under a long-term rice-wheat cropping system in the semi-arid Indo-Gangetic plains with different tillage-water-nutrient management scenarios. They used MBC, dehydrogenase activity (DHA), soil respiration, PMN, and qCO_2 as quality indicators. In addition to the various indicators discussed above, Stefanoski et al. (2016) used macroporosity, microporosity, SHC, MS, effective saturation, aggregate size distribution, ASI, exchangeable Ca and Mg, exchangeable acidity, potential acidity, aluminum saturation, basal respiration, C stock, and N stock also as potential soil quality indicators. Apart from the above-mentioned indicators that need quantitative measurement in the laboratory, there are more generalized indicators like the visual indicators, which help to detect or identify the current state of the soil resources. Unlike the quantitative ones, observations of the visual indicators can be undertaken by a layman and can have wider acceptability to common masses. Some of these visual indicators are changes in soil color, above-ground vegetation and weed species, earthworm population, signs of soil erosion, water stagnation or undulations in topography, etc. (USDA 2001). Synthesizing the numerous studies help us in identifying some soil properties, which are widely adopted and used as soil quality indicators across the world, maybe due to their ease of measurement as well as higher sensitivity to variations in management practices (Table 11.1). The various standard available protocols for measuring these widely adopted indicators and their relation to various soil management practices are also mentioned in Table 11.1.

11.3 Soil Quality Assessment

Soil quality assessment is required to assess the sustainability of soils under the present ecosystem as well as to predict the sustainability of the ecosystem in the future for the present environmental conditions. Unsustainable use of land resources leads to degradation of soil, which results in a decline in the functionality of soils such as crop productivity, hydrological cycle, water quality, biochemical cycle, and soil quality. Soil quality parameters are in general defined by considering the sustainability of soils under changing management practices or based on soil resilience under varying environmental conditions (Hartemink 1998). Physical, chemical, and biological parameters of soils of natural undisturbed lands are considered as the highest soil quality and hence used as reference level (Doran et al. 1994; Mitran et al. 2018).

Precise assessment of soil quality requires a systematic method to measure and interpret soil properties. These properties vary with agroecosystems to serve as soil quality indicators (Granatstein and Bezdicek 1992). Soil quality indicators refer to soil processes and properties that are sensitive to changes in soil functions. These indicators should be simple, sensitive, and measurable to use for soil quality assessment. Soil quality indicators are comprised of physical, chemical, and biological properties of soil. There are sets of soil quality indicators proposed to assess soil quality (Doran and Parkin 1994; Karlen et al. 1997). Researchers have used various evaluation methods to assess soil quality such as soil quality card design and test kit (Ditzler and Tugel 2002), indicator kriging, soil quality indices (Doran et al. 1994; Doran and Jones 1996), and soil quality models (Larson and Pierce 1994). Among these methods, soil quality indices are the most widely used due to their ease to application in a quantitative manner (Andrews et al. 2002). Soil quality indices are based on indicators of site-specific soil conditions under specific soil management practices. They reflect the integrated effects of dynamic and inherent soil properties under the specific management practices over the period (Wang and Gong 1998; Arshad and Martin, 2002). There is no universally accepted method for developing soil quality indices. Several researchers have evaluated soil quality and proposed a self-defined indicator method and equation in developing soil quality indices (Sun et al. 2003; Zhang et al. 2004). There are various quantitative soil quality assessment methods to evaluate soil quality. These are classified under two groups: (i) soil quality index (SQI)-based approach and (ii) soil quality modelling approaches. They are discussed below.

11.3.1 Soil Quality Indices

Soil quality indices integrate different physical, chemical, and biological soil properties. There are various soil physical indicators such as soil aggregate stability, BD, porosity, infiltration rate, hydraulic conductivity, effective soil depth, and WHC of

Table 11.1 Standard protocols to measure various soil quality indicators

Sl no.	Soil quality indicator	Measurement technique	References	Remarks
Physical soil quality indicators				
1.	Soil texture	Hydrometer method	Bouyoucos (1951)	Affects water holding capacity, drainage and soil erodibility
2.	Soil depth	Field method	USDA, 2001 Soil quality test Kit guide	Rooting depth, water availability to plant growth
3.	Coarse fragments	Field method		Provide aeration and drainage
4.	Bulk density	Cylindrical core method	Arshad et al. (1997)	Soil compaction
5.	Aggregate stability	Wet sieving	Kemper and Rosenau (1986)	Resistance to soil erosion
6.	Available water capacity	Pressure plate apparatus	USDA NRCS (2005)	Soil moisture retention and its availability to plant growth
7.	Infiltration and hydraulic conductivity	Double-ring infiltrometer, tension infiltrometer	Lowery et al. (1996)	Water movement at surface and subsurface layer
Chemical soil quality indicators				
8.	Soil pH	pH meters	Brady and Weil (2002)	Nutrients availability and land degradation
9.	Electrical conductivity	Conductivity meters	Brady and Weil (2002)	Soluble salt concentration in the soil solution
10.	Cation exchange capacity	Standard analytical procedures	Jackson (1973)	Nutrient holding capacity and soil fertility
11.	Available nutrients	Standard analytical procedures	Jackson (1973)	Nutrient supplying capacity to support plant growth
12.	Soil organic carbon	Wet oxidation/ digestion, dry combustion	Walkley and Black, 1934; Sikora and Stott (1996).	Influence the measured soil properties, most important indicator
Biological soil quality indicators				
13.	Soil respiration	CO_2 evolution	Parkin et al. (1997)	Overall microbial activity; related to organic matter recycling
14.	Microbial biomass carbon	Fumigation-extraction	Horwath and Paul. (1994)	Organic matter and nutrient recycling

(continued)

Table 11.1 (continued)

Sl no.	Soil quality indicator	Measurement technique	References	Remarks
15.	Potentially mineralizable nitrogen	Aerobic and anaerobic incubation methods	Drinkwater et al. (1996)	Easily available N in the soil
16.	Soil enzymes (dehydrogenase, phosphatases, urease, arylsulphatase, β-glucosidase, FDAse, etc.)	Standard protocols for measuring various soil enzymatic activities	Tabatabai (1994)	Indicates nutrient as well as organic matter cycling processes
17.	Earthworms	Numerical counting	USDA (2001a, b) Soil quality test Kit guide	Related to biological activity/diversity as well as the detoxifying ability of soil

the soil, which are commonly used. Whereas, most important chemical indicators used are soil pH, EC, CEC, nutrient availability, and deficiency/toxicity of micronutrients in the soil. The most relevant biological indicators used are SOM, MBC, soil respiration, or soil enzyme activities. Optimal integration of these soil properties improves crop productivity, water use efficiency, nutrient availability, and sustainability of agro-ecosystems. Soil quality indicators vary with soil types, climatic condition, and land use/land cover and management types. Various soil quality indices commonly used to assess soil quality can be discussed as follows:

11.3.1.1 Simple Ratio Based Index

SOC is considered as the most sensitive soil parameter as an indicator of soil quality. Anderson and Domsch (1985) described a simple ratio of MBC upon TOC as an indicator to assess soil quality, which is a more sensitive index compared to changes in TOC contents. The MBC values change much more rapidly in response to management regimes compared to soil organic matter (Powlson and Jenkinson 1981). Thus, early stages of soil degradation may be easily identified by variations in microbial biomass rather than changes in SOM, which is more stable and subjected to fewer variations.

11.3.1.2 Multiparametric Soil Quality Index

A framework based on weighted integration of normalized scoring functions for evaluating a production system's effect on soil quality was proposed by Karlen and Stott (1994). In this method, the value of each soil parameter is assigned between 0 and 1 following a standardized scoring function method. The weight score for each parameter was assigned based on the experience of the researcher where no

mathematical method was used. It was primarily proposed to demonstrate the methodology to compute SQI using major soil functions. It intends to suggest an index to evaluate soil conditions with an environmental point of view. It will provide the overall soil quality score based on the sum of all function scores. It is described as:

$$\text{Soil Quality} = W * Q_{we} + W * Q_{wma} + Q * Q_{rd} + Q * Q_{fqp} \quad (11.1)$$

where Q_{we} is the rating of the ability of soil to facilitate entry of water into soil, Q_{wma} is the rating of the ability of soil to facilitate water movement/transfer and absorption, Q_{rd} is the rating of the ability of soil to resist degradation, Q_{fqp} is the rating of the ability of soil to sustain plant growth, and W is the numerical weight assigned to each soil function.

11.3.1.3 NIR Spectra for Measurement of Soil Quality

Reflectance spectroscopy techniques involving the visible (VIS, 400–700 nm), near-infrared (NIR, 700–1100 nm), and shortwave infrared (SWIR, 1100–2500 nm) spectra can be used for assessing soil quality (Ben-Dor and Banin 1995). Current developments in soil analysis reveal that reflectance spectroscopy is a vigorous diagnostic technique suited for swift and concurrent analysis of the soil characteristics with several levels of estimation accuracy (Awiti et al. 2008; Cécillon et al. 2009). It is emerging as a powerful methodology for soil quality assessment which is rapid and inexpensive. It provides consistent quantification of specific soil functions or ecosystem services as a combined measure of soil quality. It can be used to characterize areas based on their degradation status as well as for evaluating the outcome of an environmental factor on soil quality. Laboratory-based NIR spectra characterization offers a cost-effective solution for monitoring and assessment of soil quality. It can be observed through an aerial survey or high-resolution satellite observations which increases the spatial coverage and sampling frequency. NIR imagery acts as an innovative tool for the spatial estimation of various soil threats in ecologically sensitive areas. Shepherd and Walsh (2002) demonstrated a reflectance spectroscopy-based scheme to use soil spectral libraries for fast non-destructive determination of soil properties. Statistical models were developed for SOC, TN, EC, and clay contents for different land uses and landscape types. Similarly, IR spectroscopy can also be used for predicting biological soil properties (Terhoeven-Urselmans et al. 2008).

11.3.1.4 Spectral Soil Quality Index (SSQI)

An SSQI is proposed as an analytic tool for assessing soil quality. In this method, distinct spectral characteristics of physical, chemical, and biological soil attributes

are derived based on reflectance spectroscopy. These spectral characteristics are combined to specify how well the soil is functioning for a particular use. A partial least squares-discriminant analysis (PLS-DA), a linear regression technique, is used most commonly to compute the alterations in soil quality under the changed land uses in various ecosystems (Singh et al. 2005). This technique was used for classifying various soil types, based on their properties (physical, biological, and chemical) as well as for the identification of relative changes (Carroll et al. 2006). Awiti et al. (2008) classified degraded soil classes in a tropical forest-cropland using discriminant analysis. The PLS-DA output generated was used to formulate a scoring function for evaluating soil quality only by spectral differences. A spectral fertility index was developed to study the impact of land-use changes and time elapsed after the conversion of forest on soil conditions in Madagascar by Vågen et al. (2006). Paz-Kagan et al. (2014) compared the soil quality and developed SSQI in various LULC such as agro-pastoral, traditional grazing and afforestation that were changed from managed to unmanaged or vice versa at the fringe of the northern Negev Desert, Israel. They have also developed and implemented an SSQI using field-, lab-, and image-based spectral information in two anthropogenically induced land-use changes sites located in Israel and Germany (Paz-Kagan et al. 2015).

11.3.1.5 Fertility Capability Soil Classification (FCC) System

The FCC system is the beginning of soil quality assessment in tropics, which is the most useful approach of quantitative soil quality assessment in the tropics. FCC is different from soil quality, which is in many occasions a challenging concept to put in practice. Soil taxonomy and quantitative topsoil properties primarily form the basis of FCC. It does not consider annually changing soil attributes. It takes into account dynamic soil attributes (showing the temporal variation over years/decades with management), as well as inherent ones (that remain unaltered over a century). FCC can take either positive or negative values based on the land use as well as the temporal/spatial scales in consideration. The FCC system comprises two levels: The first level is described by type/substrata type of topsoil and subsoil texture. The second level describes condition modifier defined by 17 modifiers to delimit specific soil conditions affecting plant growth with quantitative limits (Sanchez et al. 2003).

11.3.1.6 Soil Quality Index

The SMAF was used to calculate an SQI. SQI estimation is an indirect method based on the weighted integration of soil quality indicators. It is a widely accepted method as it provides an opportunity for detecting the systematic intricacy of soil productivity under managed as well as natural ecosystems. Many quantitative models such as integrated quality index (IQI) and Nemoro quality index (NQI) have been developed for calculation of SQI. By definition, the IQI model is described as the sum total of equivalent weight values of all the chosen indicators. It employs a

simple system of scoring where equal weights are assigned to all the quality indicators (Doran and Parkin 1994). The NQI model developed by Nemoro does not use the indicator weights; rather it considers the mean and the lowest indicator scores and portrays the law of the minimum in crop production (Han and Wu 1994; Qin and Zhao 2000). The most widely adopted approach of soil quality indices involves scoring functions and corresponding weightage for each soil property (Andrews et al. 2004). SQI calculation involves three steps: soil quality indicator selection, scoring of indicator and weightage of each soil quality indicators, and then integration into a soil quality index. The MDS for SQI calculation was identified based on the correlation of indicators with ease of measurement (Andrews et al. 2002; Govaerts et al. 2006). Many times, soil quality indicators are also selected based on expert opinion (Herrick et al. 2002). Principal component analysis (PCA) is a method used to identify suitable physical, chemical, and biological indicators in the ecosystem for soil quality assessment (Govaerts et al. 2006). It aims to decrease the data dimensionality while retaining the maximum possible variation present in the dataset. The score value of each soil quality indicator is estimated using scoring functions. A simple nonlinear polynomial framework was used for defining the scoring functions. Each soil property value was converted into a unitless score (0–1) using a scoring algorithm (Karlen et al. 2001, 2003). Three kinds of scoring functions were considered: (i) more is better, (ii) less is better—lower asymptote (positive slope), and (iii) an optimum midpoint Gaussian function. The curve shapes for different soil properties are obtained from the literature (Masto et al. 2007, 2008). The analytical hierarchy process (AHP) is a method commonly used to assign indicator weights (Qi et al. 2009). AHP is used to measure the degree of consistency; and if found unacceptable, pairwise comparisons can be revised (Saaty 1990). AHP rules are applied to derive the final weightage ratings. Numerical weights of each indicator are multiplied by the corresponding indicator scores (estimated using standardized scoring functions which normalize indicator measurements between 0 and 1.0) to yield index values. The index values range between 0 and 1. Soils with low values indicate poor soils, whereas high values indicate healthy soils (Gugino et al. 2009).

SQI is computed as a function of summation of the product of weight and score of each indicator:

$$SQI = \sum_{i=1}^{n} (\mathrm{W_i x\ S_i}) \tag{11.2}$$

where w is the weight assigned for each soil quality indicator through AHP, S is the score value of each indicator, and n is a number of soil samples in each ecosystem/land use type.

11.3.2 Modelling Soil Quality

SOC is one of the most commonly acknowledged indicators of soil quality. It acts as a functioning part of the ecosystem and improves various soil characteristics like soil structure, fertility, and water storage capacity. SOC content is controlled by various natural (land cover and/or vegetation, soil parent material, climate, and topography) and human-induced factors (land degradation, land use, and management) (Jones et al. 2004). Numerous researchers used a modelling approach to assess soil quality in various ecosystems characterized as natural and managed ecosystems. It can be grouped into (i) modelling change in SOC, (ii) modelling crop simulation yield, and (iii) modelling soil erosion.

11.3.2.1 Modelling Change in SOC

The SOC pool is a key indicator of soil quality. It is one of the most active soil biological parameters that is vital for the sustainability of agricultural systems. It plays a central role in several agricultural and ecological processes associated with soil fertility, carbon (C) cycling, and soil-atmosphere interactions, including CO_2 sequestration. Information on SOC content in soils is quite important to determine soil quality in natural as well as managed ecosystems. Change in SOC content in soil provides a vital clue to land use and management changes. SOC contents vary with various land-use types. There are several process-based soil C models which require many detailed parameters as model inputs, which are not easily available at large scale. With the help of these models, dynamics of soil C under diverse environmental and management conditions over large spatial and temporal scales can be captured and represented. Soil C models are described as below:

11.3.2.1.1 RothC Model

The Rothamsted carbon model (RothC) is widely used to simulate soil C dynamics in cropland and other land-use systems and management practices. It can predict reasonably good results of SOC dynamics. The model takes into account monthly climate data of mean air temperature, precipitation, potential evapotranspiration, and soil data to simulate the C pool in the landscape. The annual amount of crop residue and roots are computed based on crop yield data. C:N ratio of different types of manures is defined. The amount of above-ground biomass returned to the soil after harvest is also defined. It helps to evaluate the performance of the cropping system in soil C sequestration potential and SOC change that serves as an indicator of soil quality. SOC change depicts the balance of C input and its output after decomposition. Roth C model has been developed to simulate soil SOM turnover in uplands soils. The model needs to be calibrated with long-term experimental data in diverse climate, soil, and management practices. The model was tested for 16 long-term

experimental sites and reported a good performance in representing the SOC dynamics under various treatments across the sites (Wang et al. 2016). Bhattacharyya et al. (2011) used the Roth C model to simulate the SOC changes under different soil and climate conditions with different cropping systems. Wang et al. (2017) used state-of-the-art databases of soil and climate variables to simulate SOC density using Roth C model in croplands of major cereal cropping systems in the world.

11.3.2.1.2 CENTURY Model

The CENTURY model is a site-specific complex model used to simulate C, N, P, and S dynamics in the soil (Smith et al. 2009). It has been primarily developed for grassland and later expanded to the agricultural system and forest system. The model includes several sub-models such as the SOM sub-model, water budget, and plant production sub-model. The model uses a monthly time-step weather input of mean monthly minimum and maximum temperature, and monthly precipitation. It uses site-specific information and initial condition of soil parameters (texture, depth, BD, total C and N) and crop growing parameters (sowing date, fertilization, harvesting period, and crop varieties). The model simulates the steady-state SOM level and provides information on SOM turnover levels in varying climate and management practices over diverse landscapes. Several researchers used this model to study the increase in average soil C density under improved management (Ogle et al. 2010; Yu et al. 2012; Lugato et al. 2014). Gupta and Kumar (2017) used the CENTURY model to simulate climate change impact on soil C sequestration in croplands of mid-Himalaya, Uttarakhand, India. Di Tizio and Grego (2006) used the CENTURY model for annual C balance in agricultural lands under organic and conventional management. The study revealed that the loss of soil C depends on the management types, weather, and physical characteristics of soils.

11.3.2.2 Crop Simulation Models

Crop growth models simulate soil and plant processes to approximate crop biomass and yield for a given period. These models are process-based models that require a large number of soil, plant, and weather input parameters to compute processes on the daily time step. These models can be classified into field-scale and regional-scale models. Field-scale model comprehensively simulates plant functions at site-specific soil and weather conditions, whereas the regional-scale model simulates plant processes by establishing a crop-climate relationship at a broader scale. Crop growth models account for spatial and temporal variability of soils at large scale and could be used as a soil quality assessment tool. Traditional land evaluation methods are based on the physico-chemical properties of soils and used as a land quality assessment tool. Crop growth models simulate crop growth processes, and crop yield is used as biological indicators of soil quality assessment. Process-based crop

Table 11.2 List of crop simulation models used in soil quality assessment

Crop simulation models	Sources
Decision Support System for Agro-technology Transfer (**DSSAT**)	*http://dssat.net*
Environmental Policy Integrated Climate **(EPIC)**	*https://epicapex.tamu.edu*
FarmSim: Wageningen—model library	*http://models.pps.wur.nl/node/961 http://www.fasset.dk*
General Large Area Model **(GLAM)**	*https://www.see.leeds.ac.uk/research/icas/research-themes/climate-change-andimpacts/Climate-impacts/glam*
WOFOST: Wageningen—model library	*http://www.wageningenur.nl/en/Expertise-Services/Research-Institutes/alterra/Facilities-products/software-and-models/WOFOST.Htm*
ORYZAv3	*https://sites.google.com/a/irri.org/oryza2000/about-oryza-version-3*
Soil Water Atmosphere Plant (**SWAP**)	*http://www.swap.alterra.nl*

growth models (e.g. World Food Studies simulation model (WOFOST), global circulation models (GCMS)) based on soil processes and plant physiology have been used to predict crop yields (Kasampalis et al. 2018). Decision Support System for Agro-technology Transfer (DSSAT) model has been parameterized to simulate crop yield for several crops (Jones et al. 2003). Rossiter (2003) described various crop growth models and their biophysical models in land evaluation. Some of the crop simulations models that can be used for soil quality assessment are listed in Table 11.2.

11.3.2.3 Modelling Soil Erosion

Land degradation due to soil erosion processes is a major problem in the world. It removes soil nutrients including SOC from the surface soil and adversely affects soil quality and productivity. Eroded lands face soil quality issues of severe rates of soil erosion, depletion of SOM, and reduction of soil fertility and crop productivity (Doran and Parkin 1994; Karlen et al. 2003). Field surveys are conducted to assess soil quality through a paired comparison of soil samples collected from eroded and non-eroded lands. It also enables to detect differences in soil management practices. Proper soil samplings at point or landscape level are conducted to make an overall assessment of soil quality (Cambardella et al. 2004). There are several soil erosion models, including empirical to process-based, available to estimate soil erosion rates under different land use/land cover types in diverse landscape and management conditions in various climatic regions. These erosion models have provided insight into understanding soil erosion processes and characterizing processes influencing soil properties at landscape level under various ecosystems. Process-based erosion models simulate surface runoff generation processes and their impact on the spatial

distribution of soil nutrients in the landscape. Thus, these models can serve as an important tool for assessing soil quality. Several researchers have integrated these models with GIS to predict the spatial pattern of soil erosion and the distribution of sediments in the landscape. Erosion models helped in understanding soil erosion and sedimentation processes in detail as well as in assessing on-site soil erosion and its influence on soil quality. Soil erosion models are grouped into empirical and physically based process models. Major empirical models are Universal Soil Loss Equation (USLE), it was modified as Modified Universal Soil Loss Equation (MUSLE) and later revised as Revised Universal Soil Loss Equation (RUSLE). Empirical models are easy to apply and require less data for soil loss estimation, whereas process-based models are complex and require detail data of climate, soil, terrain, vegetation, and management practices (Merrit et al. 2003). Empirical model RUSLE 2 was primarily developed to compute soil erosion due to sheet and rill erosion processes in the croplands. Later, it was further extended to compute soil condition index (SCI) and soil tillage intensity rating (STIR). SCI value is influenced by soil erosion, organic matter decomposition, tillage operations, and management practices. USDA-ARS (2008) is using the SCI as a tool for soil organic management, and it can be used as an indicator of soil quality. RUSLE 2 model requires the input of climate, soil texture, slope steepness, slope length, management practices, vegetation cover, and application of organic manures for computation of SCI.

Wilson et al. (2009) used process-based Water Erosion Prediction Project (WEPP) and CENTURY SOM dynamics models to study soil C loss in the agricultural field of the watershed. They evaluated change in SOM with soil erosion scenarios in the field using historical and current crop management practices. Erosion Productivity Impact Calculator (EPIC) model (Williams 1990) was used to predict the impact of soil erosion on crop productivity. It simulates major soil and water processes related to crop growth. It also simulates the impact of atmospheric CO_2 level on crop yield and soil C sequestration. Wang et al. (2006) used EPIC to simulate wheat yields, sediment loss, organic N and P, soluble P, and NO_3-N losses in six cultivated small watersheds. The EPIC model was later renamed as the Environmental Policy Integrated Climate model by incorporating environmental modules in the model (Mitchell et al. 1991). Thus, these erosion models emerged as a potential tool in characterizing and quantifying soil quality parameters and assessing the impact of land-use systems and management types on soil quality.

11.4 Geospatial Methods in Soil-Landscape Delineations for Soil Quality Assessment

11.4.1 Visual Method of Analysis

Geospatial techniques using various RS data have been widely adopted for soil survey at different scales as well as mapping of various soil quality parameters.

Dwivedi (2017) provided a detailed review of RS for various soil-related applications. Among the various applications of geospatial technology, the use of RS data for soil surveys including the delineation of soil mapping units needs special mention. It involves the delineation of soil scape boundaries, which act as sampling units for soil survey, soil profile study, and characterization of various soil properties leading to soil resource inventory. A detailed description and knowledge about the different kinds of soils and their geographic distribution are essential prerequisites for rational land use planning, improved agricultural production, and identification of the potentialities and limitations of different areas.

The soil-scape boundary delineation and mapping using RS data are based on physiographic soil analysis, where different physiographic units are delineated to account for the climate, soils, vegetation, geology, water, surface form, and their interrelationships. The different factors involved in physiographic processes approximately correspond to the different soil-forming factors; hence, knowledge regarding physiographic processes serves to indicate the broad general pattern of soil development. This approach is based on the concept that analogous physiographic processes at two widely diverse places are anticipated to support almost alike soil-forming processes resulting in similar soils with broad general characteristics. Similarly, the spatial variations in surface features such as vegetation, topography, relief, and slope can also aid in the delineation of soil boundaries, due to their relation with physiographic processes. Various landforms or surficial features of the earth at different scales and resolutions can be easily identified by the interpretation of various remote sensing data products which helps in reconstructing and studying the dominant physiographic processes at different locations. The soils within different physiographic units will be studied in detail to characterize the soil properties. Detailed study and interpretation of RS images help us in the identification and geomorphic description of landforms with varying origin such as structural origin, denudational origin, fluvial origin, and aeolian origin. The delineated landforms will be further subdivided systematically based on relief as well as land use/land cover. This accounts for various soil farming factors influencing variations in soil properties especially landform (parent material), relief (topography), and land use/land cover (vegetation). Whereas in the case of smaller spatial extents, time, parent material, and climate being almost identical, the soil property variations can be credited to variations in relief along with vegetation factors (Dobos et al. 2000; Srivastava and Saxena 2004). Thus, the delineated physiographic units will have similar soil forming factors and will result in similar soils due to the similar pedogenic processes.

Detailed scale (cadastral-level) soil mapping can be achieved by delineating various landforms through the integration of information derived from the 3D perspective view of different slope class areas, employing high-resolution Cartosat-1 DEM following visual interpretation (Nagaraju et al. 2014). The landforms were further segmented into different precise land use and land cover classes using Cartostat-1 sharpened LISS IV image. The physiography-land use (PLU) units generated by integrating slope, landform, and LULC information were more or less internally homogenous in terms of factors of soil formation and served as soil

boundaries for further soil sampling as well as classification. Chattaraj et al. (2017) developed a semi-automated object-based modelling methodology for landform classification as well as delineation. They employed geospatial object-based image analysis (GEOBIA) technique with knowledge-based modelling. Landform classification was carried out through a multiscale mapping workflow comprising various procedures, viz. digital terrain analysis, multiresolution segmentation (MRS) (using raster datasets of Cartosat-1 Digital terrain model and IRS P6 LISS IV images as input), knowledge-based landform classification, and accuracy assessment.

11.4.2 Digital Method of Analysis

Digital soil mapping (DSM) refers to an innovative technique for mapping primary as well as secondary (derived from primary properties) soil properties or soil classes employing spatial inference models. It is defined as the "computer-assisted production of digital maps of soil types as well as soil properties using various mathematical/statistical models, which combine information from soil observations with the information contained in correlated environmental variables and remote sensing images" (McBratney et al. 2003). Digital soil mapping can aid in extrapolating point-scale information to bigger areas. It offers a unique opportunity to tide over the scales between ground-based soil properties (point or field data) to model for larger extents. DSM attempts to integrate RS data derived soil-related information with proximally sensed as well as conventionally estimated soil property data at bigger spatial scales. The forthcoming studies will focus on improving the amalgamation of data derived from proximal as well as remote sensing through scaling-based methods to make the best use of all available data sources (Mulder et al. 2011). DSM can also be used for upscaling from field observations to more regional areas. It makes use of various RS data including hyperspectral images, field measurements, and spectroscopy in combination with various processing algorithms (including statistical, mathematical, and machine learning) for extrapolating field-collected information to the scale of remote sensing data.

Various environmental covariates or so-called *scorpan* factors (an acronym for the various factors for soil attribute prediction, i.e. "soil, climate, organisms, parent materials, age, and spatial position") have been suggested by McBratney et al. (2003). They can be obtained in digital form from various sources like remote sensing images, digital elevation models, and existing soil maps. The DEM-derived terrain parameters help us in quantifying the (geo) morphology of the terrain (soil scape or soil landscape), thus accounting for accretion and deposition potential, as well as to adjust the effect of climatic elements on the local topography. The RS images of different resolutions reveal and help us to capture the overall variability in environmental conditions, form, and state of the vegetation affected by various soil properties, colour, surface roughness, moisture content, and other soil surface features. Many researchers have used these numerous environmental covariates for the generation as well as updation of soil maps in raster format at

different resolutions, employing various spatial soil prediction functions (Minasny et al. 2008). Several procedures of kriging, as well as decision tree-based analysis (classification/regression trees), have been used together with various RS data for predicting soil properties at unvisited locations pointing towards attaining continuous area coverage (Mulder et al. 2011).

Several regression models correlating DEM-derived terrain parameters with soil properties have been reported with a high degree of success (Oldak et al. 2002). Mehammednur Seid et al. (2013) provided spatial distribution information of soil properties using topographic parameters along with the normalized vegetation index (NDVI) employing clustering and other statistical techniques. A methodology for automatic soil texture mapping by integrating ground, satellite, and ancillary data was successfully developed and employed by Maselli et al. (2008). Artificial neural networks (ANN) and decision trees are the novel methods extensively used in soil studies, especially for predicting soil properties. ANN modelling can predict soil types at locations devoid of any existing soil maps, by integrating soil map data from other regions with similar landscape characteristics known to be accountable for the spatial variability of soils. Zhao et al. (2009) predicted soil texture at improved resolution using a combination of soil attributes (from existing coarser-resolution soil maps) and various DEM-derived terrain indices employing ANN modelling technique. Ugbaje and Reuter (2013) described a methodology to employ DSM procedures for predicting available water capacity of soils making use of pedotransfer functions (PTFs). DSM has been used to predict pH, bulk density, soil texture, and organic carbon (OC) content using different environmental covariates as probable predictors including terrain parameters, land cover information/images, vegetation indices (e.g. NDVI), and land surface temperature. Regional-scale soil parameter prediction has been reported by Martelet et al. (2013). Casa et al. (2013) estimated and mapped soil properties at field scale by utilizing and comparing different methodologies, integrating information obtained from hyperspectral RS data (vegetation/bare soil images) with geophysical data. Kalambukattu et al. (2018) mapped various soil quality parameters in a hilly watershed using remote sensing–derived inputs using ANN technique. They were able to map spatial SOC distribution and other nutrients using various spectral and terrain indices. Dharumarajan et al. (2019) have discussed the need and importance of digital soil mapping in India with special emphasis on soil quality parameters. They had given an account of the limited attempts done in India for digital soil mapping of soil quality parameters along with the approaches for achieving the digital soil map of India.

11.5 Soil Quality Assessment in a Watershed: A Case Study

The present study was aimed to assess soil quality of landform types in a watershed of a mountainous ecosystem with objectives to identify soil quality indicators and to compute relative SQI of various landform types in the watershed (Roy 2014).

11.5.1 Experimental Site

The watershed located in one of the mountainous districts of Tehri Garhwal, Uttarakhand State, India extends between 78°22′47“ E to 78°30’ E longitudes and 30°30’29.33”N to 30°22′47”N latitudes. The geographic area of the study area is 46.14 km^2. Paddy and maize are grown in summer (kharif), whereas wheat is cultivated during winter (Rabi) season. The soil of the area is varying from loam, sandy loam, to silt loam.

11.5.2 Methodology

CartoDEM digital elevation model was used for slope analysis and landforms delineation in the watershed. Remote sensing data IRS LISS III acquired of March 2014 was used to prepare land use/land cover. Garmin GPS was used to record the geographic location of the soil sampling sites in the watershed. A brief description of the methodology is discussed below.

11.5.2.1 Delineation of Landform Types in the Watershed

CartoDEM was used to delineate landform elements based on TPI and slope classes in GIS environment. TPI is an algorithm increasingly used to measure topographic slope positions and to automate landform classifications. Positive TPI value represents ridges, which are higher than the average of their surroundings, and negative TPI value represents valleys, which are lower than the average of their surroundings. TPI value near zero represents a flat area or areas of constant slopes. Thus, the watershed was delineated into landform types of the valley, lower slope, mid-slope, and upper slope (Fig. 11.2).

11.5.2.2 Soil Sampling

Soil samples were collected from each landform types, namely, valley, lower slope, mid-slope, and upper slope. Three transects were selected in the watershed. Soil samples from 45 sites of surface (0–20 cm) and subsurface (20–50) were collected. There were 6 sites in the upper slope and 9, 20, and 10 sites, respectively, in mid, lower, and toe slopes. Soils were analysed for the physical properties (coarse fragments, soil depth, bulk density, sand, silt, clay, and stable aggregates) and chemical properties (pH, EC, CEC, TC, TN, available P, available K, and S).

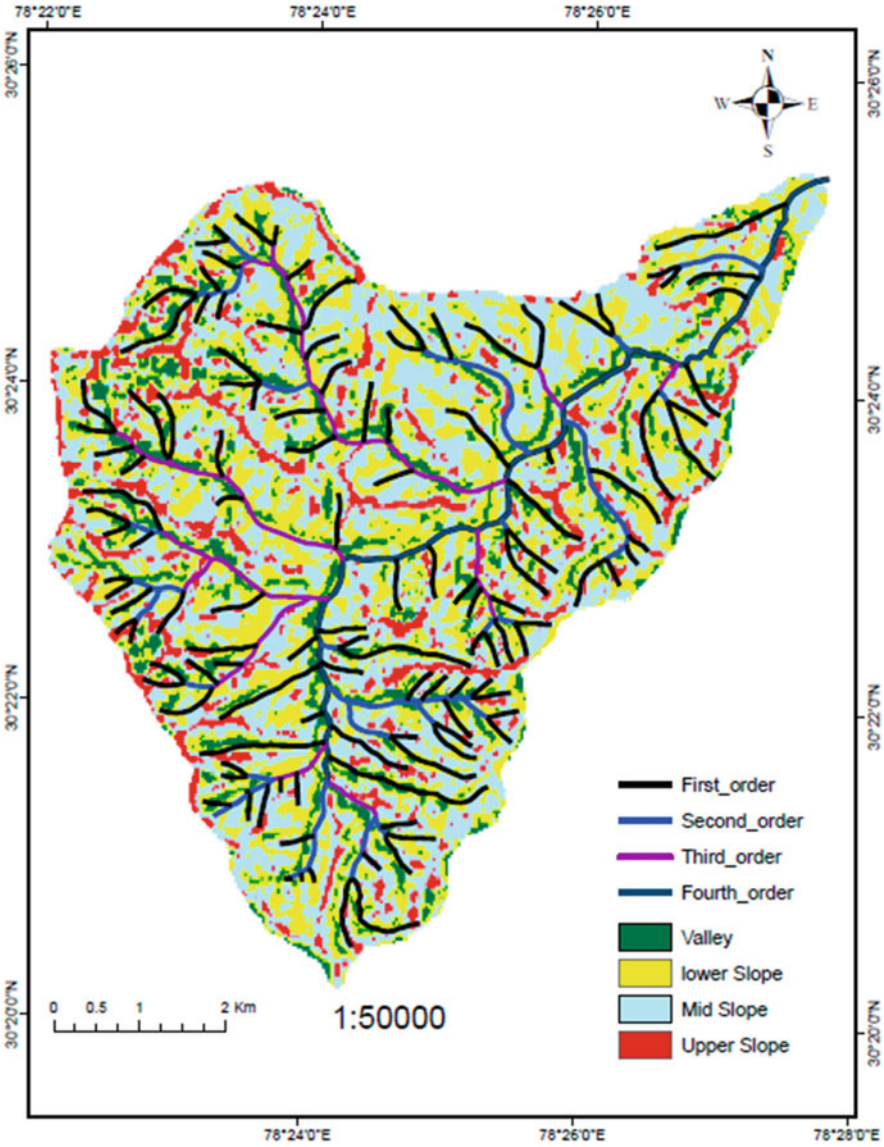

Fig. 11.2 Landform units delineated in the watershed

11.5.2.3 Soil Quality Assessment

11.5.2.3.1 Identification of Soil Quality Indicators

After analysing soil samples, PCA was used for minimum data set selection or identifying suitable indicators. PCA converts the correlated set of data to uncorrelated set and thus reduces data redundancy. Soil parameters with Eigenvalue more than one were selected as the most suitable indicators. These indicators are the most uncorrelated set of parameters among all that have been selected for computing soil quality index.

11.5.2.3.2 Assigning Weightage to the Indicators

AHP, a multi-criteria decision-making (MCDM), was used in assigning weight to the indicators. It uses pairwise comparison which relies on the judgments of experts to weigh priority wise.

11.5.2.3.3 Scoring to the Indicators

Soil data were scaled based on the importance of parameters. Some parameters are better if they are more in soil, and some are better if they are less in soil. Simply, indicators were ranked based on its importance for soil functions. If the value of the soil parameters such as OC, CEC, aggregate stability, OC, N, P, and K are more in soil, then the soil is represented as good, and if bulk density, coarse fragment, and silt values are less in soil, then it is good. Therefore, the values of OC, silt, clay, CEC, N, K, aggregate stability, and soil depth were divided by the highest value for normalizing the score, and bulk density, coarse fragment, silt values were divided with the lowest values for the parameters in the landscape. For indicators such as pH, "higher is better" up to a threshold value (e.g. 7 for pH) than scored as lower is better above the threshold (Diack and Stott 2001; Andrews et al. 2002).

Thereafter, SQI (Wu and Wang 2007) was computed as a function of summation of weight multiplied by the score of each indicator:

$$SQI = \sum_{i=1}^{n} (W_i x\ S_i) \tag{11.3}$$

where w is the weight assigned for each indicator which is done through AHP, S is the score, and n is a number of samples in each landform types.

11.5.2.4 Soil Quality Index

PCA was carried out for selecting suitable soil quality indicators. A total of 11 indicators (parameters) such as OC, TN, soil depth, pH, silt, clay content, bulk density, coarse fragments, CEC, available K, and aggregates stability were selected. Scores to each indicator were computed following the scaling method. AHP analysis was carried out to determine the weight for soil indicators. The SQI was computed for agricultural lands for landform types. SQI for the valley, lower slope, mid-slope, and the upper slope is 0.71, 0.68, 0.67, and 0.65, respectively. Soils of toe slope (valley) had the highest soil quality followed by a lower, mid, and upper slope. SQI values of the landform types revealed its sustainability state of soils in the watershed of the mountainous ecosystem. Soil quality evaluation at the hill slope scale will serve as an important mean to prepare effective land use and management plan in the watershed.

11.6 Assessing Spatial Variability of Soil Quality Attributes in a Watershed: A Case Study

11.6.1 Experimental Site

The study was conducted in a hilly watershed in the mid-Himalayan region of Himachal Pradesh, India, to assess the spatial distribution of different soil quality parameters including SOC, SOC stratification ratio, and C: N ratio (Kalambukattu et al. 2018a, b). Grid sampling approach was used for the collection of soil samples during the fallow period.

11.6.2 Method of Approach

The collected soil samples were preprocessed and analysed for estimation of various soil quality indicators like pH, EC, SOC, N, P, and K as well as soil texture. In contrast, other parameters like SOC stratification ratio and C:N ratio were computed using the estimated values. Subsequently, SQI was also calculated using different quality indicators employing AHP. Inverse distance weighted (IDW) interpolation method was used for mapping the spatial distribution of SOC content, SOC stratification ratio, CN ratio, and SQI in the study area.

11.6.3 Salient Findings

SOC concentration was found to be decreasing with soil depth all over the study area and varied significantly ($P < 0.01$) between the first two depths (0–15 cm and 15–30 cm). The values of the SOC stratification ratio exceeded 1.2 in the majority area within the watershed representing an overall improvement in soil quality. C:N ratio values appeared to be <12:1, indicating improved organic matter mineralization rates as well as higher soil quality. The spatial distribution of SOC stratification ratio, and SQI in the study area is presented in Figs. 11.3 and 11.4. A perusal of the SQI spatial distribution revealed that approximately 76% of the study area had SQI

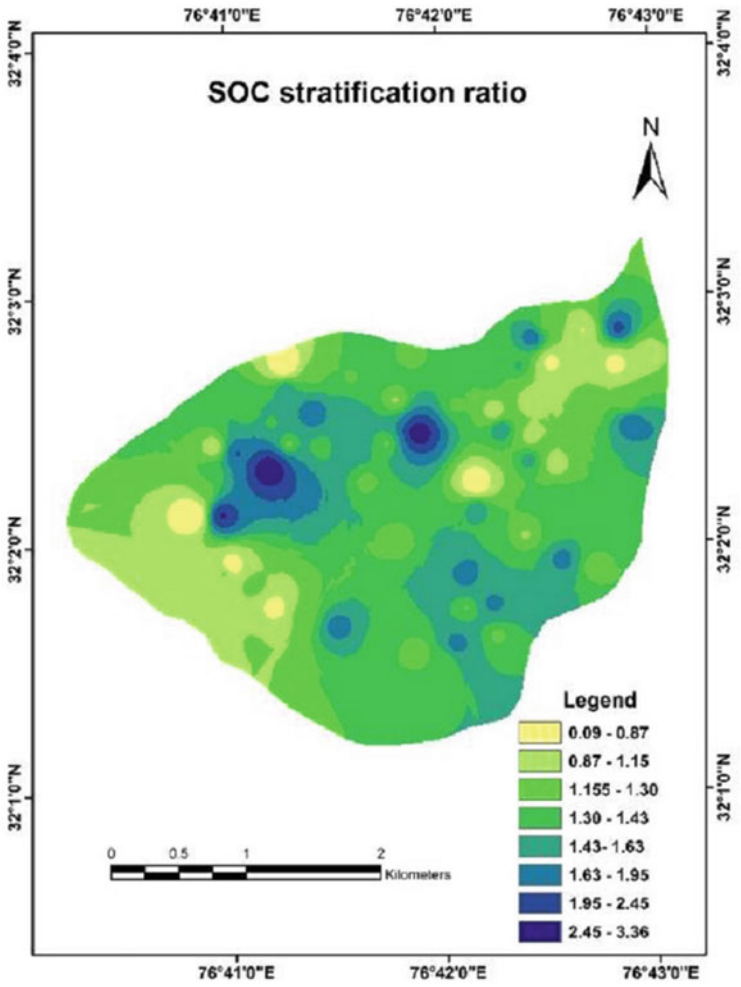

Fig. 11.3 Spatial distribution of SOC stratification ratio

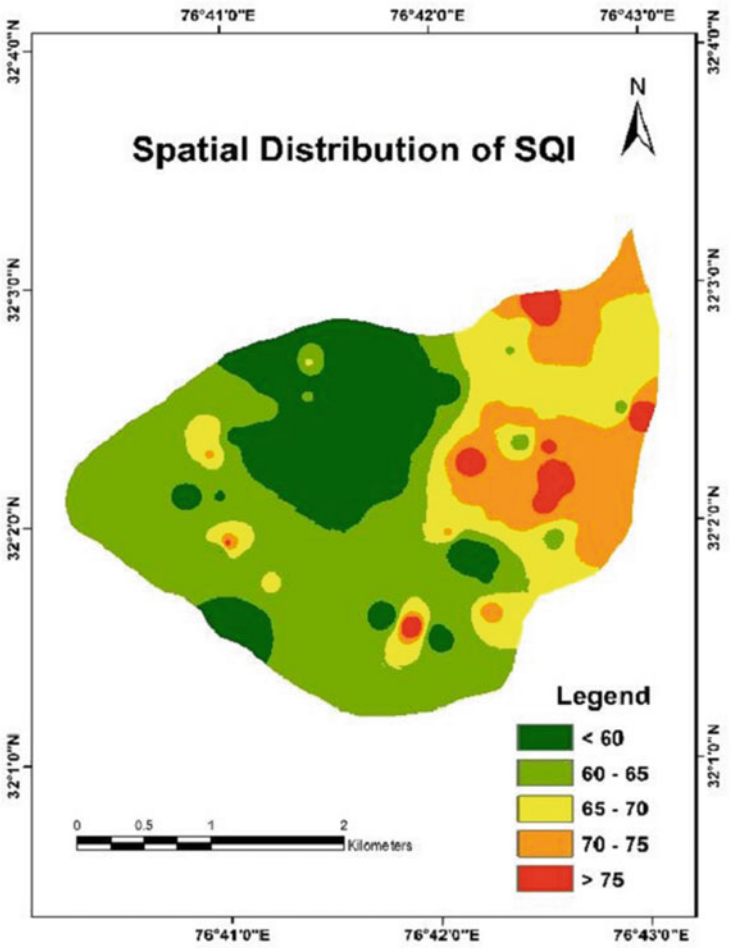

Fig. 11.4 Spatial distribution of SQI

values ranging from 60 to 75, whereas 22.16% area had SQI values lower than 60 and 2.59% area were found to have SQI values greater than 75. Overall, a high degree of soil quality was found to exist in the higher elevation zones of the study area. Majority of the watershed area had SQI values around 60%, which demands improved management strategies for enhancing the quality of the soil. The spatial mapping of SQI values will help us in identifying priority areas for better management as well as resource allocation for maintaining crop productivity and soil health.

11.7 Conclusion

Soil quality assessment is of particular importance to assess the sustainability of soils under the present ecosystem as well as to forecast the resilience of the ecosystem under the environmental constraints. It is a concept that integrates soil physical, biological, and chemical factors into a framework for soil resource assessment. Several physical, chemical, and biological indicators are used to assess soil quality from a crop production perspective. Among these indicators, biological indicators are considered as most sensitive to change. The primary role of remote sensing in land resource management is to provide information related to terrain, land, and soil under various land use land cover.

SQI methods are widely being used to assess soil quality at present as they are easy to use and quantitatively flexible. Soil quality indices are especially relevant to soil management practices because they use site-specific indicators of soil conditions. Recently, the geospatial modelling approach involving modelling change in SOC and crop simulation yield and soil erosion modelling approaches have been attempted by various researchers. SOC and N stock are also used as potential indicators of soil quality. The chapter discusses two case studies: (i) one study assessing soil quality by characterization of soil and terrain parameters and computing SQI by selecting minimum soil dataset in a watershed where PCA was used to find suitable indicators of soil quality and weights were assigned using AHP method and (ii) another study that investigated the spatial distribution of SOC, CN ratio, and SOC stratification ratio and other soil quality parameters in a small hilly watershed. Soil quality parameters such as pH, EC, SOC, N, P, K, and soil texture were studied.

References

Anderson TH, Domsch KH (1985) Determination of ecophysiological maintenance carbon requirements of soil microorganisms in a dormant state. Biol Fertil Soils 1(2):81–89

Andrews SS, Mitchell JP, Mancinelli R, Karlen DL, Hartz TK, Horwath WR, Pettygrove GS, Scow KM, Munk DS (2002) On-farm assessment of soil quality in California's central valley. Agron J 94:12–23

Andrews SS, Karlen DL, Cambardella CA (2004) The soil management assessment framework. Soil Sci Soc Am J 68(6):1945–1962

Arshad MA, Martin S (2002) Identifying critical limits for soil quality indicators in agroecosystems. Agric Ecosyst Environ 88(2):153–160

Arshad MA, Lowery B, Grossman B (1997) Physical tests for monitoring soil quality. Methods for assessing soil quality. Physical tests for monitoring soil quality. In: Doran JW, Jones AJ (eds) Methods for assessing soil quality. Soil Science Society of America, Madison, pp 123–141

Awiti AO, Walsh MG, Shepherd KD, Kinyamario J (2008) Soil condition classification using infrared spectroscopy: a proposition for assessment of soil condition along a tropical forest-cropland chronosequence. Geoderma 143(1–2):73–84

Basak N, Datta A, Mitran T, Roy SS, Saha B, Biswas S, Mandal B (2016) Assessing soil-quality indices for subtropical rice-based cropping systems in India. Soil Res 54(1):20–29

Ben-Dor E, Banin A (1995) Near-infrared analysis (Nira) as a method to simultaneously evaluate spectral featureless constituents in soils. Soil Sci 159(4):259–270

Bhaduri D, Purakayastha TJ, Patra AK, Singh M, Wilson BR (2017) Biological indicators of soil quality in a long-term rice-wheat system on the Indo-Gangetic plain: combined effect of tillage–water–nutrient management. Environ Earth Sci 76(5):202

Bhattacharyya T, Pal DK, Deshmukh AS, Deshmukh RR, Ray SK, Chandran P, Mandal C, Telpande B, Nimje AM, Tiwary P (2011) Evaluation of RothC model using four long term fertilizer experiments in black soils, India. Agric Ecosyst Environ 144(1):222–234

Biswas S, Hazra GC, Purakayastha TJ, Saha N, Mitran T, Roy SS, Basak N, Mandal B (2017) Establishment of critical limits of indicators and indices of soil quality in rice-rice cropping systems under different soil orders. Geoderma 292:34–48

Bouyoucos GJ (1951) A recalibration of the hydrometer method for making mechanical analysis of soils. Agron J 43(9):434–438

Brady N, Weil RR (2002) The nature and properties of soils, 13th edn. Prentice-Hall, New Jersey, p 598p

Bünemann EK, Bongiorno G, Bai Z, Creamer RE, De Deyn G, de Goede R, Fleskens L, Geissen V, Kuyper TW, Mäder P, Pulleman M (2018) Soil quality – a critical review. Soil Biol Biochem 120:105–125

Cambardella CA, Moorman TB, Andrews SS, Karlen DL (2004) Watershed-scale assessment of soil quality in the loess hills of Southwest Iowa. Soil Til e Res 78(2):237–247

Carroll S, Goonetilleke A, Khalil WA, Frost R (2006) Assessment via discriminant analysis of soil suitability for effluent renovation using undisturbed soil columns. Geoderma 131(1–2):201–217

Casa R, Castaldi F, Pascucci S, Basso B, Pignatti S (2013) Geophysical and hyperspectral data fusion techniques for in-field estimation of soil properties. Vadose Zone J 12(4)

Cécillon L, Barthès BG, Gomez C, Ertlen D, Génot V, Hedde M, Stevens A, Brun JJ (2009) Assessment and monitoring of soil quality using near-infrared reflectance spectroscopy (NIRS). European J Soil Sci 60(5):770–784

Chattaraj S, Srivastava R, Barthwal AK, Giri JD, Mohekar DS, Obi Reddy GP, Daripa A, Chatterji S, Singh SK (2017) Semi-automated object-based landform classification modeling in a part of the Deccan plateau of Central India. Int J Remote Sens 38(17):4855–4867

De la Rosa D, Sobral R (2008) Soil quality and methods for its assessment. In: Braimoh AK, Vlek PLG (eds) Land use and soil resources. Springer, Dordrecht

Dharumarajan S, Hegde R, Janani N, Singh SK (2019) The need for digital soil mapping in India. Geoderma Regional. Elsevier B.V

Di Tizio A, Grego S (2006) Soil organic carbon balance and CO2 emission from agricultural Italian land modeling with CENTURY. Acts of International Workshop of Development of Models and Forest Soil Surveys for Monitoring of Soil Carbon, Koli, Finland, 5–8 April

Diack M, Stott DE (2001) Development of a soil quality index for the Chalmers Silty Clay Loam from the Midwest USA, in 10th International Soil Conservation Organization Meeting. Purdue University: USDA-ARS National Soil Erosion Research Laboratory, pp 550–555

Ditzler CA, Tugel AJ (2002) Soil quality field tools. Agron J 94(1):33–38

Dobos E, Micheli E, Baumgardner MF, Biehl L, Helt T (2000) Use of combined digital elevation model and satellite radiometric data for regional soil mapping. Geoderma 97(3–4):367–391

Doran JW, Jones AJ (eds) (1996) Methods for assessing soil quality. Soil Sci Soc Am Special Pub 49:217–229

Doran JW, Parkin TB (1994) Defining and assessing soil quality. In: Doran JW, Coleman DC, Bezdicek DF, Stewart BA (eds) Defining soil quality for a sustainable environment. SSSA Special Publication 35, Madison, pp 3–21

Doran J, Coleman D, Bezdicek D, Stewart B (1994) A framework for evaluating physical and chemical indicators of soil quality

Drinkwater LE, Cambardella CA, Reeder JD, Rice CW (1996) Potentially mineralizable nitrogen as an indicator of biologically active soil nitrogen. In: Doran v and Jones AJ (eds.) Methods for assessing soil quality. Soil Sci Soc of America, Special Publication 49: 217–229

Dwivedi RS (2001) Soil resources mapping: a remote sensing perspective. Remote Sens Rev 20 (2):89–122

Dwivedi RS (2017) Remote sensing of soil / springer 13806

Ezeaku PI (2015) Evaluation of agro-ecological approach to soil quality assessment for sustainable land use and management systems. Academic J 10(15):501–512

FAO (1976) A framework for land evaluation. FAO soils bulletin 32, soil resources development and conservation service land and water development division, FAO and Agriculture Organization of The United Nations, Rome 1976

Franzluebbers AJ, Haney RL (2006) Assessing soil quality in organic agriculture. Critical Issues Report 2006.2. The Organic Center, Enterprise, OR

Govaerts B, Sayre KD, Deckers J (2006) A minimum data set for soil quality assessment of wheat and maize cropping in the highlands of Mexico. Soil Til Res 87(2):163–174

Granatstein D, Bezdicek DF (1992) The need for a soil quality index: local and regional perspectives. Am J Alt Agric 7(1–2):12–16

Gugino BK, Idowu OJ, Schindelbeck RR, van Es HM, Wolfe DW, Moebius Clune BN, Thies JE, Abawi GS (2009) Cornell Soil Health Assessment Training Manual, Edition 2.0. Cornell University, Geneva, NY

Gupta S, Kumar S (2017) Simulating climate change impact on soil carbon sequestration in agroecosystem of mid-Himalayan landscape using CENTURY model. Environ Earth Sci 76(11):394

Han WJ, Wu QT (1994) A primary approach on the quantitative assessment of soil quality. Chin J Soil Sci 25:245–247

Hartemink AE (1998) Soil chemical and physical properties as indicators of sustainable land management under sugar cane in Papua New Guinea. Geoderma 85(4):283–306

Herrick JE (2000) Soil quality: an indicator of sustainable land management? Appl Soil Ecol 15 (1):75–83

Herrick JE, Brown JR, Tugel AJ, Shaver PL, Havstad KM (2002) Application of soil quality to monitoring and management: paradigms from rangeland ecology. Agron J 94(1):3–11

Horwath WR, Paul EA (1994) Microbial Biomasss. In: Methods of soil analysis, Part 2. Microbiological and biochemical properties, SSSA Book Series No. 5. SSSA, Madison, pp 753–773

Imaz MJ, Virto I, Bescansa P, Enrique A, Fernandez-Ugalde O, Karlen DL (2010) Soil quality indicator response to tillage and residue management on semi-arid Mediterranean cropland. Soil Til Res 107(1):17–25

Jackson ML (1973) Soil chemical analysis. Prentice Hall of India Pvt. Ltd, New Delhi

Jaenicke EC (1998) From the ground up: exploring soil Quality's contribution to environmental health (p. 42). Greenbelt

Jones JW, Hoogenboom G, Porter CH, Boote KJ, Batchelor WD, Hunt LA, Wilkens PW, Singh U, Gijsman AJ, Ritchie JT (2003) The DSSAT cropping system model. European J Agron 18 (3–4):235–265

Jones RJA, Hiederer R, Rusco E, Loveland PJ, Montanarella L (2004) The map of organic carbon in topsoils in Europe, Version 1.2, September 2003: Explanation of Special Publication Ispra 2004 No.72 (S.P.I.04.72). European Soil Bureau Research Report No.17, EUR 21209 EN, and 1 map in ISO B1 format. Office for Official Publications of the European Communities, Luxembourg. 26 pp

Kalambukattu JG, Kumar S, Ghotekar YS (2018a) Spatial variability analysis of soil quality parameters in a watershed of Sub-Himalayan landscape-a case study. Eurasian J Soil Sci 7 (3):238–250

Kalambukattu JG, Kumar S, Raj RA (2018b) Digital soil mapping in a Himalayan watershed using remote sensing and terrain parameters employing artificial neural network model. Environ Earth Sci 77(5):203

Karlen DL, Stott DE (1994) A framework for evaluating physical and chemical indicators of soil quality. Defining Soil Quality Sustain Environ 35:53–72

Karlen DL, Mausbach MJ, Doran JW, Cline RG, Harris RF, Schuman GE (1997) Soil quality: a concept, definition, and framework for evaluation (a guest editorial). Soil Sci Soc Am J 61 (1):4–10

Karlen DL, Andrews SS, Doran JW (2001) Soil quality: current concepts and applications. Academic Press, Adva Agron, pp 1–40

Karlen DL, Ditzler CA, Andrews SS (2003) Soil quality: why and how? Geoderma 114 (3–4):145–156

Kasampalis DA, Alexandridis TK, Deva C, Challinor A, Moshou D, Zalidis G (2018) Contribution of remote sensing on crop models: a review. J Imaging 4(4):52

Kemper WD, Rosenau RC (1986) Aggregate stability and size distribution. Methods of soil analysis. Part 1 Physical Mineral Methods 5:425–442

Lal R (2015) Restoring soil quality to mitigate soil degradation. Sustainability 7(5):5875–5895

Larson WE, Pierce FJ (1994) The dynamics of soil quality as a measure of sustainable management. In: Doran JW, Coleman DC, Bezdicek DF, Stewart BA (eds) Defining soil quality for a sustainable environment, SSSA- Special Publication 35 edn. Soil Science Society of America, Madison, pp 37–51

Li H, Chen X, Cai X, He L, Huang W (2005) Assessment of soil quality using GIS & RS. In Proceedings. 2005 IEEE International Geoscience and Remote Sensing Symposium, 2005. IG ARSS'05. Vol. 4, pp. 2972–2975)

Lowery B, Hickey WJ, Arshad MA, Lal R (1996) Soil water parameters and soil quality. In: Doran JW, Jones AJ (eds) Methods for assessing soil quality, Madison, pp 143–155

Lugato E, Bampa F, Panagos P, Montanarella L, Jones A (2014) Potential carbon sequestration of European arable soils estimated by modelling a comprehensive set of management practices. Glob Chang Biol 20(11):3557–3567

Luo Z, Gan Y, Niu Y, Zhang R, Li L, Cai L, Xie J (2017) Soil quality indicators and crop yield under long-term tillage systems. Exp Agril 53(4):497–511

Martelet G, Drufin S, Tourliere B, Saby NP, Perrin J, Deparis J, Prognon F, Jolivet C, Ratié C, Arrouays D (2013) Regional regolith parameter prediction using the proxy of airborne gamma ray spectrometry. Vadose Zone J 1:12(4

Maselli F, Gardin L, Bottai L (2008) Automatic mapping of soil texture through the integration of ground, satellite and ancillary data. Int J Rem Sens 29(19):5555–5569

Masto RE, Chhonkar PK, Singh D, Patra AK (2007) Soil quality response to long term nutrient and crop management on a semi-arid Inceptisol. Agric Ecosyst Environ 118(1–4):130–142

Masto RE, Chhonkar PK, Singh D, Patra AK (2008) Alternative soil quality indices for evaluating the effect of intensive cropping, fertilization and manuring for 31 years in the semi-arid soils of India. Environ Monit Assess 136(1–3):419–435

McBratney AB, Santos MM, Minasny B (2003) On digital soil mapping. Geoderma 117(1–2):3–52

Meena RS, Mitran T, Kumar S, Yadav G, Bohra JS, Datta R (2018) Application of remote sensing for sustainable agriculture and forest management. Informat Proce Agricult 5:295–297

Meena RS, Kumar V, Yadav GS, Mitran T (2018a) Response and interaction of Bradyrhizobium japonicum and Arbuscular mycorrhizal fungi in the soybean rhizosphere: a review. Plant Growth Regul 84:207–223

Meena RS, Lal R, Yadav GS (2020) Long term impacts of topsoil depthand amendments on soil physical and hydrological properties of anAlfisol in Central Ohio, USA. Geoderma 363:1141164

Mehammednur Seid N, Yitaferu B, Kibret K, Ziadat F (2013) Soil-landscape modeling and remote sensing to provide spatial representation of soil attributes for an Ethiopian watershed. Appl Environ Soil Sci 2013. https://doi.org/10.1155/2013/798094

Merritt WS, Letcher RA, Jakeman AJ (2003) A review of erosion and sediment transport models. Environ Modell Software 18(8–9):761–799

Miller BA (2017) Geographic information systems and spatial statistics applied for soil mapping. In: Soil mapping and process modeling for sustainable land use management. Elsevier, Amsterdam, pp 127–149

Minasny B, McBratney AB, Salvador-Blanes S (2008) Quantitative models for pedogenesis—a review. Geoderma 144(1–2):140–157
Mitarn T, Lal R, Mishra U, Meena RS, Ravisankar T, Sreenivas (2018) Climate Change Impact on Soil Carbon Stocks in India. In: Lal R and Stewart BA (Eds) Advances in soil science, soil and climate, pp 291–308
Mitchell G, Griggs RH, Benson V, Williams J (1991) The EPIC model, environmental policy integrated climate, formerly erosion productivity impact calculator. EPIC User's guide, version. 1991; 5300
Mukherjee A, Lal R (2014) Comparison of soil quality index using three methods. PLoS One 9(8)
Mulder VL, De Bruin S, Schaepman ME, Mayr TR (2011) The use of remote sensing in soil and terrain mapping—a review. Geoderma 162(1–2):1–9
Nagaraju MS, Kumar N, Srivastava R, Das SN (2014) Cadastral-level soil mapping in basaltic terrain using Cartosat-1-derived products. Int J Remote Sens 35(10):3764–3781
NRC, National Research Council (1993) Soil and water quality: an agenda for agriculture. National Academic Press, Washington, DC
Ogle SM, Breidt FJ, Easter M, Williams S, Killian K, Paustian K (2010) Scale and uncertainty in modeled soil organic carbon stock changes for US croplands using a process-based model. Glob Chang Biol 16(2):810–822
Oldak A, Jackson TJ, Pachepsky Y (2002) Using GIS in passive microwave soil moisture mapping and geostatistical analysis. Int J Geogr Inf Sci 16(7):681–698
Parkin TB, Doran JW, Franco-Vizcaíno E (1997) Field and laboratory tests of soil respiration. Methods for assessing soil quality. 49:231–45
Paz-Kagan T, Shachak M, Zaady E, Karnieli A (2014) A spectral soil quality index (SSQI) for characterizing soil function in areas of changed land use. Geoderma 230:171–184
Paz-Kagan T, Zaady E, Salbach C, Schmidt A, Lausch A, Zacharias S, Notesco G, Ben-Dor E, Karnieli A (2015) Mapping the spectral soil quality index (SSQI) using airborne imaging spectroscopy. Remote Sens 7(11):15748–15781
Powlson DS, Jenkinson DS (1981) A comparison of the organic matter, biomass, adenosine triphosphate, and mineralizable nitrogen contents of ploughed and direct drilled soils. J Agric Sci 97(3):713–721
Qi Y, Darilek JL, Huang B, Zhao Y, Sun W, Gu Z (2009) Evaluating soil quality indices in an agricultural region of Jiangsu Province, China. Geoderma 149(3–4):325–334
Qin MZ, Zhao J (2000) Strategies for sustainable use and characteristics of soil quality changes in urban-rural marginal area. Acta Geogr Sinica-Chinese Edition 55(5):545–554
Rezaei SA, Gilkes RJ, Andrews SS (2006) A minimum data set for assessing soil quality in rangelands. Geoderma 136(1–2):229–234
Rossiter DG (2003). Land use, land cover and soil sciences – Vol. II – biophysical models in land evaluation. EOLSS Publishers Co. Ltd. (UK), https://www.eolss.net/
Roy S (2014) Developing a framework for soil quality assessment in a watershed of mountainous ecosystem using geo-spatial approach (M. Tech Thesis), Agriculture and Soils Department, Indian Institute of Remote Sensing, Dehradun, India
Saaty TL (1990) How to make a decision: the analytic hierarchy process. European J Operat Res 48:9–26
Sanchez PA, Palm CA, Buol SW (2003) Fertility capability soil classification: a tool to help assess soil quality in the tropics. Geoderma 114(3–4):157–185
Schiewe J (2003) Concepts and techniques of geographic information systems. By CP Lo and Albert KW Yeung (Upper Saddle River, New Jersey: Prentice Hall, 2002).[pp. xii+ 492]. ISBN: 0-13-080427-4. Price US $71 Hardback. Int J Geogr Inf Sci 17(8):819–820
Shepherd KD, Walsh MG (2002) Development of reflectance spectral libraries for characterization of soil properties. Soil Sci Soc Am J 66(3):988–998
Sikora LJ, Stott DE (1996) Soil organic carbon and nitrogen. In: Doran JW, Jones AJ (eds) Methods for assessing soil quality. Soil Science Society of America, Madison, pp 157–167

Sims JT, Cunningham SD, Sumner ME (1997) Assessing soil quality for environmental purposes: roles and challenges for soil scientists. J Environ Qual 26(1):20–25
Singh KP, Malik A, Mohan D, Sinha S, Singh VK (2005) Chemometric data analysis of pollutants in wastewater—a case study. Anal Chim Acta 532(1):15–25
Smith WN, Grant BB, Desjardins RL, Qian B, Hutchinson J, Gameda S (2009) Potential impact of climate change on carbon in agricultural soils in Canada 2000–2099. Climat Chan 93 (3–4):319–333
Sofi JA, Bhat AG, Kirmai NA, Wani JA, Lone AH, Ganie MA, Dar GI (2016) Soil quality index as affected by different cropping systems in northwestern Himalayas. Environ Monit Assessment 188(3):161
Srivastava R, Saxena RK (2004) Technique of large-scale soil mapping in basaltic terrain using satellite remote sensing data. Int J Remote Sens 25(4):679–688
Stefanoski DC, de Figueiredo CC, Santos GG, Marchão RL (2016) Selecting soil quality indicators for different soil management systems in the Brazilian Cerrado. Pesquisa Agropecuaria Brasileira 51(9):1643–1651
Stott DE, Cambardella CA, Tomer MD, Karlen DL, Wolf R (2011) A soil quality assessment within the Iowa River South Fork watershed. Soil Sci Soc Am J 75(6):2271–2282
Sun B, Zhou S, Zhao Q (2003) Evaluation of spatial and temporal changes of soil quality based on geostatistical analysis in the hill region of subtropical China. Geoderma 115(1–2):85–99
Tabatabai MA (1994) Soil enzymes. In: Weaver RW et al (eds) Methods of soil analysis. Part 2. Microbiological and biochemical properties, pp 775–833
Terhoeven-Urselmans T, Schmidt H, Joergensen RG, Ludwig B (2008) Usefulness of near infrared spectroscopy to determine biological and chemical soil properties: importance of sample pre-treatment. Soil Biol Biochem 40(5):1178–1188
Ugbaje SU, Reuter HI (2013) Functional digital soil mapping for the prediction of available water capacity in Nigeria using legacy data. Vadose Zone J 12(4)
USDA (2001a) Guidelines for Soil Quality Assessment in Conservation Planning. Soil Quality Institute USDA, Natural Resources Conservation Service Available at: https://www.nrcs.usda.gov/wps/portal/nrcs/main/soils/health/assessment/
USDA (2001b). Soil quality test kit guide. Soil Quality Institute, (August), 82. https://doi.org/10.1037/t15144-000
USDA (2006) Soil quality institute. Natural resources conservation service. Available at http://soils.usda.gov/sqi/
USDA (2008) Overview of RUSLE2. Available on-line at: http://www.ars.usda.gov/research/docs.htm?docid=6010&pf=1&cg_id=0 (verified 2/08)
USDA NRCS (2005). National Soil Survey Handbook, title 430-VI. Soil Properties and Qualities (Part 618), Available Water Capacity (618.05). Online at: http://soils.usda.gov/technical/handbook
Vågen TG, Shepherd KD, Walsh MG (2006) Sensing landscape level change in soil fertility following deforestation and conversion in the highlands of Madagascar using Vis-NIR spectroscopy. Geoderma 133(3–4):281–294
Viscarra Rossel RA, Walvoort DJJ, McBratney AB, Janik LJ, Skjemstad JO (2006) Visible, near infrared, mid infrared or combined diffuse reflectance spectroscopy for simultaneous assessment of various soil properties. Geoderma 131(1–2):59–75. https://doi.org/10.1016/j.geoderma.2005.03.007
Walkley A, Black IA (1934) An examination of the Degtjareff method for determining soil organic matter, and a proposed modification of the chromic acid titration method. Soil Sci 37(1):29–38
Wang X, Gong Z (1998) Assessment and analysis of soil quality changes after eleven years of reclamation in subtropical China. Geoderma 81(3–4):339–355
Wang X, Harmel RD, Williams JR, Harman WL (2006) Evaluation of EPIC for assessing crop yield, runoff, sediment and nutrient losses from watersheds with poultry litter fertilization. Trans ASABE 49(1):47–59

Wang G, Luo Z, Han P, Chen H, Xu J (2016) Critical carbon input to maintain current soil organic carbon stocks in global wheat systems. Sci Rep 6(1):1–8

Wang G, Zhang W, Sun W, Li T, Han P (2017) Modeling soil organic carbon dynamics and their driving factors in the main global cereal cropping systems. Atmos Chem Phys 17 (19):11849–11859

Williams J (1990) The Erosion-Productivity Impact Calculator (EPIC) model: a case history. Philos Trans Biol Sci 329(1255):421–428

Wilson CG, Papanicolaou AN, Abaci O (2009) SOM dynamics and erosion in an agricultural test field of the Clear Creek, IA watershed. Hydrol Earth Syst Sci Discuss 6(2):1581–1619

Wu Q, Wang M (2007) A framework for risk assessment on soil erosion by water using an integrated and systematic approach. J Hydrol 337(1–2):11–21

Yu Y, Huang Y, Zhang W (2012) Modeling soil organic carbon change in croplands of China, 1980–2009. Global Planet Change 82:115–128

Zhang B, Zhang Y, Chen D, White RE, Li Y (2004) A quantitative evaluation system of soil productivity for intensive agriculture in China. Geoderma 123(3–4):319–331

Zhao Z, Chow TL, Rees HW, Yang Q, Xing Z, Meng FR (2009) Predict soil texture distributions using an artificial neural network model. Comput Electron Agric 65(1):36–48

Chapter 12
Land Degradation Assessment Using Geospatial Techniques

Arijit Barman, Nirmalendu Basak, Bhaskar Narjary, and Tarik Mitran

Contents

Abstract Land degradation is a thoughtful threat involved in reducing area and productivity of 13.4 billion ha in the global cultivable land. The genesis and distribution of different types of land degradation processes depend on climate, topography, vegetative cover, parent material (salty or acidic), and groundwater (saline, sodic, or heavy metals/metalloid). Above all, human-induced degradation of land has been exaggerated recently. These changes in land degradation can be

A. Barman (✉) · N. Basak · B. Narjary
ICAR-Central Soil Salinity Research Institute, Karnal, Haryana, India
e-mail: arijit.barman@icar.gov.in; nirmalendu.basak@icar.gov.in; bhaskar.narjary@icar.gov.in

T. Mitran
Soil and Land Resources Assessment Division, National Remote Sensing Centre, Department of Space, ISRO, Hyderabad, Telangana, India
e-mail: tarikmitran@nrsc.gov.in

T. Mitran et al. (eds.), *Geospatial Technologies for Crops and Soils*,
https://doi.org/10.1007/978-981-15-6864-0_12

monitored and assessed through geospatial techniques such as remote sensing (RS) and geographic information system (GIS) with fine spatial and spectral resolution imageries. The advanced techniques such as microwave, hyperspectral, and proximal ground-based sensor data with multivariate statistical algorithms have increased the efficiency of classification and mapping of degraded lands. The values of different parameters extracted from thematic map of the terrain, surface, hydrology, and spectral ratio indices of multispectral, hyperspectral images are used as an input parameter for the generation of a digital soil map. The digital soil map with seasonal/temporal variation (possible with fine temporal resolution) conveys detailed information regarding the study of changes, characterization, causes, protection, and reclamation of the land degradation processes. The method of real-time monitoring and assessment of land degradation using RS/GIS techniques is cost-effective, fast, and accurate and indicates land/resource management quickly to secure the food, water, and environmental security. This chapter summarizes the comprehensive understanding of the extent, type, cause of land degradation processes, and indicators of land degradation as well as assessment and monitoring of such through advanced remote sensing techniques.

Keywords Degraded soils · Ground-based sensor · Geographic information system · Hyperspectral · Multispectral · Synthetic aperture radar · Temporal variation

Abbreviation

ANN	Artificial Neural Networks
ASTER	Advanced Spaceborne Thermal Emission and Reflection Radiometer
AVHRR	Advanced Very High Resolution Radiometer
BART	Bayesian Additive Regression Trees
CT	Classification Tree
DEM	Digital Elevation Model
ESP	Exchangeable Sodium Percentage
ETM+	Enhanced Thematic Mapper Plus
GBM	Gradient Boosting Machines
GIS	Geographic Information System
HRS	Hyperspectral Remote Sensing
IRS	Indian Remote Sensing
LDN	Land Degradation Neutrality
LISS	Linear Imaging Self Scanning
MODIS	Moderate Resolution Imaging Spectroradiometer
MSS	Multispectral Scanner System
NDSI	Normalized Difference Salinity Index
NDVI	Normalized Difference Vegetation Index
NDWI	Normalized Difference Water Index
NIR	Near Infrared
PCR	Principal Component Regression

PLSR	Partial Least Squares Regression
RF	Random Forest
RS	Remote Sensing
RT	Regression Tree
SAR	Synthetic Aperture Radar
SAVI	Soil-Adjusted Vegetation Index
SI	Salinity Index
SPAD	Soil Plant Analysis Development
SPOT	Système Pour l'Observation de la Terre
SVM	Support Vector Machine
SVR	Support Vector Regression
SWIR	Shortwave Infrared
TDR	Time-Domain Reflectometry
TM	Thematic Mapper
UNCCD	United Nations Convention to Combat Desertification
VI	Vegetation Index
VNIR	Visible and Near Infrared

12.1 Introduction

Land degradation is a challenge for the existence, prosperity, and future of any civilization. Currently, several types of land degradation are major threats for the developing countries for declining productivity of soil, water, pastureland, agricultural, and economic growth further arising of conflict at a regional level and question of security of livelihood (Reddy 2003). Agricultural production is deleteriously affected due to inappropriate land care strategies in maximum portions of the world (FAO 2005; Lambin and Meyfroidt 2011; Lambin et al. 2013). Sometimes, direct land degradation may appear in expanding the area under desertification in semi-arid and arid climatic region, frequent and intense drought occurrence, extreme types of water, and wind erosion promote a severe amount topsoil loss and flooding leads to a reduction of soil productivity, alterations of soil properties, biodiversity deterioration and encourages the loss of soil organic carbon (Foley et al. 2005; Gibbs et al. 2010; Lambin and Meyfroidt 2011). The main physical agents of land degradation are water, wind, expansion of the desert and flood, etc. Among these wind erosion, high wind velocity and intense heat carry the top fertile soils from one area to other sites, and soil nutrients are lost carried out to certain distance, and subsoil gets exposed and soil loss with productivity due to lost away of fertile soil. The secondary land degradation arises mainly due to the rapid development of irrigation infrastructure without the optimum implementation of irrigation practices, and drainage measures have caused a rise in the water table, and consequent widespread waterlogging and salinization in several arid and semi-arid regions in the world (Tyagi 1998). Agricultural intensification arises stress on soil resources,

the decline in soil quality, and overexploitation of groundwater. Such intensification increases the cost of cultivation, decrease/deposition of nutrient content, the decline in organic carbon of soil, distortion of soil structural, the addition of salts and toxic chemicals, and decline in soil resilience and resistance (Lal and Stewart 1990; Basak et al. 2014; Bhattacharyya et al. 2015). Land productivity from all aspects has been reduced by human intervention during land preparation, overexploitation of vegetation, and overgrazing, leading to soil quality deterioration (UNEP 1992; Holm et al. 2003; Kniivila 2004). The extent of land degradation varies from region to region and rapidly changes with time. There is a problem with the availability of clear information on the extent of land degradation, neither worldwide nor a particular country (FAO 2008; Bindraban et al. 2012; Mitran et al. 2018). Monitoring of land degradation depends on visual and digital analysis of an image, ground-truthing of soil, water, the pattern of the river, water bodies, land surface, land cover, natural vegetation, crops, temperature, rainfall pattern and shift, the presence of salts, toxic pollutants and determination of the source of contaminants and pollutants. Therefore, to cope with the adverse effect of land degradation, undertaking RS and GIS applications is vital for rapid and real-time estimation and assessment of the extent, type, and nature of degraded lands. Assessment, monitoring, and rehabilitation of degraded lands are the options to minimize the gap between supply and demand of our daily needs and improve agricultural productivity, strengthening the economy of agrarian countries. The digital soil maps with seasonal/time variation (possible with fine temporal resolution) give detailed information regarding changes, characterization, causes, protection, and reclamation of the land degradation process. Land degradation is a thoughtful threat which involved in reducing area and productivity of 13.4 billion ha in the global cultivable land. Space Applications Centre of India (SAC) (2016) reported that out of the total geographic area (TGA), 96.4 Mha (29.3%) areas come under the land degradation process in India. Change analysis after 10 years reported that 1.95 Mha lands have been reclaimed and around half million ha land reduced its severity level from high to medium, whereas 0.75 Mha land converted to high severity level from low in India. The genesis and distribution of different types of land degradation processes depend on climate, topography, vegetative cover, parent material (salty or acidic), and groundwater (saline, sodic, or heavy metals/metalloids). Above all, human-induced degradation of land has been exaggerated recently. These changes in land degradation can be monitored and assessed using different techniques of RS and GIS with fine spatial- and spectral-resolution imagery. The advanced techniques such as microwave, hyperspectral, and proximal ground-based sensor data such as multispectral, hyperspectral, microwave, and ground-based sensor, viz. EM38, time-domain reflectometry (TDR), spectroradiometer, ground-penetrating radar (GPR), resistivity meter, soil plant analysis development (SPAD), green shaker, and chlorophyll meter, with multivariate statistical algorithm (principal component regression (PCR), partial least-squares regression (PLSR), random forest (RF), support vector machine (SVM), etc.), have increased the efficiency of classification and mapping of degraded lands. The values of different parameters, extracted from thematic map of the terrain, surface and hydrology, and spectral ratio indices [normalized difference vegetation

index (NDVI), soil-adjusted vegetation index (SAVI), normalized difference water index (NDWI), etc.] of multispectral, hyperspectral images, are used as an input parameter for the generation of a digital soil map. The method of real-time monitoring and assessment of land degradation using RS/GIS techniques is cost-effective, fast, and accurate and indicates land/resources management quickly to secure the food, water, and environmental security. Land degradation is a thoughtful threat which involved in reducing area and productivity of 13.4 billion ha in the global cultivable land. The genesis and distribution of different types of land degradation processes depend on climate, topography, vegetative cover, parent material (salty or acidic), and groundwater (saline, sodic, or heavy metals). Above all, human-induced degradation of land has been exaggerated recently. These changes in land degradation can be monitored and assessed through geospatial techniques such as RS and GIS with fine spatial- and spectral-resolution imageries. The advanced techniques such as microwave, hyperspectral, and proximal ground-based sensor data with multivariate statistical algorithm have increased the efficiency of classification and mapping of degraded lands. The values of different parameters, extracted from thematic map of the terrain, surface, hydrology, and spectral ratio indices of multispectral, hyperspectral images, are used as an input parameter for the generation of a digital soil map. This digital soil map with seasonal/temporal variation gives detailed information regarding changes, characterization, causes, protection, and reclamation of the land degradation processes. This chapter summarizes the comprehensive understanding of the extent, type, cause of land degradation processes, and indicators of land degradation as well as assessment and monitoring of such through advanced remote sensing techniques.

12.2 Geographical Extent of Land Degradation: Global and Indian Perspective

The estimated global total degraded land area was varied from 0.99 to >6.0 billion ha (UNCCD 2017). These huge discrepancies among researchers are mainly due to their approaches and lack of cohesiveness. In a worldwide, mainly, three methodologies have been followed to estimate degraded lands, i.e. expert view, RS observation, and biophysical models. Global-estimated land degradation by these approaches is presented in Table 12.1.

According to the Global Assessment of Human-Induced Soil Degradation (Bridges and Oldeman 1999), globally, ~15% of the land was found to be degraded. Among the various agents, soil erosion, nutrient loss, salinity, soil physical problems, and chemical contamination degrade 83, 4, 4, 4, and 1% of the land, respectively. In South Asia, 43% of the agricultural land was degraded. Among this strongly degraded land was 31.0 Mha, and moderately degraded land was 63.0 Mha. The severely affected country was Iran (94% of agricultural land under

Table 12.1 Percent of degraded lands based on three methodologies

	Expert opinion			Satellite observation	Biophysical models
Area	Dregne and Chou (1992)	GLASOD	FAO TerraSTAT	GLADA	Cai et al. (2011)
Africa	29.12	26.40	19.90	24.09	13.32
Asia	37.36	37.25	40.73	33.28	49.45
Australia and Pacific	10.47	0.49	5.99	8.61	1.31
Europe	2.62	12.99	6.56	2.37	10.49
North America	11.94	11.51	12.96	17.12	9.69
South America	8.52	11.43	13.86	14.53	15.74

Modified, Gibbs and Salmon (2015)
GLASOD Global Assessment of Soil Degradation, *FAO* Food and Agriculture Organization, *GLADA* Global Assessment of Land Degradation and Improvement

degradation), and the least affected was Bhutan (10%). Only because of land degradation South Asian countries are losing US$10 billion annually.

Land degradation assessment using satellite remote sensing helped to present precisely the spatial distribution of global degraded lands. However, the main limitation of this method is to separate saline and naturally low productive areas from those human degraded lands. However, it was observed that soil degradation information derived from RS imageries in slightly and moderately degraded areas was less accurate. This limits the perspective of RS for land degradation assessment specifically in the low to moderately degraded areas. Based on NDVI imageries on land productivity, GLADA estimated a falling inclination of net primary productivity (NPP) over 21% of global land area, ranging from tropical Africa, Southeast Asia, Australia, and North America. In the biophysical approach of land degradation assessment, cropping suitability of land was combined with productivity. Based on this approach, Cai et al. (2011) reported that globally, 1.0 billion ha of lands (approximation) were affected by various types of land degradation and of which China and India contained nearly 490.0 Mha of degraded lands.

Unlike the world database, in India, a systematic approach has been followed for estimating degraded land. According to the latest land degradation assessment (SAC 2016) in 2013, 96.4 million hectares of land area affected by land degradation, representing 29.3% of India's total land area. Around 24.0% of the total geographic area was degraded mainly in the arid and semi-arid regions of India (Rajasthan, Jharkhand, Maharashtra, Gujarat, etc.). Although 1.95 Mha of land was reclaimed within 2003–2005 to 2011–2013, surprisingly, it was observed that during the same period, 3.63 Mha of productive land had undergone degradation. From 2003 to 2013, severe land degradation (11.03 to 4.34%) was observed in the states of Delhi, Nagaland, Tripura, Mizoram, and Himachal Pradesh, whereas maximum land reclamation (0.11 to 1.27%) was noticed in Odisha, Rajasthan, Telangana, and Uttar Pradesh. Among all the land degradation processes, water erosion contributed the

Table 12.2 Process wise land degradation status during 2003 and 2013 in India (percent of total area under desertification, modified, SAC 2016)

Process of land degradation	Degraded land area (%)	
	2003	2013
Deforestation	29.92	30.39
Water erosion	37.67	37.45
Wind erosion	19.41	18.91
Salinity	4.24	3.81
Waterlogging	0.63	0.67
Frost shattering	3.29	3.46
Mass movement	0.89	0.96
Manmade	0.39	0.43
Barren/rocky	1.99	1.96
Settlement	1.57	1.95

most (37.0%), followed by deforestation (30%) and wind erosion (19%) (Table 12.2). During 2003–2013, an area under desertification increased from 81.5 to 82.6 Mha. Wind erosion is the main significant process of desertification in the arid region, while deforestation and water erosion are the main process of degradation in the regions of semi-arid and dry subhumid.

In recent estimates (SAC 2016) of salt-affected land, only 3.67 Mha areas were affected by salinity and alkalinity. But these estimates have a huge deviation from the earlier estimates (6.73 Mha) done by National Remote Sensing Centre (NRSC), Central Soil Salinity Research Institute (CSSRI), and National Bureau of Soil Survey and Land Use Planning (NBSSLUP). They have used LANDSAT satellite data corresponding to 1996 along with soil chemical analysis data and estimated the total salt-affected area of 6.73 Mha and out of which saline soil cover 2.9 Mha and sodic soil cover 3.7 Mha in India (Mandal et al. 2010). This large difference in totality as well as on the spatial distribution of salt-affected degraded lands illustrates the scalability of the problem and the necessity of accurate data and techniques for estimation salt-affected areas.

12.3 Land Degradation Processes

The project of GLASOD (Oldeman et al. 1991) distinguishes four types of soil degradation around the world such as water erosion, wind erosion, chemical degradation (salinization/alkalization, acidification), and physical degradation (glacial, waterlogging), but nowadays, anthropogenic factors become more dominant due to pressure of burgeoning population. In India, NRSC (2010) had used a 13-fold major category to generate wasteland (degraded land) map at 1:250,000 and

1:50,000 scale using visual and digital remote sensing techniques) under National Wastelands Monitoring Project. These 13-fold major categories are as follows:

1. Gullied and/or ravinous (eroded) lands
2. Undulating uplands with or without scrub
3. Marshy and water stagnated land
4. Coastal or inland salinity/alkalinity affected lands
5. Shifting cultivation area
6. Degraded informed forest land
7. Pastures/grazing land degradation
8. Degraded non-forest plantation area
9. Sandy areas in the desert or coastal region
10. Wasteland in the industrial/mining area
11. Barren/sheet/stony rocky area
12. Sloppy (steep) areas
13. Snow/glacial areas

These 13-fold categories can be broadly grouped as water and wind erosion, waterlogging, salinization/alkalization, acidification, glacial, anthropogenic, and others.

12.3.1 Water Erosion

Worldwide water erosion is an important hazard, and annually, ~24 billion tonnes of top fertile soil is washed away (FAO 2011; Meena et al. 2018). This soil erosion also aggravated a loss of 1100 Mt. C into the atmosphere and conjointly erosion-induced transportation loss of 300–800 Mt. C to the ocean through soil loss (Lal 2011). Besides organic C loss, water erosion also results in losses of inherent and applied nutrients, the soil compacted as top fertile soil eroded out, loss in soil biodiversity, and chances of contamination with heavy metals and pesticides. Water erosion negatively affects crop productivity. It has an important threat to the security of food, livelihood, and environment in a country. In India, around 13.4 Mt. (≈205.32 billion rupees) of annual productions are lost due to water erosion (Sharda et al. 2010). The climatic, physiographic, and parent material characteristics show a 32% water erosion registered for the southern plateau region, while north India claimed 68% registered water erosion (NAAS 2017). In north India, the Brahmaputra, the Ganges, and the Indus, rivers which flow the northern Himalayan region, jointly contribute half of the total gross erosion in India.

12.3.2 Wind Erosion

Wind erosion is the process of movement of soil particles by strong wind regime which cross over the critical velocity for beginning the movement of soil particles (Samra et al. 2012). The topsoil erosion disturbs the soil air composition, soil temperature and water status, microbial respiration, and carbon storage in soils. In the region of semi-arid and arid, nearly devoid of native or planted vegetation with high wind velocity tends to wind erosion. The single grained sandy soils are most prone to this erosion. The finer soil particle and externally applied soil nutrients are carried out to a certain distance, and subsoil get exposed and soil loss with productivity due to blown away of fertile soil. The Sahelian Africa (Sterk 2003), northern China (Yan et al. 2005), and North-western Thar Desert of India are severely affected by wind erosion.

12.3.3 Chemical Degradation

Soils that need unusual management are collectively known as chemically degraded soil or problem soils. These types of soils are characterized by the excess or deficiency of some characteristics parameters and making it barren or less productive soil. These soils are affected by different degrees of soil degradation problems.

12.3.3.1 Salinization/Alkalization

The higher content of electrolytes (cations and anions) causes the problem of salinity. The presence of salts causes the high osmotic potential results in plants and native soil microbes start experiencing severe water stress due to the physiological unavailability of water. Further, antagonism relation between electrolytes (Cl^- and $H_2PO_4^-$), (Cl^- and NO_3^-), (Cl^- and SO_4^{2-}), and (Na^+ and K^+) affects the normal nutrition of the plant, whereas high pH_s and alkalinity ($pH_s > 8.5$) and exchangeable sodium percent ($> 15\%$) create the problem of the low permeability of water and air entry in soil due to dispersion of aggregates and clay particles. The hard crust on the surface delays seedling emergence. The toxic concentration of alkaline anion (HCO_3^- and CO_3^{2-}) causes a deficiency of N, Zn, and Fe (Rai et al. 2020; Basak et al. 2020).

12.3.3.2 Acidification

Soil having pH ranges from 4.5 to 6.5 categorized as acid soil. The deficiency of P, Ca, and Mg and excess of Al^{3+}, Fe^{3+}, and Mn^{3+} cause root injury and soil limited soil biological activity.

12.3.3.3 Physical Degradation

The unfavourable soil physical conditions make soil underproductive. The major soil physical constrains are soil compaction due to mechanical impedance, crust formation, hardening and sealing of topsoil, low water retention and highly permeable soil, shallow soils, and slowly permeable soil.

12.3.3.4 Waterlogged Soil

Water table rises to such an extent that the root zone becomes saturated with water. Impair in aeration results in poor crop growth and limited nutrient uptake. The nitrification process is badly affected.

12.3.4 Anthropogenic and Agricultural Activity

The populous country (like India and China) achieves security for food production by an intensification of agriculture. This intensification and associated food security are accomplished with a huge challenge and a serious deterioration and degradation of soil and land quality. Burgeoning population drastically shrinks the land availability (land-human ratio) in India with land availability decline 0.34 ha in 1961–52 to 0.14 ha in 2012–2013 and expected it will decline further. Therefore, it is inevitable to raise in more pressure for finite soil resources and prone to degradation for perceive agricultural productivity, sustaining economic growth (IPES-Food 2019). High fertilizer consumption for agriculture intensification increases its negative fates, a possibility for its indiscriminate use also enhanced with attendant loss of efficiency and imbalances in rates of the fertilizing nutrients particularly NPK. Such imbalances in fertilization eventually cause deterioration in the health of soils and the environment simultaneously. Symptoms of such deterioration of soil health are captured by different researchers computing soil quality index under various fertilization treatments and cropping systems in a large number of long-term fertility experiments in diverse agroclimatic areas (Basak and Mandal 2019).

The important key visual interpretation feature of several types of land degradation depends on colour, texture, pattern, size, shape, association, etc. Identification of different land degradation process depends on different types of land degradation.

Table 12.3 Keys of visual image analysis for different land degradation

Process	Colour	Shape	Texture	Pattern
Water erosion	Slightly brighter/brighter grey to dark grey than surrounding land	Irregular	Smooth/ medium to course	Contiguous/discrete patches to contiguous patches
Wind erosion	Light grey/yellow to pink mottles	Irregular/ regular	Smooth/ medium to course	Contiguous/discrete patches/ mottling
Waterlogging	dark or shaded blue/grey	Irregular/ regular	Smooth	Discrete/contiguous patches
Salinization/ alkalization	Light grey/greyish white to white/dull white	Irregular	Smooth	Discrete patches
Acidification	Green/black shades	Irregular	Smooth-medium	Contiguous/discrete patches/ mottled
Anthropogenic (industrial effluent, mining, brick factory)	Shaded/dull white, grey, blue to yellow, red, black	Irregular/ Regular	Smooth-medium	Contiguous/discrete/Isolated patches

Modified, Ravishankar and Sreenivas (2010)

The false colour composite (FCC) image helps to identify the different types of land degradation processes. Some of the important visual interpretation features of land degradation process have been presented in Table 12.3.

12.4 Causes of Land Degradation Process

The causes of land degradation are directly/indirectly linked to human activities. The pressure of the population in a rural and urban area with the development of the economy pressurizes the change of land use, leading to the function and productivity degradation of an ecosystem (Cherlet et al. 2018). Removal of soil covers by the means of overgrazing, deforestation and deterioration of soil health by agricultural activity overdose of fertilizer, and nutrient mining for supporting the increasing demand of national are the core reasons for land degradation. Man-made soil deterioration rate has been projected based on changes in local population densities (both human and animal) and/or in relation to mechanization, agricultural expansion, fertilizer use, etc. during 10 years. The reason for land degradation differs from country to country (Table 12.4). Deforestation followed by agriculture is the dominant cause of degradation in Asia and South America, whereas, in Africa and South America, it is overgrazing and agriculture, respectively. Australia and New Zealand of the Oceania continent are the main contributors to overgrazing. Overutilization by woodcutting for fuel purposes is very high in lower developing continents, while this scenario is absent in developed continents, where other causes of degradation became prominent (Table 12.4).

Table 12.4 Sources of human-induced land degradation (percent of total human-induced degraded land; Modified, Oldeman 1992)

Area	Deforestation	Overutilization	Overgrazing	Agricultural practices	Mechanization
Asia	15.17	2.34	10.03	10.38	0.05
Europe	4.27	0.05	2.54	3.26	1.07
Africa	3.41	3.21	12.37	6.16	–
North America	0.20	–	1.48	3.21	–
Central America	0.71	0.56	0.46	1.42	–
South America	5.09	0.61	3.46	3.26	–
Oceania	0.61	–	4.22	0.41	–
World	29.47	6.77	34.55	28.09	1.12

Gao and Liu (2010) reported that overgrazing, intensive cultivation, unnecessary reclamation of grassland for farming, and deforestation leads to the worsened degradation situation. They reported that land degraded area increased from 2400 to 4214 km^2 due to soil salinization, waterlogging, and desertification. A different agricultural activity like deforestation, overgrazing, excessive irrigation, groundwater withdrawal, intensive tillage operation with heavy agriculture machinery, crop residue burning and low return of organic input, impaired irrigation, drainage, and water management, monoculture and faulty crop rotation, and misuse of pesticide further aggravated the degradation (Bhattacharyya et al. 2015).

12.5 Indicators of Land Degradation Assessment

Identification of potential indicators of land degradation followed by empirical verification with ground-truthing and remote sensing data are used to measure and monitor spatial and seasonal variability of degraded land. The most important indicators are:

- Sparse vegetation/increased bare ground
- Increased soil looseness
- Reduction of soil organic matter
- The non-uniform rainfall distribution pattern
- High concentration of salts in soil surface
- Water stagnation on the soil surface
- Reduction of rain use efficiency (annual sum NDVI/annual rainfall)
- Reduction of energy use efficiency (annual sum NDVI/annual accrued temperature)

Most of these indicators directly or indirectly linked with the influence of vegetation which varies with the season, crop, and degree of maturity of the vegetation, soil and climate, and the kind of vegetative material, namely, roots, plant tops, and plant residues. Residue from vegetation protects the surface soil from raindrop impact and recovers the soil structure and organic carbon. Soil erosion can be reduced by control tillage and residue management practices. The major efforts of vegetation in reducing erosion are as follows:

- Surface sealing and runoff are reduced by the interception of rainfall by reducing the raindrop energy.
- Decreased surface velocity retards erosion and nutrient.
- Vegetation cover serves as a physical limit of soil displacement.
- Soil physical properties like porosity, structure, and aggregation are improved by root and crop residue.
- Improve soil biological activity.
- Water stagnation on the soil surface is reduced by plant transpiration and favour for the agroforestry system which reduces runoff and improves the soil storage capacity.
- Vegetation cover checks the evaporation and breaks the capillary rise of water; as a result, salt accumulation is reduced on the surface soil.

Besides vegetation cover, other indicators like inherent soil properties, slope, topographic position, volume, intensity and frequency characteristics of rain, and wind speed influence the degree of degradation.

12.6 Land Degradation Assessment Using RS and GIS Techniques

Degraded land in arid and semiarid regions creates a severe problem. Several researchers (FAO 2005; Lambin and Meyfroidt 2011; Lambin et al. 2013; Gelfand et al. 2013) reported that in many parts of the world, agricultural lands are shrinking and not enough to satisfy the demand of our daily need. Land scarcity becomes more vulnerable under the pressure of population growth especially, in the south-eastern countryside of Asia. In this scenario, degraded lands minimize the land scarcity problem by meeting the demand for food. However, regular monitoring and assessment of these lands in a spatiotemporal scale is a very difficult task. Many different approaches have been adopted by different researchers to monitor its type, extent, degree, rate, and causes; these can be grouped as (1) expert opinion during the survey and used to quantify the area and mapped; (2) biophysical modelling based on auxiliary parameters that indicate the crop productivity, which can be used as a proxy for assessment of degraded land; (3) abandonment of agricultural lands due to some economic, political, and low productive issue—these lands converted to a wasteland. All of these approaches take more time, capital, and labour; and (4) the

satellite-based approach comes to frontline due to the advancement of the satellite, software, and a new algorithm for estimating the area of degraded land and also can be assessed the cause of area extension. But the problem of delineation of degraded land using advanced different RS and GIS techniques has been overcome efficiently and very useful for monitoring purposes (Khan et al. 2005). The different features on the earth's surface can be identified using different RS data (Metternicht and Zinck 2003).

12.6.1 Aerial Image Processing

Colour/or tone, texture, pattern, association, and size of the vegetative canopy on aerial photographs and satellite images help directly or indirectly to detect the type of soil degradation. Among aerial and satellite images, the areal image is the old technique of RS, and even today, it is used intensively for detailed study. To monitor the land degradation (salt-affected lands and waterlogged lands) from a small distance, (fine) resolution imaging/non-imaging sensor is mounted on drone with GPS to scan at a fixed time and space resolution and capture detailed information about degraded land. This areal image is used to confirm the data interpretation along with RS images and served as supplement image (Haseena et al. 2013). Salt-affected soil surface is generally appeared as smoother and discrete patches over normal soil surfaces and gives high reflectance value in VNIR (visible and near-infrared) region (Dehni and Lounis 2012; Srivastava et al. 2017). But in waste or degraded land, the reflection is reduced in the VNIR region (Mandal 2019). However, the aerial photograph will be most useful in conjunction with other ground- and satellite-based RS techniques.

12.6.2 Satellite Image Processing

Land degradation differs from space to space and also with seasons which can be characterized by spatial, spectral, and temporal characteristics of different surface features (Metternicht and Zinck 2008). Defining land degradation and mapping criteria become more difficult when both surfaces, as well as subsurface variability, are considered. Notably, RS and GIS techniques with ground-based sensors are fetching popularize over conventional techniques for its fast assessment and estimation of land degradation for monitoring and mapping purposes. Both passive/active RS sensors are classified as multispectral, hyperspectral, and microwave sensors. Their amalgamation for assessment and prediction of degraded land has defined an extraordinary ability to monitor and map.

12.6.2.1 Multispectral Imagery

Integrated approach (Douaoui et al. 2006; Farifteh et al. 2006a, b; Eldeiry and Garcia 2008) of multispectral sensors (Landsat MSS, TM, ETM+, SPOT-XS, MODIS, Sentinel, Terra-ASTER, IRS-LISS-III and IV, IKONOS, Quick Bird, Hyperion, and World Vision satellite images) with ancillary information like terrain model data, spatial model data, geography survey data, and field information can increase the accuracy of degraded soil mapping (Setia et al. 2013; Rawat et al. 2018). Nowadays, multispectral advanced sensors capture images with fine (<1.0 m) spatial resolution, whereas course spatial with a high-spectral-resolution image can be fused with pan band, which has a fine spatial resolution; in this way, both spatial and spectral resolution of any image can be improved and subsequently become easy to update the information of slight to severe degree of degradation at fine scale in a very economical mode.

There was a 40% increase in salt-affected soils and waterlogged areas observed in Punjab within 5 years using IRS imageries under a project funded by the World Bank (Sethi et al. 2006). GIS platform with RS techniques was utilized for incorporating both non-spatial and spatial attributes, which were recorded from different sources like proximal sensing instrument, traditional laboratory analysis, and other sources to generate the spatiotemporal database and quantification of problem soil-related parameters through multivariate statistical modelling (Singh et al. 2010; Sethi et al. 2014). Digital image processing with visual interpretation and capturing of the spectral signature of salt-affected soils, waterlogged soil, vegetation, crop and sandy soils on multispectral FCC imagery with reference of NDVI (NIR-R/NIR + R), VI (NIR/R), etc. spectral index map are used to discriminate normal and stressed crops. Image classification techniques like maximum likelihood, random forest, and principal component classification with advance PCR, PLSR, and ANN algorithm and black box model (classification tree, regression tree, decision tree, etc.) have been used and optimized for monitoring and mapping of degraded soil (Metternicht and Zinck 2003; Dwivedi et al. 2008).

Waterlogged and salt-affected soils are mainly governed by groundwater quality and its depth. But to monitor the hydrogeological parameter, using RS imagery is very difficult. However, Sander (2007) predicted the depth and availability of water table through lineament analysis on RS imagery along with DEM image analysis using surface and hydrology tools of GIS. Currently, the temporal resolution of the satellite has been improved which helps to monitor the waterlogged status at different seasons. Techniques of RS and GIS become very handy to inaccessible areas within a short time and explore and evaluate the groundwater resources (Chowdhury et al. 2003). Hydrological with RS data had significantly used to explore aquifer geometry, details, and groundwater quality (Jha et al. 2007). Dubey and Sharma (2002) used a factor analytical model to establish a programming system to decide on the groundwater pollution potential with the help of RS, GIS, and auxiliary data. Satellite imagery and ancillary data have used in a GIS-based groundwater prediction model which enabled the prediction of the risk of

salinization by the prediction of groundwater level in the region of Murray Valley Irrigation Region of New South Wales, Australia (Lamble and Fraser 2002).

12.6.2.2 Hyperspectral Imagery

Most broadband data mainly multispectral data, derived from satellite-like Sentinel, AVHRR, IRS, SPOT, Landsat, etc., quantify the reflected radiation at a wide spectral band from surface features. Hyperspectral imagery (narrowband data) capture the reflected radiation at a sequence of 1.0 nm spectral bands. That's why one pixel of the hyperspectral image can supply huge information regarding any surface characteristics due to its high spectral resolution at a 1.0 nm interval, despite 30.0 m spatial resolution (Hyperion). A number of the spectral bands do not prove a sensor as a hyperspectral sensor. The main characteristic of a hyperspectral sensor is that it should be narrow (<10.0 nm) and produce contiguous spectral information. Spectra of soil, vegetation, and mineral have unique absorption drop at a different wavelength (Fig. 12.1a). Absorption peak shifted to higher wavelength with the increase of moisture content (Fig. 12.1b) and reflectance values in same soil are reduced with the increase of volumetric moisture content (Das et al. 2015; Fabre et al. 2015). These unique characteristics of spectra help to identify and quantify different properties of a certain material. Hyperspectral data/images can identify the different field crop canopy, in marginally and severely degraded areas, whereas multispectral images classify different vegetative growth and salinity intensity based on different spectral indices, and mapping of salt-affected soils is prepared maximum based on poor vegetative growth.

12.6.2.2.1 Spectral Libraries

Problem soil measurement using optical sensing (e.g. VNIR, SWIR) involves the fine-tuning of spectra for a degraded soil-related parameter using different multivariate statistical models. Existing spectral libraries (ESLs) and site-specific developed

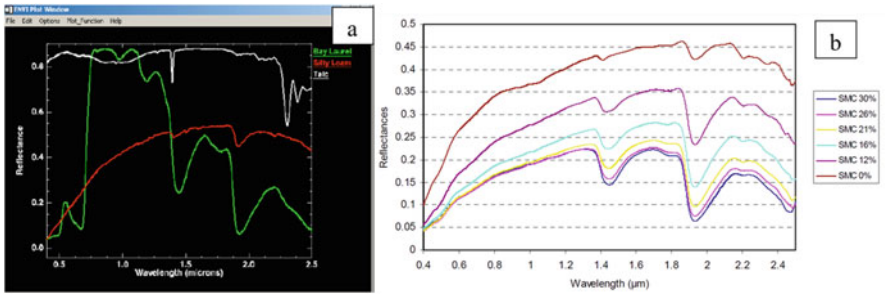

Fig. 12.1 Different spectra recorded by a spectroradiometer (**a**) for a vegetative cover, soil, talc mineral; (**b**) for soil with different moisture content. (Adopted, Fabre et al. 2015)

spectral libraries based on local soil samples (LSLs) are used for model fine-tuning (Shepherd and Walsh 2002; Viscarra Rossel and Webster 2012; Stevens et al. 2013). Nowadays, during the purchase of spectroradiometer, these ESL is supplied with instrumental software, which can be directly used for the prediction of different parameters without any analysis cost, whereas laboratory analysis cost is involved for LSL to develop an accurate (unbiased) local spectral model (Guerrero et al. 2014; Clairotte et al. 2016). Many researchers (Shepherd and Walsh 2002; Brown et al. 2006; Viscarra Rossel et al. 2016) reported that large capital is required to develop a regional-, country-, and global-level soil spectral library; that's why the cost is involved to utilize these developed spectral model for the calibration of the local spectral model. These developed spectral libraries reduce the laboratory analysis cost, time, and labour and make popularize the soil spectroscopy. In India, full-range (350.0–2500.0 nm) soil spectral library was prepared by Saxena et al. (2005) based on collected soil samples from different agroecological zones of the country. Similarly, Das et al. (2015) reported unique spectral characteristics of different soil orders of aridisols, inceptisols, alfisols, vertisols, and laterite soil across India. Vertisols have less reflectance value, whereas inceptisols have high reflectance value due to less clay content. Curcio et al. (2013) reported the all measured reflectance with average values for each soil groups. The soil texture varied from clay to clay loam, loam to sandy loam, and clay to silty clay loam for Pietranera, Dirillo, and Bompensiere soil of Sicily, Italy.

12.6.2.2.2 Methodology of Salt-Affected Soil Characterization and Mapping using HRS

Planning of salt-affected/problem soil mapping is a very difficult task due to the complexity of salt composition and its development process (salinization) along with seasonal and spatial variability. Identification of severely affected salt-affected soils using RS imagery is very easy for high reflectance value, whereas mixed reflectance value is recorded in the case of slight and moderately salt-affected soils for its association with soil, water, and crop canopy cover. New advanced methodology for salt-affected soil mapping and characterization was developed by CSSRI using multispectral, hyperspectral, proximal sensing for ground truth and different linear, non-linear, and black-box modelling of spectra for quantification of parameters. More than 90% of spatial variability of salt-affected soil parameters such as EC_e, saturated extract Cl^-, CO_3^{2-}, HCO_3^-, and Na^+ (me L^{-1}) can be predicted by hyperspectral modelling. Prominent absorption drops of 1.4, 1.9, and 2.2 μm were found in salt-affected soils of Haryana. Absorption drops at 1.9 μm shifted to higher waveband with the increase of salt concentration. The proposed methodology was found useful for delineating salt-affected soils from the space platform (Fig. 12.2).

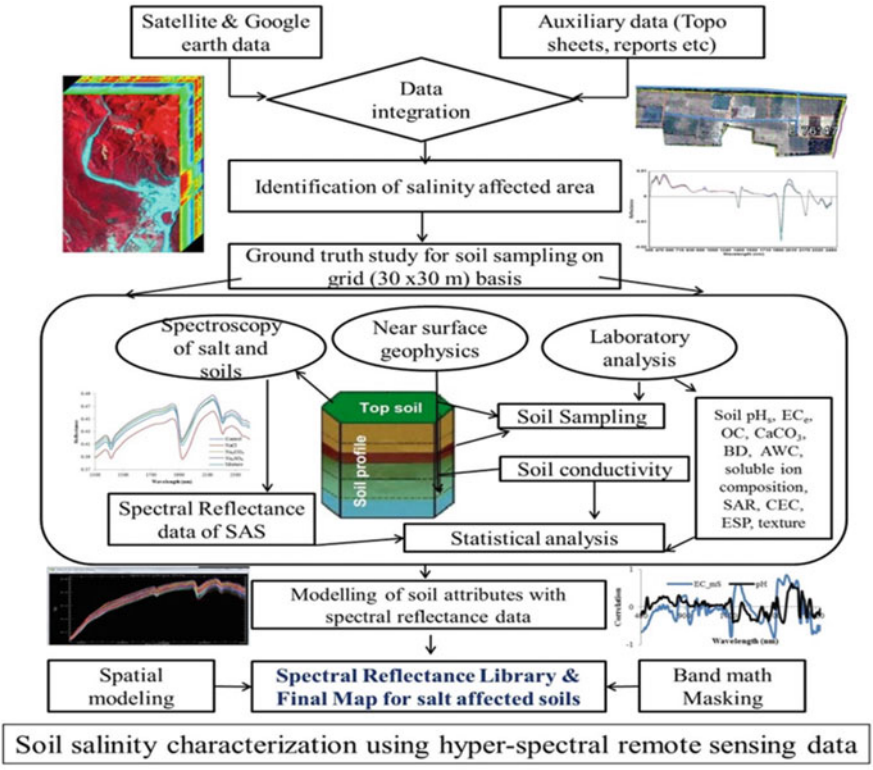

Fig. 12.2 Methodology for characterizing SAS using spectral data. (Adopted, Barman et al. 2017)

12.6.2.2.3 Prediction of Soil Attributes Based on Reflectance Data

Developed spectral models (Shepherd and Walsh 2002; Farifteh et al. 2004, 2006a, b, 2007, 2008; Wang et al. 2012; Mitran et al. 2015; Srivastava et al. 2017) by several workers using soil reflectance values and soil attributes were effectively used to predict different soil parameters. The multivariate spectral model has a huge potential to distinguish the type of land degradation in a precise region (Leone and Sommer 2000). Hyperspectral techniques with multi-temporal images solve the problem of similarity among salt-affected soil, sandy soil, and settlement (Lu et al. 2005; Farifteh et al. 2007). Representative waveband needs to be collected from mixed spectral tones of soil and crop cover to reduce errors in the NIR, red, and green bands, used for FCC image during classification (Rao et al. 1995; Metternicht and Zinck 2003; Farifteh et al. 2006a, b, 2008). Distinctive spectral reflectance in the VNIR region is reduced by hydrated evaporative minerals in salt-affected soils (Farifteh et al. 2008). A significant absorption drop was found at 505, 920, 1415, 1915, and 2205 nm. But there was a difference within the spectra of pure salt and

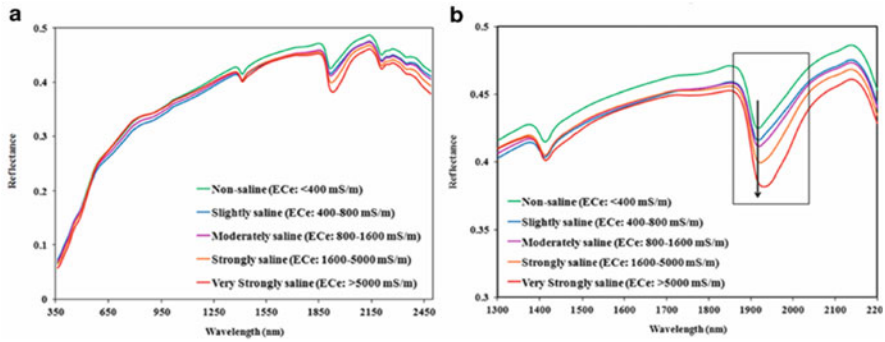

Fig. 12.3 Soil spectra with different salinity classes based on EC_e (dS m^{-1}) in the optical region (**a**) and shifting of absorption drop to higher wavelength with increase of salt concentration (**b**). (Adopted, Srivastava et al. 2017)

mixed salt with soil and/or associated with other minerals. In general, identification of degraded lands on an RS image faces the following problems:

(a) Absence of crust
(b) Mixing of degraded soil signature with others like sand and settlements
(c) Mixing of soil and vegetation cover
(d) Presence of soil moisture

Therefore, indirect mapping of degraded lands based on the vegetative spectral signature, affected by problem soil, increases the accuracy of mapping. Taylor and Dehaan (2000) reported that the decreasing trend of the reflection curve was observed in the NIR region (800–1300 nm). Different types of vegetation like vegetation under stress, narrow or broad leaves, cereal or legume, etc. can be studied using fine spectral resolution (Dehaan and Taylor 2001). High reflectance in the visible region over the NIR region of stressed vegetation (Weiss et al. 2001) helps to identify the different soil-related stress (Tilley et al. 2007). Hyperspectral images, i.e. Hyperion data (Weng et al. 2008), HyMAP (Dehaan and Taylor 2003), ASTER (Melendez-Pastor et al. 2010), and different indices of problem soil such as normalized difference vegetation index (NDVI), salinity index (SI), normalized difference salinity index (NDSI) (Huete 1998; Huete et al. 2003), and soil-adjusted vegetation index (SAVI) using Landsat imagery (Bannari et al. 2008; Jabbar and Chen 2008; Odeh and Onus 2008) can identify the different category of SAS. Kumar et al. (2015) showed a significant coefficient of determination ($R^2 > 0.75$) with soil salinity-related parameter (EC_e, SAR, and ESP). In India, NBSS&LUP (2006) developed a national soil spectral library, including problem soils, and this library can be used to increase the precision of degraded soil map. Srivastava et al. (2017) showed the effect of different salt concentrations based on EC_e (mS m^{-1}) in the optical region on soil spectral signature (Fig. 12.3a). The variation of absorption peak (on first derivative spectra) was more prominent at 1.4, 1.9, and 2.2 μm. There was a shifting of

absorption drop to a higher wavelength with an increase of salt concentration at 1.9 μm (Fig. 12.3b).

12.6.2.3 Microwave Sensors in Land Degradation Assessment

Microwave RS, i.e. synthetic aperture radar (SAR) data, has huge potential in the delineation of saline/sodic and waterlogged soils despite cloudy weather conditions (Metternicht 1998; Bell et al. 2001; Metternicht and Zinck 2003). The information from the SAR image has huge potential in the mapping of environmental change. The microwave RS (backscattering) works based on the principle of dielectric constant-polarization (Engman 1991), the roughness of features, wavelength or frequency (Evans et al. 1992), slope, and orientation, i.e. look angle. The results of small perturbation model (SPM), physical optics (PO), semi-empirical polarimetric model (SEPM), Dubois model (DM), and other algorithms were compared with soil texture, salinity, frequency, moisture content, and vegetation canopy parameters to estimate imaginary part of the dielectric constant of soil. The real part of the radar backscattering model is associated with moisture content, whereas the imaginary part is responsible for salt concentration. These soil properties depend on the backscattering coefficient which depends on the dielectric constant of soil, and this dielectric property depends on free water, bound water, air, and soil solids. Soil salinity mainly depends on free water content. Low-frequency (L-band or high-wavelength) microwave RS (active/passive) is best for the mapping of surface salt-affected soil (Dongryeol 2003). The sensitivity of imaginary soil dielectric constant proportionately correlates with salinity and moisture (Sreenivas et al. 1995). Jain (2011) measured the dielectric constant by inversed co-polarized techniques from SAR images and reported that this technique identifies soil salinity (EC) in Unnao district of Uttar Pradesh, India. The derived radar attributes have also potential in the mapping of degraded soil in an irrigated condition of Chubut, Argentina (Del Valle et al. 2009). There is a possibility to differentiate the salinity from sodicity using L waveband under wet soil regimes. Long wavelength of microwave RS can penetrate soil and vegetation. The soil penetration depends on profile moisture, but long wavelength, i.e. P (30.0–100.0 cm wavelength) and L bands (15.0–30.0 cm wavelength), has high energy to penetrate the feature over C band (3.8–7.5 cm wavelength) (Bell et al. 2001; Lasne et al. 2008). These SAR images are validated using radiometers (ground-based microwave) for the study of degraded soils. Chakraborty et al. (2013) enlisted the area of applicability of Indian radar satellite (RISAT-1) with HH, VV, HV, and VH polarizations, and these are vegetation, crop monitoring, flood mapping, salinity monitoring, degraded soil mapping, forestry study, soil moisture study, estimation of rice productivity, geology study, sea ice, and coastal monitoring.

12.6.3 Ground-Based Sensing

Data from space-based satellite images can be validated by ground-based imaging/non-imaging data. These ground-based advanced electronic sensors and other proximal devices such as electromagnetic/electrical probes, time-domain reflectometry—TDR (emissivity), resistivity tool, salinity and moisture sensors (electrochemical), chlorophyll meter (optical), and ground-penetrating radar with GPS devices are used to record data from less height of the feature surface at the field for the mapping and monitoring of degraded status. Ground-penetrating radar and TDR are indirectly linked with soil surface/underground moisture and salt concentration. These handy tools are very cost-effective (Aldabaa et al. 2015) and can be mapped and/or in situ monitor based on an empirical site-specific model of infiltration and profile moisture (French and Binley 2004; Jayawickreme et al. 2008), EC, and resistivity model (Slater and Sandberg 2000; Kemna et al. 2002) with less time and capital (Hamed et al. 2003; Robinson et al. 2003). The ground-penetrating radar (for groundwater survey) can sense the little variation in salt and water movement at $<$30.0 m soil depth (Ludwig et al. 2011); however, this tool shows its difficulty in soil with EC $>$ 4.0 dS m^{-1} and SAR $>$ 13.0 due to high attenuation of backscattering. Goldshleger et al. (2010) generated a 3D map of land degradation in cropland using hyperspectral RS, frequency-domain electromagnetic induction (FDEM). and ground-based radar data. Sethi et al. (2014) estimated soil and plant properties using IRS and ground data to manage the problem soils of Haryana, India. Multispectral image with DEM gives more information regarding paleo-drainage patterns, sunken area, playas, and catchment areas which are very useful to estimate the water accumulation, recharging potential during heavy rainfall (Kwarteng 2002). Guo et al. (2015) reported that backscattering coefficient from HH polarization of ALOS/PALSAR radar imagery and apparent electrical conductivity (EC_a) value of EM38 sensor were imported to ArcGIS platform to perform the spatial model with a geostatistical tool to know the variability of moisture and salt concentration of soil, respectively, in reclaimed coastal of south Hangzhou Gulf. Traditional laboratory determination of salinity and sodicity are costly and laborious and requires intensive time to get desired information. Electromagnetic (EM) induction techniques are nowadays widely used as an alternative tool for collecting information on soil properties relevant to salinity and sodicity. Recently, in India, geophysical EM induction techniques were used to characterize soil salinity and their extent and represent soil salinity three-dimensionally (Narjary et al. 2017, 2019; Koganti et al. 2018). But lots of research is required to standardize and development of models to get its effective application for degradation land mapping and monitoring.

12.6.4 Methodology of Land Degradation Mapping: Visual Interpretation and Digital Approaches

Multispectral imageries of three different crop growing periods (*kharif*, *rabi*, and *zaid*) can be used as input to identify the seasonal variation of land degradation (Fig. 12.4) using an on-screen digitization technique (SAC 2016; NRSC 2020). These satellite data are processed in image processing software with the help of image enhancement, visual interpretation, spectral ratio, and ancillary information/ legacy data as thematic maps, existing LULC, wasteland map, and other printed material. Satellite image processing and interpretation are very important for the identification of ground-truth sample collection. Different types of land degradation can be visually identified based on colour/tone, texture, pattern, size, shape, and association (explained in Sect 12.3.4). Collected soil samples are analysed for pH_s, EC_e texture, organic carbon, exchangeable cation and anion, $CaCO_3$ percentage, etc. These are used to develop the final land degradation map after the validation and accuracy assessment.

However, various digital approaches have also been adopted for qualitative and quantitative assessment of degraded soils by various researcher across the world

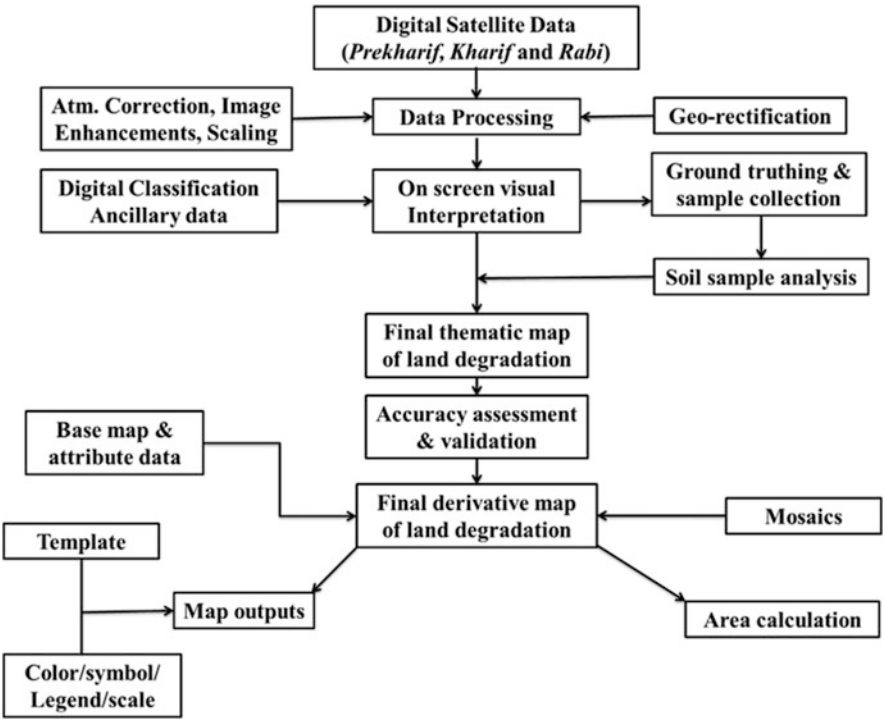

Fig. 12.4 Methodology of land degradation mapping. (Modified, Ravishankar and Sreenivas 2010)

Table 12.5 Methodology and remote sensing data used in different studies for land degradation assessment

Land degradation processes	Study area	Method	Data used	References
All land degradation processes	India	On-screen visual interpretation along with soil sample analysis	IRS AWiFS (1:500 K)	SAC (2016)
All land degradation processes	India	On-screen visual interpretation along with soil sample analysis	LISS-III (1:50 K)	NRSC (2015, 2020)
Soil salinity Mapping	Bhavnagar, Gujarat	Spectral angle mapper algorithm	Hyperion data	Mitran et al. (2015)
Soil moisture and salinity stress	Dharmapuri, India	Microwave and multispectral model	Radar Imaging Satellite and Landsat data	Periasamy and Shanmugam (2017)
Surface waterlogging	Rohtak, India	Thresholding of NDWI for optical image and Sigma0 for SAR images	Sentinel 2 MSS images and Sentinel 1A SAR images	Kaushik et al. (2018)
Dynamics of waterlogged area	Bangladesh	Random forest classification based on training pixel	Landsat imageries (Time series)	Islam et al. (2018)
Saline soil map	SE Spain	Matched filtering (MF) and mixture-tuned MF	ASTER Images	Melendez-Pastor et al. (2010)
Hydro saline land degradation	Faisalabad, Pakistan	Salinity indices and digital image processing	IRS-1B	Khan et al. (2005)
Salinity stress	Hakim Farabi Farming in Iran	Hyperspectral vegetation indices	Hyperion image	Hamzeh et al. (2013)
Wind erosion hazard mapping	Laghouat region (Algeria)	Fuzzy logic approach	Landsat 8 OLI images	Saadoud et al. (2018)
Soil wind erosion	Inner Mongolia, China	Improved AHP and a weighted summation method	AVHRR and MODIS NDVI	Zhou et al. (2015)
Acid sludge concentration in soil	Balikpapan, East Kalimantan (Indonesian)	NDVI method	Landsat images	Haryani et al. (2017)
Acid mine drainage map	Mpumalanga Province of South Africa	Spectral signatures of jarosite and haematite	Landsat 8	Sakala et al. (2017)
Trace metal content in Soils	New York	Correlation analysis (surrogate)	ASD data	Wu et al. (2010)

(continued)

Table 12.5 (continued)

Land degradation processes	Study area	Method	Data used	References
Soil loss by water erosion	Australia	Factors of RUSLE estimation to model soil loss by water erosion	SRTM and MODIS data	Teng et al. (2016)
Deforestation detection	Viti Levu Island, Fiji	MulTiFuse approach for detecting deforestation	Landsat and SAR time series	Reiche et al. (2015)

(Table. 12.5). They have used multispectral, hyperspectral, and microwave satellite datasets to map degraded soil through different modelling techniques. A number of researchers have used various hyperspectral based indices and algorithm to assess and map soil salinity at regional scale (Melendez-Pastor et al. 2010; Hamzeh et al. 2013; Mitran et al. 2015). Saadoud et al. (2018) generated wind erosion hazard map at Laghouat region in Algeria using Landsat 8 OLI data using the fuzzy logic approach. Teng et al. (2016) assessed soil loss by water erosion in Australia using SRTM and MODIS data using an universal soil loss equation. Dynamics of waterlogged area was mapped by Islam et al. (2018) using Landsat time-series datasets through random forest classification technique. Kaushik et al. (2018) were used NDWI thresholding method on optical image and SAR images of Sentinel 1 and 2 to map surface waterlogging in parts of Rohtak, Haryana, India.

12.6.5 Assessing Spatial and Temporal Pattern of Salt-Affected Soils: A Case Study

12.6.5.1 Study area

An experiment was conducted by CSSRI in the Nain experimental farm of Panipat, Haryana (between 29°18′37.93″N longitude to 29°19′20.86″N latitude and 76°47′08.62″N longitude and 76°48′21.79″E longitude) states of India to study the changing pattern of salinity/sodicity through RS and GIS using field-based observation.

12.6.5.2 Data and Methodology

The high temporal resolution of any satellite images helps to monitor the extent and pattern of degraded land over a time period in a specific region. Hence, different seasonal satellite datasets of years 2011–2012 and 2017–2018 (here, IRS LISS III and Landsat satellite imageries) of a year were collected and corrected by the removal of the effects of sun elevation angle, atmospheric influences, and normalization of radiometric differences for comparing the land degradation. The satellite

data was used to identify the salt-affected soils at the study site through visual interpretation technique. After the identification of the area, the soil samples were collected. The sampling time and weather condition have a great impact on the increment of area. Hence, the surface (0–15 cm) soil samples were collected during April–May during 2011–2012 and 2017–2018, and that time salt has been accumulated to the surface due to high evaporative demand during hot dry weather condition.

The soil samples were analysed for pH_s and EC_e using standard protocols. The spatial interpolation technique, i.e. ordinary kriging, was used to create spatial soil pH_s and EC_e map of the experimental site for 2011–12 and 2017–18. Both the maps were used to assess the changes in soil salinity and sodicity over 6 year period.

12.6.5.3 Salient Findings

The spatial pattern of EC_e and pH_s of the study site is presented in Fig. 12.5. Results of the study show that the extent of soil salinity increased by 8.3 and 15.8% (Table 12.6) over 6 years period in moderate (EC_e 8.0–30.0 dS m^{-1}) and strong ($EC_e > 30.0$ dS m^{-1}) salinity region, respectively, whereas, the extent of pH_s increased by 28.9 and 20.3% (Table 12.6) over 6 years period, in the region where pH_s ranges from 8.2–8.5 and > 8.5, respectively.

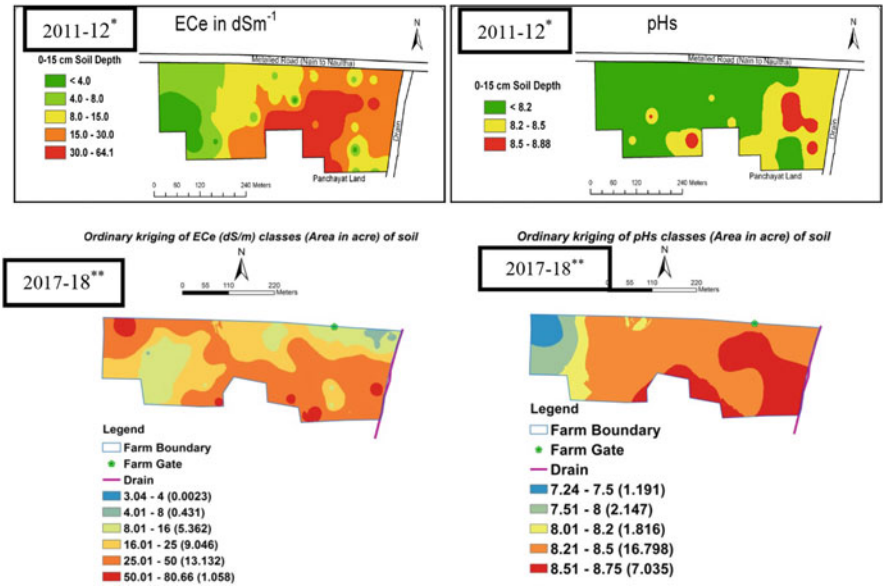

Fig. 12.5 Changes of salinity/sodicity after 6 years. (Adopted, *Mandal et al. 2013 and **CSSRI 2018)

Table 12.6 Changes of surface soil salinity and sodicity over 6 years

Soil properties	Range in property	Percent of the total area (2011–12*)	Percent of the total area (2017–18)	Δ_6% area
pH_s	<8.2	67	17.8	49.2
	8.2–8.5	29	57.9	(+) 28.9
	>8.5	4	24.3	(+) 20.3
EC_e (dS m^{-1})	<4.0	8.7	0.01	8.69
	4.0 to 8.0	16.9	1.49	15.41
	8.0 to 15.0	25.4	15.4	10
	15.0–30.0	31.2	49.5	(+) 18.3
	>30	17.8	33.6	(+) 15.8

Adopted, CSSRI (2018) and *Mandal et al. (2013)

12.7 Conclusions and Future Perspectives

Remotely sensed data become more efficient when it combines with numerical modelling. Predictive models to estimate degraded soil-related parameters are empirical and site-specific in nature and have limited applicability beyond the area of development, but for qualitative assessment of degraded soil for mapping, monitoring and some management practices can be done using multispectral imagery, and its accuracy can be improved by using hyperspectral, radar, and ground-based sensor. So, there is a need to develop methodologies for rapid detection and mapping of salt-affected soil by integrating satellite RS with ground-based proximal sensors. Ground truthing is a must for removing the confusion of mixed pixel or signatures and also used for accuracy assessment in the mapping of degraded soil. All spectral, GPS, and ground-based sensor data are imported to a GIS platform which provides an efficient handling and management system for handling large and complex databases for land degradation assessment studies. Predicting warmer temperatures, change of rainfall distribution pattern and intensity, rising sea level, etc. leads to a change in the extent of degraded land. Therefore, monitor and assessment of degraded soil of any country becomes a flagship program after a minimum of 3–5 years interval due to a change of climatic scenarios. With the growing interest on high-resolution satellite imagery data applicability, rapid assessment of soil salinity, sodicity, acidity, waterlogged, and wasteland through visual and digital models that are encouraging as it assists in real-time precise monitoring of degraded soil over the spatiotemporal context and also helps in the collection of spectral signature, facilitating the farmers to manage more effectively and efficiently based on the mobile-based decision support system in regional language. As a new step of the digital era, digital soil mapping of a country gives the detailed information of each point of the map and stored spectral library in Web-GIS server help to retrieve any information or parameters related to degraded soils. The collaboration of different sensors (e.g. optical, microwave, and

thermal sensors) and platforms (e.g. ground-based, air-based, and space-based sensing) improves the accuracy and reproducibility of degraded soil map in time. In 2015, United Nations Convention to Combat Desertification (UNCCD) has developed Land Degradation Neutrality (LDN) programme in collaboration with multiple international partners (over 120 countries) and committed to setting LDN targets, and out of these, 80 countries have already set their target. The LDN target follows the Sustainable Development Goal (SDG) target 15.3 which states to achieve a land degradation-neutral world by combating desertification and restoration of degraded land and soil by 2030. In this scenario India sets its target to restore degraded lands from 21 Mha to 26 Mha, by 2030 (Press Information Bureau, Ministry of Environment, Forest and Climate Change, GOI, 2019). Geospatial techniques can play a meaningful role in support to achieve LDN target through the qualitative and quantitative assessment of land resources which are necessary to the ecosystem functions and services and enhance food security and production by the reclamation and restoration process.

Acknowledgements The authors are thankful to PME (No.-Research Article/83/2019) and Director, ICAR-Central Soil Salinity Research Institute, Karnal, Haryana, and Head of Soil and Crop Management for sustain encouragement for writing the chapter. The authors also gratefully acknowledge Dr s. Madhurama Sethi, Rajeev Srivastava and AK Mandal for their constructive support.

References

Aldabaa AAA, Weindorf DC, Chakraborty S, Sharma A, Li B (2015) Combination of proximal and remote sensing methods for rapid soil salinity quantification. Geoderma 239–240:34–46

Bannari A, Guedona AM, El-Hartib A, Cherkaouic FZ, El-Ghmari A (2008) Characterization of slightly and moderately saline and sodic soils in irrigated agricultural land using simulated data of advanced land imaging (EO-1) sensor. Commun Soil Sci Plant Anal 39(19–20):2795–2811

Barman A, Mandal AK, Srivastava R, Yadav RK, Sharma PC (2017) Soil salinity characterization using hyper-spectral remote sensing data. ICAR News 23(4):11–12

Basak N, Mandal B (2019) Soil quality management through carbon farming under intensive agriculture systems. Indian J Fertil 14(12):54–64

Basak N, Datta A, Mandal A, Ghoshal SK, Mandal B (2014) Improving quality and resilience of soils under rice-based cropping systems. Indian Farming 64(1):10–13

Basak N, Barman A, Sundha P, Rai AK (2020) Recent trends in soil salinity appraisal and management. In: Rakshit A, Ghosh S, Chakraborty S, Philip V, Datta A (eds) Soil analysis: recent trends and applications. Springer, Singapore, pp 143–162

Bell D, Menges C, Ahmad W, Van Zyl JJ (2001) The application of dielectric retrieval algorithms for mapping soil salinity in a tropical coastal environment using airborne polarimetric SAR. Remote Sens Environ 75:375–384

Bhattacharyya R, Ghosh BN, Mishra PK, Mandal B, Rao CS, Sarkar D, Das K, Anil KS, Lalitha M, Hati KM, Franzluebbers AJ (2015) Soil degradation in India: challenges and potential solutions. Sustainability 7:3528–3570

Bindraban PS, van der Velde M, Ye L, van den Berg M, Materechera S, Kiba DI, Tamene L, Ragnarsdóttir KV, Jongschaap R, Hoogmoed M, Hoogmoed W (2012) Assessing the impact of soil degradation on food production. Curr Opin Environ Sustain 4(5):478–488

Bridges EM, Oldeman LR (1999) Global assessment of human induced soil degradation. Arid Soil Res Rehabil 13(4):319–325

Brown DJ, Shepherd KD, Walsh MG, Dewayne MM, Reinsch TG (2006) Global soil characterization with VNIR diffuse reflectance spectroscopy. Geoderma 132(3–4):273–290

Cai X, Zhang X, Wang D (2011) Land availability for biofuel production. Environ Sci Technol 45 (1):334–339

Chakraborty M, Panigrahy S, Rajawat AS, Kumar R, Murthy TVR, Haldar D, Chakraborty A, Kumar T, Rode S, Kumar H, Mahapatra M, Kundu S (2013) Initial results using RISAT-1 C-band SAR data. Curr Sci 104(4):491–501

Cherlet M, Hutchinson C, Reynolds J, Hill J, Sommer S, von Maltitz G (2018) World atlas of desertification. Publication office of the European Union, Luxembourg

Chowdhury A, Jha MK, Machiwal D (2003) Application of remote sensing and GIS in groundwater studies: an overview. In: Proceedings of the International Conference on Water & Environment (WE-2003), Ground Water Pollution, December 15–18, MP, India, pp 39–50

Clairotte M, Grinand C, Kouakoua E, Thebault A, Saby NPA, Bernoux M, Barthes BG (2016) National calibration of soil organic carbon concentration using diffuse infrared reflectance spectroscopy. Geoderma 276:41–52

CSSRI (2018) Annual Report 2017–18. Central Soil Salinity Research Institute, Karnal, India

Curcio D, Ciraolo G, D'Asaro F, Minacapilli M (2013) Prediction of soil texture distributions using VNIR-SWIR reflectance spectroscopy. Procedia Environ Sci 19(494):494–503

Das BS, Sarathjith MC, Santra P, Sahoo RN, Srivastava R, Routray A, Ray SS (2015) Hyperspectral remote sensing: opportunities, status and challenges for rapid soil assessment in India. Curr Sci 10:860–868

Dehaan RL, Taylor GR (2001) Mapping irrigation-induced salinity with hyperspectral imagery. In: Proceedings of the international geoscience and remote sensing symposium, IGARSS '01, IEEE International, pp 293–295

Dehaan R, Taylor GR (2003) Image-derived spectral end members as indicators of salinization. Int J Remote Sens 24(4):775–794

Dehni A, Lounis M (2012) Remote sensing techniques for salt affected soil mapping: application to the Oran region of Algeria. Procedia Eng 33:188–198

Del Valle HF, Blanco PD, Sione W, Rostagno CM, Elissalde N (2009) Assessment of salt affected soils using multisensory radar data-a case study from Northeastern Patagonia (Argentina). In: Metternicht G, Zinck JA (eds) Remote sensing of soil salinization: impact on land management. CRC Press, Boca Raton, pp 155–173

Dongryeol R (2003) Microwave emission of high-saline soils. Lecture at Merit Melbourne Engineering Research Institute, Melbourne

Douaoui AEK, Nicolas H, Walter C (2006) Detecting salinity hazards within a semiarid context by means of combining soil and remote-sensing data. Geoderma 134(1–2):217–230

Dregne HE, Chou NT (1992) Global desertification dimensions and costs. Degradation & Restoration of Arid Lands:73–92

Dubey OP, Sharma DC (2002) Integrated remote sensing and factor analytic GIS model for evaluating groundwater pollution potential

Dwivedi RS, Kothapalli RV, Singh AN (2008) Generation of farm level information on salt-affected soils using IKONOS-II multispectral data. In: Metternicht G, Zinck JA (eds) Remote sensing of soil salinization: impact on land management. CRC Press, Taylor & Francis, Boca Raton

Eldeiry A, Garcia LA (2008) Detecting soil salinity in alfalfa fields using spatial modeling and remote sensing. Soil Sci Soc Am J 72(1):201–211

Engman ET (1991) Applications of microwave remote sensing of soil moisture for water resources and agriculture. Remote Sens Environ 35:213–226

Evans DL, Farr TG, Van Zyl JJ (1992) Estimates of surface roughness derived from synthetic aperture radar (SAR) data. IEEE Trans Geosci Remote Sens 30(2):382–389

Fabre S, Briottet X, Lesaignoux A (2015) Estimation of soil moisture content from the spectral reflectance of bare soils in the 0.4–2.5 μm domain. Sensors 15(2):3262–3281

FAO (2005) The state of food insecurity in the world 2005: Eradicating world hunger e key to achieving the millennium development goals

FAO (2011) The State of the World's Land and Water Resources for Food and Agriculture (SOLAW): managing systems at risk. FAO, Rome, p 50

Farifteh J, Bouma A, Van Der Meijde M (2004) A new approach in the detection of salt affected soils; integrating surface and subsurface measurements. Poster presented at "Near surface 2004", 10th EAGE European Meeting of Environmental and Engineering Geophysics, Utrecht, The Netherlands

Farifteh J, Van der Meer F, Carranza EJM (2006a) Similarity measures for spectral discrimination of salt-affected soils. Int J Remote Sens 28:5273–5293

Farifteh J, Farshada A, George RJ (2006b) Assessing salt-affected soils using remote sensing, solute modelling, and geophysics. Geoderma 130:191–206

Farifteh J, Van Der Meer F, Atzberger C, Carranza EJM (2007) Quantitative analysis of salt affected soil reflectance spectra: a comparison of two adaptive methods (PLSR and ANN). Remote Sens Environ 110:59–78

Farifteh J, Van Der Meer F, Van Der Meijde M, Atzberger C (2008) Spectral characteristics of salt-affected soils: a laboratory experiment. Geoderma 145:196–206

Foley JA, DeFries R, Asner GP, Barford C, Bonan G, Carpenter SR, Chapin FS, Coe MT, Daily GC, Gibbs HK, Helkowski JH (2005) Global consequences of land use. Science 309 (5734):570–574

Food and Agriculture Organization (2008) The state of food and agriculture, Biofuels: Prospects, risks and opportunities, pp 1–138

French H, Binley A (2004) Snowmelt infiltration: monitoring temporal and spatial variability using time-lapse electrical resistivity. J Hydrol 297:174–186

Gao J, Liu Y (2010) Determination of land degradation causes in Tongyu County, Northeast China via land cover change detection. Int J Appl Earth Obs Geoinform 12(1):9–16

Gelfand I, Sahajpal R, Zhang X, Izaurralde RC, Gross KL, Robertson GP (2013) Sustainable bioenergy production from marginal lands in the US Midwest. Nature 493(7433):514–517

Gibbs HK, Salmon JM (2015) Mapping the world's degraded lands. Appl Geogr 57:12–21

Gibbs HK, Ruesch AS, Achard F, Clayton MK, Holmgren P, Ramankutty N, Foley JA (2010) Tropical forests were the primary sources of new agricultural land in the 1980s and 1990s. Proc Natl Acad Sci 107(38):16732–16737

Goldshleger N, Ben-Dor E, Lugassi R, Eshel G (2010) Soil degradation monitoring by remote sensing: examples with three degradation processes. Soil Sci Soc Am J 74:1433–1445

Guerrero C, Stenberg B, Wetterlind J, Viscarra Rossel RA, Maestre FT, Mouazen AM, Zornoza R, Ruiz-Sinoga JD, Kuang B (2014) Assessment of soil organic carbon at local scale with spiked NIR calibrations: effects of selection and extra weighting on the spiking subset. Eur J Soil Sci 65:248–263

Guo Y, Shi Z, Huang J, Zhou L, Zhou Y, Wang L (2015) Characterization of field scale soil variability using remotely and proximally sensed data and response surface method. Stoch Environ Res Risk Assess, Springer, Berlin/Heidelberg

Hamed Y, Persson M, Berndtsson R (2003) Soil solution electrical conductivity measurements using different dielectric techniques. Soil Sci Soc Am J 67:1071–1078

Hamzeh S, Naseri AA, Alavipanah SK, Mojaradi B, Bartholomeus HM, Clevers JG, Behzad M (2013) Estimating salinity stress in sugarcane fields with spaceborne hyperspectral vegetation indices. Int J Appl Earth Obs Geoinform 21:282–290

Haryani NS, Sulma S, Pasaribu JM (2017) Detection of acid sludge contaminated area based on Normalized Difference Vegetation Index (NDVI) value. Int J Remote Sens Earth Sci 11 (1):21–32

Haseena HK, Kiran BR, Shankar MK (2013) Application of aerial photography & remote sensing in environmental and geological interpretations in India-An Overview. Int J Environ Biol 3 (3):100–114

Holm A, Cridland S, Roderick M (2003) The use of time-integrated NOAA NDVI data and rainfall to assess landscape degradation in the arid shrub land of Western Australia. Remote Sens Environ 85(2):145–158

Huete AR (1998) A soil-adjusted vegetation index (SAVI). Remote Sens Environ 25:295–309

Huete A, Miura T, Gao X (2003) Land cover conversion and degradation analyses through coupled soil–plant biophysical parameters derived from Hyperspectral EO-1 Hyperion. IEEE Trans Geosci Remote Sen 41:1268–1276

IPES-Food (2019) From uniformity to diversity: a paradigm shift from industrial agriculture to diversified agro-ecological systems. International Panel of Experts on Sustainable Food Systems. http://www.ipes-food.org/img/upload/files/UniformityToDiversityFULL

Islam MR, Abdullah HM, Ahmed ZU, Islam I, Ferdush J, Miah MG, Miah MM (2018) Monitoring the spatiotemporal dynamics of waterlogged area in southwestern Bangladesh using time series Landsat imagery. Remote Sens Appl Soc Environ 9:52–59

Jabbar MT, Chen X (2008) Land degradation due to salinization in arid and semi-arid regions with the aid of geo-information techniques. Geo-Spatial Inform Sci 11(2):112–120

Jain R (2011) Feasibility study on potential use of microwave SAR data in soil salinity induced land degradation assessment. M.Tech thesis, Andhra University, pp 1–97

Jayawickreme DH, Van Dam RL, Hyndman DW (2008) Subsurface imaging of vegetation, climate, and root-zone moisture interactions. Geophys Res Lett 35(18)

Jha MK, Chowdhury A, Chowdary VM, Peiffer S (2007) Groundwater management and development by integrated remote sensing and geographic information systems: prospects and constraints. Water Resour Manag 21(2):427–467

Kaushik S, Dhote PR, Thakur PK, Aggarwal SP (2018) Assessing the impact of canal network on surface waterlogging using remote sensing datasets in Rohtak district, Haryana. Int Arch Photogramm Remote Sens Spatial Inform Sci XLII-5:261–266

Kemna A, Vanderborght J, Kulessa B, Vereecken H (2002) Imaging and characterisation of subsurface solute transport using electrical resistivity tomography (ERT) and equivalent transport models. J Hydrol 267:125–146

Khan NM, Rastoskuev VV, Sato Y, Shiozawa S (2005) Assessment of hydrosaline land degradation by using a simple approach of remote sensing indicators. Agric Water Manag 77:96–109

Kniivila M (2004) Land degradation and land use/cover data sources. Working Document. United Nations: Department of Economic and Social Affairs, Statistics Division

Koganti T, Najary B, Pathan A, Huang J, Triantafilis J (2018) Quantitative mapping of soil salinity using the DUALEM -21S instrument and EM inversion software. Land Degarad Dev 29:1768–1781

Kumar S, Ghosh G, Saha SK (2015) Hyperspectral remote sensing data derived spectral indices in characterizing salt-affected soils: a case study of Indo-Gangetic plains of India. Environ Earth Sci 73(7):3229–3308

Kwarteng AY (2002) Utilization of remote sensing and GIS for groundwater exploration. In: Singh S, Al-Rashed M (eds) Kuwait Sherif. Groundwater hydrology, Balkema, pp 157–178

Lal R (2011) Soil carbon sequestration. SOLAW background thematic report- TR04B, Food and Agriculture Organization of the United Nations, Rome, p 36

Lal R, Stewart BA (1990) Soil degradation: a global threat. Adv Soil Sci 11:XIII–XVIII

Lambin EF, Meyfroidt P (2011) Global land use change, economic globalization, and the looming land scarcity. Proc Natl Acad Sci 108(9):3465–3472

Lambin EF, Gibbs HK, Ferreira L, Grau R, Mayaux P, Meyfroidt P, Morton DC, Rudel TK, Gasparri I, Munger J (2013) Estimating the world's potentially available cropland using a bottom-up approach. Glob Environ Chang 23(5):892–901

Lamble P, Fraser D (2002) Creation of a GIS-based predictive model for groundwater in the Murray Valley irrigation region (NSW). Cartography 31(1):33–44

Lasne Y, Paillou P, Ruffie G, Serradilla C, Demontoux F, Freeman A, Farr T, Mcdonald K, Chapman B, Malezieu X (2008) Effect of salinity on the dielectric properties of geological materials: implication for soil moisture detection by means of remote sensing. IEEE Trans Geosci Remote Sens 46(6):1674–1688

Leone AP, Sommer S (2000) Multivariate analysis of laboratory spectra for the assessment of soil development and soil degradation in the Southern Apennine (Italy). Remote Sens Environ 72:346–359

Lu N, Zhang Z, Gao Y (2005) Recognition and mapping of soil salinization in arid environment with hyperspectral data. Proc. IGARSS 2005. IEEE Int 6:4520–4523

Ludwig R, Gerhards H, Klenk, P, Wollschläger U, Buchner J (2011) Electromagnetic methods in applied geophysics. Institute of Environmental Physics, Heidelberg University, p 1–59

Mandal AK (2019) Modern technologies for diagnosis and prognosis of salt-affected soils and poor-quality waters. In: Dagar J, Yadav R, Sharma P (eds) Research Developments in Saline Agriculture. Springer, Singapore, pp 95–152

Mandal AK, Sharma RC, Singh G, Dagar JC (2010) Computerized database on salt affected soils in India, Technical Bull./2/2010. CSSRI, Karnal, p 28

Mandal AK, Sethi M, Yaduvanshi NPS, Yadav RK, Bundela DS, Chaudhari SK, Anil C, Sharma DK (2013) Salt affected soils of Nain experimental farm: site characteristics, reclaimability & potential use. Tech Bull, CSSRI, Karnal 03:34

Meena RS, Mitran T, Kumar S, Yadav G, Bohra JS, Datta R (2018) Application of remote sensing for sustainable agriculture and forest management. Informat Proc Agric 5:295–297

Melendez-Pastor I, Navarro-Pedreño J, Koch M, Gómez I (2010) Applying imaging spectroscopy techniques to map saline soils with ASTER images. Geoderma 158:55–65

Metternicht GI (1998) Fuzzy classification of JERS-1 SAR data: an evaluation of its performance for soil salinity mapping. Ecol Model 111:61–74

Metternicht GI, Zinck JA (2003) Remote sensing of soil salinity: potentials and constraints. Remote Sens Environ 85:1–20

Metternicht GI, Zinck JA (eds) (2008) Remote sensing of soil salinization: impact on land management. CRC Press, Taylor & Francis, Boca Raton, p 377

Mitran T, Ravisankar T, Fyzee MA, Suresh JR, Sujatha G, Sreenivas K (2015) Retrieval of soil physicochemical properties towards assessing salt-affected soils using Hyperspectral Data. Geocarto Int 30(6):701–721

Mitran T, Lal R, Mishra U, Meena RS, Ravisankar T, Sreenivas K (2018) Climate change impact on soil carbon stocks in India. In: Lal R, Stewart BA (eds) Advances in soil science, Soil and climate, pp 291–308

NAAS (2017) Mitigating land degradation due to water erosion. Policy Paper No. 88 National Academy of Agricultural Sciences, New Delhi, p 20

Narjary B, Jangra P, Abhishek R, Kumar N, Raju R, Thimappa K, Meena RL, Kumar S, Kumar P, Chichmatalpure AR, Kamra SK (2017) Quantitative assessment of soil salinity using electromagnetic induction technique and geostatistical approach. J Soil Salin Water Qual 9:156–166

Narjary B, Meena MD, Kumar S, Kamra SK, Sharma DK, Triantafilis J (2019) Digital mapping of soil salinity at various depths using an EM38. Soil Use Manag 35:232–244

NBSS&LUP (2006) Soils of India. NBSS Pub. 94. National Bureau of Soil Survey and Land Use Planning, Nagpur, India

NRSC (2010) Wasteland Atlas of India. National Remote Sensing Centre, ISRO, Hyderabad, p 140

NRSC (2015) Land degradation Atlas of India. National Remote Sensing Centre, ISRO, Hyderabad

NRSC (2020) Land degradation Atlas of India. National Remote Sensing Centre, ISRO, Hyderabad

Odeh IO, Onus A (2008) Spatial analysis of soil salinity and soil structural stability in a semiarid region of New South Wales, Australia. Environ Manag 42(2):265

Oldeman LR, Hakkeling RTA, Sombroek WG (1991) World map of the status of human-induced soil degradation: An explanatory note (GLASOD project). ISRIC, Wageninen, the Netherlands and UNEP, Nairobi, Kenya

Oldeman LR (1992) Global extent of soil degradation. In: Bi-Annual Report 1991–1992. ISRIC, Wageningen, pp 19–36

Periasamy S, Shanmugam RS (2017) Multispectral and microwave remote sensing models to survey soil moisture and salinity. Land Degrad Dev 28(4):1412–1425
Rai AK, Basak N, Sundha P (2020) Chemistry of salt-affected soils. In: Minhas PS et al (eds) Salinity management in India. Central Soil Salinity Research Institute, Karnal, Haryana. (Submitted to ICAR, New Delhi)
Rao BRM, Ravisankar T, Dwivedi RS, Thammappa SS, Venkataratnam L, Sharma RC, Das SN (1995) Spectral behaviour of salt-affected soils. Int J Remote Sens 16:2125–2136
Ravishankar T, Sreenivas K (2010) Soils and land degradation. In: Roy PS, Dwivedi RS, Vijayan D (eds) Remote sensing applications. NRSC, ISRO, Hyderabad, pp 81–107
Rawat KS, Mishra SV, Singh SK (2018) Integration of earth observation data and spatial approach to delineate and manage Aeolian Sand-Affected Wasteland in Highly Productive Lands of Haryana, India. Int J Geoph 1–7 https://doi.org/10.1155/2018/2847504
Reddy VR (2003) Land degradation in India extent, costs and determinants. Econ Polit Wkly 38 (44):4700–4713
Reiche J, Verbesselt J, Hoekman D, Herold M (2015) Fusing Landsat and SAR time series to detect deforestation in the tropics. Remote Sens Environ 156:276–293
Robinson DA, Jones SB, Wraith JM, Or D, Friedman SP (2003) A review of advances in dielectric and electrical conductivity measurements in soils using time domain reflectometry. Vadose Zone J 2:444–475
Saadoud D, Hassani M, Peinado FJ, Guettouche MS (2018) Application of fuzzy logic approach for wind erosion hazard mapping in Laghouat region (Algeria) using remote sensing and GIS. Aeolian Res 32:24–34
SAC (2016) Desertification and land degradation Atlas of India (Based on IRS AWiFS data of 2011–13 and 2003–05). Space Applications Centre, ISRO, Ahmedabad, p 219
Sakala E, Fourie F, Gomo M, Coetzee H (2017) Mapping surface sources of acid mine drainage using remote sensing: case study of the Witbank, Ermelo and Highveld coalfields. Mine Water and Circular Economy, Lappeenranta, pp 1246–1253
Samra JS, Sharma UC, Dadhwal KS (2012) Soil erosion and soil conservation. In: Goswami NN et al (eds) Fundamentals of soil science, p 725
Sander P (2007) Lineaments in groundwater exploration: a review of applications and limitations. Hydrogeol J 15(1):71–74
Saxena RK, Srivastava R Verma KS (2005) Spectral library of Indian Soils. Tech. Bull. No. 5, NATP, National Bureau of Soil Survey and Land Use Planning, Nagpur, India
Sethi M, Dasog GS, Van Lieshout A, Salimath SB (2006) Salinity appraisal using IRS images in Shorapur Taluka, Upper Krishna Irrigation Project-Phase I, Gulbarga District, Karnataka, India. Int J Remote Sens 27:2917–2926
Sethi M, Bundela D, Yadav RK, Manjit S (2014) Development of Spectral Reflectance Methods and Low Cost Sensors for Real-Time Application of Variable Rate Inputs in Precision Farming, Component 4 of NAIP, NAIP, ICAR Final Report
Setia R, Lewis M, Marschner P, Raja Segaran R, Summers D, Chittleborough D (2013) Severity of salinity accurately detected and classified on a paddock scale with high resolution multispectral satellite imagery. Land Degrad Dev 24(4):375–384
Sharda VN, Dogra P, Prakash C (2010) Assessment of production losses due to water erosion in rainfed areas of India. J Soil Water Conserv 65(2):79–91
Shepherd KD, Walsh MG (2002) Development of reflectance spectral libraries for characterization of soil properties. Soil Sci Soc Am J 66:988–998
Singh G, Bundela DS, Sethi M, Lal K, Kamra SK (2010) Remote sensing and GIS for appraisal of salt-affected soils in India. J Environ Qual 39(1):5–15
Slater LD, Sandberg SK (2000) Resistivity and induced polarization monitoring of salt transport under natural hydraulic gradients. Geophysics 65:408–420
Sreenivas K, Venkataratnam L, Narasimha Rao PV (1995) Dielectric properties of salt-affected soils. Int J Remote Sens 16:641–649
Srivastava R, Sethi M, Yadav RK, Bundela DS, Singh M, Chattaraj S, Singh SK, Nasre RA, Bishnoi SR, Dhale S, Mohekar DS, Barthwal AK (2017) Visible-Near Infrared Reflectance

Spectroscopy for Rapid Characterization of Salt-Affected Soil in the Indo-Gangetic Plains of Haryana, India. J Indian Soc Remote Sens 45(2):307–315
Sterk G (2003) Causes, consequences and control of wind Erosion in Sahelian Africa: a review. Land Degrad Develop 14:95–108
Stevens A, Nocita M, Toth G, Montanarella L, van Wesemael B (2013) Prediction of soil organic carbon at the European scale by visible and near infra red reflectance spectroscopy. PLoS One 8: e66409
Taylor G, Dehaan R (2000) Salinity mapping with hyperspectral imagery. In: 14th International conference, Applied Geologic Remote Sensing, Springer, Netherlands, Las Vegas, pp 512–519
Teng H, Rossel RA, Shi Z, Behrens T, Chappell A, Bui E (2016) Assimilating satellite imagery and visible–near infrared spectroscopy to model and map soil loss by water erosion in Australia. Environ Model Softw 77:156–167
Tilley DR, Ahmed M, Son JH, Badrinarayanan H (2007) Hyperspectral reflectance response of freshwater macrophytes to salinity in a brackish subtropical marsh. J Environ Qual 36:780–789
Tyagi NK (1998) Improvement of irrigation system for control of salinity. In: Tyagi NK, Minhas PS (eds) Agricultural salinity management in India. ICAR-CSSRI, Karnal, pp 309–324
UNCCD (2017) Global land outlook. Germany, pp. 336
UNEP (1992) World Atlas of desertification. London, Edward Arnold, p 69
Viscarra Rossel R, Webster R (2012) Predicting soil properties from the Australian soil visible-near infrared spectroscopic database. Eur J Soil Sci 63:848–860
Viscarra Rossel R, Behrens T, Ben-Dor E, Brown DJ, Demattê JA, Shepherd KD, Shi Z, Stenberg B, Stevens A, Adamchuk V, Aïchi H (2016) A global spectral library to characterize the world's soil. Earth Sci Rev 155:198–230
Wang Q, Li P, Chen X (2012) Modeling salinity effects on soil reflectance under various moisture conditions and its inverse application: a laboratory experiment. Geoderma 170:103–111
Weiss E, Marsh SE, Pfirman ES (2001) Application of NOAA-AVHRR NDVI time-series data to assess changes in Saudi Arabia's Rangelands. Int J Remote Sens 22(6):1005–1027
Weng Y, Gong P, Zhu Z (2008) Soil salt content estimation in the Yellow River Delta with satellite hyperspectral data. Canadian J Remote Sens 34(3):259–270
Wu CY, Jacobson AR, Laba M, Kim B, Baveye PC (2010) Surrogate correlations and near-infrared diffuse reflectance sensing of trace metal content in soils. Water Air Soil Pollut 209 (1–4):377–390
Yan H, Wang S, Wang C, Zhang G, Patel N (2005) Losses of soil organic carbon under wind erosion in China. Glob Chang Biol 11:828–840
Zhou Y, Guo B, Wang S, Tao H (2015) An estimation method of soil wind erosion in Inner Mongolia of China based on geographic information system and remote sensing. J Arid Land 7 (3):304–317

Chapter 13
Groundwater Management for Irrigated Agriculture Through Geospatial Techniques

Rajarshi Saha, Tarik Mitran, Suryadipta Mukherjee, Iswar Chandra Das, and K. Vinod Kumar

Contents

Abstract Groundwater irrigation plays an important role in sustainable agricultural development through protective shield during droughts and dry spells and intensifying and diversifying of the cropping system. The measuring, monitoring, and

R. Saha (✉) · S. Mukherjee · I. C. Das · K. V. Kumar
Geosciences Group, National Remote Sensing Centre, Department of Space, ISRO, Hyderabad, Telangana, India
e-mail: rajarshi_s@nrsc.gov.in; das_ic@nrsc.gov.in; vinodkumar_k@nrsc.gov.in

T. Mitran
Soil and Land Resources Assessment Division, National Remote Sensing Centre, Department of Space, ISRO, Hyderabad, Telangana, India
e-mail: tarikmitran@nrsc.gov.in

T. Mitran et al. (eds.), *Geospatial Technologies for Crops and Soils*,
https://doi.org/10.1007/978-981-15-6864-0_13

modeling of groundwater availability, condition, and distribution are the major step to formulate a sustainable groundwater management plan for agricultural use. The conventional methods to manage groundwater are tedious and costly. However, the modernization of geospatial techniques, namely, remote sensing (RS), geographic information system (GIS), Global Positioning System (GPS), etc., along with differential proximity sensing has enabled groundwater management both spatially and temporally. It can help in surveying, analyzing, detecting, differentiating, characterizing, mapping, monitoring, and modeling of the groundwater quantity, quality, distribution, extent, and association of groundwater resources. The major interventions of geospatial techniques in groundwater management are groundwater quality assessment, spatial zonation for irrigation, groundwater prospects mapping, dynamicity of groundwater storage, saltwater intrusion, etc. These applications have made a huge impact on groundwater management for crop and land resources on a sustainable basis. The multiparametric approach of geospatial techniques can minimize the time, labor, and money and thereby enable quick decision-making for efficient water resources management. However RS data has some inherent limitations of spatial, spectral, and temporal resolution, which sometimes makes it difficult to understand and asses the groundwater condition. Still, it is very important for the areas/regions especially developing nations where data scarcity in terms of quantity and quality is often an obstacle for solving real-world water problems. This chapter highlights the various approaches of groundwater management for irrigated agriculture using geospatial tools and techniques.

Keywords Geographic information system · Groundwater irrigation · Groundwater prospects · Groundwater sustainability · Remote sensing

Abbreviations

BIS	Bureau of Indian Standards
DC	Dharwar Craton
EC	Electrical Conductivity
EMAG	Earth Magnetic Anomaly Grid
EO	Earth Observation
ERT	Electrical Resistivity Tomography
EVI	Enhanced Vegetation Index
FAO	Food and Agricultural Organization
FCC	False Color Composite
GIS	Geographic Information System
GPR	Ground Penetrating Radar
GRACE	Gravity Recovery and Climate Experiment
GWP	Groundwater Potential
IDW	Inverse Distance Weighted
LISA	Local Indicators of Spatial Autocorrelations
LULC	Land Use and Land Cover

NDMI	Normalized Difference Moisture Index
NDVI	Normalized Difference Vegetation Index
NDWI	Normalized Difference Water Index
NGLM	National Geomorphological Layer Mapping
NRDWP	National Rural Drinking Water Program
OECD	Organization for Economic Co-operation and Development
RSC	Residual Sodium Carbonate
SAR	Sodium Absorption Ratio
SWIR	Shortwave Infrared
TDS	Total Dissolved Solids
TWS	Total Water Storage
VNIR	Visible and Near-Infrared

13.1 Introduction

Groundwater is the portion of water present below the Earth's surface in pore spaces of soil/unconsolidated rocks and in the fractures/fissures of crystalline rock formations, etc. Groundwater constitutes about 30% of the world's freshwater supply, which is about 0.76% of the entire world's available water (Gleick 1993). Groundwater distribution in the globe is heterogeneous and varied both spatially and temporally. Diverse geomorphic conditions along with uneven precipitation type may be the reason. The fracture/lineament distribution, variation in lithology and geomorphology, and hydrological characteristics produce heterogeneous and inconsistent yield as well as the depth of groundwater. Groundwater serves as a dependable source of water for various purposes including irrigated agriculture and domestic and industrial uses. It is the major contributor in areas with high populations, irrigated agriculture, and insufficient surface water resources (Shah et al. 2001). The use of groundwater for agricultural irrigation overthrows the rest of other uses (Burke 2002). The world has witnessed the rapid growth of groundwater irrigation for crops over the past five to six decades (Shah 2014). Asia has contributed about 70% of this groundwater for irrigation use leading to substantial improvement in agriculture and food security (Siebert et al. 2010). This has positively impacted the economic growth and improves millions of household financial condition from poverty. It balanced marginal to submarginal farming by mitigating drought effects, allowing farmers to intensifying, diversifying, and changing in cropping patterns. It has also allowed farmers to adopt cultivation of high-value crops, multiple cropping, etc.

The innovation in tubewells and pumping technologies has excelled in the growth of groundwater irrigation. As a part of a long-established practice, groundwater use was initially limited to arid regions and rechargeable shallow alluvial aquifers of Ganga and parts of the Indus river basin. However, with the progress of time, it has rapidly spread over other regions with diverse environmental and geological setup. It

got spread to hard rock terrains of peninsular India to the hot and humid southeastern Asian countries and northeastern part of Sri Lanka, where aquifer storage is inconsistent with low yield (Shah 2010). It was observed that in Indian subcontinent, annual groundwater abstraction increased from 10–20 km^3 before 1950 to 240–260 km^3 in 2009 (Shah 2010). European countries like Spain had experienced a huge demand increase in groundwater draft for agricultural irrigation purposes from 2 km^3 during 1960 to 6 km^3 during 2000 (Martinez-Cortina and Hernandez-Mora 2003). South Asian countries' groundwater irrigation development has reached a plateau, whereas in countries in sub-Saharan Africa, Southeast Asia, and South America, groundwater use is just beginning to grow (Barker and Molle 2005; Giordano 2006; Shah 2010; Shah 2014). The Food and Agricultural Organization (FAO) reported that groundwater irrigates around one-third of the world's total irrigated area out of that more than 70% area belongs to Asia (Siebert et al. 2010). However the estimates provided by South Asian countries like India and China show a periodical upward revise trend of groundwater-irrigated area over surface water-irrigated area (Shah 2010). These data indicate that in Asia groundwater-irrigated area is significantly greater than FAO estimates.

Excel in groundwater irrigation is the result of a high demand from agricultural industries. This is due to the stability provided by groundwater during drought season and contribution over dry land which helps in crop intensification and diversification (Tsur 1990). These also all affect countries' agricultural and socio-economic development. Groundwater irrigation has created many dry season crops in several South Asian countries (Barker and Molle 2005). Vietnam became the largest producer of pepper and robusta coffee by adopting groundwater irrigation (Zhu et al. 2007). Groundwater irrigation has enabled and intensified pre-summer Boro rice cultivation in Bangladesh, which revolutionizes the country from food borrower to a rice exporter (Palmer-Jones 1999). It has positively impacted the economy by raising the land value in the USA and Spain (Lee and Bagley 1972; Garrido et al. 2006).

Groundwater monitoring and management is very crucial for sustainable agriculture and economic growth of a country. Hence, continuous monitoring of such is required both spatially and temporally at global or regional scale. As the conventional methods are laborious, costly, and time-consuming, geospatial techniques can play a meaningful role. Remote sensing (RS) and geographic information systems (GIS) are very useful to extract information on groundwater-irrigated areas and their historical evolution (Sharma et al. 2018). However, use of only RS data in case of precise estimation of groundwater irrigation is very difficult as fragmented land-holdings, intense cloud cover in tropical regions, issues with satellite data resolution and repeativity, and spectral and spatial heterogeneity of crops (Velpuri et al. 2009; Thenkabail et al. 2009a, b). Nowadays census-based data along with sensing-based approaches have been used to generate groundwater-irrigated land statistics at a regional or national scale. But there are variations in data used, method of approaches, and results (Thenkabail et al. 2005; Thenkabail et al. 2009a, b). Interpolation methods are commonly used to assess spatial variability of groundwater (Corwin and Lesch 2005; Gunarathna et al. 2016). But such approaches may not be

enough to understand the spatial and temporal distribution of water to formulate groundwater management plans for agricultural purposes. Even though there is a huge advancement in the RS imaging capabilities, accurate identification and monitoring is still an enormous challenge for groundwater resources, i.e., managing at micro-watershed level (Robert et al. 2017). Besides, various other socioeconomic factors along with diversified farming practices increase the difficulty in assessing groundwater-irrigated areas. Thus integrated use of RS and GIS is needed with various optical indices, classification algorithms, data assimilation, as well as data modeling (Gunaalan et al. 2018). Satellite image-derived indices were mostly used by various researchers to differentiate between irrigated and nonirrigated cropland area. These are generally dependent on spatial, spectral, and temporal differences water and/or vegetation cover (Jin and Sader 2005; Dutrieux et al. 2016; Ambika et al. 2016). Normalized Differential Moisture Index (NDMI) (Jackson et al. 2004; Jin and Sader 2005; Dutrieux et al. 2016) and Normalized Differential Vegetation Index (NDVI) were generally used to identify the irrigated cropland and land use and land cover (LULC) classification at different scales using various spatiotemporal resolution satellite images (Thenkabail et al. 2010; Dhiman 2012; Ambika et al. 2016). However multiple indices (vegetation, surface moisture, and surface temperature)-based approach is mostly preferable for irrigated and nonirrigated cropland classification (Ozdogan and Gutman 2008; Shahriar Pervez et al. 2014). The temporal NDVI and Enhanced Vegetation Index (EVI) data are commonly used to represent seasonal rhythms and phenological variations for different land-use types which showcase the groundwater irrigation impact (Jin and Sader 2005).

Groundwater occurrence and distribution vary spatially and temporarily depending upon lithology-geomorphology, hydrogeology, lineament/fracture distribution, and stream/drainage network and which eventually control its yield and depth. This spatiotemporal variability along with other associated factors makes it very complicated and time-consuming to identify its occurrence by conventional field mapping. The integration of RS and GIS with filed data could provide various impact components of groundwater occurrence and its movement depending on geology, geomorphology, soils, LULC, drainage, and lineaments (Jha et al. 2007). Modernization and sophistication in RS and GIS can help to integrate the data collected from various sources and methods. Many researchers have used such data to delineate groundwater prospects zones in different geological terrains (Prasad et al. 2008; Chowdhury et al. 2009; Rashid et al. 2012; Magesh et al. 2012; Adiat et al. 2012; Satapathy and Syed 2015; Agarwal and Garg 2016; Das et al. 2017; Ahmed and Mansor 2018). This chapter highlights the aptness of the geospatial technologies for groundwater irrigation and its positive impact on the socioeconomic environment through agriculture and food security. It also gives an insight into the groundwater usage regime that fits well with a nation's hydrogeological and socio-ecological reality.

13.2 Groundwater Usages in Irrigated Agriculture: Global Scenario

It is essential to manage groundwater resources to stabilize and increase agricultural production. Groundwater has contributed significantly toward agricultural transformation in Asia, the Middle East, and North African countries over the last five to six decades. A total of 38% of the world's irrigated area is currently supported by groundwater irrigation (Siebert et al. 2013). Groundwater contributes 13% of world total food production and 44% of world total irrigated food production (CGIAR 2017). The dependence on groundwater irrigation for crops is highest in South Asia followed by East Asia, Organization for Economic Co-operation and Development (OECD) countries, and East African and North African countries, respectively (Fig. 13.1).

Nowadays most countries like the USA, China, India, Spain, Bangladesh, Vietnam, and many African countries are managing groundwater resources for sustainable agricultural production (Shah 2014). This social and economic well-being by agriculture was associated with a high increase of groundwater abstraction (Shah 2010). Thus the global usages of groundwater for irrigation purposes show a steep increase (Fig. 13.2). As per FAO estimates, earth's total irrigated area is 307 million ha (Mha) out of which around 90% area belongs to Asia and America (Siebert et al. 2013). Table 13.1 represents the total area equipped with irrigation as well as area with surface and groundwater irrigation. In America, Asia and Europe the usage of groundwater for irrigation purpose are around 47, 38 and 31%, respectively, but in other continents, it is less than 25% (Fig. 13.3). Africa has a large potential for groundwater irrigation across the continent. Recent studies show that the semiarid Sahel and the eastern regions, stretching from Ethiopia to Zimbabwe, may have significant potential for groundwater irrigation (CGIAR 2017). Large portions of the region in Southern and Northern Africa have overexploited the groundwater

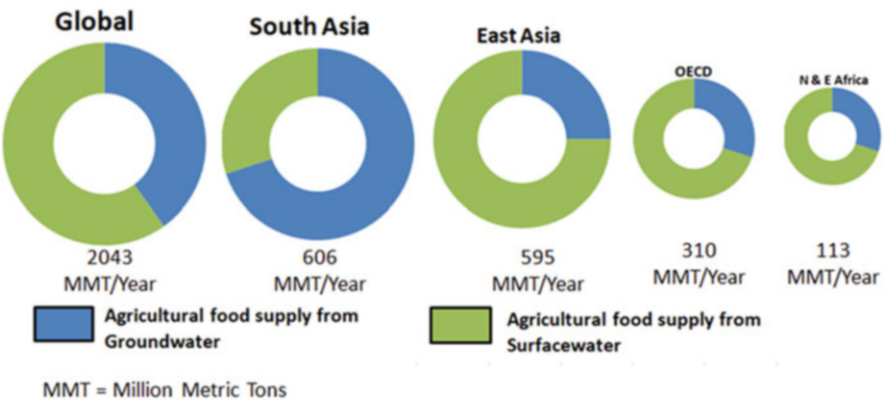

Fig. 13.1 Global scenario of dependence on groundwater irrigation for agriculture. (Modified, CGIAR 2017)

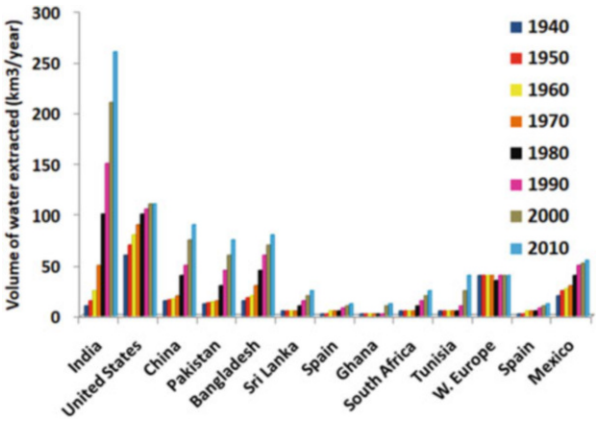

Fig. 13.2 Growth trends of global groundwater use

resources without considering the recharging capacities of aquifers and other geo-environmental factors (Shah et al. 2001; Hamed et al. 2014;Ahmed et al. 2014; Closas and Villholth 2016).

This has potentially ended the sustainable development of groundwater irrigation (Altchenko and Villholth 2015). Several studies have indicated that many Southern African countries are at greater risk of climate change and groundwater drought in the future (Villholth et al. 2013). Asia's groundwater-irrigated area contributes to almost 70% of the world's groundwater-irrigated area (Siebert et al. 2013). Asia demonstrates a blended representation of areas with potential and overexploited groundwater irrigation (Shah 2014). Countries like India, China, Pakistan, Bangladesh, and Sri Lanka where groundwater irrigation experienced rapid increases show a mixed picture of potential and overexploited areas (CGWB 2011; CGIAR 2017). In parts of South and Western India, extensive use exhausted the groundwater resources. However, there is plenty of opportunity for groundwater irrigation in Northeastern India. In India and Bangladesh, the uses of groundwater for irrigation are more than 60% (www.fao.org) of total irrigated areas. However, the statistics are on the lower side in countries like Afghanistan, Sri Lanka, and Indonesia (Fig. 13.4).

In Northern America, groundwater-irrigated area is around 59% of the total irrigated area, while it is on the lower side in Central and Southern America. However, Europe shows a very diverse picture of groundwater irrigation. In Eastern Europe, the groundwater-irrigated areas are around 10%, while in Central and Western Europe, it shows a higher value. Countries like Germany, the UK, and Spain show a prosperous picture on groundwater irrigation (Fig. 13.4). In Australia groundwater irrigation is around one-fourth of total irrigated land of the country.

Table 13.1 Total area equipped for irrigation and area with surface and groundwater irrigation (Adopted, Siebert et al. 2013)

Area equipped for irrigation (ha)				
Region	Total	Area equipped with groundwater	Irrigation with surface water	% area under groundwater irrigation
Northern Africa	6,400,826	2,113,437	4,273,626	33
Sub-Saharan Africa	7,148,268	399,210	6,747,858	6
Africa total	13,549,094	2,512,647	11,021,483	19
Central America and Caribbean	1,865,268	651,185	1,214,083	35
Northern America	36,411,337	21,355,866	15,055,471	59
Southern America	13,055,707	2,235,854	10,819,854	17
America total	51,332,312	24,242,905	27,089,407	47
Central Asia	13,657,552	1,085,033	12,572,518	8
Middle East	24,083,108	10,747,301	13,130,305	45
Southern and Eastern Asia	175,983,556	68,929,063	107,054,494	39
Asia total	213,724,215	80,761,397	132,757,317	38
Eastern Europe	5,198,729	494,759	4,703,970	10
Western and Central Europe	19,138,579	7,004,714	12,133,292	37
Europe total	24,337,308	7,499,473	16,837,262	31
Australia and New Zealand	4,688,259	1,135,787	3,478,479	24
Other Pacific Islands	4471	759	3712	17
Oceania total	4,692,730	1,136,546	3,482,191	24
World	307,635,659	116,152,968	191,187,660	38

13.3 Sources of Groundwater for Agricultural Use

The source of groundwater origin is from rainfall, lakes, rivers, streams snow, and ice, which is a part of the water cycle. Groundwater is the part of the water that is present beneath Earth's surface in soil pore spaces and in the fractures/fissures of rock formations, etc. below the zone of aeration (Todd 1980). This zone of aeration is nothing but the region between the earth's surface and the water table. Below the zone of aeration, the earth rock strata or sedimentary layer holds a considerable amount of water; this is called an aquifer. Aquifers are of porous which allows water

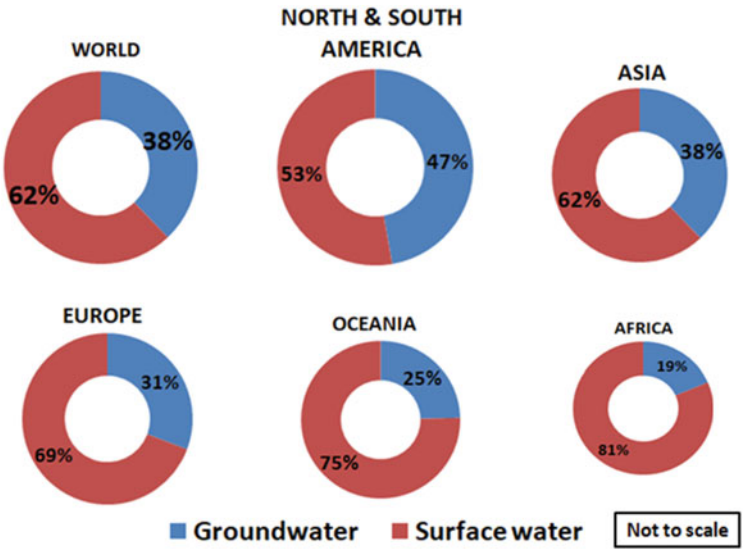

Fig. 13.3 Continent-wise groundwater vs surface water irrigation area. (Data source: www.fao.org)

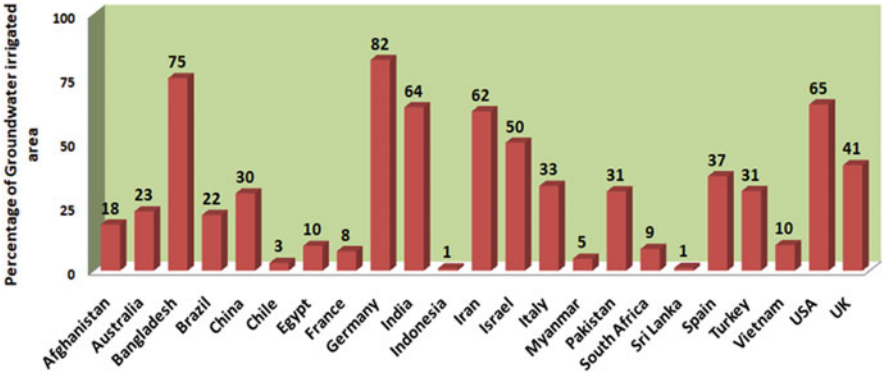

Fig. 13.4 Country-wise groundwater-irrigated area (%) with respect to total irrigated area. (Data source: www.fao.org)

to flow or percolate. Depending upon the nature of flow or recharge, aquifers are characterized. Surface water when directly flows to the aquifer-saturated zone is called unconfined aquifer or vadose zone (Fig. 13.5a). If the aquifer is sealed with impermeable layers at the bottom and top, it is called confined aquifers. These impermeable layers with very low porosity are called aquitard, and if it stops, the flow is called aquiclude.

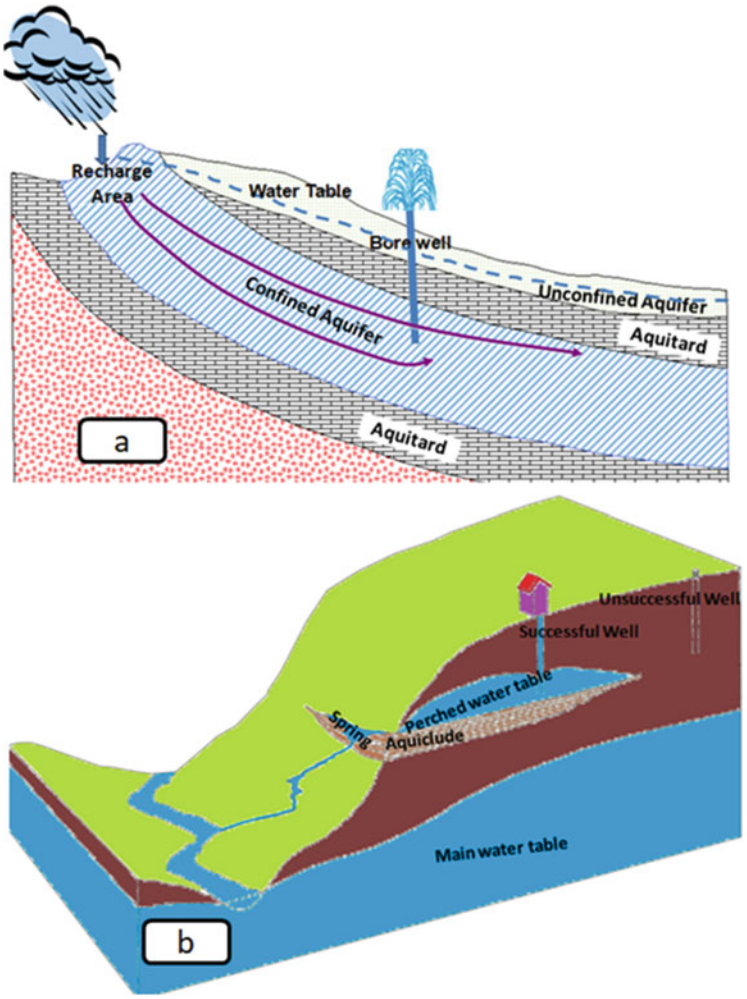

Fig. 13.5 (**a**) Schematic diagram of confined and unconfined aquifer with recharge zone; (**b**) schematic diagram of perched water table, springs, successful and unsuccessful wells

Groundwater constitutes about 30% of the world's freshwater supply, which is about 0.76% of the entire world's available water (Gleick 1993; USGS 2020). Groundwater resources in the world are heterogeneously distributed both spatially and temporally. Diverse geomorphic and lithological conditions along with uneven precipitation type give rise to the heterogeneous distribution of groundwater (Preeja et al. 2011; Saha et al. 2018). The fracture/lineament distribution system, variation in lithology and geomorphology, and hydrological characteristics produce heterogeneous and inconsistent yield as well as the depth of groundwater. Furthermore, groundwater occurrence and distribution in hard rock terrain is much more complicated than the soft rock terrain. The majority of groundwater use for agricultural

irrigation are from various groundwater resources, like unconfined aquifer sources by dug well and hand pumps, confined aquifer sources through bore well, and perennial and seasonal spring's water in hilly terrains. Usually, in the soft rock terrains of alluvium zones, sandy aquifers of semiarid to arid regions water are of unconfined condition. The water from the confined aquifers mainly hard rock terrains of arid to the semiarid region is used by bore-well pumping technologies. These unconfined and confined waters of these aquifers are used for sustainable agricultural purposes where surface water is unavailable and during droughts as well as spells. In the hilly regions, perennial and seasonal spring water (Fig. 13.5b) is channelized to the agricultural fields for usage, when a surface water source is unavailable. There are many other sources of groundwater like well in the perched water table and artesian wells groundwater, and qanat well is used for agricultural usage. In this way groundwater plays a pivotal part in socioeconomic development in arid to semiarid region by backing agricultural activities; otherwise it couldn't sustain.

13.4 Groundwater Management Through Conventional Methods

There are various conventional groundwater management practices that have been used across the world since ancient times (Fig. 13.6). These practices are usually dependent on local socioeconomic environmental factors linked with surface and groundwater extraction and management. In many countries such as Spain, Morocco, Iran, and Syria and Central and Eastern Asia, a conventional water extraction and transporting technique called "qanat" is prevalent for a long period of time (Hartl 1989; Canvas 2014). This is a subsurface mildly sloping tunnel constructed to guide water from high elevated region to habitations situated below (Fig. 13.7a). Qanat is also called khettara in Morocco and kariz (kahrez) in Central and Eastern Asia including China. In Spain it is known as galerias (Taghavi-Jeloudar et al. 2013; Canvas 2014). This system has been operating for centuries to extend well-being of life in deserts (Hartl 1989; Canvas 2014). Traditional practices in Borana and Konso communities of Ethiopia include Ella (wells) and Harta (ponds) (Behailu et al. 2016).

The primary cause of conventional water management is water shortage and the need for survival. In arid regions where rainfall is low and the temperature is extremely high with a deeper groundwater table (~300 m), qanat is the only means of harvesting water for domestic and irrigational use (Taghavi-Jeloudar 2013; Canavas 2014). In the semiarid regions where rainfall is erratic, rainwater harvesting techniques such as the construction of ponds, check dams, nala bundh, nala pluge, etc. allowing runoff to percolate into shallow unconfined aquifers are practiced for centuries to secure the water needs of respective communities (Akpinar Ferrand and Cecunjanin 2014). The conventional groundwater management systems are related

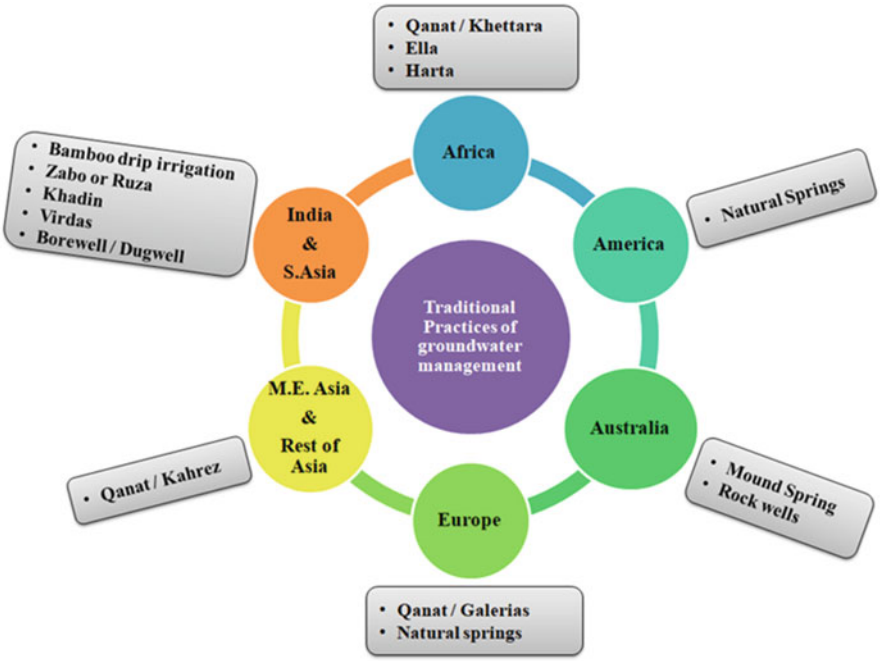

Fig. 13.6 Conventional groundwater management practices around the world

to water sources which include springs, shallow wells, and deep wells in Borana and qanat systems which are very much existent in the developing countries. Many European countries such as Sweden and Finland traditional beliefs governed their water management practices (Katko 2000; Knutsson 2014). The various sources to procure water were public wells and natural springs, and their management was governed by local customs.

In countries like India and China, groundwater harvesting techniques have been used for over 4000 years to meet the domestic and agricultural demand (Oweis et al. 2004). The major traditional practices used in India are as follows:

I. **Bamboo Drip Irrigation System**: This system of water conservation uses bamboo pipes to distribute spring water. Different diameter bamboo is used in perennial as well as seasonal springs for irrigation purposes in northeastern state of Meghalaya (Singh and Gupta 2002).
II. **Zabo:** It is also known as "Ruza," a unique combination of water conservation with animal care, forests, and agriculture. Practiced in Nagaland (Singh and Gupta 2002).
III. **Khadin:** In this water conservation technique, surface runoff is stored for agricultural purposes. An embankment is usually constructed around the

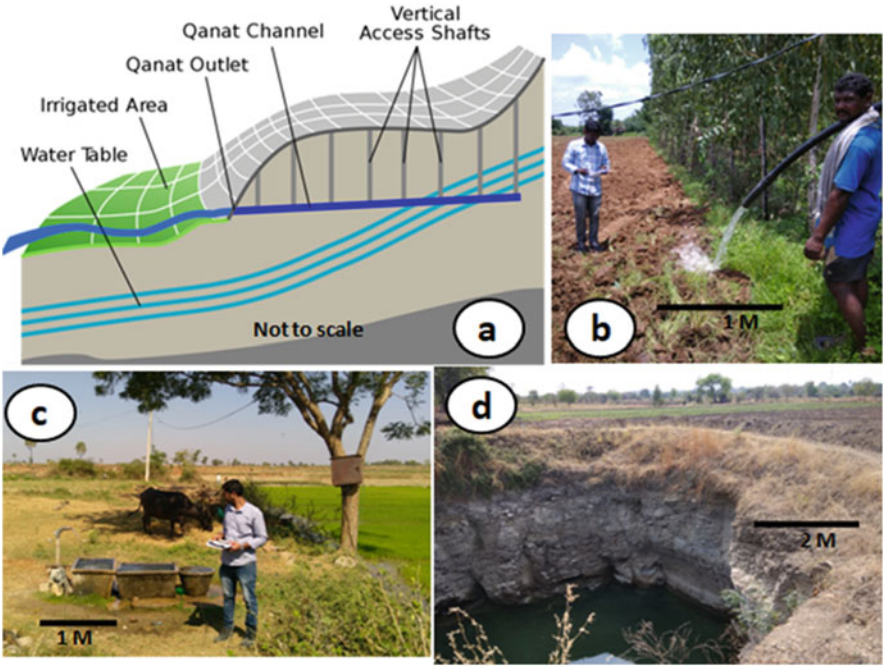

Fig. 13.7 (**a**) Schematic diagram of qanat well (Adopted, Wikipedia); (**b** and **c**) Representing bore-well-driven groundwater irrigation techniques in peninsular India; (**d**) Representing dug well irrigation system in Basaltic terrains of India

slope to collect and distribute groundwater to the agricultural fields. Generally a dug well is constructed nearby to get advantage from groundwater recharging. This practice is usually seen in arid regions of Rajasthan (Kolarkar et al. 1983).

IV. **Virdas:** Developed by Maldhari nomadic tribes of Rann of Kutch, these are shallow wells dug within a natural depression (jheel). It is an intelligent way to extract freshwater from saline groundwater (Machiwal et al. 2018).
V. **Bore Well and Dug Well:** Bore wells are constructed and used for flooding irrigation where there is plenty of groundwater (Fig. 13.7b–d).

The USA is predominantly surface water-dependent; hence, traditional methods of groundwater conservation are not used so much. One of the very popular conventional methods of groundwater irrigation in Australia is a mound spring. Carbonated water fed these springs which later rises to the surface through fissure/cracks in the overlying strata (Michael et al. 2018). Another traditional method of using groundwater is through rock wells, which are open entries to fractured rock aquifers.

13.5 Role of Geospatial Technologies in Groundwater Management for Irrigated Agriculture

Geospatial technologies have demonstrated huge potential in agricultural groundwater management. Lithology, geomorphology, structure along with physical processes such as climatic control, weathering pattern, and erosional agents acting upon a terrain for a substantial period control the terrain's groundwater regime. With the remarkable progress in RS technologies, satellite data of various electromagnetic wavelengths, types, and resolution gives valuable information about groundwater occurrence and distribution either directly or indirectly. Even though much of the earth surface is covered by soil or vegetation, RS has capabilities to provide subsurface aquifer information up to an assertive level (Rose and Krishnan 2009; Muralitharan and Palanivel 2015). This can provide indirect information on groundwater potential. RS along with GIS-integrated studies provide a double dimension, firstly, to visualize any earth feature in variable spectral, temporal, and spatial resolution and, secondly, to overcome the inaccessibility and duration of field investigation. Various decisive geospatial indicators may be of direct, indirect, or derived in nature and provide the probable location of groundwater occurrence as well as its variability (Fig. 13.8) for agricultural use.

Optical RS data can provide qualitative and quantitative information on tone, texture, pattern, shape, size, shadow, association, and resolution which are very essential in groundwater prospects study (Navalgund et al. 2007; Bennia et al. 2013).

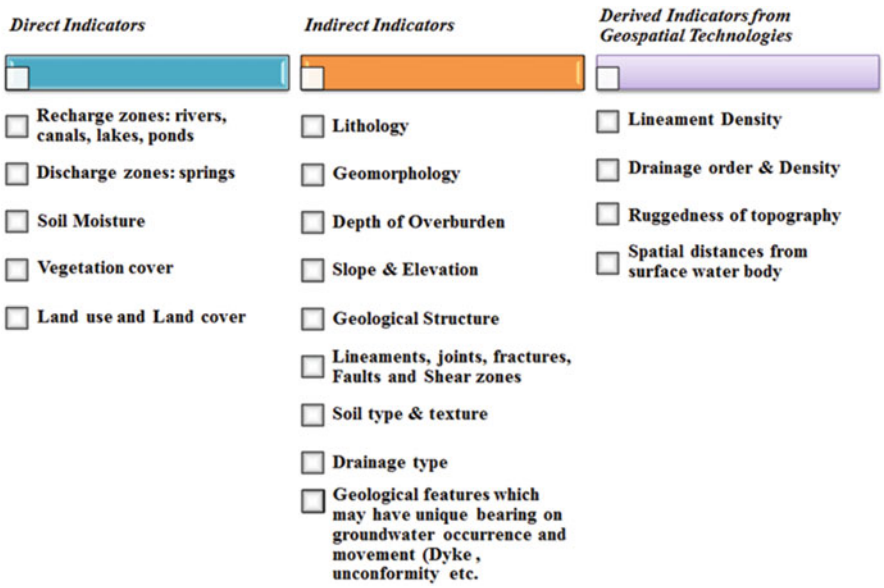

Fig. 13.8 List of decisive geospatial indicators for groundwater prospecting. (Ellyett and Pratt 1975; Singhal and Gupta 2010; Gupta 2003)

Lithological characteristic, moisture content, porosity, etc. of an aquifer can be characterized through tonal variations of satellite images, which give potential groundwater site information (Solomon and Quiel 2006; Adham et al. 2010; Abdalla 2012). Integrated use of RS elements such as texture, pattern, etc. and resolution can provide information on geomorphology, geological structures, the extent of major lineaments, change in moisture content, and hydrogeological characteristics. These eventually indicate the spatial and temporal variability of groundwater occurrence as well as distribution. Thermal RS data has shown enormous potential in determining lithotypes, major geological structures, buried lineament, soil moisture, canal, water body seepages, etc., which provides information of probable water-bearing horizons (Gupta 2003). Hyperspectral RS data provides information on an altered and lateritic zone within the earth's surface, thus providing indirect evidence of unconfined storage of water (Jensen 2016). Microwave RS data is very useful in delineating major litho units, mapping, and identification of major structural discontinuities like fold, fault, joint planes, and shear zones as well as the orientation of bedding plain, dipping strata, etc. (Lillesand et al. 2015). These determine the lithological, geomorphological, and structural variability of the earth's surface for identification as well as an understanding of aquifer heterogeneity and diversity. Eventually, this diversity and heterogeneity denote differential yield and depth of groundwater. Different geospatial sensors are capable to capture variable magnetic anomalies arising from geological features that enhance or reduce the local magnetic fields. The quantification and interpretation of these magnetic anomalies provide variable information on conduits and barriers (fracture, lineament, and dyke) of groundwater movement and characterization of aquifers (Subrahmanyam and Rao 2009). Gravity data from Gravity Recovery and Climate Experiment (GRACE) satellite is useful to calculate the change in total water storage (Tiwari et al. 2011; Dasgupta et al. 2014). The assimilation of additional datasets (evapotranspiration, runoff, precipitation, soil moisture) along with gravity data helps to find out a change in storage and temporal variability of groundwater. This is particularly useful in the modeling of groundwater impact assessment and depletion studies (Rodell et al. 2009; Feng et al. 2013) due to abstraction. Digital elevation model (DEM) also provides valuable information about physiography of any area, which helps in the delineation of geomorphic control on groundwater (Vittala et al. 2006; Singh et al. 2015). NDVI, NDMI, and other various satellite-derived parameters as well as indices are useful in differentiating irrigated cropland and LULC (Seeyan et al. 2014; Sharma et al. 2018).

13.6 Application of Geospatial Technologies for Groundwater Management

Geospatial technologies applications are very crucial in mapping, monitoring, and modeling of natural resources, especially for groundwater as it is very dynamic (Teeuw 1995). The systematic and integrated use of RS and GIS along with other

ancillary information provide decisive information about groundwater studies (Naqa et al. 2009; Dar et al. 2010; Gupta and Srivastava 2010). Remotely sensed earth observation (EO) datasets are valuable sources for creating major geospatial indicators for groundwater occurrence and distribution (Ganapuram et al. 2009; Shaban 2010). The list of satellite data and sensors used for water management is presented in Table 13.2. The major applications of geospatial techniques in agricultural groundwater management are described as follows.

13.6.1 Groundwater Prospects Mapping for Site Suitability

The role of remotely sensed EO data and GIS in groundwater targeting and prospecting is enormous both locally and regionally (Prithviraj 1980; Parker 1988, Das et al. 1997; Thomas et al. 1999; Pratap et al. 2000; Sreedevi et al. 2005; Elbeih 2015; Naghibi et al. 2016; Gopinathan et al. 2019; Haque et al. 2020). Groundwater is very dynamic and multidisciplinary and acts as an integrated function of geology, geomorphology, structure, hydrology, slope, elevation, and LULC. RS data provides information about these decisive factors which directly or indirectly govern the movement and occurrence of groundwater within the aquifer (Gupta 2003; Jha et al. 2007; Machiwal et al. 2011). These factors can control the groundwater regime both quantitatively and qualitatively. Geospatial techniques can provide an efficient platform through GIS where all the satellite-derived thematic layers are integrated with large ancillary information and spatial and nonspatial data to delineate suitable groundwater prospects zone for irrigation (Stafford 1991, Machiwal et al. 2011; NRDWP 2012). The integration of RS data along with electrical resistivity tomography (ERT) is very efficient to assess the geo-structural settings and groundwater prospects with subsurface perspective, finer resolution, and larger coverage (Stan and Stan-Kleczek 2014). Thermal remote-sensed data can provide a regional and local flow of groundwater (Thakur et al. 2017). Integrated modeling (1D, 2D, and 3D) of thermal RS data along with groundwater prospects data and GPS-based field observations can provide groundwater zonation with more spatial and temporal accuracy (Gao 2002).

13.6.2 Dynamicity of Groundwater Storage

GRACE satellite data gives temporal gravity field and total water storage (TWS) dynamics of the entire Earth, with a coarse spatial resolution ~300 kilometers. Geospatial techniques make it possible to integrate GRACE data with various hydrological models for a better understanding of hydro-dynamicity, with higher accuracy at a regional scale (Swenson et al. 2003; Wahr et al. 2004). Modernization of geospatial technologies has provided quantitative dynamicity of groundwater storage and its impact using GRACE data (Rodell et al. 2009; Tiwari et al. 2011;

Table 13.2 The list of satellite data and sensor used for groundwater management

Sl No.	Satellite/ sensor/ geophysical sensor	Resolution	Band specification	Uses in groundwater management	Source
1	IRS 1C/D; Resourcesat-1 and Resourcesat-2 (LISS-III)	23.5 m	Consists of four spectral bands B2 (green; 0.52–0.59 μm), B3 (red; 0.62–0.68 μm), B4 (NIR; 0.77–0.86 μm), and B5 (SWIR; 1.55–1.70 μm) Repeativity 24 days	Thematic mapping of decisive spatial layers which controls the groundwater occurrence and movement. Indices like NDVI, NDWI, NDMI	bhuvan.nrsc.gov.in
2	Cartosat-1 DEM	10 m	Consists of a single panchromatic band with circular accuracy of 15 m and vertical accuracy of 10 m	Topographic controls in GWP mapping	bhuvan.nrsc.gov.in
3	Landsat-8/ OLI	15 m for Pan 30 m for visible, NIR, SWIR 100 m for thermal	Different bands 11 spectral bands (0.433–0.453; 0.450–0.515; 0.525–0.600; 0.630–0.680; 0.845–0.885; 1.560–1.660; 2.100–2.300; 1.360–1.390; 10.6–11.2; 11.5–12.5; 0.500–0.680 in μm)	Thematic mapping of decisive spatial layers which controls the groundwater occurrence and movement. Indices like NDVI, NDWI, NDMI, and EVI, regional and local flow of groundwater	www.usgs.gov
4	ASTER TM	15 m for Pan 30 m for visible, NIR, SWIR 90 m for thermal	Different bands 14 spectral bands (0.520–0.60; 0.630–0.690; 0.760–0.860; 1.600–1.700; 2.145–2.185; 2.185–2.225, 2.235–2.285; 2.295–2.365; 2.360–2.430; 8.125–8.475; 8.475–8.825; 8.925–9.27; 10.250–10.950; 10.950–11.650 in μm)	Thematic mapping of decisive spatial layers which controls the groundwater occurrence and movement. Indices like NDVI, NDWI, NDMI, and EVI, regional and local flow of groundwater	asterweb.jpl.nasa.gov

(continued)

Table 13.2 (continued)

Sl No.	Satellite/ sensor/ geophysical sensor	Resolution	Band specification	Uses in groundwater management	Source
5	GRACE	~330 km	Earth gravity anomaly	Dynamicity of ground water storage	gracefo.jpl.nasa.gov
6	EMAG2	~3.5 km	Magnetic anomaly grids compiled from satellite, ship, and airborne magnetic measurement	Magnetic anomalies provide variable information on conduits and barrier (fracture, lineament, and dyke)	www.ngdc.noaa.gov/geomag/emag2
7	GPR	Depth of penetration up to 40 m	Multifrequency (25, 80, 200, 400, 600, and 900 MHz)	Saltwater intrusion and coastal geomorphology study	Jol and Smith (1991), Neal and Roberts (2000a, b) and Bennett et al. (2009)

Longuevergne et al. 2010; Chinnasamy et al. 2013). Determination of groundwater storage both qualitatively and quantitatively at finer temporal and spatial scale is challenging because of the limitations of data. The coarse GRACE data can be integrated with other hydrological parameters having finer spatial resolution to determine a change in groundwater storage for a better understanding of groundwater management (Bates et al. 2007; Dasgupta et al. 2014). Magnetic anomaly data quantification and interpretation provide variable information on conduits and barriers (fracture, lineament, and dyke) of groundwater movement and characterization of aquifers (Subrahmanyam and Rao 2009).

13.6.3 Assessing Spatial Variability of Groundwater Quality Using GIS

Water quality depends upon various biological, physical, and chemical characteristics (Apha 2005). Irrigation water quality mainly depends upon physical and chemical parameters. The methods for suitability assessment of irrigated water include the following: (i) calculation of sodium, borate, and chloride ion and excessive presence of these affects sensitive crops (Wilcox 1955; Todd 1980); (ii) residual sodium carbonate (RSC) indicates alkalinity hazard (Richards 1954); (iii) trace elements and toxicity affect susceptible crops (Ayers and Westcot 1994); (iv) sodium absorption ratio (SAR) indicates sodium hazard affects infiltration rate of water into the soil (Richards 1954); and (v) electrical conductivity (EC) and total dissolved solids (TDS) indicate salinity hazard affects crop water availability (Wilcox 1955). GIS

enabled the interpolation techniques by which spatial distribution maps of water quality elements (field-collected and lab-analyzed data) can be prepared. Such spatial maps are useful to formulate irrigation management plans for agricultural crops. The spatial distribution of water quality parameters by inverse distance weighted (IDW) method demonstrates accurate estimation (Corwin and Lesch 2005; Asadi et al. 2007; Mir et al. 2017). These interpolation results can be classified based on national or international irrigational quality standards (FAO 1985; BIS 2002) for suitability zonation as per groundwater quality (Richards 1954; Wilcox 1955; Donen 1964; Ayers and Westcot 1985). Gradient analysis methods provide spatial variability patterns more accurately of key elements, where the boundary conditions are heterogeneous. It generally creates multiple ring buffers around the point known point origin (Chen et al. 2016; Ranagalage et al. 2017). Local indicators of spatial autocorrelations (LISA) is a dimension of spatial relationships; it creates clusters of key elements under the assumption that a spatial pattern is a nonrandom distribution, which enables us to understand the spatial relationship (Anselin 1995; Anselin et al. 2010; Guo et al. 2015). These techniques help to know the spatial extent, inter-variability, relationship, and distributions of quality parameters of groundwater for irrigation purposes, which eventually allow us to map, monitor, and measure irrigation suitability spatially.

13.6.4 Assessment and Monitoring of Saltwater Intrusion

The coastal aquifers occupy some of the most potential aquifer systems in the world, but they are very vulnerable to seawater intrusion and salinity hazard from the host aquifer lithology (Frind 1982; Jalali 2007; Das et al. 2016). These external factors determine the quality of groundwater in coastal aquifers. The lowering of groundwater table by excessive abstraction, sea-level rise, and nonscientific processes of pumping groundwater by puncturing both fresh and saline aquifers are the main causes of seawater intrusion (Lee and Song 2007; Werner and Simmons 2009; Sebben et al. 2015). Apart from this geology, geomorphology, lineament, change in land-use pattern, and drainage also play a major role in seawater intrusion (Custodio and Bruggeman 1987; Dagan and Zeitoun 1998; Held et al. 2005; Kerrou and Renard 2010). Multifrequency ground-penetrating radar (GPR) is one of the major geophysical techniques used in groundwater studies by many researchers (Beres and Haeni 1991; de Menezes Travassos and Menezes (2004); Doolittle et al. 2006). It gives a good knowledge about coastal aquifer subsurface geology, which controls groundwater occurrence (Leatherman 1987). GPR measures and maps the water table indirectly by responding to the saturated conditions within or near the top of the capillary fringe (Doolittle et al. 2006). GPR has also been used to define recharge and discharge areas, identify groundwater flow patterns, and understand near-surface hydrological conditions (Steenhuis et al. 1990; Beres and Haeni 1991). GPR profiles of various frequencies provide a continuous image of the subsurface, from which groundwater depth to the water table and interface between

saltwater and freshwater can be determined (Lee and Song 2007). GPR detects the electrical discontinuities both in liquid and solid medium in shallow subsurface conditions (Neal 2004). Differences in the dielectric constant usually cause strong reflections from lithological boundaries in the subsurface (Jol and Smith 1995). Besides, saline water attenuates and absorbs the GPR signal. This helps in the identification of saltwater intrusion, depth of fresh- and saltwater interface zone, and magnitude of the intrusion (Lee and Song, 2007). This helps in understanding the coastal aquifer characteristics for groundwater management.

13.7 Assessing Site Suitability for Groundwater Irrigation Using Geospatial Techniques: A Case Study

Identifying the groundwater in hard rock terrain is one of the major challenging tasks for hydrogeologists in the groundwater research domain. The objective of the present case study is to identify suitable sites for groundwater irrigation in a peninsular gneissic terrain, part of Dharwar Craton, India. The complexity of geology and structural origin of the study area is the major obstacle to delineate suitable groundwater prospects zone. Accordingly, a systematic procedure of geospatial techniques was adopted by integrating various thematic inventory and remotely sensed data in conjunction with limited field observations. The results highlight the importance of geospatial techniques to understand/identify suitable sites for groundwater for irrigated agriculture.

13.7.1 Study Area: Location and Hydrogeological Setup

The study area Palcherla watershed is a part of the granodiorite and hornblende-biotite gneissic province of Dharwar Craton (DC). It is situated in the Anantapur district of Andhra Pradesh, India, with latitude-longitude ranges between 14°20′00″ N to 14°36′30″ N and 77°21′30″ E to 77°34′30″ E (Fig. 13.9). The study area is a macro-watershed covering 214 sq. Km. The study area represents undulating topography, where the elevation ranges from 294 m to 593 m above mean sea level (MSL) (Fig. 13.10f). It demonstrates gently to the moderately dipping slope of 2–10°, but in some places, the slope is greater than 15° (Fig. 13.10b). The lithology of the site consists of granodiorite and hornblende-biotite gneisses of Archean age, which is crosscut by basic dolerite dikes of Paleocene to Cretaceous age. The field evidence also supported the fact that the host rocks gneiss was intruded by basic dolerite dykes at a later stage (Fig. 13.10a). The presence of metabasaltic rock of Archean age is also observed in the study area (Taylor et al. 1984; Rao et al. 1992). The lithology of this watershed is constituted by medium- to coarse-grained gneisses with very little porosity. The area shows predominantly pediplains of various depths weathering

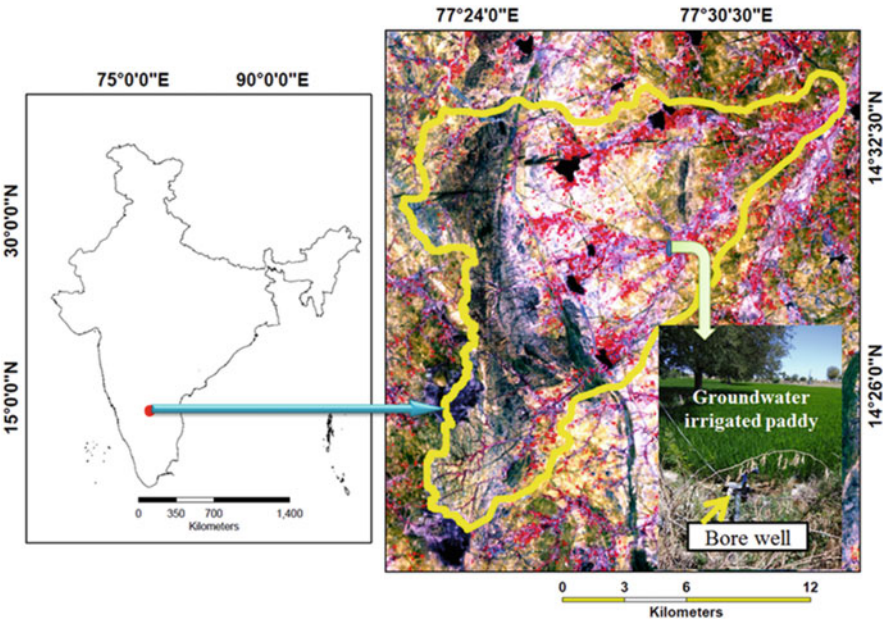

Fig. 13.9 Location of the study area. (It is shown in Resourcesat-2 LISS-III FCC composite with field photograph of bore-well irrigation)

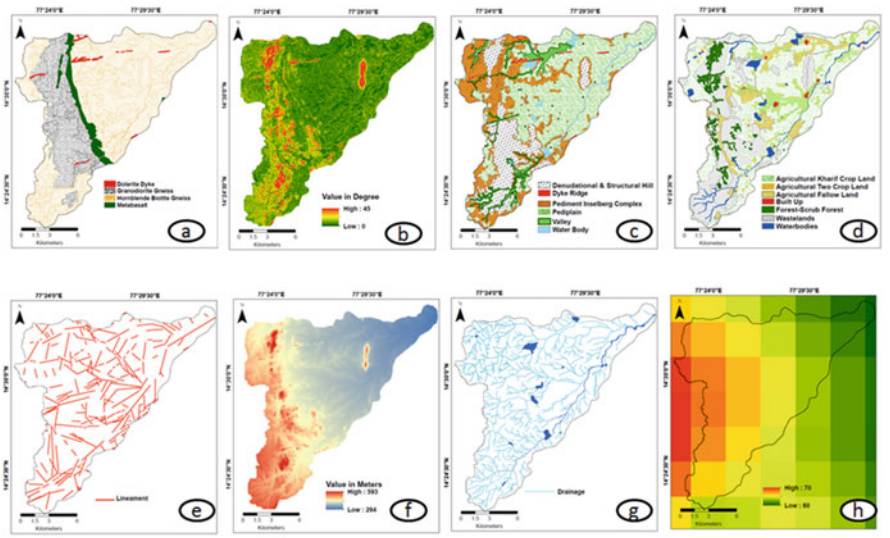

Fig. 13.10 (**a**) Lithology map showing the variation of different gneissic rocks and metabasalts; (**b**) slope map representing the slope variation in degrees; (**c**) geomorphology map showing different geomorphic features; (**d**) LULC map represents different patterns; (**e**) spatial distribution of lineaments; (**f**) variation of elevation in meters; (**g**) distribution of drainage and water body; and (**h**) EMAG2 data showing variation in earth magnetic anomaly datasets and method of approach

thickness, ranging between less than a meter and 30 m, and structural as well as residual hills. The weathered pediplains are mostly of shallow depths; only in some parts, it demonstrates moderate to a deeper thickness of overburden. The overburden material consists of particles of variable size and textures ranging from clay soil to gravelly soil to loamy soil. The hills are mainly of two types of residual hills which represent severe weathering pattern and hills with prominent structural control. The rest of the study area is covered by a pediment inselberg complex, valley fills (Fig. 13.10c) (NRDWP 2012; NGLM 2005). Regional lineament pattern reveals NE-SW and NNW-SEE trend (Fig. 13.10e). Dendritic to a sub-dendritic pattern of drainages is observed with streams trending in a NE-SW direction and very few tanks in this watershed region (Fig. 13.10g). LULC pattern of the study area shows a majority of the area comes under wasteland, followed by single-crop, double-crop, and fallow agricultural land; the rest is covered with forest and built-up area (Fig. 13.10d) (LULC 2015–2016).

13.7.2 Datasets and Method of Approach

13.7.2.1 Satellite Data

Resourcesat-2 LISS-III satellite data with a spatial resolution of 23.5 m was used in the current study (bhuvan.nrsc.gov.in). The false-color composite (FCC) data along with Cartosat DEM (10 m spatial resolution) (bhuvan.nrsc.gov.in) was used to generate various thematic layers related to geology, geomorphology, and hydrology. EMAG2 (Earth Magnetic Anomaly Grid) data (~3.5 km) was (www.ngdc.noaa.gov/geomag/emag2) integrated with the hydrogeomorphic unit to get the suitable site for groundwater irrigation purposes. These anomaly data grids provide insightful knowledge into subsurface structures which mostly act as conduits and barrier for groundwater movement.

13.7.2.2 Field and Ancillary Data

The field-based observations, i.e., GPS location, groundwater yield depth, geological formation, geomorphology, and LULC, were collected from the study site. These datasets were integrated with geospatial information to create site suitability map for groundwater irrigation. A set of field observations were also used to validate the site suitability map derived through geospatial techniques. To gain knowledge about the hydrogeological characteristics of the study area, hydrogeomorphology maps (NRDWP 2012), available well-drilled data, reports (CGWB 2013), and historical records were also collected from various sources. Such information gives an insight into aquifer characteristics in a holistic manner.

13.7.2.3 Method of Approach

The brief methodology of the study is presented in Fig. 13.11. The LISS-III image was processed and enhanced to bring the spectral and spatial variability between the features. The various thematic layers related to geology, geomorphology, structure, hydrology, slope, elevation, and LULC were prepared using LISS-III data and DEM. All the thematic layers were integrated into a GIS environment based on their relative importance in the spatiotemporal occurrence of groundwater (Fig. 13.11) to delineate the hydrogeomorphic unit. These different hydrogeomorphic units were later combined with the earth's magnetic anomaly data and field observation. The integration of satellite imagery-DEM-derived thematic layers, ancillary datasets, and field information has been made in a GIS platform to delineate suitable sites for groundwater irrigation.

13.7.3 Salient Findings

The site suitability zonation map of groundwater for the study site is presented in Fig. 13.12. The map consists of four suitability classes: (i) highly suitable, (ii) moderately suitable, (iii) slightly suitable, and (iv) unsuitable (Fig. 13.12). The spatial distribution shows that the slightly suitable and unsuitable zones are mainly concentrated in the western side of the watershed. Result shows that around half of the watershed is unsuitable or slightly suitable for groundwater irrigation for agriculture. These zones mainly consist of a structural or residual hill, where soil cover is

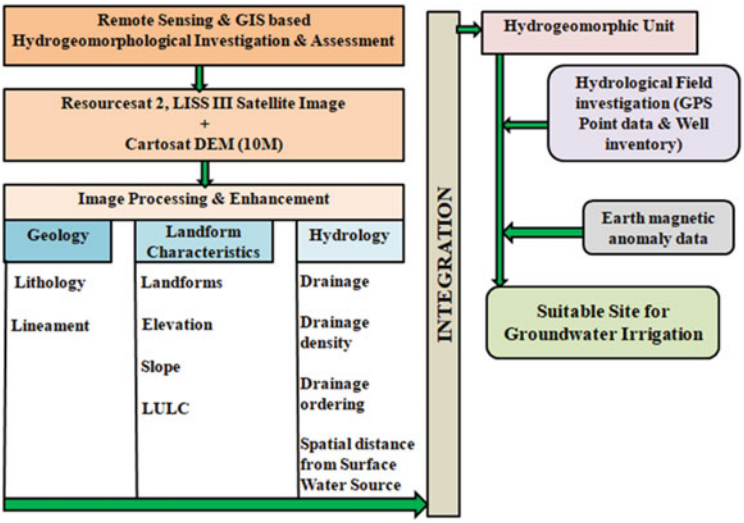

Fig. 13.11 Brief methodology of the study

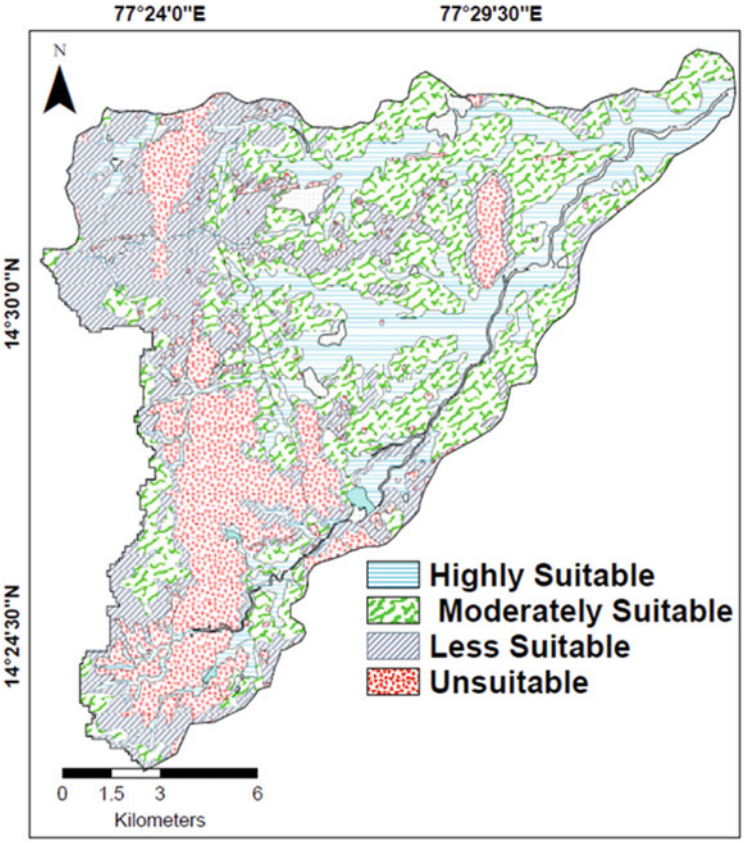

Fig. 13.12 Site suitability zonation map of groundwater for irrigation

almost nil for any agriculture vis-à-vis no groundwater source is available. The spatial distribution also shows the areas which are highly suitable to moderately suitable are the zones of weathered pediplains and valleys with the presence of a considerable amount of weathered overburdens/soils. These areas are usually characterized by a gentle slope, high lineament, and drainage density as well as high prospects for groundwater irrigation. The findings of the study area are in good agreement with the field observations and available data from different sources.

The study area Palcherla is a dry macro-watershed covering 214 sq. km which is part of the gneissic province of Dharwar Craton facing water shortage for irrigation purposes for the past few years. The overdependence on agriculture and unpredictable retreating monsoon has worsened the scenario. The result of the present case study can guide the groundwater irrigational practices in the study area as well as similar geological provinces. This study using geospatial techniques involving RS and GIS data interpretation with minimum groundwater field survey can drastically reduce the time, labor, and money and enables quick solution. Even

though there are several limitations, the methods and results of the study show the potentialities of geospatial tools and techniques for solving real-world water problems.

13.8 Groundwater Management for Irrigated Agriculture Using Geospatial Approaches: Current Status and Challenges

The integrated use of geospatial tools and techniques are encouraging enough to be used in different groundwater management plans (Srivastava et al. 2011; Srivastava et al. 2012a, b). This involves the assimilation of near real-time information and their various utilizations (Yaduvanshi et al. 2015). The use of geospatial technologies are cheaper, more efficient, and time effective than conventional approaches (Okoye and Koeln 2003) and can be used for automated analysis using different approaches and modeling techniques. Advanced modeling is carried out to improve the knowledge about the quality/quantity of groundwater and related studies, such as prediction studies on how the vegetation changes with change in parameters of groundwater. Many advanced nations conduct drone surveys to generate real-time datasets which help in better monitoring of water resources (Lally et al. 2019). The mapping of groundwater resources in arid regions is well documented from Namibia (https://cals.arizona.edu/OALS/ALN/aln51/ednote51.html), America, and other countries. India is emerging as a global player in utilizing geospatial technologies to map groundwater potential zones as demonstrated by the National Rural Drinking Water Programme (NRDWP 2012). According to the survey carried out by Devex and CRS (2019), geospatial analysis and mapping will be the fourth major sector which will have a great impact in the development sector, in the coming 5 years with the Asia Pacific being the most accepted region (geospatialworld.net).

However, there are several limitations associated with the use of space-based sensors for groundwater monitoring. A huge volume of datasets needs to be monitored and is essential for real-time monitoring purposes. The remotely sensed data should be properly calibrated and validated with ground truth data (reference data). Another challenge in RS is the unavailability of spatiotemporal datasets with low revisit time. Besides, the RS datasets should be available in different formats so that it can be processed in different software with ease. The majority of the satellites have a short life span barring a few which makes it difficult to analyze changes over a while for impact assessment studies. Most of the commercially available satellites with high temporal resolution provide medium spatial resolution datasets which are sometimes inefficient in monitoring small irrigated landholdings. Besides, people are largely unaware of the benefits of geospatial technologies and are afraid to use them. Very high-resolution datasets with high temporal resolution are essential to carry out water management-related studies and policymaking decisions. Lack of

skilled personnel is another challenge; hence hands-on training should be given to handle the datasets and process them which are essential at a grassroots level.

13.9 Conclusions and Future Perspectives

All over the world, groundwater irrigation provides a significant contribution to food security and socioeconomic development. Various scientific and conventional approaches have been adopted for groundwater irrigational practices. The use of geospatial technology in groundwater irrigation and management has grown very rapidly in the last two and half decades. The use of geospatial techniques by integrating EO data derived inputs as well as other ancillary information in a GIS platform to measure, monitor, and model the groundwater and provide another dimension to groundwater irrigation for agricultural purposes. The multiparametric approach of geospatial techniques can minimize the time, labor, and money and thereby enable quick decision-making for efficient water resources management. But RS data have some inherent limitations of spatial, spectral, and temporal resolution, which sometimes makes it difficult to understand and asses the groundwater condition as it is not directly visible and present below the Earth's surface in pore spaces of soil/unconsolidated rocks and in the fractures/fissures of crystalline rock formations, etc. In spite of limitations, the conjunctive use of RS data along with other ground-based and available ancillary information makes it a valuable practical tool. Thus it is very important for the areas/regions especially developing nations where data scarcity in terms of quantity and quality is often an obstacle for solving real-world water problems. But this advancement has a potential seed of a grave danger hiding. The ever-increasing dependence on groundwater and scientific as well as technological advancement of its abstraction has resulted in indiscriminate extraction without due regard to the recharging capacities of aquifers and other geo-environmental factors. This may result in further depletion of groundwater sources globally by impacting sustainability. Hence the groundwater extraction should be made with proper regards to recharge, and overexploitation should be curtailed to create a sustainable scenario.

References

Abdalla F (2012) Mapping of groundwater prospective zones using remote sensing and GIS techniques: a case study from the Central Eastern Desert. Egypt J Afr Earth Sci 70:8–17

Adham MI, Jahan CS, Mazumder QH, Hossain MMA, Haque AM (2010) Study on groundwater recharge potentiality of Barind Tract, Rajshahi District, Bangladesh using GIS and remote sensing technique. J Geol Soc India 75(2):432–438

Adiat KAN, Nawawi MNM, Abdullah K (2012) Assessing the accuracy of GIS-based elementary multi criteria decision analysis as a spatial prediction tool–a case of predicting potential zones of sustainable groundwater resources. J Hydrol 440:75–89

Agarwal R, Garg PK (2016) Remote sensing and GIS-based groundwater potential and recharge zones mapping using multicriteria decision-making technique. Water Res Manag 30 (1):243–260

Ahmed JB II, Mansor S (2018) Overview of the application of geospatial technology to groundwater potential mapping in Nigeria. Arab J Geo 11(17):504

Ahmed M, Sultan M, Wahr J, Yan E (2014) The use of GRACE data to monitor natural and anthropogenic induced variations in water availability across Africa. Earth-Sci Rev 136:289–300

Akpinar Ferrand E, Cecunjanin F (2014) Potential of rainwater harvesting in a thirsty world: a survey of ancient and traditional rainwater harvesting applications. Geogr Compass 8 (6):395–413

Altchenko Y, Villholth KG (2015) Mapping irrigation potential from renewable groundwater in Africa–a quantitative hydrological approach. Hydrol Earth Syst Sci 19(2):1055–1067

Ambika AK, Wardlow B, Mishra V (2016) Remotely sensed high resolution irrigated area mapping in India for 2000 to 2015. Scientific Data 3(1):1–4

Anselin L (1995) Local indicators of spatial association—LISA. Geogr Anal:93–115

Anselin L, Syabri I, Kho Y (2010) GeoDa: an introduction to spatial data analysis. In: Handbook of applied spatial analysis. Springer, Berlin, pp 73–89

APHA(American Public Health Association)/AWWA(American Water Works Association)/WEF (Water Environment Federation) (2005) Standard methods for the examination of water and wastewater, vol 21. pp 258–259

Asadi SS, Vuppala P, Reddy MA (2007) Remote sensing and GIS techniques for evaluation of groundwater quality in municipal corporation of Hyderabad (Zone-V), India. Int J Environ Res Public Health 4(1):45–52

asterweb.jpl.nasa.gov

Ayers RS, Westcot DW (1985) Water quality for irrigation. FAO irrigation and drainage paper 20

Ayers RS, Westcot DW (1994) Food, agriculture organization of the United Nations (FAO), water quality for agriculture. Irrigation and Drainage, Rome, Paper 29:77044–77042

Barker R, Molle F (2005) Perspectives on Asian irrigation. In: Asian irrigation in transition: responding to challenges. Sage, New Delhi, pp 45–78

Bates P, Han S, Alsdorf D, Seo K (2007) Influence of the Amazon floodwave on the intra-basin variability of GRACE water storage estimates. AGU Fall Meeting Abstracts

Behailu BM, Pietilä PE, Katko TS (2016) Indigenous practices of water management for sustainable services: case of Borana and Konso, Ethiopia. Sage Open 6(4):2158244016682292

Bennett MR, Cassidy NJ, Pile J (2009) Internal structure of a barrier beach as revealed by ground penetrating radar (GPR): Chesil beach, UK. Geomorphology 104(3-4):218–229

Bennia A, Srivastav SK, Chatterjee RS (2013) Groundwater investigations using optical and microwave remote sensing data in Solani Watershed, India. In: Landslide science and practice. Springer, Berlin, pp 95–100

Beres M Jr, Haeni FP (1991) Application of ground-penetrating-radar Methods in Hydrogeologie Studies. Groundwater 29(3):375–386

bhuvan.nrsc.gov.in (Land Use and Land Cover Mapping 2015–2016 [LULC])

bhuvan.nrsc.gov.in (National Geomorphological and Lineament mapping 2005 [NGLM])

bhuvan.nrsc.gov.in (National Rural Drinking Water Programme, 2012[NRDWP])

BIS (Bureau of Indian Standards) (2002) Tolerance limits of selected water quality parameters for inland surface water prescribed for different uses by Bureau of Indian Standards in India. Bureau of Indian Standards, New Delhi

Burke JJ (2002) Groundwater for irrigation: productivity gains and the need to manage hydro-environmental risk. In: Intensive use of groundwater challenges and opportunities. Balkema Publishers, Lisse, p 478

Canavas C (2014) Public awareness and safeguarding traditional knowledge: challenges and conflicts in preserving and representing kārīz/kǎnérjǐng in Xinjiang, PR China. Water Sci Technol Water Supply 14(5):758–765

CGIAR Research Program on Water, Land and Ecosystems (WLE)(2017) Building resilience through sustainable groundwater use. Colombo, Sri Lanka: International Water Management Institute (IWMI). CGIAR Research Program on Water, Land and Ecosystems (WLE) 12p (WLE Towards Sustainable Intensification: Insights and Solutions Brief 1)

Chen X, Zhou W, Pickett ST, Li W, Han L (2016) Spatial-temporal variations of water quality and its relationship to land use and land cover in Beijing, China. Int J Environ Res Pub Health 13 (5):449

Chinnasamy P, Hubbart JA, Agoramoorthy G (2013) Using remote sensing data to improve groundwater supply estimations in Gujarat, India. Earth Interact 17(1):1–7

Chowdhury A, Jha MK, Chowdary VM, Mal BC (2009) Integrated remote sensing and GIS-based approach for assessing groundwater potential in West Medinipur district, West Bengal, India. Int J Rem Sens 30(1):231–250

Closas A, Villholth KG (2016) Aquifer contracts: a means to solving groundwater over-exploitation in Morocco?. International Water Management Institute (IWMI)

Corwin DL, Lesch SM (2005) Characterizing soil spatial variability with apparent soil electrical conductivity: I. Survey protocols. Comput Electron Agric 1;46(1-3):103–33

Custodio E, Bruggeman GA (1987) Groundwater problems in coastal areas. Studies and reports in hydrology (UNESCO)

Dagan G, Zeitoun DG (1998) Free-surface flow toward a well and interface upconing in stratified aquifers of random conductivity. Water resources research 34(11):3191–3196

Dar IA, Sankar K, Dar MA (2010) Remote sensing technology and geographic information system modeling: an integrated approach towards the mapping of groundwater potential zones in Hardrock terrain, Mamundiyar basin. J Hydrol 394(3-4):285–295

Das PP, Sahoo HK, Mohapatra PP (2016) Hydrogeochemical evolution and potability evaluation of saline contaminated coastal aquifer system of Rajnagar, Odisha, India: a geospatial perspective. J Earth Syst Sci 125(6):1157–1174

Das S, Behera SC, Kar A, Narendra P, Guha S (1997) Hydrogeomorphological mapping in ground water exploration using remotely sensed data—a case study in Keonjhar district, Orissa. J Indian Soc Remote Sens 25(4):247–259

Das S, Gupta A, Ghosh S (2017) Exploring groundwater potential zones using MIF technique in semi-arid region: a case study of Hingoli district, Maharashtra. Spat Inf Res 25(6):749–756

Dasgupta S, Das IC, Subramanian SK, Dadhwal VK (2014) Space-based gravity data analysis for groundwater storage estimation in the Gangetic plain, India. Curr Sci 10:832–844

de Menezes TJ, Menezes PD (2004) GPR exploration for groundwater in a crystalline rock terrain. J Appl Geophys 55(3–4):239–248

Dhiman SC (2012) Aquifer systems of India. CGWB, Ministry of Water Resources, Gov of India, New Delhi

Doneen LD (1964) Notes on water quality in agriculture. Published as a water science and engineering paper 4001, Department of Water Sciences and Engineering, University of California, Davis p 48

Doolittle JA, Jenkinson B, Hopkins D, Ulmer M, Tuttle W (2006) Hydropedological investigations with ground-penetrating radar (GPR): estimating water-table depths and local ground-water flow pattern in areas of coarse-textured soils. Geoderma 131(3-4):317–329

Dutrieux LP, Jakovac CC, Latifah SH, Kooistra L (2016) Reconstructing land use history from Landsat time-series: case study of a swidden agriculture system in Brazil. Int J Appl Earth Obs Geoinf 47:112–124

El-Naqa A, Hammouri N, Ibrahim K, El-Taj M (2009) Integrated approach for groundwater exploration in WadiAraba using remote sensing and GIS. Jordan J Civil Eng 3(3):229–243

Elbeih SF (2015) An overview of integrated remote sensing and GIS for groundwater mapping in Egypt. Ain Shams Eng J 6(1):1–5

Ellyett CD, Pratt DA (1975) A review of the potential applications of remote sensing techniques to hydrogeological studies in Australia. Australian Government Publishing Service, Canberra

FAO (1985) Water quality for agriculture. Irrigation and drainage paper no. 29. Rev. 1. Rome, 182 pp

Feng W, Zhong M, Lemoine JM, Biancale R, Hsu HT, Xia J (2013) Evaluation of groundwater depletion in North China using the Gravity Recovery and Climate Experiment (GRACE) data and ground-based measurements. Water Resour Res 49(4):2110–2118

Frind EO (1982) Seawater intrusion in continuous coastal aquifer-aquitard systems. Adv Water Res 5(2):89–97

Ganapuram S, Kumar GV, Krishna IM, Kahya E, Demirel MC (2009) Mapping of groundwater potential zones in the Musi basin using remote sensing data and GIS. Adv Eng Softw 40 (7):506–518

Gao J (2002) Integration of GPS with remote sensing and GIS: reality and prospect. Photogr Eng Remote Sen 68(5):447–454

Garrido A, Martínez-Santos P, Llamas MR (2006) Groundwater irrigation and its implications for water policy in semiarid countries: the Spanish experience. Hydrogeol J 14(3):340

Giordano M (2006) Agricultural groundwater use and rural livelihoods in sub-Saharan Africa: a first-cut assessment. Hydrogeol J14(3):310–318

Gleick PH (1993) Water in crisis. Pacific Institute for Studies in Dev., Environment and Security. Stockholm Env. Institute 9:473

Gopinathan P, Nandini CV, Parthiban S, Sathish S, Singh AK, Singh PK (2019) A geo-spatial approach to perceive the groundwater regime of hard rock terrain-a case study from Morappur area, Dharmapuri district, South India. Groundwater Sustain Devel 10:100316

Gunaalan K, Ranagalage M, Gunarathna MH, Kumari MK, Vithanage M, Srivaratharasan T, Saravanan S, Warnasuriya TW (2018) Application of geospatial techniques for groundwater quality and availability assessment: a case study in Jaffna Peninsula, Sri Lanka. ISPRS Int J Geo-Inform 7(1):20

Gunarathna MH, Nirmanee KG, Kumari MK (2016) Geostatistical analysis of spatial and seasonal variation of groundwater level: a comprehensive study in Malwathu Oya cascade-I, Anuradhapura, Sri Lanka. Int Res J Environ Sci 5(8):29–36

Guo G, Wu Z, Xiao R, Chen Y, Liu X, Zhang X (2015) Impacts of urban biophysical composition on land surface temperature in urban heat island clusters. Landscape and Urban Planning 135:1–10

Gupta M, Srivastava PK (2010) Integrating GIS and remote sensing for identification of groundwater potential zones in the hilly terrain of Pavagarh, Gujarat, India. Water Int 35(2):233–245

Gupta RP (2003) Remote Sens Geol. Heidelberg: Springer-Verlag 10:978-973

Hamed Y, Ahmadi R, Hadji R, Mokadem N, Dhia HB, Ali W (2014) Groundwater evolution of the Continental Intercalaire aquifer of Southern Tunisia and a part of Southern Algeria: use of geochemical and isotopic indicators. Desalination and Water Treatment 52(10-12):1990–1996

Haque S, Kannaujiya S, Taloor AK, Keshri D, Bhunia RK, Ray PK, Chauhan P (2020) Identification of groundwater resource zone in the active tectonic region of Himalaya through earth observatory techniques. Groundwater Sustain Dev 10:100337

Hartl M (1989) Qanats in the Najafabad valley. In: Qanats, kariz and khattara: traditional water systems in the Middle East and North Africa, pp 119–135

Held R, Attinger S, Kinzelbach W (2005) Homogenization and effective parameters for the Henry problem in heterogeneous formations. Water Resour Res 41(11)

Jackson TJ, Chen D, Cosh M, Li F, Anderson M, Walthall C, Doriaswamy P, Hunt ER (2004) Vegetation water content mapping using Landsat data derived normalized difference water index for corn and soybeans. Rem Sens Environ 92(4):475–482

Jalali M (2007) Salinization of groundwater in arid and semi-arid zones: an example from Tajarak, western Iran. Environ Geol 52(6):1133–1149

Jensen JR (2016) Introductory digital image processing: a remote sensing perspective, 4th edn. Pearson Education, Glenview

Jha MK, Chowdhury A, Chowdary VM, Peiffer S (2007) Groundwater management and development by integrated remote sensing and geographic information systems: prospects and constraints. Water Resour Manag 21(2):427–467
Jin S, Sader SA (2005) Comparison of time series tasseled cap wetness and the normalized difference moisture index in detecting forest disturbances. Remote Sen Environ 94(3):364–372
Jol HM, Smith DG (1991) Ground penetrating radar of northern lacustrine deltas. Can J Earth Sci 28 (12):1939–1947
Jol HM, Smith DG (1995) Ground penetrating radar surveys of peatlands for oilfield pipelines in Canada. J Appl Geoph 34(2):109–123
Katko TS (2000) Water!: evolution of water supply and sanitation in Finland from the mid-1800s to 2000. Finnish Water and Waste Water Works Association, Helsinki
Kerrou J, Renard P (2010) A numerical analysis of dimensionality and heterogeneity effects on advective dispersive seawater intrusion processes. Hydrogeol J 18(1):55–72
Knutsson G (2014) The role of springs in the history of Sweden. Vatten—J Water Manag Res 70:79–86
Kolarkar AS, Murthy KN, Singh N (1983) Khadin—a method of harvesting water for agriculture in the Thar Desert. J Arid Environ 6(1):59–66
Lally HT, O'Connor I, Jensen OP, Graham CT (2019) Can drones be used to conduct water sampling in aquatic environments? A review. Science of the total environment 670:569–575
Leatherman SP (1987) Coastal geomorphological applications of ground-penetrating radar. J Coast Res:397–399
Lee JY, Song SH (2007) Evaluation of groundwater quality in coastal areas: implications for sustainable agriculture. Environ Geol 52(7):1231–1242
Lee SH, Bagley ES (1972) Ground Water and Land Values in Southwestern Kansas a. Groundwater 10(6):27–36
Lillesand T, Kiefer RW, Chipman J (2015) Remote sensing and image interpretation. Wiley, Hoboken
Longuevergne L, Scanlon BR, Wilson CR (2010) GRACE Hydrological estimates for small basins: evaluating processing approaches on the High Plains Aquifer, USA. Water Resour Res 46(11)
Machiwal D, Jha MK, Mal BC (2011) Assessment of groundwater potential in a semi-arid region of India using remote sensing, GIS and MCDM techniques. Water Resour Res 25(5):1359–1386
Machiwal D, Kumar S, Sharma GK, Jat SR, Dayal D (2018) Studying an indigenous rainwater harvesting system in Banni grassland of Kachchh, India. Indian J Tradit Knowl 17(3):559–568
Magesh NS, Chandrasekar N, Soundranayagam JP (2012) Delineation of groundwater potential zones in Theni district, Tamil Nadu, using remote sensing, GIS and MIF techniques. Geosci Front 3(2):189–196
Martinez Cortina L, Hernandez Mora N (2003) The role of groundwater in Spain's water policy. Water Int 28(3):313–320
Mir A, Piri J, Kisi O (2017) Spatial monitoring and zoning water quality of Sistan River in the wet and dry years using GIS and geostatistics. Comput Electron Agric 135:38–50
Muralitharan J, Palanivel K (2015) Groundwater targeting using remote sensing, geographical information system and analytical hierarchy process method in hard rock aquifer system, Karur district, Tamil Nadu, India. Earth Sci Inform 8(4):827–842
Naghibi SA, Pourghasemi HR, Dixon B (2016) GIS-based groundwater potential mapping using boosted regression tree, classification and regression tree, and random forest machine learning models in Iran. Environ Monit Assess 188(1):44
Navalgund RR, Jayaraman V, Roy PS (2007) Remote sensing applications: an overview. Curr Sci 00113891:93(12)
Neal A (2004) Ground-penetrating radar and its use in sedimentology: principles, problems and progress. Earth-Sci Rev 66(3-4):261–330
Neal A, Roberts CL (2000a) Applications of ground-penetrating radar (GPR) to sedimentological, geomorphological and geoarchaeological studies in coastal environments. Geol Soc Lond Spec Publ 175(1):139–171

Neal A, Roberts CL (2000b) Applications of ground-penetrating radar (GPR) to sedimentological, geomorphological and geoarchaeological studies in coastal environments. Geol Soc Lond Spec Publ 175(1):139–171

Okoye MA, Koeln GT (2003) Remote sending (satellite) system technologies. Environmental Monitoring I, Encyclopedia of Life Support Systems (EOLSS)

Oweis T, Hachum A, Bruggeman A (2004) Indigenous water-harvesting systems in West Asia and North Africa. Indigenous water-harvesting systems in West Asia and North Africa

Ozdogan M, Gutman G (2008) A new methodology to map irrigated areas using multi-temporal MODIS and ancillary data: an application example in the continental US. Remote Sens Environ 112(9):3520–3537

Palmer-Jones R (1999) Slowdown in agricultural growth in Bangladesh: neither a good description nor a description good to give. In: Sonar Bangla? Agricultural growth and agrarian change in West Bengal and Bangladesh. Sage, London, pp 92–136

Parker D (1988) In: Stewert JB, Engman ET (eds) Innovations in geographic information systems, vol 3. Taylor and Francis, London

Pervez MS, Budde M, Rowland J (2014) Mapping irrigated areas in Afghanistan over the past decade using MODIS NDVI. Remote Sens Environ 149:155–165

Prasad RK, Mondal NC, Banerjee P, Nandakumar MV, Singh VS (2008) Deciphering potential groundwater zone in hard rock through the application of GIS. Environ Geol 55(3):467–475

Pratap K, Ravindran KV, Prabakaran B (2000) Groundwater prospect zoning using remote sensing and geographical information system: a case study in Dala-Renukoot area, Sonbhadra district, Uttar Pradesh. J Indian Soc Remote Sens 28(4):249–263

Preeja KR, Joseph S, Thomas J, Vijith H (2011) Identification of groundwater potential zones of a tropical river basin (Kerala, India) using remote sensing and GIS techniques. J Indian Soc Remote Sens 39(1):83–94

Prithviraj N (1980) Geomorphic studies in Sarada river basin, Vishakapattanam District, Andhra Pradesh, India (Doctoral dissertation, Ph.D thesis (unpublished), Andhra University, Visakhapatnam, India)

Ranagalage M, Estoque RC, Murayama Y (2017) An urban heat island study of the Colombo metropolitan area, Sri Lanka, based on Landsat data (1997–2017). ISPRS Int J Geo-Inform 6 (7):189

Rao S, Divakara Rao V, Govil PK, Balaram V, PANTULU GC (1992) Geochemical and Sr-isotopic signatures in the 2.6 By Lepakshi granite, Anantapur district, Andhra Pradesh: implications for its origin and evolution. Indian Miner 46(3-4):289–302

Rashid M, Lone MA, Ahmed S (2012) Integrating geospatial and ground geophysical information as guidelines for groundwater potential zones in hard rock terrains of south India. Environ Monit Assess 184(8):4829–4839

Richards LA (1954) Diagnosis and improvement of saline and alkali soils. LWW

Robert M, Thomas A, Sekhar M, Badiger S, Ruiz L, Willaume M, Leenhardt D, Bergez JE (2017) Farm typology in the Berambadi Watershed (India): farming systems are determined by farm size and access to groundwater. Water 9(1):51

Rodell M, Velicogna I, Famiglietti JS (2009) Satellite-based estimates of groundwater depletion in India. Nature 460(7258):999–1002

Rose RS, Krishnan N (2009) Spatial analysis of groundwater potential using remote sensing and GIS in the Kanyakumari and Nambiyar basins, India. J Indian Soc Remote Sens 37(4):681–692

Saha R, Kumar GP, Pandiri M, Das IC, Rao PN, Reddy KS, Kumar KV (2018) Knowledge guided integrated geo-hydrological, geo-mathematical and GIS based groundwater draft estimation modelling in Budhan Pochampalli Watershed, Nalgonda District, Telangana State, India. Earth Sci India 11(4)

Satapathy I, Syed TH (2015) Characterization of groundwater potential and artificial recharge sites in Bokaro District, Jharkhand (India), using remote sensing and GIS-based techniques. Environ Earth Sci 74(5):4215–4232

Sebben ML, Werner AD, Graf T (2015) Seawater intrusion in fractured coastal aquifers: a preliminary numerical investigation using a fractured Henry problem. Adv Water Res 85:93–108

Seeyan S, Merkel B, Abo R (2014) Investigation of the relationship between groundwater level fluctuation and vegetation cover by using NDVI for Shaqlawa Basin, Kurdistan Region-Iraq. J Geogr Geol 6(3):187

Shaban A (2010) Support of space techniques for groundwater exploration in Lebanon. J Water Res Protect 2(5):469

Shah T (2010) Taming the anarchy: groundwater governance in South Asia. Routledge

Shah T (2014) Groundwater governance and irrigated agriculture. Global Water Partnership (GWP), Stockholm

Shah T, Molden D, Sakthivadivel R, Seckler D (2001) Global groundwater situation: opportunities and challenges. Econ Polit Wkly 36:4142–4150

Sharma AK, Hubert-Moy L, Buvaneshwari S, Sekhar M, Ruiz L, Bandyopadhyay S, Corgne S (2018) Irrigation history estimation using multitemporal landsat satellite images: application to an intensive groundwater irrigated agricultural watershed in India. Remote Sens 10(6):893

Siebert S, Burke J, Faures JM, Frenken K, Hoogeveen J, Döll P, Portmann FT (2010) Groundwater use for irrigation—a global inventory. Hydrology and earth system sciences 14(10):1863–1880

Siebert S, Henrich V, Frenken K, Burke J (2013) Update of the digital global map of irrigation areas to version 5. Rheinische Friedrich-Wilhelms-Universität, Bonn, Germany and Food and Agriculture Organization of the United Nations, Rome

Singh KV, Setia R, Sahoo S, Prasad A, Pateriya B (2015) Evaluation of NDWI and MNDWI for assessment of waterlogging by integrating digital elevation model and groundwater level. Geocarto Int 30(6):650–661

Singh RA, Gupta RC (2002) Traditional land and water management systems of North-East hill region. Indian J Tradit Knowl 1(1):32–39

Singhal BB, Gupta RP (2010) Applied hydrogeology of fractured rocks. Springer Science & Business Media, Dordrecht

Solomon S, Quiel F (2006) Groundwater study using remote sensing and geographic information systems (GIS) in the central highlands of Eritrea. Hydrogeol J 14(6):1029–1041

Sreedevi PD, Subrahmanyam K, Ahmed S (2005) Integrated approach for delineating potential zones to explore for groundwater in the Pageru River basin, Cuddapah District, Andhra Pradesh, India. Hydrogeol J 13(3):534–543

Srivastava PK, Gupta M, Mukherjee S (2012a) Mapping spatial distribution of pollutants in groundwater of a tropical area of India using remote sensing and GIS. Appl Geomatics 4 (1):21–32

Srivastava PK, Han D, Gupta M, Mukherjee S (2012b) Integrated framework for monitoring groundwater pollution using a geographical information system and multivariate analysis. Hydrol Sci J 57(7):1453–1472

Srivastava PK, Mukherjee S, Gupta M, Singh SK (2011) Characterizing monsoonal variation on water quality index of River Mahi in India using geographical information system. Water Quality, Exposure and Health 2(3-4):193–203

Stafford DB (ed) (1991) Civil engineering applications of remote sensing and geographic information systems. ASCE, New York

Stan D, Stan-Kłeczek I (2014) Application of electrical resistivity tomography to map lithological differences and subsurface structures (Eastern Sudetes, Czech Republic). Geomorphology 221:113–123

Steenhuis TS, Kung KJ, Cathles LM (1990) Finding layers in the soil. Ground-penetrating radar as a tool in studies of groundwater contamination. Cornell Eng Quart 25(1):15–19

Subrahmanyam M, Rao TP (2009) Interpretation of magnetic anomalies using some simple characteristic positions over tabular bodies. Explor Geophys 40(3):265–276

Swenson S, Wahr J, Milly PC (2003) Estimated accuracies of regional water storage variations inferred from the Gravity Recovery and Climate Experiment (GRACE). Water Resour Res 39 (8)

Taghavi-Jeloudar M, Han M, Davoudi M, Kim M (2013) Review of ancient wisdom of Qanat, and suggestions for future water management. Environ Eng Res 18(2):57–63

Taylor PN, Chadwick B, Moorbath S, Ramakrishnan M, Viswanatha MN (1984) Petrography, chemistry and isotopic ages of Peninsular Gneiss, Dharwar acid volcanic rocks and the Chitradurga Granite with special reference to the late Archean evolution of the Karnataka Craton, southern India. Precambrian Research 23(3-4):349–375

Teeuw RM (1995) Groundwater exploration using remote sensing and a low-cost geographical information system. Hydrogeol J 3(3):21–30

Thakur JK, Singh SK, Ekanthalu VS (2017) Integrating remote sensing, geographic information systems and global positioning system techniques with hydrological modeling. Appl Water Sci 7(4):1595–1608

Thenkabail PS, Biradar CM, Noojipady P, Dheeravath V, Li Y, Velpuri M, Gumma M, Gangalakunta OR, Turral H, Cai X, Vithanage J (2009a) Global irrigated area map (GIAM), derived from remote sensing, for the end of the last millennium. Int J Remote Sens 30 (14):3679–3733

Thenkabail PS, Dheeravath V, Biradar CM, Gangalakunta OR, Noojipady P, Gurappa C, Velpuri M, Gumma M, Li Y (2009b) Irrigated area maps and statistics of India using remote sensing and national statistics. Remote Sens 1(2):50–67

Thenkabail PS, Hanjra MA, Dheeravath V, Gumma M (2010) A holistic view of global croplands and their water use for ensuring global food security in the 21st century through advanced remote sensing and non-remote sensing approaches. Remote Sens 2(1):211–261

Thenkabail PS, Schull M, Turral H (2005) Ganges and Indus river basin land use/land cover (LULC) and irrigated area mapping using continuous streams of MODIS data. Remote Sens Environ 95(3):317–341

Thomas A, Sharma PK, Sharma MK, Sood A (1999) Hydrogeomorphological mapping in assessing ground water by using remote sensing data—a case study in lehra gaga block, sangrur district, Punjab. J Indian Soc Remote Sen 27(1):31

Tiwari VM, Wahr JM, Swenson S, Singh B (2011) Land water storage variation over Southern India from space gravimetry. Curr Sci 101:536–540

Todd DK (1980) Groundwater hydrogeology, 2nd edn. Wiley, New York, p 537

Tsur Y (1990) The stabilization role of groundwater when surface water supplies are uncertain: the implications for groundwater development. Water Resour Res 26(5):811–818

Velpuri NM, Thenkabail PS, Gumma MK, Biradar C, Dheeravath V, Noojipady P, Yuanjie L (2009) Influence of resolution in irrigated area mapping and area estimation. Photogramm Eng Remote Sens 75(12):1383–1395

Villholth KG, Tøttrup C, Stendel M, Maherry A (2013) Integrated mapping of groundwater drought risk in the Southern African Development Community (SADC) region. Hydrogeology J 21 (4):863–885

Vittala SS, Govindaiah S, Honne Gowda H (2006) Digital Elevation Model (DEM) for identification of groundwater prospective zones. J Indian Soc Remote Sens 34:305–310

Wahr J, Swenson S, Zlotnicki V, Velicogna I (2004) Time-variable gravity from GRACE: first results. Geophys Res Lett 31(11)

Werner AD, Simmons CT (2009) Impact of sea level rise on sea water intrusion in coastal aquifers. Groundwater 47(2):197–204

Wilcox L (1955) Classification and use of irrigation waters. US Department of Agriculture

www.cals.arizona.edu/OALS/ALN/aln51/ednote51.html

www.cgwb.gov.in/District_Profile/AP/Ananthapur.pdf (Central Ground Water Board (2013) Brochure Anantapur District, Andhra Pradesh Southern Region, Hyderabad)

www.cgwb.gov.in/MAP/CATEGON%202011.jpg (Central Ground Water Board, 2011)

www.commons.wikimedia.org/wiki/File:Qanat-3.svg

www.fao.org/aquastat/en/geospatial-information/global-maps-irrigated-areas/irrigation-by-country
www.geospatialworld.net (Devex and CRS, 2019).
www.ngdc.noaa.gov/geomag/emag2
www.usgs.gov
www.usgs.gov. Retrieved 2020-03-18 “Where is Earth’s Water?”
Yaduvanshi A, Srivastava PK, Pandey AC (2015) Integrating TRMM and MODIS satellite with socio-economic vulnerability for monitoring drought risk over a tropical region of India. Phys Chem Earth Parts A/B/C 83:14–27
Zhu T, Ringler C, Cai X (2007) Energy price and groundwater extraction for agriculture: exploring the energy-water-food nexus at the global and basin levels. In: International Conference of Linkages between Energy and Water Management for Agriculture in Developing Countries, Hyderabad, India

Chapter 14
Assessment of Urban Sprawl Impact on Agricultural Land Use Using Geospatial Techniques

Kuntal Ganguly, Shewli Shabnam, Srabani Das, and Tarik Mitran

Contents

K. Ganguly (✉)
Cognizant Technology Solutions, Hyderabad, India
e-mail: kuntal.ganguly@cognizant.com

S. Shabnam
Bidhannagar College, Kolkata, West Bengal, India

S. Das
Indian Institute of Engineering Science and Technology, Kolkata, West Bengal, India

T. Mitran
Soil and Land Resources Assessment Division, National Remote Sensing Centre, Department of Space, ISRO, Hyderabad, Telangana, India
e-mail: tarikmitran@nrsc.gov.in

T. Mitran et al. (eds.), *Geospatial Technologies for Crops and Soils*,
https://doi.org/10.1007/978-981-15-6864-0_14

Abstract The number of city dwellers around the world is expected to increase about 2.5 billion between 2018 and 2050. This increment will lead to urban sprawl which is associated with destruction of agricultural lands, loss of fertile soils and reduction in food production. Already around 3–4% reduction of global crop production has been reported, in which Africa tops the list with 9% loss followed by Asia (5–6%). Hence, impact assessment of urban sprawl on agricultural land uses at both regional and global scale is required. The data from global satellite imageries and new geospatial technologies can play a crucial role in facilitating the impact assessments with precision and regularity. Remote Sensing (RS) and Geographic Information System (GIS) coupled with various modelling techniques have been proved to be an efficient tool for the analysis of land use/land cover (LULC). Such modelling approaches can be utilized to explore potential future impact of urban expansion on croplands and evaluate potential trade-offs between different land demands and thus are helpful for informed decision-making. This chapter emphasizes on the usage of RS and GIS to address the impact of urbanization on agricultural lands.

Keywords Cropland · Global land use change · Geographic information system · Land use/land cover · Remote sensing · Spatial statistics · Urban expansion

Abbreviations

ANN	Artificial Neural Network
CAPRI	Common Agricultural Policy Regionalized Impact model
CLUE	Conversion of Land Use and its Effects modelling framework
ETM	Enhanced Thematic Mapper
GDP	Gross Domestic Product
GILA	Greater Ibadan-Lagos-Accra
GIS	Geographic Information System
HAF	Harvested Area Fraction
IAMs	Integrated Assessment Models
IRS	Indian Remote Sensing Satellite
ISRO	Indian Space Research Organization
KH	Key Hole
Landsat	Land Satellite
LandSHIFT	Land Simulation to Harmonize and Integrate Freshwater Availability and the Terrestrial Environment
LST	Land Surface Temperatures
LULC	Land Use and Land Cover
LULCC	Land Use and Land Cover Change
LUS	Land Use Systems
LUSD	Land Use Scenario Dynamics
MA	Metropolis Area
Mha	Million Hectares

MSS	Multispectral Scanner System
MUR	Mega Urban Region
MURs	Mega Urban Regions
NDVI	Normalized Difference Vegetation Index
NRSC	National Remote Sensing Centre
NUTS	Nomenclature of Territorial Units for Statistics
RMS	Root Mean Square
RS	Remote Sensing
SALU	Sudano-Sahelian Countries of Africa
SAVI	Soil-Adjusted Vegetation Index
SSPs	Socioeconomic Pathways
TGA	Total Geographical Area
TM	Thematic Mapper
TM	Thematic Mapper
UTM	Universal Transverse Mercator
WGS	World Geodetic Survey

14.1 Introduction

The processes of industrialization, urbanization and globalization together have posed mounting environmental problems in the present world. These include the change in climate; scarcity of freshwater; desertification; pollution of soil, air and water through contamination of hazardous waste; loss of biodiversity; and many more which are creating hindrances to sustainable development (Mitran et al. 2018). Therefore, at present, environmental assessments are gaining significance in the urban planning processes around the world. Around 1800 AD, only 3% of the world's population resided in urban centres. It increased to 14% in 1900 and in 2000 it reached to 47% (World Bank 2013). However, the rate of urbanization is not the same throughout the world. In 2018, almost 82% of population of North America lived in urban areas, whereas the corresponding figure was 50% in Asia; but at present, the pace of urbanization is higher in developing nations. From 1990 to 2018, the average annual rate of urbanization in high-income nations was 0.32%, while in China it was 2.9% (United Nations 2019). Although 68.8% of population in India were living in rural areas in 2011, the pace of urbanization is increasing in the country. India's urban population increased by 31.8% between 2001 and 2011, while the rural population increased by just 12.18% during this period (Chand et al. 2017). As per the Census of India, 79 million individuals lived in urban regions in 1961 and it had gone up to 377 million in 2011. Only 23 metropolis areas (MA_s) existed in India in 1991 which increased to 46 in 2011 (Chandramouli and General 2011). Rapid urbanization is associated with tremendous growth of population and construction exercises in urban areas, resulting in an exceptional loss of urban green spaces and expansion of the impervious region. Nevertheless, short-term and unsystematic planning approaches of cities lead to urban sprawl, resulting in

deterioration in the social, economic and ecological sustainability of the city (Islam and Ahmed 2011). Hence there is a need for continuous monitoring of such changes through a systematic approach.

The recent advancement of geospatial technologies including RS and GIS can play a meaningful role in land use/land cover (LULC) assessment. The various spatial and temporal satellite images have been widely used by many researchers to monitor the land use and land cover changes as due to urban growth. Such information is also used to retrieve various biophysical attributes of land such as land surface temperatures (LST), vegetation abundances and built-up indices which are good indicators to measure an urban ecosystem condition (Streutker 2002; Sobrino et al. 2004; Xu 2008a, b; Lu and Weng 2009; Tooke et al. 2009; Zhang et al. 2009). Villages in India are embracing the urban way of life and have capitulated to the present advancement exercises. These villages are located at the peri-urban or fringe areas and getting acclimatized with the developing urban communities and advancement of "new towns". At a certain point when urban communities slowly spread out over the hinterlands due to excessive population pressure, villages in the fringe areas get transformed at a slow pace. These areas have comprehensively alluded to a rural-urban fringe. The rural-urban fringe which is the territory at the edge of a city has become an inexorably well-known region for economic developments. In India, rivalry for land in these areas increased significantly during the 1990s. Here, the land is less expensive as compared to the core of the city. Therefore, various service centres, offices, manufacturing units, etc. which were situated in the prime downtown areas moved to these territories as their past areas lacked space for extension. These rural-urban periphery zones also attract shopping centres, business parks and amusement facilities like golf courses.

An eccentricity of Indian urban system is the villages in periurban areas where the prime change occurs in the landscape segment. Most of the Indian urban areas are not continuous uninterrupted urban agglomerations. One can find the remnants of villages inside the built-up areas of the Indian city. These remnants are the signs of existence of villages in those areas which were consumed in the process of urban expansion of the concerned city or advancement of new towns. The expansion of the city immerses the villages by transforming their land form agricultural use to urban use. Thus, urban encroachment brings in extraordinary changes in the economic base of the communities which ultimately convert the villages into urban systems. However, the physical and social patterns of the villages change just in a relative sense. In the developing countries like India, the rural areas which are brought under urban fold can't be immediately acclimatized to the new urban form of development (Shaw 2020).

Urban sprawl takes a wide range of forms, including residential buildings, industrial compounds, infrastructural development, agricultural land, etc. The toll of urban sprawl is heavily paid by agricultural lands. Loss of agricultural land as a result of urban sprawl has become a global phenomenon tormenting all countries of the world, rich or poor. It is influencing urban communities as well as suburban and rural areas, as it is responsible for the loss of cropland, asset exhaustion and the

decay of old urban centres. Urban sprawl, actually, consumes vast amount of land under agriculture or forest cover.

Ideally, economic data shows agricultural lands present in urban areas are mainly exposed to marginalization leading to the weakening of productive, social and environmental functions of farmers (Lovell 2010; Zasada 2011). The most important negative consequence of the process of urbanization is the acquisition of productive land, in particular the loss of highly fertile land (Mazzocchi et al. 2013; Huang et al. 2015; Busko and Szafranska 2018). The reduction of cultivable fertile lands is mainly noticeable in developing nations (Su et al. 2011; Deng et al. 2015) but is also occurring in Europe (Wojciech et al. 2020). It is evident from the research conducted as a part of the project "Peri-urban Land Use Relationships Strategies and Sustainability Assessment Tools for Urban-Rural Linkages (PLUREL)" (Piorr et al. 2011). It has been identified that the process of rapid urbanization is bringing significant changes in available spaces and causing degradation of quality of the MAs. Research shows areas that are arable, open and environment friendly, mostly preferable for building house infrastructure and business centres (Piorr et al. 2011; Mazzocchi et al. 2013). Research performed in Poland also highlights the fact that the contemporary farmlands in and around metropolitan areas are kept as a reserve for more profit-gaining activities (Lorens and Martyniuk 2010; Krzyk et al. 2013).

14.2 Factors Influencing Land Use Changes with Special Reference to Farmland

To analyse the factors of influencing the proportion of agricultural land in urban region, both internal and exterior factors are significant (Mazzocchi et al. 2013). Factors can be categorized into socioeconomic issues, natural constraint (geophysical), institutional structure and causes associated with unadapted agricultural arrangement, particularly, land fragmentation (Mitsuda and Ito 2011; Huang et al. 2015; Deng et al. 2015).

Drivers for land use may be categorized into four types such as (a) socioeconomic aspects that exhibit the influence of the urbanization process, (b) ecological and permanent geographic features, (c) traits of agricultural system and (d) the institutional structure (Table 14.1). Let us discuss some of the factors in brief. Firstly, let us analyse the role of socioeconomic factors on the changing nature of land use. The socioeconomic factors refer to demographic and economic factors that are influencing urban sprawl. Pressure of population in metropolitan cities changes agricultural land into urban tracts, and the inherent limitation of cultivation makes transformation easy (Mazzocchi et al. 2013). The need for space for humans to work and live is accelerated by rapid population growth and (Huang et al. 2015) through in-migration (Zasada 2011). Huge population growth in the cities due to more opportunities for employment (Ravetz et al. 2013) leads to the changes in urban land use. According

Table 14.1 Factors influencing land use/land cover change

Drivers	Important entities	Impact on agriculture	References
Demographic character	Density of population	The increase in density of population, net migration and rate of unemployment stipulate people to go for nonagricultural activities which result in the conversion of the agricultural land into nonfarm uses	Zasada et al. (2011), Ravetz et al. (2013), Huang et al. (2015) and Deng et al. (2015)
	Combination of in-migration and out-migration rate		
	Rate of employment generation		
	Labour characteristics		
Geographical factors	Proximity to market	Infrastructural development creates better access to market which in turn influences the cropping pattern in the region. Proximity to market also changes the land use pattern from agricultural to nonagricultural as the latter brings higher rent for every unit of surface area	Gellrich (2007), Mitsuda and Ito (2011), Diogo et al. (2015), Deng et al. (2015) and Huang et al. (2015)
	Road networks		
	Infrastructure		
	Environmental condition		
Socioeconomic factors	Commercial crops	Due to export potentiality, farmers shift towards commercial crops such as cotton, sugarcane, etc. Cities which act as market centres of these crops grow with time and influence the conversion of agricultural land into built-up areas	Lambin and Meyfroidt (2010), Mitsuda and Ito (2011) and Dang and Kawasaki (2017)
	Export potentiality		
	Urban population		
Institutional factors	Government policies	Effective policies and programmes of the government and legal support may influence the decision-making of individuals that can restrict the conversion of agricultural land into nonagricultural uses	Van Rij et al. (2008), Pölling et al. (2016) and Busko and Szafranska (2018)
	Spatial planning		
	Land conversion		

to Alonso (1964) and Konagaya (1999), in the areas where population density is very high and nonagricultural enterprises are prevalent, there would be minimum share of agricultural land as economic worth of urban land use is higher than agricultural land use.

Another important factor that influences urban land use is environmental and fixed geographic features. The pattern of land use is controlled by urban proximity as well as by the distance from port and roadway (Mitsuda and Ito 2011; Deng et al.

2015), environmental conditions and quality of agricultural products including climate, availability of water and the type of land (Gellrich 2007; Huang et al. 2015). In which specific way a land owner will utilize its land depends on the remoteness of a land from markets (von Thünian ideas) and the "nature" of land in terms of geophysical features (Ricardian ideas) (Gellrich 2007). Intense competition for plots in "ideal" location (near the market place, by rivers, at airports, at ports, etc.) raises the demands of the plots. Subsequently, in accordance with the theory of utility maximization, the land will be allocated to people who can offer high economic rents. Only when high return from land is guaranteed, a person will invest considerable amount of money to buy that land or take lease of that land.

The pattern of land use is also determined by the characteristics of agricultural system. Low return from agriculture due to faulty farm structure (prevalence of small farms and land fragmentation) forces the land owner, first, to keep it unutilized and then convert it to nonagricultural uses (Mazzocchi et al. 2013; Xie et al. 2014). Grădinaru et al. (2015), as well as Hagedorn (2004), in their respective study found that the problem of fragmentation of farms was particularly prevalent in Poland. Additionally, Wästfelt and Zhang (2016) pointed out that, due to high price of land in urban region, it was not possible for the cultivators to increase the area of production, and they had to remain satisfied with lower economic rents. Previously, Sinclair and Thünen (1976) opined that, with the spreading of urban land use, the chances of maintaining agricultural production or increasing its intensity would be lesser in the future.

The final and most important factor is the institutional framework which plays a vital role in preserving agricultural land in metropolitan regions (Van Rij et al. 2008). For example, government departments in many places formulate laws to protect green areas (Pölling et al. 2016), make suitable provision in development strategy (e.g. not allowing a good quality of land to be abandoned) and limit the spatial expansion of cities to check the function of market mechanism, i.e. the effect of economic rents (Huang et al. 2015).

14.3 Loss of Agricultural Lands Due to Urbanization: Global Estimates

More than 60% of the irrigated cropland in the world is located in the vicinity of urban areas, emphasizing significant contest for land between urban and agricultural uses. A number of studies show that rapid urban growth over the past 30 years has resulted in the shrinking of cropland worldwide, including China, India, the USA, Turkey, Egypt and other countries (Chen 2007; Bagan and Yamagata 2014; Ahmad et al. 2016). The loss of agricultural land has direct impact on production of food grains and livelihood security (Brook and Davila 2000) in many countries. Unfortunately, not adequate efforts are made to study and understand the impact of future urban expansion on farmland. Nevertheless, we cannot deny the possibility of major

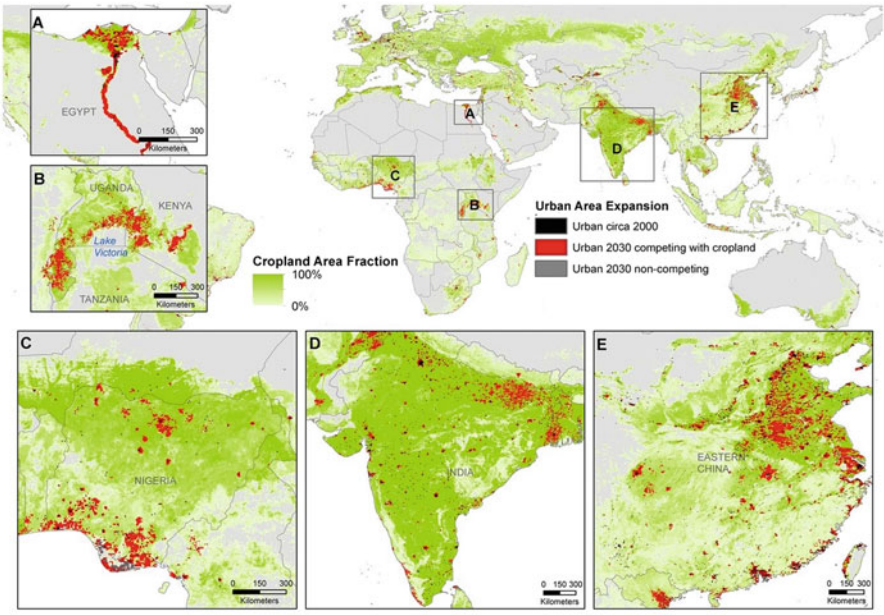

Fig. 14.1 Map shows future urban growth until 2030 and probable agricultural loss. Competing areas (red) hold farmlands but have a high likelihood (>75%) of becoming urbanized by 2030. (A–E) show hot spots of rapid urban growth areas. (Adopted, d'Amour et al. 2016, 2017)

land conflicts between nonfarm and agricultural uses in the transition of mega urbanization. Seto and Ramankutty (2016) predicted that in the future most of the urban expansion will occur in Africa and Asia, often in places characterized by high level of poverty and systemic interruption in the food system (d'Amour et al. 2016). In many countries, the economic importance of agriculture is tremendous as it ensures economic growth by providing considerable amount of employment and holding a large share in the gross domestic product (GDP) at national level. Hence, it is necessary to evaluate the impact of urban expansion on agricultural land at regional, national, subnational level and global scale to recognize the possible areas of conflicts as well as strategies to pursue sustainable form of urban expansion.

It is expected that in the future urban expansion will take place in areas which are at present under cultivation (Fig. 14.1). In 2000, around 46 million hectares (Mha) of croplands equivalent to 3.2% (3.0–3.8%) of presently available cropland were situated in places which are most likely to be grown as urban area by 2020 (d'Amour et al. 2016). However, potential of urban agriculture has been recognized recently and it is practised in many cities. d'Amour et al. (2016) observed that 36% of urban (on average) places were utilized for cultivation. According to them, this percentage of urban agriculture should prevail when urban area expands, but always there would be regional variation (e.g. 32% in Africa and 41% in Asia). Following those prevailing cropland fractions, between 2000 and 2030, total cropland loss would

Table 14.2 Impact of urban area expansion on crop production at country and regional level

Country/ region	Total urban expansion (in km^2)	Production loss (in %)	References
World	346,491	3.7	d'Amour et al. (2016), d'Amour et al. (2017) and He et al. (2019)
Asia	144,186	5.6	
Africa	19,897	8.9	
Europe	39,861	1.2	
America	199,253	1.3	
Australia	8350	0.2	
China	66,351	8.7	
India	14,438	3.9	
USA	66,389	0.7	
Brazil	28,817	2.4	
Vietnam	4499	15.9	
Mexico	7928	3.7	
Indonesia	4391	2.3	

amount to 2.0% (1.8–2.4%) of the global total, i.e. 30 Mha (27–35 Mha), and the countries like Pakistan, China and Vietnam would experience the fraction ranging between 5% and 10%.

Globally, the cumulative effect of urban growth on cropland was well marked, but at regional level, the impact would be critical and differentiated. In case of moderate urbanization, Asia and Africa together would account for around 80% (24 Mha) of the total global cropland loss. In Africa, three regions, namely, Nigeria, Egypt and the region surrounding Lake Victoria Basin, would be severely affected (Fig. 14.1). On the other hand, in Asia, major cropland loss would be visible along coastlines and river valleys, many of which are located at the transition zone of mega urban regions (MURs), such as the Bohai Economic Rim and the Yangtze River Delta in China, Java Island in Indonesia, etc.

China is experiencing tremendous rate of urban growth, but the urban area is expanding at the expense of country's most productive agricultural tract (d'Amour et al. 2017). It would possibly pose severe threat to domestic food production in the future. India, Brazil and the USA would also experience loss of agricultural land, but in contrast to China, urban expansion in these countries would not probably touch big tracts of croplands, so there would be lesser chance of drastic drop in domestic crop production (Table 14.2).

Future urban growth will continue to take place on primary croplands. According to d'Amour et al. (2017), due to expansion of urban area, there would be a loss of 3.7% in crop production by the end of 2030. On an average, the farmland lost due to urban growth was 1.77 times more productive than the average global croplands. Other studies (Chen 2007; Bagan and Yamagata 2014; Ahmad et al. 2016) have also confirmed the fact that farmlands surrounding urban agglomerations possessed higher productivity than average. Their analyses also revealed that Africa and Asia were expected to face 8.9% and 5.6% of global production losses, respectively

(Table 14.2). Globally, there are very few countries where agricultural productivity of urban farmland is below national average (e.g. the USA). China and India's urbanization is likely to be continued but with various spatial pattern and growth dynamics. In China, cropping areas are concentrated along the coastal tracts which are expected to be affected by 2030 due to urban expansion. In India, the urban extent was quite small (3 Mha) compared to China (8 Mha) in 2000. In India, the net expansion of urban area until 2030 is expected to cover 3–4 Mha which would be almost double in case of China (7–8 Mha). In 2012, China's urban population has surpassed its rural counterpart; and by 2050 it is projected that three fourths of the country's population will reside in urban areas. In 2011, the proportion of urban population in India was around 31% which is expected to be 50% by 2050. Moreover, in 2011, 79% of India's urban population lived in cities with 100,000 population or fewer, and 52% of the total population of India lived in villages and towns (urban sprawl) that had population below 5000 (Mitra et al. 2016). As per the study, cropland loss is not going to harm India by 2030 as it is only about 2% (d'Amour et al. 2016; d'Amour et al. 2017); however, other studies have suggested that in the future, urban expansion can accelerate the risk of cropland loss and the rate of cropland destruction would be much faster than rate of urban growth (Pandey and Seto 2015).

In African countries, cropland loss varies over the space. Unlike China, in Africa major urban areas are expected to grow along the coastal areas, whereas most of the farmlands have inland location (d'Amour et al. 2017). The situation is still not less troublesome because in another study it has been estimated that 11% area under soybean, 14% under maize, 19% under rice and 26% area under wheat production will be urbanized by 2030 (d'Amour et al. 2016). On the other hand, in Asia, the corresponding crop area loss is predicted as 7%, 10%, 9% and 13%, respectively, due to urban expansion. However, in arid zones of Africa, cropland is going to be relatively less affected by urbanization (Fig. 14.1). In the developed countries, the situation is not so grim. Therefore, urbanization is definitely going to effect the staple food production in Asia and Africa. However, in the developed world, impact of future urbanization on staple food crops would be less. In the USA it would be around 1 to 2%, in Europe 2 to 3%, and in Australasia it will be less than 1 percent.

Tremendous cropland loss has been observed for urban megalopolis and an increasing often spreading over 10,000 sq. km with population over than 20 million (d'Amour et al. 2016). As per the case studies of Doos (2002) and d'Amour et al. (2016), Divine et al. (2019), principal farming lands are highly susceptible to conversion in expansion regions with estimated farmland losses between 0.1 and 1.2 Mha. According to d'Amour et al. (2016) in mega urban regions (MURs) of Bangladesh, Indonesia and India, the relative productivity is <2 pico-calories (Pcal), whereas the relative productivity in MURs of China is 1.05–22.05 Pcal.

To comprehend the evolving MURs agricultural production system patterns, the harvested area fraction (HAF) was analysed. According to the analysis, the aggregated HAF of the crops in majority of the MURs is very high. The combined HAF of rice and wheat in the Yangtze River Delta around Shanghai MURs accounts for 50% of total area harvested in competing areas, whereas it is quite small in the USA,

Japan and Brazil as these areas produce other foodstuffs like vegetables. HAF is also small in the Greater Ibadan-Lagos-Accra (GILA) corridor in Western Africa as crops produced in this area do not contribute much to diets.

It has already been mentioned that loss of farmland is a direct effect of urban expansion. MURs most of the times contain multiple urban centres, with fertile farmland spread all through the urban framework. However, there are regions with a single principal urban centre, like Greater Delhi where croplands surround the urban centre. In this case there exists little possibility for the formation of extensive continuous urban tract. As per Pandey and Seto (2015), agricultural land in these regions will continue to be transformed, but not at a similar pace like multi-nodal urban regions.

Let us look at another problem of urban expansion faced by the farmers living in urban sprawls. In this region the remaining croplands and farmers suffer from scarcity of water and climate hazards. Dewan et al. (2012) reported that the urban growth into the Ganges-Brahmaputra Delta is responsible for the loss of wetlands and drying up of water bodies which otherwise helps to protect flood. Excessive extraction of groundwater for urban development and transformation of cropland is creating obstacles for compaction and aggradations of sediments which is ultimately leading to the sinking of Ganga-Brahmaputra Delta. As a result, with the adverse effect of climate change, this delta becomes more prone to hazard due to rise in sea level (Higgins et al. 2014).

Climatic hazards not will only pose a threat towards urban areas but to the rest of the croplands in this delta region which produce rice (HAF of rice >83%), the main staple food of this region. The rise in sea level and submergence of land is a matter of concern for Greater Cairo because the significant part of Nile Delta is about to sink below sea level (Syviski et al. 2009) and expected to sink further (Syvitski et al. 2009). In this case another problem is that the amount of sediment discharged from the southern dams is decreasing day by day. It will enhance the pressure on the delta, which will ultimately reduce the size of delta (Redeker and Kantoush 2014). Study shows that extremely fertile farmlands along the Nile have been changed into urban tracts although they are the primary source of the food supply for the people of this region (combined HAF for wheat and maize, 49%).

14.4 Assessing Impact of Urbanization on Agricultural Land: Geospatial Approaches

The geospatial data fill the information gaps by asking the following questions: (i) Which parts of the croplands are more prone to transformation because of potential urban growth? (ii) What is estimation of cropland loss in the future, particularly main cropland, due to urban expansion? (iii) What will be the impact of cropland loss on the total agricultural area and economic significance of agriculture in different countries?

The understanding of "hidden linkages" between urbanization and food systems is the key for sustainability in the era of mega urbanization (Seto and Ramankutty 2016). It is not possible to stop urbanization but we must focus on where and how to maintain cropland for producing food. Hence this food system includes fabrication, refining, disposition, utilization and disposal of wastes just like other related directive establishments and activities (Pothikuchi and Kaufman 2000). Presently satellite imageries are used to study urban sprawl and changes in other LULC. Alqurashi et al. (2016) analysed the urban expansion and changes in land cover in five Middle East cities using an object-based image analysis approach. Cao et al. (2018) performed a study on urban expansion and its consequences on land use changes utilizing radar graph as well as inclination bearing techniques and landscape metrics. Liu et al. (2016) examined urban extension in China in recent decades utilizing satellite imageries. Gumma et al. (2011) made a study on urban extension and wastewater-irrigated areas in Hyderabad, India, using Landsat images. Many of these studies used Landsat imageries to analyse the changes with time. Using sophisticated techniques of satellite image analysis, a number of studies have demonstrated the mapping processes of agricultural areas (Thiruvengadachari and Sakthivadivel 1997; Sakthivadivel et al. 1999; Bastiaanssen et al. 2002; Velpuri et al. 2009). Parece and Campbell (2013) designated urban impervious surfaces of Roanoke in the USA utilizing Landsat imagery and high-resolution aerial photographs. Myint et al. (2011) specifically classified land use pattern utilizing high spatial resolution imagery and object-based classification. Zhang et al. (2017) evaluated the effects of urban growth on ecosystem services through various models. For example, he used shared socioeconomic pathways (SSPs) and the land use scenario dynamics-urban (LUSD-urban) model for his study. However, mapping of urban agricultural areas, particularly fragmented irrigated areas, is a challenge because of the differing scope of irrigated plot sizes, crops and water sources used by farmers (Draeger 1976; Gaur et al. 2008). Another popular indicator to observe cropland and LULC changes over a set period is Normalized Difference Vegetation Index (NDVI), and it has been used in many studies (Gumma et al. 2011; Gray and Bilsborrow 2014).

14.4.1 Selection of Geospatial Data and Scale of Mapping Through the Understanding of Land Use Functions

Land cover indicates the physical type or surface qualities of land (e.g. forest or the existence of any construction). Therefore, during fieldwork or through remote sensing, one can directly recognize land cover. In contrast, land use describes the economic and social functions of land or how humans are utilizing the land. Land use systems exist when land uses are systematically linked through temporal or

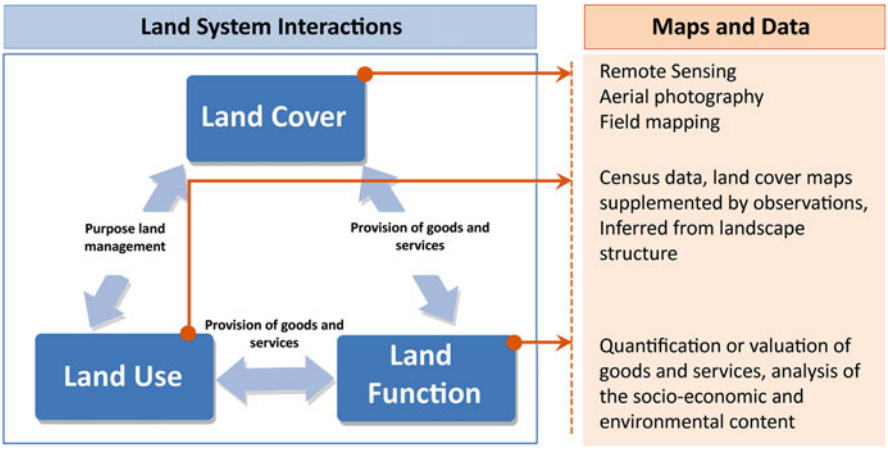

Fig. 14.2 Correlation between land cover, land use and land function and possible methods to collect spatial data. (Modified, Verburg et al. 2009)

spatial interactions such as crop rotation (Fig. 14.2). Land cover observations (e.g. satellite imageries) alone are normally not enough to detect and analyse such land use systems.

Additional socioeconomic data (e.g. harvest statistics) are necessary to assess these systems (Kruska et al. 2003). At a landscape level, there may be various interrelated land use systems which offer a variety of products and services to society (Verburg et al. 2009). The ability of the land to supply goods and services is referred to as land use functions or ecosystem functions (de Groot 1992; de Groot 2006; Verburg et al. 2009). In geospatial studies choice of appropriate data on the basis of scale is of utmost importance. The scale of a geospatial analysis sets limits of information contents and the degree of reality with which it can be delineated on the map. A multi-scale view of remote sensing (RS) data analysis for urban expansion and land use change has been illustrated in Table 14.3 for the mapping and investigation of urban land use dynamics. It has highlighted four levels of geographical scale. Each scale determines their spatial characteristics and is associated with specific urban dynamics. Besides, each scale is influenced by different drivers and factors of growth and shows scale-specific effects and patterns as a result of the process separation. Based on the framework, we examine scale issues related to both RS data analysis and modelling of urban change dynamics (Herold et al. 2002).

Table 14.3 A multi-scale framework for the mapping and analysis of urban land use change using remote sensing

Spatial extent	Change dynamic	Mapping entity	Spatial resolution	Mapping intervals
Global level	Trend of urbanization globally Uneven development Regional polarization	Spatial extent of urban area	1 km	10–50 ys
Superregional level				
National/country level	Formation of exhubs/edge cities Urban deconcentration Counter-urbanization		30 m	5–10 ys
City level	Intra-urban land use conversion Socioeconomic segregation	Urban land cover objects (vegetation patches, buildings, etc.)	5 m	2–5 ys
District/block level	Housing/land development Neighbourhood changes		1 m	1–2 ys

14.4.2 Land Use Models

Land use models can broadly be understood as tools that help us in understanding and analysing complex linkages and feedbacks between various operators of land use change. However, there are a number of definitions of land use models. Heistermann et al. (2006) define a land use model as an instrument to figure out the change of area allocated to at least one specific type of land use. Verburg et al. (2004) define a land use model as a device to carry on the analysis of the cause and effects of land use dynamics.

Models that are capable of capturing (reproducing) aspects of the complex dynamics involved in land use change can support understanding of these dynamics. Land use models may be applied to project demand for land for specific purposes and where resulting land use changes will occur given different boundary conditions. They can, therefore, help in understanding the drivers of land use change and identify the areas that are likely to be under the greatest pressure and can, thus, provide support to land use and policy decisions. Land use models can also be used to explore alternative futures using scenarios. However, not all land use models can be used for scenario analysis. Models that are dependent merely on an extrapolation of trends in land use change may not be appropriate for scenario analysis as they are only applicable within the range of land use changes on which they are based (Verburg et al. 2004).

Because of the significance of monitoring the effect of urbanization on the physical condition, many scientists have shown interest in urban extension and land use dynamic analysis and developed prediction models. Various types of such models have been distinguished in the writing. Important among them are (i) urban spatial change or land use models (Wray and Cheruiyot 2015) and (ii) urban growth prediction models (Triantakonstantis 2012). These models may have

common objectives, but they differ in terms of methodology and/or theoretical assumptions. Heistermann et al. (2006) reviewed land use models at continental to global scales and categorize them into (a) geographic land use models, including empirical-statistical and rule-based or process-based models, (b) economic land use models and (c) integrated models. Geographic models are those that allocate area or commodity demand on suitable locations based on local characteristics. Economic models apply supply and demand of land-intensive commodities as the basis for allotment of land (albeit at large geographical scales), while integrated models combine these two approaches. It incorporates economic analysis of world markets and policies to measure demand and supply and also geographic analysis for allotment of land under different uses.

14.4.2.1 Geographic Model

14.4.2.1.1 Empirical-Statistical Models

The CLUE (Conversion of Land Use and its Effects modelling framework) model framework (Veldkamp and Fresco 1996) is probably the most well-known and most frequently used land use model globally. Over the years, the model has evolved, and different versions have been developed (CLUE, CLUE-s, Dyna-CLUE and CLUE-Scanner). The key assumption underlying the CLUE models is that observed spatial relations between land use types and possible explanatory factors signify currently active processes and remain valid in the future. Logistic regression is used to derive relationships between observed land use and spatial variables.

14.4.2.1.2 Rule-Based/Process-Based Models

In contrast to empirical-statistical models that are based on statistical relationships between drivers and historical land use changes, rule- or process-based models reproduce processes dealing with the interaction of different elements forming a system (Lambin et al. 2000). For example, the SALU (Sudano-sahelian countries of Africa) model (Stéphenne and Lambin 2001) simulates spatially explicit changes of land use at a coarse resolution for the Sahel zone using a series of agricultural land use transformations that are typical for many regions, because agricultural development at the most extensive technological level is followed by agricultural intensification once a land threshold is reached.

14.4.2.2 Land System Models

Land system models are also classed as integrated models as they combine economic and environmental processes. An example of the land system approach is the model developed by Letourneau et al. (2012). They have used a land use system (LUS) approach to model the change of land at global level. The LUS are combinations of land cover, land use (such as livestock, cropland and pasture), population and accessibility and were modelled at 5 arc minute resolution (~10 × 10 km). Regions and management intensities are controlled by global economic models based on global trends and the choice between land cover change and intensification of agriculture. This approach is advocated for better understanding of the land-sharing/land-sparing debate as it can show regionally variable outcomes of expansion of arable land based on local aspects that either restrain or endorse land system conversion (Phalan et al. 2011; Tscharntke et al. 2012; van Asselen and Verburg 2013).

Another example of a land use system model is the LandSHIFT (Land Simulation to Harmonize and Integrate Freshwater Availability and the Terrestrial Environment) model framework (Schaldach et al. 2006). LandSHIFT is an instrument for medium-term scenario analysis (20–50 years). It helps in assessing environmental impact of land use change, and the model simulates spatial-temporal dynamics of settlement, farming and livestock grazing. Land use system is at the core of LandSHIFT as it combines model components representing anthropogenic and environmental systems.

14.4.2.3 Economic Land Use Models

In economic models, demand and supply functions for tradable commodities are recognized as the main drivers of land use change. Among such models, the Common Agricultural Policy Regionalized Impact (CAPRI) model is an agricultural economic model developed to assess agricultural policies within the European Union (Britz 2005). The model links approximately 280 administrative regions at the NUTS-2 (Nomenclature of Territorial Units for Statistics) level with a global agricultural trade model. For each of the NUTS-2 regions, CAPRI simulates changes in crop areas and yields for 35 crops, herd sizes of 13 animal groups as well as feeding and fertilizing practice. It also includes fallow land that exhausts the available agricultural area. Economic land use models have the advantage that they can persistently deal with demand, supply and trade via price mechanisms. However, they are often unable to explain supply-side constraints (such as behaviour not related to price mechanisms) as well as incorporate the effect of demand on real land use change processes.

Table 14.4 Urban growth indicators and their respective models (Modified, Musa et al. 2017)

Models	Urban growth indicators	References
Fractals	Remoteness from central business district (CBD), nearness to urban functionaries, neighbourhood quality and land use types	Batty and Longely (1986)
Agent based	Land use category, size of population and its density, distance from noise levels, shops; entry permission to green/vegetated areas and transportation zone	Bharat et al. (2016)
Artificial neural networks	Elevation, gradient, population growth per annum, category of land parcels, propinquity to roads, service facility and built-up areas	Wang and Mountrakis (2011)
Cellular automata	Distance to centre of the town, railways and roadways, as well as land use and terrain category	Vaz and Arsanjani (2015)
Decision trees	Development type; elevation; gradient/slope; interior/exterior subregions; land use category; accessibility to entertainment zone; large industries; rivers/streams/canals; primary, secondary and minor roads; kernal densities of croplands; residential zones; urban expansion area; education facilities; ponds or lakes; lands for cultivation and natural green space/vegetation	Jin and Mountrakis (2013)
Linear/logistic regression	Coordinates (x, y), land use category, gradient, restricted location, size of population, nearness to main active business/commercial/financial centres, nearness to urban centres and roadways	Alsharif and Pradhan (2014)

14.4.2.4 Integrated Land Use Models

Integrated land use models are models that combine both economic and environmental factors and thus overcome the limitations associated with purely geographical and economic land use models. Integrated assessment models (IAMs) are typically large-scale models that combine natural and human subsystems and can thus be classified as a type of integrated models although they are not specifically focused on land use modelling. The Model of Agricultural Production and its Impact on the Environment (Lotze-Campen et al. 2008) is a global, spatially explicit model of land use change. The model concentrates on agricultural production along with land and water for the most important crop and livestock production and covers ten economic regions of the world. The model develops land use patterns for grid cells at a resolution of three by three degrees (ca. 300 × 300 km at the equator) incorporating regional economic conditions and spatially explicit data on potential crop yields and land and water constraints. The main urban development indicators come from socioeconomic exercises which obviously could impact changes in land use and urban development design.

So, different models use different indicators to predict urban expansion. These explain the variation in their performances. Important models explaining urban growth and indicators used in those models are presented in Table 14.4.

14.5 The Impact of Urbanization on Land Transformation with Special Reference to Cropland: A Case Study

In India the land use pattern is changing rapidly as the result of urban growth. The impact of urbanization on agricultural land in the last 50 years (1965–2014) in parts of Pune, Maharashtra, is presented here as a case study.

14.5.1 Study Area

The study was conducted in a section of Pune district covering four taluks, namely, Haveli, Khed, Marvel and Mulshi, and spreading over an area of about 5533 km^2 (Fig. 14.3).

The study region is traversed by three main rivers, namely, Pavana, Mula and Mutha. The study area is situated at the lap of hills bordering the west. Steep slopes and rocky red soils add geomorphologic characteristics to this region. The alluvial deposits along the bank of the rivers contain sand, gravels, fine silts and clays.

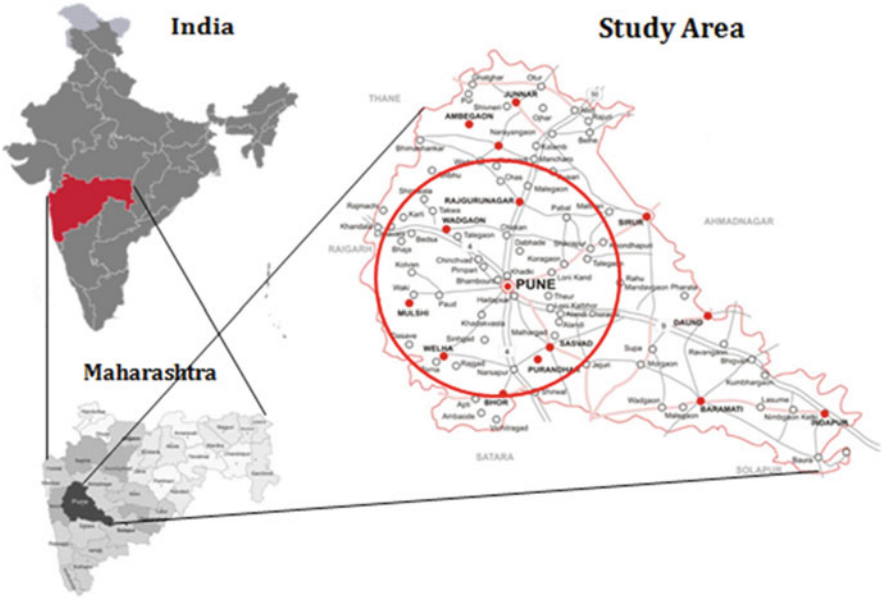

Fig. 14.3 Location of the study area

14.5.2 Datasets Used and Method of Approach

The geometrically corrected satellite datasets such as Landsat MSS, Landsat TM, Landsat ETM+, Landsat 8, and IRS Resourcesat 2 LISS-3 have been examined for this study. The list of satellite data used and their specification is presented in Table 14.5. The declassified CORONA image was also used after geometric correction with a root mean square error of 0.238. The Universal Transverse Mercator (UTM) Zone 43 N' coordinate system and WGS-84 datum were used for all the images. The boundaries of the villages correspond to the cadastral boundaries. These boundaries were utilized to analyse LULC at village level.

Present study includes creation of geospatial outputs following data preparation, processing and in-depth research; the workflow of the study is presented in Fig. 14.4.

Table 14.5 Satellite image specifications

Sensor types	Sensors	Platforms	Spatial resolutions (in meter)	Operational from
Multispectral	MSS	Landsat 1	60	4 Feb 1973
				17 Mar 1981
	TM	Landsat 5	30	22 Mar 1992
	ETM+	Landsat 7		27 Mar 2002
		Landsat 8		4 Apr 2014
	Resourcesat 2, LISS-3	IRS	23.5	17 Mar 2012
Panchromatic	KH-A.B	CORONA	2.5	11 Nov 1965

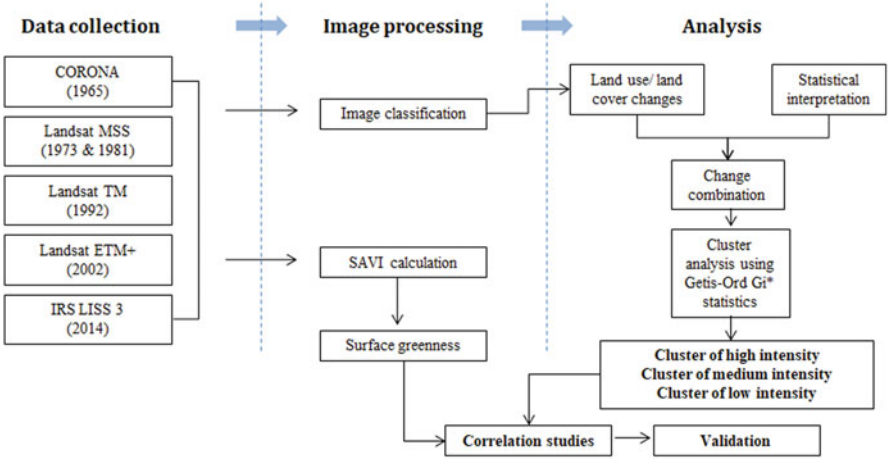

Fig. 14.4 Workflow of the study

14.5.3 Land Use/Land Cover Classification

Satellite image classification is the base of all land cover analysis. In the present study, object-based classification system was adopted to classify LULC for better accuracy (Ganguly et al. 2016). This technique depends on the interpreter who uses visual cues such as tone, texture, shape, pattern and relationship to other objects to make out the differences in land cover classes (NRSC 2010). The classification scheme, at level 2 classes, was used which is neither very detailed nor much generalized (Table 14.6). This classification scheme was based on the LULC classification system developed by National Remote Sensing Centre (NRSC), India. It was used to build a pan-India LULC 1:50000 Atlas in 2011. The LULC classified maps were prepared for six different years, i.e. 1965, 1973, 1981, 1992, 2002 and 2014 (Fig. 14.5).

14.5.4 Assessment of LULC Change Dynamics and Statistical Interpretations

The classified LULC maps were analysed for the past 50 years (Fig. 14.5). Based on the available data, the individual LULC class area and change statistics were generated for 6 years, i.e. 1965, 1973, 1981, 1992, 2002 and 2014 (Table 14.7).

Table 14.6 Basis of land use/land cover classification

LULC category	Description
Urban	Residential, commercial and mixed built-up areas, public facilities, green or vegetated landscapes, utilities and facilities, transportation and recreational facilities, reclaimed zones
Rural	Large-/small-size built-up areas, associated mainly with agricultural lands and noncommercial allied sectors. Generally grouped or cluster in form and scattered
Industrial	Industrial buildings, dumps of ash and cooling ponds, quarries, brick kilns, gravel and sandpits, dump of industrial raw materials, etc.
Cropland	Standing or growing crops, agricultural plantations
Fallow lands	Bare lands with no crops, taken up for agricultural use but temporarily left uncultivated for more than a year
Forests	A large area with more than 10% of tree canopy cover (more than 0.5 ha of area). Includes forest plantation and scrub kind of forests
Tree clads	Tree or woody vegetation outside of designated forest
Wastelands	Lands which are un-capable for cultivation, degraded due to natural causes. It includes saline land, rocky barren area, gullied/ravinous land, Ranna, shrubs
River	Consistent or inconsistent flow of water through a definite channel into sea/lake/inland basin/marsh
Water bodies	Surface water (permanent/seasonal) like dam, reservoir, tanks, lakes and ponds

Adopted, NRSC (2010)

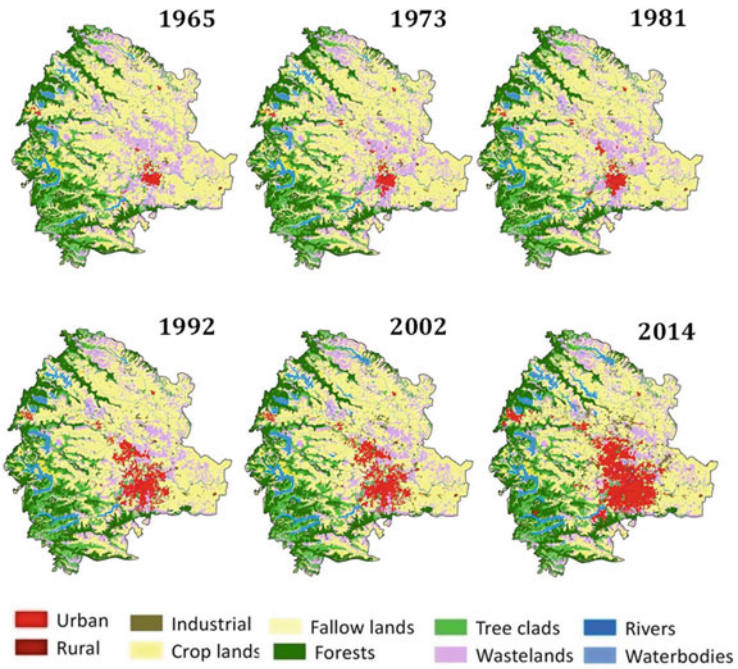

Fig. 14.5 Land use and land cover change map

Table 14.7 Land use/land cover changes from 1965 to 2014 (in km^2)

LULC class	Year 1965	Year 1973	Year 1981	Year 1992	Year 2002	Year 2014
Urban	45.69	55.71	63.16	231.0	250.49	456.6
Rural	4.44	5.80	6.15	6.79	16.25	18.33
Industrial	8.04	16.1	17.84	23.44	41.64	98.7
Forest	905.98	905.9	905.9	905.9	905.8	898.4
Tree clad	604.33	604.3	604.3	603.18	605.9	598.02
Cropland	2538.10	2519.2	2509.8	2347.3	2311.5	2154.8
Fallow land	191.25	191.2	191.2	239.2	222.7	181.0
Plantation	39.06	39.06	39.06	39.06	38.36	37.09
Wastelands	1017.5	1018.4	1018.4	904.8	885.1	806.4
River	57.66	57.67	57.67	55.94	54.40	49.73
Water body	121.13	121.1	121.1	160.2	192.48	233.4

Table 14.8 shows that between 1965 and 2014, the land use pattern in this region has changed drastically. It is found that urban and industrial zones have been expanded substantially as compared to other land use classes. However, the maximum growth was noticed during 1992 to 2014. The rate of increment in urban built-up and industrial area during this period was 8 times higher than the previous decades. As a result constant decreases in croplands were also observed between

Table 14.8 Land use/land cover interclass changes from 1965 to 2014 (in km^2)

(1965–2014)												
						2014						
1965	Urban	Rural	Industries	**Croplands**	Fallow lands	Plantation	Forests	Tree clads	Wastelands	River	Water bodies	**(1965) Total**
Urban	45.69											45.7
Rural	2.21	2.2			0.03							4.44
Industries	0.03		8.01									8.04
Croplands	219.18	6.46	29.18	**2151.79**	49.55				1.71	0.05	80.18	2538.1
Fallow lands	40.41	3	12.1	**0.1**	131.46						4.18	191.25
Plantation			1.97			37.09						39.06
Forests	1.39		2.72				898.18		3.52	0.01	0.16	905.9
Tree clads	0.1	0.39	0.37	**1.4**				595.29	0.1		6.68	604.3
Wastelands	147.29	6.28	46.32	**1.34**	0.03		0.4	2.73	799.79	0.03	13.38	1017.5
River				**0.2**					0.02	50.03	7.41	57.66
Water bodies											121.13	121.1
(2014) Total	456.3	18.33	100.67	2154.8	181.07	37.09	898.6	598.02	805.1	50.12	233.1	5533.27

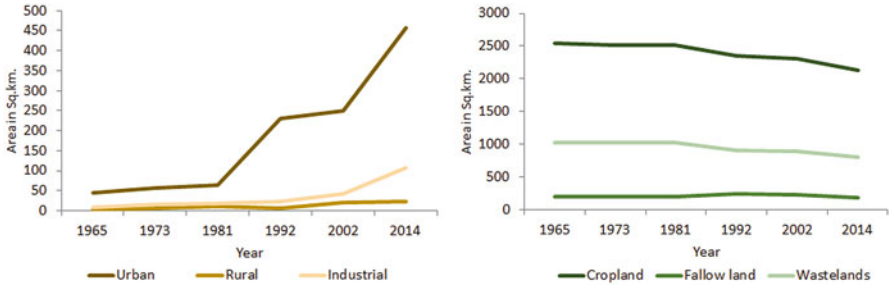

Fig. 14.6 Temporal changes in LULC from 1965 to 2014

1992 and 2014. A significant amount of change was found in case of wastelands, the area of which decreased around 200 km^2 between 1981 and 2014. Besides, construction of new reservoirs in this area brought significant changes in land cover by increasing water bodies during 1965 to 2014.

A comparison between temporal changes in area under built-ups, agricultural lands and wastelands from 1965 to 2014 is presented in Fig. 14.6. Besides, the interclass changes of LULC classes were also compared and presented in Table 14.8. The comparison between built-up area and agriculture shows opposite trend as the expansion in urban areas has caused a remarkable reduction in the amount of agricultural lands and wastelands (Fig. 14.6). The maximum changes in LULC were observed in urban areas (456.3 km2) due to newly constructed water bodies (233.12 km2) and industrial expansion (100.67 km2).

14.5.5 Optimization of Geospatial Techniques

In this study, geostatistical measures with spatial technique named as spatial autocorrelation were implemented. The basic principle of spatial autocorrelation in geospatial statistics is the task of assemblage a set of items in a way that intends to put together or cluster items into the same group that is more analogous to each other than other groups. It is defined as the interrelation between variables assembling together through space. It assesses the efficiency of spatial correlation and executes the theory of entropy. As per this technique, the presence of any orderly pattern in the spatial distribution of a variable is said to be spatially correlated, and the correlation is positive if surrounding areas are similar. On the other hand, if the adjacent areas are dissimilar and random patterns are exhibited with no significant spatial cluster, it is said to be negatively correlated. However, in spatial statistics cluster analysis is not able to elucidate the reason of importance of location which carries statistically considerable cluster of LULCC. These clusters have maximum rate of transformation than other locations. This technique fails to recognize components that force changes in LULC.

14.5.5.1 Spatial Autocorrelation Using Statistical Method

Gi-statistics was developed by Getis and Ord (Getis and Ord 1992; Ord and Getis 1995) that represent a global spatial autocorrelation (SA) index. Applicability lies in its discerning cluster structures of high or low concentration. The simple form of this method has been suggested by Songchitruksa and Zeng (2010) in the following manner:

$$\mathrm{Gi}^* = \frac{\sum_{j=1}^{n} W_{ij} x_j}{\sum_{j=1}^{n} x_j} \tag{14.1}$$

where Gi* = SA statistic of an event i over n events

w_{ij} = measure of the spatial proximity between regions i and j
x_j = magnitude of the variable x at events j over all n

The standardized Gi* is a Z-value which can be expressed as follows:

$$Z(\mathrm{Gi}^*) = \frac{\sum_{j=1}^{n} w_{ij} x_j - \overline{\mathbf{x}} \sum_{j=1}^{n} w_{ij}^2}{s \sqrt{\frac{n \sum_{j=1}^{n} w_{ij}^2 - \left(\sum_{j=1}^{n} w_{ij} \right)^2}{n-1}}} \tag{14.2}$$

The Gi value close to "0" represents a random distribution of events. A high positive and negative absolute value indicates the clusters of transforming land with high- and low-value events, respectively (Manepalli et al. 2011).

14.5.6 GIS Database Design for Spatial Statistical Model

GIS database is advantageous as one can utilize the data more efficiently without altering the original dataset. In this study, the classified dataset was redefined in the form of land use/land cover change combinations to execute spatial database queries more accurately. For computational advantage of Getis-Ord Gi* model in ArcGIS 10.2.1, a unique value was assigned to all the LULCC combinations (Ganguly et al. 2016). The returned Gi* value for each polygon in the dataset was further used for ordinary kriging to ascertain a contiguous map for showcasing all other prediction points through the chosen model. The resultant Gi* score helps to categorize the study area into hot and cold spots. The hot spot represents the maximum spatial change area, whereas the cold spots is the minimum spatial change area. This was

further categorized into high-, medium- and low-intensity zones on the basis of its scores.

14.5.7 Zonation of Land Use Change Clusters

In this study, regions with higher concentration of LULCC clusters have been identified using the Z-score. The nature of hot spots from 1965 to 2014 was identified using GIS-based kriging interpolation technique which helps to categorize the whole study area into three zones as high-, medium- and low-intensity clusters (Fig. 14.7).

Clusters where land transformation had taken place after 1992 were identified as high-intensity zones. In this zone adjacent villages near to Pune and Pimpri-Chinchwad city areas showed continuous and higher rates of LULCC since 1992 (Fig. 14.8). Along with rapid urbanization, vigorous industrialization had also changed the land use pattern in this zone. As a result, higher rate of reduction in croplands and wastelands was noticed.

It was observed from the analysis of land transformation of the past five decades (1965–2014) that about 190 new villages surrounding of Pune city experienced a higher concentration of LULCC after 1992. There was a marginal increase (2% of the total geographical area (TGA)) in urban built-up area during 1965 to 1992.

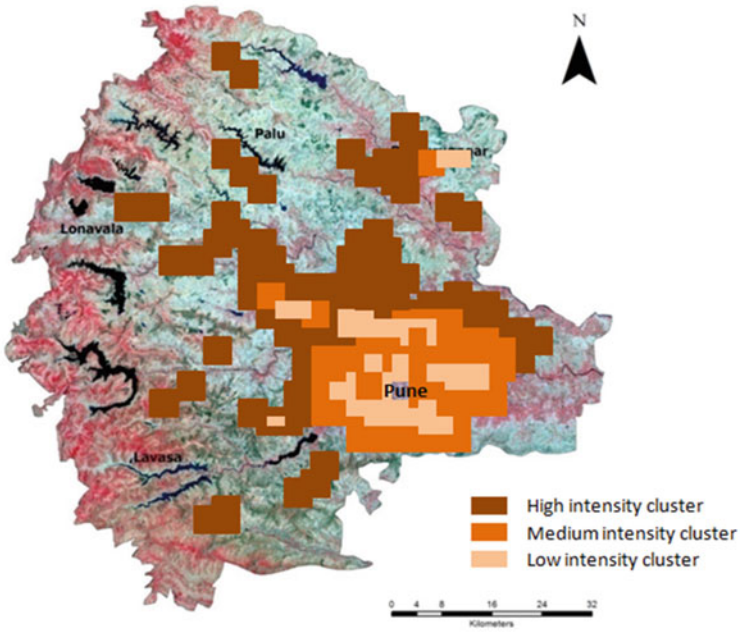

Fig. 14.7 Zonation of LULCC intensity

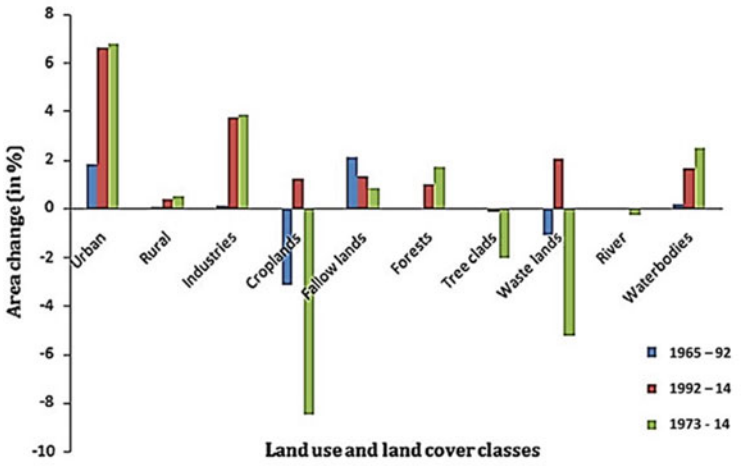

Fig. 14.8 Changes in LULC in villages under high-intensity cluster

Compared to this period, the increase was more than three times (more than 6.5% of TGA) between 1992 and 2014. Likewise, industrial area increased from less than 1% to nearly 4% of the TGA during the last 50 years. A considerable decrease (9% of TGA) in agricultural land was also noticed. Similarly, an area comprising 6% of TGA was transformed from wastelands to urban built-up area during the last 40 years. The medium-intensity cluster represents the areas which are already developed zone and still expanding rapidly and filling up all empty lands due to urban expansion. Figure 14.9 shows the changes in LULC in villages under medium-intensity cluster. A higher rate of urbanization (~40%) and marginal changes in industrial expansion (below 5%) were observed in medium-intensity cluster. A significant decrease of area under croplands and wastelands was also observed between 1965 and 2014. The low-intensity cluster represents the areas having very less changes during the last 20 years. The low-intensity clusters practically represent nonprogressive zone.

It was found that in the study region during 1965 to 2014, urban area and industrial area recorded an increase of 1.5%. Although here the loss of cropland and wasteland proceeds with supplementary hot spot, yet the extent of transformation was not consequential.

14.5.8 Temporal Variations in Surface Greenness During 1973 to 2014

To assess the temporal variation of surface greenness due to urban expansion in the study region, the Soil-Adjusted Vegetation Index (SAVI) has been calculated from the satellite images (Ganguly et al. 2014). SAVI can overcome the effects of soil

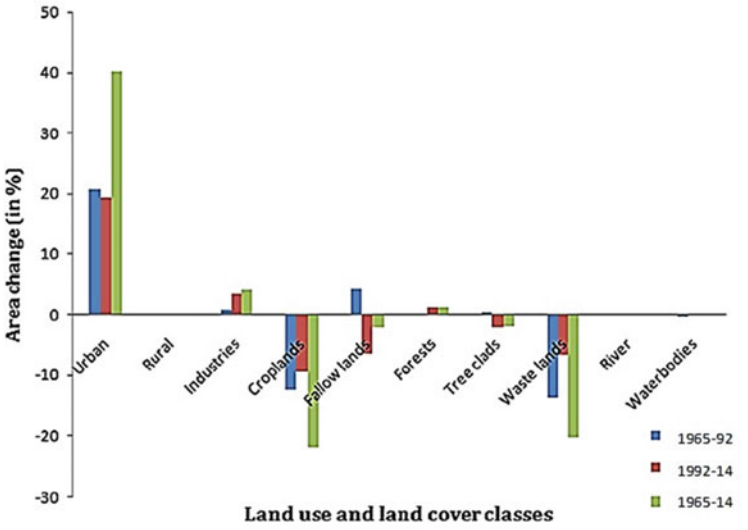

Fig. 14.9 Changes in LULC in villages under medium-intensity cluster

pixel by using a canopy background adjustment factor. An optimal value of 0.5 has been suggested by Huete and Huete (1988) to account for first-order soil background variations. It can be best used in areas with sparse vegetation and where soil is visible through the canopy. It is computed in the following manner:

$$\text{SAVI} = \frac{1.5 * (\text{NIR} - \text{RED})}{(\text{NIR} + \text{RED} + 0.5)} \tag{14.3}$$

The value of SAVI ranges from −1 to +1. The positive values signify wet area or greenness and negative values indicate less vegetation. The images obtained from SAVI model can visually distinguish vegetated and non-vegetated areas. SAVI results often get affected by sparse vegetation characteristic. However a gradual decreasing trend in greenness was noticed in SAVI images from 1973 to 2014.

Results of the study area show considerable amount of greenness with a very high SAVI value (0.92) in 1973. However a reduction of greenness was observed in 1992 (SAVI = 0.76). Thereafter a gradual decrease of SAVI indicates very low vegetation cover (SAVI = 0.2) in 2014 (Fig. 14.10).

Correlation analysis was carried out to understand the relationship between greenness and impervious surface. A negative correlation ($R^2 = -0.61$) between the above two parameters was found which reflects that 61.6 percent variation in vegetation cover in the study region was due to the presence of impervious surface/ built-up areas (Fig. 14.11).

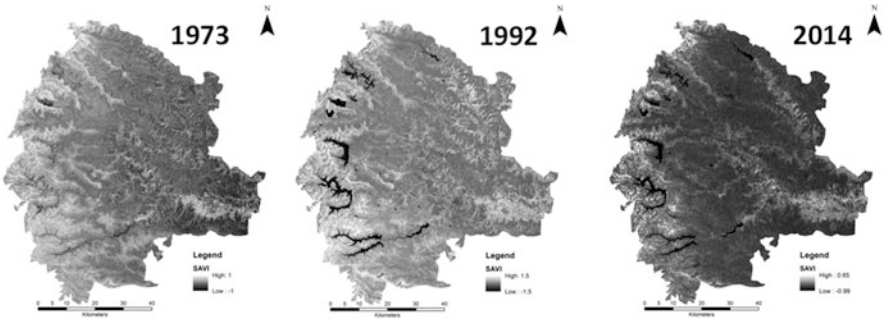

Fig. 14.10 Calculated SAVI showing changes in greenness over time

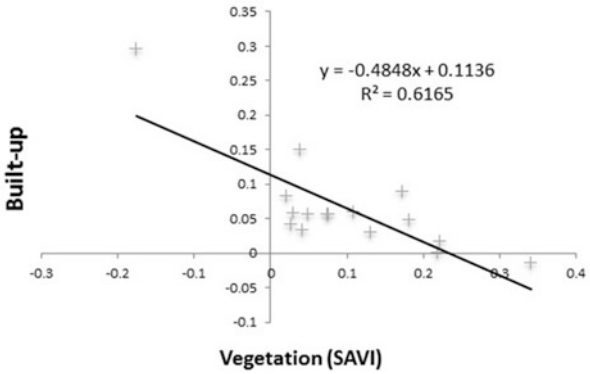

Fig. 14.11 Relationship between built-up area and vegetation

14.5.9 Conclusions and Future Perspectives

According to Global Land Outlook report published by United Nations (Al Malalha 2016), an estimated 30 Mha of global area is expected to be urbanized by 2030. Asia and Africa are projected to lead the chart. Together they are predicted to account for nearly 80% of the global cropland loss due to urban expansion. Hence a continuous monitoring is required to identify the impact of urban sprawl on agricultural land at both regional and global level. However, systematic studies using traditional techniques have become time-consuming and burdensome over the years. The uses of RS and GIS have generated ample scopes to analyse the current situations rapidly and create a spatial forecasting system for better decision-making processes. The various spatial modelling tools and approaches have been used by many researchers to determine the potential impact of urbanization on cropland. Different GIS and RS modelling approaches under various scenarios show a declining trend in croplands in the future. Forecasting the potential changes in land use is generally a multistep

approach which involves several datasets, models and assessment methods, introducing and propagating uncertainty at each step. However, land use modelling is very complex and in most cases requires significant expertise and capacity in terms of understanding of drivers, spatial data analysis and statistical relationships. The choice of land use model to be used in a project, therefore, depends on the scale, scope and purpose of the study as well as the resources and capacity available. There are many existing models of land use which can be used for LULCC analysis within a range of future scenarios.

References

Ahmad S, Avtar R, Sethi M, Surjan A (2016) Delhi's land cover change in post transit era. Cities 50:111–118

Al Malalha M (2016) Global land outlook Writeshop: summary of discussions

Alonso W (1964) Location and land use. Harvard University Press, Cambridge, MA. ISBN 9780674730854

Alqurashi AF, Kumar L, Al-Ghamdi KA (2016) Spatiotemporal modeling of urban growth predictions based on driving force factors in five Saudi Arabian cities. ISPRS Int J Geo Infor 5 (8):139

Alsharif AA, Pradhan B (2014) Urban sprawl analysis of Tripoli Metropolitan city (Libya) using remote sensing data and multivariate logistic regression model. J Indian Soc Remote Sens 42 (1):149–163

Bagan H, Yamagata Y (2014) Land-cover change analysis in 50 global cities by using a combination of Landsat data and analysis of grid cells. Environ Res Lett 9(6):64015

Bastiaanssen WG, Molden DJ, Makin IW (2002) Remote sensing for irrigated agriculture: examples from research and possible applications. Agric Water Manag 46(2):137–155

Batty M, Longley PA (1986) The fractal simulation of urban structure. Environ Plan 18 (9):1143–1179

Bharath AH, Vinay S, Ramachandra TV (2016) Agent-based modelling urban dynamics of Bhopal, India. J Settlements Spat Plan 7(1):1–4

Britz W (2005) CAPRI modelling system documentation (Common Agricultural Policy Regional Impact Analysis). Bonn. http://www.ilr.uni-bonn.de/agpo/rsrch/capri

Brook RM, Dávila JD (2000) The peri-urban interface: a tale of two cities. School of Agricultural and Forest Sciences, University of Wales, Bangor

Busko M, Szafranska B (2018) Analysis of changes in land use patterns pursuant to the conversion of agricultural land to non-agricultural use in the context of the sustainable development of the Malopolska region. Sustainability 10:136

Cao H, Liu J, Fu C, Zhang W, Wang G, Yang G, Luo L (2018) Urban expansion and its impact on the land use pattern in Xishuangbanna since the reform and opening up of China. Remote Sens 9 (2):137

Chand R, Srivastava S, Singh J (2017) Changing structure of rural economy of India implications for employment and growth. 2:2018. https://doi.org/10.13140/RG.2.2.17270.09280

Chandramouli C, General R (2011) Census of India 2011. Provisional population totals, vol 2011. Government of India, New Delhi, pp 409–413

Chen J (2007) Rapid urbanization in China: a real challenge to soil protection and food security. Catena 69(1):1–15

d'Amour CB, Wenz L, Kalkuhl M, Steckel JC, Creutzig F (2016) Teleconnected food supply shocks. Environ Res Lett 11(3):366–379

d'Amour CB, Reitsma F, Baiocchi G, Barthel S, Güneralp B, Erb KH, Haberl H, Creutzig F, Seto KC (2017) Future urban land expansion and implications for global croplands. Proc Natl Acad Sci 114(34):8939–8944

Dang AN, Kawasaki A (2017) Integrating biophysical and socio-economic factors for land-use and land-cover change projection in agricultural economic regions. Ecol Model 344:29–37

De Groot RS (1992) Functions of nature: evaluation of nature in environmental planning, management and decision-making. Wolters Noordhoff B.V, Groningen

De Groot R (2006) Function-analysis and valuation as a tool to assess land use conflicts in planning for sustainable, multi-functional landscapes. Landsc Urban Plan 75(3–4):175–186

Deng X, Huang J, Rozelle S, Zhang J, Li Z (2015) Impact of urbanization on cultivated land changes in China. Land Use Policy 45:1–7

Dewan AM, Yamaguchi Y, Rahman MZ (2012) Dynamics of land use/cover changes and the analysis of landscape fragmentation in Dhaka Metropolitan, Bangladesh. Geogr J 77 (3):315–330

Diogo V, Koomen E, Kuhlman T (2015) An economic theory-based explanatory model of agricultural land-use patterns: the Netherlands as a case study. Agric Syst 139:1–16

Divine OA, Felix A, Bernice N (2019) Perspectives on agricultural land use conversion and food security in rural Ghana. Science 1:14

Döös BR (2002) Population growth and loss of arable land. Glob Environ Chang 12(4):303–311

Draeger WC (1976) Machine-assisted analysis of Landsat data in the study of crop-soils relationships. US Geological Survey, Sioux Falls

Ganguly K, Ravi Shankar G (2014) Geo-environmental appraisal for studying urban environment and its associated biophysical parameters using remote sensing and GIS technique. Int Arch Photogramm Remote Sens XL-8:717–724

Ganguly K, Kumar R, Reddy KM, Rao PJ, Saxena MR, Ravi Shankar G (2016) Optimization of spatial statistical approaches to identify land use/land cover change hot spots of Pune region of Maharashtra using Remote Sensing and GIS techniques. Geocarto Int 32(7):777–796

Gaur A, Biggs TW, Gumma MK, Parthasaradhi G, Turral H (2008) Water scarcity effects on equitable water distribution and land use in a major irrigation project—case study in India. J Irrig Drain Eng 4(1):26–35

Gellrich M (2007) Zimmermann, N.E. Investigating the regional-scale pattern of agricultural land abandonment in the Swiss mountains: a spatial statistical modelling approach. Landsc Urban Plan 79:65–76

Getis A Ord JK (1992) The analysis of spatial association by use of distance statistics. Geogr Anal 24:189–206

Getis A, Ord JK (1992) The analysis of spatial association by use of distance statistics. Geogr Anal 24:189–206

Grădinaru SR, Iojă CI, Onose DA, Gavrilidis AA, Pătru-Stupariu I, Kienast F, Hersperger AM (2015) Land abandonment as a precursor of built-up development at the sprawling periphery of former socialist cities. Ecol Indic 57:305–313

Gray CL, Bilsborrow RE (2014) Consequences of out-migration for land use in rural Ecuador. Land Use Policy 36:182–191

Gumma KM, Van Rooijen D, Nelson A, Thenkabail PS, Aakuraju RV, Amerasinghe P (2011) Expansion of urban area and wastewater irrigated rice area in Hyderabad, India. Irrig Drain Syst 25(3):135–149

Hagedorn K (2004) Property rights reform on agricultural land in Central and Eastern Europe. Q J Int Agric 43(4):409–438

He C, Liu Z, Gou S, Zhang Q, Zhang J, Xu L (2019) Detection global urban expansion over the last three decades using fully convolutional network. Environ Res Lett 14(3):034008

Heistermann M, Müller C, Ronneberger K (2006) Land in sight? Achievements, deficits and potentials of continental to global scale land-use modeling. Agric Ecosyst Environ 114 (2–4):141–158

Herold M, Clarke KC, Menz G (2002) A multi-scale framework for mapping and analysis of the spatial and temporal pattern of urban growth. In: 22nd EARSEL Symposium "Geoinformation for European-wide integration" Proceedings, Prague 2002 Jun.

Higgins SA, Overeem I, Steckler MS, Syvitski JPM, Seeber L, Akhter SH (2014) InSAR measurements of compaction and subsidence in the Ganges-Brahmaputra Delta, Bangladesh. J Geophys Res Earth Surf 119(8):1768–1781

Huang D, Jin H, Zhao X, Liu S (2015) Factors influencing the conversion of arable land to urban use and policy implications in Beijing, China. Sustainability 7:180–194

Huete A, Huete AR (1988) A soil-adjusted vegetation index (SAVI). Remote Sensing of Environment. Remote Sens Environ 25:295–309

Islam MS, Ahmed R (2011) Land use change prediction in Dhaka city using GIS aided Markov chain modeling. J Life Earth Sci 6:81–89

Jin H, Mountrakis G (2013) Integration of urban growth modelling products with image-based urban change analysis. Int J Remote Sens 34(15):5468–5486

Konagaya K (1999) The generalised Thunen Alonso model for land use change in Sumatra Island. Geogr Environ Model 3:145–162

Kruska RL, Reid RS, Thornton PK, Henninger N, Kristjanson PM (2003) Mapping livestock-oriented agricultural production systems for the developing world. Agric Syst 77(1):39–63

Krzyk P, Tokarczuk T, Heczko-Hyłowa E, Ziobrowski Z (2013) Obszary rolne jako element struktury przestrzennej miast–problemy planistyczne. Instytut Rozwoju Miast, Kraków, p 175

Lambin EF, Meyfroidt P (2010) Land use transitions: socio-ecological feedback versus socio-economic change. Land Use Policy 27(2):108–118

Lambin EF, Rounsevell MDA, Geist HJ (2000) Are agricultural land-use models able to predict changes in land-use intensity? Agric Ecosyst Environ 82:321–331

Letourneau A, Verburg PH, Stehfest E (2012) A land-use systems approach to represent land-use dynamics at continental and global scales. Environ Model Softw 33:61–79

Liu X, Derudder B, Wu K (2016) Measuring polycentric urban development in China: an intercity transportation network perspective. Reg Stud 50(8):1302–1315

Lorens P, Martyniuk-Pe ̨czek J (2010) Zarza ̨dzanie Rozwojem Przestrzennym Miast; Wydawnictwo Urbanista: Gdan ́sk, Poland, pp 16–42. ISBN 978-83-89649-30-0

Lotze-Campen H, Müller C, Bondeau A, Rost S, Popp A, Lucht W (2008) Global food demand, productivity growth, and the scarcity of land and water resources: a spatially explicit mathematical programming approach. Agric Econ 39:325–338

Lovell ST (2010) Multifunctional urban agriculture for sustainable land use planning in the United States. Sustainability 2:2499–2522

Lu D, Weng Q (2009) Extraction of urban impervious surfaces from an IKONOS image. Int J Remote Sen 30(5):1297–1311

Manepalli URR, Bham GH, Kandada S (2011) Evaluation of Hot spot identification using kernel density estimation and Getis–Ord (Gi*) on I-630. In: 3rd International Conference on Road Safety and Simulation. 2011 Sept 14–16, Indianapolis

Mazzocchi C, Sali G, Corsi S (2013) Land use conversion in metropolitan areas and the permanence of agriculture: Sensitivity Index of Agricultural Land (SIAL), a tool for territorial analysis. Land Use Policy 35:155–162

Mitarn T, Lal R, Mishra U, Meena RS, Ravisankar T, Sreenivas (2018) Climate change impact on soil carbon stocks in India. In: Lal R, Stewart BA (eds) Advances in soil science, soil and climate, pp 291–308

Mitra C, Pandey B, Allen NB, Seto KC (2016) Contemporary urbanization in India. In: The Routledge handbook of urbanization and global environmental change. Routledge, London, pp 64–76

Mitsuda Y, Ito S (2011) A review of spatial-explicit factors determining spatial distribution of land use/land-use change. Landsc Ecol Eng 7:117–125

Musa SI, Hashim M, Reba MN (2017) A review of geospatial-based urban growth models and modelling initiatives. Geocarto Int 32(8):813–833

Myint SW, Gober P, Brazel A, Clarke SG, Weng Q (2011) Per-pixel vs. object-based classification of urban land cover extraction using high spatial resolution imagery. Remote Sens Environ 115 (5):1145–1161

National Remote Sensing Centre (2010) Indian Space Research Organisation (ISRO), Ebook on remote sensing applications. National Remote Sensing Centre, Hyderabad. Available at: http://www.nrsc.gov.in/pdf/Chap_2_LULC.pdf
Ord JK, Getis A (1995) Local spatial autocorrelation statistics: distributional issues and an application. Geogr Anal 27:286–306
Pandey B, Seto KC (2015) Urbanization and agricultural land loss in India: comparing satellite estimates with census data. J Environ Manag 148:53–66
Parece TE, Campbell JB (2013) Comparing urban impervious surface identification using Landsat and high resolution aerial photography. Remote Sens 5(10):4942–4960
Phalan B, Onial M, Balmford A, Green RE (2011) Reconciling food production and biodiversity conservation: land sharing and land sparing compared. Science 333(6047):1289–1291
Piorr A, Ravetz J, Tosics I (2011) Peri-urbanisation in Europe: towards European policies to sustain urban-rural futures; forest and landscape. University of Copenhagen, Copenhagen, pp 30–42. ISBN 8779035345
Pölling B, Mergenthaler M, Lorleberg W (2016) Professional urban agriculture and its characteristic business models in Metropolis Ruhr, Germany. Land Use Policy 58:366–379
Pothukuchi K, Kaufman JL (2000) The food system: a stranger to the planning field. J Am Plan Assoc 66(2):113–124
Ravetz J, Fertner C, Nielsen TS (2013) The dynamics of peri-urbanization. In: Peri-urban futures: scenarios and models for land use change in Europe. Springer, Berlin/Heidelberg, pp 13–44. ISBN 978-3-642-30528-3
Redeker C, Kantoush SA (2014) The Nile Delta: urbanizing on diminishing resources. Built Environ 40(2):201–212
Sakthivadivel R, De Fraiture C, Molden DJ, Perry C, Kloezen W (1999) Indicators of land and water productivity in irrigated agriculture. Int J Water Resour Dev 15(1–2):161–179
Schaldach R, Alcamo J, Heistermann M (2006) The multiple-scale land use change model LandShift: a scenario analysis of land use change and environmental consequences in Africa. In: Voinov A, Jakeman AJ, Rizzoli AE (eds) Proceedings of the iEMSs Third Biennial Meeting: "Summit on Environmental Modelling and Software". International Environmental Modelling and Software Society, Burlington, USA, July 2006
Seto KC, Ramankutty N (2016) Hidden linkages between urbanization and food systems. Science 352(6288):943–945
Shaw D (2020) City building on the eastern frontier: sorting the New Nineteenth-Century City. JHU Press
Sinclair R, Thünen V (1976) Urban sprawl. Ann Assoc Am Geogr 57:72–87
Sobrino JA, Jime'nez-Muoz JC, Paolini L (2004) Land surface temperature retrieval from landsat TM5. Remote Sens Environ 90(4):434–446
Songchitruksa P, Zeng X (2010) Getis–Ord spatial statistics for identifying hot spots using incident management data. In: Transportation Research Board (TRB) 89th Annual Meeting; 2010 Jan 10–14; Washington, DC
Stéphenne N, Lambin EF (2001) A dynamic simulation model of land-use changes in Sudano-sahelian countries of Africa (SALU). Agric Ecosyst Environ 85(1–3):145–161
Streutker DR (2002) A remote sensing study of the urban heat island of Houston, Texas. Int J Remote Sens 23(13):2595–2608
Su SL, Jiang ZL, Zhang Q, Zhang YA (2011) Transformation of agricultural landscapes under rapid urbanization: a threat to sustainability in Hang-Jia-Hu region, China. Appl Geogr 31:439–449
Syvitski JP, Kettner AJ, Overeem I, Hutton EW, Hannon MT, Brakenridge GR, Day J, Vörösmarty C, Saito Y, Giosan L, Nicholls RJ (2009) Sinking deltas due to human activities. Nat Geosci 2(10):681–686
Thiruvengadachari S, Sakthivadivel R (1997) Satellite remote sensing for assessment of irrigation system performance: a case study in India. IWMI, Colombo
Tooke TR, Coops NC, Christen A, Voogt JA (2009) Extracting urban vegetation characteristics using spectral mixture analysis and decision tree classifications. Remote Sens Environ 113 (2):398–407

Triantakonstantis D (2012) Urban growth prediction: a review of computational models and human perceptions. J Geogr Inf Syst 4:555–587
Tscharntke T, Clough Y, Wanger TC, Jackson L, Motzke I, Perfecto I, Vandermeer J, Whitbread A (2012) Global food security, biodiversity conservation and the future of agricultural intensification. Biol Conserv 151(1):53–59
United Nations (2019) World urbanization prospects, the 2018 revision. Department of Economic and Social Affairs, United Nations, New York
Van Asselen S, Verburg PH (2013) Land cover change or land-use intensification: simulating land system change with a global-scale land change model. Glob Chang Biol 19(12):3648–3667
Van Rij E, Dekkers J, Koomen E (2008) Analysing the success of open space preservation in the Netherlands: the Midden-Delfland case. Tijdschr Econ Soc Geogr 99:115–124
Vaz E, Arsanjani JJ (2015) Predicting urban growth of the greater Toronto area-coupling a Markov cellular automata with document meta-analysis. J Environ Inf 25(2):71–80
Veldkamp A, Fresco LO (1996) CLUE-CR: an integrated multi-scale model to simulate land use change scenarios in Costa Rica. Ecol Model 91(1–3):231–248
Velpuri NM, Thenkabail PS, Gumma MK, Biradar C, Dheeravath V, Noojipady P, Yuanjie L (2009) Influence of resolution in irrigated area mapping and area estimation. Photogramm Eng Remote Sens 75(12):1383–1395
Verburg PH, Schot PP, Dijst MJ, Veldkamp A (2004) Land use change modelling: current practice and research priorities. Geogr J 61(4):309–324
Verburg PH, van de Steeg J, Veldkamp A, Willemen L (2009) From land cover change to land function dynamics: a major challenge to improve land characterization. J Environ 90 (3):1327–1335
Wang J, Mountrakis G (2011) Developing a multi-network urbanization model: a case study of urban growth in Denver, Colorado. Inte J Geogr Inf Sci 25(2):229–253
Wästfelt A, Zhang Q (2016) Reclaiming localisation for revitalising agriculture: a case study of peri-urban agricultural change in Gothenburg, Sweden. J Rural Stud 47:172–185
Wojciech Z, Kamil K, Bogusława BZ (2020) Intensity and driving forces of land abandonment in Eastern Poland. Appl Sci 10:3500
World Bank (2013) Urbanization and economic growth. Report, Urban China, pp 81–261
Wray C, Cheruiyot K (2015) Key challenges and potential urban modelling opportunities in South Africa, with specific reference to the Gauteng City-region. South Afr J Geom 4(1):14–35
Xie H, Wang P, Yao G (2014) Exploring the dynamic mechanisms of farmland abandonment based on a spatially explicit economic model for environmental sustainability: a case study in Jiangxi Province, China. Sustainability 6:1260–1282
Xu HQ (2008a) A new remote sensing index for fastly extracting impervious surface information. Geom Inf Sci Wuhan Univ 33:1150–1153
Xu HQ (2008b) A new index for delineating built-up land features in satellite imagery. Int J Remote Sens 29(14):269–4276
Zasada I (2011) Multifunctional peri-urban agriculture—a review of societal demands and the provision of goods and services by farming. Land Use Policy 28:639–648
Zasada I, Fertner C, Piorr A, Nielsen TS (2011) Peri-urbanisation and multifunctional adaptation of agriculture around Copenhagen. Dan J Geogr 111:59–72
Zhang YS, Odeh IOA, Han CF (2009) Bi-temporal characterization of land surface temperature in relation to impervious surface area, NDVI and NDBI, using a sub-pixel image analysis. Int J Appl Earth Obs 11(4):256–264
Zhang D, Huang Q, He C, Wu J (2017) Impacts of urban expansion on ecosystem services in the Beijing-Tianjin-Hebei urban agglomeration, China: a scenario analysis based on the Shared Socioeconomic Pathways. Resou Conserv Recycl 125:115–130